

# **Orthogonal pathway design for eco-efficient biocatalytic monomer production from cyclohexane**

Dissertation

zur Erlangung des Doktorgrades der Naturwissenschaften (Dr. rer. nat.)

der Naturwissenschaftlichen Fakultät I - Biowissenschaften -

der Martin-Luther-Universität Halle-Wittenberg,

vorgelegt von

Frau M. Sc. Lisa Bretschneider geb. Schäfer

geboren am 22.10.1992 in Riesa

Gutachter: Prof. Dr. Bruno Bühler

Prof. Dr. Nick Wierckx

Prof. Dr. Markus Pietzsch

Tag der Verteidigung: 14.10.2021



# Acknowledgements

First, I want to thank my doctoral father Prof. Bruno Bühler. Thank you for allowing me to develop my scientific and personal skills and your guidance throughout these three years. Discussions with you were always helpful to get new ideas and a deeper understanding of my research.

I also thank our head of department Prof. Andreas Schmid for sharing his expertise and new impulses during our scientific seminars.

I want to express special thanks to my second supervisor Dr. Rohan Karande who gave me motivation, encouragement, and excitement. Your ideas and visions significantly contributed to this thesis.

I am very thankful that I had the opportunity to accomplish my thesis in the frame of the ERA-IB project PolyBugs headed by Prof. Katja Bühler. It was a pleasure to work in this interdisciplinary research environment and I thank all collaborators from Lisbon, Marl, Hamburg, and Trondheim. I express my gratitude to Prof. Nick Wierckx and Prof. Markus Pietzsch for their willingness to review my thesis.

My special thanks go to Inge for being the best lab partner I can imagine. We grew side by side and gave each other the strength to manage every difficult situation throughout these years. It is a great feeling to work (and live) with a friend and share coffee breaks, grief, and happiness.

I want to thank my students Nathalie Becker, Friedrike Nintzel, Golnaz Memari, Afaq Ahmed, and Martin Wegner who contributed to this thesis with valuable experimental work and helped me to manage the different parts of this thesis.

I enjoyed the supportive and joyful atmosphere in the Solar Materials group and would like to thank all (former) colleagues: Adrian, Amelie, Anja, Anna, Bin, Caro (Bertelmann and Ruhl), Christian (David and Dusny), Eleni, Fabian, Franz, Hans, Heiko, Katharina, Kristin, Jacky, Jenny, Jens, Jochen, Jörg, Magda, Mahir, Martin (Lindmeyer and Schirmer), Pål, Paul, Peter, Robert, Ron, Samuel, Sara, Sebastian, Seung Jae, Sonja, Stephan, Tim, and Vu.

Ganz besonders möchte ich meiner Familie für ihren Zuspruch und ihre Unterstützung danken und dass sie den Glauben an mich nie verloren haben. Danke, Alex, dass du in dieser Zeit nicht nur mein Ehemann geworden bist, sondern zeitweise mein Leben organisiert und mich während meiner Arbeitswochenenden auf jegliche Weise unterstützt hast. Danke, dass du da bist!



# Table of contents

<b>Acknowledgements</b>	<b>I</b>
<b>Table of contents</b>	<b>III</b>
<b>Summary</b>	<b>V</b>
<b>Zusammenfassung</b>	<b>VII</b>
<b>List of abbreviations</b>	<b>IX</b>
<b>Chapter 1</b> General Introduction	<b>1</b>
<b>Chapter 2</b> Results	<b>27</b>
<b>Chapter 2.1</b> Maximizing biocatalytic cyclohexane hydroxylation by modulating cytochrome P450 monooxygenase expression in <i>P. taiwanensis</i> VLB120	<b>28</b>
<b>Chapter 2.2</b> Characterization of different biocatalyst formats for BVMO-catalyzed cyclohexanone oxidation	<b>29</b>
<b>Chapter 2.3</b> Rational engineering of a multi-step biocatalytic cascade for the conversion of cyclohexane to polycaprolactone monomers in <i>Pseudomonas taiwanensis</i>	<b>30</b>
<b>Chapter 2.4</b> Conversion of cyclohexane to 6-hydroxyhexanoic acid using recombinant <i>Pseudomonas taiwanensis</i> in a stirred-tank bioreactor	<b>31</b>
<b>Chapter 2.5</b> One-pot synthesis of 6-aminohexanoic acid from cyclohexane using mixed-species cultures	<b>51</b>
<b>Chapter 2.6</b> Rational orthologous pathway and biochemical process engineering for adipic acid production using <i>Pseudomonas taiwanensis</i> VLB120	<b>52</b>
<b>Chapter 3</b> General Discussion and Conclusions	<b>75</b>
<b>References</b>	<b>89</b>
<b>Appendix</b>	<b>103</b>
1 Front. Bioeng. Biotechnol. (2020), 8, art. 140, incl. Supplementary Material	<b>104</b>
2 Biotechnol. Bioeng. (2021), incl. Supplementary Material	<b>129</b>
3 Biotechnol. J. (2020), 15(11), art. 2000091, incl. Supplementary Material	<b>154</b>
4 Front. Catal. (2021) Supplementary Material	<b>175</b>

5 Microb. Biotechnol. (2021), 14(3), p. 1011-1025, incl. Supplementary Material	179
6 Supplementary Material for Chapter 2.6	209
<b>Curriculum Vitae</b>	<b>218</b>
<b>Selbstständigkeitserklärung</b>	<b>220</b>

# Summary

Plastics are found in every aspect of human life and have applications in packaging, electronics, transport, construction, and textile manufacturing. Polyesters such as polycaprolactone and polyamides like nylons are the most important synthetic fibers. However, the production of the monomers, for instance,  $\epsilon$ -caprolactone ( $\epsilon$ -CL), 6-hydroxyhexanoic acid (6HA), 6-aminohexanoic acid (6AHA), and adipic acid (AA), are associated with severe environmental concerns. Their production from the crude oil derived cyclohexane comprises several steps at elevated temperature and pressure and produces hazardous by-products such as the greenhouse gas nitrous oxide and heavy metals. Consequently, there is a demand for greener and more efficient production routes. Biocatalytic processes and, more specifically whole-cell biotransformations, are operated under mild conditions and can be engineered as cascade reactions enabling one-pot processes. Therefore, bioprocesses offer enormous potential to save time, energy, and waste, allowing for ecological and economical solutions. In this thesis, recombinant *Pseudomonas taiwanensis* VLB120 strains harboring different *in vivo* enzymatic cascades to produce the monomers  $\epsilon$ -CL, 6HA, 6AHA, and AA were generated, optimized, and evaluated under process conditions.

The synthetic pathway to produce  $\epsilon$ -CL is composed of the P450 monooxygenase Cyp, the alcohol dehydrogenase CDH, and the Baeyer-Villiger monooxygenase CHMO all originating from the bacterium *Acidovorax* CHX100. Analysis of the cascade enzymes revealed that Cyp-catalyzed cyclohexane oxidation constitutes the rate-limiting step. Genetic alterations involving transcriptional, translational, and gene dosage engineering enabled a 2.5-fold increase of whole-cell activity to  $55 \text{ U g}_{\text{CDW}}^{-1}$  than the control strain. The characterization of the CHMO in different biocatalyst formats, i.e., isolated enzyme, suspended whole cells, and biofilms demonstrated its broad substrate spectrum and favorable properties of suspended whole cells. The efficient regeneration of cofactors via the central carbon metabolism makes this format highly promising from a kinetics perspective.

The entire 3-step cascade was built based on this catalyst resulting in specific  $\epsilon$ -CL formation activity of  $43 \text{ U g}_{\text{CDW}}^{-1}$ . Intrinsic hydrolases of *P. taiwanensis* causing 6HA accumulation reduced the  $\epsilon$ -CL yield to 80 %. Albeit, polycaprolactone might also be synthesized from 6HA in a polycondensation reaction. The cascade's amendment with the *Acidovorax* lactonase gave 100 % cyclohexane conversion and 100 % 6HA yield in 5 mM shake-flask experiments showing similar whole-cell activities. After the proof-of-concept, reaction and process engineering in a stirred-tank reactor were pursued. Feeding of cyclohexane via the air phase enabled a specific product yield of  $0.4 \text{ g}_{6\text{HA}} \text{ g}_{\text{CDW}}^{-1}$  and a final 6HA titer of  $3.3 \text{ g L}^{-1}$ . Cyclohexane toxicity and product inhibition were found to be the main factors responsible for decreasing biocatalyst activities. Further efforts involving precise cyclohexane monitoring and in situ product removal are required to stabilize the process and enhance product titer.

The synthesis of the nylon 6 monomer 6AHA from cyclohexane is possible via 6HA and two additional enzymes catalyzing further oxidation and subsequent amination. High metabolic burden and expression issues of the six enzymes in *P. taiwanensis* favored a mixed-species approach by utilizing the polycaprolactone monomer-producing strains combined with *Escherichia coli* strains containing the corresponding downstream cascade.  $\epsilon$ -CL was found to be the better 'shuttle molecule' than 6HA enabling higher 6AHA formation rates and yields. Optimization of oxygen feeding, biomass concentrations, and cyclohexane mass transfer led to complete substrate conversion with 86 % 6AHA yield and an initial specific 6AHA formation rate of  $7.7 \pm 0.1 \text{ U g}_{\text{CDW}}^{-1}$ .

Genetic engineering of plasmid harboring the *Acidovorax*-derived alcohol and aldehyde dehydrogenase genes and its introduction into the 6HA-producing *P. taiwanensis* gave rise to the nylon 6,6 monomer AA. Induced resting cells turned out to be most promising in terms of stability and activity ( $49 \text{ U g}_{\text{CDW}}^{-1}$ ) and were applied in a stirred-tank reactor. During the induction and production phase, glucose excess conditions enhanced the average productivity ( $1.3 \text{ g L}^{-1} \text{ h}^{-1}$ ) and final AA titer to  $10.2 \text{ g L}^{-1}$ . Downstream-processing of the reactor broth resulted in  $3.4 \text{ g AA}$  with a purity of 96 %. Cyclohexane recycling, as well as improved purification techniques, need to be investigated and optimized to enhance the yield on the substrate.

In conclusion, this thesis exploits the potential of whole-cell catalysis for cascade reactions allowing one-pot conversions with high activities and superior conversions. The entire biocatalysis cycle from enzyme selection, genetic engineering, and investigation of different biocatalyst systems towards reaction and process engineering has been conducted. For the first time, 6AHA could be synthesized from cyclohexane. The achieved AA titer and productivity are the highest reported so far and constitute the first one-species approach for this reaction. Taken together, these findings support the development of eco-efficient monomer production routes allowing the sustainable use of resources.



# Zusammenfassung

Kunststoffe, die man in jedem Lebensbereich findet, haben Verwendung im Verpackungswesen, in der Elektronik, im Transport, im Bauwesen und in der Textilindustrie. Polyester wie Polycaprolacton und Polyamide wie Nylon stellen die wichtigsten synthetischen Fasern dar. Jedoch ist die Produktion deren Monomere, z.B.  $\epsilon$ -Caprolacton ( $\epsilon$ -CL), 6-Hydroxyhexansäure (6HA), 6-Aminohexansäure (6AHA) und Adipinsäure (AA) mit gravierenden Umweltschädigungen verbunden. Deren Herstellung basiert auf Cyclohexan, welches aus Erdöl gewonnen wird, und beinhaltet mehrere Produktionsschritte bei hoher Temperatur und hohem Druck und produziert zudem giftige Nebenprodukte wie das Treibhausgas Distickstoffoxid sowie Schwermetalle. Dadurch entsteht eine erhöhte Nachfrage nach grünen und effizienteren Produktionsrouten. Biokatalytische Prozesse – insbesondere Ganzzellbiotransformationen – werden unter milden Bedingungen betrieben und können als Reaktionskaskade konzipiert sein, sodass nur ein Reaktionsgefäß benötigt wird. Deshalb eröffnen Bioprozesse ein enormes Potenzial, um Zeit, Energie und Müll einzusparen, was gleichzeitig ökologische und ökonomische Lösungen erlaubt. In dieser Arbeit wurden verschiedene rekombinante *Pseudomonas taiwanensis* VLB120-Stämme, welche *in vivo* Kaskaden beherbergen, um Monomere zu produzieren, generiert, optimiert und unter Prozessbedingungen evaluiert.

Der synthetische Weg, um  $\epsilon$ -CL zu produzieren, besteht aus der P450-Monooxygenase Cyp, der Alkoholdehydrogenase CDH und der Baeyer-Villiger-Monooxygenase CHMO, welche alle aus dem Bakterium *Acidovorax* CHX100 stammen. Eine Analyse der Kaskadenenzyme zeigte, dass die Cyp-katalysierte Cyclohexanoxidation geschwindigkeitsbestimmend ist. Genetische Veränderungen, welche die Transkription, Translation und Gendosierung zum Ziel hatten, ermöglichten einen 2,5-fachen Anstieg der Ganzzellaktivität auf  $55 \text{ U g}_{\text{CDW}}^{-1}$  im Vergleich zum Kontrollstamm. Die Charakterisierung der CHMO in Form verschiedener Katalysatorformate – als isoliertes Enzym, als suspendierte Ganzzellen, und als Biofilm – demonstrierte das breite Substratspektrum und die vorteilhaften Eigenschaften suspendierter Ganzzellen. Die effiziente Regenerierung von Kofaktoren über den zentralen Kohlenstoffmetabolismus begünstigt dieses Format von einer kinetischen Perspektive. Die gesamte 3-Schritt-kaskade wurde basierend auf diesem Format aufgebaut und resultierte in einer spezifischen  $\epsilon$ -CL-Bildungsaktivität von  $43 \text{ U g}_{\text{CDW}}^{-1}$ . Intrinsische Hydrolasen von *P. taiwanensis*, welche eine 6HA-Akkumulation herbeiführten, reduzierten den  $\epsilon$ -CL-Ertrag auf 80 %. Polycaprolacton kann jedoch auch in einer Polykondensationsreaktion aus 6HA synthetisiert werden. Das Ergänzen der Kaskade um die *Acidovorax*-Lactonase ergab eine 100 %ige Cyclohexanumsetzung und 100 % 6HA-Ertrag in 5 mM Schüttelkolbenexperimenten mit gleich hohen Aktivitäten. Nachfolgend wurden Reaktions- und Prozesstechnik in einem Rührkesselreaktor evaluiert. Das Zufüttern von Cyclohexan über die Gasphase resultierte in einem spezifischen Produktertrag von  $0,4 \text{ g}_{6\text{HA}} \text{ g}_{\text{CDW}}^{-1}$  und einem finalen 6HA-Titer von  $3,3 \text{ g L}^{-1}$ . Es stellte sich heraus, dass die Cyclohexantoxizität sowie Produktinhibierung die hauptsächlichen limitierenden Faktoren für die abnehmende Biokatalysatoraktivität sind. Weitere Bemühungen, welche die präzise Kontrolle der Cyclohexanconzentration und *in situ*-Produktentfernung beinhalten, sind notwendig, um den Prozess zu stabilisieren und den Produkttiter zu erhöhen.

Die Synthese des Nylon 6-Monomers 6AHA aus Cyclohexan über 6HA benötigt zwei zusätzliche Enzyme, welche die weitere Oxidation und nachfolgende Aminierung katalysieren, möglich. Die gesteigerte metabolische Last und Expressionsprobleme der sechs Enzyme in *P. taiwanensis* fa-

vorisierten einen Ansatz, bestehend aus verschiedenen Spezies (mixed-species) unter Verwendung der *Pseudomonas*-Stämme, welche Monomere für Polycaprolacton produzieren, sowie *Escherichia coli*-Stämme, welche die weiterführende Kaskade beherbergen. Dabei wurde herausgefunden, dass  $\epsilon$ -CL das bessere Transfermolekül im Vergleich zu 6HA ist, da höhere 6AHA-Bildungsraten und Erträge damit erzielt wurden. Die Optimierung der Sauerstoffzugabe, der Zellkonzentration sowie des Cyclohexanmassentransfers führte zu einer vollständigen Substratumwandlung mit einem 6AHA-Ertrag von 86 % und einer initialen spezifischen 6HA-Bildungsrate von  $7.7 \pm 0.1 \text{ U g}_{\text{CDW}}^{-1}$ .

Die genetische Manipulation eines Plasmids, welcher die aus *Acidovorax* stammenden Alcohol- und Aldehydhydrogenasegene beherbergt, und dessen Einführung in den 6HA-produzierenden *P. taiwanensis* ermöglichten die Produktion des Nylon 6,6-Monomers AA. Induzierte ruhende Zellen stellten sich aufgrund ihrer Stabilität und Aktivität ( $49 \text{ U g}_{\text{CDW}}^{-1}$ ) als vielversprechend heraus, weshalb sie in einem Rührkesselreaktorexperiment benutzt wurden. Ein Glukoseüberschuss während der Induktions- und Produktionsphase erhöhte die durchschnittliche Produktivität ( $1.3 \text{ g L}^{-1} \text{ h}^{-1}$ ) und den finalen AA-Titer auf  $10.2 \text{ g L}^{-1}$ . Aus der Aufreinigung der Reaktorbrühe resultierten  $3.4 \text{ g AA}$ , welche eine Reinheit von 96 % hatten. Die Wiederverwendung von Cyclohexan sowie verbesserte Aufreinigungstechniken sind notwendig, um den Ertrag – bezogen auf das Substrat – zu erhöhen. Zusammenfassend lässt sich feststellen, dass diese Arbeit das Potenzial der Ganzzellkatalyse für Kaskadenreaktionen, welche nur in einem Reaktionsgefäß stattfinden, mit hohen Aktivitäten und verbesserten Umsetzungen erforscht. Der gesamte Prozess umfasste die Auswahl von Enzymen, genetische Manipulation der Konstrukte, die Evaluierung verschiedener Biokatalysatorsysteme sowie Reaktions- und Prozesstechnik. Zum ersten Mal konnte 6AHA aus Cyclohexan synthetisiert werden. Die erreichten AA-Titer und -Produktivitäten sind die höchsten, welche bis jetzt erreicht wurden, und demonstrieren die erste Kaskade in nur einem Stamm. Folglich tragen diese Erkenntnisse dazu bei, dass ökoeffiziente Monomerproduktionsprozesse erreichbar sind, sodass Ressourcen nachhaltig genutzt werden können.

# List of abbreviations

SI-units and abbreviations will not be listed in this index.

%	Percent
°C	Degree Celsius
6AHA	6-Aminohexanoic acid
6HA	6-Hydroxyhexanoic acid
7HA	7-Aminoheptanoic acid
AA	Adipic acid
AlcDH	Alcohol dehydrogenase
AldDH	Aldehyde dehydrogenase
aq.	aqueous
BVMO	Baeyer-Villiger-Monooxygenase
Cam	Chloramphenicol
CDH	Cyclohexanol dehydrogenase
CDW	Cell dry weight
$\epsilon$ -CL	$\epsilon$ -caprolactone
Cyp	Cytochrome P450 monooxygenase
DCPK	Dicyclopropyl ketone
DINP	Diisononyl phthalate
DGC	Diguanylate cyclase
DSP	Downstream processing
<i>et al.</i>	<i>Et alii, et aliae, et alia</i>
Fd	Ferredoxin
Fd Red	Ferredoxin reductase
FID	Flame ionization detector
GC	Gas chromatography
GCA	Growing cell assay
Gm	Gentamycin
HPLC	High pressure liquid chromatography
IPTG	Isopropyl- $\beta$ -D-thiogalactopyranoside
$k_{cat}$	Turnover number
$K_i$	Inhibition constant
$K_M$	Michaelis-Menten constant
Km	Kanamycin
KPi	Potassium phosphate
$K_S$	apparent substrate uptake constant
LacI <sup>(q)</sup>	Lac repressor (with stronger promoter)
Lact	Lactonase
LB	Lysogeny broth
logP	Logarithmic octanol-water coefficient
M	Molar

NAD(P/H)	(Reduced) nicotinamide adenine dinucleotide (phosphate)
OD <sub>450</sub>	Optical density at 450 nm
PA	Pimelic acid
P <sub>alk</sub>	<i>alk</i> promoter
pH	Negative decadic logarithm of the hydrogen ion concentration
P <sub>lac</sub>	<i>lac</i> promoter
pO <sub>2</sub>	Partial pressure of oxygen
P <sub>tac</sub>	<i>tac</i> promoter
P <sub>trc</sub>	<i>trc</i> promoter
PTV	Programmed temperature vaporizer
R	resistance
RB	Riesenberg
RBS	Ribosomal binding site
RCA	Resting cell assay
RI	Refractive index
rpm	Revolutions per minute
RT	Room temperature
SDS-PAGE	Sodium dodecyl sulphate-polyacrylamide gel electrophoresis
sp.	species
STR	Stirred-tank reactor
Strep	Streptomycin
TTN	Total turnover number
U	Unit [1 μmol product per min]
UV	Ultraviolet
v/v	volume/volume
w/v	weight/volume
WT	wild-type
Y	Yield

# **Chapter 1**

## **General Introduction**

## 1.1 The concept of green and sustainable chemistry with a focus on polymers

### 1.1.1 The principles of green chemistry and sustainable chemistry

Human development and prosperity are connected to industrial processes relying on fossil resources as energy sources and raw materials. However, these activities have profoundly affected the Earth, defining a new human-dominated geological epoch – the Anthropocene (Lewis & Maslin, 2015). Within the last decade, people have realized that these resources from Nature are limited and global warming needs to be reduced/stopped. The term “green chemistry” was defined by Anastas & Warner (1998) and refers to “the design, development, and implementation of chemical processes and products to reduce or eliminate substances hazardous to human health and the environment”. It thereby focuses on preventing pollution and hazards across all life-cycle stages of a chemical process, which is economically viable (Anastas & Eghbali, 2010). Nevertheless, green chemistry mainly tries to optimize the process itself and does not consider remediation strategies. Additionally, it lacks an implicit economic component, which was criticized by industry (Sheldon, 2018).

These shortcomings are addressed by “sustainability,” which is defined as a “development that meets the needs of the present generation without compromising the ability of future generations to meet their own needs” (World Commission on Environment and Development, 1987). Two main implications have been suggested by Graedel (2002): (1) natural resources should be drawn at rates ensuring their supply over the long term, and (2) wastes and residues should be generated at rates not higher than can readily be assimilated by the natural environment. Consequently, sustainable chemistry also considers longer periods, broader spaces, and complex interactions (Graedel, 2002). Thus, the current use of fossil resources is unsustainable. On the one hand, coal, gas, and oil are depleted at a far higher rate than they are generated, and on the other hand, the carbon dioxide produced cannot be entirely assimilated (Sheldon, 2018).

To achieve the goal of green and sustainable chemistry, alternative synthesis routes and production processes are required. Biotechnology has many intrinsic advantages in the context of a more environmentally friendly concept for industrial applications, which will be discussed in the next section.

### 1.1.2 The role of biotechnology

Biotechnology is defined as “any technological application that uses biological systems, living organisms, or derivatives thereof, to make or modify products or processes for specific use” by the Convention on Biological Diversity of the United Nations (United Nations, 1992). The most popular classification of biotechnology relies on a color code. Among others, the four most important sectors are: green biotechnology involving plant engineering and agricultural developments; blue biotechnology referring to marine and aquatic applications; red biotechnology devoted to medicine and health; and white biotechnology comprising the vast field of industrial applications (Kafarski, 2012). Biocatalysis constitutes the most important branch of industrial biotechnology. It encompasses all processes making use of enzymes or microorganisms as natural catalysts. The latter is termed whole-cell biocatalysis and can further be subdivided into fermentations and biotransformations. Fermentation processes rely on the same substrate for the formation of biomass and the desired product. In biotransformations, an additional compound is fed, which serves as a substrate for the desired reaction or reaction cascade, whereas, in the case of whole-cell biocatalysts, a substrate for cell metabolism may be required to support cell maintenance, growth, enzyme reactivation/synthesis,

and/or the supply of reduction equivalents. The transition from enzyme-catalyzed biotransformations via metabolism-dependent biotransformations to fermentations can also be considered a continuum (Schrewe *et al.*, 2013a).

The major part of the waste generated in the organic synthesis can be attributed to the use of predominantly inorganic compounds as catalysts and co-substrates as well as to solvent use (Leak *et al.*, 2009). In biocatalysis, the biodegradable catalyst (cell or enzyme) is renewable or derived from a renewable resource, and the reactions are carried out under mild conditions (pH, ambient pressure, and temperature) in water as an environmentally friendly solvent (Sheldon, 2012). Biocatalysis fulfills 10 out of 12 principles for green chemistry; the remaining two concern the product, which can be diverse (Anastas & Warner, 1998; Sheldon & Woodley, 2018). Furthermore, similar reaction conditions to be applied for various biocatalytic reactions facilitate one-pot multistep reaction schemes, i.e., cascades (Chapters 2.3, 2.4, 2.5, 2.6; Sheldon & Woodley (2018)). Due to these criteria, Sheldon & Woodley (2018) concluded that biocatalysis is a truly green and sustainable technology. However, biocatalytic processes consume resources and produce waste, making a quantitative assessment necessary to take into account down-stream processing, regeneration systems, and solvents for commonly used multiphase systems (Kuhn *et al.*, 2010; Ni *et al.*, 2014). Certainly, biotechnology has the potential to allow for environmentally benign reactions and therefore contributes to greener chemistry. Still, one has to face the enormous challenge of economic feasibility by reaction and catalyst engineering to make the process cost-efficient.

Especially the production of polymers that are used in all aspects of human life offers great potential for greener production routes. The replacement of traditional energy- and waste-intensive processes with sustainable alternatives would be a huge step toward achieving sustainability. The problems associated with the current polymer production and potential solutions are summarized in the next section.

### 1.1.3 (Bio)polymer production

Natural polymers such as silk, rubber, and cellulose (Figure 1.1) have been used by humans long before the first evidence of the chain structures was discovered by Staudinger and colleagues (Morawetz, 1987). Today, polymers are defined as macromolecules “of high relative molecular mass, the structure of which essentially comprises the multiple repetitions of units derived, actually or conceptually, from molecules of low relative molecular mass” by the IUPAC (Jenkins *et al.*, 1996).

The first polymer science efforts aimed at modifying natural polymeric materials and, afterward, imitating these (Mülhaupt, 2004). The sophisticated structural design of biological polymers within living cells that act as sensors, actuators, or processors opened the field of bioinspired macromolecular chemistry, which is still an active field of research (Mülhaupt, 2010). In 1907, the first commercially used synthetic polymer Bakelite<sup>TM</sup> was invented by reacting phenol with formaldehyde (Braun & Collin, 2010). Since then, various polymers were commercialized based on fossil-derived monomers and emerging technologies (Mülhaupt (2013); Figure 1.1).

Nowadays, polyamides (nylons) and polyesters have the highest demand among synthetic fibers and constitute 80 % of the worldwide production (Bellussi & Perego, 2000). Nylons 6 and 6,6 have applications in automotive engineering, consumer products, and packaging and comprise 95 % of the total polyamide market (Weissermel & Arpe, 2003). The corresponding monomers  $\epsilon$ -caprolactam,

adipic acid (AA), and hexamethylenediamine have a high yearly demand of over 8 million tons - the first two belong to the top 50 chemicals (Wittcoff *et al.*, 2012).

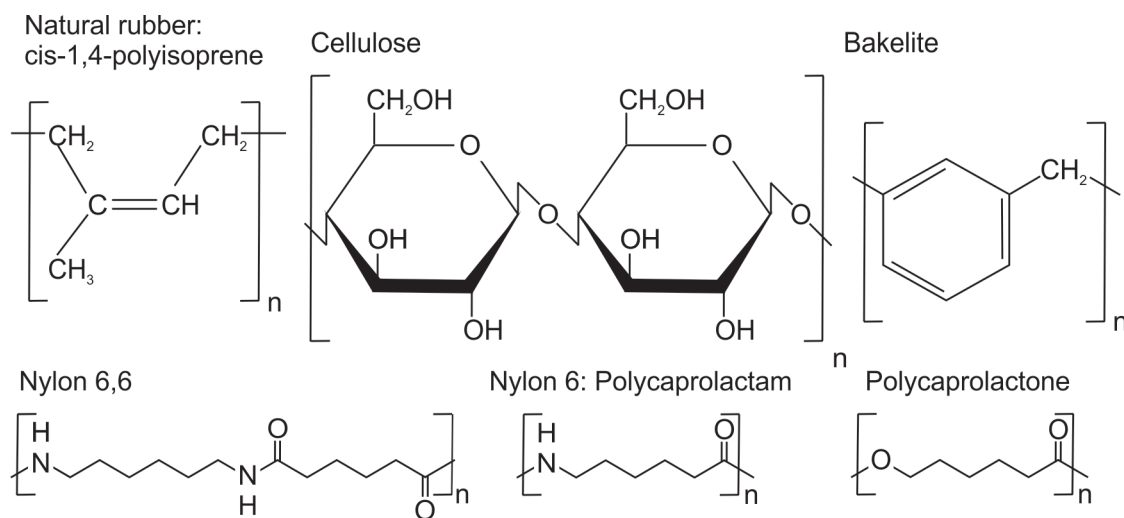


**Figure 1.1: Structures of polymers.** Depicted are natural (rubber, cellulose) as well as artificial (Bakelite, Nylon, polycaprolactone) polymers.

In the following, the traditional production routes and associated problems for these monomers are briefly summarized according to Wittcoff *et al.* (2012). The most widely used starting compound is cyclohexane, which is obtained via the hydrogenation of benzene. Cyclohexane oxidation to KA (ketone/alcohol) oil, a mixture of cyclohexanol and cyclohexanone, at 10-15 bar and 150 °C applying a metal catalyst reaches per pass conversions of 10-12 %. KA oil undergoes oxidation to AA utilizing nitric acid as oxidant and a copper catalyst enabling high selectivity but low per pass conversion of 12 %. The major issue for AA synthesis is the evolution of nitrous oxide as a by-product with three times higher global warming potential than carbon dioxide. AA then serves as the substrate for hexamethylenediamine synthesis by ammoniation to adiponitrile at 275 °C in the presence of strong acids and its subsequent hydrogenation.  $\epsilon$ -caprolactam production starts from cyclohexanone, which needs to be separated from cyclohexanol in KA oil. Using hydroxylamine sulfate and sulfuric acid, an oxime is formed, which undergoes Beckmann rearrangement yielding  $\epsilon$ -caprolactam. Thereby, vast amounts of nitrous waste are generated in the form of ammonium sulfate. Additionally, hydroxylamine, which quickly decomposes to the explosive ammonium nitrile, poses a hazard.

In summary, the inevitable application of metal catalysts and acids implies handling, safety, and corrosion issues. Additionally, waste and side products have adverse environmental effects. Many process steps, often at high temperatures and pressure, require significant energy input (Bellussi & Perego, 2000). Consequently, the development of sustainable and green process alternatives demands massive changes in the process concept. For this purpose, two major approaches can be followed. The more demanding approach includes a change in the primary substrate source away from crude oil. Alternatively, more eco-efficient production processes can be developed based on the same starting substrate. Both options are discussed in the following sections.



### 1.1.3.1 Bio-based monomers and polymers

The ideal vision for green and sustainable plastics would be their generation from renewable feedstocks such as biomass. After use, these bioplastics can be biologically or thermally degraded, yielding reusable monomers or water and carbon dioxide, which in turn serve as electron and carbon sources for biomass growth, thereby closing the circle (Mülhaupt, 2013). Several efforts have been made to employ natural polymers or improve the production of bio-monomers. These efforts are often combined with a biotechnological and therefore “greener” production route.

Cellulose, starch, chitosan, proteins, and lignin are naturally occurring polymers. Due to their inferior mechanical properties compared to commercial plastics, they primarily have specialized applications as blends, coatings, medical products, or food additives (Klemm *et al.*, 2005; Janssen & Moscicki, 2009; Mülhaupt, 2013). The most promising biopolymers for larger volume applications are biopolyesters, i.e., poly(hydroxy alcanoates) (PHAs) produced as storage compounds in bacteria. Their variable architecture allows them to exhibit different properties in terms of stiffness and elasticity (Mülhaupt, 2013). The low abundance of naturally occurring biopolymers associated with increased purification costs makes them less attractive for commercial applications. However, a more promising approach uses renewable feedstocks to produce potentially new monomers that are excreted from cells, are much easier to purify, and then are fed into optimized polymerization processes (Mülhaupt, 2013).

Promising feedstocks include starch, fructose, glucose, ethanol, virgin oils, and glycerol (Beerthuis *et al.*, 2015). It has been shown that the acrylic acid precursor propylene can be chemically synthesized from bioethanol (Iwamoto *et al.*, 2013). A direct route from the biodiesel by-product glycerol resulted in a yield of 34 % (Chiericato *et al.*, 2012). The resulting monomers and polymers are identical to the non-renewable ones and therefore have the same applications in synthetic rubber, absorbents, and plastics (Beerthuis *et al.*, 2015). There are also possible routes for renewable AA. Although lignin can be reacted to phenol to yield bio-based KA oil, the process would still rely on nitric acid oxidation (Beerthuis *et al.*, 2015). A more elegant alternative is the biosynthetic conversion of lignin monomers to *cis,cis*-muconic acid (Kohlstedt *et al.*, 2018), which can be hydrogenated to AA with a 97 % yield (Beerthuis *et al.*, 2015). Another example is the selective oxidation of glucose to glucaric acid and its subsequent reduction to AA with a theoretical yield of 59 % (Beerthuis *et al.*, 2015). Lysine constitutes another feasible biological resource for  $\epsilon$ -caprolactam, as it already possesses the required chemical functionalities and can be further processed with a yield of 75 % (Beerthuis *et al.*, 2015). Recently, a fermentation strategy starting from glucose for 6-aminocaproic acid (6AHA), the linear form of caprolactam, has been reported with a final titer of 160 mg L<sup>-1</sup> in lab-scale batch fermentation (Turk *et al.*, 2016).

There are several examples of already commercialized bio-based polymers. The fermentation of dextrose to L-lactic acid and its subsequent reaction to lactide followed by ring-opening polymerization allowed tailored architectures (Drumright *et al.*, 2000). It is available under its trade name Ingeo™ and has wide-spread applications as 3D printing molds, packaging material, disposable tableware, and medical implants. Therefore, it has a unique role as a biodegradable polymer. Other examples are the PlantBottle™ consisting of 100 % bio-based ethylene glycol and terephthalic acid, and Green Polyethylene™ derived from sugarcane bioethanol (Mülhaupt, 2013). DuPont produces 1,3-propanediol – a monomer for polypropylene terephthalate (Serona®)- from glucose with a capacity

of 45,000 tons year<sup>-1</sup> employing a recombinant *E. coli* strain (Du & Webb, 2011). Evonik Industries operates a pilot plant for polyamide 12 production in a biotransformation process with renewable fatty acid methyl esters as substrates (EVONIK Industries AG, 2013; Ladkau, 2015).

The primary issue of bio-based monomers and polymers arises from the competition with food production, resulting in rising costs for essential products (Mülhaupt, 2013). Possible consequences are deforestation, intensified farming, and fertilizers accompanied by the emission of the greenhouse gas nitrous oxide. This scenario is referred to as the “green paradox” (Sinn, 2012). Thus, a crucial measure of green polymers is the optimization of their production processes.

### 1.1.3.2 Development of greener production processes

The polymerization of monomers to polymers is generally considered to be green as this process is carried out in the melt or gas phase without solvent use and waste generation (Mülhaupt, 2013). The potential for more sustainable strategies lies in the monomer synthesis. The chemical industry deploys 12 % of the total fossil feedstocks used, with equal shares used as raw materials and energy generation (Mecking, 2004). The majority of plastics have an oil-like degree of reduction and energy content, which makes the use of oil as raw material sustainable in contrast to burning it as an energy carrier (Mülhaupt, 2013). The production of polylactic acid (PLA) from renewable resources by Cargill-Dow consumes 57 MJ energy equivalents of fossil fuels for fertilizer and pesticide synthesis, workup, transport, and the polymer production itself, while the same amount of PET requires 80 MJ with half of it serving as raw material (Mecking, 2004; Vink *et al.*, 2003). The high energy content of polymers can be exploited to recycle monomers from consumer products. It has been demonstrated that nylon carpets can be decomposed to caprolactam at moderate pressure and temperature with a yield of 90 % and a high potential to be improved further (Braun *et al.*, 1999). Thereby, recycling can reduce the impact of non-renewable energy, acidification, and smog air and attenuate the global warming potential by 13.5 % (Binder *et al.*, 2010). Overall, monomer recycling offers excellent potential by reducing waste, co-substrates from fossil origin (e.g., hydroxylamine), and energy requirements of the whole process (temperature, pressure). This complies with the green chemistry principles of atom efficiency, prevention, and energy efficiency (Anastas & Warner, 1998). Additionally, recycling allows the sustainable use of petroleum feedstocks (Graedel, 2002).

Biotransformations can achieve sustainable processes based on fossil feedstocks. Typically, they are operated at ambient pressure and temperature, and required medium components (e.g., buffer salts, trace elements) have the potential to be partly reused (Sheldon, 2012). The biotransformation substrate is converted to the desired product by enzymes, and ideally, only water and oxygen are required as readily available co-substrates. However, enzyme production, irrespective if whole cells or isolated enzymes are employed, requires an energy and carbon source, typically sugars. This, although at a reduced extent, again constitutes a possible competition with the food industry, which can be circumvented by engineering bacteria to use waste products like molasses or corn oil (Chaudhry *et al.*, 2011). As another promising alternative, phototrophic microorganisms can be used with light as an energy source and carbon dioxide as a carbon source. In contrast to heterotrophic bacteria, phototrophs generate reduction equivalents (mainly NADPH) from water in the photosynthetic light reaction (Ducat *et al.*, 2011). In the past years, several biotechnological synthesis routes for monomers and polymers have been developed. Their economic feasibility and possible contribution to a green

economy will be discussed in the next section.

### 1.1.3.3 Comparison of traditional production routes and new concepts

The assessment of environmental impact, sustainability, and greenness of a process necessitates life-cycle assessment (LCA) techniques. Hong & Xu (2012) analyzed the current chemical caprolactam production in China. It has a global warming potential of 7.5 t carbon dioxide equivalents per ton product and an energy demand of 156 GJ ton<sup>-1</sup>, with electricity and steam being the main contributions. Benzene, sodium hydroxide, hydrogen peroxide, and sulfuric acid constitute the primary raw materials required. The highest benefit would be an efficiency increase in terms of increasing the yield on benzene. An alternative chemo-enzymatic route for the production of  $\epsilon$ -caprolactone ( $\epsilon$ -CL) has been presented by Thaore *et al.* (2018). The enzymatic hydrolysis of milled corn starch yields glucose, which is chemically converted to  $\epsilon$ -CL by dehydrogenation via 5-hydroxymethylfurfural. The emission of carbon dioxide (1557 kg ton<sup>-1</sup>) could be significantly reduced compared to the conventional process. The main issues remaining included low yields (with levulinic acid and formic acid as by-products) and high solvent utilization so that a minimal selling price of 1618 US\$ ton<sup>-1</sup> is required. Dros *et al.* (2015) proposed three routes for the production of hexamethylenediamine via 5-hydroxymethylfurfural from high fructose syrup. The fossil route outcompetes all of the proposed bio-based routes with a price of 1.84 € compared to at least 2.13 € kg<sup>-1</sup> due to low yields and fructose's high price. Additionally, the bio-based routes produced 8 kg of carbon dioxide equivalents compared to only 6 for the chemical process. The authors reasoned that the high number for the bio-based route could be attributed to the high amounts of water and steam needed and maize's low crop yield. Only when considering the polymer as carbon sink (2.3 kg carbon dioxide equivalents) the bio-based process has advantages in terms of environmental impact. This process is not viable until inexpensive and environmentally friendly building blocks (e.g. lignocellulosic waste) are available and the energy input can be reduced. The highest environmental impact in the current AA production is attributed to the emission of nitrous oxide. Although chemical decomposition could theoretically reduce it by over 99 %, only 80 % are realized on average, so that 60.2 kg<sub>N<sub>2</sub>O</sub> ton<sub>AA</sub><sup>-1</sup> are produced (Shimizu *et al.*, 2000). Van Duuren *et al.* (2011a) performed an LCA for the biotransformation of different petro- or bio-based substrates to *cis,cis*-muconic acid, which can be hydrogenated to AA, employing *P. putida*. A high impact of energy demand and emissions could be attributed to the glucose demand and sodium hydroxide required for pH regulation. In contrast to benzoic acid or toluene as pure petrochemical feedstocks, impure aromatics appeared feasible. Bio-based phenols from lignin were proposed as a sustainable solution with a 57 % decrease in cumulative energy demand (from 104.2 to 45.8 GJ ton<sup>-1</sup>) and an 80 % decrease in greenhouse gas emissions (Corona *et al.*, 2018). Irrespective of the feedstock, the biotransformation approach reduced the carbon dioxide emissions by 17.4 CO<sub>2</sub> equivalents. The authors suggest that the most significant improvement of the environmental impact is the increase of the final *cis,cis*-muconic acid titer by metabolic engineering of the cell.

In conclusion, the optimization or replacement of conventional industrial production processes offers excellent potential to reduce the global warming potential of polymer synthesis. Thereby, the establishment of energy-efficient production routes based on cheap carbon sources constitutes the major challenge. This challenge can be met by multistep biotransformation approaches, especially those based on living whole-cell biocatalysts containing an orthogonal monomer synthesis pathway.

However, the respective strain and process design are challenging, which will be addressed in the next chapter.

## 1.2 Biocatalytic cascade reactions

### 1.2.1 Definition and types of cascade reactions

Nature and, more specifically, microbial cells create an enormous diversity of compounds and synthesis strategies. The entire metabolism relies on natural catalysts – i.e., enzymes – arranged in complex reaction cascades – i.e., the metabolic pathways – to ensure the cell's survival (Garcia-Junceda, 2008). The first studied biocatalytic cascade reaction was the fermentation of sugars leading to the discovery of glycolysis and the respective enzymes (Buchner, 1897). Cascade reactions are defined as “chemical transformations in which the starting substrate is designed to (or happens to) undergo a reaction whose product becomes the substrate for the next step, [...] and so on until a product stable to the reaction conditions is reached” (Nicolaou & Chen, 2009). In this context, spontaneous reactions of unstable intermediates and transformations, which are supplied with some substrates at later stages of the reaction, are included, as long as they are carried out concurrently in the same reaction vessel (Ricca *et al.*, 2011).

One classification of cascade reactions relies on respective design principles (Ricca *et al.* (2011); Figure 1.2). A linear cascade constitutes a reaction sequence in which one substrate is converted into one product via intermediate(s). The coupling with further reactions for cofactor or cosubstrate regeneration or by-product removal results in an orthogonal cascade. It is also possible to couple two reactions via these cosubstrates or cofactors in a parallel reaction yielding two products. In cyclic cascades, a substrate mixture (e.g., a racemate) is applied, where one substrate is transformed into an intermediate and shuttled back so that the desired compound is enriched.

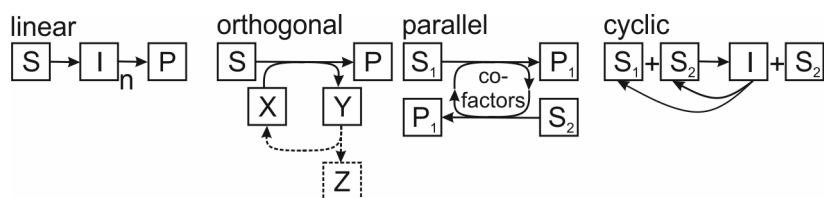


**Figure 1.2: Four designs of cascade reactions.** Orthogonal and parallel cascades are closely related and only differ in the economic value of the substances, which is high for both products in the case of parallel cascades. In orthogonal cascades, the by-products are usually discarded (according to Ricca *et al.* (2011))

Biocatalytic cascades were designed for the synthesis of bulk chemicals, e.g., monomers for nylon synthesis (Ladkau *et al.*, 2016; Müller *et al.*, 2016; Schrewe *et al.*, 2013a), and fine chemicals, e.g., chiral compounds derived from asymmetric alkene functionalization (Wu *et al.*, 2016b). Applications of cascade reactions in the synthesis of value-added compounds are superior compared to step-by-step approaches. It is unnecessary to purify intermediates, which reduces the amount of waste, solvents, catalysts, operating time, and costs (Muschiol *et al.*, 2015; Nicolaou & Chen, 2009). The next enzyme directly converts unstable or toxic intermediates within the cell (Ricca *et al.*, 2011). Toxic substances can be provided *in situ* instead of being supplied in bulk amounts (Schrittwieser *et al.*, 2017). Besides, linear cascades are a tool to drive reversible reactions towards completion if the reaction product is

directly converted by the next enzyme catalyzing an irreversible reaction (Ricca *et al.*, 2011). This is especially helpful in implementing oxidation-reduction cascades that often involve equilibrium reactions catalyzed by dehydrogenases (Schrittwieser *et al.*, 2011). Thereby, high atom economy, conversion, and overall yields can be achieved (Denard *et al.*, 2013; Muschiol *et al.*, 2015). Cascade reactions are generally considered a means to achieve green chemistry with a high potential for economic feasibility (Nicolaou & Chen, 2009). The concept of sustainability is met as the amount of required raw materials is substantially decreased, and (fossil) energy requirements and operating expenses are reduced (Oberleitner *et al.*, 2013). Biocatalysts are intrinsically “green” and compatible with each other (Ricca *et al.*, 2011).

The sequential action of different enzymes allows for the construction of highly functionalized molecules from readily available starting materials, thereby increasing complexity (Simon *et al.*, 2013). Additionally, cascades allow for retrosynthetic approaches, where the molecule of interest is decomposed to different functional units to identify suitable catalysts for key bond-forming steps (Turner & O’Reilly, 2013). As a result of this reverse design starting from the target product, entirely new molecules not occurring in nature can be assembled, and pathways or enzymes from different species be combined (Ladkau *et al.*, 2014; Wu & Li, 2018).

The advantages mentioned above can only be exploited if all enzymes of the cascade act in a concerted manner as the activity of one enzyme relies on the action of the previous. Thus, to construct an efficient cascade, several challenges need to be overcome and reasonable decisions must be made.

### 1.2.2 Challenges and optimization strategies for the implementation of *in vivo* cascades

The first decision to be made when it comes to cascade reactions concerns the catalyst format. Usually, two different formats are considered: whole cells or isolated enzymes, which can be immobilized or suspended. At first glance, the *in vitro* combination of several enzymes with defined activities might appear straightforward and easier regarding the balancing of enzymatic ratios (Muschiol *et al.*, 2015). However, each enzyme has to be purified separately, consuming resources, energy, and time. Additionally, cascades often require expensive cofactors, which need to be supplied in stoichiometric amounts or regenerated. These aspects add complexity and economic inefficiency to an initially simple system (Bayer *et al.*, 2015).

In contrast, whole cells harbor the enzymes within the cell with microreactor-type function so that reaction steps are efficiently coupled, and down-stream processing is only necessary at the end of the reaction. Additionally, the cellular environment provides appropriate conditions for the enzymes, and cofactors can be supplied and regenerated via cellular metabolism (Blank *et al.*, 2010). Co-localization of enzymes within the cell decreases diffusion distances (Schrewe *et al.*, 2013a; Wachtmeister & Rother, 2016; Wu & Li, 2018). The so-called substrate channeling occurring within distances of 10 nm is crucial to ensure that diffusion from one active site to the other is faster than catalytic rates (Wheeldon *et al.*, 2016). Permeabilized cells can be considered an intermediate biocatalyst format, which does not rely on cellular transport processes (uptake and secretion of substrates and products). However, they can neither provide metabolism-based cofactor recycling, metabolite supply, or enzyme re-synthesis nor protect enzymes from harsh reaction conditions, e.g., solvents or reactive oxygen species (Krauser *et al.*, 2013). Although *in vivo* cascades require elaborate design, their intriguing

advantages significantly contribute to green and sustainable production routes. Whole-cell biocatalytic cascades and their design constitute the topic of this thesis.

Establishing a concerted action of several enzymes *in vivo* can be a complicated task having in mind that nature optimized cascades over millions of years towards highly efficient networks with growth and reproduction as primary targets (Bayer *et al.*, 2015). Besides genetic and regulatory engineering efforts, suitable reaction conditions must be identified to sustain all enzymes' activity and selectivity within the cascade (Denard *et al.*, 2013). The entire cascade needs to be thermodynamically feasible, with the last step preferably being exergonic (most preferably irreversible) to favor product formation (France *et al.*, 2017). The total turnover number of the overall cascade is determined by the least stable enzyme, which needs to be identified as well as the enzyme catalyzing the rate-limiting step (Schrittwiesser *et al.*, 2017). Muschiol *et al.* (2015) pointed out four main challenges associated with whole-cell cascades: (1) the host background potentially leading to side reactions; (2) growth deficiency associated with the increased metabolic burden; (3) the balance of expression levels; and (4) overcoming of the diffusion barrier. The balancing of enzyme levels is challenging due to the different maximal activities and operational stabilities (Rudroff, 2019). The metabolic burden induced by the formation of reactive compounds (such as reactive oxygen species) and the withdrawal of cellular resources (amino acids, coenzymes) for recombinant enzyme synthesis and operation can result in a detrimental competition between metabolic and pathway demands (Rudroff, 2019). Organic co-solvents applied for hydrophobic substrates or products can solve diffusion and/or toxicity issues but need to be tolerated by the cell (Schrittwiesser *et al.*, 2017).

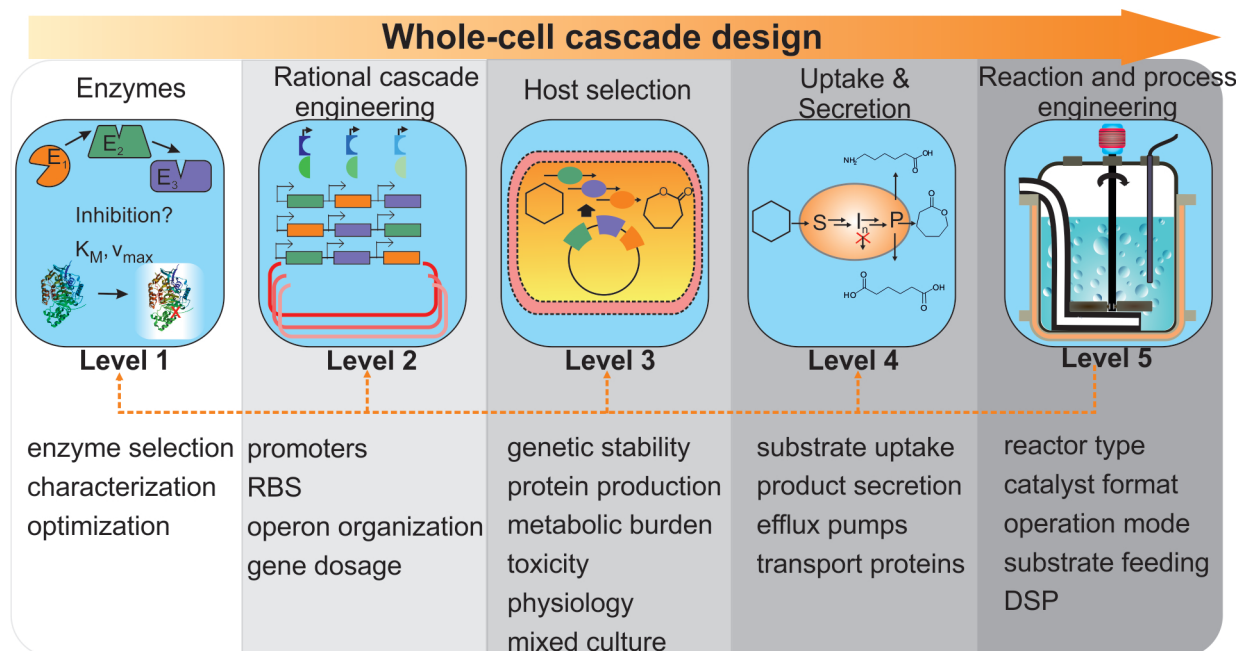


**Figure 1.3: Overall structure of whole-cell cascade design.** The different levels are depicted with the main tasks, criteria, and necessary decisions.

Until now, most publications on biocatalytic cascade reactions represent proof-of-concept studies (Rudroff, 2019). The mentioned challenges can be tackled on several levels to establish an industrially

applicable process employing whole cells. The following subsections introduce these levels and highlight the optimization potential based on selected examples (Figure 1.3).

### 1.2.2.1 Level 1: Enzymes choice, characterization, and optimization

The design of both *in vivo* and *in vitro* cascades starts with selecting appropriate enzymes that catalyze the desired reactions. The cascade may rely on natural biosynthetic pathways or sections thereof or can be assembled, potentially combining enzymes from different species in a retrosynthetic approach (Ladkau *et al.*, 2014). The native 4-step L-carnitine synthesis pathway of *Agrobacterium* sp. has been employed by Lonza for an industrial L-carnitine production process at a scale of  $>100$  t year<sup>-1</sup> (Breuer *et al.*, 2004; Meyer & Robins, 2005). Upon recombinant expression, the enzymes catalyzing the three initial steps of the cyclohexane degradation pathway identified in *Acidovorax* sp. CHX100, which has been isolated from a biotrickling filter, were successfully employed for heterologous whole-cell multistep biotransformations, e.g., cyclohexane conversion to  $\epsilon$ -CL (Karande *et al.*, 2017; Salamanca & Engesser, 2014). The advantage of such cascades relying on native pathways or sections lies in the parallel evolution of cooperating enzymes, thus making efficient use of cellular resources and profit from compatible reaction conditions. However, some molecules are rather complex or do not exist in nature, making it necessary to combine enzymes from different organisms. Siirola *et al.* (2013) combined a hydrolase, an esterase, and a transaminase from three different species to synthesize complex 3-substituted cyclohexylamine derivatives with two stereocenters from bicyclic diketones with conversions up to 99 %. The nylon building block 12-aminododecanoic acid methyl ester could be generated from renewable dodecanoic methyl ester (DAME) employing enzymes from the alkane degradation pathway of *P. putida* GPo1 combined with a  $\omega$ -transaminase from *C. violaceum* and an alanine dehydrogenase from *B. subtilis* for amino-donor (alanine) regeneration (Ladkau *et al.*, 2016; Schrewe *et al.*, 2013b).

Cascade enzymes should be well characterized in terms of intracellular stability, optimal operation conditions, and kinetics, including possible inhibitions, to enable their efficient coupling under optimal reaction conditions (Rudroff, 2019). E.g., Baeyer-Villiger monooxygenases (BVMOs), which are often employed in cascade reactions *inter alia* profiting from the irreversibility of the oxygenation-type of reaction, are prone to substrate and/ or product inhibition (Alphand *et al.*, 2003). The knowledge of kinetic data ( $K_M$ ,  $K_I$ ,  $v_{max}$ ) for individual reaction steps allows for the development of kinetic models to elucidate required enzyme ratios and to optimize process performance (Milker *et al.*, 2017; Scherkus *et al.*, 2017). Schrewe *et al.* (2014) used the activities and kinetics of individual reaction steps to tune the product pattern for DAME oxidation.

The optimization of individual enzymes within a cascade typically aims to increase enzyme stability, specificity, and/or activity to improve overall cascade performance (Bornscheuer *et al.*, 2012). Site-directed mutagenesis and directed evolution thereby allow for such changes in enzyme properties (Arnold, 1998; Bornscheuer *et al.*, 2012). One of the best-studied enzymes employed in redox biocatalysis is the cytochrome P450 monooxygenase BM3 originating from *Bacillus megaterium*. It has been subject to various mutations targeting cofactor utilization, stability, and substrate scope (Whitehouse *et al.*, 2012). Staudt *et al.* (2013) selected one BM3 variant that accepts cycloalkanes and, together with an alcohol dehydrogenase (ADH), converts them to respective ketones. However, the BM3 and, consequently, the whole cascade suffered from low activities and instability, constituting

further engineering targets. An  $\omega$ -transaminase from *P. denitrificans* was subjected to site-directed mutagenesis to synthesize a diamine from isosorbide (Lerchner *et al.*, 2013). The transaminase retained high catalytic activity, but the cascade accumulated the amino alcohol intermediate as the subsequent ADH did not accept this alcohol as a substrate. The creation of fusion proteins constitutes a promising approach to increase stability and improve substrate channeling. Aalbers & Fraaije (2017) fused an ADH to a cyclohexanone monooxygenase, resulting in high enzyme stability and >99 % conversion of 200 mM cyclohexanol to  $\epsilon$ -CL.

The selection of appropriate enzymes for the desired cascade and their optimization in terms of stability and kinetics typically is followed via an iterative approach. Having promising enzyme candidates in hand, the next step is their production, which, in the case of *in vivo* cascades, includes the fine-tuning of their intracellular levels. From now on, whole-cell biocatalytic reactions as designed in Chapters 2.3, 2.5, and 2.6 are in focus.

### 1.2.2.2 Level 2: Rational cascade engineering

The successful implementation of *in vivo* cascade reactions requires the fine-tuning of the expression levels of all involved proteins to allow for streamlined production of the desired compound without accumulation of intermediates and thus facilitating downstream processing and prevent potentially toxic effects (Jeschek *et al.*, 2017; Muschiol *et al.*, 2015; Rudroff, 2019). However, the optimum expression levels often depend on the genetic background of the strain (Alper *et al.*, 2005), interconnecting cascade engineering, and host selection. There are four main strategies to manipulate protein abundance in the cell (Jeschek *et al.*, 2017).

Whole-cell biocatalysis often is based on heterologous proteins, which exhibit the desired activities and substrate scope. However, a differing **codon usage** among the strain, from which the introduced gene originates, and the host strain might limit the produced protein amount due to differing tRNA abundances and synthesis rates of amino-acylated tRNAs (Welch *et al.*, 2009a). The goal is to design an “optimal gene” composed of codons enabling the synthesis of high levels of active enzyme in the chosen expression environment (Welch *et al.*, 2009b).

**Gene dosage** variation constitutes a simple approach to fine-tune enzyme amounts within the cell. The gene dosage can range from single copies to multiple thousands on multi-copy plasmids. Genome integration is generally regarded to result in higher genetic stability and makes antibiotic selection markers dispensable. By now, it is also possible to achieve multiple targeted insertions in yeast by exploiting the multi-copy delta-sequences (Yuan & Ching, 2014). The presence of the multi-copy rRNA operons in *Pseudomonas* allows for multiple integrations of heterologous constructs that are stable for over 160 generations (Otto *et al.*, 2019). Although the maintenance of plasmids causes a higher metabolic burden for the cells often associated with decreased plasmid stability (Silva *et al.*, 2012), the remarkable number of available origins of replication allows setting the desired copy number. The use of broad-host-range origins, e.g., RSF1010, enables testing the respective constructs in several hosts (Bagdasarian *et al.*, 1981). The copy numbers range from one, e.g., for bacterial artificial chromosomes (Shizuya *et al.*, 1992), over a few, e.g., for the RK2 origin (Thomas *et al.*, 1984), to several hundreds, e.g., for the pUC plasmids (Lin-Chao *et al.*, 1992). Recently, the “Standard European Vector Architecture” (SEVA) database has been developed, enabling a standardized vector construction with nine different origins of replication for different bacterial species (Martínez-García



*et al.*, 2015; Silva-Rocha *et al.*, 2013). DIAL (different allele) *E. coli* strains allow for copy number adjustment between 1 and 250 depending on the host background's choice with varying expression levels of the *trans*-acting replication factor (Kittleson *et al.*, 2011). This approach was successfully employed to optimize the five-step production of violacein in complex medium. To synthesize benzoic acid from L-phenylalanine, Zhou *et al.* (2020a) created 4 modules each on a different plasmid encoding for 9 genes in total. By testing 4 different origins of replication, they could choose the best producer accumulating 122 mM benzoic acid with 98 % conversion.

**Transcriptional engineering** is the most popular strategy to fine-tune expression levels and is mainly achieved by promoter engineering (Alper *et al.*, 2005). There are six different inducible regulation systems available in the pSEVA collection allowing for the transcript level variation by changing the inducer concentrations (Martínez-García *et al.*, 2015). The drawback of this method is that it involves the additional expression of repressors/activators, which can cause a severe metabolic burden, especially when multiple systems are employed to express different pathway components (Jeschek *et al.*, 2017). Another possibility is the use of constitutive promoters that do not allow to separate biomass and protein production, potentially leading to hampered growth and thus whole-cell biocatalyst synthesis. Several promoter libraries have been developed that are spanning multiple orders of magnitude in expression levels. Xu *et al.* (2017) created a promoter library to investigate the optimal gene expression pattern of the five genes necessary to produce violacein in *E. coli* and thereby improved the product titer 3.2-fold. Similarly, it has been shown that succinate production by *E. coli* could be enhanced by 37 % testing a promoter library with strengths ranging from 0.8 to 100 % compared to the *trc* promoter (Yu *et al.*, 2016). Zhou *et al.* (2015a) developed a model for promoter engineering as well as process condition adaptation and thereby could increase the 6-step synthesis of 6AHA from  $\alpha$ -ketoglutarate from 9 to 48 g L<sup>-1</sup>. It is also possible to unlock complex phenotypes by altering the general transcription machinery through sigma-factor engineering (Alper & Stephanopoulos, 2007). However, this will affect all transcripts in the cell and does not explicitly target one module or enzymatic step. Pflieger *et al.* (2006) demonstrated that the engineering of intergenic regions within operons enabled to vary expression over a 100-fold range in prokaryotes and eukaryotes. Precise engineering of secondary structures in the mRNA and placing RNase E sites also tuned the gene expression (Smolke *et al.*, 2000). The latter approaches are less established but offer vast potential for the future.

In bacteria, manipulating the ribosomal binding site (RBS) containing the Shine-Dalgarno sequence is a useful **translational engineering** tool. It is especially valuable for cascade reactions, as each gene can be targeted separately, and just very few base pair changes are required (Jeschek *et al.*, 2016). It was first described by Wang *et al.* (2009), who altered 24 genetic components in the lycopene synthesis pathway resulting in a five-fold titer improvement. The "RBS library Calculator" gave access to RBSs across a 10,000-fold protein expression space and was tested in six Gram-positive and Gram-negative bacterial strains in plasmids as well as genomes (Farasat *et al.*, 2014). The yield of the seven-step astaxanthin biosynthesis pathway in *E. coli* could be increased 4-fold by testing six different RBS strengths for each gene (Zelcbuch *et al.*, 2013). By now, computational tools are available, e.g., the algorithms RedLibs enables the rational design of smart libraries and has been successfully employed for the two-step violacein production in *E. coli* (Jeschek *et al.*, 2016).

However, often a combinatorial approach involving several of the above-described strategies at the

same time is necessary Jeschek *et al.* (2017). The development of sophisticated *in silico* prediction tools allows to minimize the experimental effort to a few promising alternatives and reduces the search space. Multivariate modular metabolic engineering optimizes metabolic pathways and strains based on the expression of pathway components and enables stable and high flux through this pathway (Biggs *et al.*, 2014). Smanski *et al.* (2014) inserted the *Klebsiella oxytoca* nitrogen fixation (*nif*) gene cluster (16 genes, 103 parts) in *E. coli*. They could achieve 57% of wild-type activity by altering the operon organization, terminator number, RBSs, and promoter strength and number.

As stated above, the assembly of enzymatic reaction cascades *in vivo* is strongly host-dependent. Therefore, host selection and cascade engineering are interconnected and should be considered in a concerted way.

### 1.2.2.3 Level 3: Selection of the host organism

#### 1.2.2.3.1 Selection criteria

The improvement of heterologous gene expression has focused on optimizing the introduced DNA sequence rather than selecting an appropriate host strain. Very few attempts questioned which could be the optimal host for specific purposes (Martínez-García *et al.*, 2014). Nature is still the best source for novel enzymatic functions, and especially cascade reactions have been optimized by evolution (Muschiol *et al.*, 2015), thereby allowing for balanced enzyme ratios and proper folding, possibly involving chaperones and posttranslational modifications. The exploitation of native pathways converting non-native substrates was demonstrated before (Ladkau *et al.*, 2014). Lonza optimized the two-step biotransformation of 2-cyanopyrazine to 5-hydroxypyrazine-2-carboxylic acid in *Agrobacterium* sp. DSM 6366, reaching a total yield of 80 % and average productivity of 1.3 g L<sup>-1</sup> h<sup>-1</sup> (Wieser *et al.*, 1997). However, native hosts often comprise downstream enzymes responsible for further modifications of the desired product. The knock-out of these enzymes is an option that enabled the efficient 4-step conversion of 4-butyrobetaine to L-carnitine in *Agrobacterium* sp. HK13 with a yield of 99.5 % and average productivity of 1.4 g L<sup>-1</sup> h<sup>-1</sup> (Breuer *et al.*, 2004; Meyer & Robins, 2005). A typical technical production system heavily differs from the natural environment implying non-optimal or even toxic conditions (Volmer *et al.*, 2015). Thus, the utilization of enzymes in their native hosts is often associated with low growth rates and/or does not allow for sufficient productivity and stability in an industrial process setting (de Carvalho, 2017), which favors the use of well-known and cultivable host organisms and heterologous gene expression.

Due to its well-studied genetic background and many available genetic tools, *E. coli* is the most widely used platform organism for whole-cell biocatalysis (Lin & Tao, 2017). Like in the case of other classical biotechnological workhorses such as *Bacillus subtilis*, *Saccharomyces cerevisiae*, or *Corynebacterium glutamicum*, its “domestication” in terms of targeted engineering and well-known cultivation conditions and properties allows for efficient process optimization.

High **genetic stability** of the host strain is critical to allow for stable catalysis over different generations. The ability to evolve during a bioprocess is generally undesired due to unpredictable changes over time (Keasling, 2008). It has been shown that IS-elements can inactivate ectopic genes accounting for up to 25 % of random mutations. By generating an IS-free *E. coli* strain, unstable genetic constructs could also be maintained over prolonged periods (Umenhoffer *et al.*, 2010). Additionally, eliminating stress-inducible error-prone DNA-polymerases resulted in decreased genetic variation (Csörgő *et al.*,

2012). The prophage deletion in *C. glutamicum* resulted in improved growth and 30 % increased biotransformation efficiency (Baumgart *et al.*, 2013).

**Transcription, translation, and proper protein folding** are pre-conditions to obtain active whole-cell catalysts. Misfolding of proteins in *E. coli* increases in the presence of high inducer concentrations and strong promoters and can lead to inclusion body formation (Baneyx & Mujacic, 2004). Also, the formation of disulfide bonds is not possible in the reducing cytoplasm of *E. coli*. It has been shown that engineered variants of the chaperones GroEL/S can assist in folding of recombinant proteins (Wang *et al.*, 2002). Also, functional N-linked glycosylation was achieved in *E. coli* by transferring the respective genes from *Campylobacter jejuni* (Wacker *et al.*, 2002).

The introduction of additional enzymatic functions drains cellular resources and therefore leads to an increased **metabolic burden**. The high energy demand for recombinant protein production can divert ATP away from biomass formation (Hoffmann & Rinas, 2004). Respective flux (re)balancing can and has to be tackled via synthetic biology approaches (Anderson *et al.*, 2010). Oxidoreductase catalysis often depends on redox cofactors NAD(P/H) that also are involved in cellular maintenance metabolism and biomass formation. Therefore, regeneration systems might be required to sustain heterologous reactions. The introduction of an NADP<sup>+</sup>-dependent glucose dehydrogenase resulted in a seven-fold higher  $\alpha$ -pinene oxyfunctionalization yield based on a BM3 mutant in *E. coli* (Schewe *et al.*, 2008).

The **toxicity of substrates, intermediates, or products** differs among host organisms. Cascade reactions involve multiple intermediates, of which some might be toxic to the cell (Lin & Tao, 2017). Avoiding the accumulation of such intermediates is thus key for the design of *in vivo* cascades. The tolerance of microorganisms to chemicals is often a multigenic trait involving molecular pumps, membrane properties, energy metabolism, and cell size and shape (Nicolaou *et al.*, 2010). One typical example is the generation of ethanol-tolerant yeasts for the food industry and biofuel production (Alper *et al.*, 2006; Casey & Ingledew, 1986). Organic solvents with a logP<sub>OW</sub> between 1.5 and 4.0 are incredibly toxic to microorganisms due to their intercalation in cellular membranes. Several Gram-negative strains, e.g., from the genus *Pseudomonas*, have developed sophisticated solvent-efflux systems to survive in such environments (Ramos *et al.* (2002)).

The selected host organism should ideally synthesize all necessary enzymes, precursors, and cofactors and efficiently use them to ensure **physiological compatibility**. The recombinant expression of cytochrome P450 monooxygenases in *E. coli* requires the addition of the heme precursor 5-aminolevulinic acid or the introduction of HemA catalyzing the rate-limiting step in heme biosynthesis (Jansson *et al.*, 2000; Julsing *et al.*, 2008). Other hosts like *P. putida* do not require these measures as they natively provide higher heme levels (van Beilen *et al.*, 2005). Styrene epoxidation in *E. coli* JM101 allowed for doubled yields on glucose compared to *P. taiwanensis* VLB120 in half of the reaction time due to the high energy demand of solvent-tolerance mechanisms in the VLB120 strain in two-liquid biotransformations under the same conditions (Kuhn *et al.*, 2012a).

There is a growing demand for creating generic **chassis cells** serving as a production platform for tailored bioprocesses (Vickers *et al.*, 2010). The goal is to remove competing carbon and electron sinks, reduce regulatory issues, and increase the cell's general controllability. However, process conditions and objectives heavily differ among different applications (Volmer *et al.*, 2015; Wynands *et al.*, 2019), making it necessary to have a repertoire of chassis strains to fall back on or to choose

the best suited from (Martínez-García & de Lorenzo, 2017).

### 1.2.2.3.2 The genus *Pseudomonas* and *P. taiwanensis* VLB120

The genus *Pseudomonas* was first proposed in 1894 based on morphological observations associated with motility and the formation of spore-like structures (Migula, 1895). An accurate classification within the group of Gram-negative, aerobic  $\gamma$ -Proteobacteria was only possible with 16S-rRNA data (Palleroni *et al.*, 1973), and the previously described spore-like structures turned out to be granules of storage compounds (Palleroni, 2010).

Today, *Pseudomonas* species are known to colonize almost any environmental niche in soil, water, plants, and animals (Silby *et al.*, 2011) due to their metabolic versatility and genomic plasticity (Dos Santos *et al.*, 2004). They can withstand exogenous and endogenous stresses and produce a wide range of bioactive compounds (Nikel *et al.*, 2014). Glucose catabolism is carried out exclusively through the Entner-Doudoroff pathway due to the absence of 6-phosphofructokinase in most pseudomonads allowing them to generate high amounts of reduction equivalents to manage, primarily oxidative-stress related insults (Chavarría *et al.*, 2013). Consequently, enzymatic pathways can be expressed, which other hosts cannot cope with (Martínez-García *et al.*, 2014). It has been found that all pseudomonads share 1,491 genes (Loper *et al.*, 2012). Some species are capable of using more than 100 different sources of carbon and energy (Timmis, 2002) or tolerate extreme environmental conditions, e.g., high temperature, extreme pH, or the presence of low-logP organic solvents (Poblete-Castro *et al.*, 2012) (logP corresponds to the logarithm of the partition coefficient in an octanol-water two-liquid phase system and is a general measure for hydrophobicity) (Sangster, 1997). Therefore, they are a source for synthetically interesting enzymes like oxidoreductases, sulfur metabolism proteins, and efflux pumps (Dos Santos *et al.*, 2004). Consequently, their remarkable flexibility and unique enzyme repertoire make Pseudomonads highly interesting for industrial biotechnology and bioremediation applications (Timmis, 2002).

Non-pathogenic, solvent-tolerant *Pseudomonas* species can grow in the presence of and even produce high amounts of toxic chemicals (Tiso *et al.*, 2014). Biocatalytic conversions have been carried out mainly employing specimens of the huge variety of *P. putida* strains (Nikel *et al.*, 2016), but also other *Pseudomonas* strains showed high application potential. E.g., *P. taiwanensis* VLB120 (Köhler *et al.*, 2013) was isolated from forest soil via selection for growth on styrene as sole carbon source (Panke *et al.*, 1998). It is equipped with solvent tolerance mechanisms, including the organic solvent efflux pumps TtgABC and TtgGHI encoded on a megaplasmid (Köhler *et al.*, 2013). These features allow its growth in the presence of low-logP solvents such as octanol, styrene, and cyclohexane (Volmer, 2016). It has already been employed for enantioselective styrene epoxidation (Panke *et al.*, 1998; Park *et al.*, 2007; Volmer *et al.*, 2014), phenol production (Wynands *et al.*, 2018), isobutyric acid synthesis (Lang *et al.*, 2014), and cyclohexane conversion (Karande *et al.*, 2017, 2016). Moreover, its capability to form biofilms allows for its application in novel reactor concepts such as capillary reactors (Hoschek *et al.*, 2019a; Karande *et al.*, 2016). Recently, chassis strains with different solvent tolerance levels enabling higher growth rates and biomass yields became available (Wynands *et al.*, 2019). These features demonstrate the potential of *P. taiwanensis* VLB120 as a host for biocatalytic applications in industrial biotechnology.

### 1.2.2.3.3 Mixed-species approaches allow distributing multi-step cascades

The engineering of *in vivo* cascades involving several recombinant proteins poses a severe metabolic burden on the host cell (Rudroff, 2019). Despite the availability of sophisticated expression systems and genetic manipulation techniques, some proteins cannot or only poorly be produced in typical host organisms, which may preclude certain enzyme combinations in the same host strain. In recent years, these observations made mixed-culture approaches prevalent in the field of industrial biotechnology. However, spontaneous fermentations by consortia are long known in the food industry (Sabra & Zeng, 2014), anaerobic processes for, e.g., biogas production (Ozbayram *et al.*, 2018), and nitrification by ammonium-oxidizers and nitrite-oxidizers, which constitutes an essential part of the global nitrogen cycle (Bock & Wagner, 2006). The definition of mixed-cultures in biocatalysis and metabolic engineering is the modularization of a complete biosynthetic pathway into two or more different species or strains (Jones & Wang, 2018; Zhang & Wang, 2016). In a broader sense, co-cultures profiting from other metabolic features of co-cultivated strains are included, such as a stable catalytic biofilm of *Synechocystis* sp. PCC 6803 and *P. taiwanensis* VLB120. Whereas the heterotrophic VLB120 strain was mainly responsible for biofilm formation, the cyanobacterium allowed photoautotrophic cyclohexane hydroxylation with a productivity of  $3.76 \text{ g}_{\text{cyclohexanol}} \text{ m}^{-2} \text{ day}^{-1}$  that could be maintained for one month (Hoschek *et al.*, 2019a). Polycultures are often referred to when more than two species/strains are involved, e.g., for the *de novo* synthesis of anthocyanin with four *E. coli* strains collectively expressing 15 pathway enzymes (Jones *et al.*, 2017).

There are several advantages of mixed-cultures compared to axenic cultures with a complete pathway in one strain. Complicated biosynthetic pathways with many heterologous genes consume cellular resources and pose severe metabolic burdens associated with impaired growth and/or low flux towards the desired product (Wu *et al.*, 2016a). Cellular fitness is improved by staying within the strain's metabolic capacities when the pathway is split between more organisms (Zhang & Wang, 2016). Furthermore, the complexity of enzyme balancing by tedious genetic engineering (see above) can be reduced by manipulating the mixed-culture composition and thereby pathway enzyme abundances through the inoculation ratio (Jones *et al.*, 2016) or sequential addition of the strains (Saini *et al.*, 2015). Membranes can act as a physical separation to enclose enzymes protecting the substrate from unwanted side reactions. The 4-hydroxyphenylacetate-3-hydroxylase HpaBC has a broad substrate spectrum and synthesizes by-products from different phenols (Chen *et al.*, 2017). Via the separation of tyrosine deamination and subsequent hydroxylation by HpaBC in a second strain, a 12-fold increased final caffeic acid titer was achieved. However, such modular compartmentalization avoiding cross-talk between different modules is restricted to molecules that cannot diffuse freely between the strains (Zhang & Wang, 2016). Also, the optimal cellular background can differ for individual pathway modules. For example, *S. cerevisiae* was chosen to functionally produce a eukaryotic cytochrome P450 monooxygenase and hydroxylate taxadiene excreted by the co-cultured *E. coli* (Zhou *et al.*, 2015b). Besides, co-cultures can be employed to foster the efficient use of different carbon sources in complex mixtures, e.g., molasses, lignin, or other waste products (Zhang & Wang, 2016). Finally, one module can be combined with different downstream modules increasing the product spectrum and allowing for tailored biosynthesis following a “plug-and-play” principle (Zhang & Wang, 2016). Industrial processes need to be robust and reproducible. Therefore, systems for the controlled cultivation of microbial consortia are required to promote the growth of all involved species to the

necessary extent (Sabra *et al.*, 2010). Understanding population dynamics by mathematical modeling (Bernstein & Carlson, 2012) and studying the interactions between the strains employed is crucial (Sabra *et al.*, 2010), especially in fermentation approaches. The application of resting cells that do not produce biomass as a by-product often allows for enhanced cofactor regeneration and higher specific whole-cell activities (Blank *et al.*, 2008a; Julsing *et al.*, 2012a). Furthermore, this approach facilitates preserving a stable consortium composition over time and the titration of production rates of different steps by adjusting the strain ratio (Willrodt *et al.*, 2015a). This concept has been successfully employed to synthesize xylitol from D-arabitol with wild-type *Gluconobacter oxydans* in co-culture with *E. coli* expressing a xylitol dehydrogenase enabling a 3-fold yield increase up to  $0.837 \text{ g}_{\text{xylitol}} \text{ g}_{\text{D-arabitol}}^{-1}$  compared to the single strain approach (Qi *et al.*, 2016). In limonene producing recombinant *E. coli* BL21, only low cytochrome P450 monooxygenase-mediated limonene hydroxylation activities were obtained in resting cells. A mixed-species approach with *E. coli* MG1655 exhibiting high Cyp levels was successfully chosen to give access to perillyl acetate from glucose with an activity of  $0.11 \text{ U g}_{\text{CDW}}^{-1}$  Willrodt *et al.* (2015a). Before transfer to the resting cell state, each species can be cultivated separately with individually fine-tuned inducer concentration, time of induction, and medium composition to achieve optimal enzyme amounts within the cells.

The co-culture approach's foremost challenges include finding the optimal ratio of the different microorganisms and their maintenance over the whole reaction period. Also, the reaction conditions have to be chosen in a way that is optimal for all strains. However, the critical issue for an efficient flux towards the desired product is the mass transfer of substrates and pathway intermediates (the so-called shuttling compounds) into and out of the cells, which can already be challenging in axenic cultures. The next section will discuss substrate uptake and product secretion as key challenges in whole-cell biocatalysis.

#### 1.2.2.4 Level 4: Substrate uptake and product secretion

Uptake of nutrients, secretion of waste, containment of appropriate intracellular metabolite concentrations, and protection against toxic agents are the major functions of the cell envelope (Chen, 2007). Thus, the often non-natural and toxic substrates and products in biotechnological applications can suffer from uptake and secretion issues. This constitutes a significant challenge in whole-cell catalysis and can result in enzymatic rates one to two orders of magnitudes lower than those obtained with isolated enzymes (Chen, 2007). The bacterial cell envelopes of Gram-positive bacteria (e.g., *Firmicutes*, *Actinobacteria*) and Gram-negative bacteria (e.g., *E. coli*, *Pseudomonas*) have distinct features (Silhavy *et al.*, 2010). Both contain an inner phospholipid bilayer and a peptidoglycan layer that is much thicker in Gram-positive bacteria being the principal constituent of their cell wall. Hydrophobic molecules pass the inner membrane by relatively fast passive diffusion, whereas hydrophilic molecules rely on specific transport proteins that reside in the inner membrane (Chen, 2007). Gram-negative bacteria feature only a thin peptidoglycan layer surrounded by an additional outer membrane (OM) with lipopolysaccharides (LPS) facing outwards and making them less permeable to various, predominantly hydrophobic molecules (Leive, 1974). The mechanically robust peptidoglycan wall does not constitute an effective diffusion barrier due to its coarse meshwork (Nikaido, 1994). OMs densely packed with LPS constitute a barrier for hydrophilic and hydrophobic molecules (Chen, 2007). The diffusion rate of hydrophobic molecules through the OM is 50 to 100 times slower than

through the phospholipid bilayer (Vaara *et al.*, 1990) due to the ordered quasicrystalline arrangement of the LPS Vaara (1993). Uptake is possible through non-specific, typically hydrophilic porin channels found in all Gram-negative bacteria (Nikaido, 2003), which have an opening of only 7 to 10 Å in *E. coli* (Cowan *et al.*, 1992), allowing the entrance of molecules smaller than 600 Da (Denyer & Maillard, 2002). Charged amino acids in the porins favor the access of hydrophilic molecules (Nikaido, 1994), impeding the diffusion of hydrophobic molecules smaller than 600 Da (down to ~120 Da; with a logP > 3-4). In summary, diffusion through both membranes is reasonably fast for molecules with a logP between 1 and 4.

In the ideal case, the production rate only depends on intracellular enzyme activities and not on substrate uptake into the cell (Chen, 2007). Similarly, product export should be faster than the production rate to avoid intracellular accumulation and, eventually, the inhibition of target reactions. Common strategies to promote such transfer over cellular membranes include solvent (e.g., ethanol, toluene), detergent (e.g., Triton X-100, rhamnolipids), or salt (e.g., 0.5 M NaCl) treatment, freeze-thaw cycles, electroporation, or ion complexation by EDTA - all of them problematic in large-scale applications (Chen, 2007; Julsing *et al.*, 2012b) and potentially harmful to cellular metabolism and thus whole-cell activity (Schrewe *et al.*, 2013a). It has been shown that a mutation in Braun's lipoprotein in *E. coli* cells could enhance the rate of toluene and ethylbenzene oxidation 6-fold. The availability of sequenced genomes and genetic engineering techniques allows engineering specific transporters and pores to facilitate the transport over the inner or outer membrane. Especially pseudomonads constitute a valuable source for membrane proteins as they grow on a wide range of substrates, including hydrophobic ones (Hancock *et al.*, 1990; Timmis, 2002). One example is the *P. putida* GPO1 derived outer membrane protein AlkL facilitating the transport of hydrophobic molecules such as monoterpenes (Cornelissen *et al.*, 2013), fatty acid methyl esters (Julsing *et al.*, 2012b), and alkanes (Grant *et al.*, 2014) into *E. coli*, by restructuring a barrel extension formed by its extracellular loops (Schubeis *et al.*, 2020). Enhanced expression of the *E. coli* OM fatty acid transporter FadL resulted in 5.5-fold increased biotransformation of long-chain hydroxy acids (Jeon *et al.*, 2018).

In summary, the substrate's and product's biochemical properties dictate the efficiency of transport over the cell envelope. The implementation of membrane proteins or the use of strains that express these transporters can significantly enhance whole-cell biocatalytic performance. However, the increased uptake of these often toxic compounds can hamper cellular functions due to fast energy loss, protein misfolding, membrane disintegration, or inhibited metabolism (Julsing *et al.*, 2012b; Schrewe *et al.*, 2014). This requires the fine-tuning of expression levels and sophisticated process engineering. Reaction engineering employing the optimized catalyst and upscaling towards an industrial process will be discussed in the next section.

#### 1.2.2.5 Level 5: Optimization of process parameters and transfer to industrial settings

The ultimate goal of each biocatalytic reaction is its transfer into a bioreactor format, which can be operated to produce industrially relevant amounts of the chemical. A bioreactor constitutes a device or system that supports a biologically active environment (Jenkins *et al.*, 1996). They have several advantages compared to shake flasks, including maintenance of defined conditions, e.g., temperature and pH, controllable aeration, better mixing fostering efficient mass transfer inside and among different liquid and gaseous phases, usually higher working volumes, and, consequently, the operation at

higher biomass concentrations. Whereas new bioreactor types are continuously developed, the most common include stirred tank (STR), bubble column, packed bed, membrane, and tubular reactors (Spier *et al.* (2011), Figure 1.4)

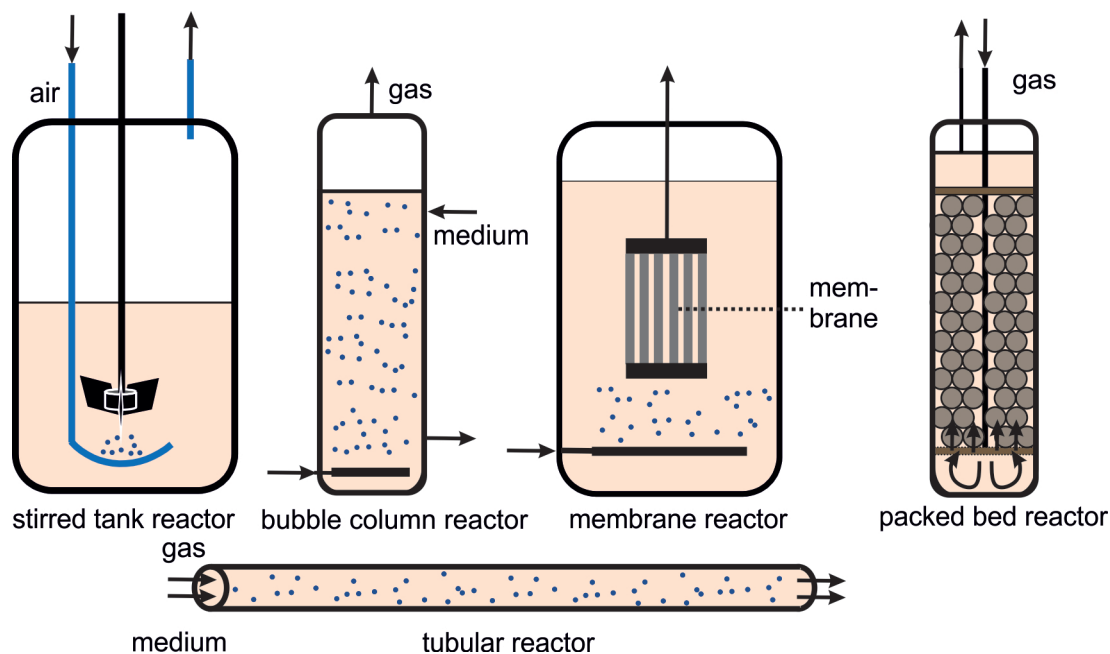


**Figure 1.4: Selected reactor types for biotechnological processes.** In- and outflow are depicted as arrows.

**Catalyst format.** Whole-cell biocatalysts can be applied as growing, non-growing but living (resting), and dead cells. Growing cells utilize the provided carbon and energy source to support both product and biomass formation in parallel. This often results in a higher growth substrate demand and implicates the advantage of constant protein re-synthesis that is of the utmost importance when unstable enzymes are involved in complex cascade reactions. Processes based on growing cells typically are strongly affected by metabolic carbon and energy fluxes or redox states (Kadisich *et al.*, 2017b). One example is microbial overflow metabolism in *E. coli* leading to acetate accumulation, which can inhibit microbial growth and metabolism and reduce product yields on growth substrates such as glucose (Nakano *et al.*, 1997). Whereas the use of dead cells precludes any dependency on metabolism, resting cells still provide an active basic carbon metabolism with limited enzyme resynthesis capacity. The resting cell status is induced by limiting one or more nutrient sources other than the energy source, often accomplished in a nitrogen-free buffer (Kadisich *et al.*, 2017b). One pre-requisite is the catalysis by inherently stable enzymes allowing for higher product yields and easier handling (de Carvalho, 2017). Applying resting *E. coli* cells catalyzing Baeyer-Villiger monooxygenase-mediated cyclohexanone oxidation, Walton & Stewart (2002) achieved a productivity of  $0.79 \text{ g}_{\epsilon\text{-CL}} \text{ L}^{-1} \text{ h}^{-1}$ . This output is one order of magnitude higher than what they achieved with growing cells, which showed slightly higher specific whole-cell activities. The choice of the whole-cell biocatalyst format depends on relevant process parameters and properties of the enzymatic reactions applied. A bioprocess can be run with suspended or immobilized cells, whereas the first is still more common. However, immobilized cell formats can facilitate continuous operation and down-stream



processing and improve process durability. One example is biofilms in capillary reactors, where cells immobilize themselves utilizing extracellular polymeric substances. Such a setup allowed continuous cyclohexane oxidation at average productivity of  $0.4 \text{ g}_{\text{cyclohexanol}} \text{ L}_{\text{tube}}^{-1} \text{ h}^{-1}$  for 18 days (Karande *et al.*, 2016).

**Operation mode for cellular growth.** In bioprocesses, the growth phase and the production phase might occur simultaneously or successively. Bioreactors can be operated in batch, fed-batch, and continuous mode and are usually different for growth and biotransformation. In batch-mode, a defined amount of growth substrate is added at the beginning of the process, and the cells convert and grow in a non-substrate-limited mode until substrate depletion when the process is usually stopped. A fed-batch can be conducted after a batch process to reach higher cell densities (Kuhn *et al.*, 2012b). A defined growth rate is set by substrate- or nutrient limitation, which can be advisable to avoid catabolite repression or substrate inhibition (Hewitt *et al.*, 1999). This was demonstrated for lactic acid production from a xylose/glucose mixture employing *Enterococcus mundtii* (Abdel-Rahman *et al.*, 2015). The fed-batch cultivation reduced by-products and catabolite repression by glucose, reaching a final titer of  $129 \text{ g L}^{-1}$  and a productivity of  $5.6 \text{ g L}^{-1} \text{ h}^{-1}$  in this fermentation. However, styrene epoxidation employing *P. taiwanensis* VLB120 reached higher specific activities ( $180 \text{ U g}_{\text{CDW}}^{-1}$ ) in batch cultivation than a glucose-limited fed-batch, possibly due to a higher strain-inherent metabolic capacity of unlimited cells (Volmer *et al.*, 2019). In continuous processes, nutrients are supplied to the cells via an inflow, and at the same time, the volume is maintained constant by an outflow. In chemostats, a defined dilution rate is set so that cell concentration and reactants remain constant (steady-state) (Kadisich *et al.*, 2017b). The establishment of such a process requires precise organization and technical control (Croughan *et al.*, 2015), and often lower product concentrations, yields, and productivities are achieved (Lee & Kim, 2015). For example, Li *et al.* (2011) observed that butanol production in *C. acetobutylicum* reached the highest yield and productivity in continuous mode ( $0.21 \text{ g}_{\text{butanol}} \text{ g}_{\text{glucose}}^{-1}; 0.81 \text{ g L}^{-1} \text{ h}^{-1}$ ) due to the prevention of acidogenesis. However, a 30 % lower titer ( $8.35 \text{ g L}^{-1}$ ) compared to fed-batch cultures was observed. Biofilm capillary reactors are also cultivated in continuous mode to achieve high-cell-density and subsequently production rates (Heuschkel *et al.*, 2019).

**Substrate feeding of the biotransformation substrate.** The biotransformation substrate might be supplied in batch, fed-batch, or continuous mode and is independent of the operation mode for growth. Often, biotransformation substrates are toxic to cells and/or poorly water-soluble, requiring appropriate feeding. Thereby, one has to consider whole-cell kinetics (Figure 1.5), especially in terms of substrate limitation and inhibitions, which becomes even more complex when cascade reactions are employed (Ringborg & Woodley, 2016). Ideally, the substrate is fed, allowing a zero-order reaction running at  $v_{\text{max}}$ . Many hydrocarbon substrates, e.g., aromatics, (cyclo)alkanes, and terpenes, exhibit a logP between 1 and 4 and are considered to be highly toxic for microbial cells (de Bont, 1998). They intercalate into cellular membranes leading to increased membrane permeability, leakage of central metabolites, metabolism breakdown, and ultimately cell death at membrane concentrations higher than 300-400 mM (Kratzer *et al.*, 2015; Sikkema *et al.*, 1994). For example, cyclohexane with a logP of 3.44 and a very low water solubility of 0.683 mM (Sikkema *et al.*, 1994) can be fed via cyclohexane-saturated air as successfully demonstrated by Hoschek *et al.* (2019a) for mixed-species capillary biofilm reactors. *In situ* substrate feeding and product extraction via an adsorbent resin

was achieved for the Baeyer-Villiger oxidation of (–)-(1S,5R)-bicyclo[3.2.0]hept-2-en-6-one reaching a yield of 75-80 % (Hilker *et al.*, 2008). Scherkus *et al.* (2017) optimized the cyclohexanol feeding regime based on a kinetic model. The two-step conversion to  $\epsilon$ -CL enabled 100 % yield in fed-batch mode (100 mM) compared to 50 % in batch mode, which was also 28 % slower. A second liquid organic phase in two-liquid phase (2LP) systems enables *in situ* feeding of toxic and/or hydrophobic substrates as well as direct product extraction, similarly as described above for adsorbent resins. In 2LP systems, the partition coefficient between the two phases dictates the aqueous reactant concentrations. Extensive work has been dedicated to 2LP biotransformations of aliphatic and aromatic compounds (Bühler & Schmid, 2004; Hoschek *et al.*, 2019b; Witholt *et al.*, 1990), such as the enantiospecific epoxidation of styrene (Julsing *et al.*, 2012a; Panke *et al.*, 2002; Volmer *et al.*, 2019).

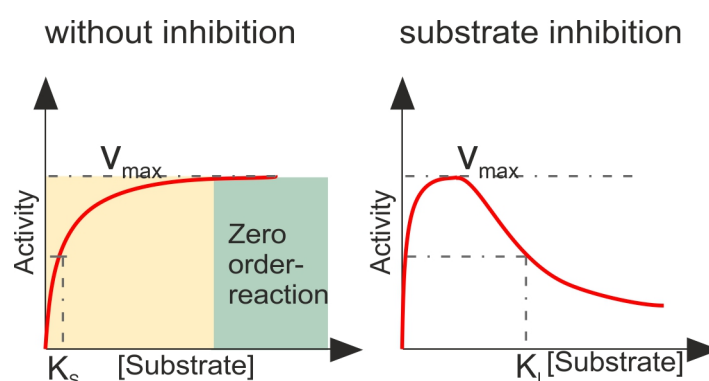


**Figure 1.5: Whole-cell kinetics without inhibition and substrate inhibition.** Kinetics correspond to Michaelis-Menten kinetics for enzymes. The apparent substrate uptake constant  $K_S$  (concentration at which whole cells show half-maximal activity) is also used in the Monod-kinetics for microbial growth and is analogous to  $K_M$ .

**Down-stream processing (DSP).** This term includes all steps necessary to obtain a packaged product after the fermentation or biotransformation process. This also includes separation of the catalyst from the broth or cell disruption if the product accumulates intracellularly. DSP often dominates production costs in biopharmaceuticals production and accounts for 20-40 % for bulk chemicals (Straathof, 2011), making *in situ* product removal (ISPR) attractive. ISPR enables the avoidance of toxic effects and reaction equilibria shifts, leading to increased yields, product titers, and productivities, and constitutes a first product separation step (Lye & Woodley, 1999). DSP is an integral part of process engineering and has been optimized for proteins (e.g., antibodies) employing chromatographic techniques (Flickinger, M. C. (ed.), 2013), which can also be applied for other biotechnological products (Kalyanpur, 2002). For some compounds, already established unit operations from the chemical industry can be used and adapted. However, DSP offers enormous potentials for more eco-efficient solutions, but dedicated research in this field remains scarce.

### 1.3 State-of-the-art biotechnological C6 monomer synthesis

The industrial production of the monomers  $\epsilon$ -CL, 6AHA, and AA suffers from severe environmental issues as respective processes were mainly optimized for cost and not for energy/environmental efficiency (Wittcoff *et al.*, 2012). Several biocatalytic processes were published to realize more eco-efficient production processes at ambient pressure and temperature.

Whole-cell synthesis of the polycaprolactone (PCL) monomers  $\epsilon$ -CL or **6-hydroxyhexanoic acid (6HA)** was realized from cyclohexanol (Kohl *et al.*, 2018; M enil *et al.*, 2019; Srinivasamurthy *et al.*, 2019). The highest productivity of  $1.1 \text{ g L}^{-1} \text{ h}^{-1}$  and an  $\epsilon$ -CL concentration of 185 mM (99.6 % conversion) was achieved by Srinivasamurthy *et al.* (2020) employing recombinant *E. coli* cells expressing a two-step cascade. Cyclohexanol is more expensive than cyclohexane because it involves a first typically unspecific and environmentally problematic chemical cyclohexane oxidation step (Wittcoff *et al.*, 2012). For the first time, Pennec *et al.* (2015a) realized a 3-step cascade reaction from cyclohexane to yield  $\epsilon$ -CL employing isolated enzymes. The low productivity of  $0.1 \text{ g L}^{-1} \text{ h}^{-1}$  and low cyclohexane conversion of 3 % (final concentration 5.2 mM) could be attributed to mass transfer issues and instability of the enzymes. Karande *et al.* (2017) engineered such a 3-step cascade in *P. taiwanensis* VLB120. The whole-cell biocatalytic approach enabled a productivity of  $0.46 \text{ g L}^{-1} \text{ h}^{-1}$  and a final product concentration of 20 mM (10 % conversion). Hydrolysis of  $\epsilon$ -CL by host-intrinsic enzymes resulted in a product mixture also containing 6HA, which complicates DSP. Additionally, the expensive growth substrate citrate and the volatile inducer dicyclopropylketone are unfavorable for industrial processes.

Until now, only two biocatalytic cascade synthesis concepts for the nylon 6 monomer **6AHA** are available. Sattler *et al.* (2014) assembled a 5-step cascade employing isolated enzymes that could produce 12 mM 6AHA (65 % conversion, 37 % specificity). They had to cap the carboxylic acid moiety as a methyl ester to overcome inhibition of the selected alcohol dehydrogenase. The presence of methanol in the reaction harmed enzyme stability, especially of the BVMO. Turk *et al.* (2016) engineered a fermentative pathway known from methanogenic archaea in *E. coli*. However, only  $160 \text{ mg L}^{-1}$  6AHA were produced from glucose within 72 h. Interestingly, Fedorchuk *et al.* (2019) published a strategy to transform AA into 6AHA by a carboxylic acid reductase combined with a transaminase enabling conversion of 95 %.

Whereas the synthesis concepts of  $\epsilon$ -CL/6HA and 6AHA were solely based on cyclohexane-derived compounds, the biocatalytic routes are more diverse for **AA**. Wang *et al.* (2020) developed a consortium consisting of three recombinant *E. coli* strains expressing eight recombinant enzymes in total. For the first time, they could show AA synthesis from cyclohexane enabling productivity of  $0.25 \text{ g L}^{-1} \text{ h}^{-1}$  and a final AA titer of  $4.5 \text{ g L}^{-1}$  (31 % yield on the substrate). Other production routes starting from glucose, glycerol, or lignin-derived aromatics were developed but only reached titers of up to  $2.5 \text{ g L}^{-1}$  AA (Cheong *et al.*, 2016; Clomburg *et al.*, 2015; Niu *et al.*, 2020; Yu *et al.*, 2014). Zhou *et al.* (2020b) and Zhao *et al.* (2018) reconstructed the reversed adipate degradation pathway from *Thermobifida fusca* in *E. coli* enabling AA titers of 58 and  $68 \text{ g L}^{-1}$  in a complex medium with a maximal yield of  $0.38 \text{ g}_{\text{AA}} \text{ g}_{\text{glycerol}}^{-1}$ . Other biosynthetic routes target *cis,cis*-muconic acid or glucaric acid production, which can be hydrogenated to AA with 97 % yield (Beerthuis *et al.*, 2015; Vardon *et al.*, 2016). Kohlstedt *et al.* (2018) engineered *P. putida* to produce *cis,cis*-muconic acid from lignin-derived catechol enabling a productivity of  $1.0 \text{ g L}^{-1} \text{ h}^{-1}$  and a final titer of  $64.2 \text{ g L}^{-1}$ . Until now, only one of these approaches has been transferred to the pilot-scale (Kohlstedt *et al.*, 2018), whereas the majority of these synthesis concepts were only proof-of-concept studies due to low activities and/or stabilities.

### 1.4 Scope of the thesis

As stated previously, biotechnological monomer production has been in focus for almost ten years. The oil-like energy content of most plastics makes the use of fossil resources as substrates sustainable and effective (Mülhaupt, 2013). This thesis aims at the biotechnological production of the PCL monomers  $\epsilon$ -CL or 6HA, the nylon 6 monomer 6AHA, and the nylon 6,6 monomer AA from cyclohexane by using biocatalytic cascades in whole-cells (Figure 1.6). Until now, most strategies started from cyclohexanol, which is less volatile and less toxic to cells and, therefore, easier to handle. The main research question relates to the efficient design of whole-cell biocatalytic cascade reactions, which requires the optimized expression of pathway genes, the evaluation of different cell formats and physiological conditions, and the assessment of the technical applicability in a bioreactor. This also includes reaction engineering overcoming the toxic effect of cyclohexane and at the same time ensuring sufficient mass transfer of this volatile compound. This thesis builds on a *P. taiwanensis* VLB120 whole-cell catalyst developed by Karande *et al.* (2017) for the synthesis of  $\epsilon$ -CL, improves biocatalytic activity and streamlined production of PCL monomers. This is the basis for the amendment of the cascade to either yield the nylon monomers 6AHA or AA.

The low biocatalytic activity achieved by Karande *et al.* (2017) could be attributed to the rate-limiting first reaction step catalyzed by a cytochrome P450 monooxygenase (Cyp). **Chapter 2.1** comprises the development of *P. taiwanensis* VLB120 pSEVA\_Cyp – a biocatalyst with improved Cyp activity, which grows on the cheaper substrate glucose, and is induced by the nonvolatile IPTG. Different genetic elements are engineered to understand the relationship between expression strength, active protein amount, and whole-cell activity. **Chapter 2.2** focuses on the characterization of the third cascade enzyme - the Baeyer-Villiger monooxygenase (CHMO) – and evaluates three different catalyst formats, i.e., the isolated enzyme, whole cells, and a biofilm concerning their kinetic properties. Advantages and disadvantages are discussed, which allow selecting the biocatalyst format based on desired process parameters. **Chapter 2.3** combines the findings of chapters 2.1 and 2.2, shows the development of two *P. taiwanensis* strains, either producing  $\epsilon$ -CL or 6HA from cyclohexane. Rational cascade assembly based on enzyme properties is conducted to enhance biocatalytic activities and prevent intermediate and side-product formation. **Chapter 2.4** further details the 6HA-producing biocatalyst in different physiological states and long-term biotransformation assays. Finally, a stirred-tank bioreactor process is established via a gaseous cyclohexane feed to find a compromise between substrate toxicity and mass transfer into the reactor. **Chapter 2.5** shows the development of a mixed-species concept to synthesize 6AHA combining the strains developed in chapter 2.3 with *E. coli* harboring downstream enzymes. Reaction engineering targeting cyclohexane toxicity, cyclohexane as well as oxygen mass transfer, and adjustment of reaction rates focuses on maximizing cyclohexane conversion and 6AHA yield. **Chapter 2.6** makes use of the knowledge generated in chapters 2.3 and 2.4 and demonstrates the development of a *P. taiwanensis* VLB120 strain inheriting a 6-step enzymatic cascade for AA synthesis, which was transferred to a lab-scale bioreactor involving product purification. **Chapter 3** generally discusses how efficient cascade design was realized in this thesis and compares the presented synthesis concepts to other polymer building block production processes.

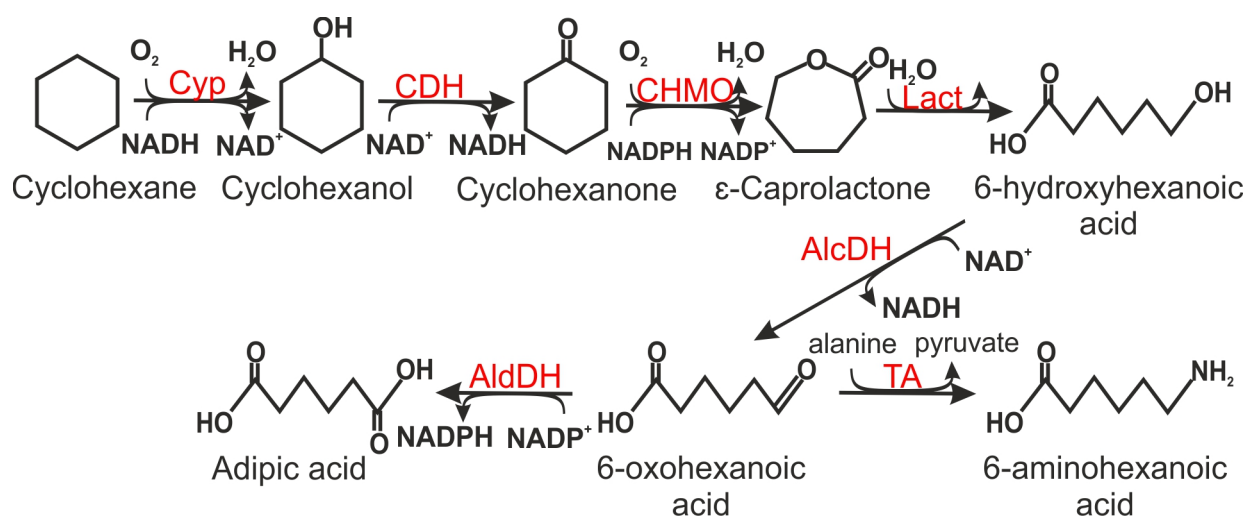


**Figure 1.6: Envisaged enzymatic cascade for the production of the key monomers  $\epsilon$ -caprolactone ( $\epsilon$ -CL), 6-hydroxyhexanoic acid (6HA), 6-aminohexanoic acid (6AHA), and adipic acid (AA).** The cascade is composed of a Cytochrome P450 monooxygenase (Cyp), a cyclohexanol dehydrogenase (CDH), and a cyclohexanone monooxygenase (CHMO), a lactonase (Lact), an alcohol dehydrogenase (AlcDH), and an aldehyde dehydrogenase (AldDH)/ a transaminase (TA).

This thesis is submitted as a cumulative work comprising 6 publications designated as research chapters 2.1 to 2.6. The status of the publications is summarized below:

Chapter 2.1: published in *Frontiers in Bioengineering and Biotechnology* (2020)

Chapter 2.2: published in *Biotechnology & Bioengineering* (2021)

Chapter 2.3: published in *Biotechnology Journal* (2020)

Chapter 2.4: published in *Frontiers in Catalysis* (2021)

Chapter 2.5: published in *Microbial Biotechnology* (2021)

Chapter 2.6: submitted to *Metabolic Engineering* (2021)



## **Chapter 2**

### **Results**

## Chapter 2.1

# Maximizing biocatalytic cyclohexane hydroxylation by modulating cytochrome P450 monooxygenase expression in *P. taiwanensis* VLB120

Lisa Bretschneider, Rohan Karande, Bruno Bühler

### Short Summary

Cytochrome P450 monooxygenases (Cyps) effectively catalyze the regiospecific oxyfunctionalization of inert C-H bonds under mild conditions. Due to their cofactor dependency and instability in isolated form, oxygenases are preferably applied in living microbial cells with *Pseudomonas* strains constituting potent host organisms for Cyps. This study presents a holistic genetic engineering approach, considering gene dosage, transcriptional, and translational levels, to engineer an effective Cyp-based whole-cell biocatalyst, building on recombinant *Pseudomonas taiwanensis* VLB120 for cyclohexane hydroxylation. A *lac*-based regulation system turned out to be favorable in terms of orthogonality to the host regulatory network and enabled a remarkable specific whole-cell activity of 34 U g<sub>CDW</sub><sup>-1</sup>. The evaluation of different ribosomal binding sites revealed that a moderate translation rate was favorable in terms of the specific activity. An increase in gene dosage did only slightly elevate the hydroxylation activity, but severely impaired growth and resulted in a large fraction of inactive Cyp. Finally, the introduction of a terminator reduced leakiness. The optimized strain *P. taiwanensis* VLB120 pSEVA\_Cyp allowed for a hydroxylation activity of 55 U g<sub>CDW</sub><sup>-1</sup>. Applying 5 mM cyclohexane, molar conversion and biomass-specific yields of 82.5 % and 2.46 mmol<sub>cyclohexanol</sub> g<sub>biomass</sub><sup>-1</sup> were achieved, respectively. The strain now serves as a platform to design *in vivo* cascades and bioprocesses for the production of polymer building blocks such as  $\epsilon$ -caprolactone ( $\epsilon$ -CL).

Published in:

*Frontiers in Bioengineering and Biotechnology*, 2020, 8, 140. doi: <https://doi.org/10.3389/fbioe.2020.00140>

The full publication incl. Supplementary Material can be found in the Appendix Section 1.



## Chapter 2.2

# Characterization of different biocatalyst formats for BVMO-catalyzed cyclohexanone oxidation

Lisa Bretschneider, Ingeborg Heuschkel, Afaq Ahmed, Katja Bühler, Rohan Karande, Bruno Bühler

### Short Summary

Cyclohexanone monooxygenase (CHMO), a member of the Baeyer-Villiger monooxygenase family, is a versatile biocatalyst that efficiently catalyzes the conversion of cyclic ketones to lactones. In this study, an *Acidovorax*-derived CHMO gene was expressed in *Pseudomonas taiwanensis* VLB120. Upon purification, the enzyme was characterized *in vitro* and shown to feature a broad substrate spectrum and up to 100 % conversion in 6 h. Further, we determined and compared the cyclohexanone conversion kinetics for different CHMO-biocatalyst formats, i.e., isolated enzyme, suspended whole cells, and biofilms, the latter two based on recombinant CHMO-containing *P. taiwanensis* VLB120. Biofilms showed less favorable values for  $K_S$  (9.3-fold higher) and  $k_{cat}$  (4.8-fold lower) compared to corresponding  $K_M$  and  $k_{cat}$  values of isolated CHMO, but a favorable  $K_I$  for cyclohexanone (5.3-fold higher). The unfavorable  $K_S$  and  $k_{cat}$  values are related to mass transfer- and possibly heterogeneity issues and deserve further investigation and engineering, in order to exploit the high potential of biofilms regarding process stability. Suspended cells showed an only 1.8-fold higher  $K_S$ , but 1.3- and 4.2-fold higher  $k_{cat}$  and  $K_I$  values than isolated CHMO. This together with the efficient NADPH regeneration via glucose metabolism makes this format highly promising from a kinetics perspective.

Published in:

*Biotechnology & Bioengineering*, **2021**, 118(7), 2719-2733. doi: <https://doi.org/10.1002/bit.27791>

The full publication incl. Supplementary Material can be found in the Appendix Section 2.

## Chapter 2.3

# Rational engineering of a multi-step biocatalytic cascade for the conversion of cyclohexane to polycaprolactone monomers in

## *Pseudomonas taiwanensis*

Lisa Bretschneider, Katja Bühler, Rohan Karande, Bruno Bühler

### Short Summary

The current industrial production of polymer building blocks such as  $\epsilon$ -capro-lactone ( $\epsilon$ -CL) and 6-hydroxyhexanoic acid (6HA) is a multi-step process associated with critical environmental issues such as the generation of toxic waste and high energy consumption. Consequently, there is a demand for more eco-efficient and sustainable production routes. This study deals with the generation of a platform organism that converts cyclohexane to such polymer building blocks without the formation of by-products and under environmentally benign conditions. Based on kinetic and thermodynamic analyses of the individual enzymatic steps, we rationally engineered a 4-step enzymatic cascade in *Pseudomonas taiwanensis* VLB120 via stepwise biocatalyst improvement on the genetic level. We found that the intermediate product cyclohexanol severely inhibits the cascade and optimized the cascade by enhancing the expression level of downstream enzymes. The integration of a lactonase enabled exclusive 6HA formation without side products. The resulting biocatalyst showed a high activity of  $44.8 \pm 0.2 \text{ U g}_{\text{CDW}}^{-1}$  and fully converted 5 mM cyclohexane to 6HA within 3 h. This platform organism can now serve as a basis for the development of greener production processes for polycaprolactone (PCL) and related polymers.

Published in:

*Biotechnology Journal*, **2020**, 15(11), 2000091. doi: <https://doi.org/10.1002/biot.202000091>

The full publication incl. Supplementary Material can be found in the Appendix Section 3.

## Chapter 2.4

### Conversion of cyclohexane to 6-hydroxyhexanoic acid using recombinant *Pseudomonas taiwanensis* in a stirred-tank bioreactor

Lisa Bretschneider, Ingeborg Heuschkel, Martin Wegner, Martin Lindmeyer, Katja Bühler, Rohan Karande, Bruno Bühler

#### Abstract

6-Hydroxyhexanoic acid (6HA) represents a polymer building block for the biodegradable polymer polycaprolactone (PCL). Alternatively to energy- and emission-intensive multistep chemical synthesis, it can be synthesized directly from cyclohexane in one step by recombinant *Pseudomonas taiwanensis* harboring a 4-step enzymatic cascade without the accumulation of any intermediate. In the present work, we performed a physiological characterization of this strain in different growth media and evaluated resulting whole-cell activities. RB and M9\* media led to reduced gluconate accumulation from glucose compared to M9 medium and allowed specific activities up to  $37.5 \pm 0.4 \text{ U g}_{\text{CDW}}^{-1}$  for 6HA synthesis. However, 50 % of the specific activity was lost within 1 h in metabolically active resting cells, specifying growing cells or induced resting cells as favored options for long-term biotransformation. Further, the whole-cell biocatalyst was evaluated in a stirred tank bioreactor setup with a continuous cyclohexane supply via the gas phase. At cyclohexane feed rates of 0.276 and 1.626  $\text{mmol min}^{-1} \text{ L}^{-1}$ , whole-cell biotransformation occurred at first-order and zero-order rates, respectively. A final 6HA concentration of 25 mM ( $3.3 \text{ g L}^{-1}$ ) and a specific product yield of  $0.4 \text{ g g}_{\text{CDW}}^{-1}$  were achieved with the higher feed rate. Substrate limitation, product inhibition, and toxification by cyclohexane were identified as critical factors limiting biocatalytic performance. Future research efforts on these factors and precise adjustment of the cyclohexane feed combined with an *insitu* product removal strategy are discussed as promising strategies to enhance biocatalyst durability and product titer and thus to enable the development of a sustainable multistep whole-cell process.

Published in:

*Frontiers in Catalysis*, 2021, 1, 683248. doi: <https://doi.org/10.3389/fctls.2021.683248>

The Supplementary Material can be found in the Appendix Section 4.

### 2.4.1 Introduction

Biodegradable polymers such as PCL, polyhydroxyalkanoates, and polylactic acid are gaining interest due to the high ecological footprint of non-degradable plastics. PCL polymerization typically is accomplished either via ring-opening polymerization of  $\epsilon$ -caprolactone ( $\epsilon$ -CL) or polycondensation of 6HA (Labet & Thielemans, 2009). However, the conventional monomer production processes starting from cyclohexane are associated with multiple reaction steps involving the isolation of intermediates, high temperature and pressure variations, and usage of toxic and explosive chemicals (Wittcoff *et al.*, 2012). Monomer production in "one pot" under mild conditions, e.g. in a bioprocess, would relieve such critical aspects. In this context, the production of  $\epsilon$ -CL and 6HA from cyclohexanol with recombinant *E. coli* has been reported (Srinivasamurthy *et al.*, 2019, 2020). In our previous work, a 4-step enzymatic cascade for the conversion of cyclohexane via cyclohexanol, cyclohexanone, and  $\epsilon$ -CL to 6HA acid has been rationally engineered in *P. taiwanensis* VLB120. A high overall specific activity of  $44 \text{ U g}_{\text{CDW}}^{-1}$  and complete conversion of 5 mM cyclohexane to 6HA have been achieved in Chapter 2.3. This study now reports on the evaluation of this promising strain regarding its performance under process conditions, including respective biochemical engineering.

The catalytic performance of microorganisms depends on the production of functional enzymes and relies on the cellular machinery fueling enzyme synthesis as well as the reaction itself with energy and reduction equivalents. Specifically, heterologous pathways involving oxidoreductases typically are connected to cellular metabolism via co-substrates in the form of redox cofactors. The metabolic activity necessary to provide energy and redox equivalents is closely linked to the physiological state of cells and thus cultivation conditions. The use of growing cells on the one hand enables efficient (re)synthesis of enzymes and energy carriers and therefore can convey superior biocatalyst stability, but, on the other hand, can suffer from a trade-off between demands for biomass synthesis and redox biocatalysis (Peralta-Yahya *et al.*, 2012). The use of metabolically active but non-growing (resting) cells, a condition induced by the lack or depletion of, e.g., nitrogen or magnesium sources in the medium (Harder & Dijkhuizen, 1983), has resulted in superior whole-cell activities for redox biocatalysis compared to growing cells (Bühler *et al.*, 2008; Julsing *et al.*, 2012a). Depending on the reaction(s) to be catalyzed, resting cells can be easier to handle and reusable, but often suffer from poor stability (Julsing *et al.*, 2012a; Zhang *et al.*, 2012). Recently, mixed-species concepts have been used to produce the monomers adipic acid, 6-aminohexanoic acid or 1,6-hexanediol from cyclohexane (Wang *et al.*, 2020; Zhang *et al.*, 2020; Bretschneider *et al.*, 2021).

A major challenge regarding the biocatalytic cyclohexane conversion relates to the physio-chemical properties of the substrate. With its high vapor pressure (77 mm Hg) and low water solubility ( $55 \text{ mg L}^{-1}$ ,  $650 \text{ }\mu\text{M}$ ), cyclohexane constitutes a highly volatile compound under standard conditions (Henry's law constant  $K_{\text{air/water}} = 0.15 \text{ atm m}^3 \text{ mol}^{-1}$ ) (ChemSpider, 2020). Such toxicity issues can be avoided via substrate feeding strategies. A non-water-miscible second organic phase can act as a substrate reservoir, continuously supplying the substrate to appropriate aqueous concentrations (Lilly, 1982; Van Sonsbeek *et al.*, 1993). This two-liquid phase concept has been successfully applied for styrene epoxidation (Volmer *et al.*, 2019), toluene hydroxylation (Collins *et al.*, 1995; Willrodt *et al.*, 2015b), and multistep pseudocomene oxidation (Bühler *et al.*, 2003). Alternatively, the substrate can be fed in liquid form via a pump (Srinivasamurthy *et al.*, 2019) or via the gas phase (Karande *et al.*, 2016). Moreover, some bacterial strains are known to feature adaptive solvent tolerance mechanisms

involving, e.g., solvent efflux systems and/or the alteration of membrane fluidity and surface properties, which qualifies them as promising hosts for applications involving toxic reactants and products (Inoue & Horikoshi, 1989; Heipieper *et al.*, 2007). *P. taiwanensis* VLB120 exhibits such features, primarily encoded on its megaplasmid (Köhler *et al.*, 2013).

The goal of this study was to evaluate the bioconversion of cyclohexane to 6HA on a bioreactor scale, with recombinant *P. taiwanensis*\_6HA as biocatalyst (Chapter 2.3). Its biocatalytic performance was investigated in growing and resting cell formats (Figure 2.4.1). Further, the catalytic potential of resting cells was evaluated in bioreactor setups with cyclohexane fed via the gas phase.

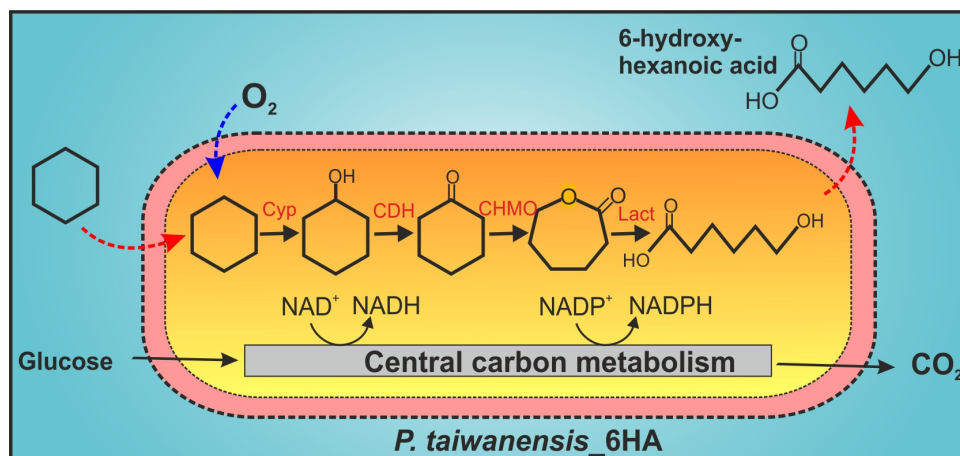


**Figure 2.4.1:** Biocatalytic cascade for 6-hydroxyhexanoic acid (6HA) synthesis from cyclohexane by *P. taiwanensis*\_6HA. Cyclohexane is successively converted to cyclohexanol, cyclohexanone,  $\epsilon$ -caprolactone ( $\epsilon$ -CL), and 6HA by a cytochrome P450 monooxygenase (Cyp), a cyclohexanol dehydrogenase (CDH), a cyclohexanone monooxygenase (CHMO), and a lactonase (Lact), respectively. Cyclohexane is a small (84 Da) and hydrophobic molecule, and can rapidly pass the outer and inner membrane of *P. taiwanensis* (Chen, 2007; Nikaido, 2003). The mode of 6HA export is unknown but possibly involves active transport due to its charged character at pH 7.2.

## 2.4.2 Materials and Methods

### 2.4.2.1 Bacterial strains, plasmids, media, and chemicals

Microbial strains and plasmids used in this work are listed in Table 2.4.1. Cells were grown in lysogeny broth (LB), M9 (Sambrook & Russell, 2001), M9\* (Panke *et al.*, 1999), or RB medium (Riesenberg *et al.*, 1991; Volmer *et al.*, 2019) at a pH of 7.2 (adjusted with 10 M NaOH) and supplemented with 0.5 % (w/v) glucose as sole carbon and energy source. Kanamycin ( $50 \mu\text{g mL}^{-1}$ ) was applied for selection when necessary. Unless stated otherwise, all chemicals were purchased from Sigma-Aldrich (Steinheim, Germany) or Carl Roth (Karlsruhe, Germany) in the highest purity available and used without further purification. 6HA was acquired from abcr (Karlsruhe, Germany). Molecular biology methods and plasmid construction are explained in detail in chapter 2.1 and 3.7.

### 2.4.2.2 Growth of bacterial cultures

Cultivations were carried out at  $30 \text{ }^\circ\text{C}$  and 200 rpm in a Multitron shaker (Infors, Bottmingen, Switzerland). Pre-cultivation generally was started with a LB culture ( $\sim 20$  h), from which a minimal medium pre-culture (1 % v/v) was inoculated and incubated for another 20 h. The latter culture was used to inoculate the main culture to an optical density at 450 nm ( $\text{OD}_{450}$ ) of 0.2. Heterologous gene

expression was induced with 1 mM isopropyl- $\beta$ -d-1-thiogalactopyranoside (IPTG) when the cultures reached an OD<sub>450</sub> of ~0.5. Incubation was continued for maximally 7.5 h.

**Table 2.4.1:** Strains and plasmids used in this chapter.

Strain/Plasmid	Characteristics	Reference
<b>Strains</b>		
<i>E. coli</i> DH5 $\alpha$	<i>supE44</i> $\Delta$ <i>lacU169</i> ( <i>q80lacZ</i> $\Delta$ M15) <i>hsdR17 recA1 endA1 gyrA96 thi-1 relA1</i>	Hanahan (1983)
<i>P. taiwanensis</i> VLB120	solvent tolerant, styrene degrading bacterium, isolated from forest soil	Köhler <i>et al.</i> (2013)
<b>Plasmids</b>		
pSEVA244_Cyp	pRO1600 and ColE1 ori, <i>lac</i> -regulatory system ( <i>lacI<sup>q</sup></i> , P <sub>trc</sub> ), BBa_B0015 terminator, RBS*, Cyp genes from <i>Acidovorax</i> sp.	Chapter 2.1
pSEVA244_CDH	pRO1600 and ColE1 ori, <i>lac</i> -regulatory system ( <i>lacI<sup>q</sup></i> , P <sub>trc</sub> ), BBa_B0015 terminator, RBS*, CDH gene from <i>Acidovorax</i> sp.	Chapter 2.3
pSEVA244_CHMO	pRO1600 and ColE1 ori, <i>lac</i> -regulatory system ( <i>lacI<sup>q</sup></i> , P <sub>trc</sub> ), BBa_B0015 terminator, RBS*, CHMO gene from <i>Acidovorax</i> sp.	Chapter 2.3
pSEVA244_Lact	pRO1600 and ColE1 ori, <i>lac</i> -regulatory system ( <i>lacI<sup>q</sup></i> , P <sub>trc</sub> ), BBa_B0015 terminator, RBS*, Lact gene from <i>Acidovorax</i> sp.	This chapter
pSEVA_6HA_2	ColE1/pRO1600 ori, carries <i>lacI<sup>q</sup></i> , P <sub>trc</sub> promoter, Cyp genes, P <sub>trc</sub> , <i>cdh</i> , <i>chmo</i> , <i>lact</i> , Km <sup>R</sup>	Chapter 2.3

### 2.4.2.3 Evaluation of induction kinetics

Main cultures were harvested after induction in time intervals of 90 min by centrifugation (RT, 5,000 g, 10 min) and resuspended in 10 mL potassium phosphate buffer containing 1 % (w/v) glucose (Kpi-g) to a final cell concentration of 0.5 g<sub>CDW</sub> L<sup>-1</sup>. The cell suspension was transferred to 100 mL baffled screw-capped shake flasks and equilibrated for 10 min at 30 °C, 250 rpm. Biotransformations were started by adding 5.46  $\mu$ L pure cyclohexane (corresponds to 5 mM with respect to the aqueous phase volume) to the flask, which then was tightly closed. The assay was stopped after 10 min by pipetting 1 mL of sample either into 1 M HCl (100  $\mu$ L) to reach a pH of 3, followed by centrifugation and storage at -20 °C for HPLC analysis, or into 0.5 mL ice-cold diethyl ether containing 0.2 mM n-decane as an internal standard. The latter sample was extracted via 2 min of vortexing. After short centrifugation, the organic phase was dried over water-free Na<sub>2</sub>SO<sub>4</sub> and transferred to a GC vial for analysis.

### 2.4.2.4 Long-term biotransformations on shake flask scale

Cells were harvested via centrifugation (10 min, RT, 5,000 g) after 6 h of induction in RB- or M9\*-shake flask cultures and resuspended to a final biomass concentration of 0.5 g<sub>CDW</sub> L<sup>-1</sup> in 20 mL of either Kpi-g, Kpi-g containing 1 mM IPTG (Kpi-g-I), or the respective growth medium containing 1 mM IPTG. After equilibration in 100 mL baffled and screw-capped shake flasks, 10.9  $\mu$ L cyclohexane (5 mM referring to aqueous phase volume) were added to start the reaction. Sampling of ca. 2.1 mL liquid volume was carried out by syringe through a silicone/PTFE septum after 10, 60, 110, and 160 min reaction time. One mL each was extracted with 0.5 mL diethyl ether or diluted with 1 M HCL

(100  $\mu\text{L}$  for Kpi and RB medium, 200  $\mu\text{L}$  for M9\* medium) for GC and HPLC analysis, respectively, as described above. Additionally,  $\text{OD}_{450}$  was determined, and 100  $\mu\text{L}$  gas samples were taken with a gas tight-glass syringe (Hamilton, Reno, NV).

#### 2.4.2.5 Toxicity assay

Cyclohexane toxicity was evaluated based on its influence on the growth rate of *P. taiwanensis* VLB120. Cells were pre-cultivated as described above and inoculated in M9\* main cultures to an  $\text{OD}_{450}$  of 0.1. Different cyclohexane amounts were added after 4 h of cultivation, and flasks were closed air-tight. Sampling was performed with a syringe through a septum in the lid. Growth was followed via  $\text{OD}_{450}$  measurement for 7 h. Aqueous cyclohexane concentrations were estimated via the Henry coefficient and verified via GC.

#### 2.4.2.6 Product inhibition assay

*P. taiwanensis*\_6HA was cultivated as described above and harvested after 4 h of induction. Cells were resuspended in 6 mL Kpi-g buffer containing defined 6HA concentrations (pH readjusted to 7.4) to a biomass concentration of 1.5  $\text{g}_{\text{CDW}} \text{L}^{-1}$  and transferred into 100 mL screw-capped Erlenmeyer flasks. Afterward, 1 mL was sampled, and the cells were equilibrated for 10 min at 30 °C. Biotransformations were started by adding 5.5  $\mu\text{L}$  pure cyclohexane and stopped after 1 h for HPLC and GC analysis as described before.

#### 2.4.2.7 Inhibition of single enzymes by 6HA

*P. taiwanensis* VLB120 containing plasmids pSEVA\_Cyp, pSEVA\_CDH, pSEVA\_CHMO, or pSEVA\_Lact were cultivated in M9\* medium as described above and harvested after 6 h of induction. Cells were resuspended to a biomass concentration of 0.25  $\text{g}_{\text{CDW}} \text{L}^{-1}$  in Kpi-g buffer containing defined 6HA concentrations (pH readjusted to 7.4). Then, 10 mL cell suspension were transferred into 100 mL screw-capped Erlenmeyer flasks (*P. taiwanensis* VLB120 with pSEVA\_Cyp / pSEVA\_Lact) or 1 mL cell suspension into 2 mL reaction tubes (*P. taiwanensis* VLB120 with pSEVA\_CDH / pSEVA\_CHMO). The cells were equilibrated for 10 min at 30 °C, and biotransformations were started by adding 5 mM substrate with respect to the aqueous phase volume (cyclohexane for pSEVA\_Cyp, cyclohexanol for pSEVA\_CDH, cyclohexanone for pSEVA\_CHMO) or 10 mM  $\epsilon$ -CL for pSEVA\_Lact. The reactions were stopped after 5 or 10 min reaction time and prepared for GC and HPLC analysis as described above.

#### 2.4.2.8 Bioreactor experiments

Bioreactor experiments were conducted in a 3.6 L stirred-tank Labfors 5 bioreactor controlled via Iris software (Infors AG, Bottmingen, Switzerland). Precultivations were performed in LB and RB media as described above. RB pre-cultures were used to inoculate bioreactors containing 1 L RB-medium (10  $\text{g} \text{L}^{-1}$  glucose, pH=7.2, 1.2 vvm aeration, 30 °C, 1,500 rpm stirrer speed). The pH was automatically controlled via the addition of 25 % (v/v) ammonia and 30 % (w/v) phosphoric acid. Batch cultivation was carried out until glucose depletion (cell concentration 3  $\text{g}_{\text{CDW}} \text{L}^{-1}$ ) and followed by exponential feeding of a solution containing 730  $\text{g} \text{L}^{-1}$  glucose and 19.6  $\text{g} \text{L}^{-1}$   $\text{MgSO}_4 \cdot 7 \text{H}_2\text{O}$  to maintain a specific growth rate  $\mu$  of 0.1  $\text{h}^{-1}$  until a biomass concentration of 13  $\text{g}_{\text{CDW}} \text{L}^{-1}$  was reached. For the last 4-6 h, cells were induced with 1 mM IPTG. Then, cells were harvested by centrifugation (3,124 g, RT, 30 min)

and resuspended in 1 L Kpi-g-I buffer to a final cell concentration of 10 g<sub>CDW</sub> L<sup>-1</sup>. The pH was set to 7.4 and automatically controlled via the addition of 10 M NaOH and 30% (w/v) phosphoric acid. After 10 min of equilibration, aeration was switched to a mix of cyclohexane-saturated air (0.051 or 0.3 L min<sup>-1</sup>) and pressurized air (1.2 L min<sup>-1</sup>). Glucose solution (730 g L<sup>-1</sup> glucose and 19.6 g L<sup>-1</sup> MgSO<sub>4</sub>·7 H<sub>2</sub>O) was fed into the reactor as given in the legends of Figures 2.4.6 and 2.4.5. A 5 mL sample was taken at each sampling point and used for GC sample preparation as described above, OD<sub>450</sub> measurement, and CO difference spectrum analysis. The rest of the sample was centrifuged (17,000 g, 4 °C, 10 min). Pellet (for SDS-PAGE) and supernatant (for HPLC analysis) were stored at -20 °C.

### 2.4.2.9 Analytical methods

Suspended biomass concentrations were determined by measuring OD<sub>450</sub> using a Libra S11 spectrophotometer (Biochrom, Cambridge, UK). For *P. taiwanensis*, one OD<sub>450</sub> unit corresponds to 0.186 g<sub>CDW</sub> L<sup>-1</sup> (Halan *et al.*, 2010). Recombinant gene expression was analyzed via SDS-PAGE according to Laemmli (Laemmli, 1970), loading 30 µg of total protein per lane, and via CO difference spectra to quantify active Cyp performed as described in chapter 2.1. Cyclohexane, cyclohexanol, cyclohexanone, and ε-CL concentrations were determined by GC and 6HA and adipic acid concentrations via HPLC as described before (Chapter 2.2).

Glucose, gluconic acid, and α-ketoglutaric acid were quantified by HPLC using a Dionex Ultimate 300 separation module (Thermo Fisher Scientific, Waltham, MA) equipped with a ligand exchange column (Hi-Plex H, 30 cm length, 7.7 mm diameter, 8 µm particle size, Agilent, Santa Clara, CA, USA). Glucose was quantified by a refractive index detector, keeping the column oven temperature constant at 15 °C and using deionized water as a mobile phase at a flow rate of 0.4 mL min<sup>-1</sup>. For gluconic acid and α-ketoglutaric acid quantification, a variable wavelength detector was operated at 210 nm, the column oven temperature was controlled at 40 °C, and 5.5 mM H<sub>2</sub>SO<sub>4</sub> in deionized water was applied as mobile phase at a flow rate of 0.4 mL min<sup>-1</sup>.

O<sub>2</sub> was quantified using a Trace 1310 gas chromatograph (Thermo Fisher Scientific) equipped with a TG-BOND Msieve 5A capillary column (30 m, I.D.: 0.32 mm, film thickness: 30 µm, Thermo Fisher Scientific) and a thermal conductivity detector operating at 100 °C with a filament temperature of 300 °C and a reference gas flow rate of 2 mL min<sup>-1</sup>. Argon gas was applied as carrier gas at a constant flow rate of 5 mL min<sup>-1</sup>. The injection temperature was set to 50 °C, and a split ratio of 2 was applied. The oven temperature was kept constant at 35 °C for 5 min. N<sub>2</sub> was used as the internal standard. The kinetic parameters  $v_{max}$ ,  $K_M$  (or  $K_S$ ), and  $K_I$  were calculated in Matlab 6.1 and fitted to the following equation using the method of least squares:

$$v_0 = \frac{v_{max}[S]}{K_S + [S] + \frac{[S]^2}{K_I}}$$

$v_0$ , initial reaction velocity given in U g<sub>CDW</sub><sup>-1</sup>;  $v_{max}$ , maximal reaction velocity; [S], aqueous cyclohexane concentration;  $K_S$ , apparent substrate uptake constant (cyclohexane concentration, at which reaction velocity is half-maximal);  $K_I$ , inhibition constant.



## 2.4.3 Results

In the previous chapter, *P. taiwanensis*\_6HA (*P. taiwanensis* VLB120 containing the plasmid pSEVA\_6HA\_2) has been developed, enabling cyclohexane conversion to 6HA as the exclusive product. In this study, it was evaluated, how and to what extent the catalytic performance of this strain can be exploited under process conditions. For this purpose, the physiology and catalytic performance of *P. taiwanensis*\_6HA was characterized in different media and physiological states with the objective to find suitable stirred-tank bioreactor (STR) setups.

### 2.4.3.1 The cultivation medium influences *P. taiwanensis*\_6HA physiology and specific activity

In a first step, *P. taiwanensis*\_6HA growth physiology and cascade activity was investigated in different standard media, i.e., M9, RB, and M9\*. As compared to M9, M9\* contains 3-fold higher phosphate salt concentrations for a higher buffering capacity (Sambrook & Russell, 2001), whereas RB medium contains more ammonium than M9 and M9\* media and intermediate phosphate concentrations (Volmer, 2016). Former studies have demonstrated that low phosphate and ammonia concentrations lead to gluconate accumulation and higher growth rates of *P. aeruginosa* and *P. taiwanensis* VLB120 (Buch *et al.*, 2008; Volmer, 2016). The impact of these factors on biocatalytic performance, however, has not been studied. Here, growth, glucose consumption, gluconate accumulation, and specific 6HA formation activities were investigated utilizing these standard media (Figures 2.4.2, S2.4.1).

**Table 2.4.2:** Selected physiological parameters for *P. taiwanensis*\_6HA growing in M9, RB, or M9\* medium with glucose (glu) as carbon source.

Medium	M9	RB	M9*
Growth rate $\mu$ [ $\text{h}^{-1}$ ]	$0.42 \pm 0.02$	$0.40 \pm 0.01$	$0.30 \pm 0.01$
Biomass yield [ $\text{g}_{\text{CDW}} \text{g}_{\text{glu}}^{-1}$ ]	$0.37 \pm 0.05$	$0.36 \pm 0.06$	$0.37 \pm 0.08$
Max. gluconate concentration [ $\text{g L}^{-1}$ ]	$3.98 \pm 0.14$	$2.28 \pm 0.11$	$0.02 \pm 0.00$
Gluconate production yield [ $\text{g}_{\text{gluconate}} \text{g}_{\text{glu}}^{-1}$ ]	$0.83 \pm 0.04$	$0.48 \pm 0.04$	$0.01 \pm 0.00$
pH increase <sup>a</sup>	$0.59 \pm 0.01$	$0.28 \pm 0.00$	$0.06 \pm 0.01$
Maximal activity [ $\text{U g}_{\text{CDW}}^{-1}$ ]	$16.7 \pm 2.4$	$37.4 \pm 7.0$	$37.5 \pm 0.4$

<sup>a</sup> between start of the cultivation and peak of gluconate accumulation

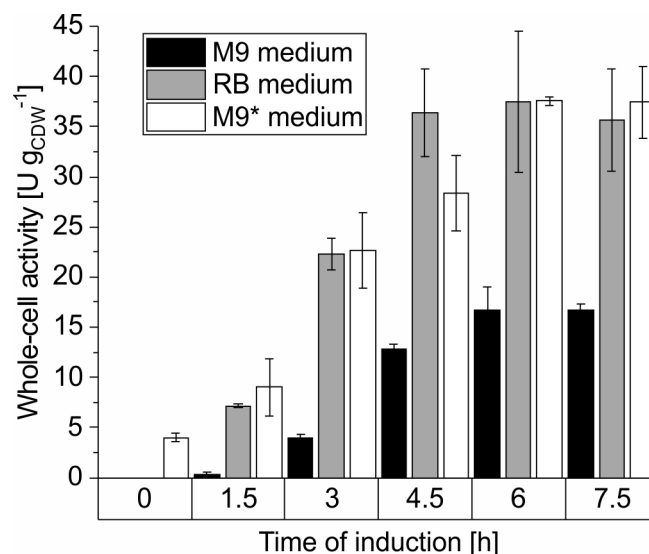


**Figure 2.4.2:** Induction studies with *P. taiwanensis\_6HA*. Cells were cultivated in M9 (black), RB (grey), or M9\* (white) medium with 0.5 % (w/v) glucose, induced by IPTG, and harvested in time intervals of 1.5 h. After resuspension in Kpi-buffer containing 1 % (w/v) glucose to a biomass concentration of 0.5 g<sub>CDW</sub> L<sup>-1</sup>, 10 mL liquid volume was transferred to a 100 mL screw-capped flask and equilibrated for 10 min at 30 °C. Reactions were started by adding 5.4 μL pure cyclohexane (corresponding to 5 mM referring to the aqueous phase volume) and stopped after 10 min. Graphs represent average values and standard deviations of two independent biological replicates. The average experimental error over all activity measurements is 15.8 %.

The *P. taiwanensis\_6HA* growth physiology differed significantly in the three media (Figure S2.4.1). The growth rate was highest in M9 medium and was only slightly lower in RB medium, but 30 % lower in M9\* medium (Table 2.4.2). Also, significant differences in gluconate accumulation were observed with negligible accumulation in M9\* medium, resulting in a relatively stable pH over the cultivation period (Figure S2.4.1). In M9 medium, however, gluconate transiently accumulated up to 4 g L<sup>-1</sup> resulting in a significant pH decrease, whereas cultivation in RB medium resulted in an intermediate gluconate accumulation. The transient gluconate accumulation did not affect the overall biomass yield, which was similar in all three media tested (Table 2.4.2).

To investigate whether these apparent physiological differences influence the catalytic performance of *P. taiwanensis\_6HA*, short-term activity assays were conducted with cells sampled during the cultivations (Figure 2.4.2). In general, similar induction kinetics (slightly faster in RB medium) were observed in all three media with the maximum specific activity reached after 6 h. The maximum activities reached in RB and M9\* medium were, however, 2-fold higher than in M9 medium, where also some leakiness was observed. This indicates that the cultivation medium significantly influenced the cell physiology and heterologous enzymes' catalytic performance and/or expression. As SDS-PAGE analysis proved inappropriate to detect expression differences among the untagged cascade enzymes, we investigated the medium effect on the expression of tagged CHMO (Figure S2.4.3). Indeed, we observed a lower CHMO expression level in M9 as compared to M9\* medium, correlating with a lower whole-cell CHMO activity, indicating a negative effect of gluconate accumulation and/or the accordingly fluctuating pH (Figure S2.4.1) on recombinant gene expression.

### 2.4.3.2 Physiological state affects the *P. taiwanensis*\_6HA catalytic activity

For styrene monooxygenase-based *in vivo* catalysis, metabolically active resting *E. coli* cells showed a higher specific activity for styrene epoxidation compared to growing cells (Julsing *et al.*, 2012a), whereas the opposite was observed with *P. taiwanensis* VLB120 $\Delta$ C (Kuhn *et al.*, 2012b,a). To investigate, whether *P. taiwanensis*\_6HA is subject to such differences, its biocatalytic performance was investigated for growing or resting cells over an extended time range. Growing cells (GCA), nitrogen-limited resting cells (RCA), and such resting cells with inducer (RCA + IPTG) grown either in RB- or M9\*-medium were applied (Figure 2.4.3). M9 medium was not tested, as only low specific activities have been obtained in the short-term assays (Figure 2.4.2). In the resting cell format, cells grown in M9\* and RB medium showed a high initial activity of  $43 \text{ U g}_{\text{CDW}}^{-1}$ , which, however, dropped by more than 50 % within the first hour of reaction and further to  $10.5 \text{ U g}_{\text{CDW}}^{-1}$  after 2 h, leading to final 6HA titers of  $1.1 \pm 0.1$  and  $1.4 \pm 0.1$  mM, respectively (Figure 2.4.3A, D).

To investigate if the whole-cell activity was maintained by continued induction in the resting cell format, we added IPTG to the resting cell suspensions and analyzed the course of their specific activities (Figure 2.4.3B, E). Again, cells grown in either medium reached initial activities of  $40 \text{ U g}_{\text{CDW}}^{-1}$ . RB grown cells showed a similar activity decrease as in the absence of IPTG, reaching a final activity of  $14.4 \pm 0.7 \text{ U g}_{\text{CDW}}^{-1}$  and a 6HA titer of  $1.5 \pm 0.1$  mM, indicating no prominent effect of the inducer. However, M9\* grown cells showed less activity drop to  $22.6 \pm 0.8 \text{ U g}_{\text{CDW}}^{-1}$  after 2 h producing  $2.2 \pm 0.1$  mM 6HA, two-fold more than in the absence of IPTG.

The initial activity of growing cells (induces with IPTG) in both media was 30 % lower than that of resting cells and dropped to  $13.2 \pm 0.4 \text{ U g}_{\text{CDW}}^{-1}$  in M9\* medium and  $16.7 \pm 0.8 \text{ U g}_{\text{CDW}}^{-1}$  in RB medium after 2 h of incubation (Figure 2.4.3C, F). The higher growth rate in RB medium resulted in a higher final 6HA concentration of  $3.1 \pm 0.1$  mM as compared to  $1.8 \pm 0.1$  mM in M9\* medium. The gas-phase  $\text{O}_2$  concentration (headspace) reached 5 % of saturation after 160 min growth in RB-medium, indicating  $\text{O}_2$  limitation as a possible reason for the activity decrease. In all other experiments shown in 2.4.3, the gas-phase  $\text{O}_2$  concentration remained above 15 % of saturation, indicating that  $\text{O}_2$  was not a major limiting factor. Cyclohexane limitation could be the possible reason for the activity decrease, as its concentration in the aqueous phase (extracellular concentration) dropped to  $50 \mu\text{M}$ . Thus, whole-cell kinetic analyses were the next step, also being crucial to optimize cyclohexane feeding for maximal 6HA production.

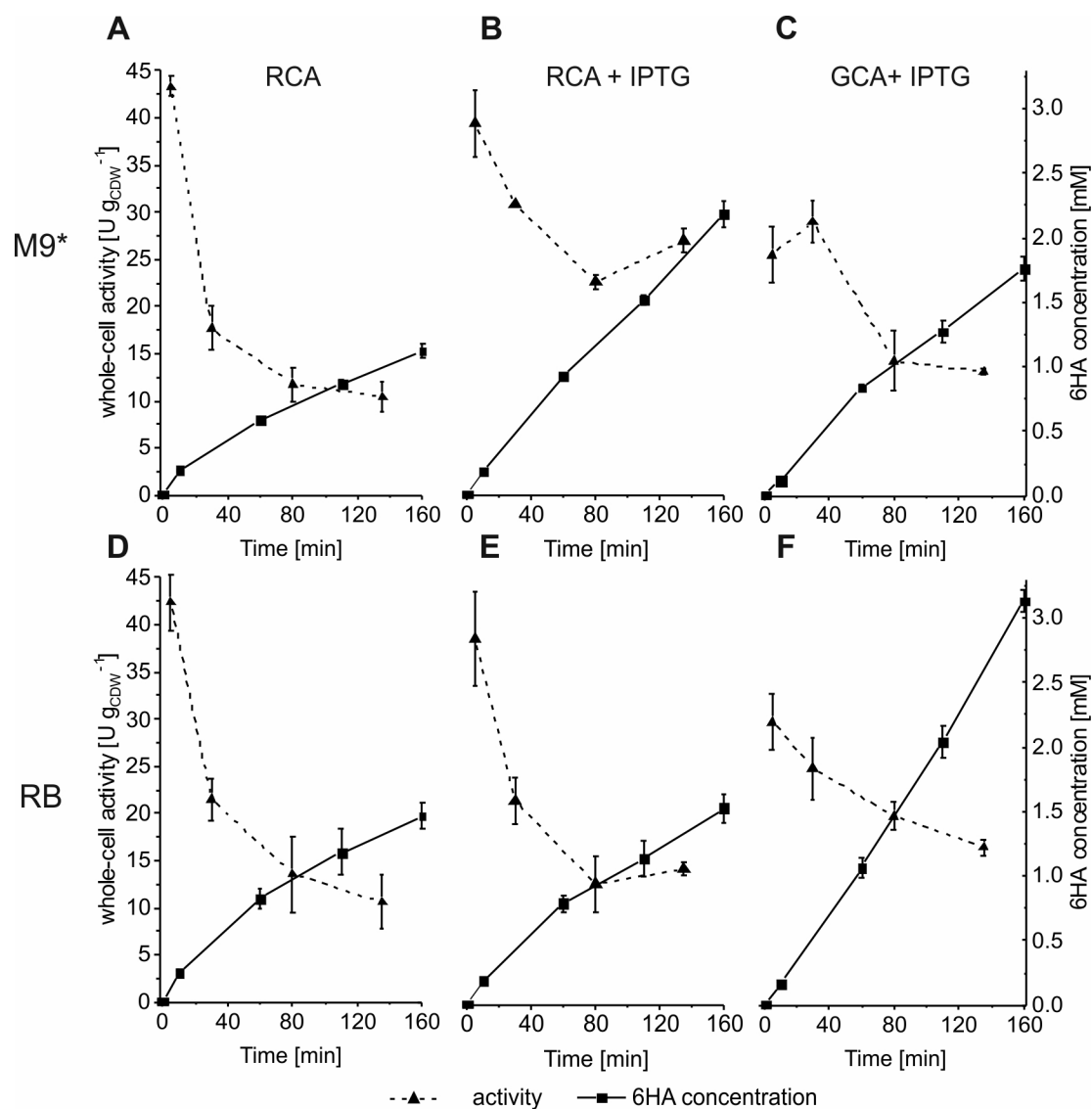


**Figure 2.4.3:** Influence of cellular physiology on specific cascade activity of *P. taiwanensis\_6HA*. Cells were cultivated in M9\* (A, B, C) or RB (D, E, F) medium with 0.5 % (w/v) glucose, induced by IPTG, and harvested 6 h after induction. Cells were either resuspended in Kpi buffer containing 1 % (w/v) glucose (A, D, RCA), Kpi-buffer containing 1 mM IPTG, and 1 % (w/v) glucose (B, E, RCA + IPTG), or fresh growth medium containing 1 mM IPTG (C, F, GCA) to a biomass concentration of 0.5 g<sub>CDW</sub> L<sup>-1</sup>. 20 mL liquid volume was transferred to 100 mL screw-capped flasks and equilibrated for 10 min at 30 °C. Reactions were started by adding 10.9 µL pure cyclohexane (corresponding to 5 mM referring to the aqueous phase volume). Sampling was conducted after 10, 60, 100, and 160 min. Graphs represent average values and standard deviations of two independent biological replicates. The average experimental errors over all measurements for the activities and 6HA concentrations are 15.2 and 6.4 %, respectively.

### 2.4.3.3 Whole-cell kinetics for cyclohexane biotransformation is subject to substrate inhibition or toxification

To understand the dependency of the whole-cell activity on the cyclohexane concentration (Karande *et al.*, 2016), the whole-cell kinetics was analyzed in resting-cell assays.

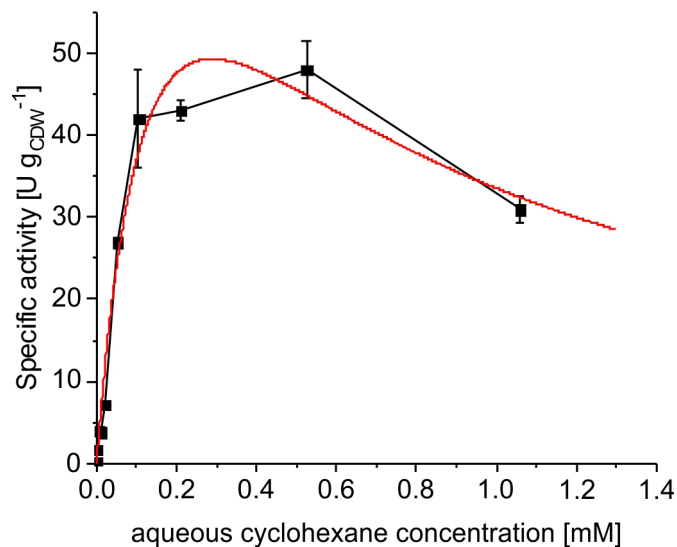


**Figure 2.4.4:** Specific 6HA formation rates as a function of the aqueous cyclohexane concentration. Cells were cultivated in M9\* medium with 0.5 % (w/v) glucose, induced by IPTG and harvested after 4 h. After resuspension in Kpi-buffer containing 1 % (w/v) glucose to a biomass concentration of  $0.5 \text{ g}_{\text{CDW}} \text{ L}^{-1}$ , 10 mL liquid volume were transferred to 100 mL screw-capped Erlenmeyer flasks and equilibrated for 10 min at 30 °C. Reactions were started by adding different volumes of pure cyclohexane and stopped after 10 min. The graph represents average values and standard deviations of two independent biological replicates for each substrate concentration. The average experimental error over all measurements for the activities is 7.6 %. Kinetic parameters and the coefficient of determination are depicted for fitting the data according to Michaelis-Menten kinetics with substrate inhibition (red line) yielding apparent values for the maximal activity  $v_{\text{max}}$ , the substrate uptake constant  $K_S$ , and the inhibition constant  $K_I$ .

A substrate inhibition type of kinetics was found, for which parameters are given in Figure 2.4.4. Indeed, the obtained substrate uptake constant  $K_S$  ( $169 \mu\text{M}$ ) indicates that substrate limitation occurs at the substrate concentrations present (and decreasing) in the experiments shown in Figure 2.4.3. Combined with substrate inhibition, this allowed for maximal activities  $\geq 40 \text{ U g}_{\text{CDW}}^{-1}$  to be achieved in an aqueous cyclohexane concentration range of  $\sim 100\text{-}500 \mu\text{M}$ , which just includes the initial aqueous substrate concentration of  $125 \mu\text{M}$  in biotransformation assays. Besides, the biomass concentration in resting cell assays dropped from  $0.54 \pm 0.01 \text{ g L}^{-1}$  to  $0.21 \pm 0.01 \text{ g L}^{-1}$  (ca. 60 %) during 10 min assay time at 1 mM aqueous cyclohexane concentration. This indicates cell toxification, which can be expected to impair metabolic and catalytic activity at high cyclohexane concentrations. In an earlier study, 70 % of the cells were reported to be permeabilized when exposed to an aqueous cyclohexane concentration of 1.1 mM (Karande *et al.*, 2016). Substrate limitation on the one hand and the strong inhibition or toxification of *P. taiwanensis*\_6HA by cyclohexane on the other hand demand a setup with a well-controlled cyclohexane supply to maximally exploit the biocatalytic capacity of the cells.

#### 2.4.3.4 Continuous cyclohexane feeding in a stirred-tank bioreactor allows 6HA production

For establishing such a controlled cyclohexane supply in a stirred-tank bioreactor under process conditions, the application of a second organic phase acting as substrate reservoir has been tested, but was not satisfactory, as even low aeration rates led to substantial cyclohexane stripping and thus to a low yield on cyclohexane and substrate limitation (Hoschek *et al.*, 2019b). Direct cyclohexane feeding may reduce stripping, but may involve a concentration gradient and cell toxification. Instead, cyclohexane feeding via the gas phase was evaluated. For this purpose, the aeration stream was saturated with

cyclohexane in a separate container leading to a gas phase concentration of  $5.42 \pm 0.04$  mM. Such cyclohexane saturated air was then mixed with pure air to create an aeration gas flow providing the desired cyclohexane amount (Figure S2.4.3). Thereby, a variation of the cyclohexane-saturated air to pure air flow rate ratio allowed tuning the gaseous cyclohexane concentration in the reactor. For the first set of experiments, we selected a cyclohexane feed rate of  $0.276 \text{ mmol min}^{-1} \text{ L}^{-1}$ , corresponding to an aqueous phase concentration of  $30 \text{ }\mu\text{M}$  upon equilibration with the gas phase. Thereby, the system was operated under substrate limitation to minimize cyclohexane toxicity effects.

Cells were first grown in batch mode in RB medium until glucose depletion and further in fed-batch mode with an exponential feed enabling  $\mu=0.1 \text{ h}^{-1}$ . During fed-batch cultivation, cells were induced for heterologous cascade gene expression, followed by harvesting and resuspension in glucose and IPTG containing Kpi-buffer. Within the first 2 h, the cell concentration increased slightly from  $9.2$  to  $11.4 \text{ g}_{\text{CDW}} \text{ L}^{-1}$ , possibly due to remaining nutrients from the cultivation medium, and then remained constant for the next 4 h (Figure 2.4.6A).  $\text{O}_2$  limitation was avoided by maintaining the dissolved oxygen concentration ( $p\text{O}_2$ ) between 20 and 50 % of saturation. Gluconate accumulated to a final concentration of  $8.5 \text{ g L}^{-1}$  after 6 h of biotransformation. Within the first 3 h, the aqueous cyclohexane concentration remained low (Figure 2.4.6B), whereas the cyclohexane-limited specific activity slightly decreased from  $-8$  to  $6 \text{ U g}_{\text{CDW}}^{-1}$ , roughly correlating to the cell density increase expected to lead to more severe substrate limitation (Figure 2.4.6C). During this time period  $-50 \text{ mmol}$  cyclohexane were fed via the gas phase and  $13.3 \pm 0.3 \text{ mmol}$  product accumulated (about 25 % conversion). After 3 h, the cyclohexane concentration increased to and stabilized at  $-18 \text{ }\mu\text{M}$ , whereas the specific activity decreased to  $-4 \text{ U g}_{\text{CDW}}^{-1}$ . This is lower than the  $10.3 \text{ U g}_{\text{CDW}}^{-1}$  expected at  $18 \text{ }\mu\text{M}$  cyclohexane according to the kinetic parameters (Figure 2.4.4) and equation 1.

Considering that no pathway intermediates accumulated, this may be due to a loss in Cyp activity (1st reaction step) or a change in cell physiology (mass transfer over cellular membranes, metabolic activity). As assessed via CO difference spectra (Figure 2.4.6C), the amount of active Cyp dropped by 30 % within the first 3 h of reaction and then remained stable, which cannot completely explain the activity course. A final product concentration of  $22.8 \pm 1.0 \text{ mM}$  was reached (Figure 2.4.6B), which includes the main product 6HA and the overoxidation product adipic acid (AA) (1.2 % of the total product). Overall, a product yield on biomass of  $0.28 \text{ g g}_{\text{CDW}}^{-1}$  and an average productivity of  $0.50 \text{ g L}^{-1} \text{ h}^{-1}$  were obtained (Table 2.4.3).

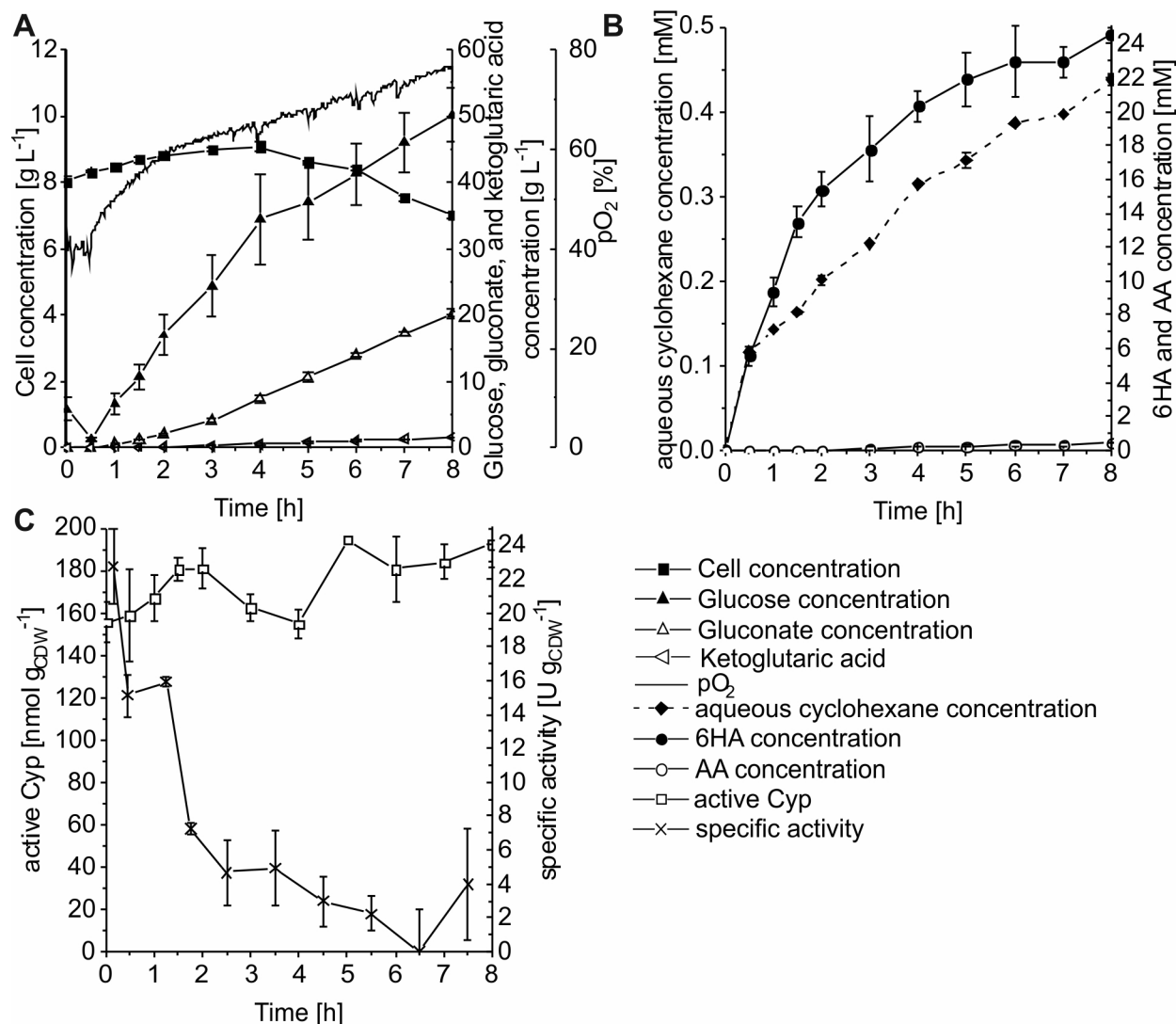


**Figure 2.4.5:** Biotransformation of cyclohexane to 6HA in a stirred-tank bioreactor with a cyclohexane feed of  $1.626 \text{ mmol min}^{-1} \text{ L}^{-1}$ . *P. taiwanensis*\_6HA was cultivated in batch mode in 1 L RB medium followed by fed-batch cultivation with exponential feeding for  $\mu=0.1 \text{ h}^{-1}$ . Cells were induced after 10 h of fed-batch cultivation and cultivated for another 3.5 h until they were harvested. The biotransformation was started with  $10 \text{ g L}^{-1}$  biomass concentration in 1 L Kpi buffer containing 1 % glucose (w/v) and 1 mM IPTG by applying a feed rate of  $1.626 \text{ mmol}_{\text{cyclohexane}} \text{ min}^{-1} \text{ L}^{-1}$  and a glucose feed rate of  $14.8 \text{ g h}^{-1}$  (started after 0.5 h). **(A)** Time courses of cell, glucose, gluconate, and dissolved oxygen ( $\text{pO}_2$ ) concentrations. **(B)** Time courses of aqueous cyclohexane, 6HA, and AA concentrations. **(C)** Time courses of active Cyp amount determined via CO difference spectra and specific activity based on 6HA and AA accumulation. Graphs represent average values and standard deviations of two technical replicates.

### 2.4.3.5 Higher cyclohexane concentrations result in enhanced initial activities but poor biocatalyst stability

To evaluate how far substrate limitation can be relieved without harming biocatalyst performance, the substrate feed rate via the gas phase was increased 6-fold, corresponding to an aqueous cyclohexane concentration of  $147 \mu\text{M}$  (see materials and methods for details).

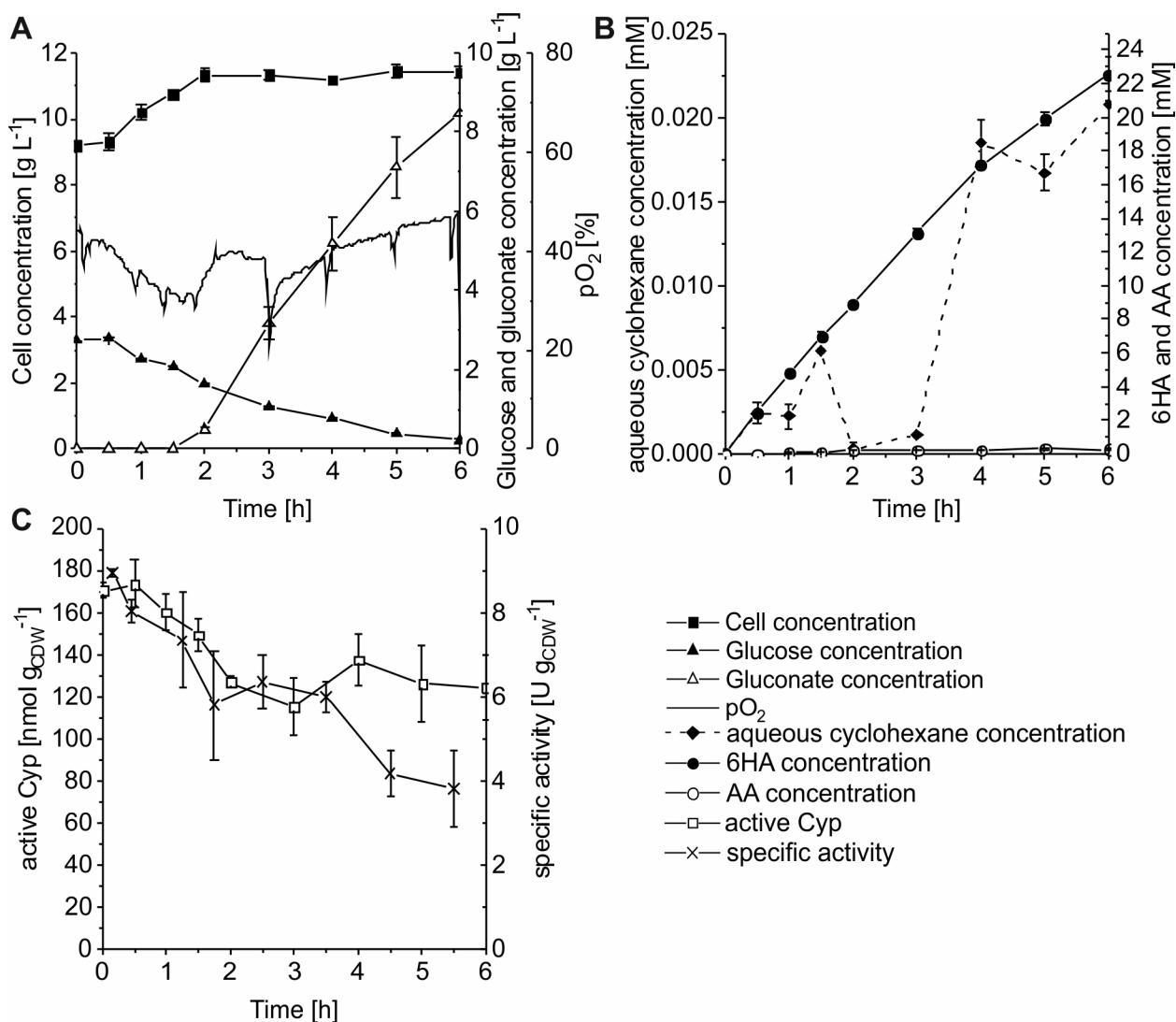


**Figure 2.4.6:** Biotransformation of cyclohexane to 6HA in a stirred-tank bioreactor with a cyclohexane feed of  $0.276 \text{ mmol min}^{-1} \text{ L}^{-1}$ . *P. taiwanensis\_6HA* was cultivated in batch mode in 1 L RB medium followed by glucose-limited fed-batch cultivation with exponential feeding for  $\mu=0.1 \text{ h}^{-1}$ . Cells were induced after 6 h of fed-batch cultivation and cultivated for another 6 h until they were harvested. Afterward, the biotransformation was started with  $10 \text{ g L}^{-1}$  biomass concentration in 1 L Kpi buffer containing 1 % glucose (w/v) and 1 mM IPTG by applying a cyclohexane feed rate of  $0.276 \text{ mmol}_{\text{cyclohexane}} \text{ min}^{-1} \text{ L}^{-1}$  and a glucose feed rate of  $7.4 \text{ g h}^{-1}$  (started after 1.5 h). **(A)** Time courses of cell, glucose, gluconate, and dissolved oxygen ( $\text{pO}_2$ ) concentrations. **(B)** Time courses of aqueous cyclohexane, 6HA, and AA concentrations. **(C)** Time courses of active Cyp amount determined via CO difference spectra and specific activity based on 6HA and AA accumulation. Graphs represent average values and standard deviations of two technical replicates.

The cell concentration increased slightly during the first 4 h from  $8$  to  $9 \text{ g}_{\text{CDW}} \text{ L}^{-1}$  but then dropped to  $7 \text{ g}_{\text{CDW}} \text{ L}^{-1}$  after 8 h (Figure 2.4.5A). Together with the continuous  $\text{pO}_2$  increase, this indicates inhibition/toxication of cell metabolism, which led to a pronounced accumulation of glucose and also gluconate (up to  $50$  and  $20 \text{ g L}^{-1}$ , respectively). Furthermore, minor  $\alpha$ -ketoglutarate formation ( $1.6 \text{ g L}^{-1}$ ) was observed. The aqueous cyclohexane concentration continuously increased from an initial value of  $0.1 \text{ mM}$  to  $0.4 \text{ mM}$  after 8 h of biotransformation (Figure 2.4.5B) indicating an increase in cyclohexane solubility due to the biology- and biotransformation-related changes in aqueous phase composition. This also has been observed before in a non-aerated STR for cyanobacteria-based cyclohexane



hydroxylation in the presence of a second organic phase (Hoschek *et al.*, 2019b). It has been shown that some microbial species, including pseudomonads, produce surfactants to increase substrate solubility and thus availability (Margaritis *et al.*, 1979; Mukherjee *et al.*, 2006). Also, the addition of hydrophobic compounds to *E. coli* cultures in an aerated STR was found to cause the appearance of a cell fraction with hydrophobic surface properties (Collins *et al.*, 2015) – another possible cause for such a solubility increase. The feed rate increase led to a 2.5-fold higher initial whole-cell activity of  $22.8 \pm 2.2 \text{ U g}_{\text{CDW}}^{-1}$ , which was followed by a more drastic decrease to  $4.7 \pm 1.9 \text{ U g}_{\text{CDW}}^{-1}$  within the first 3 h of reaction (Figure 2.4.5C), and thus did not lead to an improvement of overall biotransformation performance (Figures 2.4.6 and 2.4.5, Table 2.4.3). Interestingly, active Cyp amounts remained stable over the reaction time, and no pathway intermediates accumulated, indicating a limitation by changes in cell physiology/ metabolism and not by intracellular enzyme amounts.

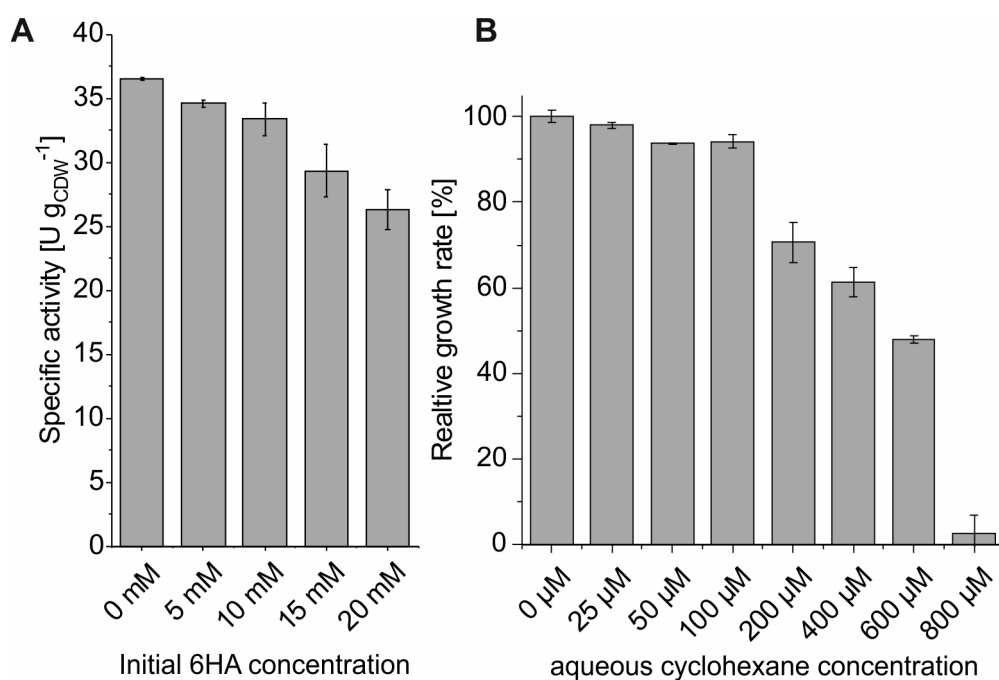


**Figure 2.4.7:** Impact of 6HA on the specific activity of *P. taiwanensis\_6HA* (A) and effect of cyclohexane on growth of *P. taiwanensis VLB120* (B). (A) Cells were cultivated in M9\*-containing shake flasks, induced for 4 h, harvested, and resuspended in Kpi-buffer (1 % glucose (w/v), varying 6HA concentrations, pH=7.4) to a biomass concentration of  $1.5 \text{ g}_{\text{CDW}} \text{ L}^{-1}$ . Biotransformations were conducted in 5 mL liquid volume within 100 mL screw-capped Erlenmeyer flasks, started by adding 5.5 μL pure cyclohexane (corresponding to 10 mM referring to the aqueous phase volume) and terminated after 1 h. (B) Relative growth rate in the presence of varying amounts of cyclohexane in M9\* medium (a growth rate of  $0.461 \pm 0.006 \text{ h}^{-1}$  represents 100%). Graphs represent average values and standard deviations of two independent biological replicates. The average experimental errors over all measurements for the specific activities and relative growth rates (except the values at 800 μM indicating complete growth inhibition) are 3.6 and 2.5%, respectively.

To identify possible reasons for the observed activity decrease, we evaluated product (6HA) inhibition and cell toxification by cyclohexane. Indeed, increasing 6HA concentrations led to decreasing specific activities (Figure 2.4.7A) and, therefore, might have contributed to the activity loss in both bioreactors. The mode of microbial 6HA export is unknown but possibly involves active transport due to its charged character at pH 7.2 Strikingly, only Cyp and lactonase were inhibited by 6HA when cells containing a single cascade enzyme were tested (Figure S2.4.4). On the other hand, cyclohexane inhibited growth

of *P. taiwanensis* VLB120 with a half-maximal growth rate observed at an aqueous cyclohexane concentration of  $\sim 450 \mu\text{M}$  (Figure 2.4.7B). Cyclohexane concentrations in the first reactor (Figure 2.4.6B) were far lower, but reached 0.4 mM in the second reactor (Figure 2.4.5B). Overall, both cyclohexane toxicity and product inhibition are factors affecting biocatalyst stability under process conditions

### 2.4.4 Discussion

PCL belongs to the group of biodegradable polymers originating from fossil resources. PCL is often used in blends and has applications in the medicinal (Serrano *et al.*, 2010), packaging (Gross & Kalra, 2002), and electronics sectors (Gao *et al.*, 2017; Labet & Thielemans, 2009). Its ester bonds are mainly responsible for its hydrolysis-based biodegradability, which depends on its molecular weight and degree of crystallinity (Gross & Kalra, 2002). At least 39 species of the bacterial classes *Firmicutes* and *Proteobacteria* have been identified to degrade PCL within several days (Tokiwa *et al.*, 2009). Recently, we have developed recombinant *P. taiwanensis* VLB120 strains that synthesize PCL monomers from cyclohexane with 100 % conversion and turnover numbers of 45,000 mol monomer per mol of Cyp, the first and rate-limiting enzyme of the engineered *in vivo* cascade (Chapter 2.3). In this work, we studied the impact of cultivation conditions on *P. taiwanensis*\_6HA growth and physiology and in turn on specific activity in order to evaluate, how and to what extent its catalytic potential can be exploited in bioreactor setups for gram-scale 6HA production from cyclohexane.

#### 2.4.4.1 Cultivation medium and conditions influence gluconate accumulation and whole-cell activity

*P. taiwanensis*\_6HA has been characterized in different media and whole-cell biocatalyst formats. M9, RB, and M9\* media are standard minimal media used to cultivate heterotrophic organisms (Riesenberg *et al.*, 1991; Sambrook & Russell, 2001). Their composition can influence cellular physiology and catalytic performance, as confirmed in this study for *P. taiwanensis*\_6HA. Cultivation of *P. aeruginosa*, *Aspergillus niger*, and *P. taiwanensis* VLB120 at low phosphate and ammonium concentrations has been reported to involve gluconate accumulation (Buch *et al.*, 2008; Müller, 1986; Volmer, 2016). We observed that gluconate accumulation could be prevented by increasing the phosphate content 3-fold in M9\* compared to M9 medium, which, however, involved a reduction in the specific growth rate (Table 2.4.2, Figure S2.4.1). With an intermediate phosphate level, RB medium leads to 40 % less gluconate accumulation compared to M9 medium, but did not significantly affect the growth rate. Gluconate is formed by the periplasmatic glucose dehydrogenase (Gcd) and diffuses via pores into the medium, where it is known to function as a phosphate solubilizer (Buch *et al.*, 2008; Del Castillo *et al.*, 2007). It has been reported that excessive gluconate formation hampered polyhydroxyalkanoate synthesis (Poblete-Castro *et al.*, 2013) and isobutyric acid production (Lang *et al.*, 2014). Although gluconate was formed in RB-medium, no difference in the specific activity of *P. taiwanensis*\_6HA was observed compared to M9\* medium (Figure 2.4.2), indicating that gluconate formation in RB medium does not affect biocatalyst performance. *P. taiwanensis*\_6HA however showed lower specific activity when grown in M9 medium (Figure 2.4.2). More pronounced gluconate formation and an unstable pH in M9 medium constitute possible reasons for such differences (Table 2.4.2, S2.4.1). Another study revealed that high growth rates observed for the fungus *Trichoderma reesei* in M9 medium

resulted in lower heterologous protein synthesis (Pakula *et al.*, 2005). Accordingly, a decrease in the heterologous protein synthesis appeared to cause the lower activity of *P. taiwanensis*\_6HA grown in an M9 medium. Overall, the M9 medium can be considered not suitable for 6HA production by *P. taiwanensis*\_6HA due to gluconate accumulation and lower specific activities. A previous study reported that metabolically active resting *E. coli* cells have a higher styrene epoxidation capacity than growing cells cultivated in RB medium (Julsing *et al.*, 2012a). Conversely, the more stable activity of growing cells made them more suitable for process setups (Kuhn *et al.*, 2012b). These results indicate that the cellular growth state significantly influences whole-cell activity, especially during long-term cultivation. Resting cells of *P. taiwanensis*\_6HA exhibited a fast drop in specific activity by more than 50 % within the first hour of reaction (Figure 2.4.3A, D). The addition of the inducer IPTG to resting cells resulted in some activity stabilization (Figure 2.4.3B, E), possibly due to protein re-synthesis based on amino acids derived from proteolysis of denatured and obsolete proteins (Konovalova *et al.*, 2014). Whereas growing cells showed lower initial activities than resting cells, their activity loss was less pronounced (Figure 2.4.3C, F), as it can be expected from their more constant and high metabolic and protein synthesis activity. However, substrate limitation, product inhibition, and/or toxification by cyclohexane cannot be excluded as additional factors leading to the observed decrease in whole-cell activities, although 6HA and aqueous cyclohexane remained low (below 3.5 mM and 125  $\mu$ M, respectively). With growing cells, RB medium appeared to be more promising compared to M9\*. Thereby, the constant volumetric product accumulation rate and low O<sub>2</sub> levels in the gas phase indicate that the slow decrease in specific activity may have been caused by an increasing O<sub>2</sub> limitation at the increasing cell concentration in shake flasks.

#### 2.4.4.2 Substrate supply and product removal as critical aspects in reaction engineering

Cyclohexane is a small (84 Da) and hydrophobic molecule, and can rapidly pass the outer and inner membrane of *P. taiwanensis* (Chen, 2007; Nikaido, 2003). In addition, its hydrophobic character ( $\log P_{\text{octanol/water}} = 3.4$ ) favors its accumulation in the cellular membrane making it extremely toxic for microorganisms (membrane disintegration at 600  $\mu$ M) (Sikkema *et al.*, 1994). Thus cyclohexane supply in a stirred-tank bioreactor is the most critical step to produce monomers. Previous studies were either performed in shake-flask experiments (Wang *et al.*, 2020; Zhang *et al.*, 2020) or started from the less toxic and less volatile substrate cyclohexanol to produce monomers via cascade reactions (Srinivasamurthy *et al.*, 2019). To exploit the catalytic performance of *P. taiwanensis*\_6HA in a controlled environment enabling high O<sub>2</sub> transfer, a continuous aeration-mediated gaseous cyclohexane feed was established for bioreactor-based biotransformations (Figure S2.4.3). Considering the resulting aqueous substrate concentrations (Figures 2.4.6B and 2.4.5B), the two different feed rates applied can be expected to involve first- and zero-order kinetics (Figure 2.4.4). Whereas the initial activity indeed was 2.5-fold higher with the higher feed rate (Figures 2.4.6C and 2.4.5C), the specific activities obtained in shake flasks were not reached, and the higher feed rate involved a relatively fast activity decrease. The stable Cyp amount during the entire non-cyclohexane-limited biotransformation (Figures 2.4.5C) indicates that product inhibition and/or an impaired metabolic activity and thus NADH regeneration possibly due to cyclohexane toxicity hampered biocatalyst activity. Cyclohexane toxicity was indeed found to be a critical factor, with the growth rate reduced by half at 450  $\mu$ M (Figure 2.4.7B), roughly corresponding to its concentration at the end of the non-cyclohexane-limited biotransformation

(Figure 2.4.5B). Such a possible toxicity effect is supported by the much less prominent activity decrease in the cyclohexane-limited biotransformation (Figure 2.4.6). Metabolic activity-related toxicity effects also have been observed for other low logP-compounds such as styrene oxide, even at apparently subtoxic levels (Kadisich *et al.*, 2017b,a; Kuhn *et al.*, 2013). Further, a contribution of product inhibition/toxicity can not be excluded (Chapter 2.3), although 6HA concentrations in the time period of the most prominent activity decrease only had a minor effect on resting cell activities (Figure 2.4.7A). In the substrate-limited biotransformation, the cyclohexanone concentration remained below 25  $\mu\text{M}$  and thus was not in the toxic range (Figure 2.4.6B). Nevertheless, a moderate activity decrease also was observed here, which, despite of the lower initial activity, still enabled a comparable final product concentration as obtained with the higher feed rate (Table 2.4.3). In this case, product inhibition, especially towards the end of the biotransformation, constitutes the most plausible reason for the moderate activity decrease (Figure 2.4.7A).

**Table 2.4.3:** Comparison of process parameters of biotransformations producing 6HA.

	Reactor I	Reactor II	Srinivasamurthy <i>et al.</i> (2019)
Volume [L]	1	1	0.5
Biotransformation time [h]	6	8	70
Substrate feed [ $\text{mmol min}^{-1} \text{L}^{-1}$ ]	0.276 <sup>a</sup>	1.626 <sup>a</sup>	0.079 <sup>b</sup>
Initial cell concentration [ $\text{g L}^{-1}$ ]	9.2	8.0	28.8
Max. cell concentration [ $\text{g L}^{-1}$ ]	11.4	9.1	n.d. <sup>c</sup>
Average productivity [ $\text{g L}^{-1} \text{h}^{-1}$ ]	0.50	0.41	0.32
Maximal activity [ $\text{U g}_{\text{CDW}}^{-1}$ ]	8.9	22.8	2.7 <sup>d</sup>
Final product concentration [mM]	22.8 <sup>e</sup>	25.0 <sup>e</sup>	168
Specific product yield [ $\text{g}_{\text{product}} \text{g}_{\text{CDW}}^{-1}$ ]	0.28	0.40	0.77
Final product titer [ $\text{g L}^{-1}$ ]	3.0	3.3	22.2
Total product [g]	3.0	3.3	11.1
Yield on substrate [%]	23	4	81 <sup>f</sup>

<sup>a</sup> referring to aqueous phase volume

<sup>b</sup> for 45 h, referring to aqueous phase volume

<sup>c</sup> not determined

<sup>d</sup> complete cyclohexanol consumption within first 12 h

<sup>e</sup> 6HA and AA are products

<sup>f</sup> isolated yield

Srinivasamurthy *et al.* (2020) developed a whole-cell process with *E. coli* and obtained 185 mM  $\epsilon$ -CL from the more expensive, but less volatile and less toxic substrate cyclohexanol. They applied a continuous substrate feed via a syringe pump and a purified lipase to obtain 6HA as main product (Srinivasamurthy *et al.*, 2019). The resulting process was stable for 70 h, resulting in 7-fold higher final product titers compared to our whole-cell process with cyclohexane as substrate (Table 2.4.3). Whereas the approach presented in this study makes use of a cheaper substrate and does not involve the addition of an expensive enzyme, process performance needs to be further improved to reach industrial relevance. Gaseous cyclohexane feeding does not allow high substrate conversion (Table 2.4.3) and thus requires cyclohexane recycling via condensation, which, however, can be considered standard technology. The optimal cyclohexane feed concentration may lie between the two tested

cyclohexane concentrations but cannot be expected to completely avoid toxicity and inhibitory effects of substrate and product. Additionally, the impact of prolonged cyclohexane exposure on whole-cell activity needs to be evaluated to fine-tune aqueous substrate concentrations. *In situ* product removal appears mandatory, which is challenging for 6HA due to its hydrophilic nature. It has been shown that solid-phase extraction could enhance the product titer up to 2000-fold (Phillips *et al.*, 2013). Additionally, the use of supercritical fluid extraction constitutes an option (Khosravi-Darani & Vasheghani-Farahani, 2005). It has been shown that *in situ* polymerization to PCL with a lipase is possible, which might be combined with product extraction into a second organic or supercritical phase (Scherkus *et al.*, 2016; Schmidt *et al.*, 2015). This second phase may also be used as a cyclohexane reservoir to alleviate its toxic effects (Hoschek *et al.*, 2019b). The use of cyclohexane as organic phase and VLB120 cells with a solvent-tolerant phenotype may constitute another option (Volmer *et al.*, 2014). However, the high energy demand for solvent tolerance (Blank *et al.*, 2008b; Kuhn *et al.*, 2012a) and the volatility and explosivity of cyclohexane in an aerated system are drawbacks of this approach.

Although growing cells have a high energy demand for growth (Bühler *et al.*, 2008) and showed lower initial activities (Figure 2.4.3), it is worth testing them for cascade reactions in a bioreactor setup, as they have been found to show less severe product inhibition/toxication (Julsing *et al.*, 2012a). This may involve an energy-dependent tolerance mechanisms and a more efficient protein re-synthesis, thereby enhancing process stability. Such a higher stability also may be realized by employing continuous biofilm capillary reactors as an alternative to STRs (Heuschkel *et al.*, 2019). Such a system has been shown to allow cyclohexane oxidation rates of  $0.4 \text{ g L}^{-1} \text{ h}^{-1}$  for several days (Karande *et al.*, 2016). A combination of heterotrophic *P. taiwanensis* with the autotrophic *Synechocystis* sp. enabled even higher stabilities and 100 % conversion of cyclohexane (Hoschek *et al.*, 2019a).

#### 2.4.4.3 Conclusion and outlook

This study reports on the successful transfer of a 4-step cascade harbored by recombinant *P. taiwanensis* VLB120 into a bioreactor format for the conversion of cyclohexane to the polymer building block 6HA and discusses encountered challenges. The cultivation medium composition was found to be a critical factor for the achievement of high whole-cell activities. Standard M9 medium was not suitable due to excessive gluconate formation from glucose, associated with lower catalytic activities. RB and M9\* media were both suitable, with RB medium enabling faster growth to higher cell densities. Metabolically active resting cells exhibited a rather fast activity decrease under reaction conditions, whereas growing cells showed more stable, but lower initial activities. The addition of inducer could stabilize resting cells, which were applied in a bioreactor setup involving a gaseous cyclohexane feed. This approach enabled a product titer of 24 mM. Further analyses showed that toxication by the substrate cyclohexane constituted a critical factor, resulting in a delicate tradeoff between substrate toxicity and substrate limitation. Also product inhibition was found to become critical at high 6HA levels. Optimization of the cyclohexane feed, gas-recycling, and *in situ* product removal, and continuous reaction formats constitute strategies to further increase yield and productivity.

### 2.4.5 Acknowledgments

LB, IH and ML were funded by the ERA-IB- Project PolyBugs ID:16006 and the Sächsisches Ministerium für Wissenschaft und Kunst (SMWK) Project ID: 100318259. We acknowledge the use of the facilities of the Centre for Biocatalysis (MiKat) at the Helmholtz Centre for Environmental Research, which is supported by European Regional Development Funds (EFRE, Europe funds Saxony) and the Helmholtz Association. The authors would like to thank Prof. Dr. Andreas Schmid for helpful discussions.

## Chapter 2.5

# One-pot synthesis of 6-aminohexanoic acid from cyclohexane using mixed-species cultures

Lisa Bretschneider, Martin Wegner, Katja Bühler, Bruno Bühler, Rohan Karande

### Short Summary

6-Aminohexanoic acid (6AHA) is a vital polymer building block for nylon 6 production and an FDA-approved orphan drug. However, its production from cyclohexane is associated with several challenges, including low conversion and yield, and severe environmental issues. We aimed at overcoming these challenges by developing a bioprocess for 6AHA synthesis. A mixed-species approach turned out to be most promising. Thereby, *Pseudomonas taiwanensis* VLB120 strains harboring an upstream cascade converting cyclohexane to either  $\epsilon$ -caprolactone ( $\epsilon$ -CL) or 6-hydroxyhexanoic acid (6HA) were combined with *Escherichia coli* JM101 strains containing the corresponding downstream cascade for the further conversion to 6AHA.  $\epsilon$ -CL was found to be a better 'shuttle molecule' than 6HA enabling higher 6AHA formation rates and yields. Mixed-species reaction performance with 4 g L<sup>-1</sup> biomass, 10 mM cyclohexane, and an air-to-aqueous phase ratio of 23 combined with a repetitive oxygen feeding strategy led to complete substrate conversion with 86 % 6AHA yield and an initial specific 6AHA formation rate of  $7.7 \pm 0.1$  U g<sub>CDW</sub><sup>-1</sup>. The same cascade enabled 49 % 7-aminoheptanoic acid yield from cycloheptane. This combination of rationally engineered strains allowed direct 6AHA production from cyclohexane in one pot with high conversion and yield under environmentally benign conditions.

Published in:

*Microbial Biotechnology*, **2021**, 14(3), 1011-1025. doi: <https://doi.org/10.1111/1751-7915.13744>

The full publication incl. Supplementary Material can be found in the Appendix Section 5.

## Chapter 2.6

# Rational orthologous pathway and biochemical process engineering for adipic acid production using *Pseudomonas taiwanensis* VLB120

Lisa Bretschneider, Ingeborg Heuschkel, Katja Bühler, Rohan Karande, Bruno Bühler

### Abstract

Microbial bioprocessing based on orthologous pathways constitutes a promising approach to replace traditional greenhouse gas- and energy-intensive production processes, e.g., for adipic acid (AA). We report the construction of a *Pseudomonas taiwanensis* strain able to efficiently convert cyclohexane to AA. For this purpose, a recently developed 6-hydroxyhexanoic acid (6HA) synthesis pathway was amended with alcohol and aldehyde dehydrogenases, for which different expression systems were tested. Thereby, genes originating from *Acidovorax* sp. CHX100 and the *XylS/Pm* regulatory system proved most efficient for the conversion of 6HA to AA as well as the overall cascade enabling an AA formation activity of up to  $48.6 \pm 0.2 \text{ U g}_{\text{CDW}}^{-1}$ . The optimization of biotransformation conditions enabled 96 % conversion of 10 mM cyclohexane with 100 % AA yield. During recombinant gene expression, the avoidance of glucose limitation was found to be crucial to enable stable AA formation. The biotransformation was then scaled from shaking flask to a 1 L bioreactor scale, at which a maximal activity of  $22.6 \pm 0.2 \text{ U g}_{\text{CDW}}^{-1}$  and an AA titer of  $10.2 \text{ g L}^{-1}$  were achieved. The principal feasibility of product isolation was shown by the purification of 3.4 g AA to a purity of 96.1 %. This study, for the first time, presents the efficient bioconversion of cyclohexane to AA by means of a single strain and thereby sets the basis for an environmentally benign production of AA and related polymers such as nylon 6,6.

Submitted to:  
*Metabolic Engineering*

The Supplementary Material can be found in the Appendix Section 6.



## 2.6.1 Introduction

AA belongs to the 50 most important chemicals by volume, with a demand of 2.6 million tons per year and a yearly growth rate of -3 % (Wittcoff *et al.*, 2012; Bart & Cavallaro, 2015b). Besides its use for the production of polyurethane applied as a foam, lubricant, or food additive, (Musser, 2011; Arpadis, 2020), more than 65 % is used to synthesize the high-volume polymer nylon 6,6 (Bart & Cavallaro, 2015a; Aversch *et al.*, 2018). Thereby, AA constitutes one of the two monomers and the precursor for the second monomer hexamethylenediamine (Bellussi & Perego, 2000). The commercial AA production process starts with the hydrogenation of benzene to cyclohexane, which is first oxidized to KA oil (ketone/alcohol oil) followed by another oxidation step to obtain AA (Bellussi & Perego, 2000; Wittcoff *et al.*, 2012). The latter step essentially relies on nitric acid as an oxidant producing the greenhouse gas nitrous oxide, for which no effectual replacement on the technical scale has been found until now (Wittcoff *et al.*, 2012). Its inefficient and ecologically harmful multi-step character makes the current AA production process, which is in place for over 70 years, incompatible with today's environmental standards (Wittcoff *et al.*, 2012; Bart & Cavallaro, 2015a). It is estimated that 10 % of the anthropogenically released N<sub>2</sub>O, which has 310 times greater global warming potential than CO<sub>2</sub>, originates from AA production (Alini *et al.*, 2007; Aversch *et al.*, 2018). Various chemical methods improving conversion or selectivity and reducing temperature or pressure have been proposed, but, however, do not solve all issues simultaneously (Bart & Cavallaro, 2015a).

Biotechnological approaches allow for high specificities and operation at ambient temperature and pH. Therefore, they entail large potential for greener production processes. Direct fermentative microbial AA synthesis from glucose was demonstrated in proof-of-concept studies albeit with low titers (2.5 g L<sup>-1</sup>) (Polen *et al.*, 2013; Yu *et al.*, 2014; Cheong *et al.*, 2016) or in complex medium (Zhao *et al.*, 2018; Zhou *et al.*, 2020b). Low productivities and yields call for further pathway and membrane transport optimization (Aversch *et al.*, 2018). Multistep biotransformations based on orthologous pathways, i.e., *in vivo* cascades, have the advantage that they run in parallel to growth metabolism using a separate substrate and only indirectly compete for the growth substrate in terms of enzyme synthesis and potentially cofactor supply. Such a strategy has been followed by Niu *et al.* (2020), who re-engineered the native degradation of aromatics in *P. putida* to enable the conversion of the lignin model compound 4-hydroxybenzoic acid to AA at reactor scale with a final titer of 2.5 g L<sup>-1</sup> and glucose as a growth substrate. Wang *et al.* (2020) reported on a mixed-species approach employing three recombinant *E. coli* strains for the biotransformation of cyclohexane to up to 4.5 g L<sup>-1</sup> AA in small-scale assays. Further improvements in product titer on bioreactor scale are necessary to achieve industrial feasibility.

It has been demonstrated that some microorganisms, including Pseudomonads (Tanaka, 1977), *Acinetobacter* (Donoghue & Trudgill, 1975), and *Nocardia globerula* (Norris & Trudgill, 1971) degrade cyclohexanol, thereby producing AA as pathway intermediate. Recently, *Acidovorax* sp. CHX100 capable to grow on cyclohexane as the sole carbon and energy source has been isolated (Salamanca & Engesser, 2014). Enzymes from its cyclohexane degradation pathway have been successfully employed in *P. taiwanensis* VLB120 to synthesize the polycaprolactone monomer 6-hydroxyhexanoic acid (6HA) from cyclohexane with 100 % conversion and yield (Chapter 2.3). In this study, we sought to engineer an AA producer based on this strain (Figure 2.6.1) and evaluate and exploit its potential in a suitable bioreactor setup, thereby closing the cycle from gene to product (Schmid *et al.*, 2001).

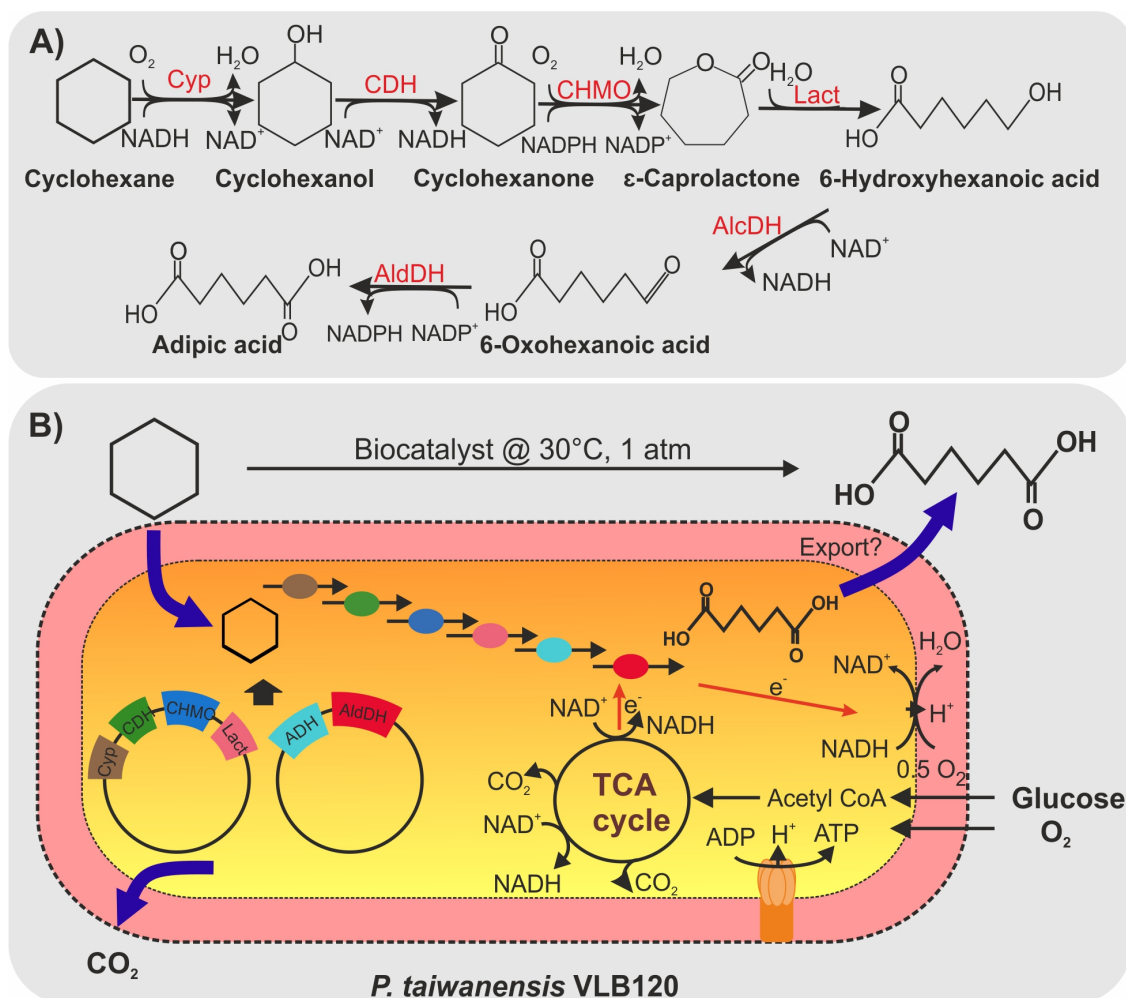


**Figure 2.6.1:** Biocatalytic synthesis of adipic acid (AA). **(A)** Biocatalytic cascade reactions for the synthesis of AA. The cascade is composed of a Cytochrome P450 monooxygenase (Cyp), a cyclohexanol dehydrogenase (CDH), and a cyclohexanone monooxygenase (CHMO), a lactonase (Lact), an alcohol dehydrogenase (ADH), and an aldehyde dehydrogenase (AldDH). **(B)** Biosynthetic genes are expressed from 2 different genetic elements in the host *P. taiwanensis* VLB120 and allow direct AA synthesis from cyclohexane at ambient pressure and temperature. The host's central metabolism provides reduction equivalents for redox reactions via the catabolism and accepts electrons via respiration (red arrows). Export systems for AA are unknown.

## 2.6.2 Materials and Methods

### 2.6.2.1 Chemicals and media

AA was purchased from AppliChem (Darmstadt, Germany). All other chemicals used in this study were obtained from Carl Roth GmbH + Co KG (Karlsruhe, Germany), Merck KGaA (Darmstadt, Germany), and Sigma Aldrich (Steinheim, Germany) in the highest purity available. Cells were grown in lysogeny broth (LB) medium (Sambrook & Russell, 2001), M9<sup>+</sup> medium (Panke *et al.*, 1999), or modified RB medium (Volmer *et al.*, 2019) with a pH of 7.2 supplemented with 0.5 % (w/v) glucose as sole carbon source. For all media, the pH was adjusted with 10 M NaOH before sterilization. Kanamycin (50  $\mu\text{g mL}^{-1}$ ), streptomycin (100  $\mu\text{g mL}^{-1}$ ), and gentamycin (50  $\mu\text{g mL}^{-1}$  for *Pseudomonas*, 10  $\mu\text{g mL}^{-1}$  for *E. coli*) were added when appropriate.

### 2.6.2.2 Strains, plasmids, and molecular biology methods

*E. coli* DH5 $\alpha$  was used for cloning purposes and *P. taiwanensis* VLB120 for biotransformations. *P. taiwanensis* VLB120\_Strep (Lindmeyer, 2016) was used in this study to prevent loss of the megaplasmid pSty encoding for solvent-tolerance genes. Streptomycin was added in LB agar plates and LB pre-cultures, but not in minimal media. Microbial strains and plasmids used in this chapter are listed in Table 2.6.1. Molecular biology methods are explained in detail in chapter 2.1 and for construction of the strains refer to Section 3.7 in the Appendix.

**Table 2.6.1:** Strains and plasmids used in this chapter. If not stated otherwise, the plasmids and strains were constructed in this chapter

Strain/Plasmid	Characteristics	Reference
<b>Strains</b>		
<i>E. coli</i> DH5 $\alpha$	<i>supE44</i> $\Delta$ <i>lacU169</i> ( $\phi$ 80 <i>lacZ</i> $\Delta$ M15) <i>hsdR17 recA1 endA1 gyrA96 thi-1 relA1</i>	Hanahan (1983)
<i>E. coli</i> DH5 $\alpha$ $\lambda$ -pir	$\lambda$ pir lysogen derivate of <i>E. coli</i> DH5 $\alpha$	Martínez-García & de Lorenzo (2011)
<i>P. taiwanensis</i> VLB120_Strep	solvent tolerant, styrene degrading bacterium, isolated from forest soil, Strep <sup>R</sup> on megaplasmid pSty	Lindmeyer (2016)
<i>Acidovorax</i> sp. CHX100	Gram-negative cyclohexane-degrading bacterium isolated from the soil and sludge of the wastewater treatment plant of the University of Stuttgart and a biotrickling filter system	(Salamanca & Engesser, 2014)
<i>P. taiwanensis</i> VLB120_Strep_ <i>lacI</i> <sup>q</sup> _ADH_AldDH	Genome-integrated <i>lac</i> -regulatory system ( <i>lacI</i> <sup>q</sup> , <i>P</i> <sub>trc</sub> ), ADH and AldDH genes from <i>Acidovorax</i> sp. (each with RBS*)	This chapter
<b>Plasmids</b>		
pSEVA244_T	pRO1600 and ColE1 oris, <i>lac</i> -regulatory system ( <i>lacI</i> <sup>q</sup> , <i>P</i> <sub>trc</sub> ), BBa_B0015 terminator, Km <sup>r</sup> , empty plasmid	Chapter 2.1
pSEVA628S	RK2 ori, <i>xyl</i> -regulatory system ( <i>XylS</i> , <i>P</i> <sub>m</sub> ), <i>I-sceI</i> , Gm <sup>R</sup>	Silva-Rocha <i>et al.</i> (2013)
pSEVA6311::DGC-244	pBBR1 ori, Cyclohexanone regulatory system ( <i>ChnR</i> , <i>P</i> <sub>chnB</sub> ), diguanylate cyclase from <i>Caulobacter crescentus</i> , Gm <sup>R</sup>	gift from Daniel Volke
pSEVA638::DGC-244	pBBR1 ori, <i>xyl</i> -regulatory system ( <i>XylS</i> , <i>P</i> <sub>m</sub> ), diguanylate cyclase from <i>Caulobacter crescentus</i> , Gm <sup>R</sup>	gift from Daniel Volke
pUC18R6K-mini-Tn7T-Gm	R6K ori, Amp <sup>R</sup> , Gm <sup>R</sup> , Tn7 transposon, for genome integration	Choi & Schweizer (2006), Addgene plasmid #65022
pTNS2	R6K ori, Amp <sup>R</sup> , transposase gene	Choi & Schweizer (2006), Addgene plasmid #64968

pJ10	pCom10 derivative, pRO1600 and ColE1 oris, <i>alk</i> -regulatory system ( <i>alkS</i> , <i>P<sub>alkB</sub></i> ), Km <sup>R</sup> , <i>alkJ</i> from <i>P. putida</i> from GPo1	Schrewe <i>et al.</i> (2013b)
pSEVA624_T	RK2 ori, <i>lac</i> -regulatory system ( <i>lacI<sup>q</sup></i> , <i>P<sub>trc</sub></i> ), BBa_B0015 terminator, Gm <sup>R</sup> , empty plasmid	This chapter
pSEVA634_T	pBBR1 ori, <i>lac</i> -regulatory system ( <i>lacI<sup>q</sup></i> , <i>P<sub>trc</sub></i> ), BBa_B0015 terminator, Gm <sup>R</sup> , empty plasmid	This chapter
pUC18_mini_Tn7_Gm_LacIq-adh-aldDH	R6K ori, Amp <sup>R</sup> , Gm <sup>R</sup> , Tn7 transposon containing ADH and AldDH encoding genes under the control of <i>P<sub>trc</sub></i> and <i>lacI<sup>q</sup></i> for genome integration	This chapter
pSEVA_6HA_2	pRO1600 and ColE1 oris, <i>lac</i> -regulatory system ( <i>lacI<sup>q</sup></i> , <i>P<sub>trc</sub></i> ), BBa_B0015 terminator, Km <sup>R</sup> , <i>Acidovorax</i> genes encoding Cyp, CDH, CHMO, and Lact (each with RBS*)	Chapter 2.3
pSEVA244_T_ADH	pRO1600 and ColE1 oris, <i>lac</i> -regulatory system ( <i>lacI<sup>q</sup></i> , <i>P<sub>trc</sub></i> ), BBa_B0015 terminator, Km <sup>R</sup> , ADH gene from <i>Acidovorax</i> (with RBS*)	This chapter
pSEVA244_T_AldDH	pRO1600 and ColE1 oris, <i>lac</i> -regulatory system ( <i>lacI<sup>q</sup></i> , <i>P<sub>trc</sub></i> ), BBa_B0015 terminator, Km <sup>R</sup> , AldDH gene from <i>Acidovorax</i> (with RBS*)	This chapter
pSEVA244_T_alkJ	pRO1600 and ColE1 oris, <i>lac</i> -regulatory system ( <i>lacI<sup>q</sup></i> , <i>P<sub>trc</sub></i> ), BBa_B0015 terminator, Km <sup>R</sup> , <i>alkJ</i> from <i>P. putida</i> GPo1 (with RBS*)	This chapter
pSEVA244_T_ADH_AldDH	pRO1600 and ColE1 oris, <i>lac</i> -regulatory system ( <i>lacI<sup>q</sup></i> , <i>P<sub>trc</sub></i> ), BBa_B0015 terminator, Km <sup>R</sup> , ADH and AldDH genes from <i>Acidovorax</i> (with RBS*)	This chapter
pSEVA244_T_alkJ_AldDH	pRO1600 and ColE1 oris, <i>lac</i> -regulatory system ( <i>lacI<sup>q</sup></i> , <i>P<sub>trc</sub></i> ), BBa_B0015 terminator, Km <sup>R</sup> , <i>alkJ</i> ( <i>P. putida</i> GPo1) and AldDH gene from <i>Acidovorax</i> (each with RBS*)	This chapter
pBL_AA_Ac	pBBR1 ori, <i>lac</i> -regulatory system ( <i>lacI<sup>q</sup></i> , <i>P<sub>trc</sub></i> ), BBa_B0015 terminator, Gm <sup>R</sup> , ADH and AldDH genes from <i>Acidovorax</i> (with RBS*)	This chapter
pBL_AA_alkJ	pBBR1 ori, <i>lac</i> -regulatory system ( <i>lacI<sup>q</sup></i> , <i>P<sub>trc</sub></i> ), BBa_B0015 terminator, Gm <sup>R</sup> , <i>alkJ</i> ( <i>P. putida</i> GPo1) and AldDH gene from <i>Acidovorax</i> (each with RBS*)	This chapter
pRKL_AA_Ac	RK2 ori, <i>lac</i> -regulatory system ( <i>lacI<sup>q</sup></i> , <i>P<sub>trc</sub></i> ), BBa_B0015 terminator, Gm <sup>R</sup> , ADH and AldDH genes from <i>Acidovorax</i> (with RBS*)	This chapter
pRKL_AA_alkJ	RK2 ori, <i>lac</i> -regulatory system ( <i>lacI<sup>q</sup></i> , <i>P<sub>trc</sub></i> ), BBa_B0015 terminator, Gm <sup>R</sup> , <i>alkJ</i> ( <i>P. putida</i> GPo1) and AldDH gene from <i>Acidovorax</i> (each with RBS*)	This chapter

---

pBX_AA_Ac	pBBR1 ori, <i>xyI</i> -regulatory system ( <i>xyIS</i> , <i>Pm</i> ), Gm <sup>R</sup> , This chapter ADH and AldDH genes from <i>Acidovorax</i> (each with RBS*)
-----------	--

---

### 2.6.2.3 Growth of bacterial cultures

Cultivations were carried out at 30 °C and 200 rpm in baffled Erlenmeyer shaking flasks with a liquid volume of maximally 20 % of the total volume in a Multitron shaker (Infors, Bottmingen, Switzerland). Microorganisms were cultivated in an LB pre-culture for -20 h, from which an M9\*- or RB-pre-culture was inoculated (1 % v/v) and incubated for another 12-16 h. This pre-culture was used to inoculate an M9\*- or RB main culture at a starting OD<sub>450</sub> of 0.2. Heterologous gene expression was induced with 1 mM isopropyl- $\beta$ -d-1-thiogalactopyranoside (IPTG) and/or 3-methylbenzoate (3MB) when the cultures reached an OD<sub>450</sub> of -0.5. After incubation for another 4 h, cells were harvested for biotransformation experiments or CO difference spectra analyses.

### 2.6.2.4 Biotransformation experiments

After cultivation as described above, *P. taiwanensis* cells were harvested by centrifugation (10 min, 5,000 g, room temperature) and resuspended in 100 mM potassium phosphate buffer (pH 7.4) supplemented with 1 % (w/v) glucose (Kpi buffer) to a cell concentration of 0.5 g<sub>CDW</sub> L<sup>-1</sup> if not stated otherwise. Optionally, IPTG and 3MB were added to the Kpi buffer (Kpi+I buffer). Biotransformations with growing cells were performed after resuspension in fresh M9\* or RB medium supplemented with 1 % (w/v) glucose, 1 mM IPTG, and 1 mM 3MB, and growth was monitored. Biotransformations were conducted in 100 mL screw-capped baffled Erlenmeyer flasks in a rotary incubator (30 °C, 200 rpm). Cell suspensions were adapted for 10 min before biotransformations were initiated by adding pure cyclohexane to a concentration of 10 mM referred to in the aqueous phase volume. The flask threads were wrapped with PTFE tape to reduce substrate loss to the environment, and the lid contained a two-layered septum with Teflon facing the inner side of the flask and silicone facing outwards. Samples (1.5 mL) were taken with a syringe at different time points. One mL sample was extracted with 0.5 mL ice-cold diethyl ether containing 0.2 mM n-decane as an internal standard. After 2 min extraction by vortexing and centrifugation, the organic phase was dried over water-free Na<sub>2</sub>SO<sub>4</sub> and then transferred to a GC vial for analysis. The rest of the samples was used for OD<sub>450</sub> measurement, and, after centrifugation (4 °C, 10 min, 17,000 g), the supernatant was stored for HPLC analysis. Gas-phase samples (100  $\mu$ L) were taken from the flask using a gas-tight syringe (Hamilton, Reno, NV).

### 2.6.2.5 Bioreactor experiments

Bioreactor experiments were conducted in 3.6 L stirred-tank Labfors 5 bioreactors and controlled via Iris software (Infors AG, Bottmingen, Switzerland). An LB pre-culture was cultivated for 20 h, from which an over-night RB-pre-culture was inoculated. This pre-culture was used to inoculate the bioreactor containing 1 L RB-medium (10 g L<sup>-1</sup> glucose, pH 7.2, 1 vvm, 30 °C, 1000 rpm stirrer speed) to an OD<sub>450</sub> of 0.35. The pH was adjusted with 12.5% ammonia and 30% phosphoric acid. Batch cultivation was carried out until carbon source depletion at a cell concentration of -4 g<sub>CDW</sub> L<sup>-1</sup>, when an exponential feed of a solution containing 730 g L<sup>-1</sup> glucose and 19.6 g L<sup>-1</sup> MgSO<sub>4</sub>·7 H<sub>2</sub>O was

applied at a rate to maintain a specific growth rate  $\mu$  of 0.15 or 0.3 h<sup>-1</sup>, and 1 mL US\* trace elements were added. When a biomass concentration of 16 or 20 g L<sup>-1</sup> was reached, the cells were harvested by centrifugation (3,124 g, RT, 30 min). Induction was performed 2 or 4 h before the harvest by adding IPTG and 3MB to a concentration of 1 mM. The cells were resuspended in 1 L Kpi+I buffer to a final concentration of 10 g<sub>CDW</sub> L<sup>-1</sup>. The pH was set to 7.4 and adjusted with 10 M NaOH and 30% phosphoric acid. The stirrer speed was increased to 1,500 rpm, and cells were equilibrated for 10 min. A cyclohexane-saturated air flow (0.25 or 0.3 L min<sup>-1</sup>) was mixed with a cyclohexane-free air flow (1 L min<sup>-1</sup>) in a mixing bottle and fed into the reactor. A 5 mL sample was taken at each sampling point, of which 2 x 1 mL was extracted for GC analysis as described above. Further analyses included OD<sub>450</sub> measurement, CO difference spectra, small-scale resting cell activity assays, and HPLC analysis of culture supernatant. Small scale resting cell activity assays were conducted in Pyrex tubes containing 1 mL Kpi buffer with cells resuspended to a concentration of 0.5 g<sub>CDW</sub> L<sup>-1</sup>. After 10 min equilibration (30 °C, 250 rpm), 1.25  $\mu$ L of pure cyclohexane were added. After 15 min, the reaction was stopped by adding 0.5 mL diethyl ether, and the sample was extracted for GC analysis or supernatant taken for HPLC analysis, respectively.

### 2.6.2.6 Purification of AA

The reactor broth was centrifuged for 30 min (RT, 2,114 g), and 500 mL of the supernatant were decolorized with 5 g activated charcoal (Merck KGaA) and incubated in a rotary shaker for 40 min (30 °C, 250 rpm). After centrifugation (30 min, 7,000 g), the supernatant was filtered (Labsolute filter paper, pore size 12-15  $\mu$ m, Th. Geyer, Renningen, Germany) and centrifuged again for 10 min at 20,000 g. The resulting supernatant was then filtered through a sterile filter (Labsolute, PES-membrane, pore size 0.2  $\mu$ m, Th. Geyer). Water was evaporated in a rotary evaporator (Heidolph, Schwabach, Germany) by slowly decreasing the pressure to ca. 100 mbar (120 rpm, 65 °C) until 75 % of the initial 500 mL liquid volume were left. The remaining liquid was acidified to pH 1.5 with 37% HCl (Figure 2.6.7A) and incubated at 4 °C for 20 h. After centrifugation (5 min, 9,000 g, RT) (Figure 2.6.7B), the supernatant was removed, and the white pellet was dried for 4 days at 60 °C (Figure 2.6.7C,D). The dried powder was dissolved in 30 mL ddH<sub>2</sub>O (60 °C, 2 h) (Figure 2.6.7E) and centrifuged for 2 min (12,000 g, RT). The resulting lower dark brown pellet was discarded, and the top layer of precipitates was harvested (Figure 2.6.7F). The remaining liquid was incubated for 30 min at 60°C and then in the fridge overnight. Emerging precipitates were dried together with the already harvested one for 3 days at 60 °C (Figure 2.6.7G).

### 2.6.2.7 Analytical methods

Suspended biomass concentrations were determined by measuring the optical density at a wavelength of 450 nm using a Libra S11 spectrophotometer (Biochrom, Cambridge, UK). One OD<sub>450</sub> unit corresponds to 0.186 g<sub>CDW</sub> L<sup>-1</sup> for *P. taiwanensis* (Halan *et al.*, 2010). Active Cyp was quantified in whole cells via CO (carbon monoxide) difference spectra obtained as described before (chapter 2.1). Concentrations of cyclohexane, cyclohexanol, cyclohexanone, and  $\epsilon$ -CL were determined via gas chromatography and 6HA and AA via HPLC as described before (Chapter 2.2). 6HA and AA were identified by HPLC-MS/MS as described in chapter 2.5. Glucose and gluconic acid were quantified by HPLC and O<sub>2</sub> via GC (Chapter 2.4).

## 2.6.3 Results

### 2.6.3.1 Finding a suitable expression system for enzymes converting 6HA to AA

A direct biocatalytic cascade / orthologous pathway from cyclohexane to AA comprises six enzymatic steps (Figure 2.6.1A). In chapter 2.3, a four-step cascade with 6HA as the exclusive product was established in *P. taiwanensis* VLB120 by introducing six genes from *Acidovorax* sp. CHX100 encoding Cyp, CDH, CHMO, and Lact in one operon under the control of the  $\text{LacI}^{\text{Q}}\text{-P}_{\text{trc}}$  regulatory system genes (designated as the upper pathway in the following). Replication of the respective plasmid pSEVA\_6HA\_2 relies on the pRO1600 origin. In the genome sequence of the same bacterium, we identified genes encoding putative alcohol (ADH) and aldehyde dehydrogenases (AldDH, for gene sequences, refer to Appendix, sections 3.7 and 3.7) in close vicinity to the genes encoding CDH, CHMO, and Lact (Figure S2.6.3)(Meyer *et al.*, 2003). ADH and AldDH were isolated after expression in *P. taiwanensis* from pSEVA244\_T\_ADH and pSEVA244\_T\_AldDH, respectively (Appendix, section 3.7). Spectrophotometric assays involving the detection of NAD(P)H formation via absorption increase at 340 nm revealed that ADH accepts 6HA as substrate with  $\text{NAD}^+$  as the preferred cofactor (no significant absorption increase with  $\text{NADP}^+$ ), leading to a fast establishment of the equilibrium between alcohol and aldehyde, as expected for this thermodynamic equilibrium lying on the side of the alcohol (Figure S2.6.1). AldDH activity was also investigated with 6HA as substrate, applying both ADH and AldDH and following a stepwise enzyme and cofactor addition approach (Figure S2.6.2). After equilibrium establishment in the presence of ADH and  $\text{NAD}^+$ , no NADH formation was observed when AldDH is added, indicating that AldDH does not accept  $\text{NAD}^+$  as an electron acceptor. However, a substantial absorption increase was observed after  $\text{NADP}^+$  addition. This absorption increase can be attributed to consecutive alcohol and aldehyde oxidation catalyzed by ADH and AldDH, respectively, giving rise to NADH and NADPH formation (Figure S2.6.2A). These results indicate that the identified ADH and AldDH efficiently catalyzed the oxidation of 6HA to AA. The apparent  $\text{NAD}^+$  and  $\text{NADP}^+$  preferences of ADH and AldDH, respectively, were confirmed by a second experiment starting with the incubation of ADH and 6HA together with  $\text{NADP}^+$ . A substantial absorption increase did not occur, also not after AldDH addition, but did occur after  $\text{NAD}^+$  addition (Figure S2.6.2B).

As an alternative alcohol dehydrogenase, we also tested the membrane-bound AlkJ from *Pseudomonas putida* GPo1 because of its ability to perform irreversible alcohol oxidation (Kirmair & Skerra, 2014; Schrewe *et al.*, 2014). We set out to create a separate operon for the ADH and AldDH genes (lower pathway) to balance their expression and activity to those of the upper pathway. To ensure compatibility with the pRO1600 replication origin present on pSEVA\_6HA\_2 (Chapter 2.3), we selected the low copy number origin RK2 and the medium copy number origin pBBR1 for respective constructs (Cook *et al.*, 2018; Aparicio *et al.*, 2019). Thereby, we employed the same  $\text{lacI}^{\text{Q}}\text{-P}_{\text{trc}}$  regulatory system as also present on pSEVA\_6HA\_2. In this first approach to establish a system for the efficient conversion of 6HA to AA *in vivo*, we thus tested 4 different constructs (Figure 2.6.2A) in *P. taiwanensis* VLB120.

In resting cell-based biotransformations, AlkJ containing strains (featuring pBL\_AA\_alkJ or pRKL\_AA\_alkJ) showed very low whole-cell activities ( $< 3 \text{ U g}_{\text{CDW}}^{-1}$ , Figure 2.6.2B), not matching the high activity of the established pathway from cyclohexane to 6HA ( $45 \text{ U g}_{\text{CDW}}^{-1}$ ). Constructs harboring the *Acidovorax* ADH instead of AlkJ (pBL\_AA\_Ac and pRKL\_AA\_Ac) enabled clearly higher activi-

ties ( $26.8 \pm 1.1$  and  $23.6 \pm 0.4$  U  $g_{CDW}^{-1}$ , respectively) and also exclusive AA formation. Genome integration of the operon containing the two *Acidovorax* dehydrogenase genes (GE\_AA\_Ac) led to a 4-fold lower activity ( $8.6 \pm 0.1$  U  $g_{CDW}^{-1}$ ), which most probably is gene copy number related. However, although good activities were obtained, they were still lower than the  $45$  U  $g_{CDW}^{-1}$  required to keep up with the established 6HA formation pathway. Thus, the *xylS*-*Pm* regulatory system from *P. putida* mt-2 was tested as an alternative for the expression of the *Acidovorax* dehydrogenase genes. The respective construct pBX\_AA\_Ac indeed enabled a clearly higher and presumably sufficient activity of  $72.9 \pm 6.0$  U  $g_{CDW}^{-1}$  (Figure 2.6.2). The three best-performing vectors, pBL\_AA\_Ac, pRKL\_AA\_Ac, and pBX\_AA\_Ac, were considered feasible candidates to be evaluated together with pSEVA\_6HA\_2 for the conversion of cyclohexane to AA.

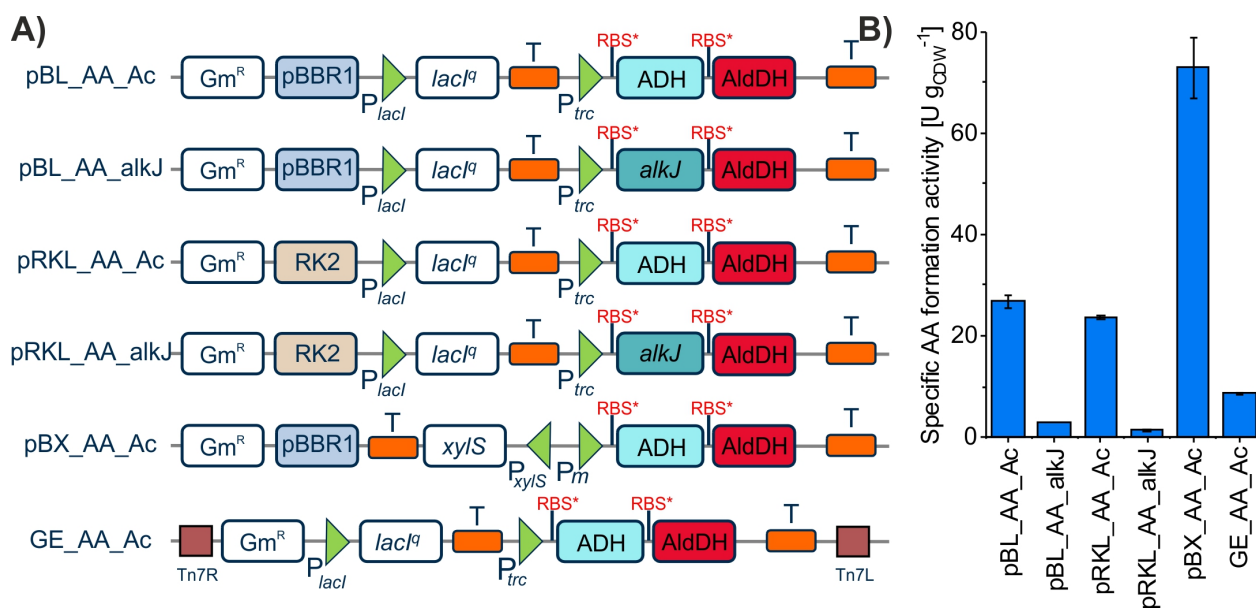


**Figure 2.6.2:** Construction and characterization of *P. taiwanensis* VLB120 strains expressing the lower cascade genes. **(A)** Graphical representation of expression constructs applied to test the conversion of 6HA to AA. Component lengths are not drawn to scale. Gm<sup>R</sup>: gentamycin resistance gene; pBBR1: pBBR1 origin of replication; RK2: RK2 origin of replication; GE: genome integration; ADH: gene no. 1088 from *Acidovorax* sp. CHX100 encoding a putative alcohol dehydrogenase; alkJ: alcohol dehydrogenase gene from *P. putida* GPo1; AldDH: gene no. 1089 from *Acidovorax* sp. CHX100 encoding a putative aldehyde dehydrogenase; P<sub>trc</sub>: P<sub>trc</sub> promoter; T: T0 terminator; *lacI*<sup>q</sup>: gene encoding *lac* repressor; P<sub>lacI</sub>: promoter of *lac* repressor gene; *xylS*: activator of *xyl* regulation system; P<sub>xylS</sub>: promoter of *xylS*; P<sub>m</sub>: promoter of the *xyl* operon encoding the *meta*-cleavage pathway from *P. putida* mt-2. **(B)** Specific activities obtained in resting cell experiments for the conversion of 6HA to AA by 6 *P. taiwanensis* VLB120 strains containing the constructs given in panel A. Reactions were started by adding 10 mM 6HA to a 0.5  $g_{CDW} L^{-1}$  cell suspension in glucose-containing KPi buffer and stopped after 1 h (see materials and methods section for experimental details). Graphs represent average values and standard deviations of two independent biological replicates. The average experimental errors over all measurements for the specific activity is 5.8 %.

### 2.6.3.2 Conversion of cyclohexane to AA by recombinant *P. taiwanensis* VLB120

In order to establish and evaluate a pathway from cyclohexane to AA, *P. taiwanensis* VLB120 (pSEVA\_6HA\_2) harboring the pathway from cyclohexane to 6HA was transformed with the plasmids pBL\_AA\_Ac, pRKL\_AA\_Ac, or pBX\_AA\_Ac. First, to assess a possible metabolic burden caused by the second plasmid encoding for two additional pathway enzymes, the growth of strains featuring different plasmid configurations after induction was compared (Figure 2.6.3A).



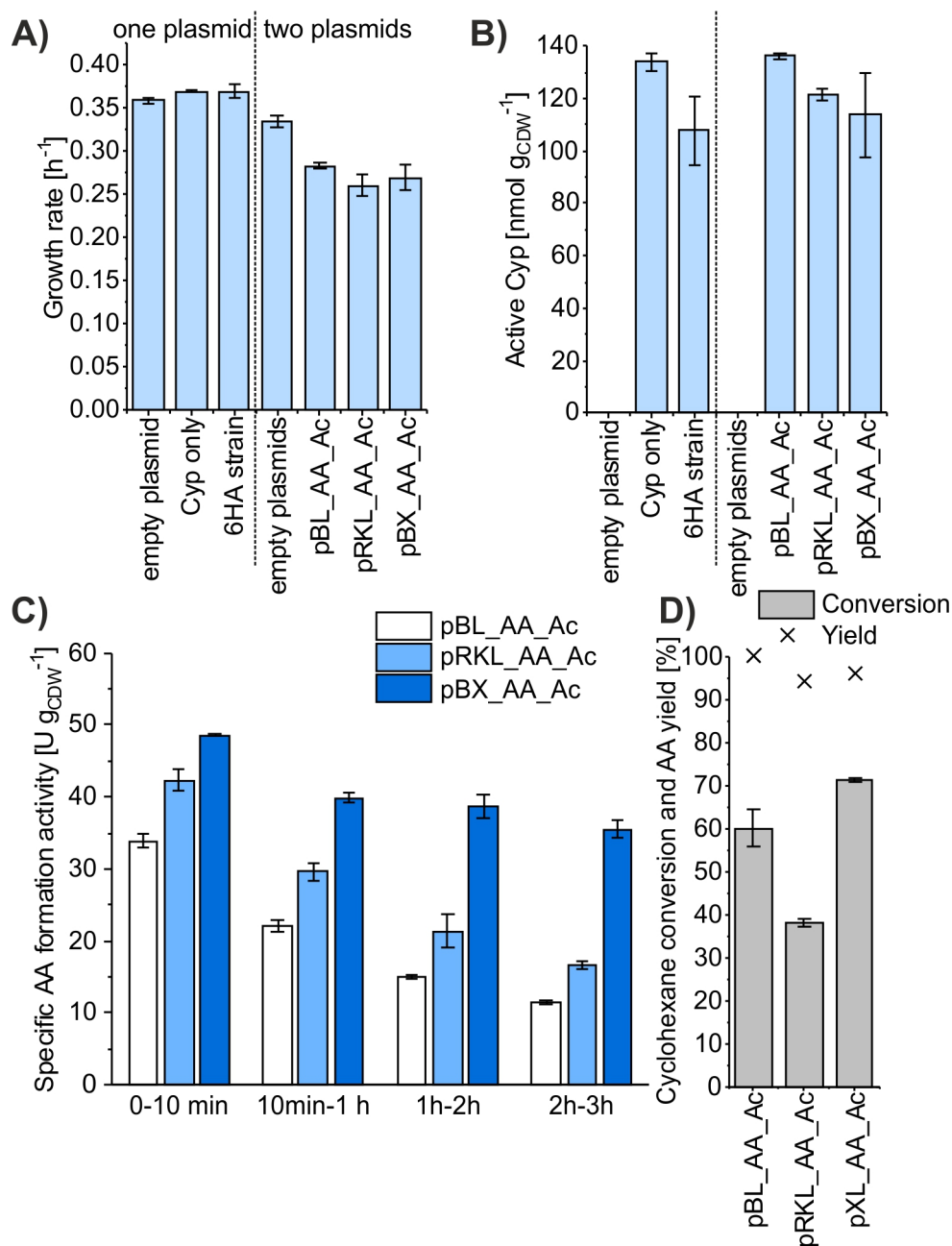


**Figure 2.6.3:** Comparison of AA producing *P. taiwanensis* VLB120 variants. **(A)** Growth rate of *P. taiwanensis* VLB120 harboring pSEVA244\_T (empty plasmid), pSEVA\_Cyp (Cyp only), pSEVA\_6HA\_2 (6HA strain), pSEVA244\_T + pSEVA634\_T (empty plasmids), pSEVA\_6HA\_2 + different plasmids as indicated in Figure 2.6.2A in M9\* medium at 30 °C after induction. **(B)** Active Cyp amounts determined via CO difference spectra after 4 h of induction of aforementioned strains. **(C)** Specific AA formation activities from cyclohexane for 3 different *P. taiwanensis* VLB120 strains within 4 different time intervals. Cells were cultivated in M9\* medium with 0.5 % (w/v) glucose, induced by IPTG (and 3MB for pBX\_AA\_Ac) for 4 h, harvested, and resuspended in KPi buffer supplemented with 1 % (w/v) glucose to a biomass concentration of 0.5 g<sub>CDW</sub> L<sup>-1</sup> in 10 mL liquid volume. Reactions were started by adding 10 μL pure cyclohexane (corresponds to 10 mM referring to the aqueous phase volume) and stopped after 10 min, 1 h, 2 h, or 3 h. **(D)** Cyclohexane conversion and AA yield on converted cyclohexane after 16 h for the experiment presented in panel C. Graphs present average values and standard deviations of two independent biological replicates. The average experimental errors over all measurements for the growth rates, Cyp amounts, specific activities, conversions, and yields are 2.7, 6.2, 3.6, 3.5, and 0.1 %, respectively.

The growth rate of *P. taiwanensis* was reduced by 10 % to  $0.33 \pm 0.1 \text{ h}^{-1}$  with an additional plasmid

(empty plasmids) compared to pSEVA244\_T as the only plasmid (empty plasmid). The expression of the two additional dehydrogenase genes further reduced the growth rate by 15-20 %. Growth rates did not differ significantly for the different expression plasmids tested for dehydrogenase production. The observed exponential growth indicates that *P. taiwanensis* can cope with the additional metabolic burden imposed by the presence of a second plasmid and the expression of the dehydrogenase genes.

The first reaction step catalyzed by Cyp was observed to be the rate-limiting step in 6HA synthesis (Chapter 2.1). Thus, the amount of active Cyp was assessed via CO difference spectra to evaluate, if and to what extent the dehydrogenase containing plasmids and respective expression compromise Cyp expression levels. Interestingly, *P. taiwanensis* (pSEVA\_6HA\_2, pBL\_AA\_Ac) exhibited a very high Cyp amount comparable to that obtained with a construct only harboring Cyp and 25 % higher than that obtained with pSEVA\_6HA\_2 only (6HA strain, Figure 2.6.3B). The introduction of pRKL\_AA\_Ac or pBX\_AA\_Ac led to slightly lower Cyp levels, which, however, were still higher than that obtained with pSEVA\_6HA\_2 only. Consequently, the second plasmid and ADH and AldDH synthesis did not lead to lower levels of Cyp, the rate-limiting first enzyme of the cascade.

All three tested strains converted cyclohexane to AA without significant accumulation of pathway intermediates such as cyclohexanol (C-ol), cyclohexanone (C-one), and  $\epsilon$ -CL. Only very low 6HA concentrations below 0.3 mM were detected indicating a balance between lower and upper pathway enzymes (Figure S2.6.4A). The lowest initial activity of  $33.9 \pm 1.0 \text{ U g}_{\text{CDW}}^{-1}$  was observed when ADH and AldDH genes were expressed from pBL\_AA\_Ac (Figure 2.6.3C), although the highest Cyp amount was detected in this strain (Figure 2.6.2B). *P. taiwanensis* VLB120 (pSEVA\_6HA\_2, pRKL\_AA\_Ac) showed an initial whole-cell activity ( $42.3 \pm 1.4 \text{ U g}_{\text{CDW}}^{-1}$ ) comparable to that of *P. taiwanensis* VLB120 (pSEVA\_6HA\_2) for 6HA synthesis from cyclohexane (Chapter 2.3). However, the strain harboring pBX\_AA\_Ac exhibited an even higher initial activity ( $48.6 \pm 0.2 \text{ U g}_{\text{CDW}}^{-1}$ ). Within 3 h, the specific activity dropped by 60-65 % except for the pBX\_AA\_Ac containing strain showing a drop by only 25 % (Figure 2.6.3C) possibly caused by substrate limitation ( $\sim 50 \mu\text{M}$  cyclohexane in aqueous phase). After 16 h, this strain also showed the highest cyclohexane conversion ranging between 38 and 71 % for the three strains (Figure 2.6.3D). As expected from the lacking accumulation of intermediates, AA yields on converted cyclohexane generally were high between 94 and 100 % (Figure 2.6.3D). Due to its relatively stable activity and the high conversion obtained, *P. taiwanensis* VLB120 (pSEVA\_6HA\_2, pBX\_AA\_Ac) was selected as the best whole-cell catalyst for further characterization.

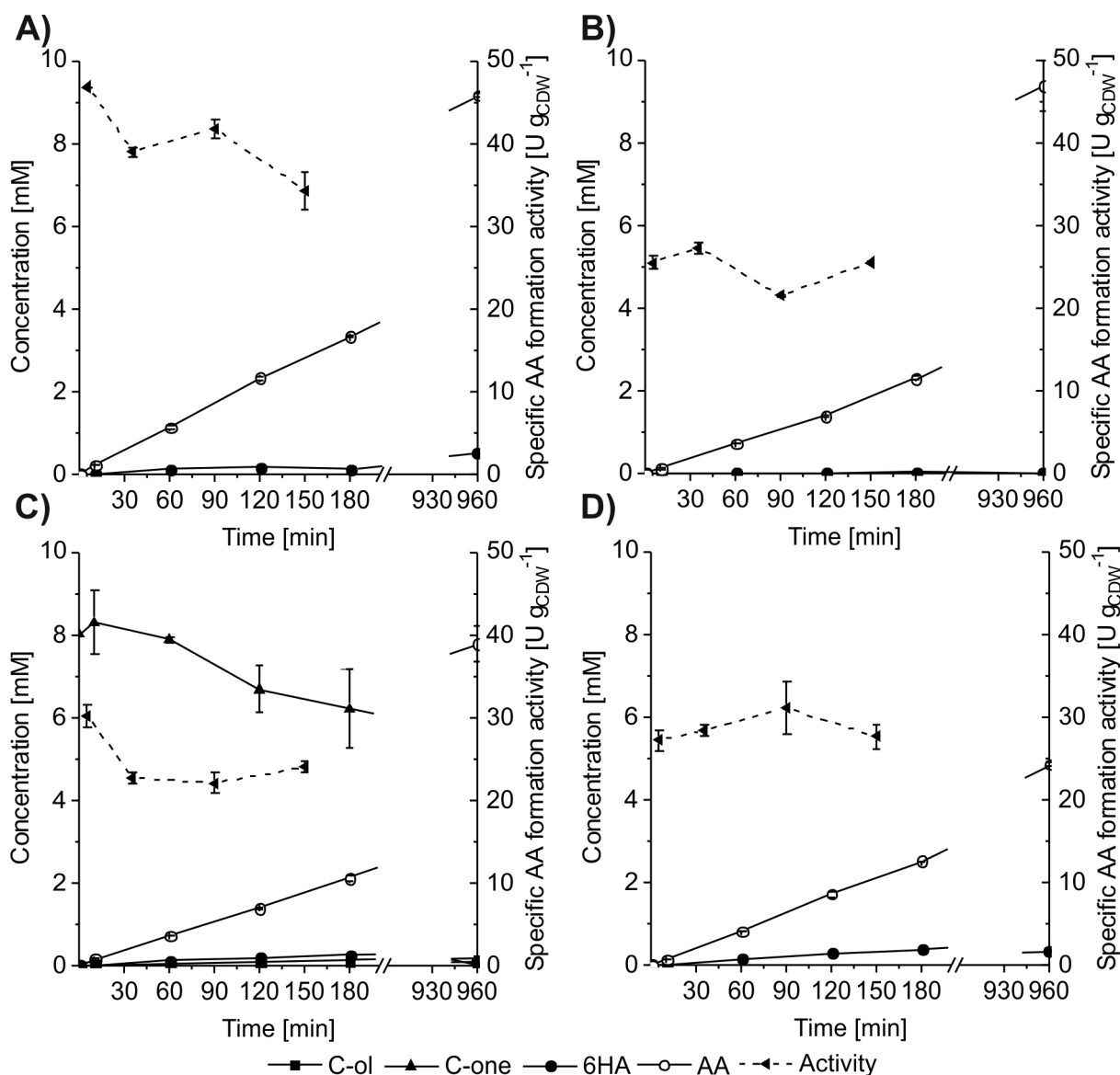


**Figure 2.6.4:** Dependency of cyclohexane conversion by *P. taiwanensis* VLB120 (pSEVA\_6HA\_2, pBX\_AA\_Ac) on reaction conditions. Time courses of cyclohexanol (C-ol), cyclohexanone (C-one), 6HA, and AA concentrations, as well as specific AA formation rates, are given. Cells were cultivated in M9\* medium with 0.5 % (w/v) glucose, induced by IPTG and 3MB for 4 h, harvested, and resuspended to a biomass concentration of  $0.5 \text{ g}_{\text{CDW}} \text{ L}^{-1}$  in (A) KPi buffer supplemented with 1 % (w/v) glucose, 1 mM IPTG, and 1 mM 3MB, (B) M9\* medium supplemented with 1 % (w/v) glucose, 1 mM IPTG, and 1 mM 3MB, or (C, D) KPi buffer in 10 mL liquid volume. Reactions were started by adding 10  $\mu\text{L}$  pure cyclohexane (A, B, D) (10 mM with respect to the aqueous phase volume) or 8 mM C-one (C) and stopped after 10 min, 1 h, 2 h, 3 h, or 16 h. Graphs represent average values and standard deviations of two independent biological replicates. The average experimental errors over all measurements for C-ol, C-one, 6HA, and AA concentrations, amounted to 38.6, 8.4, 27.6, 2.4 %, respectively, and 3.9 % for the specific activities.

### 2.6.3.3 Characterization of the AA producing strain

In order to characterize the activities of the individual reaction steps, resting-cell biotransformations were performed with the different pathway intermediates as substrates being aware of a possible uptake bias for 6HA, but not of the uncharged intermediates C-ol, C-one, and  $\epsilon\text{-CL}$  (Nikaido (1994), Table 2.6.2).

**Table 2.6.2:** Specific activities of *P. taiwanensis* VLB120 (pSEVA\_6HA\_2, pBX\_AA\_Ac) for the conversion of cyclohexane and the different cascade intermediates.

Substrate	Initial AA formation activity [U g <sub>CDW</sub> <sup>-1</sup> ]	Initial overall activity <sup>a</sup> [U g <sub>CDW</sub> <sup>-1</sup> ]	Product shares [%]		
			C-one	6HA	AA
Cyclohexane <sup>b</sup>	48.6 ± 0.2	48.6 ± 0.2	0	0	100
Cyclohexanol <sup>c</sup>	48.0 ± 2.3	72.6 ± 4.2	0.7 ± 0.0	33.3 ± 0.7	66.1 ± 0.7
Cyclohexanone <sup>d</sup>	58.5 ± 1.7	81.4 ± 1.6	n.a.	28.1 ± 0.1	71.9 ± 0.1
$\epsilon$ -Caprolactone <sup>d</sup>	40.9 ± 0.1	1,950 ± 120	n.a.	97.9 ± 0.0	2.1 ± 0.1
6HA <sup>e</sup>	39.6 ± 2.0	39.6 ± 2.0	n.a.	n.a.	100

Bioconversions with 0.25 g<sub>CDW</sub> L<sup>-1</sup> in KPi buffer supplemented with 1 % (w/v) glucose for 10 min. Average values, including standard deviations of two independent biological replicates, are given. The average error over all activity measurements is 2.7 %.

<sup>a</sup> The overall activity refers to the sum of all accumulated products.

<sup>b</sup> Addition of 10  $\mu$ L cyclohexane (10 mM referring to the aqueous phase volume); activity corresponds to the first 10 min in the experiments shown in Figure 2.6.3A.

<sup>c</sup> Maximal activity with a cyclohexanol concentration of 0.2 mM (obtained by testing different substrate concentrations)

<sup>d</sup> Addition of 5 mM substrate

<sup>e</sup> Addition of 10 mM substrate

As stated above, no intermediate products were detected with cyclohexane as substrate identifying Cyp catalyzed cyclohexane hydroxylation as the rate-limiting step. C-ol has been shown to inhibit CHMO (Chapter 2.3) so that the maximal overall activity of 73 U g<sub>CDW</sub><sup>-1</sup>, referring to the sum of all products accumulated, was observed with a low C-ol concentration of 0.2 mM. AA accounted for 66 % of total product accumulation with C-one and 6HA as the co-accumulating products indicating that CHMO and the lower pathway were limiting in this case. C-one as substrate gave rise to AA as well as 6HA as products indicating a limitation by the lower pathway. However, the 20 % elevated AA formation rate shows that the lower pathway enables somewhat faster conversion than the upper pathway, i.e., Cyp. The large discrepancy between overall and AA formation activity with  $\epsilon$ -CL as substrate relies on the high lactonase activity, whereas the rather low AA formation activity points to 6HA membrane mass transfer issues as its extrusion may hamper reuptake and conversion. A limiting 6HA uptake became apparent when 6HA was applied as substrate, leading to a 20 % lower AA formation activity as compared to the 6-step conversion of cyclohexane to AA. Therefore, enzymatic steps in this catalyst can be considered well balanced for the conversion of cyclohexane to AA, which emphasizes the streamlined nature of the pathway with minimal cellular resource dissipation for unnecessary enzyme overproduction.

In resting cell bioconversions, a decrease in whole-cell activities over time has been observed (Figure 2.6.3C). To test whether protein degradation is a critical factor, which may be overcome by continuous induction, we investigated the activity course with resting (Figure 2.6.4A) and growing cells (Figure 2.6.4B) in the presence of inducer. Resting cells revealed a similar pattern of initial activity (46.8 ± 0.1 U g<sub>CDW</sub><sup>-1</sup>) and activity loss within 3 h compared to resting cells in the absence of inducer (Figure 2.6.3C). However, after 16 h of incubation with inducers, essentially complete

conversion of supplied cyclohexane to AA was obtained (Figure 2.6.4A), which is in contrast to the bioconversion in absence of inducers (Figure 2.6.3D). Growing cells showed a 55 % lower initial activity ( $25.5 \pm 0.8 \text{ U g}_{\text{CDW}}^{-1}$ ), which remained stable and allowed close to complete conversion after 16 h (Figure 2.6.4B). Consequently, continuous induction indeed had a positive effect on biocatalyst stability and can be considered favorable in long-term bioconversion with resting as well as growing cells.

#### 2.6.3.4 The AA cascade is self-sustainable

In resting cell-based bioconversions, glucose was added to support redox metabolism, possibly crucial for redox cofactor, i.e., NAD(P/H), regeneration/balancing. However, assuming negligible uncoupling for the oxygenases, the AA cascade is NADPH neutral and produces one NADH with cyclohexane or cyclohexanone as substrate (Figure 2.6.1A). The NADH formed, may be recycled to  $\text{NAD}^+$  via respiration and thereby even support maintenance metabolism. Such cascades may thus be self-sustainable in terms of redox demands and, to some extent, even regarding catalyst maintenance.

To investigate this, we first tested if AA formation from cyclohexanone without the addition of glucose, which resulted in a 2-fold lower initial activity of  $30.2 \pm 1.3 \text{ U g}_{\text{CDW}}^{-1}$  (Figure 2.6.4C) compared to the presence of glucose (Table 2.6.2). This activity, however, was well maintained and enabled the complete conversion of 8 mM cyclohexanone to AA within 16 h with only minor amounts of 6HA remaining in the mixture as it was observed with glucose present (Figure 2.6.4). Cyclohexane conversion without glucose resulted in a stable specific AA formation activity level at  $\sim 29 \text{ U g}_{\text{CDW}}^{-1}$  over 3 h. However, after overnight incubation, a low final conversion of 52 % with 93.4 % AA yield was reached (Figure 2.6.4D). The low level of accumulated intermediates concomitantly with the complete conversion obtained for cyclohexanone conversion indicate that the first reaction step catalyzed by Cyp remained rate-limiting, pointing to Cyp instability as a limiting factor. Thus, AA synthesis from cyclohexane and cyclohexanone is self-sustainable, at least to some extent. Biocatalyst stability, however, appears to depend on cellular maintenance. Respective investigation and engineering may indeed enable redox-self-sustainable *in vivo* cascade operation.

#### 2.6.3.5 Glucose excess allows 10-gram scale production of AA in 8 hours

To exploit the catalytic performance of *P.taiwanensis* VLB120 (pSEVA\_6HA\_2, pBX\_AA\_Ac) under process conditions including high cell densities, stirred-tank bioreactor experiments were conducted. For this purpose, cells were grown in a 1 L scale in the high-cell density RB medium (Riesenberg *et al.*, 1991), first in batch and then in fed-batch mode, followed by resting cell-based bioconversions in the same stirred tank reactors at the same scale.

In a first experiment, the feed rate during fed-batch cultivation was controlled to enable glucose-limited exponential growth at a growth rate of  $0.15 \text{ h}^{-1}$  (Figure S2.6.5). After induction, cells remained glucose-limited until they were harvested. Then, a resting cell-based biotransformation was performed in Kpi buffer containing glucose and both inducers (Figure 2.6.5). Cyclohexane was fed via the gas phase at a rate of  $1.355 \text{ mmol min}^{-1} \text{ L}^{-1}$ . The initial cell concentration of  $9.5 \text{ g L}^{-1}$  decreased slightly to  $7.8 \text{ g L}^{-1}$  after 7 h of biotransformation (Figure 2.6.5A). The depletion of glucose after 3.5 h led to an immediate rise of the  $\text{pO}_2$  signal (Figure 2.6.5A) and aqueous cyclohexane concentrations (Figure 2.6.5B), which was reversed after a glucose pulse. Initial whole-cell activities of  $13.2 \pm 0.5 \text{ U g}_{\text{CDW}}^{-1}$

were stable for 2 h and after that dropped to  $-5 \text{ U g}_{\text{CDW}}^{-1}$  until the experiment was stopped after 7 h (Figure 2.6.5C).

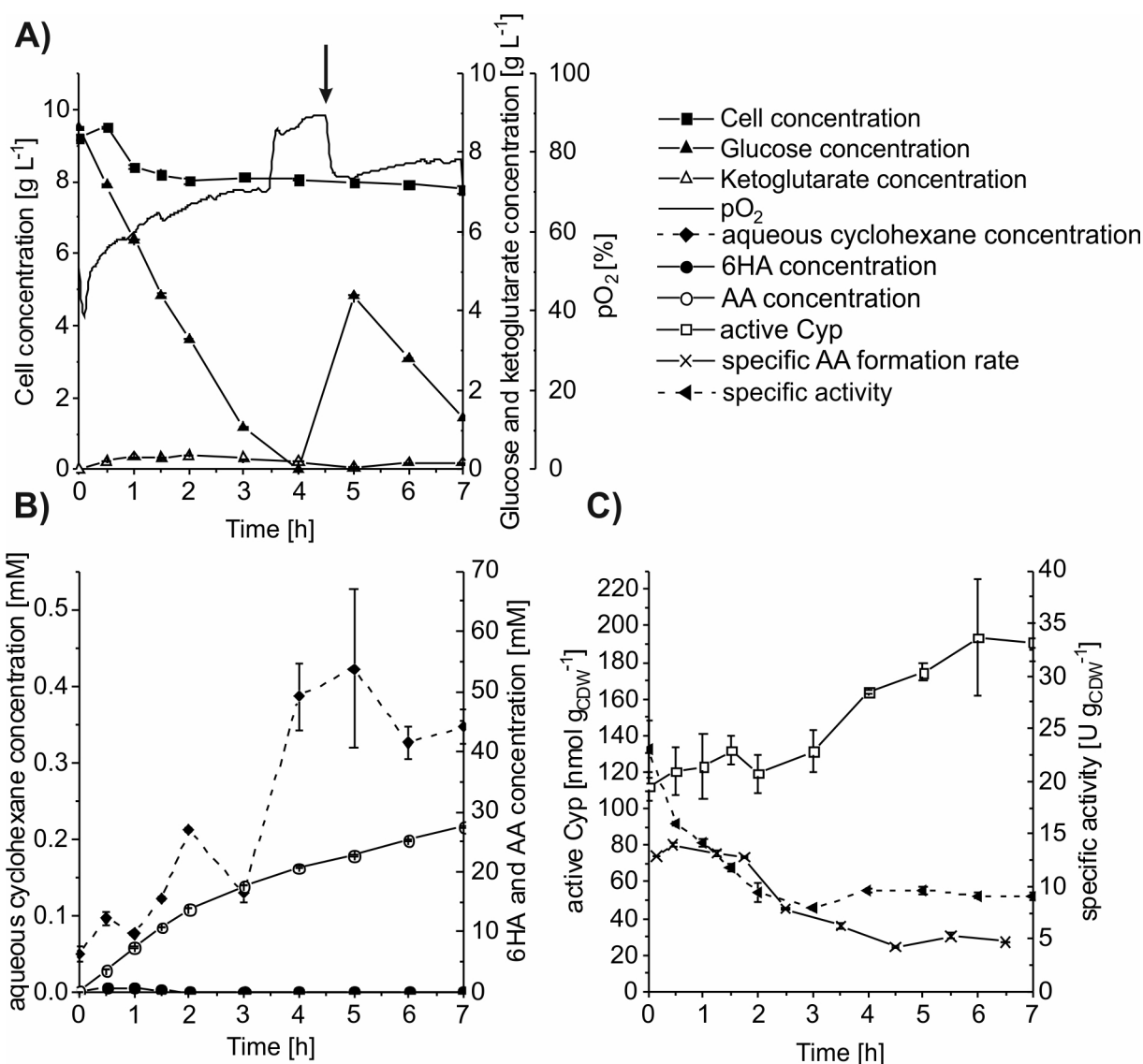


**Figure 2.6.5:** Biotransformation of cyclohexane to AA in a stirred-tank bioreactor employing resting *P. taiwanensis* VLB120 (pSEVA\_6HA\_2, pBX\_AA\_Ac) cells grown and induced under glucose-limited conditions. The cells were cultivated in batch mode until glucose depletion, followed by a fed-batch mode with an exponential feed for a  $\mu$  of  $0.15 \text{ h}^{-1}$  in 1 L RB medium (See Figure S2.6.3 for cultivation data). Cells were induced after 7 h of glucose-limited fed-batch cultivation, which was continued for another 2 h when cells were harvested and resuspended to a biomass concentration of  $10 \text{ g}_{\text{CDW}} \text{ L}^{-1}$  in 1 L Kpi buffer containing 1 % glucose (w/v), 1 mM IPTG, and 1 mM 3MB. Biotransformation was performed by applying a feed of  $1.355 \text{ mmol}_{\text{cyclohexane}} \text{ min}^{-1} \text{ L}^{-1}$  via the gas phase. The arrow in panel A indicates the addition of another  $5 \text{ g L}^{-1}$  of glucose. (A) Time courses of cell, glucose,  $\alpha$ -ketoglutarate, and dissolved oxygen ( $\text{pO}_2$ ) concentrations. (B) Time courses of aqueous cyclohexane, 6HA, and AA concentrations. (C) Time courses of active Cyp content per biomass determined via CO difference spectra, specific AA formation rate, and specific activity of cells harvested from the reactor in separate resting-cell activity assays (specific activity). Graphs represent average values and standard deviations of two technical replicates.

Interestingly, the amount of active Cyp slightly but steadily increased over time. Besides trace amounts of 6HA, no accumulation of intermediates was observed (Figure 2.6.5B), indicating that all follow-up

cascade enzymes were present in sufficient quantity. Cells sampled from the bioreactor showed an initial specific activity of  $23 \text{ U g}_{\text{CDW}}^{-1}$  in separate small-scale resting cell activity assays, which decreased to  $9 \text{ U g}_{\text{CDW}}^{-1}$  within 2 h and remained stable at this level until 7 h. At the beginning of the biotransformation, the aqueous cyclohexane concentration was below 0.1 mM (Figure 2.6.5B), indicating substrate limitation, which, however, appeared to be relieved quite fast. Towards the end, the cyclohexane concentration reached -0.4 mM, and toxicity- and/or inhibition-related effects might explain the activity decrease and the deviation in the courses of active Cyp concentration, activity in the reactor, and small-scale assays (Figure 2.6.5C). Nevertheless,  $27.5 \pm 0.1 \text{ mM}$  AA could be produced without accumulating any intermediates, which translates into an average productivity of  $0.57 \text{ g L}^{-1} \text{ h}^{-1}$  and a specific yield of  $0.48 \text{ g}_{\text{AA}} \text{ g}_{\text{CDW}}^{-1}$  (Table 2.6.3).

However, we observed 2-fold lower initial activities in separate activity assays as obtained in shaking flask experiments (Figures 2.6.4A, 2.6.5C). As the biotransformation was started when Cyp levels assessed via CO difference spectra typically saturate, an effect of the shorter induction time applied cannot be excluded. A more probable reason lies in the different growth mode applied, i.e., glucose-limited fed-batch as compared to unlimited batch growth. Volmer *et al.* (2019) showed that glucose-limited fed-batch cultivated VLB120 cells revealed lower styrene epoxidation activities than cells cultivated in an unlimited batch mode. In a second experiment, fed-batch cultivation was run with a feed enabling exponential growth at a  $\mu$  of  $0.3 \text{ h}^{-1}$ , which is slightly above the  $\mu_{\text{max}}$  obtained for induced cells in M9\* medium (Figure 2.6.2A). Whereas glucose limitation was maintained before induction, this growth rate was not maintained after induction as expected, and glucose accumulated (Figure S2.6.7). The following biotransformation was conducted as before with a slightly elevated cyclohexane feed rate of  $1.626 \text{ mmol min}^{-1} \text{ L}^{-1}$  and immediate glucose pulsing when the  $\text{pO}_2$  signal started to increase (Figure 2.6.6A). Indeed, the cells exhibited a 1.5-fold higher specific AA formation activity in separate activity assays compared to the initial activity obtained in the previous reactor experiment. Remarkably, this activity was maintained during the entire recorded biotransformation time giving an 8 h average of  $31.5 \pm 4.0 \text{ U g}_{\text{CDW}}^{-1}$  (Figure 2.6.6C). Although the amount of active Cyp remained lower than in the previous experiment (Figure 2.6.6C), specific activities in the reactor increased during the first 2 h of biotransformation in parallel to the cyclohexane concentration to  $22.6 \pm 0.2 \text{ U g}_{\text{CDW}}^{-1}$  (Figure 2.6.6B, C). Then, the activity slowly decreased to  $\sim 10 \text{ U g}_{\text{CDW}}^{-1}$  after 8 h, which might again be associated with toxic/inhibitory effects of cyclohexane. The higher overall activity allowed the accumulation of  $69.6 \pm 0.5 \text{ mM}$  ( $10.2 \pm 0.1 \text{ g L}^{-1}$ ) AA as the sole product corresponding to a doubling of average productivity, specific product yield, and yield on cyclohexane compared to the first experiment (2.6.3).

As a proof of concept, AA was then isolated from the reaction broth (Figure 2.6.7). After cell separation via centrifugation and treatment of the supernatant with active carbon for removal of colored organic substances, half of the reactor broth was concentrated and acidified to precipitate AA. After drying, a rather poor purity of 66.2 % was obtained, while 73.4 % of the AA was recovered. After the dissolution of the impure product in water at  $60 \text{ }^\circ\text{C}$  (increasing the AA solubility to  $180 \text{ g L}^{-1}$  compared to  $14 \text{ g L}^{-1}$  at  $15 \text{ }^\circ\text{C}$ ) (Musser, 2011) and centrifugation, undissolved impurities appearing as dark lower pellet were removed, whereas first AA precipitates forming during centrifugation as upper pellet were left in. After overnight incubation at  $4 \text{ }^\circ\text{C}$ , AA precipitates were dried giving rise to 3.43 g product with a purity of 96.1 %, corresponding to an isolation yield of 67.3 %.

To sum up, enzyme production during glucose excess conditions and sufficient glucose supply during the biotransformation enabled the production of the nylon monomer AA on a 10-gram scale, of which 3.4 g were isolated from 500 mL reactor broth.

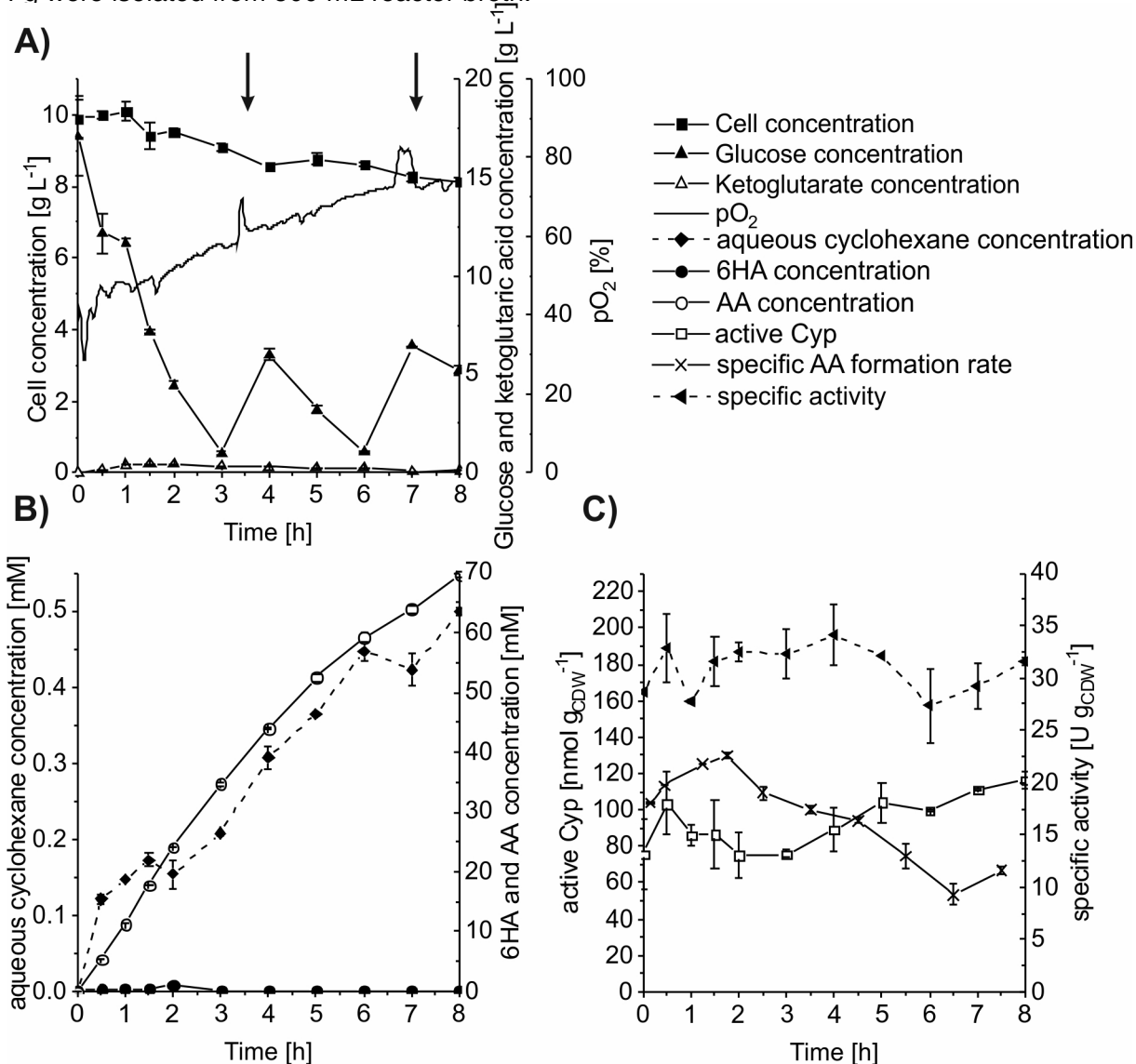


**Figure 2.6.6:** Biotransformation of cyclohexane to AA in a stirred-tank bioreactor employing resting *P. taiwanensis* VLB120 (pSEVA\_6HA\_2, pBX\_AA\_Ac) cells grown and induced under glucose-excess conditions. The cells were cultivated in a batch mode until glucose depletion, followed by a fed-batch mode with an exponential feed for a  $\mu$  of  $0.3 \text{ h}^{-1}$  in 1 L RB medium. Cells were induced after 2.5 h of fed-batch cultivation, which was continued for another 4 h, when glucose started to accumulate (see Figure S2.6.5 for cultivation data). Then, cells were harvested and resuspended to a biomass concentration of  $10 \text{ g}_{\text{CDW}} \text{ L}^{-1}$  in 1 L Kpi buffer containing 1 % glucose (w/v), 1 mM IPTG, and 1 mM 3MB. Biotransformation was performed by applying a feed of  $1.626 \text{ mmol}_{\text{cyclohexane}} \text{ min}^{-1} \text{ L}^{-1}$  via the gas phase. The arrows in panel A indicate  $5 \text{ g L}^{-1}$  glucose pulses. **(A)** Time courses of cell, glucose,  $\alpha$ -ketoglutarate, and dissolved oxygen ( $\text{pO}_2$ ) concentrations. **(B)** Time courses of aqueous cyclohexane, 6HA, and AA concentrations. **(C)** Time courses of active Cyp content per biomass determined via CO difference spectra, specific AA formation rate, and specific activity of cells harvested from the reactor in separate resting-cell activity assays (specific activity). Graphs represent average values and standard deviations of two technical replicates.



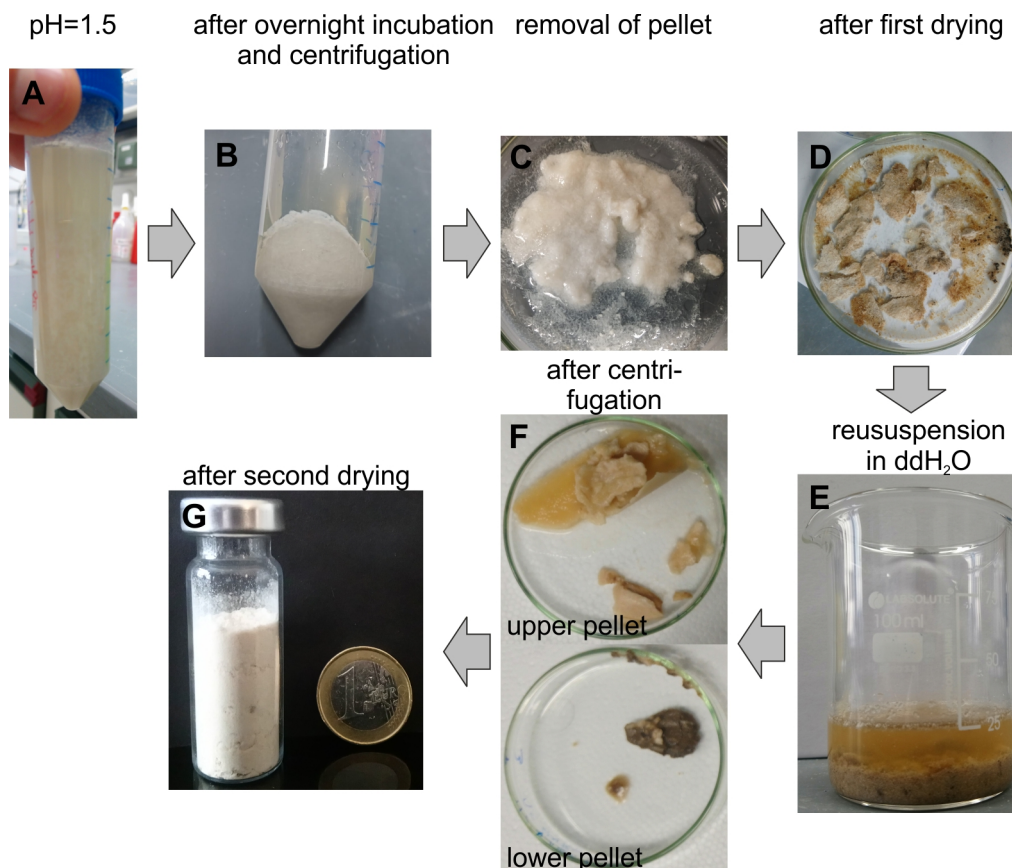


**Figure 2.6.7:** Purification of AA from the reactor broth. The images depict different steps of the purification process. (A) concentrated reactor broth after lowering the pH to 1.5; (B) precipitates after overnight incubation and subsequent centrifugation; (C) removed pellet on a glass plate; (D) product after first drying; (E) resuspended product in distilled water at 60 °C; (F) undissolved components after centrifugation; (G) product after the second drying step. The purification method is explained in detail in the Materials and Methods section 2.6.2.6.

## 2.6.4 Discussion

### 2.6.4.1 Engineering microbial hosts for direct AA synthesis

Biotechnological AA synthesis gained importance in the last 10 years due to the severe environmental concerns associated with its chemical production route (Wittcoff *et al.*, 2012). Despite the absence of enzymatic reactions leading to AA synthesis in *E. coli* and *Pseudomonads*, both species have been employed to engineer heterologous pathways (Polen *et al.*, 2013). Anabolic *de novo* production of secondary metabolites such as polyketides and non-ribosomal peptides typically suffers from low yield and productivities due to slow kinetics (Wenzel & Müller, 2005). Thus, carbon- and energy-efficient fermentative pathways are preferred and have been engineered exploiting the 6-step reverse adipate degradation pathway that is connected with the central carbon metabolism via acetyl-CoA and succinyl-CoA (Sawers & Clark, 2004; Yu *et al.*, 2014; Cheong *et al.*, 2016). Titers could be improved by genetic engineering of *E. coli* and reached 68 g L<sup>-1</sup> or 58 g L<sup>-1</sup> employing an inducible or constitutive system, respectively (Zhao *et al.*, 2018; Zhou *et al.*, 2020b). However, such production was only feasible in complex media, which are not suitable for industrial application.

Niu *et al.* (2020) demonstrated the first biotransformation approach by engineering the aromatics

degradation pathway in *P. putida* KT2440 enabling an AA titer of 2.5 g L<sup>-1</sup> (17.4 % molar yield) produced from 4-hydroxybenzoic acid. Such biotransformations are promising for bulk chemicals such as AA, because they have a theoretical yield of 100 %. However, such biotransformation approaches require a low price substrate, which is not the case for 4-hydroxybenzoic acid (Vardon *et al.*, 2015). Wang *et al.* (2020) recently presented a concept, where cheap cyclohexane was converted to AA employing three recombinant *E. coli* strains each harboring different parts of a complex reaction cascade to synthesize 31 mM AA. The complex cascade consists of 6 enzymatic steps (Figure 2.6.1A) that need to be balanced to achieve AA formation without accumulation of intermediates. This was achieved by means of the applied three-strain approach, which, however, adds complexity at cultivation and reaction levels. We have previously observed that *E. coli* cannot grow when it harbors a biocatalytic cascade for 6HA synthesis from cyclohexane (Chapter 2.5). Excess metabolic burden as well as an insufficient supply of redox equivalents can hamper the implementation of complex cascades (Chen *et al.*, 2014). Pseudomonads constitute promising alternative hosts, especially for redox reactions, due to their highly active Entner-Doudoroff and pentose phosphate pathways, enabling the efficient provision of redox equivalents, and their ability to cope with high oxidative and solvent stress (Chavarría *et al.*, 2013; Martínez-García *et al.*, 2014). Based on orthologous pathway engineering in Pseudomonads, this study for the first time reports efficient AA synthesis from cyclohexane by means of a single microbial strain.

For this purpose, *P. taiwanensis* harboring a pathway to convert cyclohexane to 6HA (Chapter 2.3) was supplied with two dehydrogenases to enable AA synthesis (Figure 2.6.1). Of the two alcohol dehydrogenases tested for the conversion of 6HA to 6-oxohexanoic acid, the NAD(H)-dependent Acidovorax ADH (Figure S2.6.1) proved superior over *P. putida*-derived AlkJ (Figure 2.6.2), although the latter catalyzes an irreversible reaction transferring substrate-derived electrons to the respiratory electron transport chain and has been shown to enable efficient aliphatic aldehyde formation (Kirmair & Skerra, 2014; Schrewe *et al.*, 2014; Ladkau *et al.*, 2016). Low-level expression, protein instability, for which indications have been reported (Schrewe *et al.*, 2014), or a low activity for the conversion of C-ol are potential reasons for the low performance obtained with AlkJ. Additionally, a substrate mass-transfer limitation to membrane-associated AlkJ (Kirmair & Skerra, 2014) cannot be excluded. The introduction of a second plasmid increased the metabolic burden as indicated by lower growth rates, which, however, did not influence the active Cyp amount (Figure 2.6.3A, B), emphasizing the potential of Pseudomonads for *in vivo* cascades / orthologous pathway engineering. Further genetic engineering, e.g., integration into the highly expressed 16S-rRNA clusters, might alleviate the metabolic burden associated with plasmid-based gene expression while retaining high whole-cell activities (Otto *et al.*, 2019). Overall, our results indicate that employing *P. taiwanensis* for cascade biocatalysis has tremendous potential to replace current industrial AA production routes.

### 2.6.4.2 Protein re-synthesis and glucose excess improve the durability of AA production

Substantial research has been devoted to different whole-cell formats and biotransformation conditions in order to optimize bioprocess performance (Willrodt *et al.*, 2015b; Kadisch *et al.*, 2017b). As observed before (Julsing *et al.*, 2012a; Kuhn *et al.*, 2012b; Willrodt *et al.*, 2016) and in chapter 2.4, high initial activities of resting cells tend to decrease in time, as it also was the case in initial cyclohexane biotransformation experiments allowing only 70 % cyclohexane conversion within 16 h (Figure 2.6.3C,

D). Fast activity loss could be minimized by adding inducers to resting cells, thus facilitating protein re-synthesis, or by the use of growing cells, although initial activities were lower in the latter case (Figure 2.6.4A, B). Based on their high metabolic activity, growing cells can efficiently resynthesize cofactors and proteins, thereby fostering biocatalyst stability, which is associated with a higher glucose demand (Kuhn *et al.*, 2012b). The up to 2-fold higher initial activities of induced resting cells compared to growing cells (Figure 2.6.4A, B) indicate that there may be competition for cellular resources among growth and the heterologous pathway as observed before for oxygenase catalysis with recombinant *E. coli* (Julsing *et al.*, 2012a). Overall, this indicates a trade-off between maximal activity and stability of the biocatalyst. Willrodt *et al.* (2016) observed that a resting state based on magnesium sulfate instead of nitrogen limitation enabled a higher stability of an *E. coli*-based biocatalyst and a 5-fold higher product yield. Such an approach may further improve the AA titer and specific whole-cell activities.

The impact of glucose availability during recombinant gene expression and biotransformation has been studied by Volmer *et al.* (2019) for styrene epoxidation employing constitutively solvent-tolerant *P. taiwanensis* VLB120 $\Delta$ C $\Delta$ ttGV. Batch cultivation enabled 4-fold higher whole-cell activities compared to glucose-limited fed-batch cultivation, where recombinant enzyme synthesis and redox cofactor regeneration were limited. Stoichiometrically, AA synthesis requires an electron acceptor due to the net production of one NADH (Figure 2.6.1B). This and the fact that cells were not glucose-limited in the resting-cell biotransformation format applied make less efficient recombinant enzyme synthesis the probable reason for the observed higher activity upon enzyme expression without glucose limitation (Figures 2.6.5 and 2.6.6).

Although the presence of AA in the culture medium did not affect initial whole-cell activities in small-scale resting cell-based biotransformations (Figure S2.6.8), a long-term effect cannot be excluded. It has been found that elevated but still subtoxic product (i.e., styrene oxide) concentrations affected *E. coli* metabolism, so that oxygenase catalysis became NADH-limited (Kuhn *et al.*, 2013). Similarly, energy metabolism and thus redox cofactor balancing may be affected by AA in the long term. Further, the mechanism of AA export is unknown but may involve active transport, as it has been demonstrated for succinate (Yu *et al.*, 2019), and thus depend on energy metabolism with glucose as the energy source. Uncoupling of the oxygenases also may cause a redox cofactor imbalance. Cyp enzymes are indeed prone to uncoupling (Balke *et al.*, 2018; Morlock *et al.*, 2018). The net production of one NADH in the cascade would however compensate Cyp uncoupling up to a rate equaling that of cyclohexane conversion. The findings that *Acidovorax* CHMO did not show uncoupling *in vitro* (Chapter 2.2) and that C-one conversion was efficient with AA as main product also in the absence of glucose (Figure 2.6.4C) indicate that cofactor balancing within these three steps including AA export worked quite well. The presence of glucose however had a stabilizing effect on the operation of the entire cascade (Figure 2.6.4), which may be due to inherent Cyp instability and inefficient resynthesis and/or uncoupling causing damage related to reactive oxygen species and possibly an NADH limitation.

Overall, glucose-limited high-cell-density fed-batch cultivation with glucose excess during recombinant protein synthesis followed by biotransformation with a high concentration of glucose-fed resting cells constitutes a promising approach simultaneously enabling high specific activities and a high stability at high cell concentrations.

## 2.6.4.3 Biotechnological AA synthesis remains challenging

Besides its direct synthesis from cheap substrates such as glucose or cyclohexane, AA can be obtained by hydrogenation of *cis,cis*-muconic acid or by deoxydehydration/hydrogenation of D-glucaric acid (Averesch *et al.*, 2018).

**Table 2.6.3:** Comparison of process parameters of biotransformations yielding AA or its precursor *cis, cis*-muconic acid (Kohlstedt *et al.*, 2018; Wang *et al.*, 2020).

	Reactor I	Reactor II	Wang <i>et al.</i> , 2020	Kohlstedt <i>et al.</i> , 2018
Product	AA	AA	AA	muconic acid
Volume [L]	1	1	0.004	0.5
Biotransformation time [h]	7	8	18/24	62
Substrate feed <sup>a</sup> [mmol min <sup>-1</sup> L <sup>-1</sup> ]	1.355	1.626	n.a. <sup>b</sup>	n.d. <sup>d</sup>
Initial cell concentration [g L <sup>-1</sup> ]	9.2	9.9	12	n.d. <sup>e</sup>
Max. cell concentration [g L <sup>-1</sup> ]	9.5	10.1	n.d. <sup>c</sup>	9.2
Average productivity [g L <sup>-1</sup> h <sup>-1</sup> ]	0.57	1.28	max. 0.25	1.04
Maximal activity [U g <sub>CDW</sub> <sup>-1</sup> ]	14.0	22.6	5.2	n.d.
Final product concentration [mM]	27.5	69.6	31/21	450
Specific product yield [g <sub>product</sub> g <sub>CDW</sub> <sup>-1</sup> ]	0.48	1.12	max. 0.38	7.0
Final product titer [g L <sup>-1</sup> ]	4.0	10.2	max. 4.49	64.2
Total product [g]	4.0	10.2	max. 0.018	32.1
Yield on substrate [%]	4.2	8.9	max. 42	100

<sup>a</sup> referring to the liquid volume of the bioreactor

<sup>b</sup> not applicable, direct addition of 50 or 100 mM cyclohexane referring to the aqueous phase volume

<sup>c</sup> not determined

<sup>d</sup> coupled to base addition and thus to the pH control

<sup>e</sup> fed-batch cultivation during biotransformation

The production of glucaric acid from glucose in *E. coli* via a 5-step heterologous pathway has been demonstrated and improved to reach a titer of 2.5 g L<sup>-1</sup> with a yield of 10 % (Moon *et al.*, 2009, 2010; Kruyer & Peralta-Yahya, 2017). A benchmarking study showed the production of 64.2 g L<sup>-1</sup> muconic acid from catechol in a fed-batch process, which could be translated to depolymerized lignin conversion enabling a titer of 13 g L<sup>-1</sup> (Kohlstedt *et al.*, 2018). The high product titer was possible as the substrate is soluble and not toxic to the cells. Until now, this is the highest titer achieved in minimal medium. As indicated above, the 6-step biotransformation of cyclohexane to AA has been successfully demonstrated in a mixed-species approach, albeit only in small-scale experiments (4 mL) (Wang *et al.*, 2020). The direct AA synthesis route presented in this paper could be realized in one species and was transferred to a 1 L bioreactor scale (Figures 2.6.5, 2.6.6). Table 2.6.3 reveals that the achieved average productivity and specific product yield obtained in our *Pseudomonas*-based one species approach surpassed the values achieved by Wang *et al.* (2020) 6-fold and 3-fold, respectively. The yield on cyclohexane is significantly lower because of the continuous feed via the gas phase instead of an initial addition and subsequent closure of the reaction vessel. Gas phase feeding thus has to involve substrate recycling from the off-gas stream. AA synthesis employing *P. taiwanensis* enabled a 25 % higher average productivity than muconic acid production (Table 2.6.3). However,

the specific product yield and final product titer remained at least 6-fold lower and may be increased by prolonging the operation time and further biocatalyst stabilization (Figures 2.6.5C, 2.6.6C). As reported for 6HA synthesis, the drop in whole-cell activity may be associated with toxification by cyclohexane (Chapter 2.4), while product inhibition can be excluded (Figure S2.6.8). Online analysis of the aqueous cyclohexane concentration coupled to a feed control constitutes a promising approach to enable high activities while maintaining the cyclohexane concentration below toxic levels. For industrial application, product titer and productivity need to be increased at least 10-fold (Straathof *et al.*, 2002). A recently reported *P. taiwanensis* VLB120 chassis strain featuring deletions in flagellar clusters and biofilm-forming genes, enhanced metabolic capacities, and proven potential for titer, yield, and productivity improvements (Wynands *et al.*, 2019) may well be a promising tool to intensify cascades involving redox reactions.

The *cis,cis*-muconic acid route is a typical example of a chemoenzymatic approach with a nearly quantitative AA yield (97 %) for muconic acid hydrogenation (Beerthuis *et al.*, 2015; Vardon *et al.*, 2016). However, muconic acid needs to be purified from the culture broth and further processed, compromising overall process efficiency (Polen *et al.*, 2013). Additionally, most of the process energy demand is attributed to the hydrogenation step, thereby affecting the ecobalance (Van Duuren *et al.*, 2011a). On the other hand, impure aromatics derived from lignin or oil distillation waste streams can be used as substrates (Van Duuren *et al.*, 2011a). Further, one-step purification of *cis,cis*-muconic acid enabled a high purity of 98 % (Kohlstedt *et al.*, 2018), which is difficult to achieve for AA due to its 20-fold higher water solubility. The preliminary AA purification approach followed in this study enabled an AA purity of 96 % but required water evaporation and additional precipitation steps limiting the recovery to 67 %. Further improvements are necessary to maximize AA recovery and purity. Options include, e.g., washing steps with ethanol to remove insoluble salts (Vardon *et al.*, 2016). Life-cycle assessment is necessary to compare both routes towards AA and find major bottlenecks.

## 2.6.5 Conclusions

In this study, a recombinant *P. taiwanensis* VLB120 strain synthesizing the nylon 6,6 polymer building block AA from cyclohexane was successfully developed. An alcohol dehydrogenase and an aldehyde dehydrogenase originating from *Acidovorax* sp. CHX100 were identified and proven appropriate to amend an existing cascade from cyclohexane to 6HA. The generation and evaluation of several different expression systems enabled the establishment of a construct enabling a high specific activity of  $50 \text{ U g}_{\text{CDW}}^{-1}$  as well as cyclohexane conversions and AA yields close to 100 %. The best-performing strain, *P. taiwanensis* VLB120 (pSEVA\_6HA\_2, pBX\_AA\_Ac) was employed in stirred-tank reactor setups. Thereby, the orthologous pathway capacity was found to be higher, when glucose-excess conditions were established during respective gene expression. Gaseous cyclohexane feeding enabled the highest AA titer obtained so far with this cheap and readily available substrate. Including a proof of principal for product isolation, this study followed a truly integrated approach, covering all the way from strain development to downstream processing, thereby paving the way towards more environmentally friendly polymer production processes.

## 2.6.6 Acknowledgments

We acknowledge the use of the facilities of the Centre for Biocatalysis (MiKat) at the Helmholtz Centre for Environmental Research, which is supported by European Regional Development Funds (EFRE,

## **Chapter 2.6** Pathway and process engineering for adipic acid production

---

Europe funds Saxony) and the Helmholtz Association. LB and IH were funded by the ERA-IB- Project PolyBugs ID:16006 and the Sächsisches Ministerium für Wissenschaft und Kunst (SMWK) Project ID: 100318259. The authors would like to thank Prof. Dr. Andreas Schmid for helpful discussions.

## **Chapter 3**

### **General Discussion and Conclusions**

In 2018, 359 Mio. t of plastics were produced with applications in all fields of life, including packaging, construction, household/leisure, the automotive industry, the electrical segment, and agriculture (PlasticsEurope, 2020). Their demand is steadily increasing with an annual growth rate of up to 8.4 % (Geyer *et al.*, 2017). Progressing global warming and climate change require sustainable production routes to ensure an intact ecosystem for future generations (Graedel, 2002). The replacement of plastic usage is no option in most application fields due to their durability, mechanical stability, and deformability. Hence, the utilization of renewable resources and/or the development of greener production routes are potential solutions. The inherent “greenness” of biotechnological production processes with operations under mild conditions in an aqueous system offers an alternative to the classic organic syntheses (Anastas & Warner, 1998; Sheldon & Woodley, 2018).

This thesis contributes to this effort by presenting biotechnological solutions for the synthesis of  $\epsilon$ -caprolactone ( $\epsilon$ -CL), 6-aminohexanoic acid (6AHA), and adipic acid (AA), which are building blocks for the biodegradable polymer polycaprolactone (PCL), nylon 6, or nylon 6,6. The challenges of biocatalytic processes and potential solutions, including implications for further improvement, are presented in the following.

### 3.1 Enzyme selection and characterization, and optimization are crucial to designing biocatalytic cascades

As in industrial catalysis, biocatalytic monomer syntheses typically have a multi-step character (Wittcoff *et al.*, 2012). Therefore, several enzymes have to act sequentially to yield the final product. In this thesis, genes originating from the cyclohexane-degrading bacterium *Acidovorax* sp. CHX100 ( $\mu=0.2 \text{ h}^{-1}$ ) were heterologously expressed in the solvent-tolerant bacterium *P. taiwanensis* VLB120 with the advantage of higher growth rates and its inability to use cyclohexane as sole carbon source (Salamanca & Engesser, 2014; Karande *et al.*, 2016). This strategy has the advantage that all enzymes are evolved to accept the respective cyclohexane-derived compounds and transform them at high catalytic rates without further enzyme engineering (Chapter 2.6). In other studies, cyclohexane hydroxylation was accomplished by mutating the *Bacillus subtilis* derived BM-3 (Pennec *et al.*, 2015a; Wang *et al.*, 2020), which, however, is prone to uncoupling (Pennec *et al.*, 2015b). Also, *B. subtilis* does not harbor further downstream enzymes. Consequently, enzymes from other hosts for further reaction steps need to be tested, e.g., CDH from *Lactococcus kefir* (Srinivasamurthy *et al.*, 2019) and CHMO from *Acinetobacter* sp. (Sattler *et al.*, 2014). Whereas the biocatalytic production of  $\epsilon$ -CL or 6AHA only was accomplished from cyclohexane-derived compounds, the AA derivative *cis,cis*-muconic acid can be accessed via the degradation pathway of aromatics (Van Duuren *et al.*, 2011b). Additionally, fermentative strategies exploiting native enzymes of the host can be used for monomer production (Ladkau *et al.*, 2016). Until now, there are no metabolic routes known to synthesize  $\epsilon$ -CL or 6AHA. Within this thesis, synthetic pathways from cyclohexane have now been established (Chapters 2.3 and 2.5). AA or its derivatives glucaric acid or *cis,cis*-muconic acid can be produced from glucose (Kruyer & Peralta-Yahya, 2017) via reversed fatty acid oxidation (Clomburg *et al.*, 2015) or TCA cycle enzymes (Yu *et al.*, 2014).

Once the enzymes are selected, it is advisable to characterize them and, if necessary, find solutions to overcome potential inhibitory effects or undesired properties (e.g., uncoupling, by-product formation). This characterization can be carried out *in vitro* as well as *in vivo*. Cyp activity has been assessed *in*



*vivo* by designing different expression plasmids to maximize the rate-limiting cyclohexane hydroxylation (Chapter 2.1). Also, the thermodynamic equilibrium of the CDH reaction was determined, which revealed that the successive enzyme CHMO needs to have high activity to allow withdrawal of cyclohexanone from the equilibrium (Chapter 2.3). More detailed characterization was carried out with CHMO (Chapters 2.2 and 2.3) because it is known that Baeyer-Villiger monooxygenases are prone to uncoupling, as well as substrate and product inhibition (Alphand *et al.*, 2003; Delgove *et al.*, 2018). Thereby, it has been found that the *Acidovorax* CHMO is less prone to uncoupling or product inhibition, whereas substrate inhibition becomes only significant at elevated concentrations. However, the *Acidovorax* CHMO is severely inhibited by cyclohexanol. Scherkus *et al.* (2017) observed product inhibition by  $\epsilon$ -CL and therefore extended the biocatalytic cascade by a lactonase enabling 24 % higher product titers. Additionally, cyclohexanol inhibition was avoided by implementing a fed-batch approach. Also in this thesis the cascade's amendment with a lactonase allowed streamlined 6HA production without inhibitory effects (Chapter 2.3). Kinetic analysis of an alcohol dehydrogenase and a CHMO revealed severe cofactor limitation under biotransformation conditions in *E. coli* (Milker *et al.*, 2017). Cofactor excess enabled an 8-fold reduction of reaction time. To rule out such constraints, it is recommended to perform a basic characterization experiment, e.g., the activity assessment of each enzymatic step beforehand to reduce the experimental effort during the cascade design process. Some proteins might require optimization to increase stability, specificity, activity, or coupling efficiency, which can be accomplished by site-directed mutagenesis (Bornscheuer *et al.*, 2012). Such engineering was not conducted in this thesis as the activity of the enzymatic steps was in the same range, and the enzymes were highly specific. However, it could be a valuable tool to increase the cascade enzymes' stability, especially of the P450 monooxygenase that often suffers from decreasing enzyme activity with time (Staudt *et al.*, 2013).

Consequently, careful enzyme selection, their characterization, and potential optimization allow to rule out obstacles beforehand, enabling the formulation of cascade design guidelines.

### 3.2 Balanced enzyme ratios are key for streamlined cascade reactions

Whereas the assembly of *in vitro* cascades is accomplished by varying the respective protein amounts, *in vivo* cascades require sophisticated genetic engineering to adjust desired protein levels within the cell (Muschiol *et al.*, 2015). At this point, cascade engineering and host selection are interconnected because the cellular metabolism differs in each bacterial species at least to a certain extent (Jeschek *et al.*, 2017). In the past years, tremendous efforts have been made to standardize expression platforms and biological parts to allow transferability.

The plasmids constructed in this thesis are based on the Standard European Vector Architecture (SEVA) (Silva-Rocha *et al.*, 2013; Martínez-García *et al.*, 2015), which allowed rapid screening of different gene dosages via the variation of the origin of replication (Chapter 2.1). The highest share of active Cyp has been detected when the genes were expressed from a medium-copy plasmid. Likewise, the gene dosage of ADH and AldDH genes was varied to match the upper cascade activity (Chapter 2.6). Genome integration resulted in activities below  $10 \text{ U g}_{\text{CDW}}^{-1}$  and therefore was considered to be unsuitable compared to plasmid-based approaches. Nevertheless, genome integration into multi-copy loci, e.g., rRNA operons, could be one alternative to switch from plasmid-based expression to the less burdensome genome-based expression (Otto *et al.*, 2019).

Translational engineering via RBS sequence variation is a relatively new tool to manipulate protein abundance *in vivo*. The Registry of Standard Biological Parts (Registry of Standard Biological Parts, 2019) lists 48 prokaryotic RBS with varying strength. Among these, three were selected in this thesis for Cyp gene expression and evaluated regarding the metabolic burden on the cell, active Cyp amount, and whole-cell activity (Chapter 2.1). The RBS with moderate strength (RBS\*) allowed the highest whole-cell activities of  $55 \text{ U g}_{\text{CDW}}^{-1}$  without severely compromising the cellular growth rate and active protein content. The availability of so-called RedLibs (Reduced Libraries) combined with *in silico* prediction tools might further reduce the experimental screening effort by allowing differential expression of pathway genes (Jeschek *et al.*, 2016).

Transcriptional engineering refers to the selection of the gene expression system as well as promoter engineering. Initially, three different gene expression systems were tested (*lac*, *tac*, *alk*), and the *lac*-regulation system resulted in the highest cyclohexane hydroxylation activity of  $35 \text{ U g}_{\text{CDW}}^{-1}$  (Chapter 2.1). Therefore, the *lacI<sup>q</sup>-P<sub>trc</sub>* system from the pSEVA collection was selected for further experiments. The insertion of a second *P<sub>trc</sub>* promoter allowed to double CDH and CHMO activities, enabling efficient conversion of cyclohexane to 6-hydroxyhexanoic acid (6HA) without accumulating intermediate products (Chapter 2.2). The extension of the cascade with the ADH and AldDH genes expressed via the *xyIS-P<sub>m</sub>* regulation system resulted in the highest cyclohexane conversion of 70 %, possibly because of less cross-talk with the *lacI<sup>q</sup>-P<sub>trc</sub>*-regulated upper cascade genes (Chapter 2.6). Transcriptional engineering performed in this thesis may be further improved by testing different promoter strengths enabling differential expression levels of each pathway gene. Recently, Köbbing *et al.* (2020) presented concatenated synthetic promoters and a method to precisely determine their activity in *Pseudomonas*. Xu *et al.* (2012) developed the so-called ePathBrick vectors for *E. coli* to customize multiple transcriptional activation or repression signals allowing the assembly of multi-step heterologous pathways. In this regard, it would be advisable to combine experimental and computational methods for genetic engineering to find the optimal gene expression pattern as demonstrated for violacein production (Xu *et al.*, 2017). This approach facilitates simultaneous modification of different genetic elements and increases the search space (Jeschek *et al.*, 2016). However, prior knowledge of enzyme properties also allowed us to rationally test other operon organizations (Chapter 2.3) and plasmid combinations (Chapter 2.6), and resulted in streamlined cascade reactions with balanced enzyme ratios.

### 3.3 Versatile host selection gives access to previously not feasible cascades

As stated earlier, the host organism influences the gene expression of cascade enzymes and provides features facilitating reaction engineering. In this thesis, *P. taiwanensis* VLB120 has been selected as the host harboring biocatalytic cascades for 6HA and AA synthesis (Chapters 2.3 and 2.6). By now, *Pseudomonas* are established in biotechnological applications, and a wide range of genetic tools is available (Nikel *et al.*, 2014). On the one hand, this strain provides high amounts of reduction equivalents (Chavarría *et al.*, 2013) and, on the other hand, harbors solvent-tolerance mechanisms to cope with toxic substrate such as cyclohexane (Volmer *et al.*, 2014). Its high metabolic versatility enabled the maintenance of pSEVA\_6HA\_2 (Chapter 2.3), resulting in whole-cell activities of up to  $45 \text{ U g}_{\text{CDW}}^{-1}$  for the conversion of cyclohexane to 6HA. It was not possible to grow *E. coli* JM101 harboring this plasmid (Chapter 2.5), which might be attributed to cofactor drainage and high metabolic

burden (Biggs *et al.*, 2016; Jones & Wang, 2018). It would also be interesting to test the constitutively solvent-tolerant variant *P. taiwanensis* VLB120 $\Delta$ ttgV, which enabled a 60 % increase of styrene epoxidation activities (Volmer *et al.*, 2019). It must be considered that solvent-tolerance mechanisms require proton motive force, potentially resulting in lower yields on glucose and specific activity but extended stability (Kuhn *et al.*, 2012a). Recently, *P. taiwanensis* VLB120 chassis strains with higher yields on the carbon source, and different solvent-tolerance levels became available (Wynands *et al.*, 2019), which might further enhance product titers of 6HA and AA (Chapters 2.4 and 2.6).

However, the assembly of a biocatalytic cascade in one host can be challenging and time-consuming and might not be successful in a straight-forward approach. The use of mixed-species strategies allows to improve the biosynthesis efficiency and gives access to entirely new molecules (Jones & Wang, 2018). These co-cultures have several advantages over monocultures and have been employed in various biotechnological processes (Table 3.1). 6AHA synthesis has been realized by mixed-species biotransformation employing *E. coli* JM101 and *P. taiwanensis* VLB120 (Chapter 2.5). The high metabolic burden in *E. coli* and the lack of AlkJ activity in *P. taiwanensis* VLB120 made single-species concepts unfeasible. A similar reasoning was applied for perillyl acetate synthesis (Willrodt *et al.*, 2015a). However, the use of multiple strains or species imposes challenges requiring a reasonable experimental design (Table 3.1). The application of growing cells necessitates control over the strain ratio, which might be accomplished by different inoculation ratios or sequential inoculation (Zhang *et al.*, 2015). In this thesis, both strains were grown separately and then combined in a resting cell approach to maintain a constant strain ratio. This concept has been demonstrated by Willrodt *et al.* (2015a) but has the disadvantage that the cultivation has to be carried out separately for each strain, which is again separated from the actual biosynthesis. Efficient secretion and uptake of the shuttling compound(s) are further crucial aspects to fully exploit the cells' potentials (Jones & Wang, 2018). Thereby, it has been found that 6HA uptake is severely compromised, and  $\epsilon$ -CL as shuttling compound enables higher 6AHA formation rates and yields (Chapter 2.5). Mixed-species approaches are extremely valuable for multi-step cascades and have the potential to broaden the substrate and product spectra.

**Table 3.1:** Selected advantages and challenges in mixed-species approaches with representative examples or solutions, respectively.

	Feature	Species or strains	Product	Example/ Solution	Reference
Advantages	Distribution of metabolic burden	3 different <i>E. coli</i> strains	AA	Only trace amounts of AA in one-species approach	Wang <i>et al.</i> (2020)
	Circumvent difficulties in gene expression and/or protein synthesis	<i>E. coli</i> and <i>P. taiwanensis</i>	6AHA	<i>E. coli</i> does not grow harboring pSEVA_6HA_2, no AlkJ activity observed in <i>P. taiwanensis</i>	Chapter 2.5
		Two <i>E. coli</i> strains	Perillyl acetate from glucose	<i>E. coli</i> BL21 DE3 for limonene fermentation, <i>E. coli</i> MG1655 for limonene hydroxylation	Willrodt <i>et al.</i> (2015)
	Compartmentalization	Two <i>E. coli</i> strains	Transformation of xylan to ethanol	Secretion of hemicellulases by one strain, uptake by second strain, and conversion to ethanol	Shin <i>et al.</i> (2010)
	Inhibitory effects of pathway intermediates	Two <i>P. putida</i> KT2440 strains	sulfur removal in aromatic heterocycles	Alleviation of 2-hydroxybiphenyl sulfinate inhibition	Martinez <i>et al.</i> (2016)
	Reduction of unwanted side reactions	Two <i>E. coli</i> strains	Monolignols from glucose	Distribution of promiscuous enzyme HpaBC and tyrosine in different bacteria	Chen <i>et al.</i> (2017)
Challenges	Tuning and maintenance of strain ratios	<i>E. coli</i> and <i>S. cerevisiae</i>	oxygenated taxanes	Xylose as carbon source only available for <i>E. coli</i> that produces acetate for <i>S. cerevisiae</i>	Zhou <i>et al.</i> (2015)
		<i>E. coli</i> and <i>P. taiwanensis</i>	6AHA	Use of resting cells	Chapter 2.5
	Similar reaction/growth conditions	two <i>E. coli</i> strains	<i>Cis,cis</i> -muconic acid from glycerol	Both strains grow in same medium under the same conditions	Zhang <i>et al.</i> (2015)
	Secretion and uptake of shuttling compound	two <i>E. coli</i> strains	6AHA	More hydrophobic $\epsilon$ -CL as shuttling compound	Chapter 2.5

### 3.4 Reaction and process engineering get the best out of the biocatalysts

Reaction engineering refers to the choice and optimization of the biocatalyst configuration (e.g., resting cells), reaction conditions (e.g., selection of medium), and the overall reaction setup (e.g., single- or multiphasic conditions) (Willrodt *et al.*, 2015b). Three different catalyst formats have been investigated

in shaking flask experiments (Chapters 2.4 and 2.6). It has been found that resting cells showed high initial activities of over  $40 \text{ U g}_{\text{CDW}}^{-1}$ , which, however, declined quickly. Such observations were reported previously for styrene epoxidation (Julsing *et al.*, 2012a). Apparently, the addition of inducers could stabilize the activity at later stages of the biotransformation, indicating protein re-synthesis. As reported previously (McIver *et al.*, 2008; Julsing *et al.*, 2012a), growing cells exhibited approximately 2-fold lower initial activities due to the trade-off between biotransformation and growth (Bühler *et al.*, 2008). This cell format had the advantage of more stable product formation rates. Compared with resting cells, the application of growing *L. brevis* cells for  $\gamma$ -aminobutyric acid production resulted in both a higher yield and an increased conversion rate (Zhang *et al.*, 2012). *P. taiwanensis*\_6HA has been characterized in three different media to evaluate its physiology and influence on whole-cell activity (Chapter 2.4). It has been found that increasing phosphate concentrations in the medium correlated with increased gluconate formation (Volmer, 2016). The lower whole-cell activities observed in M9 medium could have diverse reasons such as declining pH due to gluconate formation, less recombinant protein amounts due to higher growth rates, or a direct influence of gluconate. Growth in M9\* and RB media revealed similar activities, which led us to choose the high-cell density RB medium in reactor setups.

Assessing the influence of the reaction parameters cell concentration, oxygen mass transfer, and cyclohexane mass transfer in the mixed-species shake-flask setup (Chapter 2.5) enabled us to identify oxygen depletion as the main factor for low yields and conversion. Eventually, a reaction setup with low aqueous cyclohexane concentrations that allows full conversion with 86 % 6AHA yield was chosen. The system was, however, not optimized concerning whole-cell specific activities (max.  $7.7 \text{ U g}_{\text{CDW}}^{-1}$ ), which was also the case for AA synthesis from cyclohexane employing three recombinant *E. coli* strains (max.  $5.2 \text{ U g}_{\text{CDW}}^{-1}$ ) (Wang *et al.*, 2020). For that, an optimal strain ratio with adapted biomass concentrations has to be found to increase cyclohexane mass transfer rates leading to higher whole-cell activities.

6HA and AA production was scaled to a 1 L stirred-tank bioreactor setup (Chapters 2.4 and 2.6). The main challenge in process engineering is cyclohexane feeding due to its solubility, toxicity and volatility (ChemSpider, 2020). The hydrophilic character of AA and 6HA and cyclohexane degassing when supplied via a second organic phase (Hoschek *et al.*, 2019b) favored a single-phasic aqueous reaction system. A gaseous feed via the gas phase enabled adjustment of the aqueous cyclohexane concentration. However, the low water/gas partitioning coefficient of 0.131 (Sander, 2015) resulted in low yields on cyclohexane of max. 23 % for 6HA and 9 % for AA. This massive substrate loss does not reconcile with economic and ecological precursor production and therefore requires recycling of the gas phase. Additionally, increasing the aqueous cyclohexane concentration increases whole-cell activities as observed for the initial activities in Chapter 2.4. However, high cyclohexane amounts were toxic to cells, so that a compromise between these two influences has to be found. For that, online measurements of the gas composition, possibly via membrane-inlet mass spectrometry (Hoch & Kok, 1963), would be advantageous together with more fine-tuned cyclohexane supply rates. These are also the preconditions to test biotransformations employing growing cells, where the substrate feed has to be continuously adapted depending on cell concentration and activity. This is particularly interesting because glucose-limited fed-batch cultures showed 4-fold lower styrene epoxidation activities than batch cultures (Volmer *et al.*, 2019). Similar observations have been made

for cyclohexane conversion. Growing cells exhibited more stable product formation rates compared to resting cells (Chapters 2.4 and 2.6), and glucose excess during the recombinant protein production phase enabled 50 % higher initial activities compared to fed-batch cultivation ( $\mu=0.15 \text{ h}^{-1}$ ) (Chapter 2.6).

It would be interesting to test a completely different reactor design for these cascades. In Chapter 2.2, naturally immobilized cells in tubular bioreactors (biofilms) have been compared to suspended cells. Whereas the apparent substrate uptake constant ( $K_S$ ) was 10-fold increased, substrate inhibition was reduced. Biofilms are more resistant towards high cyclohexane concentrations (Karande *et al.*, 2016) and exhibit stable reaction rates for over one month (Hoschek *et al.*, 2019a). They offer the potential to increase the biotransformation time by allowing continuous operation. However, they need further optimization regarding upscaling (e.g., increasing the length of the capillary) and the product titer at the outlet (Karande *et al.*, 2016).

### 3.5 Comparison to other polymer-building block synthesis concepts

Biotechnological monomer production gained increasing attention during the last years (Mülhaupt, 2013; Pellis *et al.*, 2016; Kruyer & Peralta-Yahya, 2017). Table 3.2 summarizes various synthesis concepts employing microorganisms with a particular focus on polyesters and nylon monomers that were also the main products in this thesis. Although other monomers, e.g., 1,4-butanediol, are interesting monomers, respective productivities remained low (Yim *et al.*, 2011) or could not be scaled (Pellis *et al.*, 2016). Itaconic acid production from various sugars (e.g., molasses) by *Corynebacterium glutamicum* has been commercialized by Pfizer, reaching moderate space-time yield and a high titer of  $71 \text{ g L}^{-1}$  due to the long reaction time (Willke & Vorlop, 2001). Until now, the synthesis of the PCL monomers 6HA or  $\epsilon$ -CL was realized by biotransformation of cyclohexane derivatives such as cyclohexanol. Srinivasamurthy *et al.* (2019, 2020) reached 7-fold higher titers, up to 2-fold higher yields on biocatalyst, and more than 20-fold higher molar yields than the process presented in Chapter 2.4, whereas the space-time yields were comparable for 6HA production. These differences can be mainly attributed to the lower toxicity and volatility of the substrate cyclohexanol, which leads to higher catalyst stability.

Fermentative, as well as biotransformation concepts, are available for nylon monomer synthesis and start from fossil resources (e.g., cyclohexane) or renewables (e.g. lignin monomers, sugars, fatty acids) (Table 3.2). *Cis,cis*-muconic acid, which can be hydrogenated to AA, is of special interest. Biotransformations reached titers of up to  $34.5 \text{ g L}^{-1}$  (Vardon *et al.*, 2016) and a high yield on biocatalyst (Kohlstedt *et al.*, 2018). Although the productivity remained below  $0.3 \text{ g L}^{-1} \text{ h}^{-1}$ , molar yields of 90 % and higher could also be reached by continuous cultivation (Van Duuren *et al.*, 2011b). Fermentative *cis,cis*-muconic acid synthesis reached an 18-fold higher titer and 25-fold higher space-time yield with glucose as substrate compared to glycerol (Niu *et al.*, 2002; Zhang *et al.*, 2015). Direct synthesis of C5- or C6 nylon monomers has been demonstrated as well. Fermentative 6AHA synthesis, however, suffered from very low titers and space-time yields below  $0.01 \text{ g L}^{-1} \text{ h}^{-1}$  (Turk *et al.*, 2016). However, the synthesis of the amine 5-aminovalerate employing recombinant *E. coli* reached one of the highest titers and space-time yields with almost quantitative yields on the substrate (Park *et al.*, 2014). AA synthesis via biotransformation from cyclohexane (Chapter 2.6) allowed a 4-fold higher titer and 50-fold increased productivities than 4-hydroxybenzoic acid as substrate (Niu *et al.*, 2002). The

highest AA titers were achieved in fermentations of glycerol, however, in a complex medium (Zhao *et al.*, 2018; Zhou *et al.*, 2020b). The biotechnological production of long-chain nylon monomers from renewable fatty acid methyl esters with a titer of 8 g L<sup>-1</sup> and moderate yields on biocatalyst was developed by Ladkau *et al.* (2016). Interestingly, the substrate dodecanoic acid methyl ester was also employed as a constituent of the second organic phase explaining the relatively low molar yield. A benchmarking study for nylon 11 monomer synthesis has been published recently by Kim *et al.* (2020). An *E. coli* mixed-species concept and *in situ*-product removal enabled titers of above 50 g L<sup>-1</sup> resulting in the highest yields on biocatalyst and productivities reported so far. The authors could successfully isolate all three monomers and separate them from the by-product n-heptanoic acid with a purity of at least 70 %.

Until now, none of these concepts have been transferred to industry except for 12-aminododecanoic acid synthesis, where a pilot-plant was installed by Evonik Industries (EVONIK Industries AG, 2013). The diverse monomer synthesis concept available until now require an evaluation of process parameters to assess their feasibility on industrial scale.

**Table 3.2:** Comparison of selected process performance parameters of multi-step whole-cell biocatalytic monomer production processes in bioreactors at a scale of at least 0.5 L.

Polymer	Substrate	Product	Type of reaction <sup>a</sup>	Reaction time [h]	Scale [L]	Titler [g L <sup>-1</sup> ]	Yield [g product gbiocatalyst <sup>-1</sup> ]	Space-time yield [g L <sup>-1</sup> h <sup>-1</sup> ]	Molar yield [%]	Reference
Polyurethane	glucose	1,4-butanediol	F	120	1	18	n.c. <sup>b</sup>	0.15	n.c.	Yim <i>et al.</i> (2011)
	diff. sugars	itaconic acid <sup>c</sup>	F	4 days	n.a.	71	n.c.	1	n.c.	Willke <i>et al.</i> (2001)
Polyester	cyclohexanol	$\epsilon$ -CL	B	19	0.5	21.1	0.59	1.11	90	Srinivas. <i>et al.</i> (2020)
		6HA	B	70	0.5	22.2	0.77	0.32	81	Srinivas. <i>et al.</i> (2019)
	cyclohexane	B	8	8	1	3.3	0.40	0.41	4	Chapter 2.4
	catechol	B	85	30	25	2.6	0.29	0.28	>90	Kohlstedt <i>et al.</i> (2018)
	benzoate	B	124	8	34.5	n.c.	0.28	0.17	100	Vardon <i>et al.</i> (2016)
	p-coumarate	B	78.5	0.7	13.5	n.c.	0.17	0.17	67	Vardon <i>et al.</i> (2015)
Nylon 6,6	benzoate	cis,cis-muconic acid	B	25	0.75 <sup>d</sup>	n.a.	n.a.	n.a.	89	Van D. <i>et al.</i> (2011)
	glucose		F	48	2	36.8	n.c.	0.77	22	Niu <i>et al.</i> (2002)
	glycerol		F <sup>e</sup>	72	0.7	2	n.c.	0.03	10	Zhang <i>et al.</i> (2015)
	4-hydroxy benzoic acid		B	144	1	2.5	n.c.	0.02	17	Niu <i>et al.</i> (2020)
	cyclohexane	AA	B	8	1	10.2	1.12	1.28	9	Chapter 2.6
Nylon 6,5	L-lysine	5-amino-valeric acid	F	144	5	57.6	n.c.	0.4	n.c.	Zhou <i>et al.</i> (2020)
			F	100	5	68.0	n.c.	0.68	33	Zhao <i>et al.</i> (2018)
			B	24	1.8	48.0	n.c.	2.0	95	Park <i>et al.</i> (2014)
Nylon 6	glucose	6AHA	F	52	10	0.02	n.c.	<0.01	n.c.	Türk <i>et al.</i> (2016)
Nylon 12	dodecanic acid methyl ester <sup>9</sup>	12-aminododecanoic acid	B	123	15	8	ca. 0.6	0.34	4	Ladkau (2015)
Nylon 11	Ricinoleic acid	11-hydroxyundecanoic acid	B	18	1.5	51.0	2.10	4.66	84	Kim <i>et al.</i> (2020)
			B <sup>e</sup>	36	1.5	46.2	1.57	2.18	83	Kim <i>et al.</i> (2020)
			B <sup>e</sup>	38	1.5	47.1	1.59	2.09	80	Kim <i>et al.</i> (2020)



Table footnotes (previous page):

<sup>a</sup> F: fermentation; B: biotransformation

<sup>b</sup> n.c.: not calculable

<sup>c</sup> process commercialized by Pfizer

<sup>d</sup> continuous cultivation in chemostat

<sup>e</sup> mixed-species cultivation of different *E. coli* strains

<sup>f</sup> cultivation and reaction are carried out in complex medium with additional glycerol supply

<sup>g</sup> two-liquid phase cultivation: 5 L organic phase with 75 % dodecanoic acid methyl ester

### 3.6 Limitations of biotechnological monomer production for industrial applications

Biocatalytic processes transferred to industry reached titers of 50-100 g L<sup>-1</sup>, average productivities of 15 g L<sup>-1</sup> h<sup>-1</sup>, and yields above 80 % (Straathof *et al.*, 2002). Whereas titers and yields close to these limits were already achieved, especially productivities need to be enhanced at least 10-fold to meet these requirements (Table 3.2).

Due to these reactions' multi-step character, the **accumulation of intermediate/side products** is a significant factor limiting titer, yield, and productivity. Zhang *et al.* (2015) only achieved 15 % of the calculated maximal yield because of the accumulation of pathway intermediates and insufficient channeling of glycerol towards *cis,cis*-muconic acid. Fermentations generally result in lower yields (Table 3.2) because of the trade-off between cell growth and product formation. However, the *cis,cis*-muconic acid yield from glucose could be theoretically doubled (43 to 83 %) by engineering phosphoenolpyruvate-independent glucose uptake systems or greatly enhanced (to 71 %) by using alternative substrates, e.g., D-xylose (Niu *et al.*, 2002). Similarly, acetic acid production from glucose due to the crabtree effect resulted in low AA titers, which was completely prevented with glycerol as a carbon source (Zhou *et al.*, 2020b). Park *et al.* (2014) could increase the 5-aminovalerate yield from L-lysine by supplementing the feed with glucose to fulfill the cells' nutritional needs. In biotransformations, the substrate could theoretically be fully converted to the product, which was possible for *cis,cis*-muconic acid production from aromatics (Vardon *et al.*, 2016; Kohlstedt *et al.*, 2018). Extensive side-product accumulation of 69 % (Niu *et al.*, 2020) and over 90 % (Turk *et al.*, 2016) limited AA and 6AHA titers. One straight-forward approach is the choice of chemoselective enzymes (Kim *et al.* (2020), Chapters 2.3, 2.5, and 2.6). Strain development and process optimizations have the potential to allow increased conversion and selectivities. Vardon *et al.* (2015) demonstrated that the deletion of the transcriptional regulator CatR prevented further metabolism of *cis,cis*-muconic acid by *P. putida*. Side-product formation by the strains developed in this thesis could be prevented by balancing the protein ratios and therefore activities through targeted genetic engineering (Chapters 2.3 and 2.6). A similar approach was followed by Zhou *et al.* (2020b), who employed strong promoter-5'-UTR complexes to vary the gene expression of the AA synthesis pathway. The deletion of 6 genes could also double the AA titer to prevent the formation of the by-products lactic acid and butyric acid. Such engineering can be facilitated by systems biology to identify bottlenecks and degradation pathways (Yim *et al.*, 2011).

The productivity can be enhanced by increasing the **specific activity of the biocatalyst**. Niu *et al.* (2020) found that the cofactor NADH/NADPH availability limited the specific activity, which could be

enhanced by reducing the aeration rate. The introduction of a cofactor regeneration system enhanced whole-cells' catalytic activities by 50 % (Kim *et al.*, 2020). The engineering of a self-sustainable cascade reaction makes such additions dispensable (Srinivasamurthy *et al.*, 2019). In Chapter 2.6, efficient NAD<sup>+</sup> recycling via respiration was accomplished by glucose excess during the biotransformation. In addition, it would be interesting to investigate chassis organisms where unnecessary elements are deleted so that reduction equivalents can be used more efficiently. Especially in large-scale reactors, the reactor geometry, power input, and aeration play an important role in ensuring efficient mass transfer, which was found to limit whole-cell activity for 12-aminododecanoic acid production (Ladkau, 2015). Optimization of oxygen mass transfer under high cell loading enabled almost complete cyclohexanol conversion (Srinivasamurthy *et al.*, 2020). In this thesis, it has been found that the choice of the medium and the physiological state (e.g., glucose excess) can influence whole-cell activity (Chapters 2.4 and 2.6).

The **stability of the biocatalyst** directly influences the process time and, therefore, the final titer. Maintaining high activities over time might be the greatest challenge in biocatalysis. Ladkau (2015) discussed that biocatalyst destabilization might occur due to the incorporation of large amounts of heterologous enzymes into the inner (AlkB and AlkJ) and outer cell membrane (AlkL), which could be one reason of decreasing 12-aminododecanoic acid methyl ester formation activities. Kim *et al.* (2020) identified the Baeyer-Villiger monooxygenase as the limiting enzyme whose catalytic efficiency could be doubled by fusion with the maltose-binding protein leading to 1.3-fold higher titers of 11HA. Srinivasamurthy *et al.* (2020) tested different CHMO variants and could double the operational stability and increase oxidative stability. *In situ*- by-product removal of n-heptanoic acid and pyruvate (ca. 67 % of the total product) by an adsorbent resin alleviated their inhibition (Kim *et al.*, 2020). Product inhibition by  $\epsilon$ -CL could be circumvented by its hydrolysis to 6HA employing CAL-B, leading to a 2-fold higher substrate conversion (Srinivasamurthy *et al.*, 2019) similar as the intracellular hydrolase application in this thesis (Chapter 2.3). The toxification of the biocatalyst by the substrate cyclohexane can be considered the primary cause for decreasing whole-cell activities over time, which requires fine-tuned supply below the toxic range (Chapters 2.4 and 2.6) or more solvent-tolerant strains (Volmer *et al.*, 2014; Wynands *et al.*, 2019). Additionally, protein instability, especially of rate-limiting enzymes like Cyp, needs to be overcome (e.g., by protein engineering) to ensure longer process times (Chapter 2.6). Biorenewable and fossil resources are employed as **substrates** for monomer synthesis (Table 3.2). Their price needs to be significantly lower than the current monomer price, which is 2.45 \$ kg<sup>-1</sup> for AA (Straathof & Bampouli, 2017). The crude oil constituent benzene can be quickly reacted to cyclohexane with a selling price of 1.37 \$ kg<sup>-1</sup> (Straathof & Bampouli, 2017). It does not require the energy-intensive hydroxylation to cyclohexanol, which has a lower (per pass) conversion of 8-10 %, and several downstream units to separate cyclohexanol from the unreacted cyclohexane and the overoxidation product cyclohexanone (Fischer *et al.*, 2010). The use of oil in plastics is also considered sustainable due to most plastics' oil-like energy content (Mülhaupt, 2013). However, their price depends on the availability of crude oil and its market price. Ricinoleic acid is obtained from the castor plant, which grows slowly and requires labor-intensive purification (Patel *et al.*, 2016) so that it is sold at 2 \$ kg<sup>-1</sup> (PharmaCompass, 2020). The manufacturing costs of AA from D-glucose (0.5 \$ kg<sup>-1</sup>, Kuhn *et al.* (2012b)) were estimated to be 2.46 \$ kg<sup>-1</sup> (Niu *et al.*, 2002). Park *et al.* (2014) calculated that commercialization of their 5-aminovalerate process with *E. coli* is

also limited by the feedstock cost (L-lysine: 1-2 \$ kg<sup>-1</sup>). An alternative is its *in situ* provision, e.g., by co-cultivation with an engineered L-lysine-producing *C. glutamicum* strain growing on the cheaper substrate glucose. The utilization of bio-based feedstocks for chemical production competes with the food industry, possibly leading to higher food prices (Mülhaupt, 2013). A sustainable way would be to utilize waste streams e.g. glycerol or lignin from bioethanol refineries (Quispe *et al.*, 2013; Corona *et al.*, 2018). Until now, only heterotrophic processes relying on an expensive organic carbon source (e.g. glucose) for cell growth/ cofactor supply were developed. The costs could be reduced by co-cultivation with phototrophic organisms providing the organic carbon source (Hoschek *et al.*, 2019a) or implementation of such reactions in phototrophs (Straathof & Bampouli, 2017; Hoschek *et al.*, 2019b).

However, not only the process itself needs to be considered, but also **downstream costs**. Purification of the relatively insoluble products AA and *cis,cis*-muconic acid is more economical (Vardon *et al.*, 2016; Wang *et al.*, 2020) compared to 1,4-butanediol with a high water solubility and a high boiling point (Pellis *et al.*, 2016). For sugar-derived fermentation acids (e.g., succinic acid), the separation process accounts for 60 % of the final cost (Bechthold *et al.*, 2008). Although the hydrogenation of *cis,cis*-muconic acid to AA has almost quantitative yields (Niu *et al.*, 2002; Beerthuis *et al.*, 2015), it requires additional unit operations (second purification and additional chemical reactor). Therefore, it poses additional costs (Niu *et al.*, 2020), which is not the case when the monomer can be directly produced in one step (Pellis *et al.*, 2016).

In the end, a **life-cycle assessment (LCA)** considering economic and ecological feasibility of the different processes needs to be conducted to identify factors that require further improvement. Such LCA has been conducted for AA synthesis from aromatics via *cis,cis*-muconic acid (Van Duuren *et al.*, 2011a; Corona *et al.*, 2018). It has been found that lignin-derived phenol as substrate can reduce the cumulative energy demand (CED) up to 60 % compared to petrochemical benzoic acid or toluene (Van Duuren *et al.*, 2011a). However, 85 % of the CED can be attributed to hydrogenation, so that this step has a high environmental impact. Further improvements in specific activity and volumetric productivity are necessary - ideally with biomass recycling. Bio-based AA can reduce greenhouse emissions by 70 % compared to the conventional process (Wittcoff *et al.*, 2012), with the additional benefit of dramatically reduced N<sub>2</sub>O emissions (Corona *et al.*, 2018). When lignin is used as a feedstock, a critical parameter is the lignin depolymerization requiring harsh conditions (NaOH and heat), which needs to be optimized. Additionally, the engineering of more acid-tolerant microbes could significantly reduce NaOH supply during the biotransformation. Such an analysis is lacking for biocatalytic  $\epsilon$ -CL, 6HA, AA, and 6AHA production, but is necessary to evaluate and compare these different concepts.

### 3.7 Conclusion

Traditional monomer and polymer production processes rely on fossil fuels. They pose severe environmental concerns due to the generation of toxic waste, high temperatures and pressures, and low conversion and selectivities. Consequently, there is a demand for more sustainable production routes, ideally as a one-step process. Biotechnological whole-cell catalysis offers such an option by implementing multi-step pathways in one microbial whole-cell biocatalyst. In this thesis, such a concept was developed to produce the polymer precursors  $\epsilon$ -CL, 6HA, 6AHA, and AA from cyclohexane.

The enzymatic cascades were rationally assembled based on enzyme characteristics via *in vivo* gene expression and protein synthesis in the host *P. taiwanensis* VLB120. For that, different genetic engineering tools were applied to find the optimal expression system. Additionally, the enzymes were characterized *in vivo* and partially *in vitro* to enable the establishment of streamlined cascades that do not accumulate any intermediate compounds. A systematic approach to design *in vivo* cascades was followed involving physiology analysis and reaction engineering. This enabled the first biocatalytic AA synthesis from cyclohexane in only one host. The concept could be successfully scaled to a 1 L bioreactor allowing the isolation of 3.4 g AA (96 % purity based on HPLC analysis). 6AHA synthesis from cyclohexane was never shown before and could be accomplished by developing a co-culture concept with *E. coli* and *P. taiwanensis* VLB120.

Loss of cyclohexane (70-90 %) via the offgas cannot be prevented with the applied aeration-based feeding technique making a recycling of the gas-stream necessary. This and a stabilization of the whole-cell catalyst potentially via sophisticated substrate feeding strategies will pave the way to enhance final titers. Also, down-stream processing of AA requires further improvement to increase the recovery and purity of the final product.

Biotechnological monomer production is not a new concept and has been investigated employing different bacterial hosts and substrates. Most approaches use bio-renewable feedstocks such as carbohydrates or lignin-derived aromatics, but suffer from low titers or require further abiotic steps. A life-cycle assessment of these different concepts is necessary to identify bottlenecks and improve current processes. Such an analysis will show if it is sustainable to use fossil fuels in biotechnological applications.

The concepts developed in this thesis can also be adapted for other polymer building blocks or value-added compounds. In general, one-pot whole-cell biocatalytic syntheses have enormous potential to reduce capital and operational expenditures, thereby contributing to greener production routes, which gain more importance in times of climate change and global warming.

## References

- Aalbers, F.S. & Fraaije, M.W. (2017). *Applied Microbiology and Biotechnology*, 101(20):7557–7565.
- Abdel-Rahman, M.A., Xiao, Y., Tashiro, Y., Wang, Y., Zendo, T., Sakai, K., & Sonomoto, K. (2015). *Journal of Bioscience and Bioengineering*, 119(2):153–158.
- Alini, S., Basile, F., Blasioli, S., Rinaldi, C., & Vaccari, A. (2007). *Applied Catalysis B: Environmental*, 70(1-4):323–329.
- Alper, H., Fischer, C., Nevoigt, E., & Stephanopoulos, G. (2005). *Proceedings of the National Academy of Sciences of the United States of America*, 102(36):12678–12683.
- Alper, H., Moxley, J., Nevoigt, E., Fink, G.R., & Stephanopoulos, G. (2006). *Science*, 314(5805):1565–1568.
- Alper, H. & Stephanopoulos, G. (2007). *Metabolic Engineering*, 9(3):258–267.
- Alphand, V., Carrea, G., Wohlgemuth, R., Furstoss, R., & Woodley, J.M. (2003). *Trends in Biotechnology*, 21(7):318–323.
- Anastas, P. & Eghbali, N. (2010). *Chemical Society Reviews*, 39(1):301–312.
- Anastas, P.T. & Warner, J.C. (1998). *Frontiers*, 640.
- Anderson, J.C., Dueber, J.E., Leguia, M., Wu, G.C., Goler, J.A., Arkin, A.P., & Keasling, J.D. (2010). *Journal of Biological Engineering*, 4:1.
- Aparicio, T., de Lorenzo, V., & Martínez-García, E. (2019). *Biotechnology Journal*, 14(1):1800483.
- Arnold, F.H. (1998). *Accounts of Chemical Research*, 31(3):125–131.
- Arpadis (2020). Accessed: 24.09.2020, <https://www.arpadis.com/adipic-acid/>.
- Averesch, N.J., Martínez, V.S., Nielsen, L.K., & Kromer, J.O. (2018). *ACS Synthetic Biology*, 7(2):490–509.
- Bagdasarian, M., Lurz, R., Rückert, B., Franklin, F., Bagdasarian, M., Frey, J., & Timmis, K. (1981). *Gene*, 16(1-3):237–247.
- Balke, K., Beier, A., & Bornscheuer, U.T. (2018). *Biotechnology Advances*, 36(1):247–263.
- Baneyx, F. & Mujacic, M. (2004). *Nature Biotechnology*, 22(11):1399–1408.
- Bart, J.C. & Cavallaro, S. (2015a). *Industrial & Engineering Chemistry Research*, 54(1):1–46.
- Bart, J.C. & Cavallaro, S. (2015b). *Industrial Engineering Chemistry Research*, 54(2):567–576.
- Baumgart, M., Unthan, S., Rückert, C., Sivalingam, J., Grünberger, A., Kalinowski, J., Bott, M., Noack, S., & Frunzke, J. (2013). *Applied and Environmental Microbiology*, 79(19):6006–6015.
- Bayer, T., Milker, S., Wiesinger, T., Rudroff, F., & Mihovilovic, M.D. (2015). *Advanced Synthesis & Catalysis*, 357(8):1587–1618.
- Bechthold, I., Bretz, K., Kabasci, S., Kopitzky, R., & Springer, A. (2008). *Chemical Engineering & Technology*, 31(5):647–654.
- Beerthuis, R., Rothenberg, G., & Shiju, N.R. (2015). *Green Chemistry*, 17(3):1341–1361.

## References

---

- Bellussi, G. & Perego, C. (2000). *Cattech*, 4(1):4–16.
- Bernstein, H.C. & Carlson, R.P. (2012). *Computational and Structural Biotechnology Journal*, 3(4):e201210017.
- Biggs, B.W., De Paepe, B., Santos, C.N.S., De Mey, M., & Ajikumar, P.K. (2014). *Current Opinion in Biotechnology*, 29:156–162.
- Biggs, B.W., Lim, C.G., Sagliani, K., Shankar, S., Stephanopoulos, G., De Mey, M., & Ajikumar, P.K. (2016). *Proceedings of the National Academy of Sciences of the United States of America*, 113(12):3209–3214.
- Binder, M., Albrecht, S., Marincovic, C., Baer, S., McGavis, D., & Harless, D. (2010). *Poster presented at the Life Cycle Assessment X: Bridging Science, Policy, and the Public, Portland, Oregon.*
- Blank, L.M., Ebert, B.E., Buehler, K., & Bühler, B. (2010). *Antioxidants & Redox Signaling*, 13(3):349–394.
- Blank, L.M., Ebert, B.E., Bühler, B., & Schmid, A. (2008a). *Biotechnology and Bioengineering*, 100(6):1050–1065.
- Blank, L.M., Ionidis, G., Ebert, B.E., Bühler, B., & Schmid, A. (2008b). *FEBS Journal*, 275(20):5173–5190.
- Bock, E. & Wagner, M. (2006). volume 2, p. 457–495. 3rd edition. Springer, New York, NY.
- Bornscheuer, U., Huisman, G., Kazlauskas, R.J., Lutz, S., Moore, J., & Robins, K. (2012). *Nature*, 485(7397):185–194.
- Bradford, M.M. (1976). *Analytical Biochemistry*, 72(1-2):248–254.
- Braun, D. & Collin, G. (2010). *Chemie in unserer Zeit*, 44(3):190–197.
- Braun, M., Levy, A., & Sifniades, S. (1999). *Polymer-Plastics Technology and Engineering*, 38(3):471–484.
- Bretschneider, L., Wegner, M., Bühler, K., Bühler, B., & Karande, R. (2021). *Microbial Biotechnology*, 14(3):1011–1025.
- Breuer, M., Ditrich, K., Habicher, T., Hauer, B., Keßeler, M., Stürmer, R., & Zelinski, T. (2004). *Angewandte Chemie International Edition*, 43(7):788–824.
- Buch, A., Archana, G., & Kumar, G.N. (2008). *Research in Microbiology*, 159(9-10):635–642.
- Buchner, E. (1897). *Berichte der deutschen chemischen Gesellschaft*, 30(1):117–124.
- Bühler, B., Bollhalder, I., Hauer, B., Witholt, B., & Schmid, A. (2003). *Biotechnology and Bioengineering*, 81(6):683–694.
- Bühler, B., Park, J.B., Blank, L.M., & Schmid, A. (2008). *Applied and Environmental microbiology*, 74(5):1436–1446.
- Bühler, B. & Schmid, A. (2004). *Journal of Biotechnology*, 113(1-3):183–210.
- Casey, G.P. & Ingledew, W.M. (1986). *CRC Critical Reviews in Microbiology*, 13(3):219–280.
- Chaudhry, W.N., Jamil, N., Ali, I., Ayaz, M.H., & Hasnain, S. (2011). *Annals of Microbiology*, 61(3):623–629.
- Chavarría, M., Nikel, P.I., Pérez-Pantoja, D., & de Lorenzo, V. (2013). *Environmental Microbiology*, 15(6):1772–1785.
- ChemSpider (2020). Accessed: 14.10.2020, <http://www.chemspider.com/Chemical-Structure.7787.html>.
- Chen, R.R. (2007). *Applied Microbiology and Biotechnology*, 74(4):730–738.
- Chen, X., Li, S., & Liu, L. (2014). *Trends in Biotechnology*, 32(6):337–343.
- Chen, Z., Sun, X., Li, Y., Yan, Y., & Yuan, Q. (2017). *Metabolic Engineering*, 39:102–109.
- Cheong, S., Clomburg, J.M., & Gonzalez, R. (2016). *Nature Biotechnology*, 34(5):556.

- Chierogato, A., Basile, F., Concepción, P., Guidetti, S., Liosi, G., Soriano, M.D., Trevisanut, C., Cavani, F., & Nieto, J.M.L. (2012). *Catalysis Today*, 197(1):58–65.
- Choi, K.H. & Schweizer, H.P. (2006). *Nature Protocols*, 1:153–161.
- Clomburg, J.M., Blankschien, M.D., Vick, J.E., Chou, A., Kim, S., & Gonzalez, R. (2015). *Metabolic Engineering*, 28:202–212.
- Collins, A.M., Woodley, J.M., & Liddell, J.M. (1995). *Journal of Industrial Microbiology*, 14(5):382–388.
- Collins, J., Grund, M., Brandenbusch, C., Sadowski, G., Schmid, A., & Bühler, B. (2015). *Journal of Industrial Microbiology and Biotechnology*, 42(7):1011–1026.
- Cook, T.B., Rand, J.M., Nurani, W., Courtney, D.K., Liu, S.A., & Pfeleger, B.F. (2018). *Journal of Industrial Microbiology & Biotechnology*, 45(7):517–527.
- Cornelissen, S., Julsing, M.K., Volmer, J., Riechert, O., Schmid, A., & Bühler, B. (2013). *Biotechnology and bioengineering*, 110(5):1282–1292.
- Corona, A., Bidy, M.J., Vardon, D.R., Birkved, M., Hauschild, M.Z., & Beckham, G.T. (2018). *Green Chemistry*, 20(16):3857–3866.
- Cowan, S., Schirmer, T., Rummel, G., Steiert, M., Ghosh, R., Pauptit, R., Jansonius, J., & Rosenbusch, J. (1992). *Nature*, 358(6389):727–733.
- Croughan, M.S., Konstantinov, K.B., & Cooney, C. (2015). *Biotechnology and Bioengineering*, 112(4):648–651.
- Csörgő, B., Fehér, T., Tímár, E., Blattner, F.R., & Pósfai, G. (2012). *Microbial cell factories*, 11(1):11.
- de Bont, J.A. (1998). *Trends in Biotechnology*, 16(12):493–499.
- de Carvalho, C.C. (2017). *Microbial Biotechnology*, 10(2):250–263.
- Del Castillo, T., Ramos, J.L., Rodríguez-Herva, J.J., Fuhrer, T., Sauer, U., & Duque, E. (2007). *Journal of Bacteriology*, 189(14):5142–5152.
- Delgove, M.A., Elford, M.T., Bernaerts, K.V., & De Wildeman, S.M. (2018). *Journal of Chemical Technology & Biotechnology*, 93(8):2131–2140.
- Denard, C.A., Hartwig, J.F., & Zhao, H. (2013). *ACS Catalysis*, 3(12):2856–2864.
- Denyer, S.P. & Maillard, J. (2002). *Journal of Applied Microbiology*, 92(s1):35S–45S.
- Donoghue, N.A. & Trudgill, P.W. (1975). *European Journal of Biochemistry*, 60(1):1–7.
- Dos Santos, V.M., Heim, S., Moore, E., Strätz, M., & Timmis, K. (2004). *Environmental Microbiology*, 6(12):1264–1286.
- Dros, A., Larue, O., Reimond, A., De Campo, F., & Pera-Titus, M. (2015). *Green Chemistry*, 17(10):4760–4772.
- Drumright, R.E., Gruber, P.R., & Henton, D.E. (2000). *Advanced Materials*, 12(23):1841–1846.
- Du, C. & Webb, C. (2011). volume 2, book section 2.03, p. 11–23. Academic Press, Oxford.
- Ducat, D.C., Way, J.C., & Silver, P.A. (2011). *Trends in Biotechnology*, 29(2):95–103.
- EVONIK Industries AG (2013). Accessed: 07.03.2021, <https://www.vestamid.com/media/pressattachments/c239/n37328/a17972.pdf>.
- Farasat, I., Kushwaha, M., Collens, J., Easterbrook, M., Guido, M., & Salis, H.M. (2014). *Molecular Systems Biology*, 10(6):731.

## References

---

- Fedorchuk, T.P., Khusnutdinova, A.N., Evdokimova, E., Flick, R., Di Leo, R., Stogios, P., Savchenko, A., & Yakunin, A.F. (2019). *Journal of the American Chemical Society*, 142(2):1038–1048.
- Fischer, J., Lange, T., Boehling, R., Rehfinger, A., & Klemm, E. (2010). *Chemical Engineering Science*, 65(16):4866–4872.
- Flickinger, M. C. (ed.) (2013). John Wiley & Sons Inc., Hoboken, New Jersey.
- France, S.P., Hepworth, L.J., Turner, N.J., & Flitsch, S.L. (2017). *ACS Catalysis*, 7(1):710–724.
- Gao, Y., Sim, K., Yan, X., Jiang, J., Xie, J., & Yu, C. (2017). *Scientific Reports*, 7(1):947.
- Garcia-Junceda, E. (2008). WILEY-VCH Verlag GmbH & Co. KGaA, Weinheim.
- Geyer, R., Jambeck, J.R., & Law, K.L. (2017). *Science Advances*, 3(7):e1700782.
- Gibson, D.G., Young, L., Chuang, R.Y., Venter, J.C., Hutchison, C.A., & Smith, H.O. (2009). *Nature Methods*, 6(5):343–345. 10.1038/nmeth.1318.
- Graedel, T.E. (2002). book section 4, p. 56–61. Blackwell Science Ltd., Oxford.
- Grant, C., Deszcz, D., Wei, Y.C., Martinez-Torres, R.J., Morris, P., Folliard, T., Sreenivasan, R., Ward, J., Dalby, P., & Woodley, J.M. (2014). *Scientific Reports*, 4:5844.
- Gross, R.A. & Kalra, B. (2002). *Science*, 297(5582):803–807.
- Halan, B., Schmid, A., & Buehler, K. (2010). *Biotechnology and Bioengineering*, 106(4):516–527.
- Hanahan, D. (1983). *Journal of Molecular Biology*, 166(4):557–580.
- Hancock, R., Siehnel, R., & Martin, N. (1990). *Molecular Microbiology*, 4(7):1069–1075.
- Harder, W. & Dijkhuizen, L. (1983). *Annual Review of Microbiology*, 37(1):1–23.
- Heipieper, H.J., Neumann, G., Cornelissen, S., & Meinhardt, F. (2007). *Applied Microbiology and Biotechnology*, 74(5):961–973.
- Heuschkel, I., Hoschek, A., Schmid, A., Bühler, B., Karande, R., & Bühler, K. (2019). *MethodsX*, 6:1822–1831.
- Hewitt, C.J., Nebe-Von Caron, G., Nienow, A.W., & McFarlane, C.M. (1999). *Journal of Biotechnology*, 75(2-3):251–264.
- Hilker, I., Gutiérrez, M.C., Furstoss, R., Ward, J., Wohlgenuth, R., & Alphand, V. (2008). *Nature Protocols*, 3(3):546–554.
- Hoch, G. & Kok, B. (1963). *Archives of Biochemistry and Biophysics*, 101(1):160–170.
- Hoffmann, F. & Rinas, U. (2004). book section 3, p. 73–92. Series: Advances in Biochemical Engineering/Biotechnology. Springer-Verlag, Berlin/Heidelberg.
- Hong, J. & Xu, X. (2012). *Journal of Cleaner Production*, 27:103–108.
- Hoschek, A., Heuschkel, I., Schmid, A., Bühler, B., Karande, R., & Bühler, K. (2019a). *Bioresource Technology*, 282:171–178.
- Hoschek, A., Toepel, J., Hochkeppel, A., Karande, R., Bühler, B., & Schmid, A. (2019b). *Biotechnology Journal*, 14(8):1800724.
- Inoue, A. & Horikoshi, K. (1989). *Nature*, 338(6212):264–266.
- Iwamoto, M., Mizuno, S., & Tanaka, M. (2013). *Chemistry—A European Journal*, 19(22):7214–7220.



- Janssen, L. & Moscicki, L. (2009). WILEY-VCH Verlag GmbH & Co. KGaA, Weinheim.
- Jansson, I., Stoilov, I., Sarfarazi, M., & Schenkman, J.B. (2000). *Toxicology*, 144(1-3):211–219.
- Jenkins, A., Kratochvíl, P., Stepto, R., & Suter, U. (1996). *Pure and Applied Chemistry*, 68(12):2287–2311.
- Jeon, E.Y., Song, J.W., Cha, H.J., Lee, S.M., Lee, J., & Park, J.B. (2018). *Journal of Biotechnology*, 281:161–167.
- Jeschek, M., Gerngross, D., & Panke, S. (2016). *Nature Communications*, 7:11163.
- Jeschek, M., Gerngross, D., & Panke, S. (2017). *Current Opinion in Biotechnology*, 47:142–151.
- Jones, J.A., Vernacchio, V.R., Collins, S.M., Shirke, A.N., Xiu, Y., Englaender, J.A., Cress, B.F., McCutcheon, C.C., Linhardt, R.J., & Gross, R.A. (2017). *mBio*, 8(3):e00621–17.
- Jones, J.A., Vernacchio, V.R., Sinkoe, A.L., Collins, S.M., Ibrahim, M.H., Lachance, D.M., Hahn, J., & Koffas, M.A. (2016). *Metabolic Engineering*, 35:55–63.
- Jones, J.A. & Wang, X. (2018). *Current Opinion in Biotechnology*, 53:33–38.
- Julsing, M.K., Cornelissen, S., Bühler, B., & Schmid, A. (2008). *Current Opinion in Chemical Biology*, 12(2):177–186.
- Julsing, M.K., Kuhn, D., Schmid, A., & Bühler, B. (2012a). *Biotechnology and Bioengineering*, 109(5):1109–1119.
- Julsing, M.K., Schrewe, M., Cornelissen, S., Hermann, I., Schmid, A., & Bühler, B. (2012b). *Applied and Environmental Microbiology*, 78(16):5724–5733.
- Kadisch, M., Julsing, M.K., Schrewe, M., Jehmlich, N., Scheer, B., von Bergen, M., Schmid, A., & Bühler, B. (2017a). *Biotechnology and Bioengineering*, 114(4):874–884.
- Kadisch, M., Willrodt, C., Hillen, M., Bühler, B., & Schmid, A. (2017b). *Biotechnology Journal*, 12(8):1600170.
- Kafarski, P. (2012). *Chemik*, 66(8):811–6.
- Kalyanpur, M. (2002). *Molecular Biotechnology*, 22(1):87–98.
- Karande, R., Debor, L., Salamanca, D., Bogdahn, F., Engesser, K.H., Buehler, K., & Schmid, A. (2016). *Biotechnology and Bioengineering*, 113(1):52–61.
- Karande, R., Salamanca, D., Schmid, A., & Buehler, K. (2017). *Biotechnology and Bioengineering*, 115(2):312–320.
- Keasling, J.D. (2008). *ACS Chemical Biology*, 3(1):64–76.
- Khosravi-Darani, K. & Vasheghani-Farahani, E. (2005). *Critical Reviews in Biotechnology*, 25(4):231–242.
- Kim, T.H., Kang, S.H., Han, J.E., Seo, E.J., Jeon, E.Y., Choi, G.E., Park, J.B., & Oh, D.K. (2020). *ACS Catalysis*, 10(9):4871–4878.
- Kirmair, L. & Skerra, A. (2014). *Applied and Environmental Microbiology*, 80(8):2468–2477.
- Kittleson, J.T., Cheung, S., & Anderson, J. (2011). *Journal of Biological Engineering*, 5(1):10.
- Klemm, D., Heublein, B., Fink, H., & Bohn, A. (2005). *Angewandte Chemie International Edition*, 44(22):3358–3393.
- Kohl, A., Srinivasamurthy, V., Böttcher, D., Kabisch, J., & Bornscheuer, U.T. (2018). *Enzyme and Microbial Technology*, 108:53–58.
- Kohlstedt, M., Starck, S., Barton, N., Stolzenberger, J., Selzer, M., Mehlmann, K., Schneider, R., Pleissner, D., Rinkel, J., & Dickschat, J.S. (2018). *Metabolic Engineering*, 47:279–293.

## References

---

- Konovalova, A., Søgaard-Andersen, L., & Kroos, L. (2014). *FEMS Microbiology Reviews*, 38(3):493–522.
- Kratzer, R., Woodley, J.M., & Nidetzky, B. (2015). *Biotechnology Advances*, 33(8):1641–1652.
- Krauser, S., Weyler, C., Blaß, L.K., & Heinzle, E. (2013). p. 185–234. Springer-Verlag, Berlin/Heidelberg.
- Kruyer, N.S. & Peralta-Yahya, P. (2017). *Current Opinion in Biotechnology*, 45:136–143.
- Kuhn, D., Bühler, B., & Schmid, A. (2012a). *Journal of Industrial Microbiology & Biotechnology*, 39(8):1125–1133.
- Kuhn, D., Fritsch, F.S., Zhang, X., Wendisch, V.F., Blank, L.M., Bühler, B., & Schmid, A. (2013). *Journal of Biotechnology*, 163(2):194–203.
- Kuhn, D., Julsing, M.K., Heinzle, E., & Bühler, B. (2012b). *Green Chemistry*, 14(3):645–653.
- Kuhn, D., Kholiq, M.A., Heinzle, E., Bühler, B., & Schmid, A. (2010). *Green Chemistry*, 12(5):815–827.
- Köbbing, S., Blank, L.M., & Wierckx, N. (2020). *Frontiers in Bioengineering and Biotechnology*, 8:551.
- Köhler, K.A.K., Rückert, C., Schatschneider, S., Vorhölter, F.J., Szczepanowski, R., Blank, L.M., Niehaus, K., Goemann, A., Pühler, A., Kalinowski, J., & Schmid, A. (2013). *Journal of Biotechnology*, 168(4):729–730.
- Labet, M. & Thielemans, W. (2009). *Chemical Society Reviews*, 38(12):3484–3504.
- Ladkau, N. (2015). *Chemical Biotechnology*, volume 18. Shaker Verlag, Aachen.
- Ladkau, N., Assmann, M., Schrewe, M., Julsing, M.K., Schmid, A., & Bühler, B. (2016). *Metabolic Engineering*, 36:1–9.
- Ladkau, N., Schmid, A., & Bühler, B. (2014). *Current Opinion in Biotechnology*, 30:178–189.
- Laemmli, U.K. (1970). *Nature*, 227(5259):680–685.
- Lang, K., Zierow, J., Buehler, K., & Schmid, A. (2014). *Microbial Cell Factories*, 13(1):2.
- Leak, D.J., Sheldon, R.A., Woodley, J.M., & Adlercreutz, P. (2009). *Biocatalysis and Biotransformation*, 27(1):1–26.
- Lee, S.Y. & Kim, H.U. (2015). *Nature Biotechnology*, 33(10):1061–1072.
- Leive, L. (1974). *Annals of the New York Academy of Sciences*, 235(1):109–129.
- Lerchner, A., Achatz, S., Rausch, C., Haas, T., & Skerra, A. (2013). *ChemCatChem*, 5(11):3374–3383.
- Lewis, S.L. & Maslin, M.A. (2015). *Nature*, 519(7542):171–180.
- Li, S.Y., Srivastava, R., Suib, S.L., Li, Y., & Parnas, R.S. (2011). *Bioresource Technology*, 102(5):4241–4250.
- Lilly, M. (1982). *Journal of Chemical Technology and Biotechnology*, 32(1):162–169.
- Lin, B. & Tao, Y. (2017). *Microbial Cell Factories*, 16(1):106.
- Lindmeyer, M. (2016). *Chemical Biotechnology*, volume 24. Shaker Verlag, Aachen.
- Lin-Chao, S., Chen, W., & Wong, T. (1992). *Molecular Microbiology*, 6(22):3385–3393.
- Loper, J.E., Hassan, K.A., Mavrodi, D.V., & Davis, E.W. (2012). *PLoS Genetics*, 8(7):e1002784.
- Lye, G.J. & Woodley, J.M. (1999). *Trends in Biotechnology*, 17(10):395–402.
- Margaritis, A., Zajic, J., & Gerson, D. (1979). *Biotechnology and Bioengineering*, 21(7):1151–1162.
- Martínez-García, E., Aparicio, T., Goñi-Moreno, A., Fraile, S., & de Lorenzo, V. (2015). *Nucleic Acids Research*, 43(D1):D1183–D1189.

- Martínez-García, E. & de Lorenzo, V. (2011). *Environmental Microbiology*, 13(10):2702–2716.
- Martínez-García, E. & de Lorenzo, V. (2017). *Current Opinion in Biotechnology*, 47:120–132.
- Martínez-García, E., Nikel, P.I., Aparicio, T., & de Lorenzo, V. (2014). *Microbial Cell Factories*, 13(1):159.
- McIver, A.M., Garikipati, S.J., Bankole, K.S., Gyamerah, M., & Peeples, T.L. (2008). *Biotechnology Progress*, 24(3):593–598.
- Mecking, S. (2004). *Angewandte Chemie International Edition*, 43(9):1078–1085.
- Meyer, F., Goesmann, A., McHardy, A.C., Bartels, D., Bekel, T., Clausen, J., Kalinowski, J., Linke, B., Rupp, O., & Giegerich, R. (2003). *Nucleic Acids Research*, 31(8):2187–2195.
- Meyer, H.P. & Robins, K.T. (2005). *Monatshefte für Chemie/Chemical Monthly*, 136(8):1269–1277.
- Migula, W. (1895).
- Milker, S., Fink, M.J., Oberleitner, N., Rössmann, A.K., Mihovilovic, M., & Bornscheuer, U. (2017). *ChemCatChem*, 9:3420–3427.
- Moon, T.S., Dueber, J.E., Shiue, E., & Prather, K.L.J. (2010). *Metabolic Engineering*, 12(3):298–305.
- Moon, T.S., Yoon, S.H., Lanza, A.M., Roy-Mayhew, J.D., & Prather, K.L.J. (2009). *Applied and Environmental Microbiology*, 75(13):4660–4660.
- Morawetz, H. (1987). *Angewandte Chemie International Edition*, 26(2):93–97.
- Morlock, L.K., Böttcher, D., & Bornscheuer, U.T. (2018). *Applied Microbiology and Biotechnology*, 102(2):985–994.
- Mukherjee, S., Das, P., & Sen, R. (2006). *Trends in Biotechnology*, 24(11):509–515.
- Muschiol, J., Peters, C., Oberleitner, N., Mihovilovic, M.D., Bornscheuer, U.T., & Rudroff, F. (2015). *Chemical Communications*, 51(27):5798–5811.
- Musser, M.T. (2011). Wiley-VCH Verlag GmbH & Co. KGaA, Weinheim. [https://doi.org/10.1002/14356007.a08\\_217.pub2](https://doi.org/10.1002/14356007.a08_217.pub2).
- Ménil, S., Petit, J., Courvoisier-Dezord, E., Debar, A., Pellouin, V., Reignier, T., Sergent, M., Deyris, V., Duquesne, K., & de Berardinis, V. (2019). *Biotechnology and Bioengineering*, 116(11):2852–2863.
- Mülhaupt, R. (2004). *Angewandte Chemie International Edition*, 43(9):1054–1063.
- Mülhaupt, R. (2010). *Macromolecular Chemistry and Physics*, 211(2):121–126.
- Mülhaupt, R. (2013). *Macromolecular Chemistry and Physics*, 214(2):159–174.
- Müller, C.A., Weingartner, A.M., Dennig, A., Ruff, A.J., Gröger, H., & Schwaneberg, U. (2016). *Journal of Industrial Microbiology & Biotechnology*, 43(12):1641–1646.
- Müller, H.M. (1986). *Archives of Microbiology*, 144(2):151–157.
- Nakano, K., Rischke, M., Sato, S., & Märkl, H. (1997). *Applied Microbiology and Biotechnology*, 48(5):597–601.
- Ni, Y., Holtmann, D., & Hollmann, F. (2014). *ChemCatChem*, 6(4):930–943.
- Nicolaou, K. & Chen, J.S. (2009). *Chemical Society Reviews*, 38(11):2993–3009.
- Nicolaou, S.A., Gaida, S.M., & Papoutsakis, E.T. (2010). *Metabolic Engineering*, 12(4):307–331.
- Nikaido, H. (1994). *Science*, 264(5157):382–388.

## References

---

- Nikaido, H. (2003). *Microbiology and Molecular Biology Reviews*, 67(4):593–656.
- Nikel, P.I., Chavarria, M., Danchin, A., & de Lorenzo, V. (2016). *Current Opinion in Chemical Biology*, 34:20–29.
- Nikel, P.I., Martínez-García, E., & De Lorenzo, V. (2014). *Nature Reviews Microbiology*, 12(5):368–379.
- Niu, W., Draths, K., & Frost, J. (2002). *Biotechnology Progress*, 18(2):201–211.
- Niu, W., Willett, H., Mueller, J., He, X., Kramer, L., Ma, B., & Guo, J. (2020). *Metabolic Engineering*, 59:151–161.
- Norris, D. & Trudgill, P. (1971). *Biochemical Journal*, 121(3):363–370.
- Oberleitner, N., Peters, C., Muschiol, J., Kadow, M., Saß, S., Bayer, T., Schaaf, P., Iqbal, N., Rudroff, F., & Mihovilovic, M.D. (2013). *ChemCatChem*, 5(12):3524–3528.
- Otto, M., Wynands, B., Drepper, T., Jaeger, K.E., Thies, S., Loeschcke, A., Blank, L.M., & Wierckx, N. (2019). *ACS Synthetic Biology*, 8(8):1901–1912.
- Ozdayram, E.G., Kleinstuber, S., Nikolausz, M., Ince, B., & Ince, O. (2018). *Engineering in Life Sciences*, 18(7):440–446.
- Pakula, T.M., Salonen, K., Uusitalo, J., & Penttilä, M. (2005). *Microbiology*, 151(1):135–143.
- Palleroni, N., Kunisawa, R., Contopoulou, R., & Doudoroff, M. (1973). *International Journal of Systematic and Evolutionary Microbiology*, 23(4):333–339.
- Palleroni, N.J. (2010). *Environmental Microbiology*, 12(6):1377–1383.
- Panke, S., Held, M., Wubbolts, M.G., Witholt, B., & Schmid, A. (2002). *Biotechnology and Bioengineering*, 80(1):33–41.
- Panke, S., Meyer, A., Huber, C.M., Witholt, B., & Wubbolts, M.G. (1999). *Applied and Environmental Microbiology*, 65(6):2324–2332.
- Panke, S., Witholt, B., Schmid, A., & Wubbolts, M.G. (1998). *Applied and Environmental Microbiology*, 64(6):2032–2043.
- Park, J.B., Bühler, B., Panke, S., Witholt, B., & Schmid, A. (2007). *Biotechnology and Bioengineering*, 98(6):1219–1229.
- Park, S.J., Oh, Y.H., Noh, W., Kim, H.Y., Shin, J.H., Lee, E.G., Lee, S., David, Y., Baylon, M.G., & Song, B.K. (2014). *Biotechnology Journal*, 9(10):1322–1328.
- Patel, V.R., Dumancas, G.G., Viswanath, L.C.K., Maples, R., & Subong, B.J.J. (2016). *Lipid Insights*, 9:LPI–S40233.
- Pellis, A., Herrero Acero, E., Gardossi, L., Ferrario, V., & Guebitz, G.M. (2016). *Polymer International*, 65(8):861–871.
- Pennec, A., Hollmann, F., Smit, M.S., & Opperman, D.J. (2015a). *ChemCatChem*, 7(2):236–239.
- Pennec, A., Jacobs, C.L., Opperman, D.J., & Smit, M.S. (2015b). *Advanced Synthesis & Catalysis*, 357(1):118–130.
- Peralta-Yahya, P.P., Zhang, F., Del Cardayre, S.B., & Keasling, J.D. (2012). *Nature*, 488(7411):320–328.
- Pfleger, B.F., Pitera, D.J., Smolke, C.D., & Keasling, J.D. (2006). *Nature Biotechnology*, 24(8):1027–1032.
- PharmaCompass (2020). Accessed: 26.11.2020, <https://www.pharmacompass.com/price/ricinoleic-acid>.
- Phillips, T., Chase, M., Wagner, S., Renzi, C., Powell, M., DeAngelo, J., & Michels, P. (2013). *Journal of Industrial Microbiology and Biotechnology*, 40(5):411–425.
- PlasticsEurope (2020). Accessed: 19.11.2020, <https://www.plasticseurope.org/de/resources/publications/1804-plastics-facts-2019>.

- Poblete-Castro, I., Becker, J., Dohnt, K., Dos Santos, V.M., & Wittmann, C. (2012). *Applied Microbiology and Biotechnology*, 93(6):2279–2290.
- Poblete-Castro, I., Binger, D., Rodrigues, A., Becker, J., Dos Santos, V.A.M., & Wittmann, C. (2013). *Metabolic Engineering*, 15:113–123.
- Polen, T., Spelberg, M., & Bott, M. (2013). *Journal of Biotechnology*, 167(2):75–84.
- Qi, X.H., Zhu, J.F., Yun, J.H., Lin, J., Qi, Y.L., Guo, Q., & Xu, H. (2016). *Journal of Bioscience and Bioengineering*, 122(3):257–262.
- Quispe, C.A., Coronado, C.J., & Carvalho Jr, J.A. (2013). *Renewable and Sustainable Energy Reviews*, 27:475–493.
- Ramos, J.L., Duque, E., Gallegos, M.T., Godoy, P., Ramos-Gonzalez, M.I., Rojas, A., Terán, W., & Segura, A. (2002). *Annual Reviews in Microbiology*, 56(1):743–768.
- Registry of Standard Biological Parts (2019). Accessed: 19.11.2019, [http://parts.igem.org/Ribosome\\_Binding\\_Sites/Prokaryotic/Constitutive/Community\\_Collection](http://parts.igem.org/Ribosome_Binding_Sites/Prokaryotic/Constitutive/Community_Collection).
- Ricca, E., Brucher, B., & Schrittwieser, J.H. (2011). *Advanced Synthesis & Catalysis*, 353(13):2239–2262.
- Riesenber, D., Schulz, V., Knorre, W., Pohl, H.D., Korz, D., Sanders, E., Ross, A., & Deckwer, W.D. (1991). *Journal of Biotechnology*, 20(1):17–27.
- Ringborg, R.H. & Woodley, J. (2016). *Reaction Chemistry & Engineering*, 1(1):10–22.
- Rudroff, F. (2019). *Current Opinion in Chemical Biology*, 49:84–90.
- Sabra, W., Dietz, D., Tjahjajari, D., & Zeng, A. (2010). *Engineering in Life Sciences*, 10(5):407–421.
- Sabra, W. & Zeng, A.P. (2014). volume 1, book section 7, p. 205–238. 1st edition. Taylor & Francis Group, Boca Raton, FL.
- Saini, M., Chen, M.H., Chiang, C.J., & Chao, Y.P. (2015). *Metabolic Engineering*, 27:76–82.
- Salamanca, D. & Engesser, K.H. (2014). *Environmental Science and Pollution Research*, 21(22):12757–12766.
- Sambrook, J. & Russell, D.W. (2001). volume 2. Cold Spring Harbor Laboratory, Cold Spring Harbor, NY.
- Sander, R. (2015). *Atmospheric Chemistry and Physics*, 15(8):4399–4981.
- Sangster, J. (1997). *Solution Chemistry*, volume 2. John Wiley & Sons, Chichester.
- Sattler, J.H., Fuchs, M., Mutti, F.G., Grischek, B., Engel, P., Pfeffer, J., Woodley, J.M., & Kroutil, W. (2014). *Angewandte Chemie International Edition*, 53(51):14153–14157.
- Sawers, R.G. & Clark, D.P. (2004). *EcoSal Plus*, 1(1).
- Scherkus, C., Schmidt, S., Bornscheuer, U.T., Gröger, H., Kara, S., & Liese, A. (2016). *ChemCatChem*, 8(22):3446–3452.
- Scherkus, C., Schmidt, S., Bornscheuer, U.T., Gröger, H., Kara, S., & Liese, A. (2017). *Biotechnology and Bioengineering*, 114(6):1215–1221.
- Schewe, H., Kaup, B.A., & Schrader, J. (2008). *Applied Microbiology and Biotechnology*, 78(1):55–65.
- Schmid, A., Dordick, J., Hauer, B., Kiener, A., Wubbolts, M., & Witholt, B. (2001). *Nature*, 409(6817):258–268.
- Schmidt, S., Scherkus, C., Muschiol, J., Menyes, U., Winkler, T., Hummel, W., Gröger, H., Liese, A., Herz, H.G., & Bornscheuer, U.T. (2015). *Angewandte Chemie International Edition*, 54(9):2784–2787.

## References

---

- Schrewe, M., Julsing, M.K., Bühler, B., & Schmid, A. (2013a). *Chemical Society Reviews*, 42(15):6346–6377.
- Schrewe, M., Julsing, M.K., Lange, K., Czarnotta, E., Schmid, A., & Bühler, B. (2014). *Biotechnology and Bioengineering*, 111(9):1820–1830.
- Schrewe, M., Ladkau, N., Bühler, B., & Schmid, A. (2013b). *Advanced Synthesis & Catalysis*, 355(9):1693–1697.
- Schrittweiser, J.H., Sattler, J., Resch, V., Mutti, F.G., & Kroutil, W. (2011). *Current Opinion in Chemical Biology*, 15(2):249–256.
- Schrittweiser, J.H., Velikogne, S., Hall, M., & Kroutil, W. (2017). *Chemical Reviews*, 118(1):270–348.
- Schubeis, T., Le Marchand, T., Daday, C., Kopec, W., Movellan, K.T., Stanek, J., Schwarzer, T.S., Castiglione, K., de Groot, B.L., & Pintacuda, G. (2020). *Proceedings of the National Academy of Sciences of the United States of America*, 117(35):21014–21021.
- Serrano, M.C., Chung, E.J., & Ameer, G.A. (2010). *Advanced Functional Materials*, 20(2):192–208.
- Sheldon, R.A. (2012). *Chemical Society Reviews*, 41(4):1437–1451.
- Sheldon, R.A. (2018). *ACS Sustainable Chemistry & Engineering*, 6(1):32–48.
- Sheldon, R.A. & Woodley, J.M. (2018). *Chemical Reviews*, 118(2):801–838.
- Shimizu, A., Tanaka, K., & Fujimori, M. (2000). *Chemosphere-Global Change Science*, 2(3-4):425–434.
- Shizuya, H., Birren, B., Kim, U.J., Mancino, V., Slepak, T., Tachiiri, Y., & Simon, M. (1992). *Proceedings of the National Academy of Sciences of the United States of America*, 89(18):8794–8797.
- Siirola, E., Mutti, F.G., Grischek, B., Hoefler, S.F., Fabian, W.M., Grogan, G., & Kroutil, W. (2013). *Advanced Synthesis & Catalysis*, 355(9):1703–1708.
- Sikkema, J., De Bont, J., & Poolman, B. (1994). *Journal of Biological Chemistry*, 269(11):8022–8028.
- Silby, M.W., Winstanley, C., Godfrey, S.A., Levy, S.B., & Jackson, R.W. (2011). *FEMS Microbiology Reviews*, 35(4):652–680.
- Silhavy, T.J., Kahne, D., & Walker, S. (2010). *Cold Spring Harbor Perspectives in Biology*, 2(5):a000414.
- Silva, F., Queiroz, J.A., & Domingues, F.C. (2012). *Biotechnology Advances*, 30(3):691–708.
- Silva-Rocha, R., Martínez-García, E., Calles, B., Chavarría, M., Arce-Rodríguez, A., de las Heras, A., Páez-Espino, A.D., Durante-Rodríguez, G., Kim, J., Nikel, P.I., Platero, R., & de Lorenzo, V. (2013). *Nucleic Acids Research*, 41(D1):D666–D675.
- Simon, R.C., Richter, N., Busto, E., & Kroutil, W. (2013). *ACS Catalysis*, 4(1):129–143.
- Sinn, H.W. (2012). The MIT press, Cambridge, MA, London.
- Smanski, M.J., Bhatia, S., Zhao, D., Park, Y., Woodruff, L.B., Giannoukos, G., Ciulla, D., Busby, M., Calderon, J., & Nicol, R. (2014). *Nature Biotechnology*, 32(12):1241.
- Smolke, C.D., Carrier, T.A., & Keasling, J. (2000). *Applied and Environmental Microbiology*, 66(12):5399–5405.
- Spier, M.R., Vandenbergh, L., Medeiros, A.B.P., & Soccol, C.R. (2011). p. 55–90. Nova Science Publishers Inc., Hauppauge, NY.
- Srinivasamurthy, V.S., Böttcher, D., & Bornscheuer, U.T. (2019). *Zeitschrift für Naturforschung C*, 74(3-4):71–76.
- Srinivasamurthy, V.S., Böttcher, D., Engel, J., Kara, S., & Bornscheuer, U.T. (2020). *Process Biochemistry*, 88:22–30.

- Staudt, S., Burda, E., Giese, C., Müller, C.A., Marienhagen, J., Schwaneberg, U., Hummel, W., Drauz, K., & Gröger, H.** (2013). *Angewandte Chemie International Edition*, 52(8):2359–2363.
- Straathof, A.J.** (2011). volume 2, book section 2.57, p. 811–814. 2nd edition. Elsevier.
- Straathof, A.J. & Bampouli, A.** (2017). *Biofuels, Bioproducts and Biorefining*, 11(5):798–810.
- Straathof, A.J., Panke, S., & Schmid, A.** (2002). *Current Opinion in Biotechnology*, 13(6):548–556.
- Tanaka, H.** (1977). *Hakko Kogaku*, 55:62–67.
- Thaore, V., Chadwick, D., & Shah, N.** (2018). *Chemical Engineering Research and Design*, 135:140–152.
- Thomas, C.M., Cross, M.A., Hussain, A., & Smith, C.A.** (1984). *EMBO Journal*, 3(1):57–63.
- Timmis, K.N.** (2002). *Environmental Microbiology*, 4(12):779–781.
- Tiso, T., Wierckx, N., & Blank, L.** (2014). book section 10, p. 323–372. Series: Pan Stanford Series on Biocatalysis. CRC Press, Taylor & Francis Group, Boca Raton, FL.
- Tokiwa, Y., Calabia, B.P., Ugwu, C.U., & Aiba, S.** (2009). *International Journal of Molecular Sciences*, 10(9):3722–3742.
- Turk, S.C., Kloosterman, W.P., Ninaber, D.K., Kolen, K.P., Knutova, J., Suir, E., Schurmann, M., Raemakers-Franken, P.C., Muller, M., & de Wildeman, S.M.** (2016). *ACS Synthetic Biology*, 5(1):65–73.
- Turner, N.J. & O'Reilly, E.** (2013). *Nature Chemical Biology*, 9(5):285–288.
- Umenhoffer, K., Fehér, T., Balikó, G., Ayaydin, F., Pósfai, J., Blattner, F.R., & Pósfai, G.** (2010). *Microbial Cell Factories*, 9(1):38.
- United Nations** (1992). Convention on Biological Diversity.
- Vaara, M.** (1993). *Antimicrobial Agents and Chemotherapy*, 37(11):2255–2260.
- Vaara, M., Plachy, W.Z., & Nikaido, H.** (1990). *Biochimica et Biophysica Acta (BBA)-Biomembranes*, 1024(1):152–158.
- van Beilen, J.B., Holtackers, R., Lüscher, D., Bauer, U., Witholt, B., & Duetz, W.A.** (2005). *Applied and Environmental Microbiology*, 71(4):1737–1744.
- Van Duuren, J., Brehmer, B., Mars, A., Eggink, G., Dos Santos, V.M., & Sanders, J.** (2011a). *Biotechnology and Bioengineering*, 108(6):1298–1306.
- Van Duuren, J., Wijte, D., Leprince, A., Karge, B., Puchałka, J., Wery, J., Dos Santos, V.M., Eggink, G., & Mars, A.** (2011b). *Journal of Biotechnology*, 156(3):163–172.
- Van Sonsbeek, H., Beeftink, H., & Tramper, J.** (1993). *Enzyme and Microbial Technology*, 15(9):722–729.
- Vardon, D.R., Franden, M.A., Johnson, C.W., Karp, E.M., Guarnieri, M.T., Linger, J.G., Salm, M.J., Strathmann, T.J., & Beckham, G.T.** (2015). *Energy & Environmental Science*, 8(2):617–628.
- Vardon, D.R., Rorrer, N.A., Salvachúa, D., Settle, A.E., Johnson, C.W., Menart, M.J., Cleveland, N.S., Ciesielski, P.N., Steirer, K.X., & Dorgan, J.R.** (2016). *Green Chemistry*, 18(11):3397–3413.
- Vickers, C.E., Blank, L.M., & Krömer, J.O.** (2010). *Nature Chemical Biology*, 6(12):875–877.
- Vink, E.T., Rabago, K.R., Glassner, D.A., & Gruber, P.R.** (2003). *Polymer Degradation and Stability*, 80(3):403–419.
- Volmer, J.** (2016). *Chemical Biotechnology*, volume 23. Shaker Verlag, Aachen.

## References

---

- Volmer, J., Lindmeyer, M., Seipp, J., Schmid, A., & Bühler, B. (2019). *Biotechnology and Bioengineering*, 116(5):1089–1101.
- Volmer, J., Neumann, C., Bühler, B., & Schmid, A. (2014). *Applied and Environmental Microbiology*, 80(20):6539–6548.
- Volmer, J., Schmid, A., & Bühler, B. (2015). *Current Opinion in Microbiology*, 25:25–32.
- Wachtmeister, J. & Rother, D. (2016). *Current Opinion in Biotechnology*, 42:169–177.
- Wacker, M., Linton, D., Hitchen, P.G., Nita-Lazar, M., Haslam, S.M., North, S.J., Panico, M., Morris, H.R., Dell, A., & Wren, B.W. (2002). *Science*, 298(5599):1790–1793.
- Walton, A.Z. & Stewart, J.D. (2002). *Biotechnology Progress*, 18(2):262–268.
- Wang, F., Zhao, J., Li, Q., Yang, J., Li, R., Min, J., Yu, X., Zheng, G.W., Yu, H.L., & Zhai, C. (2020). *Nature Communications*, 11(1):5035.
- Wang, H.H., Isaacs, F.J., Carr, P.A., Sun, Z.Z., Xu, G., Forest, C.R., & Church, G.M. (2009). *Nature*, 460(7257):894–898.
- Wang, J.D., Herman, C., Tipton, K.A., Gross, C.A., & Weissman, J.S. (2002). *Cell*, 111(7):1027–1039.
- Weissermel, K. & Arpe, H.J. (2003). book section 10, p. 239–266. 4th edition. WILEY-VCH Verlag GmbH & Co. KGaA, Weinheim.
- Welch, M., Govindarajan, S., Ness, J.E., Villalobos, A., Gurney, A., Minshull, J., & Gustafsson, C. (2009a). *PLoS One*, 4(9):e7002.
- Welch, M., Villalobos, A., Gustafsson, C., & Minshull, J. (2009b). *Journal of the Royal Society Interface*, 6(Suppl\_4):S467–S476.
- Wenzel, S.C. & Müller, R. (2005). *Current Opinion in Chemical Biology*, 9(5):447–458.
- Wheeldon, I., Minter, S.D., Banta, S., Barton, S.C., Atanassov, P., & Sigman, M. (2016). *Nature Chemistry*, 8(4):299–309.
- Whitehouse, C.J., Bell, S.G., & Wong, L.L. (2012). *Chemical Society Reviews*, 41(3):1218–1260.
- Wieser, M., Heinzmann, K., & Kiener, A. (1997). *Applied Microbiology and Biotechnology*, 48(2):174–176.
- Willke, T. & Vorlop, K.D. (2001). *Applied Microbiology and Biotechnology*, 56(3-4):289–295.
- Willrodt, C., Hoschek, A., Bühler, B., Schmid, A., & Julsing, M.K. (2015a). *Biotechnology and Bioengineering*, 112(9):1738–1750.
- Willrodt, C., Hoschek, A., Bühler, B., Schmid, A., & Julsing, M.K. (2016). *Biotechnology and Bioengineering*, 113(6):1305–1314.
- Willrodt, C., Karande, R., Schmid, A., & Julsing, M.K. (2015b). *Current Opinion in Biotechnology*, 35:52–62.
- Witholt, B., Kingma, J., van Beilen, J.B., Kok, M., Lageveen, R.G., & Eggink, G. (1990). *Trends in Biotechnology*, 8:46–52.
- Wittcoff, H.A., Reuben, B.G., & Plotkin, J.S. (2012). John Wiley & Sons, Inc., Hoboken, NJ.
- World Commission on Environment and Development (1987).
- Wu, G., Yan, Q., Jones, J.A., Tang, Y.J., Fong, S.S., & Koffas, M.A. (2016a). *Trends in Biotechnology*, 34(8):652–664.
- Wu, S. & Li, Z. (2018). *ChemCatChem*, 10(10):2164–2178.



- Wu, S., Zhou, Y., Wang, T., Too, H.P., Wang, D.I., & Li, Z. (2016b). *Nature Communications*, 7(1):11917.
- Wynands, B., Lenzen, C., Otto, M., Koch, F., Blank, L.M., & Wierckx, N. (2018). *Metabolic Engineering*, 47:121–133.
- Wynands, B., Otto, M., Runge, N., Preckel, S., Polen, T., Blank, L.M., & Wierckx, N. (2019). *ACS Synthetic Biology*, 8(9):2036–2050.
- Xu, P., Rizzoni, E.A., Sul, S.Y., & Stephanopoulos, G. (2017). *ACS Synthetic Biology*, 6(1):148–158.
- Xu, P., Vansiri, A., Bhan, N., & Koffas, M.A. (2012). *ACS Synthetic Biology*, 1(7):256–266.
- Yim, H., Haselbeck, R., Niu, W., Pujol-Baxley, C., Burgard, A., Boldt, J., Khandurina, J., Trawick, J.D., Osterhout, R.E., & Stephen, R. (2011). *Nature Chemical Biology*, 7(7):445–452.
- Yu, J., Zhu, L., Xia, S., Li, H., Tang, Y., Liang, X., Chen, T., & Tang, Y. (2016). *Biotechnology and Bioengineering*, 113(7):1531–1541.
- Yu, J.L., Xia, X.X., Zhong, J.J., & Qian, Z.G. (2014). *Biotechnology and Bioengineering*, 111(12):2580–2586.
- Yu, Y., Zhu, X., Xu, H., & Zhang, X. (2019). *Metabolic Engineering*, 56:181–189.
- Yuan, J. & Ching, C.B. (2014). *Biotechnology and Bioengineering*, 111(3):608–617.
- Zelcbuch, L., Antonovsky, N., Bar-Even, A., Levin-Karp, A., Barenholz, U., Dayagi, M., Liebermeister, W., Flamholz, A., Noor, E., & Amram, S. (2013). *Nucleic Acids Research*, 41(9):e98.
- Zhang, H., Li, Z., Pereira, B., & Stephanopoulos, G. (2015). *Microbial Cell Factories*, 14(1):134.
- Zhang, H. & Wang, X. (2016). *Metabolic Engineering*, 37:114–121.
- Zhang, W., Lee, J.H., Younes, S.H., Tonin, F., Hagedoorn, P.L., Pichler, H., Baeg, Y., Park, J.B., Kourist, R., & Hollmann, F. (2020). *Nature Communications*, 11(1):2258.
- Zhang, Y., Song, L., Gao, Q., Yu, S.M., Li, L., & Gao, N.F. (2012). *Applied Microbiology and Biotechnology*, 94(6):1619–1627.
- Zhao, M., Huang, D., Zhang, X., Koffas, M.A., Zhou, J., & Deng, Y. (2018). *Metabolic Engineering*, 47:254–262.
- Zhou, H., Vonk, B., Roubos, J.A., Bovenberg, R.A., & Voigt, C.A. (2015a). *Nucleic Acids Research*, 43(21):10560–10570.
- Zhou, K., Qiao, K., Edgar, S., & Stephanopoulos, G. (2015b). *Nature Biotechnology*, 33(4):377–383.
- Zhou, Y., Sekar, B.S., Wu, S., & Li, Z. (2020a). *Biotechnology and Bioengineering*, 117(8):2340–2350.
- Zhou, Y., Zhao, M., Zhou, S., Zhao, Y., Li, G., & Deng, Y. (2020b). *Journal of Biotechnology*, 314-315:8–13.

## References

---

# Appendix

**1 Front. Bioeng. Biotechnol. (2020), 8, art. 140, incl. Supplementary Material**



# Maximizing Biocatalytic Cyclohexane Hydroxylation by Modulating Cytochrome P450 Monooxygenase Expression in *P. taiwanensis* VLB120

Lisa Schäfer, Rohan Karande and Bruno Bühler\*

Department of Solar Materials, Helmholtz-Centre for Environmental Research—UFZ, Leipzig, Germany

## OPEN ACCESS

### Edited by:

Zhi-Qiang Liu,  
Zhejiang University of Technology,  
China

### Reviewed by:

Elisabeth Jacobsen,  
Norwegian University of Science  
and Technology, Norway  
Artur Ribeiro,  
University of Minho, Portugal

### \*Correspondence:

Bruno Bühler  
bruno.buehler@ufz.de

### Specialty section:

This article was submitted to  
Industrial Biotechnology,  
a section of the journal  
Frontiers in Bioengineering and  
Biotechnology

Received: 29 November 2019

Accepted: 11 February 2020

Published: 27 February 2020

### Citation:

Schäfer L, Karande R and  
Bühler B (2020) Maximizing  
Biocatalytic Cyclohexane  
Hydroxylation by Modulating  
Cytochrome P450 Monooxygenase  
Expression in *P. taiwanensis* VLB120.  
*Front. Bioeng. Biotechnol.* 8:140.  
doi: 10.3389/fbioe.2020.00140

Cytochrome P450 monooxygenases (Cyps) effectively catalyze the regiospecific oxyfunctionalization of inert C–H bonds under mild conditions. Due to their cofactor dependency and instability in isolated form, oxygenases are preferably applied in living microbial cells with *Pseudomonas* strains constituting potent host organisms for Cyps. This study presents a holistic genetic engineering approach, considering gene dosage, transcriptional, and translational levels, to engineer an effective Cyp-based whole-cell biocatalyst, building on recombinant *Pseudomonas taiwanensis* VLB120 for cyclohexane hydroxylation. A *lac*-based regulation system turned out to be favorable in terms of orthogonality to the host regulatory network and enabled a remarkable specific whole-cell activity of 34 U g<sub>CDW</sub><sup>-1</sup>. The evaluation of different ribosomal binding sites (RBSs) revealed that a moderate translation rate was favorable in terms of the specific activity. An increase in gene dosage did only slightly elevate the hydroxylation activity, but severely impaired growth and resulted in a large fraction of inactive Cyp. Finally, the introduction of a terminator reduced leakiness. The optimized strain *P. taiwanensis* VLB120 pSEVA\_Cyp allowed for a hydroxylation activity of 55 U g<sub>CDW</sub><sup>-1</sup>. Applying 5 mM cyclohexane, molar conversion and biomass-specific yields of 82.5% and 2.46 mmol<sub>cyclohexanol</sub> g<sub>biomass</sub><sup>-1</sup> were achieved, respectively. The strain now serves as a platform to design *in vivo* cascades and bioprocesses for the production of polymer building blocks such as ε-caprolactone.

**Keywords:** whole-cell biocatalysis, *Pseudomonas*, CYP450 monooxygenase, cyclohexane hydroxylation, pSEVA

## INTRODUCTION

Realizing aerobic oxidation of thermodynamically stable and kinetically inert C–H bonds in cyclohexane under sustainable and environmentally safe conditions remains a major challenge in current academic and industrial research (Schuchardt et al., 2001; Cavani and Teles, 2009). Industrial-scale C6-monomer production for, e.g., Nylon 6 and Nylon 66, typically is based on the so-called liquid-phase cyclohexane oxidation (Bellussi and Perego, 2000), involving Co/Mn carboxylate salts as homogenous catalysts applied at 140–160°C and 7–20 atm with air as the oxidant (Musser, 2000). In the current industrial process, this initial cyclohexane oxyfunctionalization step, with a low yield of 6–8% for KA oil (K: cyclohexanone, A: cyclohexanol) and selectivity of 80–90% (Fischer et al., 2010), is most critical regarding economical and ecological

process efficiency. Although substantial research effort has been devoted to developing novel chemical catalysts, the control of selectivity with increased conversion continues to be challenging (Schuchardt et al., 2001). Owing to the high demand, but low price, alternative production pathways need to be developed for an economical viable production process (Schuchardt et al., 1993; Van Beilen et al., 2003; Weissemel and Arpe, 2003).

With their high selectivity and catalytic effectiveness, biocatalysts often constitute a promising alternative to chemical catalysts. This especially holds true for O<sub>2</sub>-mediated oxyfunctionalizations, which can be realized by means of oxygenases under environmentally benign non-toxic operation conditions (Leak et al., 2009). Especially the versatile cytochrome P450 monooxygenases (CyPs), which have been employed to produce high-value compounds, constitute a promising group of enzymes (Urlacher and Schmid, 2006; Julsing et al., 2008). Due to their cofactor dependency and instability in isolated form, oxygenases are preferably applied in whole microbial cells (Schrewe et al., 2013). Recently, a class I cytochrome P450 monooxygenase (Cyp)-based whole-cell biocatalyst has been reported to perform selective cycloalkane (C5–C8) oxyfunctionalization under ambient conditions (Salamanca et al., 2015; Karande et al., 2016). To this end, respective genes have been isolated from *Acidovorax* CHX100 and functionally expressed in *Pseudomonas taiwanensis* VLB120, enabling a specific whole-cell activity of 20 U g<sub>CDW</sub><sup>-1</sup> for cyclohexane oxidation. This Cyp system has also been integrated into an enzyme cascade enabling the *in vivo* synthesis of lactones from cycloalkanes at specific rates of 20–22 U g<sub>CDW</sub><sup>-1</sup>. Thereby, the Cyp activity was rate-limiting and thus constitutes the primary hurdle for establishing a viable process based on this biocatalytic approach.

The increase of gene expression levels constitutes a major strategy to improve enzyme activities *in vivo*. To this end, different approaches are followed, such as gene dosage increase by the use of vectors with high copy number (Ajikumar et al., 2010) or by integrating multiple gene copies into the genome, promoter engineering (Alper et al., 2005; Xu et al., 2013) to optimize gene transcript levels, and ribosomal binding site (RBS) engineering to optimize translation levels (Jeschek et al., 2017). In previous work, the expression plasmid pCom10, enabling expression under the control of the *alk* regulatory system from *Pseudomonas putida* GPo1, was applied for functional Cyp gene expression in *P. taiwanensis* VLB120 (Karande et al., 2016). This strain constitutes a highly interesting host strain as it can tolerate high solvent and thus substrate and product levels and provides a high metabolic capacity to support oxygenase biocatalysis also at high cell densities (Kuhn et al., 2012; Volmer et al., 2014, 2017, 2019). However, catabolite repression by glucose constitutes a major disadvantage of the pCom10 system in *Pseudomonas*, necessitating the use of a more expensive carbon and energy source such as citrate (Staijen et al., 1999). Additionally, inducers of this system such as dicyclopropylketone (DCPK) are volatile complicating its application on an industrial scale.

In this study, we set out to improve Cyp activities in *P. taiwanensis* VLB120 by tackling the challenges imposed by the expression vector pCom10\_Cyp via a holistic approach

involving transcriptional, translational, as well as gene dosage engineering (Figure 1). For this purpose, we made use of the Standard European Vector Architecture (SEVA) system (Ellis et al., 2011; Silva-Rocha et al., 2013; Martínez-García et al., 2015). Different promoter systems, RBSs, and origins of replication were evaluated by means of four readouts: growth rate, total Cyp amount in the cell, active Cyp content, and specific hydroxylation activity.

## MATERIALS AND METHODS

### Bacterial Strains, Plasmids, Media, and Chemicals

Microbial strains and plasmids used in this work are listed in Table 1. Cells were grown in lysogeny broth medium (Sambrook and Russell, 2001) or M9\* medium (Panke et al., 1999) with a pH of 7.2 supplemented with 0.5% (w/v) glucose or citrate as sole carbon source and kanamycin (50 µg mL<sup>-1</sup>) for plasmid selection. Unless stated otherwise, all chemicals were purchased from Sigma–Aldrich (Steinheim, Germany) or Carl Roth (Karlsruhe, Germany) in the highest purity available and used without further purifications.

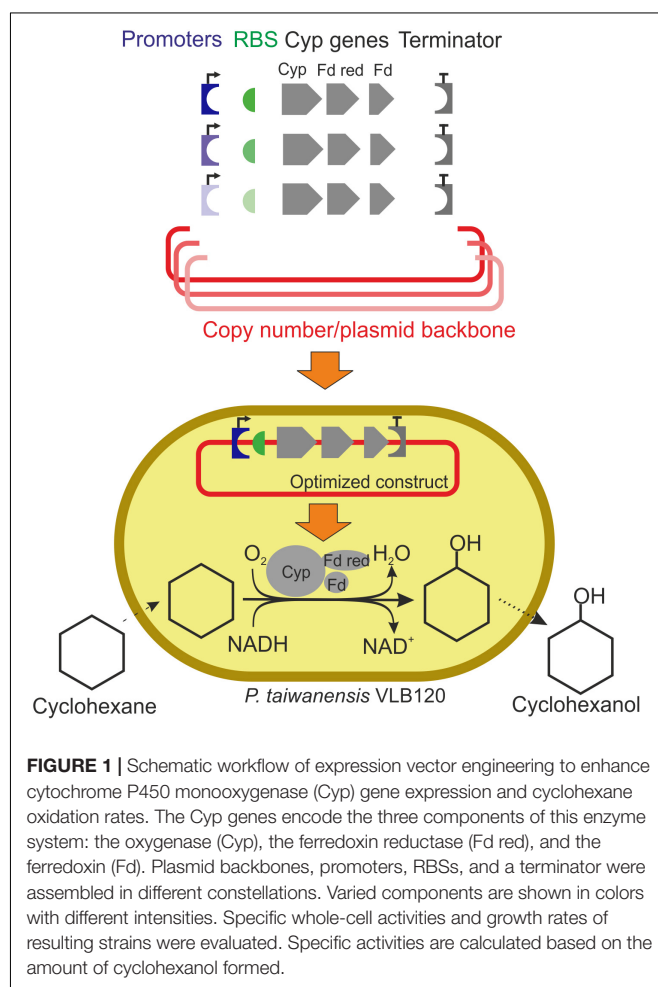


**FIGURE 1** | Schematic workflow of expression vector engineering to enhance cytochrome P450 monooxygenase (Cyp) gene expression and cyclohexane oxidation rates. The Cyp genes encode the three components of this enzyme system: the oxygenase (Cyp), the ferredoxin reductase (Fd red), and the ferredoxin (Fd). Plasmid backbones, promoters, RBSs, and a terminator were assembled in different constellations. Varied components are shown in colors with different intensities. Specific whole-cell activities and growth rates of resulting strains were evaluated. Specific activities are calculated based on the amount of cyclohexanol formed.

**TABLE 1** | Strains and plasmids used in this study.

Strain	Characteristics
<i>E. coli</i> DH5 $\alpha$ <sup>1</sup>	<i>supE44</i> $\Delta$ <i>lacU169</i> ( $\Phi$ 80 <i>lacZ</i> $\Delta$ M15) <i>hsdR17 recA1 endA1 gyrA96 thi-1 relA1</i>
<i>P. taiwanensis</i> VLB120 <sup>2</sup>	Solvent tolerant, styrene degrading bacterium, isolated from forest soil
<b>Plasmids</b>	
pCom10_lac_Cyp	pRO1600 and ColE1ori, <i>lac</i> -regulatory system ( <i>lacI</i> , <i>P<sub>lacUV5</sub></i> ), Km <sup>R</sup> , pCom10 RBS, Cyp genes from <i>Acidovorax</i> sp.
pCom10_tac_Cyp	pRO1600 and ColE1ori, <i>lac</i> -regulatory system ( <i>lacI<sup>R</sup></i> , <i>P<sub>tac</sub></i> ), Km <sup>R</sup> , pCom10 RBS, Cyp genes from <i>Acidovorax</i> sp.
pSEVA244_BB32_Cyp	pRO1600 and ColE1ori, <i>lac</i> -regulatory system ( <i>lacI<sup>R</sup></i> , <i>P<sub>tac</sub></i> ), BBa_B0032 RBS, Cyp genes from <i>Acidovorax</i> sp.
pSEVA244_BB34_Cyp	pRO1600 and ColE1ori, <i>lac</i> -regulatory system ( <i>lacI<sup>R</sup></i> , <i>P<sub>tac</sub></i> ), BBa_B0034 RBS, Cyp genes from <i>Acidovorax</i> sp.
pSEVA244_RBS* <sub>Cyp</sub>	pRO1600 and ColE1ori, <i>lac</i> -regulatory system ( <i>lacI<sup>R</sup></i> , <i>P<sub>tac</sub></i> ), RBS*, Cyp genes from <i>Acidovorax</i> sp.
pSEVA254_BB32_Cyp	RSF1010 ori, <i>lac</i> -regulatory system ( <i>lacI<sup>R</sup></i> , <i>P<sub>tac</sub></i> ), BBa_B0032 RBS, Cyp genes from <i>Acidovorax</i> sp.
pSEVA254_BB34_Cyp	RSF1010 ori, <i>lac</i> -regulatory system ( <i>lacI<sup>R</sup></i> , <i>P<sub>tac</sub></i> ), BBa_B0034 RBS, Cyp genes from <i>Acidovorax</i> sp.
pSEVA254_RBS* <sub>Cyp</sub>	RSF1010 ori, <i>lac</i> -regulatory system ( <i>lacI<sup>R</sup></i> , <i>P<sub>tac</sub></i> ), RBS*, Cyp genes from <i>Acidovorax</i> sp.
pSEVA244_T_BB34_Cyp	pRO1600 and ColE1ori, <i>lac</i> -regulatory system ( <i>lacI<sup>R</sup></i> , <i>P<sub>tac</sub></i> ), BBa_B0015 terminator, BBa_B0034 RBS, Cyp genes from <i>Acidovorax</i> sp.
pSEVA244_T_RBS* <sub>Cyp</sub> = pSEVA_Cyp	RSF1010 ori, <i>lac</i> -regulatory system ( <i>lacI<sup>R</sup></i> , <i>P<sub>tac</sub></i> ), RBS*, Cyp genes from <i>Acidovorax</i> sp.
pCom10_Cyp <sup>3</sup>	pRO1600 and ColE1 ori, <i>alk</i> -regulatory system ( <i>alkS</i> , <i>P<sub>alkB</sub></i> ), Km <sup>R</sup> , pCom10 RBS, Cyp genes from <i>Acidovorax</i> sp.

<sup>1</sup>Hanahan, 1983. <sup>2</sup>Köhler et al., 2013. <sup>3</sup>Karande et al., 2016. If not stated otherwise, the plasmids and strains were constructed in this study.

## Molecular Biology Methods

The preparation of electrocompetent *Pseudomonas* cells was performed according to Choi and Schweizer (2006), and the vectors were introduced by electroporation (2500 V, Eppendorf Eporator<sup>®</sup>, Hamburg, Germany). DNA manipulation methods and agarose gel electrophoresis were performed as described by Sambrook and Russell (2001). Enzymes (Phusion High-Fidelity Polymerase, T5 exonuclease, Taq ligase, restriction enzymes, Fast Alkaline Phosphatase) and buffers were purchased from Thermo Scientific Molecular Biology (St. Leon-Rot, Germany) or New England Biolabs (Frankfurt/Main, Germany) and oligonucleotides from Eurofins Genomics (Ebersberg, Germany). Plasmids were isolated using the peqGOLD plasmid Miniprep Kit I from peqLab (Erlangen, Germany) and purified via NucleoSpin Gel and PCR Clean-up from Macherey–Nagel (Düren, Germany) according to supplier protocols. The Gibson Master Mix was prepared according to Gibson et al. (2009). For detailed information, see **Supplementary Table S1** and **Supplementary Figure S1**.

## Growth of Bacterial Cultures

Cultivations were carried out at 30 °C and 200 rpm in a Multitron shaker (Infors, Bottmingen, Switzerland). Microorganisms were inoculated from a 10% glycerol stock in a 10 mL LB pre-culture for ca. 20 h, from which a 10 mL M9\* pre-culture (1% v/v) was inoculated and incubated for another 12–16 h. This culture was used to inoculate a 50 mL M9\* main culture to a starting OD of 0.2 or 0.4 (only for chapter transcriptional engineering). Heterologous gene expression was induced with 1 mM isopropyl  $\beta$ -D-1-thiogalactopyranoside (IPTG) for *lac*-based systems or 0.025% (v/v) DCPK for the *alk*-based system after 4 or 2.5 h (only for chapter transcriptional engineering) of cultivation. Incubation was continued for another 4–6 h, and cells were harvested for SDS-PAGE and CO difference spectra analyses and/or for resting cell assays.

## Resting Cell Assays and Bioconversion Experiments

Cells were harvested by centrifugation and resuspended to a target cell concentration (as indicated) in 100 mM potassium phosphate buffer (pH 7.4) supplemented with 1% (w/v) glucose or citrate as the source for energy and reduction equivalents. For the determination of specific whole-cell activities, the cells were diluted to two different cell concentrations, i.e., 0.2 and 0.5 g<sub>CDW</sub> L<sup>-1</sup>. In all assay setups, both gave comparable activities, which thus were averaged. The cells were transferred to baffled Erlenmeyer flasks (100 mL) or Pyrex tubes and equilibrated at 30°C for 10 min before an aqueous phase equivalent of 10 mM pure cyclohexane was added resulting in a final aqueous concentration of ~180  $\mu$ M (the major part of cyclohexane resided in the gas phase). Incubation was continued for 10 min, when the reaction was stopped. The liquid sample (1 mL) was extracted with ice-cold diethyl ether (Et<sub>2</sub>O) (1 mL) for GC analysis containing 0.2 mM n-decane as an internal standard. After 2 min extraction by vortexing and centrifugation, the organic phase was dried over anhydrous Na<sub>2</sub>SO<sub>4</sub> before it was transferred to a GC vial for analysis. The specific cyclohexane hydroxylation activity was calculated based on the formed cyclohexanol amount within 10 min of reaction per g cell dry weight (1 U = 1  $\mu$ mol cyclohexanol per min).

For the comparison of pSEVA\_Cyp and pCom10\_Cyp, 250 mL baffled Erlenmeyer flasks (300 mL total volume) were used applying a liquid volume of 40 mL with a cell concentration of 1.5 g L<sup>-1</sup>. The caps contained a septum composed of Teflon facing the inner side of the flask and silicon facing outwards. The reaction was started by adding a cyclohexane concentration of 5 mM (referred to in the aqueous phase). At each sampling point, 1.5 mL liquid volume was removed with a syringe, and gas-phase samples were taken for O<sub>2</sub> quantification. One mL of the liquid sample was extracted with 1 mL of diethyl ether for GC analysis. The substrate cyclohexane as well as cyclohexanol and the overoxidation product cyclohexanone were quantified. The conversion refers to ratio of product amount (cyclohexanol and cyclohexanone) to the known added substrate amount. The selectivity expresses the fraction of cyclohexanol of the total

product amount. The total turnover number (TTN) relates the produced amount of cyclohexanol to the active Cyp amount within the cells determined by CO difference spectra. The yield was calculated based on the formed cyclohexanol amount per g cell dry weight.

## CO Difference Spectra

Active amount of Cyp in whole cells was quantified by means of CO difference spectra previously described (Cornelissen et al., 2011, 2012). Cells were harvested and resuspended in 100 mM potassium phosphate buffer (pH = 7.4) containing 1% (w/v) glucose to obtain an OD<sub>450</sub> of 15 in a volume of 0.9 mL. This cell suspension was transferred to a plastic cuvette and supplemented with 100  $\mu$ L of fresh sodium dithionite solution (15 mg mL<sup>-1</sup>). The baseline was recorded with a UV-visible spectrophotometer (Varian, Type CARY 300, Palo Alto, CA, United States). Then, the sample was gassed with carbon monoxide (Linde AG, Munich, Germany) for 1 min and a CO difference spectrum was recorded between 350 and 600 nm. The Cyp-concentration was calculated using a molar extinction coefficient of 91 mM<sup>-1</sup> cm<sup>-1</sup> between 450 and 490 nm (Omura and Sato, 1964).

## Analytical Methods

Biomass concentrations were detected as the optical density at a wavelength of 450 nm using a Libra S11 spectrophotometer (Biochrom, Cambridge, United Kingdom). One OD<sub>450</sub> unit corresponds to 0.186 g<sub>CDW</sub> L<sup>-1</sup> (Halan et al., 2010).

Proteins were analyzed via SDS-PAGE according to Laemmli (Laemmli, 1970), loading 30  $\mu$ g of total protein per lane. Concentrations of substrates and products were determined by a GC system (Trace 1310, Thermo Scientific, Waltham, MA, United States) equipped with a flame ionization detector and a TR-5MS GC Column (dimensions: 15 m length, 0.25 mm inner diameter, Thermo Scientific) and operated with molecular nitrogen as carrier gas, 1  $\mu$ L injection volume, and splitless injection mode. The temperature profile setting was as follows: 40°C (3 min), 40–170°C (15°C min<sup>-1</sup>), 170–300°C (100°C min<sup>-1</sup>). Products were quantified based on calibration curves obtained with commercially available standards. An exemplary chromatogram is given in **Supplementary Figure S2**.

## RESULTS

In previous work, Karande et al. (2016) demonstrated that the Cyp genes from *Acidovorax* sp. CHX100 can be expressed in *P. taiwanensis* VLB120 under the control of the *alk* regulatory system from *P. putida* GPo1, enabling a resting cell activity of 20 U g<sub>CDW</sub><sup>-1</sup>. The applicability of the constructed pCom10\_Cyp expression vector in *Pseudomonas* is limited due to catabolite repression by glucose necessitating the use of more expensive carbon sources, the volatile nature of inducers, and the moderate cyclohexane oxidation activity achieved. To overcome these limitations, we followed an integrated and combinatorial approach involving transcription, translation, and gene dosage engineering based on the SEVA system (Silva-Rocha et al., 2013).

## Transcriptional (Promoter) Engineering for Efficient Cyp Gene Expression

The alteration of gene transcript levels via promoter engineering constitutes the most common strategy for the fine-tuning of expression levels (Jeschek et al., 2017). In this work, *lac*-based regulation systems (Lindmeyer et al., 2015) were tested as alternatives to the *alk* regulatory system (**Figure 2C**). The vector backbone was kept the same for better comparison. Resulting strains showed decent Cyp activity, with pCom10\_lac\_Cyp effectuating a clearly higher specific activity of 35.0  $\pm$  1.9 U g<sub>CDW</sub><sup>-1</sup> than the original construct with 22.2  $\pm$  1.9 U g<sub>CDW</sub><sup>-1</sup> and pCom10\_tac\_Cyp with 18.5  $\pm$  1.0 U g<sub>CDW</sub><sup>-1</sup> (**Figure 2B** and **Supplementary Table S2**). The strong LacI<sup>q</sup> repressor present in pCom10\_tac\_Cyp constitutes a possible reason for the lower Cyp expression level obtained with this vector (**Figure 2D**). All three strains exhibited similar Cyp-specific turnover numbers indicating that the active Cyp amount in the cells limited the cell-specific activity (**Table 2**). However, cells bearing the *lac*-based constructs exhibited severely hampered growth, which was in contrast to cells harboring the original *alk*-based vector (**Figure 2A**). To profit from the higher whole-cell activity achieved with pCom10\_lac\_Cyp and cheap glucose as a growth substrate, the growth issue needs to be addressed. To this end, we used vector parts from the SEVA platform (Silva-Rocha et al., 2013) for further engineering (see below).

## Translational (RBS) Engineering for the Fine-Tuning of Cyp Expression Levels

The engineering of the RBS constitutes another strategy to maximize expression levels and is considered a practical approach because of the small number of bases that need to be altered to achieve a wide range of expression levels (Jeschek et al., 2016). With increasing RBS strength, the protein synthesis rate is enhanced (Peretti and Bailey, 1987) in the sense of a more frequent initiation of mRNA translation. The stronger the RBS, the more ribosomes are recruited to this particular site. The RBS sequence is complementary to the 3' end of the 16S rRNA, which is identical in *Escherichia coli* and *P. taiwanensis* VLB120. We hypothesized that the relative strength of given RBSs is comparable in both strains and thus relied on the readily available expression data for *E. coli*. Three different RBSs with low (BBa\_B0032), moderate (RBS\*), and high (BBa\_B0034) strength were selected (Elowitz and Leibler, 2000; Weiss et al., 2004; Heidorn et al., 2011) based on the Registry of Standard Biological Parts, n.d.). The vector pSEVA244 containing a Kanamycin resistance gene, the pRO1600/ColE1 origin of replication, and the LacI<sup>q</sup>-*P<sub>trc</sub>* regulation system from the SEVA platform (Silva-Rocha et al., 2013) was utilized as the basis for further cloning. For all constructs, the same BioBrick scars were introduced between promoter and RBS and between RBS and start codon so that they only differ in their respective RBS sequence.

With the chosen SEVA bricks, pCom10-related issues regarding growth inhibition could successfully be overcome



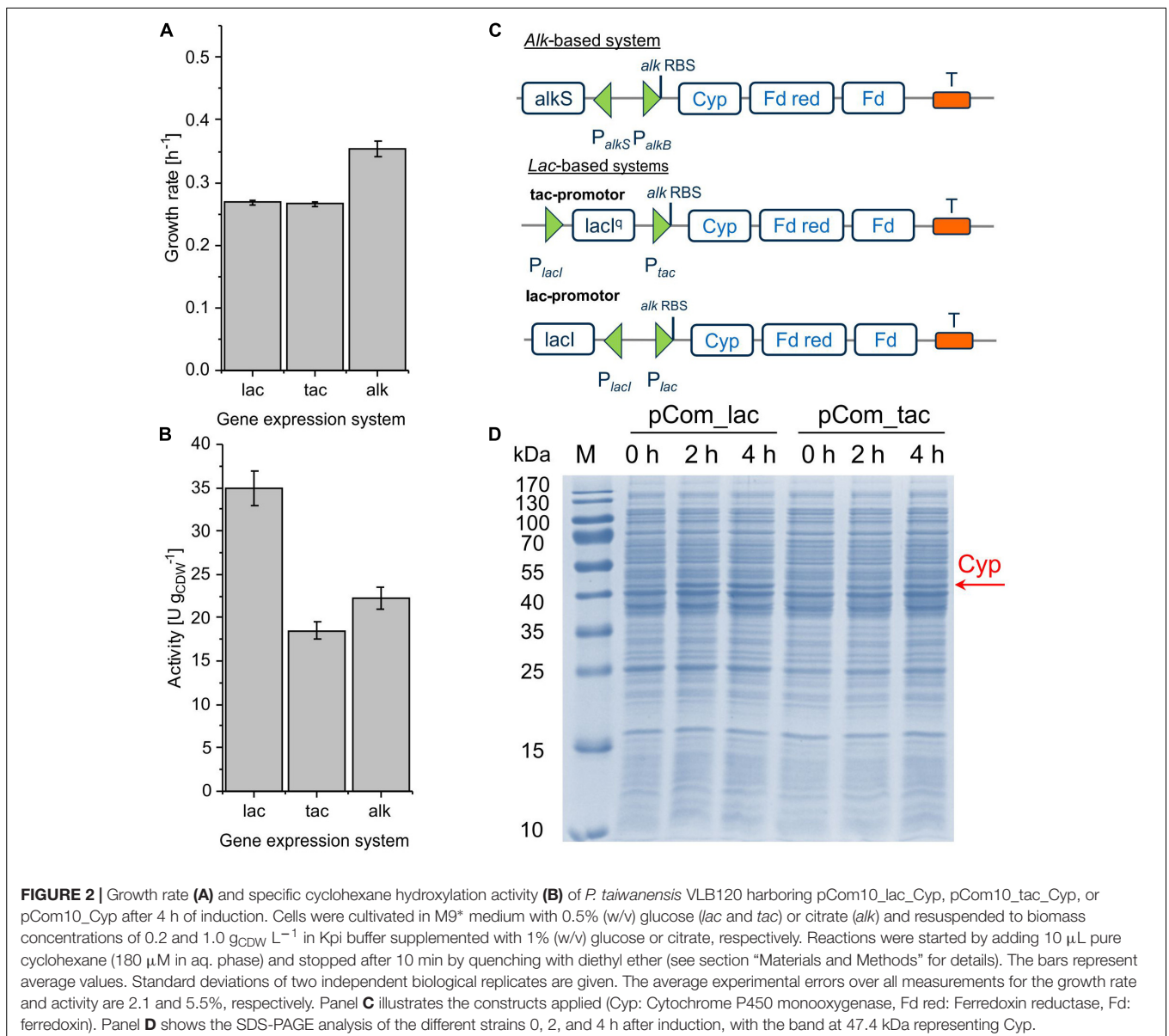


**TABLE 2 |** Specific whole-cell activities, Cyp concentrations, and Cyp turnover numbers obtained with the different expression vectors constructed.

Plasmid backbone	RBS	Activity ( $\text{U g}_{\text{CDW}}^{-1}$ )	Active Cyp concentration <sup>1</sup> ( $\text{nmol g}_{\text{CDW}}^{-1}$ )	Turnover number ( $\text{mol min}^{-1} \text{mol}^{-1}$ )
<i>ColE1/pRO1600_alk</i>	Default pCom	22.2 ± 1.2	50.6 ± 1.9	439.4 ± 40.4
<i>ColE1/pRO1600_lac</i>	Default pCom	35.0 ± 1.9	76.7 ± 11.7	455.6 ± 95.0
<i>ColE1/pRO1600_tac</i>	Default pCom	18.5 ± 1.0	42.8 ± 5.7	432.5 ± 81.1
<i>ColE1/pRO1600</i>	Weak	14.0 ± 0.9	25.4 ± 0.3	551.3 ± 29.0
	Moderate	48.4 ± 1.5	78.9 ± 4.2	613.7 ± 51.7
	Strong	4.7 ± 0.3	46.1 ± 9.6	101.5 ± 28.0
RSF1010	Weak	2.7 ± 0.7	11.3 ± 9.8	242.1 ± 266.3
	Moderate	50.7 ± 0.7	67.7 ± 7.6	749.5 ± 94.1
	Strong	49.8 ± 4.6	76.7 ± 11.7	665.5 ± 85.3
<i>ColE1/pRO1600 with terminator</i>	Moderate	42.4 ± 2.4	78.1 ± 11.7	543.3 ± 113.0
	Strong	27.3 ± 2.4	81.1 ± 6.2	336.7 ± 55.1

<sup>1</sup>CYP concentrations were obtained by CO difference spectroscopy.

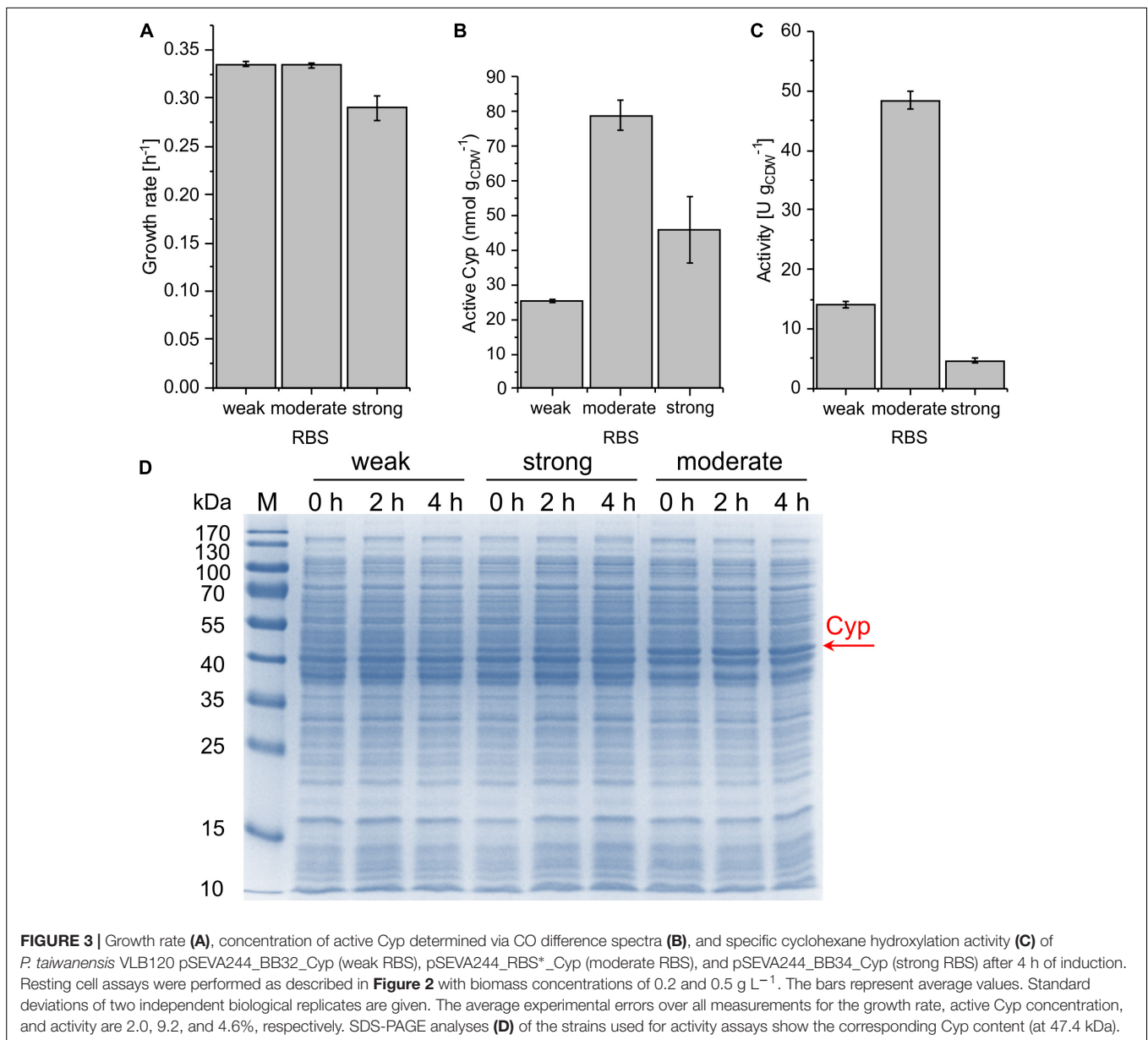


(Figure 3A). The highest specific whole-cell activity of  $48.4 \pm 1.5 \text{ U g}_{\text{CDW}}^{-1}$  was observed with the moderately strong RBS, coinciding with the highest Cyp amount on the SDS gel, the highest amount of active Cyp as determined via CO difference spectra (Figure 3 and Supplementary Table S2), and the highest turnover number (Table 2). The weakest RBS resulted in a specific activity of  $14.0 \pm 0.6 \text{ U g}_{\text{CDW}}^{-1}$ , coming along with a faint Cyp band on the SDS gel and a turnover number to that obtained with the moderate RBS. The strongest RBS resulted in a low specific activity of  $4.7 \pm 0.3 \text{ U g}_{\text{CDW}}^{-1}$  and a low turnover number for the Cyp (Table 2). Thereby, the Cyp band on the SDS-PAGE gel was stronger and the CO difference spectra-based Cyp concentration was higher compared to the weak RBS (Figure 3D). Furthermore, the slightly reduced growth rate

of the respective strain compared to the other two strains indicates that expression via the strongest RBS hampers cell physiology (Figure 3A). Obviously, most of the translated Cyp enzyme was inactive because of incorrect folding, possibly involving fast enzyme degradation. Further, its activity may have been limited by the NADH supply via the stressed cell metabolism. These results emphasize that the translation initiation rate needs to be optimized so that cell physiology can cope with additional (stress-related) demands, and to enable correct protein folding. All strains showed a high level of leakiness. Induction did not have any effect on the Cyp amount (Figure 3D). This indicates that the regulation system applied, in combination with the low plasmid copy number of 13 per cell (determined for *Pseudomonas aeruginosa*) (Farinha and

Kropinski, 1990), conveys a remarkable basal translation, irrespective of the presence of *lacI<sup>q</sup>* encoding a strong repressor of the *lac* system.

## Gene Dosage Variation for the Optimization of Cyp Gene Expression

The variation of the gene copy number constitutes another common strategy to alter the expression level and typically is realized by utilizing plasmids with different copy numbers per cell. For comparison, the ColE1/pRO1600 origins of replication used in the previous experiments (13 copies per cell in *P. aeruginosa*) (Farinha and Kropinski, 1990) were replaced by the broad-host range replication origin RSF1010. Respective copy numbers are high and mostly host-independent (Meyer, 2009), with  $130 \pm 40$  copies reported for *P. putida* KT2440 (Cook et al., 2018). The RSF1010 origin of replication was tested in combination with all three RBSs, measuring growth rate, Cyp content, and whole-cell activity (Supplementary Table S2).

The introduction of the RSF1010 origin was found to strongly influence all these parameters. Its combination with the weakest RBS led to the highest growth rate but involved a low whole-cell activity of  $2.7 \pm 0.7$  U g<sub>CDW</sub><sup>-1</sup> and no Cyp detection via SDS-PAGE (Figure 4). The combination of the RSF1010 origin with both the moderate and the strong RBS reduced the growth rate, which only was exponential until 1 h after induction (see Supplementary Figure S3). The final biomass concentration after 4 h of induction was only 0.2 g<sub>CDW</sub> L<sup>-1</sup>. However, specific whole-cell activities reached high levels of  $50.7 \pm 0.7$  and  $49.8 \pm 4.6$  U g<sub>CDW</sub><sup>-1</sup> with the moderate and the strong RBS, respectively (Figure 4C). A much stronger Cyp band was detected for the strong RBS (Figure 4D), whereas, according to CO difference spectra and turnover numbers, active Cyp concentrations were similar with these two RBSs. This indicates that, with the strong RBS, a large Cyp fraction was not appropriately processed (folding, heme incorporation, Figure 4B and Table 2). For both replication systems, the Cyp amount obtained with the moderate RBS is considered appropriate. Again, a strong leakiness was observed. The hampered growth with the high-copy plasmids (RSF1010) indicates that respective constructs and expression impose a significant metabolic burden on the cells. These results emphasize that the origin of replication is a decisive factor for stable expression and biotransformation.

## Introduction of a Terminator Eliminates Leakiness While Preserving the High Specific Activity and Wildtype-Like Growth Physiology

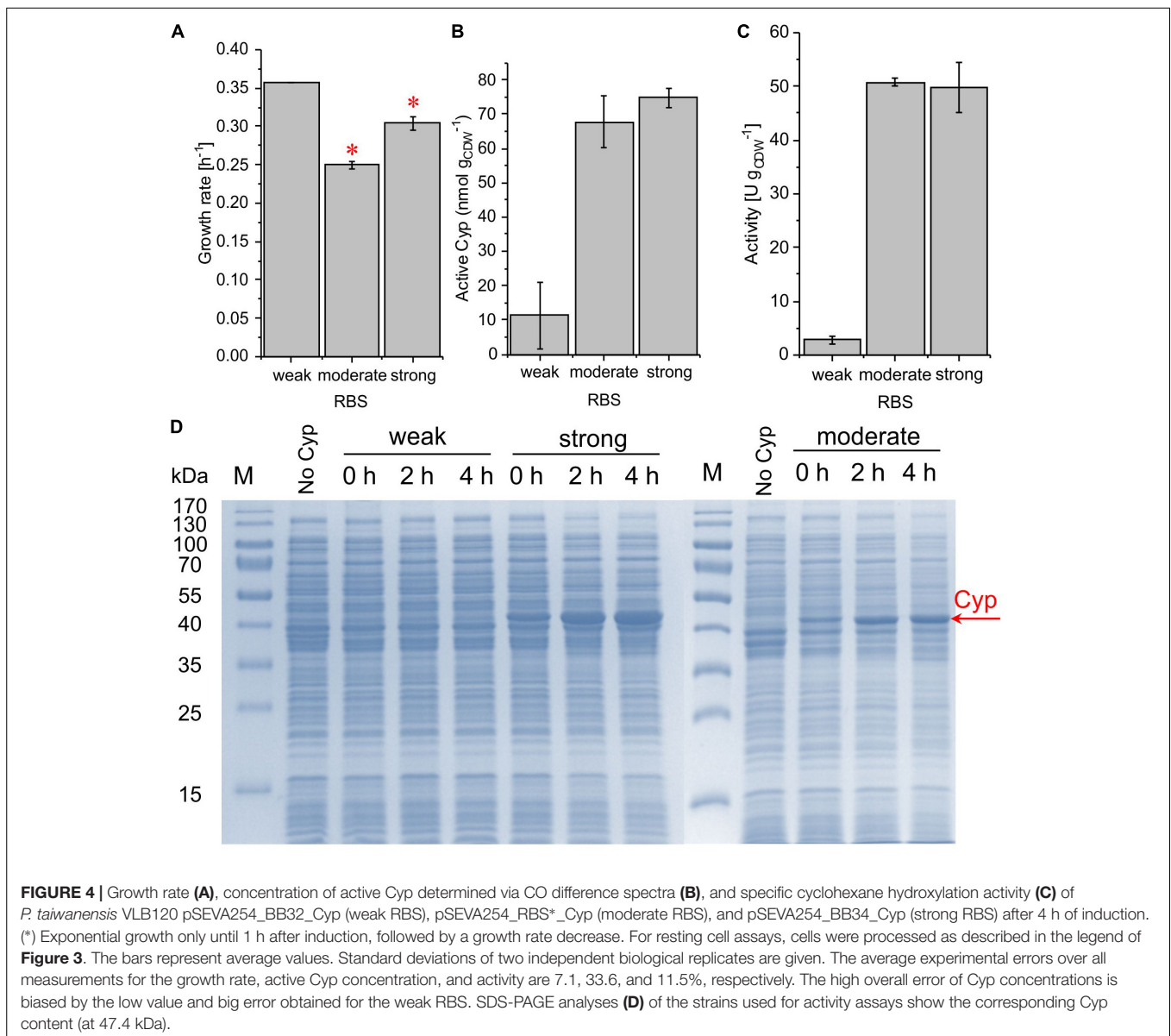
The ColE1/pRO1600 system can be considered preferable for Cyp gene expression weighing up all parameters, growth/cell physiology, Cyp expression level, and specific whole-cell activity (Table 2). However, overcoming the leakiness of the construct is necessary to gain appropriate process control. A possible read-through of the Cyp genes from the *lacI<sup>q</sup>* promoter was hypothesized to be the reason for the leakiness. To avoid such a read-through and thus leakiness, a double terminator was introduced after the *lacI<sup>q</sup>* gene (Figure 5D). Following

this approach, we investigated moderate and strong RBSs as they enabled reasonable Cyp gene expression in the constructs tested before (Figure 3D). While the transformation of RSF1010 based constructs into *P. taiwanensis* VLB120 was not successful, both ColE1/pRO1600-based constructs exhibited a remarkably enhanced tightness. With the moderate RBS, a high Cyp amount, whole-cell activity, and turnover number were obtained (Figure 5B, Table 2 and Supplementary Table S2). The strong RBS led to higher Cyp expression according to SDS-PAGE, but similar amounts of active Cyp according to CO difference spectra, again indicating non-appropriate Cyp processing (Figures 5B,E). This was further corroborated by the lower specific whole-cell activity obtained with the strong RBS compared to the moderate RBS (Figure 5C). Furthermore, the higher growth rate obtained with the moderate RBS (Figure 5A) indicates a lower metabolic burden for the cells.

The evaluation of induction kinetics with this improved construct revealed a maximal activity of  $55.6 \pm 2.4$  U g<sub>CDW</sub><sup>-1</sup> after 6 h of induction (see Supplementary Figure S4), with a slight decrease afterward. To conclude, the improved cyclohexanol producing strain shows fivefold increased activity compared to the non-induced state and exhibits the highest specific whole-cell activity obtained so far with this Cytochrome P450 monooxygenase.

## Catalytic Performance of pSEVA\_Cyp and pCom10\_Cyp Containing Strains

To evaluate the biocatalytic performance of cells containing the optimized pSEVA\_Cyp beyond their initial specific activity, comparative biotransformations of 5 mM cyclohexane were evaluated for 3 h in tightly closed flasks with 1.5 g<sub>CDW</sub> L<sup>-1</sup> of cells containing the improved pSEVA\_Cyp or pCom10\_Cyp (Supplementary Figure S5 and Supplementary Table S3). As expected, the improvement in the Cyp expression level achieved with the pSEVA\_Cyp system resulted in a 1.9-fold higher molar cyclohexane conversion yield as compared to the pCom10\_Cyp system, whereas the Cyp-related TTN was estimated to be slightly lower with the pSEVA\_Cyp system (Table 3). Whereas the selectivity for KA oil formation was 100% in both cases as cyclohexanol and the overoxidation product cyclohexanone were the only reaction products, the pSEVA\_Cyp and pCom\_Cyp systems gave rise to 89 and 96% cyclohexanol, respectively. The lower TTN and selectivity at higher cyclohexane conversion yields with the pSEVA\_Cyp system can be explained by kinetic constraints involving reinforced competition of cyclohexane and cyclohexanol for the active site at low cyclohexane concentrations as a result of gas-liquid mass transfer limitation and product inhibition, finally leading to enhanced cyclohexanol overoxidation. The overall product yield on biomass was improved 1.7-fold with the pSEVA\_Cyp system. As the next steps, a detailed characterization of whole-cell biocatalyst kinetics and a suitable feeding strategy for volatile cyclohexane will pave the way for the design of an efficient cyclohexane oxidation process.



## DISCUSSION

Cytochrome P450 monooxygenases (Cyps) are capable of catalyzing a wide range of synthetically challenging hydroxylation, epoxidation, dealkylation, and sulfoxidation reactions for the production of fine chemicals, fragrances, and pharmaceutically active compounds (Urlacher and Schmid, 2006). Although the substantial synthetic potential of Cyp has fiercely triggered respective research, Cyp applications on the industrial scale remained limited to few examples for fine chemicals and pharmaceuticals with high-value gain (Julsing et al., 2008). Limited stability, low activity, their multi-component nature, narrow substrate specificity, cofactor requirements, and the dependency on an electron source constitute the major challenges for the technical application of Cyps, especially for the million ton range production of low-priced chemicals

(Bernhardt, 2006; Lundemo and Woodley, 2015), as it is the case for cyclohexanol (Schuchardt et al., 1993; Weissermel and Arpe, 2003). The Cyp employed in this study has been isolated from *Acidovorax* sp. CHX100 and successfully heterologously expressed in *Pseudomonas* and Cyanobacteria (Karande et al., 2016; Hoschek et al., 2019). This study illustrates how holistic genetic engineering can improve the production organism.

### Genetic Engineering to Improve Expression and Activity of (Heterologous) Production Pathways

Transcriptional engineering is the most common strategy to improve expression levels (Jeschek et al., 2017). The promoter sequence itself can be engineered, which has been successfully applied for the production of the secondary metabolites lycopene

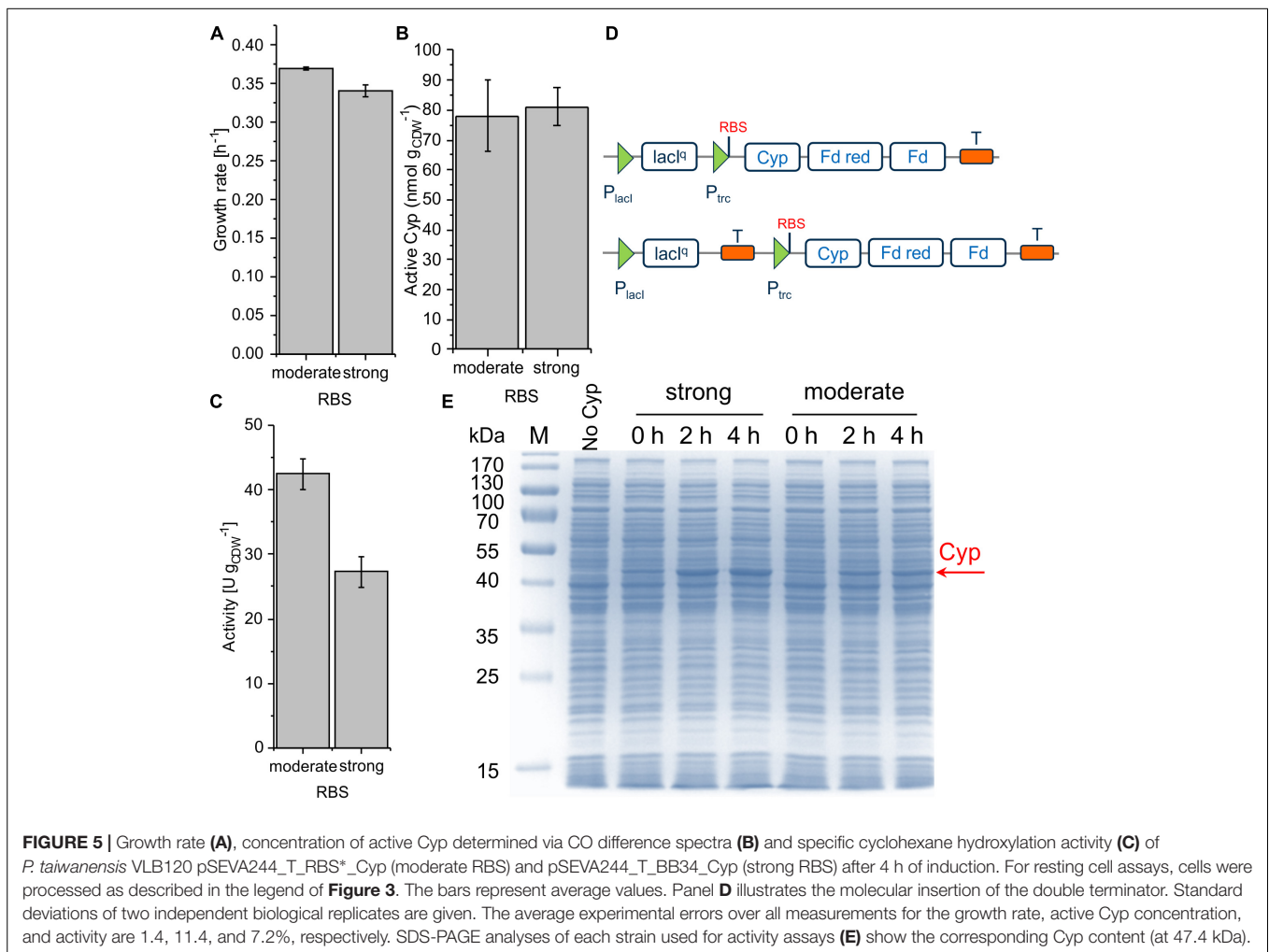


**TABLE 3 |** Comparison of molar conversion yield, selectivity, total turnover number (TTN), and yield on catalyst for cyclohexane hydroxylation using pCom10\_Cyp and pSEVA\_Cyp.

	pCom_Cyp	pSEVA_Cyp
Biotransformation time	3 h	3 h
Cyclohexane conversion [%]	44.5 ± 1.2	82.5 ± 1.1
Selectivity for cyclohexanol (for KA oil) [%]	96.1 ± 0.4 (100)	89.3 ± 0.6 (100)
Active Cyp concentration [nmol g <sub>CDW</sub> <sup>-1</sup> ]	63.3 ± 7.7	131.9 ± 4.2
TTN [mol <sub>cyclohexanol</sub> mol <sub>Cyp</sub> <sup>-1</sup> ]	22711 ± 3288	18628 ± 484
Yield [mmol <sub>cyclohexanol</sub> g <sub>CDW</sub> <sup>-1</sup> ]	1.42 ± 0.03	2.46 ± 0.01

(Alper et al., 2005) and violacein (Xu et al., 2017), where the product titer could be increased up to threefold in *E. coli*. Similarly, translational engineering (i.e., RBS engineering) was

successfully performed to increase the lycopene titer fivefold in *E. coli*. Mostly, these approaches aim at balancing the expression of different genes within a production pathway. Typically, it becomes especially important to optimize the expression level of single enzymes that govern the pathway flux (Xu et al., 2017). Oxygenases often catalyze such rate-limiting steps (Lundemo and Woodley, 2015). Lindmeyer et al. (2015) compared the *alk* regulatory system from *P. putida* GPO1 and the *lac*-system for styrene monooxygenase gene expression in different *P. putida* strains and found that the specific styrene epoxidation activities varied 1.3- to almost fivefold for *P. putida* KT2440 and *P. putida* DOT-TIE, respectively. A similar effect was observed in the present study, where the exchange of the regulation system could double the cyclohexane hydroxylation activity (Figure 2). However, the increase in activity was associated with impaired growth, indicating a negative effect of high level Cyp gene expression on cell physiology, which can be expected to affect whole-cell biocatalyst performance and stability. Our study of different RBS strengths demonstrates that the mere increase in protein amount by accelerating translation is not always associated with higher whole-cell activities (Figure 3). The strongest RBS led to reduced amounts of active Cyp and

very low activities, which emphasizes that the achievable Cyp activity does not only depend on the enzyme amount produced, but also on other factors such as the incorporation of the heme group, association with redox partners, and uncoupling. A moderately strong RBS constituted a compromise between high level expression and cell functionality and enabled a two-fold increase in activity compared to the original pCom10\_Cyp construct with still acceptable effects on cell physiology.

Apart from the promoter and RBS engineering, the gene copy number, which can be modulated via the plasmid copy number, has been found to strongly influence the achievable enzyme level in *E. coli* (Jahn et al., 2016). By expressing different modules of a Cyp-involving biosynthetic pathway from distinct plasmids in *E. coli*, taxadiene-5a-ol production titers were increased 2400-fold (Ajikumar et al., 2010). However, the maintenance of plasmids, especially those with high copy numbers, poses a high metabolic burden on the cells, which is reflected by reduced growth rates and yields on energy and carbon source (Diaz Ricci and Hernández, 2000). Respective observations also were made in this study. The combination of the high copy origin RSF1010 and the two stronger RBSs severely affected the growth of *P. taiwanensis* VLB120 upon Cyp gene expression (Figure 4). Although an activity of  $50 \text{ U g}_{\text{CDW}}^{-1}$  was obtained, a significant fraction of the produced protein appeared to be catalytically inactive. Overexpression can have severe consequences for the host as it can change the lipid composition, reduce the growth rate, and affect the strain's genetic stability (Nieboer et al., 1993; Chen et al., 1996). Additionally, oxygenase-specific issues such as uncoupling leading to the formation of reactive oxygen

species can reduce metabolic activity and cell viability in general (Kadisich et al., 2017).

In this study, the systematic combination of transcriptional, translational, and gene copy number engineering strategies finally enabled a 2.5-fold improvement of the specific hydroxylation activity of recombinant *P. taiwanensis* VLB120 while maintaining cellular fitness.

## Comparison to Other Biocatalytic Cyclohexane Hydroxylation Approaches

Cyclohexane hydroxylation is of high industrial interest, but only a few datasets for biocatalytic processes are currently available (Table 4). What they all have in common is the operation at moderate temperature and ambient pressure, which is an advantage compared to the running industrial process requiring 413–453 K and 7–20 atm (Fischer et al., 2010). The whole-cell-based approach presented in this study reached a conversion of 82.5% with a selectivity of 100% for KA oil and thus outcompeted the chemical catalyst with 8% conversion and 80% selectivity (Fischer et al., 2010). Cyclohexane hydroxylation approaches with isolated monooxygenases suffer from low product formation rates or were achieved by adding different additives (Jiang et al., 1993; Bordeaux et al., 2011; Kawakami et al., 2011). The highest specific turnover number of  $3910 \text{ mol min}^{-1} \text{ mol}^{-1}$  has been reported for a modified P450 BM3 in isolated form, but was based on the spectrophotometric determination of NADPH depletion only and thus may include significant uncoupling (Glieder et al., 2002). Besides this high value for P450 BM3, the *P. taiwanensis* VLB120 strains presented in this study showed the highest

**TABLE 4** | Literature data for cyclohexane hydroxylations.

Enzyme	Catalyst format	additives	Temperature (°C)	Reaction time	Product formation rate (mol min <sup>-1</sup> mol <sup>-1</sup> )	Total turnover number (-)	Initial activity (U g <sub>CDW</sub> <sup>-1</sup> )	Specific yield (mmol g <sub>CDW</sub> <sup>-1</sup> )	References
sMMOH	Purified enzyme	H <sub>2</sub> O <sub>2</sub>	45	10 min	0.00014	–	–	–	Jiang et al., 1993
P450 BM3	Purified enzyme	–	RT	initial	151	–	–	–	Glieder et al., 2002
P450 BM3	Purified enzyme	PFC9 <sup>a</sup>	25	10 min	108	–	–	–	Kawakami et al., 2011
Modified P450 BM3	Purified enzyme	–	RT	initial	3910 <sup>b</sup>	–	–	–	Glieder et al., 2002
Modified CYP153A13a	Purified enzyme	–	RT	2 h	3	20	–	–	Bordeaux et al., 2011
<i>P. taiwanensis</i> VLB120 pCom10_Cyp	Whole cells	–	30	3 h	336 <sup>c</sup>	22 711	20 <sup>c</sup>	1.42 <sup>d</sup>	This study
<i>P. taiwanensis</i> VLB120 pSEVA_Cyp	Whole cells	–	30	3 h	543 <sup>c</sup>	18 628	55 <sup>c</sup>	2.46 <sup>d</sup>	This study
Syn6803_CYP	Whole cells	DINP <sup>e</sup>	30	52 h	–	–	35 <sup>c</sup>	49	Hoschek et al., 2019

<sup>a</sup>Perfluorocarboxylic acid with nine carbon atoms acts as dummy substrate to provide space for cyclohexane because of the incomplete occupation of the heme cavity. <sup>b</sup>Calculated from photospectrometrically recorded NADPH depletion including possible uncoupling. <sup>c</sup>Data for the first 10 min of the reaction. <sup>d</sup>Addition of 5 mM cyclohexane as substrate. <sup>e</sup>Diisononyl phthalate added as an organic phase.

oxygenase-specific turnover rates reported so far. Whereas data on biocatalytic stability are mostly missing in previous studies, reasonable TTNs could be achieved here. These were 1000-fold higher than those obtained by Bordeaux et al. (2011) for modified CYP153A13a, indicating that the *Acidovorax* Cyp was quite well stabilized within the cellular context. Hoschek et al. (2019) set a benchmark for the utilization of the *Acidovorax* Cyp by applying it in *Synechocystis* sp. 6803 and making use of a biphasic system in a stirred-tank bioreactor with DINP as an organic phase. A specific yield of 49 mmol cyclohexanol per g cell dry weight was reached after an operation time of 52 h, once more demonstrating the potential of whole-cell biocatalysis and this enzyme. For *Synechocystis* as host strain, the achievement of high cell densities combined with sufficient light supply will be a major challenge. Besides this, the overall higher protein amounts in heterotrophic organisms still constitute a significant advantage over Cyanobacteria (Hoschek et al., 2019). The specific yields obtained in this study were lower as only 5 mM cyclohexane were provided as substrate, which was almost depleted at the end of the biotransformation with *P. taiwanensis* VLB120 pSEVA\_Cyp as biocatalyst. Consequently, as a next step, the developed biocatalyst has to be investigated in a process setup enabling longer running times and continuous cyclohexane supply as it has been done for *Synechocystis* sp. 6803. Previously, it has been shown that *P. taiwanensis* VLB120 allows for bioreactor operation at high cell densities up to 40 g<sub>biomass</sub> L<sup>-1</sup> in a two-liquid phase bioreactor setup (Kuhn et al., 2012).

## Future Perspectives

This study demonstrates that *P. taiwanensis* VLB120 is a suitable host for Cyp gene expression and the hydroxylation of alkanes. Besides its solvent-tolerance (Volmer et al., 2017), a large variety of genetic tools are now available for such *Pseudomonas* strains (Martínez-García et al., 2015). Additionally, due to their intrinsic ability to efficiently synthesize heme, the addition of a heme precursor, as it typically is necessary for *E. coli*, is not required. Until now, systematic improvement of whole-cell biocatalysts regarding specific Cyp activity mostly has been missing. Instead, protein engineering and directed evolution mainly with the camphor 5-monooxygenase P450Cam (CYP101) and P450 BM-3 (CYP102A1) have been successful in terms of improved thermostability, broader substrate spectrum, and higher turnover numbers (Appel et al., 2001; Farinas et al., 2001). This study presents an integrated and holistic genetic engineering approach toward optimal, but not necessarily maximal Cyp gene expression, in order to achieve high oxygenation yields on the substrate, biocatalyst, space, and time. This approach is necessary to meet the demands for the development of economically viable processes based on Cyps (Van Beilen et al., 2003; Lundemo and Woodley, 2015).

The improved strain *P. taiwanensis* VLB120 pSEVA\_Cyp can now be used as a starting point for the development of strains able to synthesize polymer building blocks such as  $\epsilon$ -caprolactone, 6-aminohexanoic acid, or adipic acid. For  $\epsilon$ -caprolactone synthesis, the proof of concept has already been shown by Karande et al. (2018). In this case, Cyp was the rate-limiting enzyme so that

an improved Cyp activity, as demonstrated here, constitutes an important basis for an increased overall activity of the cascade.

## CONCLUSION

In this study, we investigated Cyp gene expression and catalysis in recombinant *P. taiwanensis* VLB120 with respect to growth of the respective strain, expression levels, active Cyp amount, and specific whole-cell activities for cyclohexane hydroxylation. Recombinant *P. taiwanensis* VLB120 was systematically engineered on transcriptional, translational, as well as gene dosage levels. Thereby, a remarkable specific whole-cell biocatalyst activity of 55 U<sub>gCDW</sub><sup>-1</sup> was achieved. A compromise between expression strength and preserved enzyme functionality and cellular fitness was found to be crucial to come up with high whole-cell activities. Besides this, the optimized strain *P. taiwanensis* VLB120 pSEVA\_Cyp also showed high yields on the substrate cyclohexane and biomass. This biocatalyst shows the highest whole-cell activity for cyclohexane hydroxylation reported so far.

## DATA AVAILABILITY STATEMENT

The datasets generated for this study are available on request to the corresponding author.

## AUTHOR CONTRIBUTIONS

LS and BB designed the research. LS collected and analyzed the data. LS, RK, and BB wrote the manuscript.

## FUNDING

LS was funded from the ERA-IB-Project PolyBugs ID:16-006 and the Sächsisches Ministerium für Wissenschaft und Kunst (SMWK) Project ID: 100318259.

## ACKNOWLEDGMENTS

We acknowledge the use of the facilities of the Centre for Biocatalysis (MiKat) at the Helmholtz Centre for Environmental Research, which is supported by the European Regional Development Funds (EFRE, Europe funds Saxony) and the Helmholtz Association.

## SUPPLEMENTARY MATERIAL

The Supplementary Material for this article can be found online at: <https://www.frontiersin.org/articles/10.3389/fbioe.2020.00140/full#supplementary-material>

## REFERENCES

- Ajikumar, P. K., Xiao, W.-H., Tyo, K. E. J., Wang, Y., Simeon, F., Leonard, E., et al. (2010). Isoprenoid pathway optimization for taxol precursor overproduction in *Escherichia coli*. *Science* 330, 70–74. doi: 10.1126/science.1191652
- Alper, H., Fischer, C., Nevoigt, E., and Stephanopoulos, G. (2005). Tuning genetic control through promoter engineering. *PNAS* 102, 12678–12683. doi: 10.1073/pnas.0504604102
- Appel, D., Lutz-Wahl, S., Fischer, P., Schwaneberg, U., and Schmid, R. D. (2001). A P450 BM-3 mutant hydroxylates alkanes, cycloalkanes, arenes and heteroarenes. *J. Biotechnol.* 88, 167–171. doi: 10.1016/s0168-1656(01)00249-8
- Bellussi, G., and Perego, C. (2000). Industrial catalytic aspects of the synthesis of monomers for nylon production. *Cattech* 4, 4–16.
- Bernhardt, R. (2006). Cytochromes P450 as versatile biocatalysts. *J. Biotechnol.* 124, 128–145. doi: 10.1016/j.jbiotec.2006.01.026
- Bordeaux, M., Galarneau, A., Fajula, F., and Drone, J. (2011). A regioselective biocatalyst for alkane activation under mild conditions. *Angew. Chem.* 50, 2075–2079. doi: 10.1002/anie.201005597
- Cavani, F., and Teles, J. H. (2009). Sustainability in catalytic oxidation: an alternative approach or a structural evolution? *ChemSuschem* 2, 508–534. doi: 10.1002/cssc.200900020
- Chen, Q., Janssen, D. B., and Witholt, B. (1996). Physiological changes and *alk* gene instability in *Pseudomonas oleovorans* during induction and expression of *alk* genes. *J. Bacteriol.* 178, 5508–5512. doi: 10.1128/jb.178.18.5508-5512.1996
- Choi, K.-H., and Schweizer, H. P. (2006). mini-Tn7 insertion in bacteria with single attTn7 sites: example *Pseudomonas aeruginosa*. *Nat. Protoc.* 1:153. doi: 10.1038/nprot.2006.24
- Cook, T. B., Rand, J. M., Nurani, W., Courtney, D. K., Liu, S. A., and Pfeleger, B. F. (2018). Genetic tools for reliable gene expression and recombineering in *Pseudomonas putida*. *J. Ind. Microbiol. Biotechnol.* 45, 517–527. doi: 10.1007/s10295-017-2001-5
- Cornelissen, S., Julsing, M. K., Schmid, A., and Bühler, B. (2012). Comparison of microbial hosts and expression systems for mammalian CYP1A1 catalysis. *J. Ind. Microbiol. Biotechnol.* 39, 275–287. doi: 10.1007/s10295-011-1026-4
- Cornelissen, S., Liu, S., Deshmukh, A. T., Schmid, A., and Bühler, B. (2011). Cell physiology rather than enzyme kinetics can determine the efficiency of cytochrome P450-catalyzed C–H-oxygenation. *J. Ind. Microbiol. Biotechnol.* 38, 1359–1370. doi: 10.1007/s10295-010-0919-y
- Diaz Ricci, J. C., and Hernández, M. E. (2000). Plasmid effects on *Escherichia coli* Metabolism. *Crit. Rev. Biotechnol.* 20, 79–108.
- Ellis, T., Adie, T., and Baldwin, G. S. (2011). DNA assembly for synthetic biology: from parts to pathways and beyond. *Integr. Biol.* 3, 109–118. doi: 10.1039/c0ib00070a
- Elowitz, M. B., and Leibler, S. (2000). A synthetic oscillatory network of transcriptional regulators. *Nature* 403:335. doi: 10.1038/35002125
- Farinas, E. T., Bulter, T., and Arnold, F. H. (2001). Directed enzyme evolution. *Curr. Opin. Biotechnol.* 12, 545–551.
- Farinha, M. A., and Kropinski, A. M. (1990). Construction of broad-host-range plasmid vectors for easy visible selection and analysis of promoters. *J. Bacteriol.* 172, 3496–3499. doi: 10.1128/jb.172.6.3496-3499.1990
- Fischer, J., Lange, T., Boehling, R., Rehfinger, A., and Klemm, E. (2010). Uncatalyzed selective oxidation of liquid cyclohexane with air in a microcapillary reactor. *Chem. Eng. Sci.* 65, 4866–4872. doi: 10.1016/j.ces.2010.05.028
- Gibson, D. G., Young, L., Chuang, R.-Y., Venter, J. C., Hutchison, C. A., and Smith, H. O. (2009). Enzymatic assembly of DNA molecules up to several hundred kilobases. *Nat. Methods* 6, 343–345. doi: 10.1038/nmeth.1318
- Glieder, A., Farinas, E. T., and Arnold, F. H. (2002). Laboratory evolution of a soluble, self-sufficient, highly active alkane hydroxylase. *Nat. Biotechnol.* 20, 1135–1139. doi: 10.1038/nbt744
- Halan, B., Schmid, A., and Bühler, K. (2010). Maximizing the productivity of catalytic biofilms on solid supports in membrane aerated reactors. *Biotechnol. Bioeng.* 106, 516–527. doi: 10.1002/bit.22732
- Hanahan, D. (1983). Studies on transformation of *Escherichia coli* with plasmids. *J. Mol. Biol.* 166, 557–580. doi: 10.1016/s0022-2836(83)80284-8
- Heidorn, T., Camsund, D., Huang, H.-H., Lindberg, P., Oliveira, P., Stensjö, K., et al. (2011). “Chapter twenty-four - synthetic biology in cyanobacteria: engineering and analyzing novel functions,” in *Methods Enzymology*, ed. C. Voigt, (Cambridge, MA: Academic Press), 539–579.
- Hoschek, A., Toepel, J., Hochkeppel, A., Karande, R., Bühler, B., and Schmid, A. (2019). Light-dependent and aeration-independent gram-scale hydroxylation of cyclohexane to cyclohexanol by CYP450 harboring *Synechocystis* sp. PCC 6803. *Biotechnol. J.* 14:e1800724. doi: 10.1002/biot.201800724
- Jahn, M., Vorpahl, C., Hübschmann, T., Harms, H., and Müller, S. (2016). Copy number variability of expression plasmids determined by cell sorting and Droplet Digital PCR. *Microb. Cell Fact.* 15:211.
- Jeschek, M., Gerngross, D., and Panke, S. (2016). Rationally reduced libraries for combinatorial pathway optimization minimizing experimental effort. *Nat. Commun.* 7:11163. doi: 10.1038/ncomms11163
- Jeschek, M., Gerngross, D., and Panke, S. (2017). Combinatorial pathway optimization for streamlined metabolic engineering. *Curr. Opin. Biotechnol.* 47, 142–151. doi: 10.1016/j.copbio.2017.06.014
- Jiang, Y., Wilkins, P. C., and Dalton, H. (1993). Activation of the hydroxylase of sMMO from *Methylococcus capsulatus* (Bath) by hydrogen peroxide. *Biochim. Biophys. Acta* 1163, 105–112. doi: 10.1016/0167-4838(93)90285-y
- Julsing, M. K., Cornelissen, S., Bühler, B., and Schmid, A. (2008). Heme-iron oxygenases: powerful industrial biocatalysts? *Curr. Opin. Chem. Biol.* 12, 177–186. doi: 10.1016/j.cbpa.2008.01.029
- Kadisich, M., Willrodt, C., Hillen, M., Bühler, B., and Schmid, A. (2017). Maximizing the stability of metabolic engineering-derived whole-cell biocatalysts. *Biotechnol. J.* 12:1600170. doi: 10.1002/biot.201600170
- Karande, R., Debor, L., Salamanca, D., Bogdahn, F., Engesser, K. H., Buehler, K., et al. (2016). Continuous cyclohexane oxidation to cyclohexanol using a novel cytochrome P450 monooxygenase from *Acidovorax* sp. CHX100 in recombinant *P. taiwanensis* VLB120 biofilms. *Biotechnol. Bioeng.* 113, 52–61. doi: 10.1002/bit.25696
- Karande, R., Salamanca, D., Schmid, A., and Buehler, K. (2018). Biocatalytic conversion of cycloalkanes to lactones using an in-vivo cascade in *Pseudomonas taiwanensis* VLB120. *Biotechnol. Bioeng.* 115, 312–320. doi: 10.1002/bit.26469
- Kawakami, N., Shoji, O., and Watanabe, Y. (2011). Use of perfluorocarboxylic acids to trick cytochrome P450BM3 into initiating the hydroxylation of gaseous alkanes. *Angew. Chem.* 50, 5315–5318. doi: 10.1002/anie.201007975
- Köhler, K. A., Rückert, C., Schatschneider, S., Vorhölter, F.-J., Szczepanowski, R., Blank, L. M., et al. (2013). Complete genome sequence of *Pseudomonas* sp. strain VLB120 a solvent tolerant, styrene degrading bacterium, isolated from forest soil. *J. Biotechnol.* 168, 729–730. doi: 10.1016/j.jbiotec.2013.10.016
- Kuhn, D., Bühler, B., and Schmid, A. (2012). Production host selection for asymmetric styrene epoxidation: *Escherichia coli* vs. solvent-tolerant *Pseudomonas*. *J. Ind. Microbiol. Biotechnol.* 39, 1125–1133. doi: 10.1007/s10295-012-1126-9
- Laemmli, U. K. (1970). Cleavage of structural proteins during the assembly of the head of bacteriophage T4. *Nature* 227:680. doi: 10.1038/227680a0
- Leak, D. J., Sheldon, R. A., Woodley, J. M., and Adlercreutz, P. (2009). Biocatalysts for selective introduction of oxygen. *Biocatal. Biotransfor.* 27, 1–26. doi: 10.1080/10242420802393519
- Lindmeyer, M., Meyer, D., Kuhn, D., Bühler, B., and Schmid, A. (2015). Making variability less variable: matching expression system and host for oxygenase-based biotransformations. *J. Ind. Microbiol. Biotechnol.* 42, 851–866. doi: 10.1007/s10295-015-1615-8
- Lundemo, M. T., and Woodley, J. M. (2015). Guidelines for development and implementation of biocatalytic P450 processes. *Appl. Microbiol. Biotechnol.* 99, 2465–2483. doi: 10.1007/s00253-015-6403-x
- Martínez-García, E., Aparicio, T., Goñi-Moreno, A., Fraile, S., and De lorenzo, V. (2015). SEVA 2.0: an update of the standard european vector architecture for de-/re-construction of bacterial functionalities. *Nucleic Acids Res.* 43, D1183–D1189. doi: 10.1093/nar/gku1114
- Meyer, R. (2009). Replication and conjugative mobilization of broad host-range IncQ plasmids. *Plasmid* 62, 57–70. doi: 10.1016/j.plasmid.2009.05.001
- Musser, M. T. (2000). *Cyclohexanol and Cyclohexanone*, *Ullmann's Encyclopedia of Industrial Chemistry*. Hoboken, NJ: Wiley.
- Nieboer, M., Kingma, J., and Witholt, B. (1993). The alkane oxidation system of *Pseudomonas oleovorans*: induction of the *alk* genes in *Escherichia coli* W3110 (pGEc47) affects membrane biogenesis and results in overexpression of alkane hydroxylase in a distinct cytoplasmic membrane subfraction. *Mol. Microbiol.* 8, 1039–1051. doi: 10.1111/j.1365-2958.1993.tb01649.x



- Omura, T., and Sato, R. (1964). The carbon monoxide-binding pigment of liver microsomes I. Evidence for its hemoprotein nature. *J. Biol. Chem.* 239, 2370–2378.
- Panke, S., Meyer, A., Huber, C. M., Witholt, B., and Wubbolts, M. G. (1999). An alkane-responsive expression system for the production of fine chemicals. *Appl. Environ. Microbiol.* 65, 2324–2332. doi: 10.1128/aem.65.6.2324-2332.1999
- Peretti, S. W., and Bailey, J. E. (1987). Simulations of host–plasmid interactions in *Escherichia coli*: copy number, promoter strength, and ribosome binding site strength effects on metabolic activity and plasmid gene expression. *Biotechnol. Bioeng.* 29, 316–328. doi: 10.1002/bit.260290305
- Registry of Standard Biological Parts, (n.d.). *Ribosome Binding Sites/Prokaryotic/Constitutive/Community Collection*. Available at: [http://parts.igem.org/Ribosome\\_Binding\\_Sites/Prokaryotic/Constitutive/Community\\_Collection](http://parts.igem.org/Ribosome_Binding_Sites/Prokaryotic/Constitutive/Community_Collection) (accessed November 19, 2019).
- Salamanca, D., Karande, R., Schmid, A., and Dobsław, D. (2015). Novel cyclohexane monooxygenase from *Acidovorax* sp. CHX100. *Appl. Microbiol. Biotechnol.* 99, 6889–6897. doi: 10.1007/s00253-015-6599-9
- Sambrook, J., and Russell, D. W. (2001). *Molecular Cloning: A Laboratory Manual*. Cold Spring Harbor, NY: Cold Spring Harbor Laboratory.
- Schrewe, M., Julsing, M. K., Buehler, B., and Schmid, A. (2013). Whole-cell biocatalysis for selective and productive C–O functional group introduction and modification. *Chem. Soc. Rev.* 42, 6346–6377. doi: 10.1039/c3cs60011d
- Schuchardt, U., Cardoso, D., Sercheli, R., Pereira, R., Da Cruz, R. S., Guerreiro, M. C., et al. (2001). Cyclohexane oxidation continues to be a challenge. *Appl. Catal. A* 211, 1–17. doi: 10.1016/S0926-860X(01)00472-0
- Schuchardt, U., Carvalho, W. A., and Spinacé, E. V. (1993). Why is it interesting to study cyclohexane oxidation? *Synlett* 1993, 713–718. doi: 10.1055/s-1993-22583
- Silva-Rocha, R., Martínez-García, E., Calles, B., Chavarria, M., Arce-Rodríguez, A., De Las Heras, A., et al. (2013). The standard european vector architecture (SEVA): a coherent platform for the analysis and deployment of complex prokaryotic phenotypes. *Nucleic Acids Res.* 41, D666–D675. doi: 10.1093/nar/gks1119
- Staijen, I. E., Marcionelli, R., and Witholt, B. (1999). The PalkBFGHJKL promoter is under carbon catabolite repression control in *Pseudomonas oleovorans* but not in *Escherichia coli* alk+ recombinants. *J. Bacteriol.* 181, 1610–1616. doi: 10.1128/jb.181.5.1610-1616.1999
- Urlacher, V. B., and Schmid, R. D. (2006). Recent advances in oxygenase-catalyzed biotransformations. *Curr. Opin. Chem. Biol.* 10, 156–161. doi: 10.1016/j.cbpa.2006.02.001
- Van Beilen, J. B., Duetz, W. A., Schmid, A., and Witholt, B. (2003). Practical issues in the application of oxygenases. *Trends Biotechnol.* 21, 170–177. doi: 10.1016/S0167-7799(03)00032-5
- Volmer, J., Lindmeyer, M., Seipp, J., Schmid, A., and Bühler, B. (2019). Constitutively solvent-tolerant *Pseudomonas taiwanensis* VLB120Δ CΔ ttgV supports particularly high-styrene epoxidation activities when grown under glucose excess conditions. *Biotechnol. Bioeng.* 116, 1089–1101. doi: 10.1002/bit.26924
- Volmer, J., Neumann, C., Bühler, B., and Schmid, A. (2014). Engineering of *Pseudomonas taiwanensis* VLB120 for constitutive solvent tolerance and increased specific styrene epoxidation activity. *Appl. Environ. Microbiol.* 80, 6539–6548. doi: 10.1128/AEM.01940-14
- Volmer, J., Schmid, A., and Bühler, B. (2017). The application of constitutively solvent-tolerant *P. taiwanensis* VLB120ΔCΔttgV for stereospecific epoxidation of toxic styrene alleviates carrier solvent use. *Biotechnol. J.* 12:1600558. doi: 10.1002/biot.201600558
- Weiss, R., Knight, T., and Sussman, G. (2004). “Cellular computation and communication using engineered genetic regulatory networks,” in *Cellular Computing*, eds M. Amos, and G. Owenson, (New York, NY: Oxford University Press Inc.), 120–147.
- Weissermel, K., and Arpe, H.-J. (2003). *Industrial Organic Chemistry*, 4th Edn, Weinheim: WILEY-VCH Verlag GmbH & Co. KGaA.
- Xu, P., Gu, Q., Wang, W., Wong, L., Bower, A. G. W., Collins, C. H., et al. (2013). Modular optimization of multi-gene pathways for fatty acids production in *E. coli*. *Nat. Commun.* 4:1409. doi: 10.1038/ncomms2425
- Xu, P., Rizzoni, E. A., Sul, S.-Y., and Stephanopoulos, G. (2017). Improving metabolic pathway efficiency by statistical model-based multivariate regulatory metabolic engineering. *ACS Synth. Biol.* 6, 148–158. doi: 10.1021/acssynbio.6b00187

**Conflict of Interest:** The authors declare that the research was conducted in the absence of any commercial or financial relationships that could be construed as a potential conflict of interest.

Copyright © 2020 Schäfer, Karande and Bühler. This is an open-access article distributed under the terms of the Creative Commons Attribution License (CC BY). The use, distribution or reproduction in other forums is permitted, provided the original author(s) and the copyright owner(s) are credited and that the original publication in this journal is cited, in accordance with accepted academic practice. No use, distribution or reproduction is permitted which does not comply with these terms.

## *Supplementary Material*

### **1 Molecular biology methods**

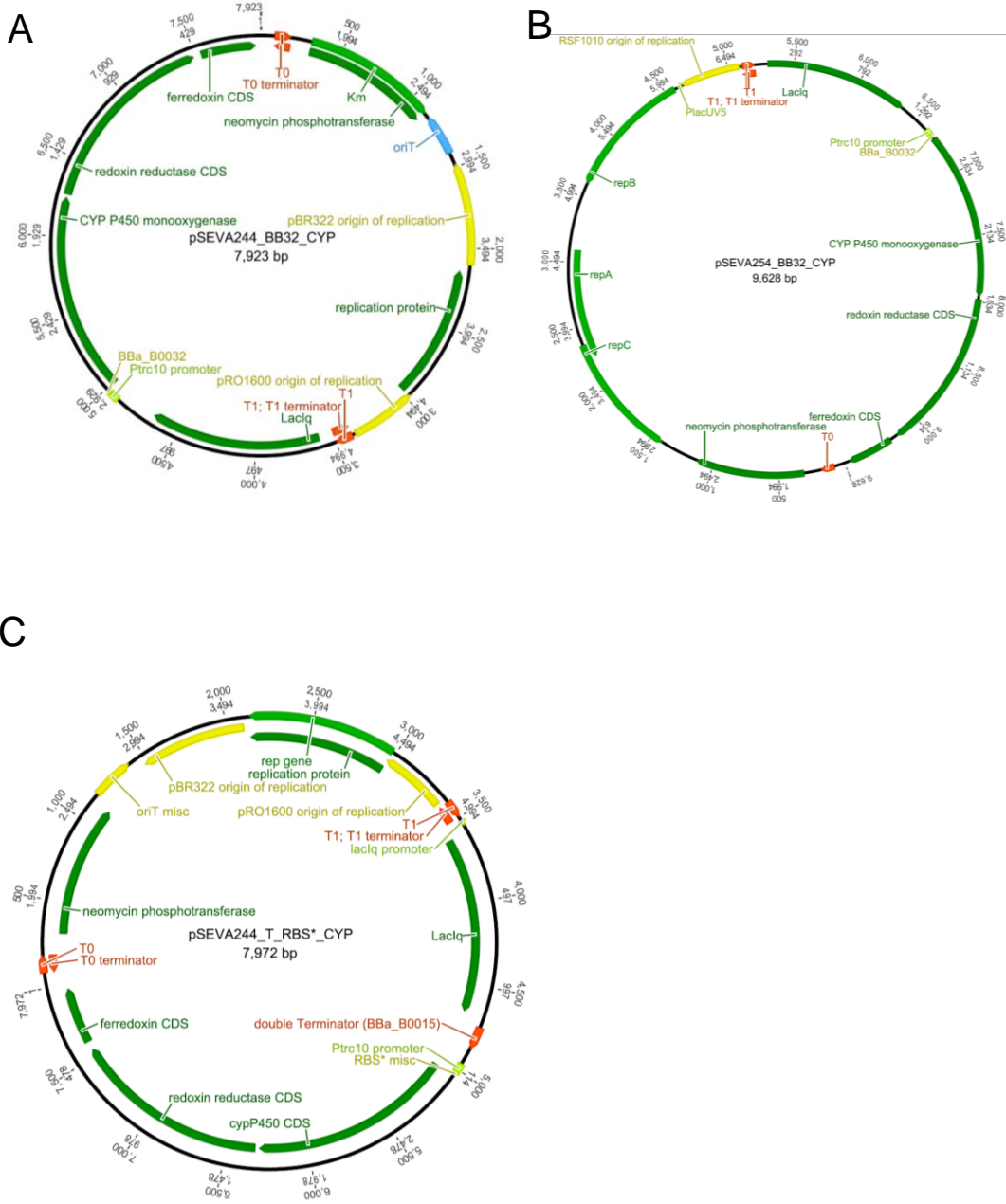
For the construction of plasmids pCom\_lac\_Cyp and pCom\_tac\_Cyp, the monooxygenase, ferredoxin and ferredoxin reductase genes were isolated from the plasmid pCapro (Karande et al., 2018) by restriction with NdeI and AscI. This purified fragment was ligated into pCom10\_lac (Lindmeyer et al., 2015b) or pCom10\_tac (Lindmeyer et al., 2015a) cut with the same enzymes, respectively.

To generate the Cyp expression vectors with different RBSs and copy numbers, pSEVA244 and pSEVA254 (Jahn et al., 2016) were employed containing a ColE1/pRO1600 or RSF1010 origin of replication and digested with XmaJI. Cyp, ferredoxin and ferredoxin reductase were amplified from pCapro with the primers listed in Table 1 (PLS005/7/8 and PLS006). The purified fragment and the vector backbone were fused by Gibson assembly.

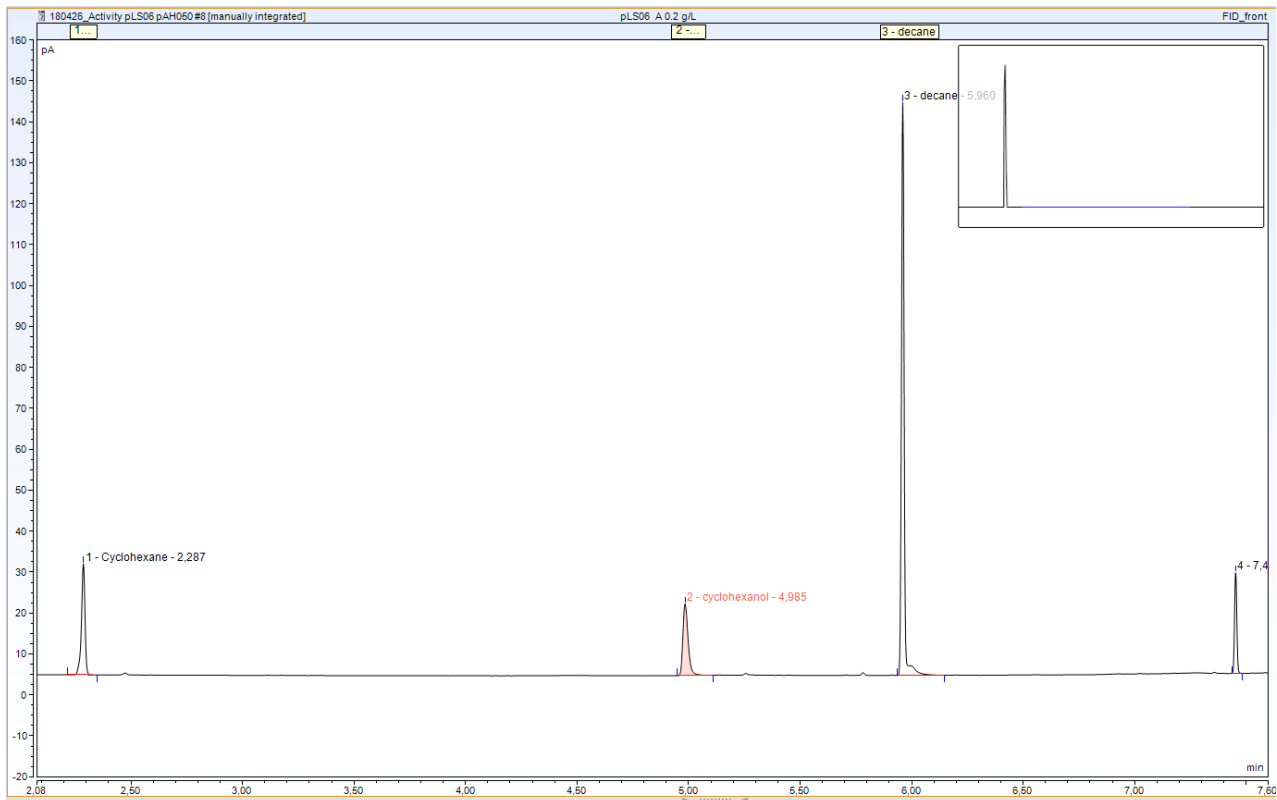
The double terminator was amplified from the vector pSB1AC3\_Ptrc1O\_GFPmut3b (Huang et al., 2010) using primers PLS009 and PLS010 (Tab. S2). A PCR with the vector pSEVA244 was conducted with primers PLS011 and PLS012 and both fragments were brought together via Gibson assembly. The Cyp genes were inserted afterwards as described above.

**Supplementary Table S1:** Primer used during the cloning. **binding region**, overlap to vector, scar,**RBS**

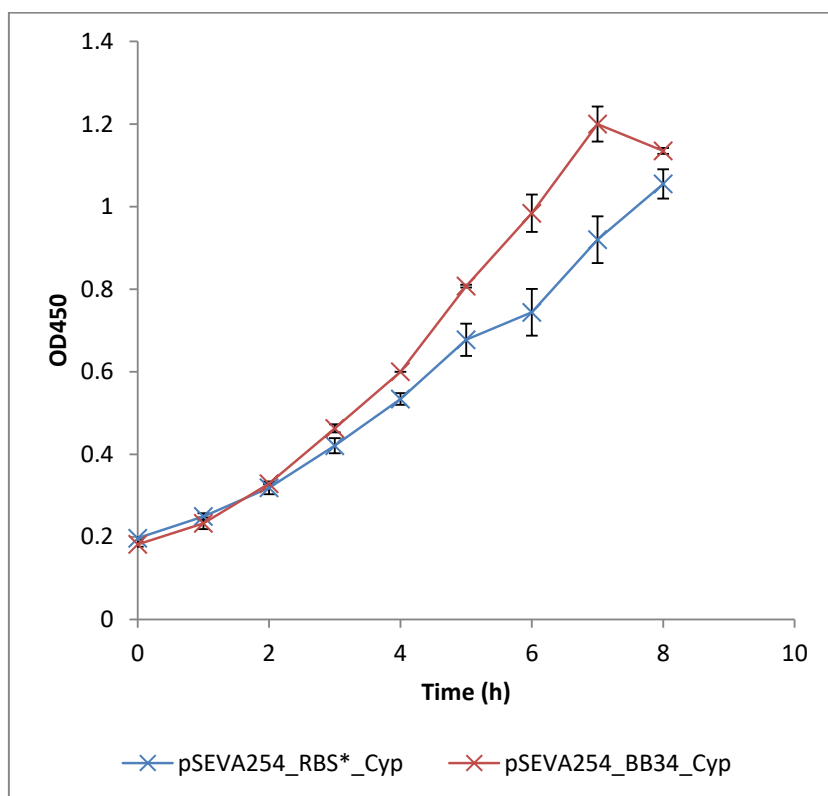
Primer#	Function	Sequence
PLS005	CYP fwd, BBa_B0032	<u>TGTGAGCGGATAACAATTCACACCTAGGAGAG</u> <b>TCACACAGGAAAG</b> TACTAGATGACTCAGACTGCTGCGGC
PLS006	CYP rev	<u>GAGCTCGAATTCGCGCGGCCGCGGCCTAGGTCAGTGCTGCCCTTGC</u> <b>G</b>
PLS007	CYP fwd, BBa_B0034	<u>TGTGAGCGGATAACAATTCACACCTAGGAGAG</u> <b>AAAGAGGAGAAAT</b> ACTAGATGACTCAGACTGCTGCGGC
PLS008	CYP fwd, RBS*	<u>TGTGAGCGGATAACAATTCACACCTAGGAGAG</u> <b>TAGTGGAGGT</b> TACT AGATGACTCAGACTGCTGCGGC
PLS009	Term fwd	<u>GATCTGGTTTGACAGCTTATCATCGCCAGGCATCAAATAAAACG</u>
PLS010	Term rev	<u>CGCCTTGAGCGACACGAATTATGCATATAAACGCAGAAAGGCC</u>
PLS011	pSEVA244 fwd	<b>TGCATAATTCGTGTCGCTC</b>
PLS012	pSEVA244 rev	<b>CGATGATAAGCTGTCAAACCAG</b>



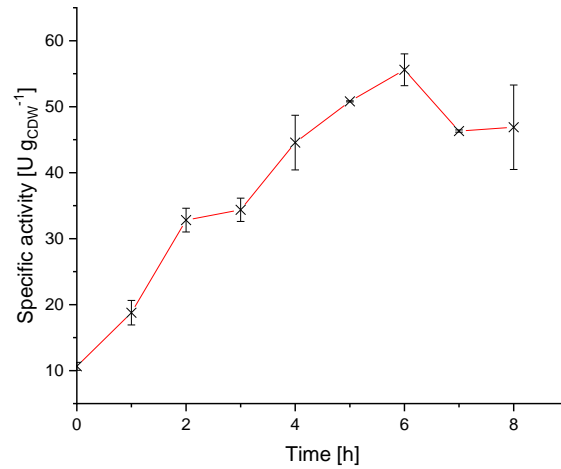
**Supplementary Figure S1.** Exemplary vector maps for pSEVA244\_RBS\_Cyp (A) pSEVA254\_RBS\_Cyp and pSEVA244\_T\_RBS\_Cyp. The vectors are based on the pSEVA collection (Silva-Rocha et al., 2013).



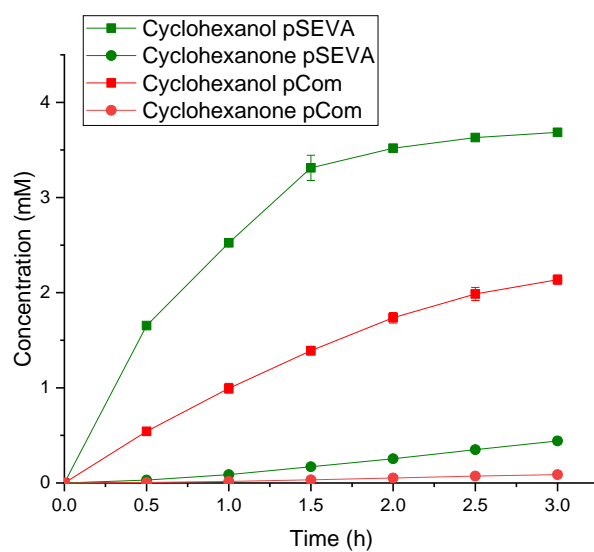
**Supplementary Figure S2: Exemplary GC chromatogram.** The GC chromatogram is shown for *P. taiwanensis* VLB120 pSEVA254\_BB34\_Cyp (see Fig. 4, strong RBS) with the retention times for cyclohexane, cyclohexanol and n-decane of 2.3, 5.0, and 6.0 min, respectively.



**Supplementary Figure S3.** Growth curves for *P. taiwanensis* VLB120 pSEVA244\_RBS\*\_Cyp and pSEVA254\_BB34\_Cyp. The cultures were induced 4 h after inoculation. Cells were cultivated in M9\* medium with 0.5 % (w/v) glucose at 30°C, 200 rpm. One OD450 unit corresponds to a biomass concentration of 0.186 g<sub>CDW</sub> L<sup>-1</sup> for *P. taiwanensis* VLB120 (Halan et al., 2010).



**Supplementary Figure S4.** Cyclohexane hydroxylation activity *P. taiwanensis* VLB120 pSEVA244\_T\_RBS\*\_Cyp (intermediate). Cells were induced 3 h after inoculation and harvested every hour for resting cell assays. For resting cell assays, cells were cultivated in M9\* medium with 0.5 % (w/v) glucose and resuspended in Kpi buffer supplemented with 1 % (w/v) respective carbon source to a biomass concentration of 0.2 g/L. Assays were performed with 1 mL of cell suspension in Pyrex tubes in a water bath, at 30°C and 250 rpm. Reactions were started by adding 1.25  $\mu$ L pure cyclohexane (liquid cyclohexane concentration is equal to 10  $\mu$ L in flasks 180  $\mu$ M in aq. phase) and stopped after 10 min by quenching with diethyl ether. The bars represent average values and standard deviations of two independent biological replicates.



**Supplementary Figure S5.** Reaction course of the biotransformation employing *P. taiwanensis* VLB120 pCom\_Cyp (red) and pSEVA\_Cyp (green). Reaction products are cyclohexanol and the overoxidation product cyclohexanone, which are quantified by GC. Reactions were started by adding pure cyclohexane to a total concentration of 5 mM (referred to in the aqueous phase). For further details see Materials and Methods section. The bars represent average values and standard deviations of two independent biological replicates.



**Raw data for results presented**

Specific activities given in Figs. 2-5 were obtained from GC-derived cyclohexanol concentrations, which were calculated based on calibration curves referring to the internal standard n-decane. Cyclohexanol concentrations, OD<sub>450</sub>-derived cell concentrations, and activity calculations are given in Table S2. Specific activities were calculated based on the produced cyclohexanol concentration within 10 min taking into account the measured cell concentration in the flask.

**Supplementary Table S2:** Raw data for Figs. 2-5.

	Construct name	Concentration	Cell concentration	Activity		
		mM	g L <sup>-1</sup>	U g <sub>CDW</sub> <sup>-1</sup>		
		in aqueous phase			Average	Standard deviation
		Cyclohexanol				
Figure 2	pCom10_lac_Cyp A	0.337	0.975	34.5	35.0	1.9
	pCom10_lac_Cyp B	0.355	0.962	36.9		
	pCom10_lac_Cyp A	0.072	0.201	35.9		
	pCom10_lac_Cyp B	0.064	0.199	32.4		
	pCom10_tac_Cyp A	0.184	0.960	19.1	18.5	1.0
	pCom10_tac_Cyp B	0.174	0.973	17.9		
	pCom10_tac_Cyp A	0.033	0.189	17.4		
	pCom10_tac_Cyp B	0.039	0.201	19.6		
	pCom10_Cyp A	0.034	0.149	22.9	22.2	1.2
	pCom10_Cyp B	0.032	0.156	20.4		
	pCom10_Cyp A	0.167	0.740	22.6		
	pCom10_Cyp B	0.171	0.748	22.9		
Figure 3	pSEVA244_BB32_Cyp A	0.024	0.166	14.7	14.0	0.6
	pSEVA244_BB32_Cyp B	0.025	0.175	14.2		
	pSEVA244_BB32_Cyp A	0.058	0.424	13.7		
	pSEVA244_BB32_Cyp B	0.060	0.448	13.4		
	pSEVA244_BB34_Cyp A	0.009	0.193	4.5	4.7	0.3
	pSEVA244_BB34_Cyp B	0.008	0.184	4.5		
	pSEVA244_BB34_Cyp A	0.025	0.478	5.2		
	pSEVA244_BB34_Cyp B	0.021	0.476	4.5		
	pSEVA244_RBS*_Cyp A	0.084	0.179	46.9	48.4	1.5
	pSEVA244_RBS*_Cyp B	0.091	0.182	50.1		
	pSEVA244_RBS*_Cyp A	0.220	0.463	47.5		
	pSEVA244_RBS*_Cyp B	0.223	0.454	49.2		
Figure	pSEVA254_BB32_Cyp A	0.007	0.211	3.3	2.7	0.7
	pSEVA254_BB32_Cyp B	0.004	0.223	1.8		
	pSEVA254_BB32_Cyp A	0.016	0.551	3.0		

	pSEVA254_BB32_Cyp B	0.016	0.526	3.0		
	pSEVA254_BB34_Cyp A	0.114	0.214	54.5	49.8	4.6
	pSEVA254_BB34_Cyp B	0.103	0.196	52.9		
	pSEVA254_BB34_Cyp A	0.164	0.355	46.7		
	pSEVA254_BB34_Cyp B	0.155	0.333	45.1		
	pSEVA254_RBS*_Cyp A	0.113	0.225	50.3	50.7	0.7
	pSEVA254_RBS*_Cyp B	0.113	0.221	50.9		
	pSEVA254_RBS*_Cyp A	0.219	0.424	51.6		
	pSEVA254_RBS*_Cyp B	0.217	0.433	50.0		
Figure 5	pSEVA244_T_BB34_Cyp A	0.145	0.588	24.7	27.3	2.4
	pSEVA244_T_BB34_Cyp B	0.153	0.588	26.0		
	pSEVA244_T_BB34_Cyp C	0.136	0.552	24.6		
	pSEVA244_T_BB34_Cyp D	0.152	0.552	27.5		
	pSEVA244_T_BB34_Cyp A	0.062	0.212	29.1		
	pSEVA244_T_BB34_Cyp B	0.067	0.212	31.8		
	pSEVA244_T_BB34_Cyp C	0.055	0.204	27.0		
	pSEVA244_T_BB34_Cyp D	0.056	0.204	27.6		
	pSEVA244_T_RBS*_Cyp A	0.343	0.565	60.7	42.4	2.4
	pSEVA244_T_RBS*_Cyp B	0.245	0.565	43.4		
	pSEVA244_T_RBS*_Cyp C	0.219	0.497	44.1		
	pSEVA244_T_RBS*_Cyp D	0.222	0.497	44.6		
	pSEVA244_T_RBS*_Cyp A	0.100	0.246	40.5		
	pSEVA244_T_RBS*_Cyp B	0.109	0.246	44.3		
	pSEVA244_T_RBS*_Cyp C	0.097	0.231	42.2		
	pSEVA244_T_RBS*_Cyp D	0.088	0.231	38.0		

## Supplementary Material

The biotransformation data given in Table 3 were obtained from GC-derived cyclohexane, cyclohexanol and cyclohexanone concentrations, which were calculated based on calibration curves referring to the internal standard n-decane. The concentrations are given in Table S3, where cyclohexanol and cyclohexanone are both considered as products of the biotransformation. The data given in Tab. 3 were calculated as described in Materials and Methods after a biotransformation time of 3 h with a cell concentration of 1.5 g L<sup>-1</sup>.

**Supplementary Table 3:** Raw data for Table 3 and Supplementary Figure S5.

Time h	Injection Name	Concentration cyclohexane			Concentration cyclohexanol			Concentration cyclohexanone			Sum of Products	
		mM			mM			mM			mM	
		in aqueous phase			in aqueous phase			in aqueous phase				
		Average	Standard deviation		Average	Standard deviation		Average	Standard deviation			
0.5	pCom t1 A	0.056	0.054	0.003	0.515	0.543	0.039	0.004	0.005	0.001	0.548	0.040
0.5	pCom t1 B	0.052			0.571			0.005				
1	pCom t2 A	0.045	0.046	0.001	0.959	0.995	0.052	0.014	0.016	0.003	1.011	0.055
1	pCom t2 B	0.047			1.032			0.019				
1.5	pCom t3 A	0.050	0.050	0.000	1.358	1.390	0.045	0.030	0.033	0.004	1.423	0.048
1.5	pCom t3 B	0.050			1.421			0.035				
2	pCom t4 A	0.040	0.043	0.004	1.698	1.737	0.055	0.048	0.052	0.006	1.789	0.062
2	pCom t4 B	0.046			1.776			0.057				
2.5	pCom t5 A	0.039	0.040	0.001	1.937	1.986	0.069	0.066	0.072	0.009	2.058	0.078
2.5	pCom t5 B	0.041			2.035			0.078				
3	pCom t6 A	0.038	0.037	0.001	2.103	2.137	0.049	0.080	0.087	0.010	2.224	0.059
3	pCom t6 B	0.036			2.172			0.094				
0.5	pSEVA t1 A	0.014	0.015	0.001	1.661	1.654	0.010	0.029	0.031	0.003	1.685	0.013
0.5	pSEVA t1 B	0.016			1.646			0.033				
1	pSEVA t2 A	0.010	0.010	0.001	2.528	2.524	0.006	0.084	0.088	0.006	2.612	0.012
1	pSEVA t2 B	0.009			2.520			0.093				
1.5	pSEVA t3 A	0.008	0.007	0.001	3.406	3.312	0.132	0.166	0.170	0.006	3.482	0.138
1.5	pSEVA t3 B	0.006			3.218			0.175				
2	pSEVA t4 A	0.005	0.005	0.000	3.531	3.518	0.019	0.242	0.255	0.018	3.772	0.037
2	pSEVA t4 B	0.005			3.504			0.267				
2.5	pSEVA t5 A	0.003	0.003	0.000	3.646	3.630	0.023	0.336	0.351	0.021	3.980	0.044
2.5	pSEVA t5 B	0.003			3.613			0.365				
3	pSEVA t6 A	0.003	0.003	0.000	3.670	3.685	0.022	0.419	0.441	0.032	4.126	0.053
3	pSEVA t6 B	0.003			3.700			0.464				

## References




- Halan, B., Schmid, A., and Buehler, K. (2010). Maximizing the productivity of catalytic biofilms on solid supports in membrane aerated reactors. *Biotechnol. Bioeng.* 106, 516-527.
- Huang, H.-H., Camsund, D., Lindblad, P., and Heidorn, T. (2010). Design and characterization of molecular tools for a Synthetic Biology approach towards developing cyanobacterial biotechnology. *Nucleic Acids Res.* 38, 2577-2593.
- Jahn, M., Vorpahl, C., Hübschmann, T., Harms, H., and Müller, S. (2016). Copy number variability of expression plasmids determined by cell sorting and Droplet Digital PCR. *Microb. Cell Fact.* 15, 211.
- Karande, R., Salamanca, D., Schmid, A., and Buehler, K. (2018). Biocatalytic conversion of cycloalkanes to lactones using an in-vivo cascade in *Pseudomonas taiwanensis* VLB120. *Biotechnol. Bioeng.* 115, 312-320.
- Lindmeyer, M., Jahn, M., Vorpahl, C., Müller, S., Schmid, A., and Bühler, B. (2015a). Variability in subpopulation formation propagates into biocatalytic variability of engineered *Pseudomonas putida* strains. *Front. Microbiol.* 6, 1042.
- Lindmeyer, M., Meyer, D., Kuhn, D., Bühler, B., and Schmid, A. (2015b). Making variability less variable: matching expression system and host for oxygenase-based biotransformations. *J. Ind. Microbiol. Biotechnol.* 42, 851-866.
- Silva-Rocha, R., Martínez-García, E., Calles, B., Chavarría, M., Arce-Rodríguez, A., De Las Heras, A., Páez-Espino, A.D., Durante-Rodríguez, G., Kim, J., Nickel, P.I., Platero, R., and De Lorenzo, V. (2013). The Standard European Vector Architecture (SEVA): a coherent platform for the analysis and deployment of complex prokaryotic phenotypes. *Nucleic Acids Res.* 41, D666-D675.

**2 Biotechnol. Bioeng. (2021), 118(7), p. 2719-2733, incl.**

**Supplementary Material**

## ARTICLE

# Characterization of different biocatalyst formats for BVMO-catalyzed cyclohexanone oxidation

Lisa Bretschneider  | Ingeborg Heuschkel | Afaq Ahmed | Katja Bühler |  
Rohan Karande  | Bruno Bühler 

Department of Solar Materials, Helmholtz-Centre for Environmental Research - UFZ, Leipzig, Germany

## Correspondence

Rohan Karande, Department of Solar Materials, Helmholtz-Centre for Environmental Research - UFZ, Leipzig, Permoserstraße 15, 04318 Leipzig, Germany. Email: rohan.karande@ufz.de

## Funding information

Sächsisches Ministerium für Wissenschaft und Kunst (SMWK), Grant/Award Number: 100318259; ERA-IB Project PolyBugs, Grant/Award Number: 16006

## Abstract

Cyclohexanone monooxygenase (CHMO), a member of the Baeyer–Villiger monooxygenase family, is a versatile biocatalyst that efficiently catalyzes the conversion of cyclic ketones to lactones. In this study, an *Acidovorax*-derived CHMO gene was expressed in *Pseudomonas taiwanensis* VLB120. Upon purification, the enzyme was characterized in vitro and shown to feature a broad substrate spectrum and up to 100% conversion in 6 h. Furthermore, we determined and compared the cyclohexanone conversion kinetics for different CHMO-biocatalyst formats, that is, isolated enzyme, suspended whole cells, and biofilms, the latter two based on recombinant CHMO-containing *P. taiwanensis* VLB120. Biofilms showed less favorable values for  $K_S$  (9.3-fold higher) and  $k_{cat}$  (4.8-fold lower) compared with corresponding  $K_M$  and  $k_{cat}$  values of isolated CHMO, but a favorable  $K_I$  for cyclohexanone (5.3-fold higher). The unfavorable  $K_S$  and  $k_{cat}$  values are related to mass transfer- and possibly heterogeneity issues and deserve further investigation and engineering, to exploit the high potential of biofilms regarding process stability. Suspended cells showed only 1.8-fold higher  $K_S$ , but 1.3- and 4.2-fold higher  $k_{cat}$  and  $K_I$  values than isolated CHMO. This together with the efficient NADPH regeneration via glucose metabolism makes this format highly promising from a kinetics perspective.

## KEYWORDS

Baeyer–Villiger monooxygenase, biocatalysis, biofilm kinetics, enzyme kinetics, whole-cell kinetics

## 1 | INTRODUCTION

In synthetic organic chemistry, the Baeyer–Villiger oxidation is known as the conversion of ketones to respective esters or lactones with peracids as typical oxygen donors (Bayer et al., 2015). However, this classical approach often suffers from low

chemo-, regio-, and enantioselectivities (Pazmino et al., 2010). Moreover, the necessity of strong chemical oxidants such as hydrogen peroxide ( $H_2O_2$ ) and *m*-chloroperoxybenzoic acid (*m*-CPBA) in combination with a Lewis acid implicates high costs and explosion risk (Grootboom & Nyokong, 2002). Baeyer–Villiger monooxygenases (BVMOs) constitute the biological alternative,

This is an open access article under the terms of the Creative Commons Attribution License, which permits use, distribution and reproduction in any medium, provided the original work is properly cited.

© 2021 The Authors. *Biotechnology and Bioengineering* published by Wiley Periodicals LLC

utilize O<sub>2</sub> as oxygen donor, and depend on NAD(P)H (Ryerson et al., 1982). They feature high regio-, stereo-, and enantioselectivities and operate under mild reaction conditions, making them an environmentally friendly alternative to the existing chemical catalytic processes (Ten Brink et al., 2004).

One of the main features of BVMOs is their broad substrate scope, also covering nonnatural substrates. Besides the carbonyl carbon in aliphatic, cyclic, and aromatic ketones, BVMOs also oxidize sulfur (Colonna et al., 1996), nitrogen (Ottolina et al., 1999), and even selenium (Latham et al., 1986) atoms. In the last two decades, extensive work has been done regarding the isolation of BVMOs and their evaluation for the generation of novel functionalities with value for the pharmaceutical, food, and fine chemical industries (Alphand et al., 2003; Fürst et al., 2019; Pazmino et al., 2010). On the downside, most BVMO-based oxidation processes suffer from low enzyme stability and inhibitory or toxic effects of substrates and/or products restricting volumetric productivities and product titers (Fürst et al., 2019).

The application of BVMOs in *in vivo* and/or immobilized formats constitutes a promising strategy to improve biocatalyst stability and total turnover number. However, a change in biocatalyst configuration can affect reaction kinetics and, consequently, reaction performance (van Beilen et al., 2003). Typically, *in vitro* kinetics are characterized under conditions that do not resemble *in vivo* environments, and thus reaction kinetics often differ among *in vitro* and *in vivo* formats (Teusink et al., 2000; Van Eunen & Bakker, 2014). Conversely, other studies that characterized *in vivo* catalytic rates found that they generally concur with *in vitro* measurements (Davidi et al., 2016; Heckmann et al., 2020). Such contradictory results also have been reported for the comparison of kinetics for suspended and immobilized microbial cells. Whereas toluene degradation kinetics were comparable in biofilms and planktonic cells (Mirpuri et al., 1997), nitriloacetate degradation activity was three-fold enhanced for sand-associated as compared with suspended cells (McFeters et al., 1990). These findings imply that similarity or differences in reaction kinetics among biocatalyst formats might be case-dependent, and point out that the determination and understanding of differences in kinetics is of significant interest for modeling biological systems and selecting the most promising biocatalyst format for technical applications.

In the present work, we aimed to understand if, to what extent, and why CHMO-reaction kinetics concur or differ among isolated enzyme-, suspended cell-, and biofilm-based formats. For this purpose, CHMO from *Acidovorax* sp. CHX100 was introduced into *Pseudomonas taiwanensis* VLB120, a solvent-tolerant strain and good biofilm former (Halan et al., 2011; Rohan Karande et al., 2014; Volmer et al., 2014). This strain was used for recombinant CHMO production and as a catalytic unit in suspended cell- and biofilm formats.

## 2 | MATERIALS AND METHODS

### 2.1 | Construction of the phylogenetic tree

Amino acid sequences of different BVMOs were aligned using the MUSCLE algorithm (Edgar, 2004). The evolutionary history was inferred by using the Maximum Likelihood method and the Whelan and Goldman model (Whelan & Goldman, 2001). The bootstrap consensus tree inferred from 500 replicates is taken to represent the evolutionary history of the taxa analyzed (Felsenstein, 1985). Branches corresponding to partitions reproduced in less than 50% bootstrap replicates are collapsed. Initial tree(s) for the heuristic search were obtained automatically by applying Neighbor-Join and BioNJ algorithms to a matrix of pairwise distances estimated using a JTT model, and then selecting the topology with a superior log likelihood value. A discrete Gamma distribution was used to model evolutionary rate differences among sites (five categories [+G, parameter = 21,745]). This analysis involved 36 amino acid sequences. There were a total of 788 positions in the final data set. Evolutionary analyses were conducted in MEGA X (Kumar et al., 2018).

### 2.2 | Chemicals, media, and bacterial strains

Unless stated otherwise, all chemicals were purchased from Sigma-Aldrich or Carl Roth in the highest purity available and used without further purification. Microbial strains and plasmids used in this study are listed in Table 1. Cells were grown in lysogeny broth (LB) medium

**TABLE 1** Strains and plasmids used in this study

Strain	Characteristics	Reference
<i>Escherichia coli</i> DH5 $\alpha$	<i>supE44</i> $\Delta$ <i>lacU169</i> ( $\Phi$ 80 <i>lacZ</i> $\Delta$ M15) <i>hsdR17 recA1 endA1 gyrA96 thi-1 relA1</i>	Hanahan (1983)
<i>Pseudomonas taiwanensis</i> VLB120	Solvent tolerant, styrene degrading bacterium, isolated from forest soil	Köhler et al. (2013)
Plasmid		
pSEVA244_T	pRO1600 and ColE1ori, <i>lac</i> -regulatory system ( <i>lacI<sup>q</sup></i> , <i>P<sub>trc</sub></i> ), BBa_B0015 terminator, RBS*, empty vector	Schäfer, Karande, et al. (2020)
pSEVA_CHMO	pRO1600 and ColE1ori, <i>lac</i> -regulatory system ( <i>lacI<sup>q</sup></i> , <i>P<sub>trc</sub></i> ), BBa_B0015 terminator, RBS*, CHMO gene from <i>Acidovorax</i> sp.	Schäfer, Bühler, et al. (2020)

(Sambrook & Russell, 2001) or M9\* medium (Panke et al., 1999) with a pH of 7.2 supplemented with 0.5% (w/v) glucose as sole carbon source and kanamycin ( $50 \mu\text{g ml}^{-1}$ ).

### 2.3 | Cultivation conditions

Cultivations were carried out at  $30^\circ\text{C}$  and 200 rpm in a Multitron shaker (Infors) utilizing baffled shake flasks. LB pre-cultures (10 ml in 100 ml flasks) incubated for ca. twenty hours typically were used to inoculate (1% v/v) M9\* pre-cultures (10 ml in 100 ml flasks), which were incubated for another 12–16 h and used to inoculate M9\* main cultures at a starting  $\text{OD}_{450}$  of 0.2 (50 ml in 500 ml flasks). Heterologous gene expression was induced by adding isopropyl  $\beta$ -d-1-thiogalactopyranoside (IPTG) to a concentration of 1 mM after 3 h of cultivation ( $\text{OD}_{450} \sim 0.5$ ). Incubation was continued for another 6 h, followed by cell harvesting via centrifugation (10 min, 5000 g) for sodium dodecyl sulfate-polyacrylamide gel electrophoresis (SDS-PAGE), resting cell assays, and/or CHMO purification. For purification, the pellet was stored at  $-20^\circ\text{C}$  until further use.

### 2.4 | Purification protocol

Cells were resuspended in 100 mM Kpi buffer (pH = 7.4) to an  $\text{OD}_{450}$  of 50 and disrupted by using a French press (Thermo Electron Corporation). The sample was passed three times at 1200 psi. The crude cell extract was centrifuged at  $10,000 \times g$  for 15 min at  $4^\circ\text{C}$ . The supernatant was loaded on a disposable plastic column (Thermo Fisher Scientific), which was packed with Strep-Tactin<sup>®</sup> Superflow<sup>®</sup> resin (IBA Life Sciences) and equilibrated following the manufacturer's instructions. The flow-through, wash, and elution fractions were collected for SDS-PAGE analysis. In total three elution fractions were collected (1.5 ml, 2 ml, and 1.5 ml). The column was regenerated and stored in the wash buffer at  $4^\circ\text{C}$  until reuse.

### 2.5 | Determination of CHMO activity

To evaluate purification efficiency and the substrate spectrum of CHMO, its activity was assayed by monitoring the decrease in NADPH absorbance at 340 nm after the addition of substrate with a Cary Bio 300 UV-visible spectrophotometer (Varian, Palo Alto, USA). Activity assays were performed at  $30^\circ\text{C}$  for at least 2 min. Assay mixtures contained 1 mM substrate, 0.2 mM NADPH, and  $20 \mu\text{l}$  enzyme solution (containing  $1.0$ – $2.7 \text{ mg}_{\text{CHMO}} \text{ ml}^{-1}$ ) in 1 ml total volume. Initial activities were calculated from the decrease of NADPH absorption at 340 nm for 60–120 s using a specific absorption coefficient of  $\epsilon = 6.22 \text{ mM}^{-1} \text{ cm}^{-1}$ . One unit of enzyme activity was defined as  $1 \mu\text{mol}$  of NADPH consumed per min.

### 2.6 | Determination of CHMO kinetics

For kinetic analyses, a cell concentration of  $0.25 \text{ g}_{\text{CDW}} \text{ L}^{-1}$  or  $20 \mu\text{l}$  of purified enzyme ( $0.98 \text{ mg CHMO ml}^{-1}$ ) were used in 100 mM potassium phosphate buffer, pH = 7.4 (Kpi buffer) supplemented with 1% (w/v) glucose for whole cells as catalysts. For the variation of cyclohexanone and NADPH concentrations, the assays were conducted in 2 ml Eppendorf reaction tubes on a thermoshaker (Thermomixer C, Eppendorf). For the variation of the  $\text{O}_2$  concentration, small glass vials with a gas-tight septum cap were used. Buffer-containing vials were incubated at  $60^\circ\text{C}$  for 10 min and then degassed with  $\text{N}_2$  for 45 s. Then, target amounts of  $\text{O}_2$  were added with a gas-tight syringe (Hamilton). The assay was started by the addition of cyclohexanone for whole cells, and of cyclohexanone and CHMO for the isolated enzyme. Reactions were carried out for 5 min and stopped by the addition of ice-cold diethyl ether containing 0.2 mM n-decane as an internal standard. After 2 min of extraction by vortexing and centrifugation, the organic phase was dried over water-free  $\text{Na}_2\text{SO}_4$  before it was transferred to a GC vial for analysis.

### 2.7 | Determination of CHMO kinetics in biofilms

The biofilm capillary reactor system and *P. taiwanensis* VLB120 (pSEVA\_CHMO) pre-cultures were prepared as reported before (Heuschkel et al., 2019). A serological pipette functioned as a capillary for biofilm growth (3 mm inner diameter, 10 cm length, Labso-lute, Th. Geyer GmbH & Co. KG). M9\* medium ( $5 \text{ g L}^{-1}$  glucose) was supplied using a peristaltic pump (530S with 205CA12 pump head, Watson-Marlow). The capillaries of the reactor system were inoculated by purging 2 ml M9\* pre-culture through the injection port. The medium flow was started 2 h after inoculation at a rate of  $150 \mu\text{l min}^{-1}$ . Air segments were introduced 2 days after inoculation at a rate of  $150 \mu\text{l min}^{-1}$ . The airflow rate was set to  $200 \mu\text{l min}^{-1}$  4 days after inoculation and increased to  $400 \mu\text{l min}^{-1}$  at Day 5. By the addition of 1 mM IPTG to the medium feed, heterologous expression of BVMO genes was induced on Day 5. Bubble traps, as well as sampling ports, were attached at the end of the capillary to enable gas and liquid sampling while injection ports were removed from the setup. The kinetics experiment was conducted on Day 6. The airflow rate was set to  $600 \mu\text{l min}^{-1}$  and feed solutions containing desired cyclohexanone concentrations were freshly prepared in separate medium bottles (Kpi buffer, pH 7.4,  $10 \text{ g L}^{-1}$  glucose, 1 mM IPTG). The desired cyclohexanone feed solution was supplied to the capillaries by using PTFE tubing and a peristaltic pump (Tygon MHLL pump tubing, IPC 4, Ismatec) at a flow rate of  $150 \mu\text{l min}^{-1}$  equaling a residence time of 5 min. Thirty-minute after the switch to cyclohexanone containing feed, a sample was collected for 15 min and directly prepared for GC (as described before) and HPLC analysis. The HPLC sample was centrifuged (10 min,  $4^\circ\text{C}$ ,  $17,000 \times g$ ). One hundred microliters of the supernatant was acidified with  $10 \mu\text{l}$  1 M HCl and subjected to HPLC analysis. The procedure was repeated



with the different feed solutions. Finally, the biomass was harvested from the capillary and dried for 5 days at 80°C for cell dry weight determination.

## 2.8 | Analytical methods

Biomass concentrations were detected as the optical density at a wavelength of 450 nm ( $OD_{450}$ ) using a Libra S11 spectrophotometer (Biochrom). One  $OD_{450}$  unit corresponds to  $0.186 \text{ g}_{\text{CDW}} \text{ L}^{-1}$  (Halan et al., 2010).

Protein concentrations were determined using BSA as protein standard (Quick Start™ Bradford Protein Assay) following the supplier's instructions. Expression patterns were analyzed via SDS-PAGE according to Laemmli (1970). CHMO was quantified by determining the integrated density of CHMO bands using ImageJ. Samples with known CHMO content were used as calibration standards to calculate the CHMO content within samples (Figure S3). Cyclohexanone and  $\epsilon$ -caprolactone were separated by Trace 1310 gas chromatographs (Thermo Fisher Scientific) equipped with a TG-5MS GC Column (15 m length, 0.25 mm inner diameter, Thermo Fisher Scientific) and operated with a split ratio of 7,  $\text{N}_2$  as carrier gas,  $1 \mu\text{l}$  injection volume, and the following temperature profile: 40°C (1 min), 40–80°C [ $10^\circ\text{C min}^{-1}$ ], 80–320 [ $100^\circ\text{C min}^{-1}$ ], 320°C [7.6 min]. Cyclohexanone and  $\epsilon$ -caprolactone were quantified via flame ionization detector based on calibration curves from commercially available standards. Selected lactones were identified by a Thermo ISQ LT single Quadrupole MS (Thermo Fisher Scientific) coupled to the same GC-setup run with Helium as carrier gas and the following temperature profile: 80°C (2 min), 80–170°C [ $10^\circ\text{C min}^{-1}$ ], 170–300°C [ $100^\circ\text{C min}^{-1}$ ], 300°C (2 min), 300–80°C [ $100^\circ\text{C min}^{-1}$ ], and 80°C (1 min). Spectra were analyzed with Chromeleon 7 (Thermo Fisher Scientific). Concentrations of 6-hydroxyhexanoic acid were quantified by HPLC as described before (Schäfer, Bühler, et al., 2020).

The kinetic parameters  $V_{\text{max}}$ ,  $K_M$  (or  $K_S$ ), and  $K_I$  were calculated in Matlab 6.1 and fitted to the following equations using the method of least squares:

(1) without substrate inhibition ( $\text{O}_2$  as limiting substrate)

$$v_0 = \frac{v_{\text{max}} \times [S]}{K_M + [S]}$$

(2) with substrate inhibition (NADPH or cyclohexanone as limiting substrate)

$$v_0 = \frac{v_{\text{max}} \times [S]}{K_M + [S] + \frac{[S]^2}{K_I}}$$

$v_0$ : initial reaction velocity given in  $\text{U mg}^{-1}$  (isolated enzyme) or  $\text{U g}_{\text{CDW}}^{-1}$  (whole-cells, biofilm);  $V_{\text{max}}$  maximal reaction velocity;  $[S]$  substrate concentration;  $K_M$  Michaelis–Menten constant (substrate concentration, at which reaction velocity is half-maximal);  $K_I$  inhibition constant.

## 3 | RESULTS

### 3.1 | Relatedness of CHMO from *Acidovorax* to other BVMOs

The BVMO gene originating from *Acidovorax* CHX100 encodes a 541 amino acid protein. Several BVMOs from different bacterial species have been isolated and characterized. A phylogenetic tree of BVMOs is depicted in Figure 1, illustrating a certain clustering in substrate specificity-related clades. Although BVMOs typically feature a large substrate spectrum, such clustering, as described previously, is a useful tool to predict substrate specificities of uncharacterized BVMOs (Rehdorf et al., 2009). The CHMO isolated from *Acidovorax* sp. CHX100 clusters in a clade together with 10 BVMOs oxidizing cyclohexanone as preferred substrate in the frame of cyclohexanol or cyclohexanone degradation by *Brachymonas petroleovorans* (Brzostowicz et al., 2005), *Acinetobacter* sp. SE19 (Cheng et al., 2000), *Acinetobacter* sp. (Chen et al., 1988), *Acidovorax* sp. CHX100, *Xanthobacter flavus* (Van Beilen et al., 2003), *Arthrobacter* sp. (Brzostowicz et al., 2005; Kim et al., 2008), and *Rhodococcus* sp. (Brzostowicz et al., 2003; Mirza et al., 2009). It has the lowest similarity with BVMOs acting on aliphatic ketones or ethionamide.

### 3.2 | CHMO gene expression in and isolation from *P. taiwanensis* VLB120

In our previous studies, the CHMO gene of *Acidovorax* sp. CHX100 was isolated and applied within an in vivo cascade to produce  $\epsilon$ -caprolactone ( $\epsilon$ -CL), 6-hydroxycaproic acid, and 6-aminocaproic acid from cyclohexane in *P. taiwanensis* VLB120 and *E. coli* (Bretschneider et al., 2021; R. Karande et al., 2017; Schäfer, Bühler, et al., 2020). Solvent-tolerant *P. taiwanensis* VLB120 is a good biofilm former and has been intensively studied regarding whole-cell redox biocatalysis (Lang et al., 2014; Volmer et al., 2014; Wynands et al., 2018). In the present work, this strain was selected for CHMO gene expression and enzyme isolation and as the host strain for kinetic studies on suspended cells and biofilms.

CHMO isolation was based on affinity chromatography making use of a C-terminal Strep-Tag fused to CHMO. CHMO gene expression slightly reduced the growth rate to  $0.33 \text{ h}^{-1}$  compared with the empty vector control ( $0.35 \text{ h}^{-1}$ , Figure 2a). SDS-PAGE analysis (Figure 2b) showed a strong band at the expected molecular weight of 59 kDa and indicated a high level of leaky expression. After induction, CHMO abundance roughly doubled over time, reaching a maximal level after 6 h, when cells were harvested for CHMO purification.

Recombinant CHMO was isolated from *P. taiwanensis* VLB120 crude-cell extracts via a one-step protocol using a Strep-tactin resin resulting in a purification factor of 8.5 and a CHMO activity of  $0.94 \text{ U mg}_{\text{CHMO}}^{-1}$  (Table 2, Figure S1). The CHMO protein in the eluted fraction leads to a light yellow-colored solution due to the tightly

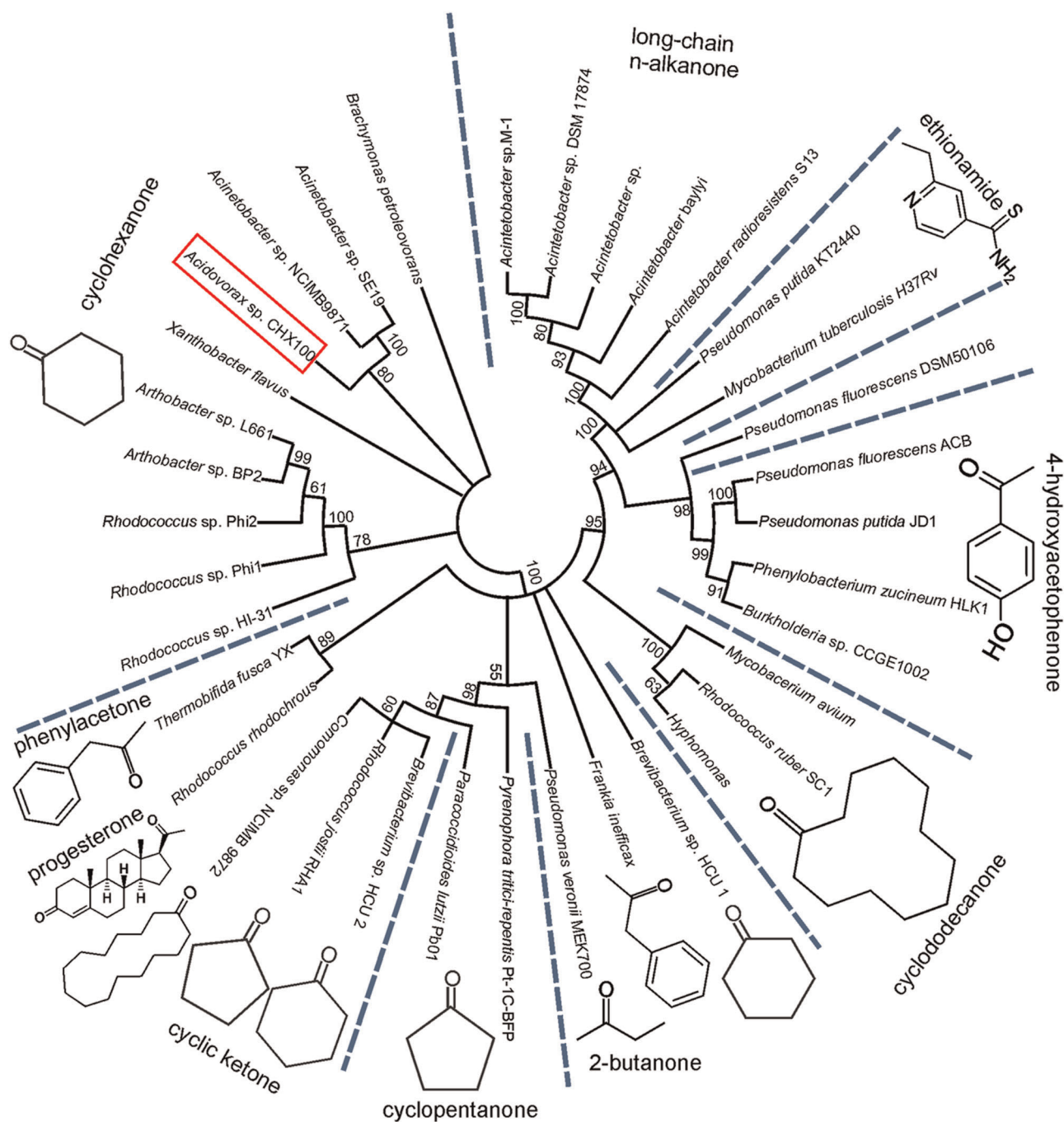


**FIGURE 1** Maximum likelihood phylogenetic tree (Bootstrap consensus tree) of Bayer-Villiger monoxygenases (BVMOs). NCBI accession numbers of protein sequences: *Brachymonas petroleovorans* (AAR99068.1), *Acinetobacter* sp. SE19 (AAG10021.1), *Acinetobacter* sp. NCIMB 9871 (BAA86293.1); *Acidovorax* sp. CHX100 (KX989890.1), *Xanthobacter flavus* (CAD10801.1), *Arthrobacter* sp. L661 (ABQ10653.1), *Arthrobacter* sp. BP2 (AAN37479.1), *Rhodococcus* sp. Phi2 (AAN37491.1), *Rhodococcus* sp. Phi1 (AAN37494.1), *Rhodococcus* sp. HI-31 (BAH56670.1), *Thermobifida fusca* YX (Q47PU3.1), *Rhodococcus rhodochrous* (BAA24454.1), *Comamonas* sp. NCIMB 9872 (BAC22652.1), *Rhodococcus jostii* RHA1 (WP\_011595904.1), *Brevibacterium* sp. HCU 2 (AAG01290.1), *Paracoccidioides lutzii* Pb01 (XP\_002792362.1), *Pyrenophora tritici-repentis* Pt-1C-BFP (XP\_001942142.1), *Pseudomonas veronii* MEK700 (ABI15711.1), *Frankia inefficax* (WP\_013424030.1), *Brevibacterium* sp. HCU 1 (AAG01289.1), *Hyphomonas* (WP\_011646304.1), *Rhodococcus ruber* SC1 (AAL14233.1), *Mycobacterium avium* (WP\_011726526.1), *Burkholderia* sp. CCGE 1002 (ADG19710.1), *Phenylobacterium zucineum* (WP\_012522360.1), *Pseudomonas putida* JD1 (FJ010625.1), *Pseudomonas fluorescens* ACB (AAK54073.1), *Pseudomonas fluorescens* DSM50106 (AAC36351.2), *Mycobacterium tuberculosis* H37Rv (NP\_218371.1), *Pseudomonas putida* KT2440 (AAN68413.1), *Acinetobacter radioresistens* S13 (GU145276.2), *Acinetobacter baylyi* (WP\_004924170.1), *Acinetobacter* sp. (WP\_000415125.1), *Acinetobacter* sp. DSM 17874 (ABQ18224.1), *Acinetobacter* sp. M-1 (ABQ18228.1) [Color figure can be viewed at [wileyonlinelibrary.com](http://wileyonlinelibrary.com)]

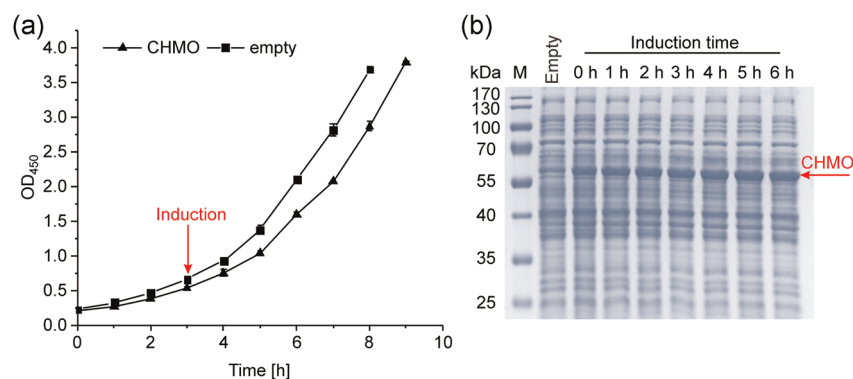


**FIGURE 2** CHMO gene expression in *Pseudomonas taiwanensis* VLB120. (a) Growth curve for IPTG-induced *P. taiwanensis* VLB120 harboring the CHMO expression plasmid pSEVA244\_CHMO (triangles) and the empty vector control pSEVA244\_T (squares). (b) SDS-PAGE of *P. taiwanensis* VLB120 harboring pSEVA244\_T or pSEVA244\_CHMO 0–6 h after IPTG addition. The size of CHMO is 58.8 kDa. CHMO, cyclohexanone monooxygenase; IPTG, isopropyl  $\beta$ -D-1-thiogalactopyranoside; SDS-PAGE, sodium dodecyl sulfate-polyacrylamide gel electrophoresis [Color figure can be viewed at [wileyonlinelibrary.com](http://wileyonlinelibrary.com)]

**TABLE 2** CHMO purification table

Purification step	Protein concentration (mg ml <sup>-1</sup> )	Volume (ml)	Total protein amount (mg)	Specific activity (U mg <sup>-1</sup> )	Yield (%)	Purification factor
Crude cell extract	8.12	5.80	47.10	0.11	100	1.00
Elution fraction 2	0.98	2.00	1.96	0.94	35.2	8.46

Note: Protein concentrations and specific activities were determined via Bradford and spectrophotometry assays, respectively. See Section 2 for details. Abbreviation: CHMO, cyclohexanone monooxygenase.

bound FAD cofactor (Fraaije et al., 2005). The absorbance spectrum of CHMO showed the two maxima at 380 and 443 nm characteristic for flavins and flavoproteins (Figure S2).

### 3.3 | Substrate spectrum and catalytic performance of CHMO

BVMOs are known to display a wide range of substrate spectra covering over 100 compounds (Mihovilovic et al., 2002). To get a rough overview on the substrate spectrum of the *Acidovorax* CHMO, activities were analyzed spectrophotometrically, that is, in terms of NADPH consumption (1 mM substrate, 2–5 min reaction time), as done in previous studies (Bisagni, Hatti-Kaul, et al., 2014; Brzostowicz et al., 2003; Trower et al., 1989). With a focus on initial activities, we investigated a large variety of substrates, including cyclic, substituted cyclic, aromatic, and alkylic ketones, as well as thioanisole, its *p*-methoxy derivative, and methyl phenyl sulfoxide. Enantio- and regioselectivities were not investigated. Chiral substrates were applied as racemates.

As expected from the involvement of CHMO in cyclohexane degradation (Salamanca & Engesser, 2014), cyclohexanone was among the best-converted substrates (Figure 3). CHMO did not show any uncoupling, neither with cyclohexanone as substrate nor without substrate (Supporting Information Section 1, Table S1). Similarly, uncoupling may not be prominent for other substrates, but cannot be

excluded. The highest activity was found for 3-methylcyclohexanone. The position of methyl substitutions of cyclohexanone strongly influenced CHMO activity with 54%, 104%, and 91% relative activity for methyl groups at positions 2, 3, and 4, respectively. Whereas the bulky substrate 3,3,5-trimethylcyclohexanone was converted with 85% relative activity, 4-tert-butylcyclohexanone reacted more slowly (12% relative activity). Alkylic ketones also were converted, but at lower rates than cyclic compounds. Even lower rates were found for benzylic ketones, whereas substrates with the carbonyl group further away from aromatic rings as, for example,  $\beta$ -tetralone (65% relative activity), were more preferred. BVMOs are well known to catalyze sulfide and sulfoxide oxidations (Bisagni, Summers, et al., 2014; Colonna et al., 1998; Zhang et al., 2018), which also was confirmed here for *Acidovorax* CHMO. Overall, CHMO showed a large substrate spectrum with high activities towards cyclic compounds with or without substitutions as well as for sulfides and sulfoxides and lower activities towards aliphatic and benzylic ketones.

The biocatalytic performance of isolated CHMO was further characterized in biotransformations conducted for 6 h with 5 mM of seven substrates from four different compound classes. All products except  $\delta$ -valerolactone, which could not be detected with the chromatographic method, were subjected to GC-MS analysis confirming their structure (Figures S4–S9). The lower conversions for  $\beta$ -tetralone (24%) and methylphenylsulfoxide (57%) (Figure 4) may be a result of the substrate and/or product inhibition or uncoupling

**FIGURE 3** Substrate spectrum of CHMO. Substrates from different compound classes were subjected to activity assays with isolated *Acidovorax* CHMO (see Section 2 for details). Specific activities were determined photometrically and normalized to the activity for cyclohexanone ( $1.06 \pm 0.08 \text{ U mg}^{-1}$ ). CHMO, cyclohexanone monooxygenase [Color figure can be viewed at [wileyonlinelibrary.com](http://wileyonlinelibrary.com)]

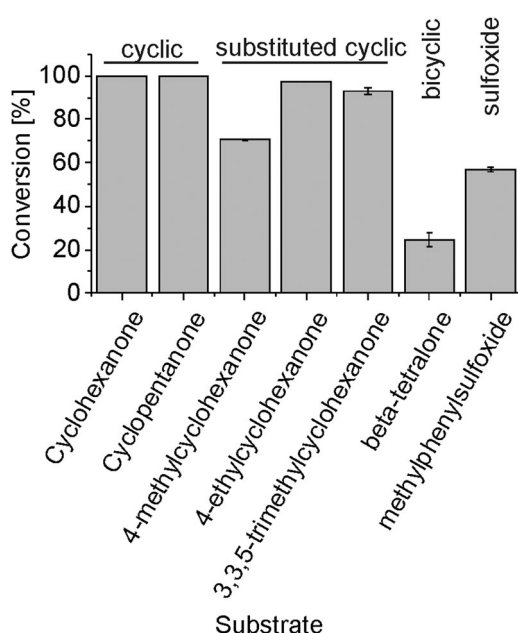
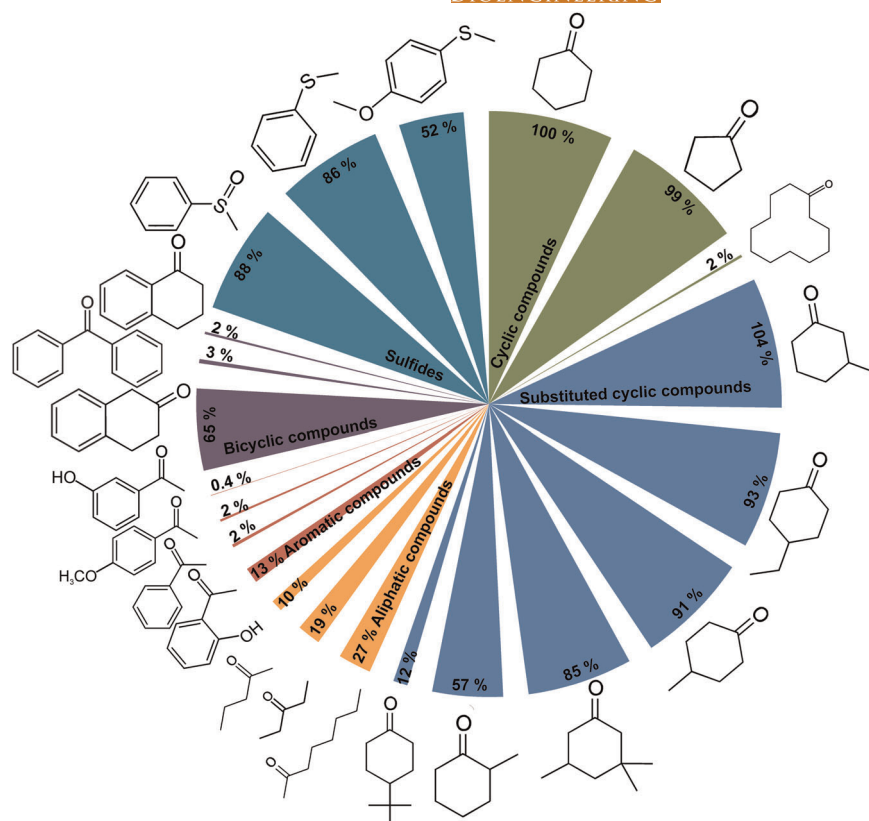


**FIGURE 4** Conversion efficiency of isolated CHMO for different substrates. Biotransformations were conducted in 1 ml reaction volume containing 5 mM substrate, 0.5 mM NADPH,  $10 \text{ g L}^{-1}$  glucose, 10 U glucose dehydrogenase for NADPH regeneration, and  $50 \mu\text{g}$  CHMO. Conversion values are given based on substrate depletion after 6 h reaction time. CHMO, cyclohexanone monooxygenase

with these substrates might be prominent leading to the formation of reactive oxygen species (ROS) and thus enzyme destabilization. The high conversions obtained for (substituted) cycloalkanes qualify them as preferred substrates of *Acidovorax*-CHMO (Figure 4).

### 3.4 | In vitro characterization of CHMO kinetics

CHMO in vitro kinetics for cyclohexanone conversion was investigated by varying either the cyclohexanone, NADPH, or  $\text{O}_2$  concentration and measuring initial reaction rates based on  $\epsilon$ -CL formation. These rates followed Michaelis–Menten kinetics with substrate inhibition for cyclohexanone and NADPH (Figure 5). Parameters were fitted utilizing the respective equations (Table 3). This leads to apparent  $K_M$  and also  $V_{\text{max}}$  and values for each substrate, as inhibition by the other substrate(s) added was not considered at this stage. Thus, the  $V_{\text{max}}$  ( $k_{\text{cat}}$ ) values obtained with the different substrates (by varying their concentrations individually) can be expected to differ. Kinetic parameters of BVMOs are commonly reported for their primary substrate (ketone) and occasionally for NADPH. Their characterization for  $\text{O}_2$  is limited due to technical restrictions. In this study, kinetics for  $\text{O}_2$  was estimated by varying  $\text{O}_2$  concentrations from 1% to 21% ( $V_{\text{O}_2}/V_{\text{N}_2}$ ) in the gas phase of closed glass vials (as detailed in Section 2).

When comparing kinetic parameters of isolated CHMO (Table 3), apparent  $k_{\text{cat}}$  values obtained with the different substrates were in the same range ( $1.15\text{--}1.21 \text{ s}^{-1}$ ), indicating no significant

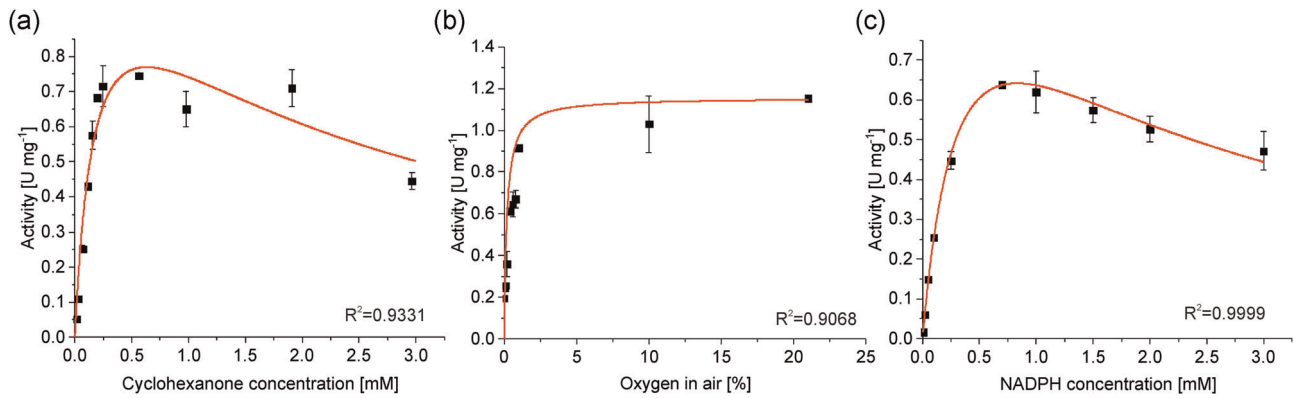


**FIGURE 5** In vitro CHMO kinetics for cyclohexanone (a), O<sub>2</sub> (b), and NADPH (c) as substrates. Experiments were conducted in 1 ml 100 mM Kpi buffer, started by the addition of 20 μg CHMO, and stopped after 5 min. (a) 0.5 mM NADPH, ambient O<sub>2</sub> concentration in gas phase; (b) 0.5 mM NADPH, 1 mM cyclohexanone; (c) 1 mM cyclohexanone, ambient O<sub>2</sub> concentration in gas phase. The red curves correspond to the Michaelis–Menten fit in Matlab. CHMO, cyclohexanone monooxygenase [Color figure can be viewed at [wileyonlinelibrary.com](http://wileyonlinelibrary.com)]

**TABLE 3** Cyclohexanone monooxygenase (CHMO) kinetics for isolated enzyme-, suspended cell-, and biofilm-based biocatalyst formats

Catalyst format	Substrate	$K_M$ or $K_S$ [μM] <sup>a</sup>	$K_I$ [mM]	$V_{max}$ [U mg <sup>-1</sup> ] or [U g <sub>CDW</sub> <sup>-1</sup> ] <sup>b</sup>	$k_{cat}$ [s <sup>-1</sup> ] <sup>c</sup>	$k_{cat}K_M^{-1}$ or $k_{cat}K_S^{-1}$ [mM <sup>-1</sup> s <sup>-1</sup> ] <sup>a</sup>
Isolated enzyme	Cyclohexanone	178 ± 38	2.24 ± 0.65	1.20 ± 0.17	1.16 ± 0.17	6.54
	NADPH	372 ± 17	1.85 ± 0.20	1.21 ± 0.04	1.17 ± 0.04	3.16
	O <sub>2</sub>	2.2 ± 0.1 (0.19%) <sup>d</sup>	n.a.	1.15 ± 0.09	1.11 ± 0.09	5.79
Suspended cells	Cyclohexanone	316 ± 21	9.43 ± 2.53	395 ± 17	1.50 ± 0.06	4.75
	O <sub>2</sub>	54 ± 1 (4.65%) <sup>d</sup>	n.a.	347 ± 5	1.31 ± 0.02	0.283
Biofilm	Cyclohexanone	1648 ± 70	11.9 ± 0.7	41 ± 1	0.24 ± 0.01	0.146

Note:  $K_M$ ,  $K_S$ ,  $V_{max}$ , and  $K_I$  values were calculated applying Michaelis–Menten fitting in Matlab from kinetic data presented in Figures 5 and 6. For NADPH and cyclohexanone, the substrate inhibition fit was used.

<sup>a</sup>For whole cell-based formats, the apparent substrate uptake constant  $K_S$  is given as the equivalent of the Michaelis–Menten constant  $K_M$  for isolated enzymes.

<sup>b</sup> $V_{max}$  values are given in U per mg protein for isolated CHMO and in U per g cell dry weight (CDW) for whole-cell-based formats.

<sup>c</sup>CHMO-related  $k_{cat}$  values for both in vivo formats were estimated based on CHMO contents of respective biomass.

<sup>d</sup>Henry's constant for O<sub>2</sub> (0.86 atm L mmol<sup>-1</sup>) was used to calculate the dissolved O<sub>2</sub> concentration in the aqueous phase assuming equilibration with the gas phase concentration. Values given in % refer to volume shares of O<sub>2</sub> in the gas phase

effect of cross inhibitions by co-substrates. This roughly fits comparing the standard co-substrate conditions applied and estimated  $K_I$  values (cyclohexanone: 1 mM,  $K_I$  = 2.24 mM; NADPH: 0.5 mM,  $K_I$  = 1.85 mM). The apparent  $K_M$  values for the different substrates, although indicating a high affinity for all three substrates, varied significantly from 2.2 to 372 μM. The lowest value was observed for O<sub>2</sub>, whereas values for cyclohexanone and NADPH were 80- and 170-fold higher, respectively (Table 3). Substrate inhibition occurred at intermediary to high NADPH and cyclohexanone levels.

### 3.5 | Characterization of CHMO kinetics in suspended cell- and biofilm formats

To compare biocatalyst formats, we aimed to estimate the kinetic parameters for suspended cells and biofilms. Cyclohexane, as well as O<sub>2</sub> concentrations, were varied to analyze the respective kinetics of

suspended cells. For the biofilm format, only kinetics for cyclohexanone were analyzed due to technical restrictions regarding the control of O<sub>2</sub> levels. In this case, a biofilm was grown for 6 days in a small plastic capillary under aqueous-air segmented flow conditions. O<sub>2</sub> supply via air segments (Heuschkel et al., 2019) was sufficient to avoid O<sub>2</sub> limitation over the entire length of the capillary. The applied Taylor flow creates convective forces within segments resulting in better mixing and enhanced mass transfer (Kashid et al., 2010). This pattern was selected to avoid concentration gradients from the bulk phase to the biofilm surface. Substrate concentration gradients from the beginning to the end of the capillary were minimized by establishing a low residence time of 5 min via tube length and flow rate adjustment.

Both in vivo formats exhibited Michaelis–Menten-type kinetics (Figure 6). The substrate uptake constant  $K_S$  of suspended cells for O<sub>2</sub> was 25-fold higher than the respective apparent  $K_M$  of isolated CHMO (Figure 6b, Table 3). Compared to the  $K_M$  value of isolated

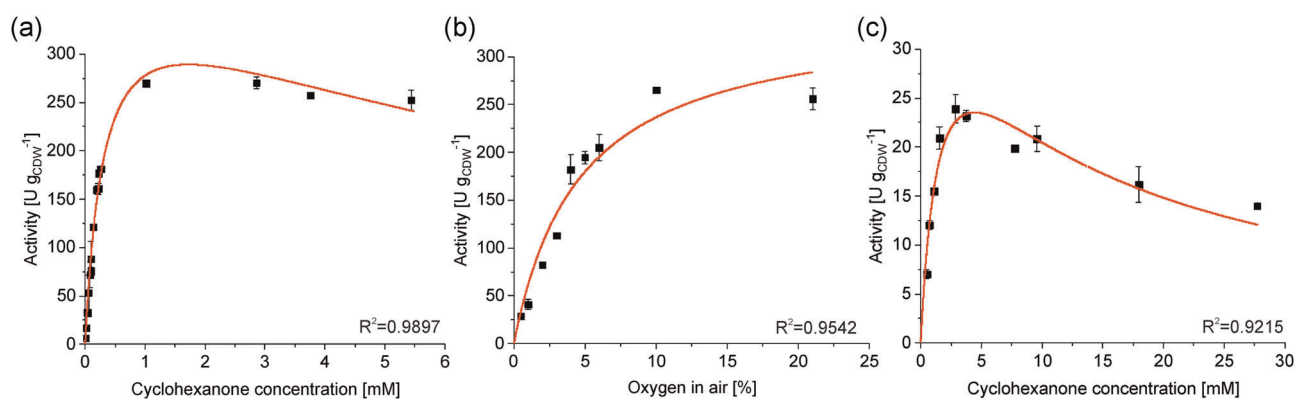


**FIGURE 6** CHMO kinetics of suspended *Pseudomonas taiwanensis* VLB 120 cells for cyclohexanone (a) and O<sub>2</sub> (b), and of *P. taiwanensis* VLB120 biofilms for cyclohexanone (c). Suspended cell experiments were conducted in 1 ml 100 mM Kpi buffer containing 10 g L<sup>-1</sup> glucose and a biomass concentration of 0.25 g<sub>CDW</sub> L<sup>-1</sup>. Biotransformations with suspended cells were started via cyclohexanone addition and stopped after 5 min reaction time. Thereby, the cyclohexanone concentration was varied at atmospheric O<sub>2</sub> concentration in the gas phase (a); (b) variation of O<sub>2</sub> concentration in the gas phase at a cyclohexanone concentration of 1 mM. (c) Biofilms were grown in serological plastic pipettes. Kpi buffer containing 10 g L<sup>-1</sup> glucose and varying cyclohexanone concentrations was used as a reaction medium. For details, refer to Section 2. The red curves correspond to the Michaelis–Menten fit in Matlab. CHMO, cyclohexanone monooxygenase [Color figure can be viewed at [wileyonlinelibrary.com](http://wileyonlinelibrary.com)]

CHMO for cyclohexanone (178 μM), the corresponding apparent  $K_S$  values were 1.8- and 9.3-fold higher for suspended cells and biofilms, respectively (Table 3). Similarly, the cyclohexanone-related substrate inhibition constants ( $K_i$ ) of suspended cells and biofilms were 4.3- and 5.3-fold higher than those of isolated CHMO. These results indicate more prominent cyclohexanone and O<sub>2</sub> mass transfer limitations towards and into cells and, especially, biofilms.

The maximal specific activity of suspended cells ( $V_{max}$ ) was almost 10-fold higher than that of the biofilm (Table 3). To further characterize this effect, CHMO-related  $k_{cat}$  values for both in vivo formats were estimated based on CHMO contents of respective biomass. The latter were derived by relating SDS-PAGE band intensities to those obtained with samples of known CHMO content (Figure S3) and assuming a total protein fraction of 55% in cell dry mass (Neidhardt et al., 1990). Remarkably, the obtained  $k_{cat}$  value for CHMO in suspended cells and cyclohexanone as substrate was 1.3-fold higher than that obtained for isolated CHMO (Table 3). In biofilms, however, this  $k_{cat}$  value was 4.8-fold lower than isolated CHMO. This result indicates that the CHMO content, as well as active enzyme fractions, were lower in biofilms than in suspended cells.

Overall, the significant differences in kinetic parameters obtained for the different CHMO biocatalyst formats emphasize that the biocatalyst format choice plays an important role regarding biocatalyst and thus bioprocess efficiency.

## 4 | DISCUSSION

### 4.1 | Characteristics of *Acidovorax* CHMO

In this study, a Type I Baeyer–Villiger monooxygenase involved in cyclohexane degradation by *Acidovorax* sp. CHX100 was isolated and

characterized (Salamanca & Engesser, 2014). The *Acidovorax* CHMO was shown to integrate well into the clustering of BVMO gene sequences according to their native substrate (Fraaije et al., 2002) (Figure 1). CHMO gene expression in *P. taiwanensis* VLB120 by means of the pSEVA244\_T vector resulted in high expression levels of the soluble protein (Figure 2) with a minor effect on growth, qualifying *P. taiwanensis* VLB120 as suitable host for CHMO synthesis. *Acidovorax* CHMO showed a large substrate spectrum as it is quite common for BVMOs (Bisagni, Hatti-Kaul, et al., 2014; Brzostowicz et al., 2003; Riebel et al., 2012), also catalyzing sulfur oxidation in substrates that are structurally different from their native substrate (Fink et al., 2012; Fraaije et al., 2005). For cyclic and substituted cyclic substrates, *Acidovorax* CHMO enabled 90%–100% conversion within 6 h of reaction (Figure 4). As observed for other CHMOs, its activity towards benzylic ketones such as acetophenone and  $\alpha$ -tetralone was very low (Riebel et al., 2012). The most studied BVMO from *Acinetobacter* has been shown to accept over 100 different substrates (Mihovilovic et al., 2002; J. D. Stewart, 1998). Other BVMOs like the phenylacetone monooxygenase from *T. fusca* have a more restricted substrate spectrum (Fraaije et al., 2005). The substrate screen given in this study revealed a versatile CHMO, of which the substrate spectrum deserves further investigation, including the determination of enantio- and regiospecificities.

The turnover numbers ( $k_{cat}$ ) of *Acidovorax* CHMO and its  $K_m$  value for the native substrate cyclohexanone are within the typical ranges reported for BVMOs (Table 4). It has to be noted that studies on BVMO kinetics often rely on spectrophotometrically analyzed NADPH oxidation and can be compromised by a possible uncoupling leading to overestimated activities. Whereas *Acidovorax* CHMO did not show uncoupling with cyclohexanone as substrate, which is in contrast to other BVMOs, for example, those originating from *T. municipale* or *Gordonia* sp. showing 11% and 19% uncoupling,

TABLE 4 Selected kinetic parameters for fungal and bacterial Baeyer–Villiger monooxygenases

Origin	Substrate	$K_{M, \text{substrate}}$ [ $\mu\text{M}$ ]	$K_{M, \text{NADPH}}$ [ $\mu\text{M}$ ]	$k_{\text{cat}}$ [ $\text{s}^{-1}$ ]	$k_{\text{cat}}/K_{M}$ [ $\text{mM}^{-1} \text{s}^{-1}$ ]	Uncoupling rate <sup>a</sup> [ $\text{s}^{-1}$ ]	Reference
<i>Acidovorax</i> sp. CHX100	Cyclohexanone	178	372	1.11–1.17	6.54	0	This study
<i>Acinetobacter</i> NCIB 9871	Cyclo-hexanone	6.3	7.3	22.2	3524	n.d. <sup>b</sup>	Donoghue et al., (1976); Kamerbeek et al. (2004)
<i>Thermocrispum</i> municipale	4-Methyl-cyclo-hexanone	<1	n.d.	1.93	>1930	0.22	Li et al. (2017)
<i>Thermobifida fusca</i>	Phenyl-acetone	59	0.7	1.9	32.0	0.02	Fraaije et al., 2005; Torres Pazmiño et al. (2008)
<i>Dietzia</i> sp. D5	Phenyl-acetone	829	11	0.634	0.8	n.d.	Bisagni, Hatti-Kaul, et al. (2014)
<i>Pseudomonas fluorescens</i> ACB	4-hydroxy-aceto-phenone	9.2	64	12.6	1,400	0.11	Kamerbeek, Janssen, et al. (2003); Kamerbeek, Olsthoorn, et al. (2003)
<i>Pseudomonas putida</i> JD1	4-hydroxy-aceto-phenone	38	n.d.	9.8	257	n.d.	Rehdorf et al. (2009)
<i>Gordonia</i> sp. TY-5	acetone	170	6.7	1.4	8.2	0.26	Fordwour et al. (2018)
<i>Aspergillus fumigatus</i> Af293	Bicycle [3.2.0]hept-2-en-6-one	119	<5	0.46	4.1	0.01	Mascotti et al. (2014)
<i>Aspergillus flavus</i>	2-octanone	10	n.d.	5.3	530	n.d.	Ferroni et al. (2016)
<i>Mycobacterium tuberculosis</i>	Ethion-amide	340	10	0.027	<0.1	n.d.	Fraaije et al. (2004)

Abbreviation: n.d., not determined.

<sup>a</sup>In the absence of substrate.

respectively (Fordwour et al., 2018; Li et al., 2017). Whereas low  $K_M$ -values for NADPH (1–64  $\mu\text{M}$ ) have been reported for other BVMOs (Table 4), *Acidovorax* CHMO exhibited a comparably high  $K_M$  (372  $\mu\text{M}$ ), which is still within the intracellular range of 120–540  $\mu\text{M}$  as determined for *E. coli* (Bennett et al., 2009; Milo et al., 2010, BNID:100146), but indicates a firm dependency of whole-cell-based CHMO-catalysis on the cellular redox state.

Substrate inhibition is a well-known phenomenon for CHMOs (Alphand et al., 2003; Delgove et al., 2018; Hilker et al., 2008) and also was found for *Acidovorax* CHMO with a  $K_I$  of 2.24 mM. For synthetic application, this demands suitable substrate feeding strategies. For CHMO<sub>*Acinetobacter*</sub> and PAMO<sub>*T.fusca*</sub>, the product NADP<sup>+</sup> has moreover been found to act as a competitive inhibitor ( $K_I = 38$  and 2.7  $\mu\text{M}$ , respectively) (Ryerson et al., 1982; Torres Pazmiño et al., 2008). Whereas such product inhibition was not found for *Acidovorax* CHMO, substrate inhibition by NADPH was apparent, which has been reported for BVMOs so far. The respective  $K_I$  (1.85 mM), however, was clearly above typically encountered intracellular NADPH concentrations, for example, 120–540  $\mu\text{M}$  in *E. coli* (Bennett et al., 2009; Milo et al., 2010, BNID:100146).

O<sub>2</sub>-related kinetic data are rarely reported for BVMOs. Ryerson et al. (1982) concluded that apparent  $K_M$ -values for O<sub>2</sub> must be below 10–15  $\mu\text{M}$  (Ryerson et al., 1982), which was experimentally proven by Torres-Pazmino et al. (2008) for PAMO ( $K_M = 10 \pm 4 \mu\text{M}$ ). The  $K_M$  of 1.1  $\mu\text{M}$  obtained in this study translates to a catalytic efficiency of 10,800 s<sup>-1</sup> M<sup>-1</sup>, which is in line with these previous studies.

## 4.2 | Kinetic parameters differ for different biocatalyst formats

In recent years, in vivo kinetic parameters and their correspondence to in vitro counterparts have been questioned and refined using omics approaches (Davidi et al., 2016; Heckmann et al., 2020). Kinetic differences occur as conditions applied in vitro often do not resemble in vivo conditions, that is, high protein concentrations and close confinement by membranes. In vivo like media have been developed to mimic cellular conditions (García-Contreras et al., 2012; Van Eunen & Bakker, 2014), which, however, was compromised by unknown biochemical factors within the cell. Conducting full quantitative proteome analysis followed by computational fluxomics for in vivo  $k_{\text{cat}}$  determination (Davidi et al., 2016) is interesting for enzymes integrated in native metabolism, but is not suitable to investigate the in vivo kinetics of heterologously enzymes, which operate orthologously to cellular metabolism and depend on substrate and product mass transfer over cellular membranes. In this study, we considered the cell as a catalyst with corresponding  $K_S$  and  $V_{\text{max}}$  values and estimated CHMO-related  $k_{\text{cat}}$  values based on the CHMO content of suspended cells and biofilms. Unlike the  $K_M$  value for isolated enzymes, the  $K_S$ -value for cellular catalysts, besides enzyme characteristics, also depends on substrate transfer over cellular membranes (Bühler et al., 2002). Although the half-saturation constants of suspended cells for cyclohexanone and O<sub>2</sub> were 1.8 and 25 times higher,

respectively than the corresponding  $K_M$ -values of isolated CHMO, they still were in the  $\mu\text{M}$  range. This can be explained by the facile diffusion of these small and hydrophobic substrates through membranes. In the case of O<sub>2</sub>, the competition for O<sub>2</sub> with respiration at the cytoplasmic membrane additionally comes into play. Some resistance of the cell envelope regarding cyclohexanone transfer can be considered the reason for the 4.2-fold higher  $K_I$  of suspended cells compared to isolated CHMO.

Despite the high  $K_M$  for NADPH (372  $\mu\text{M}$ ), the turnover number  $k_{\text{cat}}$  of CHMO was estimated to be 1.3-fold higher in suspended cells than the corresponding value of isolated CHMO. This indicates that the cells offer a sufficiently high intracellular NADPH concentration (120–540  $\mu\text{M}$  in *E. coli*) and supply (Bennett et al., 2009; Milo et al., 2010, BNID:100146). The higher  $k_{\text{cat}}$  in suspended cells can be explained by the intracellular milieu, for which enzymes are evolutionarily optimized (Cheung et al., 2005). Such conditions are difficult to realize with standard reaction buffers. Furthermore, partial enzyme denaturation during purification can affect the in vitro  $k_{\text{cat}}$  estimation. These differences among in vivo and in vitro kinetics (Table 3) can bring advantages for in vivo biocatalysis. Besides an optimal milieu enabling high enzyme stability and effective metabolism-based redox cofactor regeneration, continuous enzyme regeneration/synthesis constitutes another advantage of in vivo biocatalysis (Kadisich et al., 2017; Schrewe et al., 2013).

In biofilms, self-immobilized cells are embedded within a self-produced matrix of extra-polymeric substances (EPS). Compared with suspended cells, apparent  $K_S$  and  $K_I$  values of biofilms for cyclohexanone were 5.2- and 1.3 times higher, respectively, and the  $V_{\text{max}}$  was 9.6-fold lower, which only partially was attributed to a lower BVMO content (the  $k_{\text{cat}}$  was 6.3 time lower, Table 3). Possible reasons for these differences include the substrate mass transfer within a biofilm, which mainly depends on diffusion resulting in concentration gradients and consequently a higher apparent  $K_S$ . Further, the high heterogeneity among cells within biofilms (P. S. Stewart & Franklin, 2008; Wimpenny et al., 2000) imply that not all cells are catalytically active, resulting in a reduced  $V_{\text{max}}$ . However, planktonic cell-based kinetics are often used to model biofilm-based processes (Bakke et al., 1984; Mirpuri et al., 1997), which, as exemplified by the results obtained in this study, can lead to a substantial overestimation of biological activity.

Apart from reaction kinetics and thus the biotransformation rate, the stability of biocatalyst formats is an important parameter, as it determines the product yield on biocatalyst ( $g_{\text{product}} g_{\text{catalyst}}^{-1}$ ) and the achievable product titer (Hoschek, Heuschkel, et al., 2019; Hoschek, Toepel, et al., 2019; Kadisich et al., 2017). Thus, it will be the task of future research on the process performance of different biocatalyst formats to focus on stability aspects and combine them with rate- and specificity-related assessments (Tufvesson et al., 2011).

## 5 | CONCLUSIONS

A BVMO originating from *Acidovorax* CHX100 was heterologously expressed in *P. taiwanensis* and characterized in the isolated form. Like other BVMOs, this enzyme was found to feature a broad substrate spectrum and showed the highest activity towards



cyclic ketones. Unlike other CHMOs, no uncoupling was observed with and without cyclohexanone as substrate. Kinetics was also found to be similar as reported for other CHMOs and was characterized in detail, not only for the isolated enzyme but also for CHMO-containing suspended cells and biofilms to compare different biocatalyst formats. This kinetic assessment revealed slightly higher  $K_S$  and  $k_{cat}$  values for suspended cells compared with the  $K_M$  and  $k_{cat}$  of the isolated enzyme. Biofilms exhibited the lowest  $k_{cat}$  and the highest  $K_S$ . Both suspended cells and biofilms were significantly less susceptible to inhibition by cyclohexanone than isolated CHMO. From a kinetics point of view, the suspended-cell format can thus be considered most promising, as it efficiently exploits the enzyme capacity and NADPH regeneration via glucose metabolism. The biofilm format bears high potential regarding process stability but suffers from kinetic issues related to mass transfer and possibly heterogeneity, which deserve further research and engineering efforts.

## ACKNOWLEDGMENTS

We acknowledge the use of the facilities of the Centre for Biocatalysis (MiKat) at the Helmholtz Centre for Environmental Research, which is supported by European Regional Development Funds (EFRE, Europe funds Saxony) and the Helmholtz Association. LB and IH were funded by the ERA-IB- Project PolyBugs ID:16006 and the Sächsisches Ministerium für Wissenschaft und Kunst (SMWK) Project ID: 100318259. The authors would like to thank Prof. Dr. Andreas Schmid for helpful discussions. Access funding enabled and organized by Projekt DEAL.

## AUTHOR CONTRIBUTIONS

Lisa Bretschneider, Rohan Karande, and Bruno Bühler were involved in the conception and design of the study as well as data interpretation. Lisa Bretschneider, Ingeborg Heuschkel, and Afaq Ahmed performed experimental work and collected data. Lisa Bretschneider wrote the original draft of the manuscript. Rohan Karande and Bruno Bühler contributed in terms of article structuring and editing. All authors were involved in final editing and approved the submitted version.

## DATA AVAILABILITY STATEMENT

The data that support the findings of this study are available from the corresponding author upon reasonable request.

## ORCID

Lisa Bretschneider  <http://orcid.org/0000-0002-9149-0265>

Rohan Karande  <http://orcid.org/0000-0003-3186-4787>

Bruno Bühler  <http://orcid.org/0000-0001-6458-5739>

## REFERENCES

- Alphand, V., Carrea, G., Wohlgemuth, R., Furstoss, R., & Woodley, J. M. (2003). Towards large-scale synthetic applications of Baeyer-Villiger monooxygenases. *Trends in Biotechnology*, 21, 318–323. [https://doi.org/10.1016/S0167-7799\(03\)00144-6](https://doi.org/10.1016/S0167-7799(03)00144-6)
- Bakke, R., Trulear, M. G., Robinson, J., & Characklis, W. G. (1984). Activity of *Pseudomonas aeruginosa* in biofilms: Steady state. *Biotechnology and Bioengineering*, 26, 1418–1424. <https://doi.org/10.1002/bit.260261204>
- Bayer, T., Milker, S., Wiesinger, T., Rudroff, F., & Mihovilovic, M. D. (2015). Designer microorganisms for optimized redox cascade reactions—challenges and future perspectives. *Advanced Synthesis & Catalysis*, 357, 1587–1618. <https://doi.org/10.1002/adsc.201500202>
- Bennett, B. D., Kimball, E. H., Gao, M., Osterhout, R., Van Dien, S. J., & Rabinowitz, J. D. (2009). Absolute metabolite concentrations and implied enzyme active site occupancy in *Escherichia coli*. *Nature Chemical Biology*, 5, 593–599. <https://doi.org/10.1038/nchembio.186>
- Bisagni, S., Hatti-Kaul, R., & Mamo, G. (2014). Cloning, expression and characterization of a versatile Baeyer-Villiger monooxygenase from *Dietzia* sp. D5. *AMB Express*, 4, 23. <https://doi.org/10.1186/s13568-014-0023-1>
- Bisagni, S., Summers, B., Kara, S., Hatti-Kaul, R., Grogan, G., Mamo, G., & Hollmann, F. (2014). Exploring the substrate specificity and enantioselectivity of a Baeyer-Villiger monooxygenase from *Dietzia* sp. D5: Oxidation of sulfides and aldehydes. *Topics in Catalysis*, 57, 366–375. <https://doi.org/10.1007/s11244-013-0192-1>
- Bretschneider, L., Wegner, M., Bühler, K., Bühler, B., & Karande, R. (2021). One-pot synthesis of 6-aminohexanoic acid from cyclohexane using mixed-species cultures. *Microbial Biotechnology*, 1751–7915.13744. <https://doi.org/10.1111/1751-7915.13744>
- Brzostowicz, P. C., Walters, D. M., Jackson, R. E., Halsey, K. H., Ni, H., & Rouvière, P. E. (2005). Proposed involvement of a soluble methane monooxygenase homologue in the cyclohexane-dependent growth of a new *Brachymonas* species. *Environmental Microbiology*, 7, 179–190. <https://doi.org/10.1111/j.1462-2920.2004.00681.x>
- Brzostowicz, P. C., Walters, D. M., Thomas, S. M., Nagarajan, V., & Rouvière, P. E. (2003). mRNA differential display in a microbial enrichment culture: Simultaneous identification of three cyclohexanone monooxygenases from three species. *Applied and Environmental Microbiology*, 69, 334–342. <https://doi.org/10.1128/AEM.69.1.334-342.2003>
- Bühler, B., Witholt, B., Hauer, B., & Schmid, A. (2002). Characterization and application of xylene monooxygenase for multistep biocatalysis. *Applied and Environmental Microbiology*, 68, 560–568. <https://doi.org/10.1128/AEM.68.2.560-568.2002>
- Chen, Y., Peoples, O., & Walsh, C. (1988). *Acinetobacter* cyclohexanone monooxygenase: Gene cloning and sequence determination. *Journal of Bacteriology*, 170, 781–789. <https://doi.org/10.1128/jb.170.2.781-789.1988>
- Cheng, Q., Thomas, S. M., Kostichka, K., Valentine, J. R., & Nagarajan, V. (2000). Genetic analysis of a gene cluster for cyclohexanol oxidation in *Acinetobacter* sp. strain SE19 by in vitro transposition. *Journal of Bacteriology*, 182, 4744–4751. <https://doi.org/10.1128/JB.182.17.4744-4751.2000>
- Cheung, M. S., Klimov, D., & Thirumalai, D. (2005). Molecular crowding enhances native state stability and refolding rates of globular proteins. *Proceedings of the National Academy of Sciences of the United States of America*, 102, 4753–4758. <https://doi.org/10.1073/pnas.0409630102>
- Colonna, S., Gaggero, N., Carrea, G., & Pasta, P. (1998). Oxidation of organic cyclic sulfites to sulfates: a new reaction catalyzed by cyclohexanone monooxygenase. *Chemical Communications*, 415–416. <https://doi.org/10.1039/A707749A>
- Colonna, S., Gaggero, N., Pasta, P., & Ottolina, G. (1996). Enantioselective oxidation of sulfides to sulfoxides catalysed by bacterial cyclohexanone monooxygenases. *Chemical Communications*, 2303–2307. <https://doi.org/10.1039/CC9960002303>
- Davidi, D., Noor, E., Liebermeister, W., Bar-Even, A., Flamholz, A., Tumbler, K., Barenholz, U., Goldenfeld, M., Shlomi, T., & Milo, R. (2016). Global characterization of in vivo enzyme catalytic rates and their correspondence to in vitro  $k_{cat}$  measurements. *Proceedings of*

- the National Academy of Sciences of the United States of America, 113, 3401–3406. <https://doi.org/10.1073/pnas.1514240113>
- Delgove, M. A., Eford, M. T., Bernaerts, K. V., & De Wildeman, S. M. (2018). Application of a thermostable Baeyer–Villiger monoxygenase for the synthesis of branched polyester precursors. *Journal of Chemical Technology & Biotechnology*, 93, 2131–2140. <https://doi.org/10.1002/jctb.5623>
- Donoghue, N. A., Norris, D. B., & Trudgill, P. W. (1976). The purification and properties of cyclohexanone oxygenase from *Nocardia globerula* CL1 and *Acinetobacter* NCIB 9871. *European Journal of Biochemistry*, 63, 175–192. <https://doi.org/10.1111/j.1432-1033.1976.tb10220.x>
- Edgar, R. C. (2004). MUSCLE: Multiple sequence alignment with high accuracy and high throughput. *Nucleic Acids Research*, 32, 1792–1797. <https://doi.org/10.1093/nar/gkh340>
- Felsenstein, J. (1985). Confidence limits on phylogenies: An approach using the bootstrap. *Evolution*, 39, 783–791. <https://doi.org/10.1111/j.1558-5646.1985.tb00420.x>
- Ferroni, F. M., Tolmie, C., Smit, M. S., & Opperman, D. J. (2016). Structural and catalytic characterization of a fungal Baeyer–Villiger monoxygenase. *PLoS One*, 11, e0160186. <https://doi.org/10.1371/journal.pone.0160186>
- Fink, M. J., Rial, D. V., Kapitanova, P., Lengar, A., Rehdorf, J., Cheng, Q., Rudroff, F., & Mihovilovic, M. D. (2012). Quantitative comparison of chiral catalysts selectivity and performance: A generic concept illustrated with cyclododecanone monoxygenase as Baeyer–Villiger biocatalyst. *Advanced Synthesis & Catalysis*, 354, 3491–3500. <https://doi.org/10.1002/adsc.201200453>
- Fordwour, O. B., Luka, G., Hoofar, M., & Wolthers, K. R. (2018). Kinetic characterization of acetone monoxygenase from *Gordonia* sp. strain TY-5. *AMB Express*, 8, 181. <https://doi.org/10.1186/s13568-018-0709-x>
- Fraaije, M. W., Kamerbeek, N. M., van Berkel, W. J., & Janssen, D. B. (2002). Identification of a Baeyer–Villiger monoxygenase sequence motif. *FEBS Letters*, 518, 43–47. [https://doi.org/10.1016/S0014-5793\(02\)02623-6](https://doi.org/10.1016/S0014-5793(02)02623-6)
- Fraaije, M. W., Kamerbeek, N. M., Heidekamp, A. J., Fortin, R., & Janssen, D. B. (2004). The prodrug activator EtaA from *Mycobacterium tuberculosis* is a Baeyer–Villiger monoxygenase. *Journal of Biological Chemistry*, 279, 3354–3360. <https://doi.org/10.1074/jbc.M307770200>
- Fraaije, M. W., Wu, J., Heuts, D. P., Van Hellemond, E. W., Spelberg, J. H. L., & Janssen, D. B. (2005). Discovery of a thermostable Baeyer–Villiger monoxygenase by genome mining. *Applied Microbiology and Biotechnology*, 66, 393–400. <https://doi.org/10.1007/s00253-004-1749-5>
- Fürst, M. J., Gran-Scheuch, A., Aalbers, F. S., & Fraaije, M. W. (2019). Baeyer–Villiger monoxygenases: Tunable oxidative biocatalysts. *ACS Catalysis*, 9, 11207–11241. <https://doi.org/10.1021/acscatal.9b03396>
- Fürst, M. J., Boonstra, M., Bandstra, S., & Fraaije, M. W. (2019). Stabilization of cyclohexanone monoxygenase by computational and experimental library design. *Biotechnology and Bioengineering*, 116, 2167–2177. <https://doi.org/10.1002/bit.27022>
- García-Contreras, R., Vos, P., Westerhoff, H. V., & Booger, F. C. (2012). Why in vivo may not equal in vitro—new effectors revealed by measurement of enzymatic activities under the same in vivo-like assay conditions. *The FEBS Journal*, 279, 4145–4159. <https://doi.org/10.1111/febs.12007>
- Grootboom, N., & Nyokong, T. (2002). Iron perchlorophthalocyanine and tetrasulfophthalocyanine catalyzed oxidation of cyclohexane using hydrogen peroxide, chloroperoxybenzoic acid and tert-butylhydroperoxide as oxidants. *Journal of Molecular Catalysis A: Chemical*, 179, 113–123. [https://doi.org/10.1016/S1381-1169\(01\)00404-6](https://doi.org/10.1016/S1381-1169(01)00404-6)
- Halan, B., Schmid, A., & Buehler, K. (2010). Maximizing the productivity of catalytic biofilms on solid supports in membrane aerated reactors. *Biotechnology and Bioengineering*, 106, 516–527. <https://doi.org/10.1002/bit.22732>
- Halan, B., Schmid, A., & Buehler, K. (2011). Real-time solvent tolerance analysis of *Pseudomonas* sp. strain VLB120ΔC catalytic biofilms. *Applied and Environmental Microbiology*, 77, 1563–1571. <https://doi.org/10.1128/AEM.02498-10>
- Hanahan, D. (1983). Studies on transformation of *Escherichia coli* with plasmids. *Journal of Molecular Biology*, 166, 557–580. [https://doi.org/10.1016/s0022-2836\(83\)80284-8](https://doi.org/10.1016/s0022-2836(83)80284-8)
- Heckmann, D., Campeau, A., Lloyd, C. J., Phaneuf, P. V., Hefner, Y., Carrillo-Terrazas, M., Feist, A. M., Gonzalez, D. J., & Palsson, B. O. (2020). Kinetic profiling of metabolic specialists demonstrates stability and consistency of in vivo enzyme turnover numbers. *Proceedings of the National Academy of Sciences of the United States of America*, 117, 23182–23190. <https://doi.org/10.1073/pnas.2001562117>
- Heuschkel, I., Hoschek, A., Schmid, A., Bühler, B., Karande, R., & Bühler, K. (2019). Mixed-trophies biofilm cultivation in capillary reactors. *MethodsX*, 6, 1822–1831. <https://doi.org/10.1016/j.mex.2019.07.021>
- Hilker, I., Gutiérrez, M. C., Furstoss, R., Ward, J., Wohlgemuth, R., & Alphand, V. (2008). Preparative scale Baeyer–Villiger biooxidation at high concentration using recombinant *Escherichia coli* and in situ substrate feeding and product removal process. *Nature Protocols*, 3, 546–554. <https://doi.org/10.1038/nprot.2007.532>
- Hoschek, A., Heuschkel, I., Schmid, A., Bühler, B., Karande, R., & Bühler, K. (2019). Mixed-species biofilms for high-cell-density application of *Synechocystis* sp. PCC 6803 in capillary reactors for continuous cyclohexane oxidation to cyclohexanol. *Bioresource Technology*, 282, 171–178. <https://doi.org/10.1016/j.biortech.2019.02.093>
- Hoschek, A., Toepel, J., Hochkeppel, A., Karande, R., Bühler, B., & Schmid, A. (2019). Light-dependent and aeration-independent gram-scale hydroxylation of cyclohexane to cyclohexanol by CYP450 harboring *Synechocystis* sp. PCC 6803. *Biotechnology Journal*, 14, 1800724. <https://doi.org/10.1002/biot.201800724>
- Kadisich, M., Willrodt, C., Hillen, M., Bühler, B., & Schmid, A. (2017). Maximizing the stability of metabolic engineering-derived whole-cell biocatalysts. *Biotechnology Journal*, 12, 1600170. <https://doi.org/10.1002/biot.201600170>
- Kamerbeek, N. M., Fraaije, M. W., & Janssen, D. B. (2004). Identifying determinants of NADPH specificity in Baeyer–Villiger monoxygenases. *European Journal of Biochemistry*, 271, 2107–2116. <https://doi.org/10.1111/j.1432-1033.2004.04126.x>
- Kamerbeek, N. M., Janssen, D. B., van Berkel, W. J., & Fraaije, M. W. (2003). Baeyer–Villiger monoxygenases, an emerging family of flavin-dependent biocatalysts. *Advanced Synthesis & Catalysis*, 345, 667–678. <https://doi.org/10.1002/adsc.200303014>
- Kamerbeek, N. M., Olsthoorn, A. J., Fraaije, M. W., & Janssen, D. B. (2003). Substrate specificity and enantioselectivity of 4-hydroxyacetophenone monoxygenase. *Applied and Environmental Microbiology*, 69, 419–426. <https://doi.org/10.1128/AEM.69.1.419-426.2003>
- Karande, R., Halan, B., Schmid, A., & Buehler, K. (2014). Segmented flow is controlling growth of catalytic biofilms in continuous multiphase microreactors. *Biotechnology and Bioengineering*, 111, 1831–1840. <https://doi.org/10.1002/bit.25256>
- Karande, R., Salamanca, D., Schmid, A., & Buehler, K. (2017). Biocatalytic conversion of cycloalkanes to lactones using an in-vivo cascade in *Pseudomonas taiwanensis* VLB120. *Biotechnology and Bioengineering*, 115, 312–320. <https://doi.org/10.1002/bit.26469>
- Kashid, M. N., Gupta, A., Renken, A., & Kiwi-Minsker, L. (2010). Numbering-up and mass transfer studies of liquid–liquid two-phase microstructured reactors. *Chemical Engineering Journal*, 158, 233–240. <https://doi.org/10.1016/j.cej.2010.01.020>
- Kim, Y.-M., Jung, S.-H., Chung, Y.-H., Yu, C.-B., & Rhee, I.-K. (2008). Cloning and characterization of a cyclohexanone monoxygenase gene from *Arthrobacter* sp. L661. *Biotechnology and Bioprocess Engineering*, 13, 40–47. <https://doi.org/10.1007/s12257-007-0162-1>

- Kumar, S., Stecher, G., Li, M., Knyaz, C., & Tamura, K. (2018). MEGA X: Molecular evolutionary genetics analysis across computing platforms. *Molecular Biology and Evolution*, 35, 1547–1549. <https://doi.org/10.1093/molbev/msy096>
- Köhler, K. A. K., Rückert, C., Schatschneider, S., Vorhölter, F.-J., Szczepanowski, R., Blank, L. M., Niehaus, K., Goesmann, A., Pühler, A., Kalinowski, J., & Schmid, A. (2013). Complete genome sequence of *Pseudomonas* sp. strain VLB120 a solvent tolerant, styrene degrading bacterium, isolated from forest soil. *Journal of Biotechnology*, 168, 729–730. <https://doi.org/10.1016/j.jbiotec.2013.10.016>
- Laemmli, U. K. (1970). Cleavage of structural proteins during the assembly of the head of bacteriophage T4. *Nature*, 227, 680–685. <https://doi.org/10.1038/227680a0>
- Lang, K., Zierow, J., Buehler, K., & Schmid, A. (2014). Metabolic engineering of *Pseudomonas* sp. strain VLB120 as platform biocatalyst for the production of isobutyric acid and other secondary metabolites. *Microbial Cell Factories*, 13, 2. <https://doi.org/10.1186/1475-2859-13-2>
- Latham, J. A., Branchaud, B. P., Chen, Y.-C. J., & Walsh, C. (1986). Allylic and propargylic phenyl selenide oxygenation by cyclohexanone oxygenase: [2, 3]-sigmatropic rearrangement of the enzyme-generated selenoxide. *Journal of the Chemical Society, Chemical Communications*, 7, 528–530. <https://doi.org/10.1039/C39860000528>
- Li, G., Fürst, M. J. L. J., Mansouri, H. R., Ressmann, A. K., Ilie, A., Rudroff, F., Mihovilovic, M. D., Fraaije, M. W., & Reetz, M. T. (2017). Manipulating the stereoselectivity of the thermostable Baeyer–Villiger monooxygenase TmCHMO by directed evolution. *Organic & Biomolecular Chemistry*, 15, 9824–9829. <https://doi.org/10.1039/C7OB02692G>
- Mascotti, M. L., Kurina-Sanz, M., Ayub, M. J., & Fraaije, M. W. (2014). Insights in the kinetic mechanism of the eukaryotic Baeyer–Villiger monooxygenase BVMO<sub>Af1</sub> from *Aspergillus fumigatus* Af293. *Biochimie*, 107, 270–276. <https://doi.org/10.1016/j.biochi.2014.09.005>
- McFeters, G., Egli, T., Wilberg, E., Alder, A., Schneider, R., Suozzi, M., & Giger, W. (1990). Activity and adaptation of nitrilotriacetate (NTA)-degrading bacteria: Field and laboratory studies. *Water Research*, 24, 875–881. [https://doi.org/10.1016/0043-1354\(90\)90137-U](https://doi.org/10.1016/0043-1354(90)90137-U)
- Mihovilovic, M. D., Müller, B., & Stanetty, P. (2002). Monooxygenase-Mediated Baeyer–Villiger Oxidations. *European Journal of Organic Chemistry*, 2002, 3711–3730. [https://doi.org/10.1002/1099-0690\(200211\)2002:22%3C3711::AID-EJOC3711%3E3.0.CO;2-5](https://doi.org/10.1002/1099-0690(200211)2002:22%3C3711::AID-EJOC3711%3E3.0.CO;2-5)
- Milo, R., Jorgensen, P., Moran, U., Weber, G., & Springer, M. (2010). BioNumbers—the database of key numbers in molecular and cell biology. *Nucleic Acids Research*, 38, D750–D753. <https://doi.org/10.1093/nar/gkp889>
- Mirpuri, R., Jones, W., & Bryers, J. D. (1997). Toluene degradation kinetics for planktonic and biofilm-grown cells of *Pseudomonas putida* 54G. *Biotechnology and Bioengineering*, 53, 535–546. [https://doi.org/10.1002/\(SICI\)1097-0290\(19970320\)53:6%3C535::AID-BIT1%3E3.0.CO;2-N](https://doi.org/10.1002/(SICI)1097-0290(19970320)53:6%3C535::AID-BIT1%3E3.0.CO;2-N)
- Mirza, I. A., Yachnin, B. J., Wang, S., Grosse, S., Bergeron, H., Imura, A., Iwaki, H., Hasegawa, Y., Lau, P. C. K., & Berghuis, A. M. (2009). Crystal structures of cyclohexanone monooxygenase reveal complex domain movements and a sliding cofactor. *Journal of the American Chemical Society*, 131, 8848–8854. <https://doi.org/10.1021/ja9010578>
- Neidhardt, F., Ingraham, J., & Schaechter, M. (1990). *Physiology of the bacterial cell: A molecular approach*. Sinauer Associates Inc.
- Ottolina, G., Bianchi, S., Belloni, B., Carrea, G., & Danieli, B. (1999). First asymmetric oxidation of tertiary amines by cyclohexanone monooxygenase. *Tetrahedron Letters*, 40, 8483–8486. [https://doi.org/10.1016/S0040-4039\(99\)01780-3](https://doi.org/10.1016/S0040-4039(99)01780-3)
- Panke, S., Meyer, A., Huber, C. M., Witholt, B., & Wubbolts, M. G. (1999). An alkane-responsive expression system for the production of fine chemicals. *Applied and Environmental Microbiology*, 65, 2324–2332. <https://doi.org/10.1128/AEM.65.6.2324-2332.1999>
- Pazmino, D. E. T., Dudek, H. M., & Fraaije, M. W. (2010). Baeyer–Villiger monooxygenases: Recent advances and future challenges. *Current Opinion in Chemical Biology*, 14, 138–144. <https://doi.org/10.1016/j.cbpa.2009.11.017>
- Rehdorf, J., Zimmer, C. L., & Bornscheuer, U. T. (2009). Cloning, expression, characterization, and biocatalytic investigation of the 4-hydroxyacetophenone monooxygenase from *Pseudomonas putida* JD1. *Applied and Environmental Microbiology*, 75, 3106–3114. <https://doi.org/10.1128/aem.02707-08>
- Riebel, A., Dudek, H., De Gonzalo, G., Stepniak, P., Rychlewski, L., & Fraaije, M. (2012). Expanding the set of rhodococcal Baeyer–Villiger monooxygenases by high-throughput cloning, expression and substrate screening. *Applied Microbiology and Biotechnology*, 95, 1479–1489. <https://doi.org/10.1007/s00253-011-3823-0>
- Ryerson, C. C., Ballou, D. P., & Walsh, C. (1982). Mechanistic studies on cyclohexanone oxygenase. *Biochemistry*, 21, 2644–2655. <https://doi.org/10.1021/bi00540a011>
- Salamanca, D., & Engesser, K.-H. (2014). Isolation and characterization of two novel strains capable of using cyclohexane as carbon source. *Environmental Science and Pollution Research*, 21, 12757–12766. <https://doi.org/10.1007/s11356-014-3206-z>
- Sambrook, J., & Russell, D. W. (2001). *Molecular cloning: A laboratory manual* (Vol. 2). Cold Spring Harbor Laboratory.
- Schrewe, M., Julsing, M. K., Bühler, B., & Schmid, A. (2013). Whole-cell biocatalysis for selective and productive C–O functional group introduction and modification. *Chemical Society Reviews*, 42, 6346–6377. <https://doi.org/10.1039/c3cs60011d>
- Schäfer, L., Bühler, K., Karande, R., & Bühler, B. (2020). Rational engineering of a multi-step biocatalytic cascade for the conversion of cyclohexane to polycaprolactone monomers in *Pseudomonas taiwanensis*. *Biotechnology Journal*, 15, 2000091. <https://doi.org/10.1002/biot.202000091>
- Schäfer, L., Karande, R., & Bühler, B. (2020). Maximizing biocatalytic cyclohexane hydroxylation by modulating cytochrome P450 monooxygenase expression in *P. taiwanensis* VLB120. *Frontiers in Bioengineering and Biotechnology*, 8, 140. <https://doi.org/10.3389/fbioe.2020.00140>
- Stewart, J. D. (1998). Cyclohexanone monooxygenase: a useful asymmetric Baeyer–Villiger reactions. *Current Organic Chemistry*, 2, 195–216.
- Stewart, P. S., & Franklin, M. J. (2008). Physiological heterogeneity in biofilms. *Nature Reviews Microbiology*, 6, 199–210. <https://doi.org/10.1038/nrmicro1838>
- Ten Brink, G.-J., Arends, I., & Sheldon, R. (2004). The Baeyer–Villiger reaction: New developments toward greener procedures. *Chemical Reviews*, 104, 4105–4124. <https://doi.org/10.1021/cr030011h>
- Teusink, B., Passarge, J., Reijenga, C. A., Esgalhado, E., Van der Weijden, C. C., Schepper, M., Walsh, M. C., Bakker, B. M., van Dam, K., Westerhoff, H. V., & Snoep, J. L. (2000). Can yeast glycolysis be understood in terms of *in vitro* kinetics of the constituent enzymes? Testing biochemistry. *European Journal of Biochemistry*, 267, 5313–5329. <https://doi.org/10.1046/j.1432-1327.2000.01527.x>
- Torres Pazmiño, D. E., Baas, B.-J., Janssen, D. B., & Fraaije, M. W. (2008). Kinetic mechanism of phenylacetone monooxygenase from *Thermobifida fusca*. *Biochemistry*, 47, 4082–4093. <https://doi.org/10.1021/bi702296k>
- Trower, M. K., Buckland, R. M., & Griffin, M. (1989). Characterization of an FMN-containing cyclohexanone monooxygenase from a cyclohexane-grown *Xanthobacter* sp. *European Journal of Biochemistry*, 181, 199–206. <https://doi.org/10.1111/j.1432-1033.1989.tb14711.x>

- Tufvesson, P., Lima-Ramos, J., Jensen, J. S., Al-Haque, N., Neto, W., & Woodley, J. M. (2011). Process considerations for the asymmetric synthesis of chiral amines using transaminases. *Biotechnology and Bioengineering*, 108, 1479–1493. <https://doi.org/10.1002/bit.23154>
- Van Beilen, J. B., Duetz, W. A., Schmid, A., & Witholt, B. (2003). Practical issues in the application of oxygenases. *Trends in Biotechnology*, 21, 170–177. [https://doi.org/10.1016/S0167-7799\(03\)00032-5](https://doi.org/10.1016/S0167-7799(03)00032-5)
- Van Beilen, J. B., Mourlane, F., Seeger, M. A., Kovac, J., Li, Z., Smits, T. H. M., Fritsche, U., & Witholt, B. (2003). Cloning of Baeyer-Villiger monooxygenases from *Comamonas*, *Xanthobacter* and *Rhodococcus* using polymerase chain reaction with highly degenerate primers. *Environmental Microbiology*, 5, 174–182. <https://doi.org/10.1046/j.1462-2920.2003.00401.x>
- Van Eunen, K., & Bakker, B. M. (2014). The importance and challenges of in vivo-like enzyme kinetics. *Perspectives in Science*, 1, 126–130. <https://doi.org/10.1016/j.pisc.2014.02.011>
- Volmer, J., Neumann, C., Bühler, B., & Schmid, A. (2014). Engineering of *Pseudomonas taiwanensis* VLB120 for constitutive solvent tolerance and increased specific styrene epoxidation activity. *Applied and Environmental Microbiology*, 80, 6539–6548. <https://doi.org/10.1128/AEM.01940-14>
- Whelan, S., & Goldman, N. (2001). A general empirical model of protein evolution derived from multiple protein families using a maximum-likelihood approach. *Molecular Biology and Evolution*, 18, 691–699. <https://doi.org/10.1093/oxfordjournals.molbev.a003851>
- Wimpenny, J., Manz, W., & Szewzyk, U. (2000). Heterogeneity in biofilms. *FEMS Microbiology Reviews*, 24, 661–671. <https://doi.org/10.1111/j.1574-6976.2000.tb00565.x>
- Wynands, B., Lenzen, C., Otto, M., Koch, F., Blank, L. M., & Wierckx, N. (2018). Metabolic engineering of *Pseudomonas taiwanensis* VLB120 with minimal genomic modifications for high-yield phenol production. *Metabolic Engineering*, 47, 121–133. <https://doi.org/10.1016/j.ymben.2018.03.011>
- Zhang, Y., Liu, F., Xu, N., Wu, Y.-Q., Zheng, Y.-C., Zhao, Q., Lin, G., Yu, H. L., & Xu, J. H. (2018). Discovery of two native Baeyer-Villiger monooxygenases for asymmetric synthesis of bulky chiral sulfoxides. *Applied and Environmental Microbiology*, 84, e00638-00618 <https://doi.org/10.1128/AEM.00638-18>

#### SUPPORTING INFORMATION

Additional Supporting Information may be found online in the supporting information tab for this article.

**How to cite this article:** Bretschneider, L., Heuschkel, I., Ahmed, A., Bühler, K., Karande, R., & Bühler, B. (2021). Characterization of different biocatalyst formats for BVMO-catalyzed cyclohexanone oxidation. *Biotechnology and Bioengineering*, 1–15. <https://doi.org/10.1002/bit.27791>

## Supporting Information

### **Characterization of different biocatalyst formats for BVMO-catalyzed cyclohexanone oxidation**

#### **Table of contents**

1	Uncoupling in CHMO-catalyzed reactions.....	2
2	Supplementary Figures .....	2
3	References.....	9

## 1 Uncoupling of CHMO

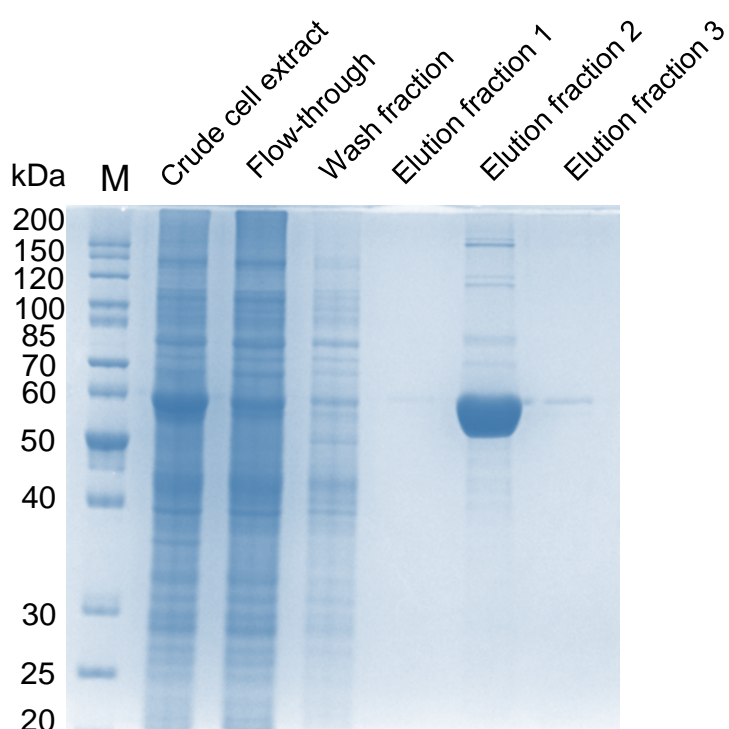
The uncoupling reaction in CHMO was investigated by quantifying NADPH consumption spectrophotometrically and product ( $\epsilon$ -caprolactone) formation by GC after 5 min reaction time (Table S1). Without substrate, no NADPH consumption and thus uncoupling was observed. Also in the presence of substrate, no uncoupling occurred, as it can be deduced from the coincident amounts of NADPH and  $\epsilon$ -caprolactone consumed.

**Table S1: Analysis of CHMO uncoupling.**

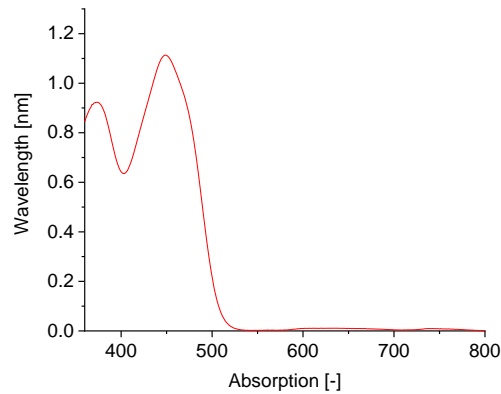
Substrate (mM)	NADPH consumed (mM)	$\epsilon$ -caprolactone (mM)
0	0	not applicable
1	$0.19 \pm 0.01$	$0.21 \pm 0.01$
3	$0.15 \pm 0.01$	$0.17 \pm 0.01$

NADPH consumption was assayed spectrophotometrically over 5 min. The same sample then was immediately quenched and extracted by diethyl ether addition, followed by GC-based  $\epsilon$ -caprolactone quantification.

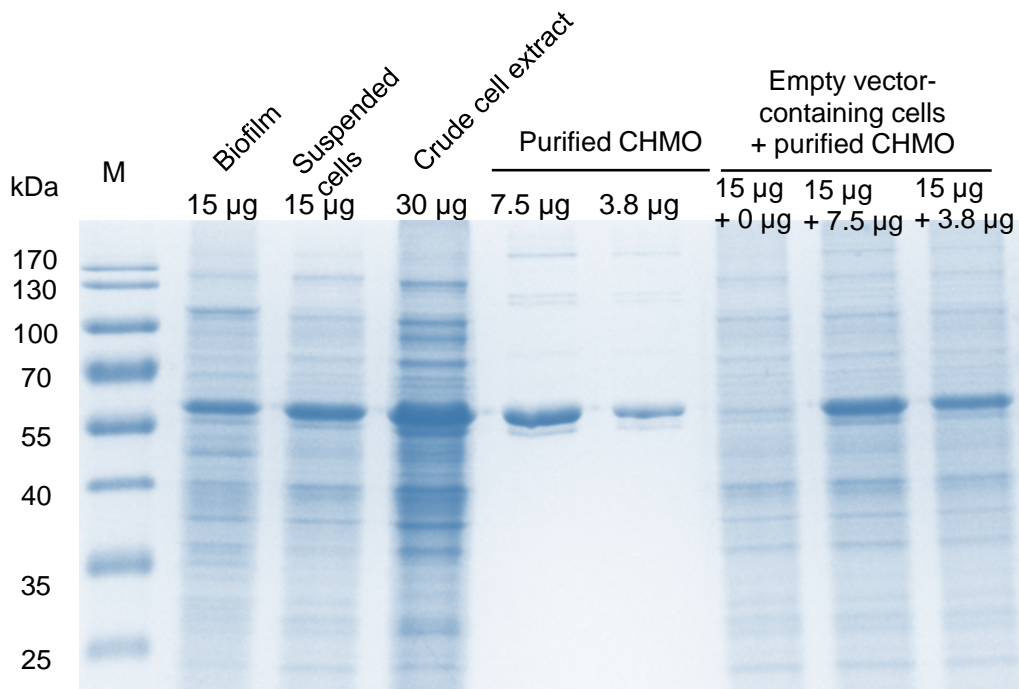
## 2 Supplementary Figures



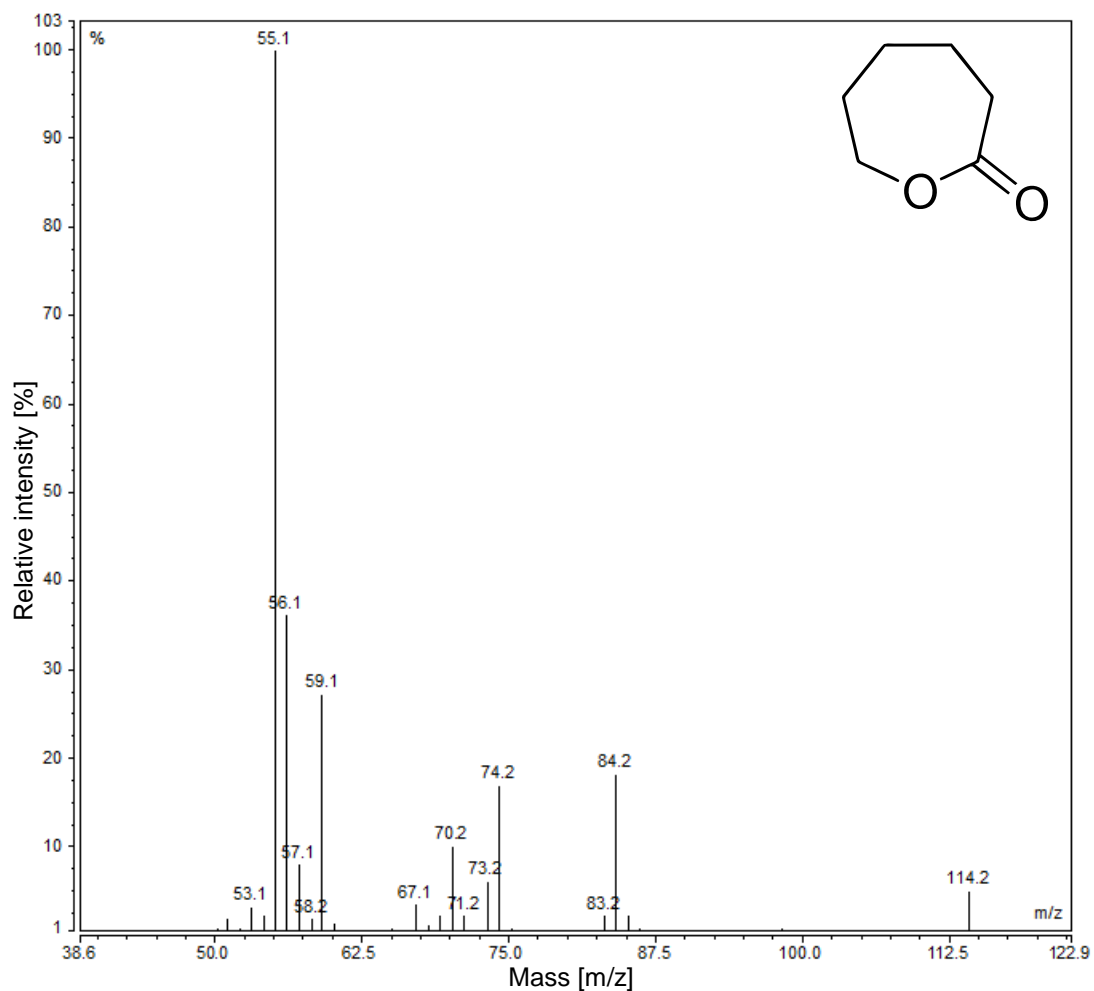
**Supplementary Figure S1: SDS-PAGE-analysis during CHMO purification.** 2 $\mu$ L of respective fractions were loaded. The gels shows the first out of five wash fractions and the three consecutively collected elution fractions (1.5 mL, 2 mL, 1.5 mL).



**Supplementary Figure S2:** Absorption spectrum of purified CHMO. The spectrum was recorded applying a CHMO concentration of  $0.5 \text{ mg mL}^{-1}$  with a Cary photometer. The absorbance spectrum shows the two maxima at 380 and 443 nm characteristic for flavins and flavoproteins (Fraaije, Wu, Heuts, Van Hellemond, Spelberg & Janssen, 2005) .

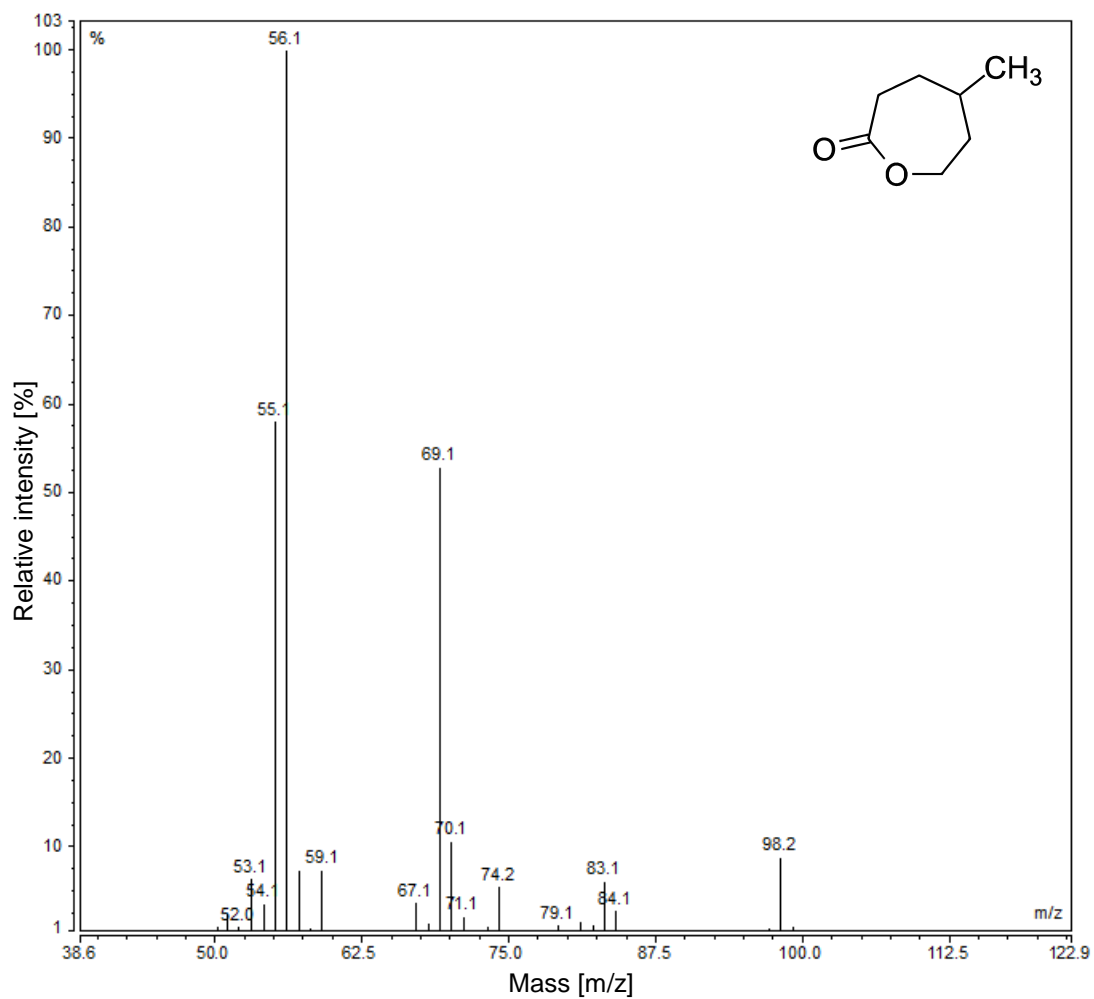


**Supplementary Figure S3: SDS-PAGE analysis to quantify cellular CHMO contents.** Biofilm and suspension derived cells were pelleted and resuspended in Kpi buffer.  $OD_{450}$ -standardized amounts of biomass were loaded on the gel. The amounts of protein and/or cells given in  $\mu\text{g}$  are derived from Bradford analysis or applying a conversion factor of  $0.186 \text{ g}_{\text{CDW}} \text{ L}^{-1}$  per  $OD_{450}$ . Samples containing defined amounts of purified CHMO were used to estimate intracellular CHMO amounts.

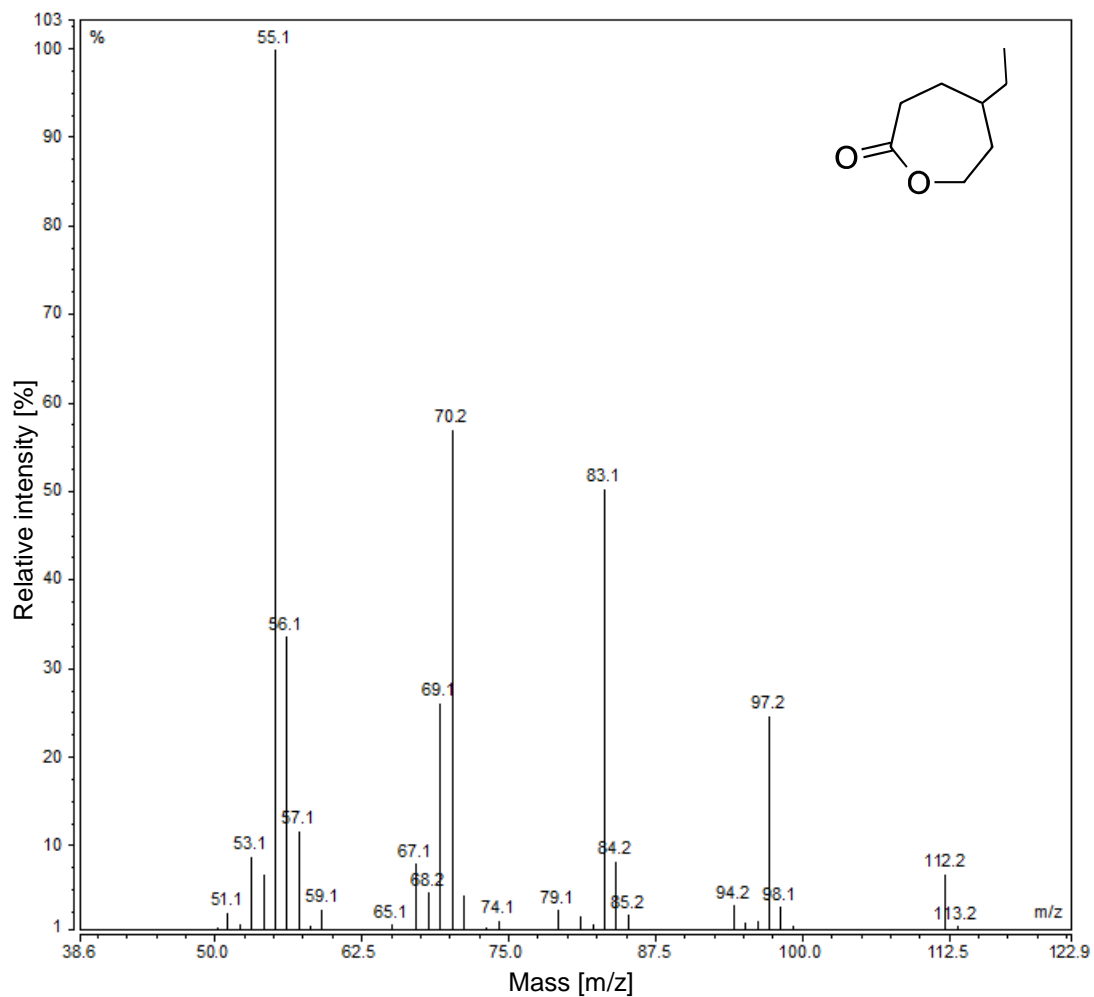


**Supplementary Figure S4:** GC-MS spectrum of  $\epsilon$ -caprolactone from cyclohexanone conversion.

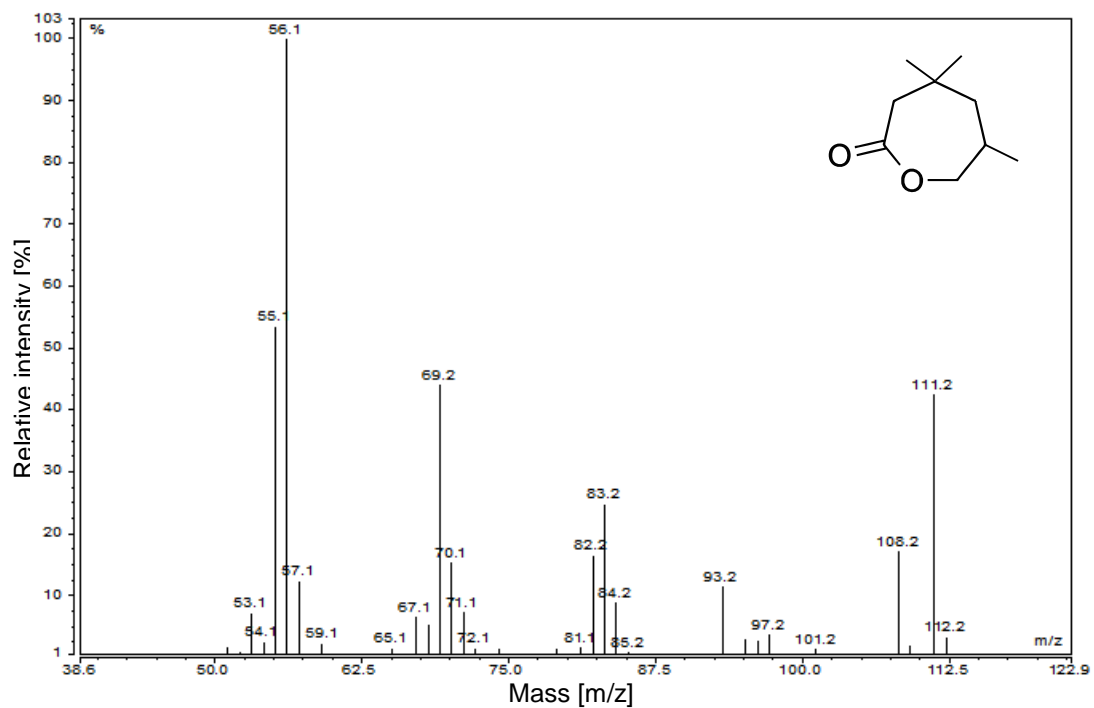




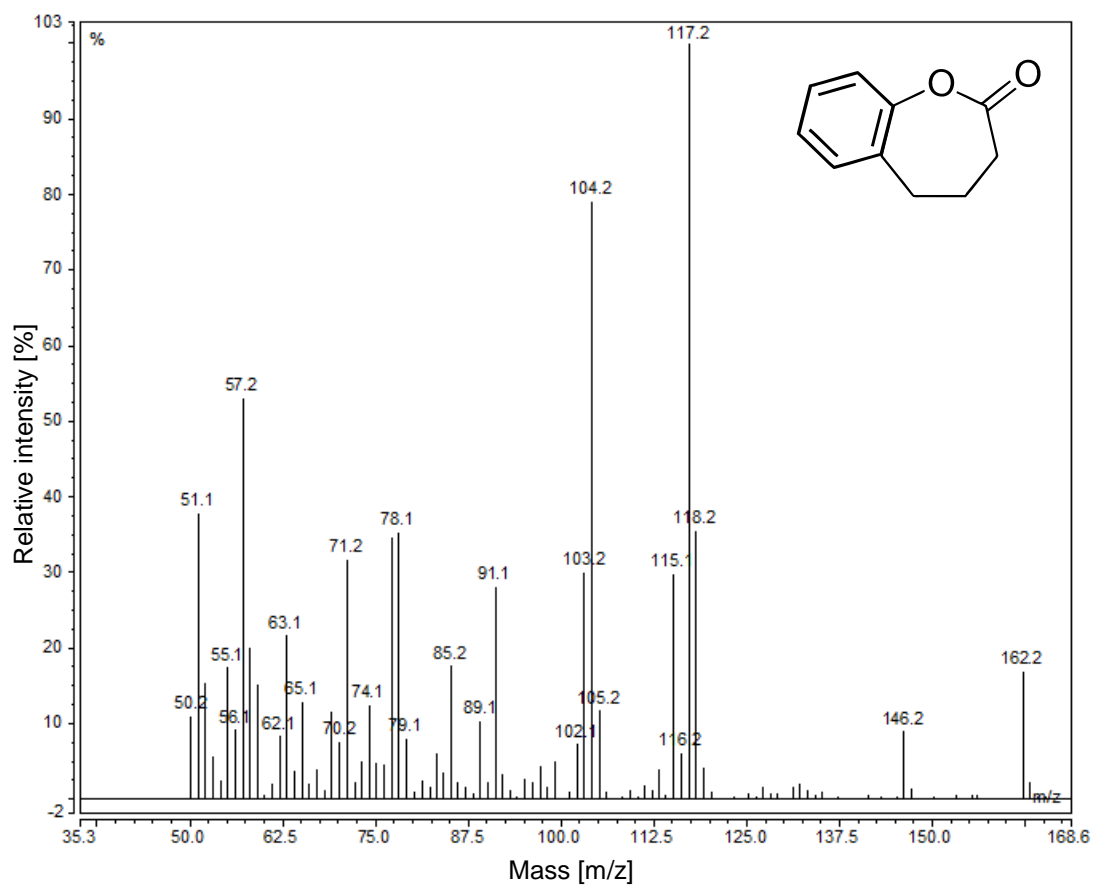
**Supplementary Figure S5:** GC-MS spectrum of 4-methylcaprolactone from 4-methylcyclohexanone conversion.



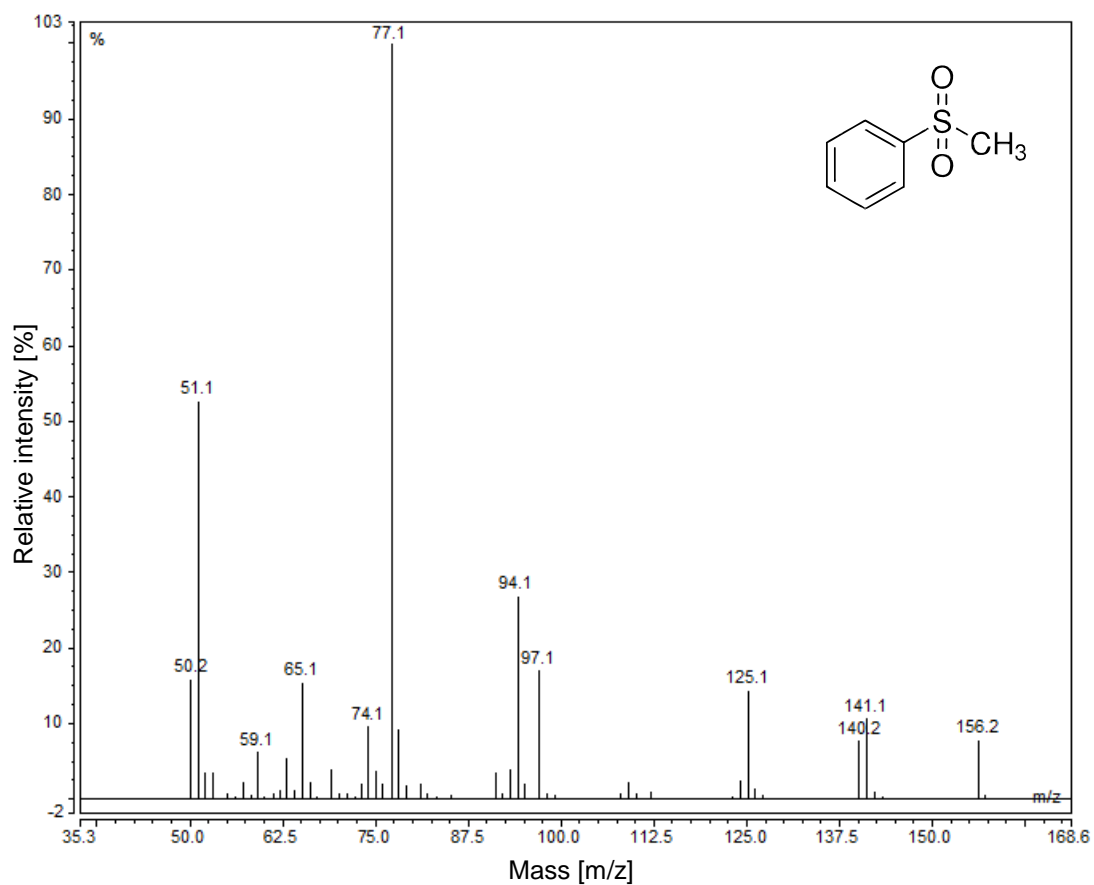
**Supplementary Figure S6:** GC-MS spectrum of 4-ethylcaprolactone from 4-ethylcyclohexanone conversion.



**Supplementary Figure S7:** GC-MS spectrum of 3,3,5-trimethylcaprolactone from 3,3,5-trimethylcyclohexanone conversion.



**Supplementary Figure S8:** GC-MS spectrum of  $\beta$ -tetralone lactone from  $\beta$ -tetralone conversion.



**Supplementary Figure S9:** GC-MS spectrum of methyl phenyl sulfone from methyl phenyl sulfoxide conversion.

### 3 References

Fraaije, M.W., Wu, J., Heuts, D.P.H. M., Van Hellemond, E. W., Spelberg, J. H. L. & Janssen, D.B. (2005). Discovery of a thermostable Baeyer–Villiger monooxygenase by genome mining. *Applied Microbiology and Biotechnology*, 66, 393-400. doi: <https://doi.org/10.1007/s00253-004-1749-5>

**3 Biotechnol. J. (2020), 15(11), art. 2000091, incl. Supplementary Material**

# Rational Engineering of a Multi-Step Biocatalytic Cascade for the Conversion of Cyclohexane to Polycaprolactone Monomers in *Pseudomonas taiwanensis*

Lisa Schäfer, Katja Bühler, Rohan Karande, and Bruno Bühler\*

The current industrial production of polymer building blocks such as  $\epsilon$ -caprolactone ( $\epsilon$ -CL) and 6-hydroxyhexanoic acid (6HA) is a multi-step process associated with critical environmental issues such as the generation of toxic waste and high energy consumption. Consequently, there is a demand for more eco-efficient and sustainable production routes. This study deals with the generation of a platform organism that converts cyclohexane to such polymer building blocks without the formation of byproducts and under environmentally benign conditions. Based on kinetic and thermodynamic analyses of the individual enzymatic steps, a 4-step enzymatic cascade in *Pseudomonas taiwanensis* VLB120 is rationally engineered via stepwise biocatalyst improvement on the genetic level. It is found that the intermediate product cyclohexanol severely inhibits the cascade which could be optimized by enhancing the expression level of downstream enzymes. The integration of a lactonase enables exclusive 6HA formation without side products. The resulting biocatalyst shows a high activity of  $44.8 \pm 0.2 \text{ U g}_{\text{CDW}}^{-1}$  and fully converts 5 mM cyclohexane to 6HA within 3 h. This platform organism can now serve as a basis for the development of greener production processes for polycaprolactone and related polymers.

origin constitute a major challenge as they introduce novel enzymatic functions into the host.<sup>[4,9]</sup> On the one hand, it is crucial to provide sufficient enzyme amounts to sustain reasonable rates. On the other hand, too much overexpression, especially of more than one gene, can severely hamper host metabolism and interfere with its stability.<sup>[10,11]</sup> Moreover, optimizations regarding the choice of the host strain, substrate uptake, and pathway flux can systematically improve in vivo cascade.<sup>[11–13,14]</sup> A holistic approach comprising catalyst and reaction engineering allows controlling the product formation patterns.<sup>[15,16]</sup>

Nowadays, plastics are ubiquitous in human life and cause severe litter problems. Thus, biodegradable polymers such as polycaprolactone (PCL), polylactic acid, and polyhydroxyalkanoate have gained importance.<sup>[17]</sup> PCL can either be synthesized by the ring-opening polymerization of  $\epsilon$ -caprolactone ( $\epsilon$ -CL) or by the polycondensation of 6-hydroxyhexanoic acid (6-HA).<sup>[18]</sup>

## 1. Introduction

In synthetic applications, cascade reactions allow for streamlined product formation via multiple reaction steps with the advantage to avoid the isolation of intermediates, thus saving resources, reagents, and time.<sup>[1]</sup> Multi-step biocatalysis employing whole cells emerged as a powerful tool for the synthesis of value-added compounds.<sup>[2–4,5]</sup> Precise and delicate fine-tuning of gene expression is required to balance individual enzyme amounts and activities for the construction of “designer cells.”<sup>[1,6,7,8]</sup> Especially “artificial cascades” employing heterologous genes of diverse

Industrially,  $\epsilon$ -CL is produced from cyclohexane through the Union Carbide Corporation (UCC) process, which suffers from serious environmental issues, a low cyclohexane conversion of 10–12%, and only moderate selectivity of 85–90%.<sup>[19,20]</sup> General advantages of biocatalysis, such as high selectivities and operation at moderate temperature and ambient pressure, have a big potential to design a more eco-efficient process. Recently, two biocatalytic approaches to synthesize  $\epsilon$ -CL from cyclohexane have been published. Pennec et al. demonstrated a one-pot reaction applying purified enzymes,<sup>[21]</sup> which, however, suffered from a low conversion of 3%. Recently, Au-doped TiO<sub>2</sub> and graphitic carbonitride photocatalysts catalyzing the oxidation of cyclohexane to cyclohexanone were combined with *E. coli* cells expressing a Baeyer–Villiger monooxygenase in a proof-of-concept study producing 0.4 mM  $\epsilon$ -CL from cyclohexane, but with a low conversion (200 mM cyclohexane employed).<sup>[22]</sup> Karande et al. generated a whole-cell biocatalyst showing superior total turnover numbers (TTN),<sup>[23]</sup> depending, however, on the expensive growth substrate citrate and the volatile inducer dicyclopropylketone. Thereby, they established a 3-step cascade in *P. taiwanensis* VLB120 by introducing cytochrome P450 monooxygenase (Cyp), cyclohexanol dehydrogenase (CDH), and Baeyer–Villiger cyclohexanone monooxygenase (CHMO) genes from

L. Schäfer, Prof. K. Bühler, Dr. R. Karande, Prof. B. Bühler  
Department of Solar Materials  
Helmholtz-Centre for Environmental Research - UFZ  
Permoserstraße 15, Leipzig, Saxony 04318, Germany  
E-mail: bruno.buehler@ufz.de

 The ORCID identification number(s) for the author(s) of this article can be found under <https://doi.org/10.1002/biot.202000091>

© 2020 The Authors. *Biotechnology Journal* published by Wiley-VCH GmbH. This is an open access article under the terms of the Creative Commons Attribution License, which permits use, distribution and reproduction in any medium, provided the original work is properly cited.

DOI: 10.1002/biot.202000091

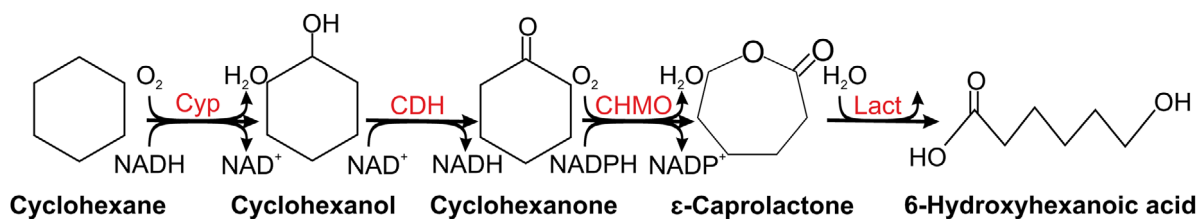


**Figure 1.** Biocatalytic cascade for the synthesis of polycaprolactone (PCL) monomers. The cascade is composed of a cytochrome P450 monooxygenase (Cyp), a cyclohexanol dehydrogenase (CDH), and a cyclohexanone monooxygenase (CHMO) for the production of  $\epsilon$ -caprolactone ( $\epsilon$ -CL).<sup>[23]</sup> Optionally, a lactonase (Lact) catalyzes the ring-opening reaction to yield 6-hydroxyhexanoic acid (6HA).

*Acidovorax* sp. CHX100 (**Figure 1**). Respective cascade development mainly focused on the monomer  $\epsilon$ -CL and gave rise to a maximal activity of  $22 \text{ Ug}_{\text{CDW}}^{-1}$ , with the first Cyp-catalyzed step being rate-limiting. The successive enzymes, CDH and CHMO exhibited much higher activities of 80 and  $170 \text{ Ug}_{\text{CDW}}^{-1}$ , respectively. In a separate study, the activity of cells containing only the Cyp could be more than doubled by expression system engineering.<sup>[24]</sup>

In this study, we set out to amend the latter system with CDH and CHMO genes and thereby achieve high respective activities, utilize glucose instead of citrate as carbon and energy source, prevent the accumulation of intermediates, and keep the expression related metabolic burden reasonably low to allow for stable catalysis. Explicitly, oxygenases such as Cyps or Baeyer-Villiger monooxygenases are prone to form reactive oxygen species via uncoupling reactions, which may hamper the catalytic prowess of the cells.<sup>[11,13]</sup> Another point to be considered is that, due to the accumulation of the hydrolysis product 6HA, the approach of Karande et al.<sup>[23]</sup> suffered from restricted cascade selectivity. We aimed to tackle all these points by rational pathway engineering including the characterization of the involved enzymes as the basis for the rational assembly of the expression system. It is thereby crucial to balance enzyme activities without dissipating the cell's resources.

## 2. Results

The construction of an efficient biocatalytic in vivo cascade necessitates a balanced expression of the cascade genes to avoid side product accumulation. Besides the well-characterized initiating Cyp,<sup>[24,25]</sup> CDH, and CHMO have been employed for PCL monomer synthesis from cyclohexane,<sup>[23]</sup> but nothing is known about respective reaction kinetics and possible inhibitions by pathway intermediates as they have been observed before, for example, for Baeyer-Villiger monooxygenases.<sup>[26,27]</sup> Consequently, CDH and CHMO were characterized as the first step in this study to support the rational engineering of a productive 3-step cascade based on the optimized Cyp-containing whole-cell biocatalyst.<sup>[24]</sup>

### 2.1. Characterization of CDH and CHMO

CDH and CHMO were cloned separately into the pSEVA244\_T vector<sup>[24]</sup> to characterize their in vivo activity. As CDH catalyzes an equilibrium reaction, the kinetic parameters were assayed for both reaction directions (**Table 1**). For the reverse reaction with cyclohexanone as substrate, CDH showed a 10 times lower  $\nu_{\text{max}}$

**Table 1.** Kinetic parameters of *P. taiwanensis* VLB 120 (pSEVA\_CDH).

Substrate <sup>a)</sup>	$\nu_{\text{max}}$ [ $\text{U g}_{\text{CDW}}^{-1}$ ]	$K_{\text{S}}$ <sup>b)</sup> [mM]	$k_{\text{cat}}$ <sup>c)</sup> [ $\text{s}^{-1}$ ]
Cyclohexanol	$296.6 \pm 15.7$	$3.57 \pm 0.26$	$2.74 \pm 0.14$
Cyclohexanone	$29.5 \pm 1.3$	$0.05 \pm 0.01$	$0.27 \pm 0.01$

<sup>a)</sup> Resting cell bioconversions were performed in 2 mL microcentrifuge tubes with a liquid volume of 1 mL and a biomass concentration of  $0.15 \text{ g}_{\text{CDW}} \text{ L}^{-1}$  for 3 min; <sup>b)</sup> Apparent substrate constant (concentration at which whole cells show half-maximal transformation rates);<sup>[28]</sup> <sup>c)</sup> Based on an estimated 5 g CDH in 100 g total cell dry weight (CDW).

compared to the forward reaction. On the other hand, the  $K_{\text{S}}$  values, corresponding to the apparent substrate uptake constant (concentration at which whole cells show half-maximal transformation rates) as it is used in the Monod-kinetics for microbial growth,<sup>[28]</sup> differed by a factor of almost 100 in favor of the reverse reaction (0.05 for cyclohexanone, 3.57 mM for cyclohexanol). The concentration of cyclohexanol and cyclohexanone in the system determine if  $\nu_{\text{max}}$  or  $K_{\text{S}}$  prevail. Furthermore, we theoretically and experimentally assessed the cyclohexanol/cyclohexanone concentration ratio at equilibrium. Utilizing the group contribution method<sup>[29]</sup> assuming a physiological intracellular NADH to NAD concentration ratio of 10.6 under aerobic conditions,<sup>[30]</sup> this ratio was determined to be 1.9 (Section S4, Supporting Information). It was confirmed experimentally by applying different initial alcohol and ketone concentrations giving a cyclohexanol/cyclohexanone concentration ratio of  $1.95 \pm 0.29$  after 16 h (Figure S2, Supporting Information). This thermodynamic preference of the backward reaction, together with the low  $K_{\text{S}}$  value for cyclohexanone emphasizes the necessity of an efficient cyclohexanone withdrawal by the successive enzyme in the cascade, that is, CHMO.

Substantial research has been conducted with a cyclohexanone monooxygenase originating from *Acinetobacter* sp.<sup>[31]</sup> Generally, the substrate as well as product toxicity, are features of Baeyer-Villiger monooxygenase-catalyzed reactions.<sup>[26,27]</sup> Substrate toxicity was generally observed at aqueous concentrations in the mM-range, which should thus be avoided during the cascade reaction. Furthermore, CHMO may be inhibited by the cascade intermediate cyclohexanol and its product  $\epsilon$ -CL. *Acidovorax* CHMO indeed was found to be highly prone to inhibition by cyclohexanol (Figure 2A). At a cyclohexanol concentration as low as 0.4 mM, the high initial CHMO activity of  $160.3 \pm 0.1 \text{ Ug}_{\text{CDW}}^{-1}$  was found to be reduced to half this rate. Cyclohexanol concentrations  $\geq 1.7 \text{ mM}$  completely abolished CHMO activity. However, up to an  $\epsilon$ -CL concentration of 17 mM, no product inhibition was found for CHMO (Figure 2B).



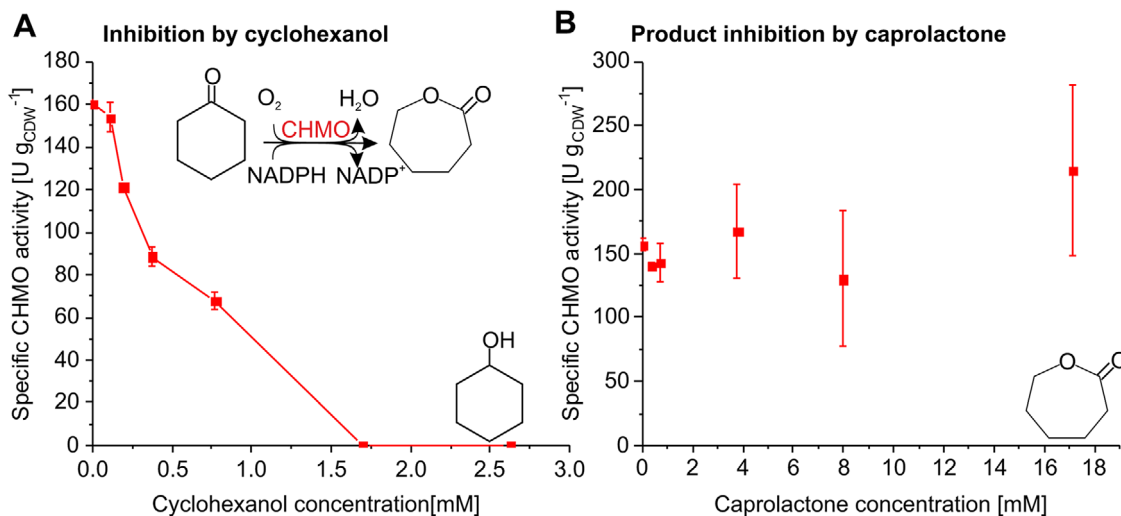


**Figure 2.** Inhibition studies with *P. taiwanensis* VLB120 (pSEVA\_CHMO). The influence of A) cyclohexanol or B) the product  $\epsilon$ -CL on specific CHMO activity was investigated in resting cell bioconversions. Cells were cultivated in M9\* medium with 0.5% (w/v) glucose, induced by isopropyl  $\beta$ -D-1-thiogalactopyranoside (IPTG) for 6 h, harvested, and resuspended in KPi-g buffer (100 mM potassium phosphate buffer supplemented with 1% (w/v) glucose) to a biomass concentration of A) 0.25 g<sub>CDW</sub> L<sup>-1</sup> in 1 mL liquid volume or B) 0.5 g<sub>CDW</sub> L<sup>-1</sup> in 10 mL liquid volume. Reactions were started by adding 3 mM cyclohexanone. Graphs represent average values and standard deviations of two independent biological replicates. The average experimental errors over all measurements for the activities in Panels A and B are 3.4% and 18.2%, respectively.

Summing up, these results emphasize that the produced cyclohexanol needs to be directly converted by CDH to avoid CHMO inhibition. High intracellular CDH and CHMO activities are important to avoid any accumulation of alcohol and ketone intermediates, as already low alcohol amounts can be expected to inherently reinforce such accumulation.

## 2.2. Assembling Caprolactone-Producing Strains

To assess CDH and CHMO gene expression to different levels, we generated two  $\epsilon$ -CL producers based on the platform organism for Cyp gene expression developed recently.<sup>[24]</sup> First, CDH and CHMO genes were placed downstream of the Cyp genes on the same operon in *P. taiwanensis* VLB120 pSEVA\_CL\_1 (Figure 3A). Consequently, one mRNA is produced, harboring all 5 genes sequentially. To enhance CDH and CHMO levels, a second strain harboring pSEVA\_CL\_2 was created. pSEVA\_CL\_2 contains a second  $P_{trc}$  promoter upstream of the CDH and CHMO genes giving rise to increased expression rates of the respective genes.

In bioconversions applying resting *P. taiwanensis* VLB120 (pSEVA\_CL\_1),  $\epsilon$ -CL accumulated up to  $1.46 \pm 0.01$  mM within 120 min, after which the reaction was stopped (Figure 3C). Besides the desired product  $\epsilon$ -CL, also the intermediate cyclohexanol was detected to a maximal concentration of 42  $\mu$ M after 60 min. Additionally, 6HA, the hydrolysis product of  $\epsilon$ -CL (Figure 1), accumulated in the culture (especially in the second hour of bioconversion) and reached a final concentration of  $0.77 \pm 0.07$  mM after 120 min. The specific overall product formation rate considering  $\epsilon$ -CL and 6HA remained quite stable at a high level ( $37.3 \pm 1.9$  U<sub>gCDW</sub><sup>-1</sup>). The same experiment employing *P. taiwanensis* VLB120 (pSEVA\_CL\_2) (Figure 3E), resulted in  $\epsilon$ -CL accumulation to a 20% higher concentration of

$1.80 \pm 0.01$  mM after 120 min and a higher specific product formation rate ( $43.4 \pm 1.9$  U<sub>gCDW</sub><sup>-1</sup>). In contrast to pSEVA\_CL\_1, the insertion of the second promoter completely prevented the emergence of cyclohexanol, whereas 6HA accumulated to a comparable concentration of 0.7 mM within 120 min. The activity increase observed in the first 10 min of both experiments (Figure 3C,E) may be attributed to the direct addition of liquid cyclohexane into the bacterial culture resulting in high local and thus toxic/inhibitory cyclohexane concentrations, which then were attenuated upon cyclohexane redistribution among gas and liquid phase.

The direct comparison of both strains carrying either pSEVA\_CL\_1 or pSEVA\_CL\_2 via SDS-PAGE showed that Cyp levels were similar, with pSEVA\_CL\_1 showing leaky expression (Figure 3B,D). CDH and CHMO levels were close to the detection limit in *P. taiwanensis* VLB120 (pSEVA\_CL\_1), whereas the insertion of the second promoter in the construct pSEVA\_CL\_2 significantly enhanced CDH and CHMO levels (Figure 3D). Assessing the initial specific activities of pSEVA\_CL\_1 containing enzymes for cyclohexane ( $37$  U<sub>gCDW</sub><sup>-1</sup>), cyclohexanol ( $39$  U<sub>gCDW</sub><sup>-1</sup>), and cyclohexanone ( $44$  U<sub>gCDW</sub><sup>-1</sup>) conversion revealed similar values for all three reaction steps (Table 2) with the CHMO activity being slightly higher than the other two. The higher CDH and CHMO content of *P. taiwanensis* VLB120 (pSEVA\_CL\_2) directly translated into higher alcohol ( $76$  U<sub>gCDW</sub><sup>-1</sup>) and ketone ( $84$  U<sub>gCDW</sub><sup>-1</sup>) conversion activities, respectively (Table 2). The introduction of the second promoter doubled the CDH and CHMO activities without affecting the amount of active Cyp in the cells (Table S4, Supporting Information). Coexpression of CDH and CHMO together with Cyp genes resulted in a 20% growth rate reduction from  $0.37 \pm 0.01$  (pSEVA\_Cyp) to  $0.29 \pm 0.01$  h<sup>-1</sup> (pSEVA\_CL\_1), indicating a metabolic burden (Table S4, Supporting Information). Concomitantly, the active Cyp content decreased by 30%. Interestingly, such decreases

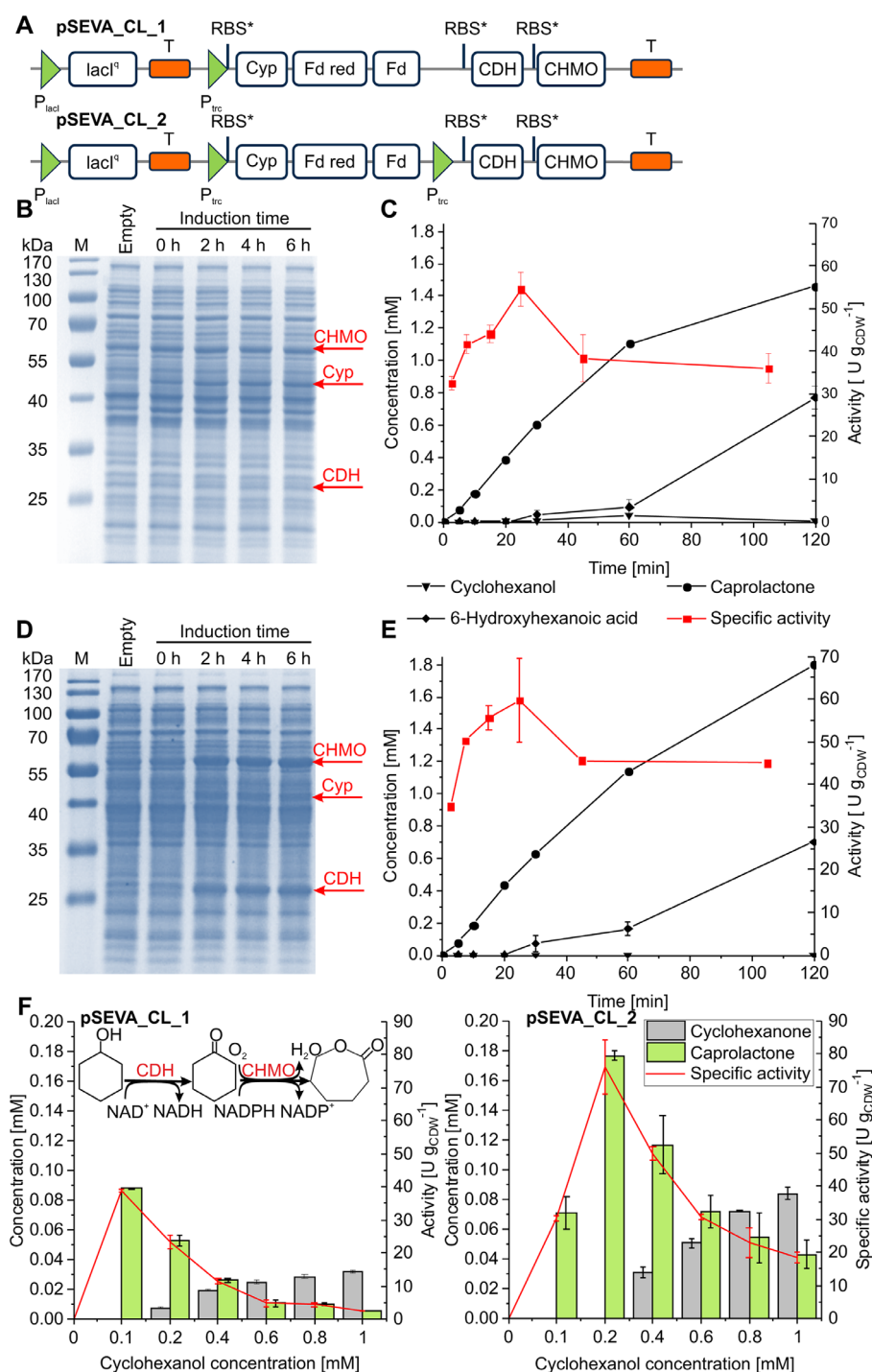


**Figure 3.** Construction and characterization of *P. taiwanensis* VLB120 A–C,F) pSEVA\_CL\_1 and A,D–F) pSEVA\_CL\_2. A) Graphical representation of expression units in the plasmids pSEVA\_CL\_1 and pSEVA\_CL\_2. B,D) SDS-PAGE analyses of *P. taiwanensis* VLB120 containing pSEVA\_CL\_1 or pSEVA\_CL\_2, respectively, showing bands for Cyp (47.4 kDa), CDH (26.5 kDa), and CHMO (58.8 kDa) after different times of induction and compared with cells containing an empty vector. C,E) Time courses for the production of cyclohexanol,  $\epsilon$ -CL, and 6HA and for whole-cell activities for the total product (sum of  $\epsilon$ -CL and 6HA) formation in resting cell bioconversions. Cells were cultivated as described in the legend of Figure 2 and induced for 4 h. Resting cell bioconversions were performed with a biomass concentration of  $0.5 \text{ g}_{\text{CDW}} \text{ L}^{-1}$  in 10 mL KPi-g buffer and started by adding  $10 \mu\text{L}$  of pure cyclohexane ( $180 \mu\text{M}$  dissolved in the aqueous phase,  $9.2 \text{ mM}$  in total concerning the aqueous phase volume). F) Resting cell bioconversions to study cascade inhibition by cyclohexanol. Varying cyclohexanol concentrations were applied in 1 mL KPi-g buffer with a cell concentration of  $0.25 \text{ g}_{\text{CDW}} \text{ L}^{-1}$ . The graphs depict cyclohexanone and  $\epsilon$ -CL concentrations as well as the whole-cell activity ( $\epsilon$ -CL formation) for an assay time of 10 min. Graphs represent average values and standard deviations of two independent biological replicates. The average experimental errors over all measurements for the concentrations of cyclohexanol, cyclohexanone,  $\epsilon$ -CL, and 6HA are 6.9%, 4.7%, 6.7%, and 35.2%, respectively, and 7.2% for the whole-cell activities.

**Table 2.** Specific activities of *P. taiwanensis* VLB120 containing different constructs for the conversion of the different cascade substrates/intermediates.

Desired product <sup>a)</sup>	Construct	Substrate	Maximal initial activity <sup>e)</sup> [ $\text{U}_{\text{gCDW}}^{-1}$ ]
$\epsilon$ -Caprolactone	pSEVA_CL_1	Cyclohexane <sup>b)</sup>	37.3 $\pm$ 0.4
		Cyclohexanol <sup>c)</sup>	38.9 $\pm$ 0.5
		Cyclohexanone <sup>d)</sup>	44.1 $\pm$ 1.0
	pSEVA_CL_2	Cyclohexane <sup>b)</sup>	43.4 $\pm$ 1.9
		Cyclohexanol <sup>c)</sup>	76.0 $\pm$ 8.3
		Cyclohexanone <sup>d)</sup>	84.1 $\pm$ 2.2
6-hydroxyhexanoic acid	pSEVA_6HA_1	Cyclohexane <sup>b)</sup>	38.0 $\pm$ 0.6
		Cyclohexanol <sup>c)</sup>	34.4 $\pm$ 1.6
		Cyclohexanone <sup>d)</sup>	46.1 $\pm$ 2.3
	pSEVA_6HA_2	$\epsilon$ -Caprolactone <sup>d)</sup>	543.8 $\pm$ 21.0
		Cyclohexane <sup>b)</sup>	44.8 $\pm$ 0.2
		Cyclohexanol <sup>c)</sup>	82.7 $\pm$ 3.5
		Cyclohexanone <sup>d)</sup>	82.9 $\pm$ 0.8
		$\epsilon$ -Caprolactone <sup>d)</sup>	836.6 $\pm$ 16.5

<sup>a)</sup> Bioconversions with  $0.5 \text{ g}_{\text{CDW}} \text{ L}^{-1}$  of cells in Erlenmeyer flasks, 10 min assay time;

<sup>b)</sup> Addition of 9.2 mM cyclohexane (180  $\mu\text{M}$  in aqueous phase), activities correspond to the first 10 min in the experiments shown in Figures 3C,E and 4C, Figure S3C, Supporting Information; <sup>c)</sup> Maximal activity obtained by testing different cyclohexanol concentrations (see also Figure 3F); <sup>d)</sup> Addition of 5 mM substrate; <sup>e)</sup> Average values for the products formed (6 HA summed up with  $\epsilon$ -CL if applicable) including standard deviations of two independent biological replicates. The average experimental errors overall measurements for the whole-cell activities with cyclohexane, cyclohexanol, cyclohexanone, and  $\epsilon$ -CL as substrates are 1.8%, 5.3%, 2.7%, and 2.9%, respectively.

in growth rate and active Cyp content were not observed with pSEVA\_CL\_2 (Table S4, Supporting Information). These results indicate that higher CDH and CHMO levels are crucial to prevent the accumulation of cascade intermediates, especially of the CHMO inhibitor cyclohexanol, and thus to drive the cascade towards  $\epsilon$ -CL formation. Furthermore, the two-operon approach reduced the metabolic burden as indicated by the growth rate of the respective strain compared to the one-operon approach.

To further characterize cyclohexanol conversion efficiencies, different cyclohexanol concentrations were added to *P. taiwanensis* VLB120 cells containing pSEVA\_CL\_1 or pSEVA\_CL\_2 (Figure 3F). With pSEVA\_CL\_1, increasing cyclohexanol led to a decrease in the initial specific  $\epsilon$ -CL formation rate and the accumulation of cyclohexanone in the culture (Figure 3F). This correlated with CHMO inhibition and only 15% of the produced cyclohexanone were converted to  $\epsilon$ -CL when 1 mM of cyclohexanol was added as substrate. For a similar cyclohexanol amount (1 mM), the elevated CDH and CHMO levels in cells carrying the pSEVA\_CL\_2 construct resulted in a stable activity of the overall cascade, giving rise to higher cyclohexanol and, subsequently, cyclohexanone conversion with 35% being converted to  $\epsilon$ -CL (Figure 3F). Cyclohexanone accumulation was only observed for initial cyclohexanol concentrations  $\geq 0.4$  mM.

In conclusion, both tested strains exhibited decent specific whole-cell activities for the entire cascade. The main difference consisted in the production of small amounts of cyclohexanol

with pSEVA\_CL\_1. Due to CHMO inhibition and CDH kinetics, cyclohexanol was found to potentially disrupt the cascade in a self-enforcing manner. However, the high CDH and CHMO expression levels in *P. taiwanensis* VLB 120 (pSEVA\_CL\_2) efficiently prevented cyclohexanol accumulation. Furthermore, the two-operon approach involved a lower metabolic burden, auguring for stable biocatalytic activities.

### 2.3. Construction and Characterization of a 6HA Producing Strain

Whereas *P. taiwanensis* VLB 120 (pSEVA\_CL\_2) showed promising properties regarding cascade activity and stability, the presence of host-intrinsic hydrolases still led to a product mix consisting of  $\epsilon$ -CL and 6HA (Figure 3C,E). An industrial production process always relies on an efficient DSP, which in turn demands the avoidance of excessive byproduct accumulation. One possibility to prevent  $\epsilon$ -CL hydrolysis is the knockout of the respective hydrolase(s) in the host strain *P. taiwanensis* VLB120. However, its genome encodes over 100 enzymes with hydrolytic activity. Consequently, identification and inactivation of the responsible enzyme(s) would be very challenging, especially as several enzymes may be involved in this reaction, possibly even in a cooperative manner. The more promising alternative is to focus on 6HA as the only reaction product, which can also serve as a monomer to produce PCL.<sup>[18]</sup> Furthermore, 6HA is significantly less toxic to the cells as compared to  $\epsilon$ -CL (Figure 4D).

Whereas concentrations of up to 20 mM 6HA did barely affect the growth, 20 mM  $\epsilon$ -CL reduced the growth rate by  $\approx 50\%$ . For 6HA, a half-maximal growth rate was observed at  $\approx 100$  mM, which in turn led to complete growth inhibition in the case of  $\epsilon$ -CL.

To push the reaction towards 6HA, an additional lactonase was included in the pSEVA\_CL\_2 construct, originating from the cyclohexane degradation pathway of *Acidovorax* sp. CHX100 (see Section S5, Supporting Information, for the nucleotide sequence), resulting in pSEVA\_6HA\_2 (Figure 4A). This construct indeed enabled the exclusive production of 6HA to a concentration of  $1.74 \pm 0.17$  mM after 2 h of reaction (Figure 4C). The high initial specific activity of  $52.5 \pm 5.0 \text{ U}_{\text{gCDW}}^{-1}$  (in the first 5 min) dropped by 50% within 30 min and then remained stable. Lactonase gene expression led to a detectable lactonase band and was found to enable a high  $\epsilon$ -CL hydrolysis activity of  $836.6 \pm 16.5 \text{ U}_{\text{gCDW}}^{-1}$ , but did not influence Cyp, CDH, or CHMO levels and activities nor the active Cyp concentration (Figure 4B, Table 2 and Table S4, Supporting Information). The growth rate during expression ( $0.37 \pm 0.01 \text{ h}^{-1}$ ) also remained comparable to that of the empty vector control (Table S4, Supporting Information). A construct pSEVA\_6HA\_1 with all genes under the control of only one promoter also was established. It again led to less favorable properties such as slower growth, (transient) cyclohexanol accumulation, and lower initial activities (Table 2 and Table S4, Figure S3, Supporting Information), confirming the superiority of the two-promoter approach.

Finally, the two strains containing two-promoter constructs for the 3- or 4-step pathway were tested for the conversion of 5 mM cyclohexane on a 40 mL scale. Both strains enabled complete conversion within 3 h with the 4-step pathway being superior

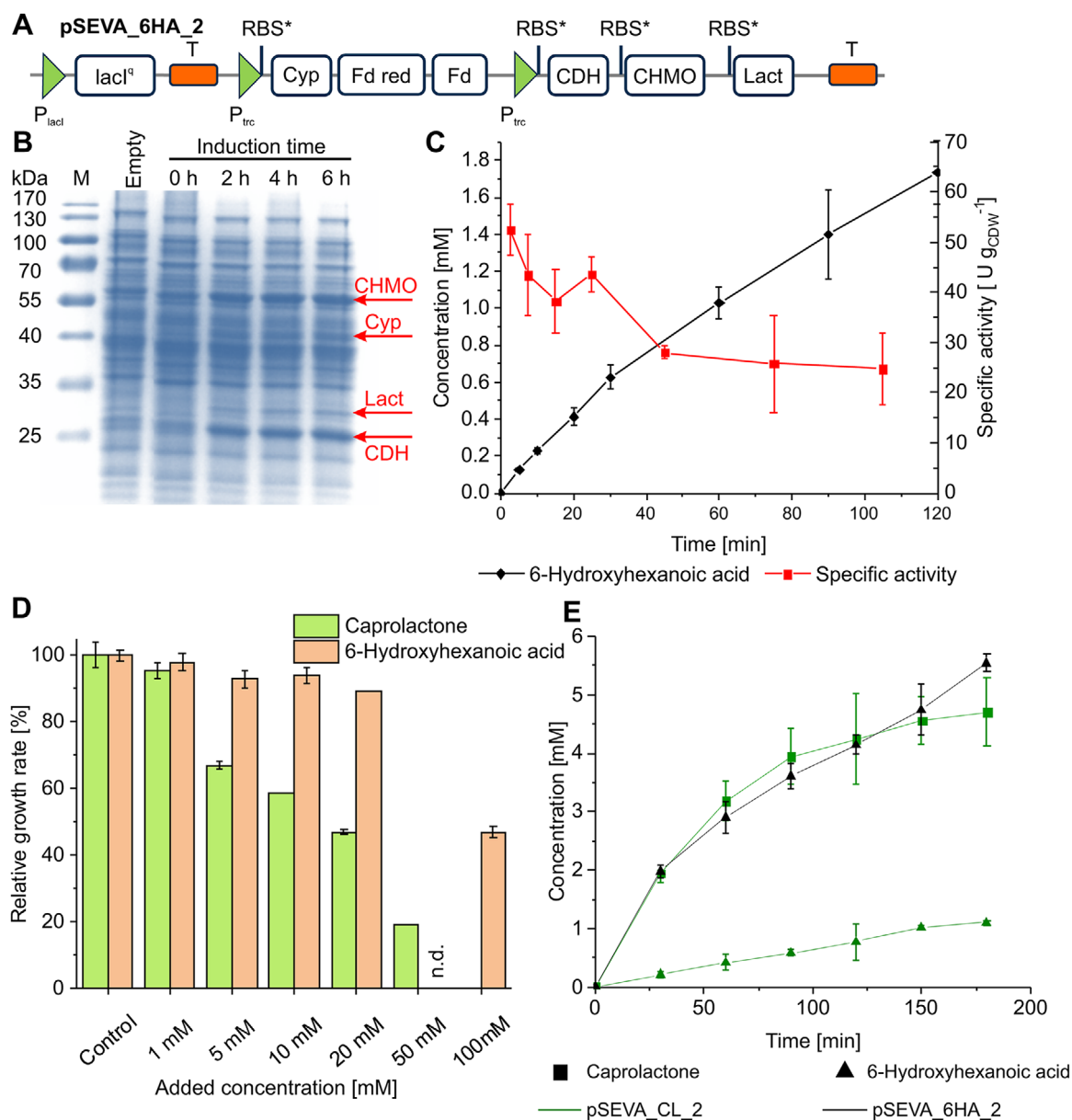


**Figure 4.** Construction and characterization of *P. taiwanensis* VLB120 (pSEVA\_6HA\_2). A) Graphical representation of expression units in the plasmid pSEVA\_6HA\_2. B) SDS-PAGE analysis showing bands for Cyp (47.4 kDa), CDH (26.5 kDa), CHMO (58.8 kDa), and Lact (32.2 kDa) after different times of induction and compared with cells containing an empty vector. C) Time courses for the 6HA concentration and the whole-cell activity for 6HA formation in resting cell bioconversions as described in the legend of Figure 3. D) Relative growth rate of *P. taiwanensis* VLB120 in the presence of varying amounts of  $\epsilon$ -CL (green) or 6HA (orange) (a growth rate of  $0.47 \pm 0.01 \text{ h}^{-1}$  represents 100%). E) Conversion of 5 mM cyclohexane by *P. taiwanensis* VLB120 containing pSEVA\_CL\_2 or pSEVA\_6HA\_2. Resting cell bioconversions were performed in 40 mL KPi-g buffer containing  $1.05 \text{ g}_{\text{CDW}} \text{ L}^{-1}$  of cells in closed 250 mL screw-capped and baffled shake flasks. Graphs represent average values and standard deviations of two independent biological replicates. The average experimental errors over all measurements for  $\epsilon$ -CL concentrations, 6HA concentrations, whole-cell activities, and relative growth rates are 11.7%, 11.6%, 17.7%, and 1.9%, respectively.

regarding selectivity (100% for 6HA) than the 3-step pathway (80% towards  $\epsilon$ -CL) (Figure 4E). The initial specific activities of *P. taiwanensis* VLB120 harboring pSEVA\_CL\_2 or pSEVA\_6HA\_2 were high and in the same range ( $68.4 \pm 6.5$  or  $61.5 \pm 3.2 \text{ U}_{\text{g}_{\text{CDW}}^{-1}}$ , respectively). The activities showed a decrease over time, most probably due to the decreasing substrate availability, giving overall activities of  $30.8 \pm 5.8$  and  $33.2 \pm 0.7 \text{ U}_{\text{g}_{\text{CDW}}^{-1}}$ ,

respectively. Consequently, complete conversion of cyclohexane to 6HA via the in vivo 4-step cascade was found to be feasible and efficient without serious impediments by enzyme kinetics or biocatalyst instability.

Overall, *P. taiwanensis* VLB120 (pSEVA\_6HA\_2) can be considered a highly promising production strain for the conversion of cyclohexane to the PCL monomer 6HA.

### 3. Discussion

The development of eco-efficient sustainable production processes has been one of the major objectives of biotechnology research over the last decade. Such promise is based on the inherent biodegradability, selectivity, and specificity of biocatalysts.<sup>[32]</sup> Biotechnological solutions already have replaced chemical processes for the production of biosurfactants, amino acids, and even complex heterocyclic compounds.<sup>[33,34]</sup> The research presented in this study aimed to set a basis for the replacement of the highly polluting UCC process<sup>[19]</sup> by developing a direct route from cyclohexane to the PCL monomer 6HA enabling full conversion.

#### 3.1. Efficient Design of In Vivo Cascades

Various factors including functional expression and stability of the cascade enzymes, toxicity of the reactants and products, equilibrium thermodynamics, cofactor regeneration, and byproduct formation should be considered for the design and construction of efficient whole-cell biotransformation pathways.<sup>[4]</sup> The final production strain developed in this study for the conversion of cyclohexane to 6HA enabled a decent activity in the 50–60  $\text{Ug}_{\text{CDW}}^{-1}$  range for the whole cascade without side product formation. It has been shown that detailed analyses of enzyme kinetics and respective reaction engineering for a 3-step cascade could efficiently enhance the conversion of several unsaturated cyclic alcohols to the corresponding lactones in vitro.<sup>[2,35]</sup> Scherkus et al. analyzed the kinetic parameters of an alcohol dehydrogenase and a CHMO for the production of 6HA from cyclohexanol with isolated enzymes.<sup>[36]</sup> Similarly to the CDH investigated in our study, the  $K_M$  value of the alcohol dehydrogenase was significantly lower for the reverse reaction, and CHMO was severely inhibited by cyclohexanol. Establishing a kinetic model enabled the setup of an efficient fed-batch process. Increasing the expression and stabilizing the activity of Baeyer–Villiger monooxygenases also led to higher 9-hydroxynonanoic acid and C11 nylon monomer concentrations in 4- and 5-step catalytic cascades, respectively.<sup>[7,16]</sup>

Whereas the balancing of enzyme ratios in vitro is a rather straight-forward approach,<sup>[2]</sup> in case of whole-cell biocatalysis, this requires fine-tuning of expression levels which, furthermore, should not drive the demand of resources beyond cellular capacities.<sup>[11]</sup> One possibility is the use of different plasmids to adjust the gene copy number,<sup>[37]</sup> which also can influence plasmid stability.<sup>[7]</sup> In our previous study, we varied copy number, RBS, and regulatory systems for Cyp gene expression.<sup>[24]</sup> The best system in terms of activity, stability, and metabolic burden was used in this study to engineer multi-gene operons. The so-called metabolic burden arises from the change in demand for (biomass) building blocks and energy (ATP, NAD(P)H) related to plasmid maintenance, gene expression, and enzyme activity and is system- and condition-dependent.<sup>[38,39]</sup> Our results indicate a gradual decrease in the growth rate with increasing operon size (Table S4, Supporting Information). For the cascade investigated, the two-operon- compared to the one-operon approach not only enabled faster growth indicating low metabolic burden, but also led to higher CDH and CHMO expression levels and cascade activities. The relation between gene organization and gene

expression is poorly understood. It has been found for *E. coli* that gene expression increases with the length of the operon resulting in more co-transcriptional translation.<sup>[40]</sup> Increased translation can result in metabolic burden and misfolded or otherwise non-functional proteins, which was found for the Cyp in our previous study.<sup>[24]</sup> Also without a terminator after the Cyp genes (Figure 3A), RNA polymerase dissociation may have been promoted by the transcription initiation machinery occupying the downstream promoter region and thereby opening up the DNA.<sup>[39]</sup> Thus, mRNAs with shorter average length can be expected for the two-promoter- as compared to the one-promoter constructs. Shorter mRNAs, in turn, have been found to show increased stability in *E. coli* cells<sup>[41]</sup> and to recruit fewer ribosomes,<sup>[40]</sup> thus decreasing the metabolic burden. In general, the metabolic burden increases with gene and operon size. It is further enhanced by some antibiotics such as kanamycin and thus tends to be high for plasmid-based expression, especially when antibiotic resistance genes are used as selection markers.<sup>[42]</sup> The two-operon approach may have profited from shorter but more stable mRNAs and can be considered suitable for efficient expression of the designed pathways in *P. taiwanensis* VLB120. For further optimization, metabolic modeling of cascades and combinatorial pathway engineering taking into account metabolic burden effects may become interesting, although these approaches still suffer from incomplete knowledge.<sup>[43–45]</sup>

#### 3.2. Production of PCL Precursors

The biocatalytic production of PCL or its precursors has been heavily investigated over the last years (Table 3). Approaches based on isolated enzymes,<sup>[21,46–50]</sup> as well as whole cells,<sup>[23,37,51–53]</sup> have successfully been established. However, most of these approaches relied on cyclohexanol as a substrate,<sup>[37,47–53]</sup> which needs to be synthesized from cyclohexane employing an ecologically critical process.<sup>[54]</sup> Additionally, inhibition of CHMO by cyclohexanol or substrate inhibition necessitated the development of suitable reaction concepts, for example, two-liquid phase<sup>[46]</sup> or fed-batch systems.<sup>[49]</sup> The highest productivity of  $1.87 \text{ g L}^{-1} \text{ h}^{-1}$  was obtained with isolated enzymes by employing an appropriate feeding strategy for the complete conversion of 283 mM cyclohexanol to 6HA<sup>[49]</sup> (Table 3). The CHMO from *Acinetobacter* heterologously expressed in *E. coli* showed the highest TTN with almost 70 000  $\text{mol}_{\epsilon\text{-CL}} \text{ mol}_{\text{CHMO}}^{-1}$ .<sup>[52]</sup> In general, whole-cell approaches show lower yields on biocatalyst, as target enzymes constitute only about 1–10% (w/w) of cells, but avoid the enormous effort to purify the enzymes. The highest  $\epsilon\text{-CL}$  yield of  $1.2 \text{ g}_{\epsilon\text{-CL}} \text{ g}_{\text{biocatalyst}}^{-1}$  with a high initial activity of  $15 \text{ Ug}_{\text{CDW}}^{-1}$  was observed by M enil et al. in complex medium.<sup>[37]</sup>

Compared to cyclohexanol, cyclohexane is an even more challenging substrate due to its high volatility and toxicity. In comparison to solvent-sensitive *E. coli* employed to convert cyclohexanol to 6HA,<sup>[53]</sup> we obtained a tenfold higher specific whole-cell activity and a similar yield on biocatalyst (Table 3). *P. taiwanensis* VLB120 is known to tolerate low-logP solvents and can, therefore, be considered suitable for the biotransformation of the more toxic substrate cyclohexane.<sup>[55–57]</sup>

**Table 3.** Comparison of biocatalytic PCL precursor synthesis approaches.

Substrate	Product	Biocatalyst <sup>a)</sup>	Time [h]	Cell concentration [g <sub>CDW</sub> L <sup>-1</sup> ]	Conversion [%]	Productivity [g L <sup>-1</sup> h <sup>-1</sup> ]	Maximal concentration [mM]	Yield [g <sub>Product</sub> g <sub>Biocatalyst</sub> <sup>-1</sup> ]	Total turnover number [mol <sub>Product</sub> mol <sub>Biocatalyst</sub> <sup>-1</sup> ]	Specific activity [U mg <sub>protein</sub> <sup>-1</sup> or [U g <sub>CDW</sub> <sup>-1</sup> ]	Reference
Cyclohexanone	<i>ε</i> -CL	E	48	n.a. <sup>b)</sup>	58.2 (48 h)	0.19 (24 h)	53	12	6000	0.05 (24h)	[46]
					42.9 (24 h)	0.13 (48 h)					
Cyclohexanol	<i>ε</i> -CL	E <sup>d)</sup>	24	n.a.	>99	0.95	200	14.9	20 000	0.09	[47]
		C	16	10	100 (16 h)	0.14 (16 h)	20	0.23	n.c. <sup>c)</sup>	13.3 (2h)	[51]
		C	20	35	80 (2 h)	0.91 (2 h)	185	0.6	69 167 <sup>g)</sup> , 38606 <sup>f)</sup>	2.1 (16h)	[52]
			24	n.a.	99.6	1.1	185	0.6	69 167 <sup>g)</sup> , 38606 <sup>f)</sup>	7	[52]
	6HA	E	24	n.a.	94	0.27	56.4	1.29 <sup>g)</sup>	690 <sup>g)</sup>	0.008 <sup>g)</sup>	[48]
		C	8	1.5	100	0.244	16	1.2	n.c.	15 (initial)	[37]
		C	70	30	84	0.8	168	0.67	n.c.	3.5	[53]
		PCL	E	20	n.a.	>99	1.87	283	n.c.	n.c.	n.c.
Cyclohexane	<i>ε</i> -CL	E	48	n.a.	99	n.c.	n.c.	n.c.	n.c.	n.c.	[50]
		E	6	n.a.	2.8	0.1	5.2	0.85 <sup>e)</sup>	822 <sup>e)</sup>	0.02 <sup>e)</sup>	[21]
		C <sup>i)</sup>	24	100	<1	0.02	0.4	0.002	n.c.	0.003 (24 h)	[22]
		C	5	6.8	10	0.46	20.1 <sup>h)</sup>	0.43	45 585 <sup>e)</sup>	12.2 (overall) 18.0 (initial)	[23]
	6HA	C	2	3.7	100	0.30	5.0 <sup>h)</sup>	0.16	16 894 <sup>e)</sup>	11.3 (overall) 22.7 (initial)	[23]
		C	3	1.05	100	0.23	5.0 <sup>h)</sup>	0.66	59 032 <sup>e)</sup>	30.8 (overall) 68.4 (initial)	This study
		C	3	1.05	100	0.24	5.5	0.68	47 900 <sup>e)</sup>	28.7 (overall) 61.5 (initial)	This study
		C	3	1.05	100	0.24	5.5	0.68	47 900 <sup>e)</sup>	28.7 (overall) 61.5 (initial)	This study

<sup>a)</sup>E = isolated enzymes, C = whole cells; <sup>b)</sup>Not applicable; <sup>c)</sup>Not calculable; <sup>d)</sup>Fusion enzyme of ADH and CHMO; <sup>e)</sup>Calculated referring to Cyp; <sup>f)</sup>Calculated referring to ADH; <sup>g)</sup>Calculated referring to CHMO; <sup>h)</sup>Total product concentration including the byproduct 6HA; <sup>i)</sup>a photocatalyst oxidizing cyclohexane to cyclohexanone combined with CHMO-containing *E. coli*.

Possible prolongation of the reaction with an appropriate substrate feeding and the application of a high-cell density setup hold big potential to further improve the product titer and the volumetric productivity.

This study, for the first time, demonstrates a whole-cell approach directly converting cyclohexane to the PCL precursor 6HA. The biotransformation to *ε*-CL presented by Karande et al.<sup>[23]</sup> could be optimized by enhancing the conversion, yield on biocatalyst, TTN, and specific activity (Table 3). In comparison with this strain, the two strains developed in this study (Table 3, entries 13–15) showed a 3-times higher specific whole-cell activity allowing for lower cell concentrations to achieve a full conversion of 5 mM cyclohexane and thereby higher yields on biocatalyst and TTN. The chemo-biocatalytic approach presented by Li et al. constitutes a proof-of-concept and suffered from low conversion and very low activities.<sup>[22]</sup> The use of isolated enzymes to convert cyclohexane to *ε*-CL suffered from low conversion and TTN, which can be attributed to mass transfer limitations or inherent instability of P450 monooxygenases.<sup>[11,21]</sup> The cellular environment allows for more stable catalytic activities with superior productivities. As a result, the main limitation for future process development is considered not to lie necessarily in the catalyst itself, but rather in the reaction engineering with cyclohexane feeding/cyclohexane mass transfer and cell toxification as critical points. This may be solved by cyclohexane feeding

potentially via the gas phase. The achieved increase in whole-cell activity and conversion, however, can be considered a huge step forward towards the establishment of an economically viable process.<sup>[58]</sup>

## 4. Conclusion

In this study, we developed the strain *P. taiwanensis* VLB120 (pSEVA\_6HA\_2) that expresses 6 genes encoding 4 enzymes able to fully convert 5 mM cyclohexane to the PCL monomer 6HA. Accumulation of intermediates and byproducts was successfully prevented, and a high cascade activity was achieved. Our study demonstrated that a balanced expression of pathway encoding genes guided by enzyme characteristics (kinetics, inhibition) allowed for streamlined production of *ε*-CL and, especially, 6HA. The constructed orthogonal pathway/cascade also can serve as a template to be amended by additional enzymes to synthesize nylon monomers such as adipic acid and 6-aminohexanoic acid. This in combination with their solvent tolerance<sup>[56,59,60]</sup> and versatility regarding reactor setups—including biofilm approaches<sup>[61–63]</sup>—qualify VLB120 strains harboring pSEVA\_CL\_2 or pSEVA\_6HA\_2 as a promising platform organism for greener polymer production routes.

## 5. Experimental Section

**Bacterial Strains, Plasmids, Media, and Chemicals:** Microbial strains and plasmids used in this work are listed in Table S1, Supporting Information. Cells were grown in lysogeny broth (LB) medium<sup>[64]</sup> or M9\* medium<sup>[65]</sup> with a pH of 7.2 supplemented with 0.5% (w/v) glucose as sole carbon and energy source. Kanamycin (50 µg mL<sup>-1</sup>) was applied for selection when necessary. Unless stated otherwise, all chemicals were purchased from Sigma-Aldrich (Steinheim, Germany) or Carl Roth (Karlsruhe, Germany) in the highest purity available and used without further purification. 6HA was acquired from abcr (Karlsruhe, Germany). Molecular biology methods are explained in detail in Section S1, Supporting Information.

**Strain Construction:** The strains and plasmids used in this study are listed in Table S1, Supporting Information. The plasmids pSEVA244\_T and pSEVA\_Cyp constituted the basis for the constructs engineered in this study and originate from Schäfer et al.<sup>[24]</sup> The primers used for such engineering are listed in Table S2, Supporting Information.

For the construction of plasmids pSEVA\_CDH and pSEVA\_Cyp\_CDH, the CDH gene was amplified from pCapro<sup>[23]</sup> using the primers PLS013 and PLS014. The resulting purified fragment was fused either to KpnI-digested pSEVA244\_T or pSEVA\_Cyp by Gibson Assembly<sup>[66]</sup> to yield pSEVA\_CDH or pSEVA\_Cyp\_CDH, respectively.

Plasmids pSEVA\_CHMO and pSEVA\_CL\_1 were assembled accordingly. The CHMO gene was amplified from pCapro with primers PLS015A and PLS016 or PLS015B and PLS016. The forward primer was different for the two constructs due to the adjustment of the 5' region (overhang to the plasmid backbone). The resulting purified fragments were fused via Gibson Assembly either to XbaI-digested pSEVA244\_T or pSEVA\_Cyp\_CDH to yield pSEVA\_CHMO or pSEVA\_CL\_1, respectively.

*Acidovorax* sp. CHX100 was cultivated for 4 days in nutrient broth (NB) medium<sup>[64]</sup> for DNA isolation performed with the peqGOLD Bacterial DNA Mini Kit (PiqLab, Erlangen, Germany). The lactonase gene was amplified with the primers PLS017B and PLS018, and Gibson Assembly of the resulting fragment and HindIII-digested pSEVA\_CL\_1 gave rise to pSEVA\_6HA\_1.

The  $P_{trc}$  promoter was amplified from pSEVA244<sup>[67]</sup> with primers PLS021 and PLS022. It was fused to EcoRI-digested pSEVA\_CL\_1 or pSEVA\_6HA\_1 via Gibson Assembly to yield pSEVA\_CL\_2 and pSEVA\_6HA\_2.

**Growth of Bacterial Cultures:** Cultivations were carried out at 30 °C and 200 rpm in a Multitron shaker (Infors, Bottmingen, Switzerland). Microorganisms were cultivated in an LB pre-culture for ≈20 h, from which an M9\* pre-culture (1% v/v) was inoculated and incubated for another 12–16 h. From this culture, an M9\* main culture was inoculated to a starting OD<sub>450</sub> of 0.2. Heterologous gene expression was induced with 1 mM isopropyl β-d-1-thiogalactopyranoside (IPTG) when the cultures reached an OD<sub>450</sub> of ≈0.5. Incubation was continued for another 4–6 h, and cells were harvested for SDS-PAGE analyses, CO spectra analyses, and/or activity or toxicity assays (see below). One OD<sub>450</sub> unit corresponds to a biomass concentration of 0.186 g<sub>CDW</sub> (grams of cell dry weight) L<sup>-1</sup>.<sup>[68]</sup> CO difference spectra (see Section S2, Supporting Information, for details) were recorded to determine the active Cyp concentrations.

**Toxicity Assay:** *P. taiwanensis* VLB120 was cultivated as described above but without induction. Different concentrations of ε-CL or 6HA were added 2 h after inoculation, and the growth rate was determined from this time point on for at least 7 h.

**Resting Cell Bioconversions:** The cells were cultivated as described above, harvested by centrifugation (10 min, 5000 × g, RT), and resuspended to a specific cell concentration in 100 mM potassium phosphate buffer (pH 7.4) supplemented with 1% (w/v) glucose (KPi-g buffer). The cells were transferred to baffled Erlenmeyer flasks (100 mL) or microcentrifuge tubes (2 mL) with liquid volumes of 10 or 1 mL and biomass concentrations of 0.5 or 0.25 g<sub>CDW</sub> L<sup>-1</sup>, respectively, equilibrated at 30 °C for 10 min (flasks in a water bath at 250 rpm; microcentrifuge tubes in a ThermoMixer C (Eppendorf, Hamburg) at 2000 rpm), then provided with the substrate (as stated in the Table and Figure legends). Biotransformations were stopped by the addition of 0.5 mL ice-cold diethyl ether containing 0.2 mM n-decane as an internal standard to 1 mL sample. After 2 min

extraction by vortexing and short centrifugation, the organic phase was dried over water-free Na<sub>2</sub>SO<sub>4</sub> before it was transferred to a GC vial for analysis. The aqueous phase was removed with a syringe from the microcentrifuge tube and stored at –20 °C for HPLC analysis. The activity is given in U<sub>g<sub>CDW</sub></sub><sup>-1</sup>, where 1 U corresponds to 1 µmol product formed within 1 min reaction time.

For the conversion of 5 mM cyclohexane (Figure 4E), 250 mL screw-capped and baffled Erlenmeyer flasks were used with a liquid volume of 40 mL and a biomass concentration of 1.05 g<sub>CDW</sub> L<sup>-1</sup>. The caps contained two septa, a Teflon septum facing the inner side of the flask, and a silicon septum facing outwards. Pure cyclohexane (21.8 µL) was added to start the reaction and the flasks were tightly closed. For each sampling point, 1.5 mL liquid volume was removed through the septa using a syringe. From this sample, 1 mL was extracted with diethyl ether for GC analysis as described above and 0.5 mL was used for HPLC analysis.

For details on analytical methods refer to Section S3, Supporting Information.

## Supporting Information

Supporting Information is available from the Wiley Online Library or from the author.

## Acknowledgements

The authors are grateful to Andreas Schmid for helpful discussions. The authors acknowledge the use of the facilities of the Centre for Biocatalysis (MiKat) at the Helmholtz Centre for Environmental Research, which is supported by European Regional Development Funds (EFRE, Europe funds Saxony) and the Helmholtz Association. L.S. was funded from the ERA-IB- Project PolyBugs ID: 16006 and the Sächsisches Ministerium für Wissenschaft und Kunst (SMWK) Project ID: 100318259.

Open access funding enabled and organized by Projekt DEAL.

## Conflict of Interest

The authors declare no conflict of interest.

## Keywords

biocatalysis, genetic engineering, in vivo cascade, polycaprolactone, *Pseudomonas*

Received: May 22, 2020  
Revised: July 13, 2020  
Published online: September 6, 2020

- [1] N. Oberleitner, C. Peters, J. Muschiol, M. Kadow, S. Saß, T. Bayer, P. Schaaf, N. Iqbal, F. Rudroff, M. D. Mihovilovic, *ChemCatChem* **2013**, *5*, 3524.
- [2] J. Muschiol, C. Peters, N. Oberleitner, M. D. Mihovilovic, U. T. Bornscheuer, F. Rudroff, *Chem. Commun.* **2015**, *51*, 5798.
- [3] N. Ladkau, A. Schmid, B. Bühler, *Curr. Opin. Biotechnol.* **2014**, *30*, 178.
- [4] J.-W. Song, J.-H. Seo, D.-K. Oh, U. T. Bornscheuer, J.-B. Park, *Catal. Sci. Technol.* **2020**, *10*, 46.
- [5] H. J. Cha, S. Y. Hwang, D. S. Lee, A. R. Kumar, Y. U. Kwon, M. Voß, E. Schuiten, U. T. Bornscheuer, F. Hollmann, D. K. Oh, J. B. Park, *Angew. Chem., Int. Ed.* **2020**, *132*, 7090.

- [6] W. Szymanski, C. P. Postema, C. Tarabiono, F. Berthiol, L. Campbell-Verduyn, S. de Wildeman, J. G. de Vries, B. L. Feringa, D. B. Janssen, *Adv. Synth. Catal.* **2010**, 352, 2111.
- [7] E.-J. Seo, C. W. Kang, J.-M. Woo, S. Jang, Y. J. Yeon, G. Y. Jung, J.-B. Park, *Metab. Eng.* **2019**, 54, 137.
- [8] W. Zhang, J.-H. Lee, S. H. Younes, F. Tonin, P.-L. Hagedoorn, H. Pichler, Y. Baeg, J.-B. Park, R. Kourist, F. Hollmann, *Nat. Commun.* **2020**, 11, 2258.
- [9] J. H. Schrittwieser, S. Velikogne, M. I. Hall, W. Kroutil, *Chem. Rev.* **2018**, 118, 270.
- [10] T. Bayer, S. Milker, T. Wiesinger, F. Rudroff, M. D. Mihovilovic, *Adv. Synth. Catal.* **2015**, 357, 1587.
- [11] M. Kadisch, C. Willrodt, M. Hillen, B. Bühler, A. Schmid, *Biotechnol. J.* **2017**, 12, 1600170.
- [12] N. Ladkau, M. Assmann, M. Schrewe, M. K. Julsing, A. Schmid, B. Bühler, *Metab. Eng.* **2016**, 36, 1.
- [13] M. Schrewe, M. K. Julsing, B. Bühler, A. Schmid, *Chem. Soc. Rev.* **2013**, 42, 6346.
- [14] E.-Y. Jeon, J.-W. Song, H.-J. Cha, S.-M. Lee, J. Lee, J.-B. Park, *J. Biotechnol.* **2018**, 281, 161.
- [15] M. Schrewe, M. K. Julsing, K. Lange, E. Czarnotta, A. Schmid, B. Bühler, *Biotechnol. Bioeng.* **2014**, 111, 1820.
- [16] T.-H. Kim, S.-H. Kang, J.-E. Han, E.-J. Seo, E.-Y. Jeon, G.-E. Choi, J.-B. Park, D.-K. Oh, *ACS Catal.* **2020**, 10, 4871.
- [17] C. K. Williams, *Chem. Soc. Rev.* **2007**, 36, 1573.
- [18] M. Labet, W. Thielemans, *Chem. Soc. Rev.* **2009**, 38, 3484.
- [19] K. Weissermel, H.-J. Arpe, in *Industrial Organic Chemistry* (Eds: K. Weissermel, H.-J. Arpe), WILEY-VCH Verlag GmbH & Co. KGaA, Weinheim, Germany **2003**, p. 239.
- [20] U. Schuchardt, D. Cardoso, R. Sercheli, R. Pereira, R. S. da Cruz, M. C. Guerreiro, D. Mandelli, E. V. Spinacé, E. L. Pires, *Appl. Catal., A* **2001**, 211, 1.
- [21] A. Penneç, F. Hollmann, M. S. Smit, D. J. Opperman, *ChemCatChem* **2015**, 7, 236.
- [22] P. Li, Y. Ma, Y. Li, X. Zhang, Y. Wang, *ChemBioChem* **2020**, 21, 1852.
- [23] R. Karande, D. Salamanca, A. Schmid, K. Buehler, *Biotechnol. Bioeng.* **2018**, 115, 312.
- [24] L. Schäfer, R. Karande, B. Bühler, *Front. Bioeng. Biotechnol.* **2020**, 8, 140.
- [25] D. Salamanca, R. Karande, A. Schmid, D. Dobsław, *Appl. Microbiol. Biotechnol.* **2015**, 99, 6889.
- [26] V. Alphand, G. Carrea, R. Wohlgemuth, R. Furstoss, J. M. Woodley, *Trends Biotechnol.* **2003**, 21, 318.
- [27] M. A. Delgove, M. T. Elford, K. V. Bernaerts, S. M. De Wildeman, *J. Chem. Technol. Biotechnol.* **2018**, 93, 2131.
- [28] B. Bühler, B. Witholt, B. Hauer, A. Schmid, *Appl. Environ. Microbiol.* **2002**, 68, 560.
- [29] M. L. Mavrouniotis, *Biotechnol. Bioeng.* **1990**, 36, 1070.
- [30] M. R. Leonardo, Y. Dailly, D. P. Clark, *J. Bacteriol.* **1996**, 178, 6013.
- [31] N. A. Donoghue, D. B. Norris, P. W. Trudgill, *Eur. J. Biochem.* **1976**, 63, 175.
- [32] E. Ricca, B. Brucher, J. H. Schrittwieser, *Adv. Synth. Catal.* **2011**, 353, 2239.
- [33] A. Schmid, J. Dordick, B. Hauer, A. Kiener, M. Wubbolts, B. Witholt, *Nature* **2001**, 409, 258.
- [34] C. Gehring, M. Wessel, S. Schaffer, O. Thum, *ChemistryOpen* **2016**, 5, 513.
- [35] N. Oberleitner, C. Peters, F. Rudroff, U. T. Bornscheuer, M. D. Mihovilovic, *J. Biotechnol.* **2014**, 192, 393.
- [36] C. Scherkus, S. Schmidt, U. T. Bornscheuer, H. Gröger, S. Kara, A. Liese, *Biotechnol. Bioeng.* **2017**, 114, 1215.
- [37] S. Ménil, J. I. Petit, E. Courvoisier-Dezord, A. Debard, V. Pellouin, T. Reignier, M. Sergent, V. Deyris, K. Duquesne, V. de Berardinis, *Biotechnol. Bioeng.* **2019**, 116, 2852.
- [38] H. Nojiri, *Curr. Opin. Biotechnol.* **2013**, 24, 423.
- [39] C. D. Smolke, J. D. Keasling, *Biotechnol. Bioeng.* **2002**, 78, 412.
- [40] H. N. Lim, Y. Lee, R. Hussein, *Proc. Natl. Acad. Sci. USA* **2011**, 108, 10626.
- [41] L. Feng, D.-K. Niu, *Biochem. Genet.* **2007**, 45, 131.
- [42] J. Mi, A. Sydow, F. Schempp, D. Becher, H. Schewe, J. Schrader, M. Buchhaupt, *J. Biotechnol.* **2016**, 231, 167.
- [43] G. Wu, Q. Yan, J. A. Jones, Y. J. Tang, S. S. Fong, M. A. Koffas, *Trends Biotechnol.* **2016**, 34, 652.
- [44] M. Jeschek, D. Gerngross, S. Panke, *Curr. Opin. Biotechnol.* **2017**, 47, 142.
- [45] M. Jeschek, D. Gerngross, S. Panke, *Nat. Commun.* **2016**, 7, 11163.
- [46] A. Bornadel, R. Hatti-Kaul, F. Hollmann, S. Kara, *Tetrahedron* **2016**, 72, 7222.
- [47] F. S. Aalbers, M. W. Fraaije, *Appl. Microbiol. Biotechnol.* **2017**, 101, 7557.
- [48] S. Staudt, U. T. Bornscheuer, U. Menyes, W. Hummel, H. Gröger, *Enzyme Microb. Technol.* **2013**, 53, 288.
- [49] C. Scherkus, S. Schmidt, U. T. Bornscheuer, H. Gröger, S. Kara, A. Liese, *ChemCatChem* **2016**, 8, 3446.
- [50] S. Schmidt, C. Scherkus, J. Muschiol, U. Menyes, T. Winkler, W. Hummel, H. Gröger, A. Liese, H.-G. Herz, U. T. Bornscheuer, *Angew. Chem.* **2015**, 54, 2784.
- [51] A. Kohl, V. Srinivasamurthy, D. Böttcher, J. Kabisch, U. T. Bornscheuer, *Enzyme Microb. Technol.* **2018**, 108, 53.
- [52] V. S. Srinivasamurthy, D. Böttcher, J. Engel, S. Kara, U. T. Bornscheuer, *Process Biochem.* **2020**, 88, 22.
- [53] V. S. Srinivasamurthy, D. Böttcher, U. T. Bornscheuer, *Z. Naturforsch., C: J. Biosci.* **2019**, 74, 71.
- [54] J. Fischer, T. Lange, R. Boehling, A. Rehfinger, E. Klemm, *Chem. Eng. Sci.* **2010**, 65, 4866.
- [55] J. Volmer, A. Schmid, B. Bühler, *Biotechnol. J.* **2017**, 12, 1600558.
- [56] J.-B. Park, B. Bühler, S. Panke, B. Witholt, A. Schmid, *Biotechnol. Bioeng.* **2007**, 98, 1219.
- [57] L. M. Blank, G. Ionidis, B. E. Ebert, B. Bühler, A. Schmid, *FEBS J.* **2008**, 275, 5173.
- [58] F. Rudroff, *Curr. Opin. Chem. Biol.* **2019**, 49, 84.
- [59] J. Volmer, C. Neumann, B. Bühler, A. Schmid, *Appl. Environ. Microbiol.* **2014**, 80, 6539.
- [60] J. Volmer, M. Lindmeyer, J. Seipp, A. Schmid, B. Bühler, *Biotechnol. Bioeng.* **2019**, 116, 1089.
- [61] A. Hoschek, I. Heuschkel, A. Schmid, B. Bühler, R. Karande, K. Buehler, *Bioresour. Technol.* **2019**, 282, 171.
- [62] B. Halan, R. Karande, K. Buehler, A. Schmid, *J. Flow Chem.* **2016**, 6, 39.
- [63] R. Karande, L. Debor, D. Salamanca, F. Bogdahn, K. H. Engesser, K. Buehler, A. Schmid, *Biotechnol. Bioeng.* **2016**, 113, 52.
- [64] J. Sambrook, D. W. Russell, *Molecular Cloning: A Laboratory Manual*, Cold Spring Harbor Laboratory Press, Cold Spring Harbor, NY **2001**.
- [65] S. Panke, A. Meyer, C. M. Huber, B. Witholt, M. G. Wubbolts, *Appl. Environ. Microbiol.* **1999**, 65, 2324.
- [66] D. G. Gibson, L. Young, R.-Y. Chuang, J. C. Venter, C. A. Hutchison, H. O. Smith, *Nat. Methods* **2009**, 6, 343.
- [67] E. Martínez-García, T. Aparicio, A. Goñi-Moreno, S. Fraile, V. de Lorenzo, *Nucleic Acids Res.* **2015**, 43, D1183.
- [68] B. Halan, A. Schmid, K. Buehler, *Biotechnol. Bioeng.* **2010**, 106, 516.



## Table of Contents

1	Molecular biology methods.....	1
2	CO difference spectra.....	3
3	Analytical methods.....	4
4	Determination of Gibbs free energy, equilibrium constant, and equilibrium concentrations for CDH reaction.....	5
5	Nucleotide sequence of lactonase gene from <i>Acidovorax</i> sp. CHX-100.....	7
6	Determination of growth rate and turnover number for Cyp.....	8
7	Construction and characterization of <i>P. taiwanensis</i> VLB120 (pSEVA_6HA_1).....	9
8	References.....	10

### 1 Molecular biology methods

The preparation of electrocompetent *Pseudomonas* cells was performed according to Choi *et al.* [1], and the vectors were introduced by electroporation (2500 V, Eppendorf Eporator®, Hamburg, Germany). DNA manipulation methods and agarose gel electrophoresis were performed as described by Sambrook and Russel [2]. Enzymes (Phusion High-Fidelity Polymerase, T5 exonuclease, *Taq* ligase, restriction enzymes, Fast Alkaline Phosphatase) and buffers were purchased from Thermo Scientific Molecular Biology (St. Leon-Rot, Germany) or New England Biolabs (Frankfurt/Main, Germany) and oligonucleotides from Eurofins Genomics (Ebersberg, Germany). Plasmids were isolated using the peqGOLD Plasmid Miniprep Kit I from peqLab (Erlangen, Germany) and purified via NucleoSpin Gel and PCR Clean-up from Macherey–Nagel (Düren, Germany) according to supplier protocols. The Gibson Master Mix was prepared according to Gibson *et al.* [3].

**Table S1:** Strains and plasmids used in this study.

	Characteristics	Reference
<b>Strains</b>		
<i>E. coli</i> DH5 $\alpha$	<i>supE44</i> $\Delta$ <i>lacU169</i> ( $\Phi$ 80 <i>lacZ</i> $\Delta$ M15) <i>hsdR17 recA1 endA1 gyrA96 thi-1 relA1</i>	[4]
<i>P. taiwanensis</i> VLB120	solvent tolerant, styrene degrading bacterium, isolated from forest soil	[5]
<b>Plasmids</b>		
pCapro	pCom10 derivative, pRO1600 and ColE1 ori, <i>alk</i> -regulatory system ( <i>alkS</i> , <i>P<sub>alk</sub></i> ), Cyp genes from <i>Acidovorax</i> sp, <i>P<sub>alk</sub></i> , CDH gene, CHMO gene	[6]
pSEVA244_T	pRO1600 and ColE1 ori, <i>lac</i> -regulatory system ( <i>lacI<sup>q</sup></i> , <i>P<sub>trc</sub></i> ), BBa_B0015 terminator, empty plasmid	[7]
pSEVA_Cyp	pRO1600 and ColE1 ori, <i>lac</i> -regulatory system ( <i>lacI<sup>q</sup></i> , <i>P<sub>trc</sub></i> ), BBa_B0015 terminator, RBS*, Cyp genes from <i>Acidovorax</i> sp.	[7]
pSEVA_CDH	pRO1600 and ColE1 ori, <i>lac</i> -regulatory system ( <i>lacI<sup>q</sup></i> , <i>P<sub>trc</sub></i> ), BBa_B0015 terminator, RBS*, CDH gene from <i>Acidovorax</i> sp.	This study
pSEVA_CHMO	pRO1600 and ColE1 ori, <i>lac</i> -regulatory system ( <i>lacI<sup>q</sup></i> , <i>P<sub>trc</sub></i> ), BBa_B0015 terminator, RBS*, CHMO gene from <i>Acidovorax</i> sp.	This study
pSEVA_Cyp_CDH	pSEVA_Cyp, CDH from <i>Acidovorax</i> sp. with RBS*	This study
pSEVA_CL_1	pSEVA_Cyp_CDH, CHMO from <i>Acidovorax</i> sp. with RBS*	This study
pSEVA_CL_2	pSEVACL_1 with additional <i>P<sub>trc</sub></i> promoter after Cyp genes	This study
pSEVA_6HA_1	pSEVA_CL_1, lactonase gene from <i>Acidovorax</i> sp. with RBS*	This study
pSEVA_6HA_2	pSEVA_6HA_1 with additional <i>P<sub>trc</sub></i> promoter after Cyp genes	This study

**Table S2:** Primers used during the cloning including the indication of the **fragment binding region** overlap to vector, **RBS**, **Stop codon**, **Strep-Tag**, and **Spacer**

Primer#	Function	Sequence
PLS013	CDH fwd	<u>GGCCGCGCGAATTCGAGCTCGGTAC</u> <b>TAGTGGAGGT</b> TACTAGATGAAACGCGTAGAAAACAAAGTG
PLS014	CDH rev	<u>TCGACTCTAGAGGATCCCCGGGTACTCAATTGGCCGTGTAGCC</u>
PLS015A	CHMO fwd for pSEVA_CHMO	<u>TTCGAGCTCGGTACCCGGGGATCCT</u> <b>TAGTGGAGGT</b> TACTAGATGAAAAAAACC <b>CAACATCTGG</b>
PLS015B	CHMO fwd for pSEVA_CL_1	<u>GGCCAATTGAGTACCCGGGGATCCT</u> <b>TAGTGGAGGT</b> TACTAGATGAAAAAAACC <b>CCAACATCTGG</b>
PLS016	CHMO rev	<u>AAGCTTGCATGCCTGCAGGTCGACT</u> <b>CTA</b> <u>TTTTTCGAACTGCGGGTGGCTCCA</u> <b>AGCGCTCTGGAATACGAAACCCTCG</b>
PLS017B	Lact fwd	AATAGAGTCGACCTGCAGGCATGCA <b>TAGTGGAGGT</b> TACTAGATGGGCACCTCACCCAATC
PLS018	Lact rev	<u>TTTTCCAGTCACGACGCGGCCGCATCAGGCGCGCTTGAACCAC</u>
PLS021	<i>P<sub>trc</sub></i> fwd	<u>CACTGACCTAGGCCGCGGCCGCGCTTGACAATTAATCATCCGG</u>
PLS022	<i>P<sub>trc</sub></i> rev	<u>GTAACCTCCACTAGTACCGAGCTCGTGTGTGAAATTGTTATCCG</u>

## 2 CO difference spectra

Active Cyp in whole cells was quantified by means of CO difference spectra as previously described [8, 9]. Cells were harvested and resuspended in 100 mM potassium phosphate buffer (pH 7.4) containing 1 % (w/v) glucose to obtain an OD<sub>450</sub> of 15 in a volume of 0.9 mL. This cell suspension was transferred to a cuvette and supplemented with 100 µL of fresh sodium dithionite solution (15 mg mL<sup>-1</sup>). The baseline was recorded with a UV-visible spectrophotometer (Varian, Type CARY 300, Palo Alto, CA, USA). Then, the sample was gassed with carbon monoxide (Linde AG, Munich, Germany) for 1 min and a CO difference spectrum was recorded between 350 and 600 nm. The Cyp-concentration was calculated using a molar extinction coefficient of 91 mM<sup>-1</sup> cm<sup>-1</sup> between 450 and 490 nm [10].

### 3 Analytical methods

Biomass concentrations were detected as the optical density at a wavelength of 450 nm using a Libra S11 spectrophotometer (Biochrom, Cambridge, UK). One OD<sub>450</sub> unit corresponds to 0.186 g<sub>CDW</sub> L<sup>-1</sup> [11].

Proteins were detected using SDS-PAGE according to Laemmli [12] with a loading of 30 µg of total protein per lane. Active Cyp was quantified in whole cells via CO difference spectra according to Schäfer et al. [7]. Concentrations of cyclohexane, cyclohexanol, cyclohexanone, and ε-CL were quantified by GC (Trace 1310, Thermo Scientific, Waltham, MA) equipped with a flame ionization detector and a TR-5MS GC Column (dimensions: 15m length, 0.25 mm inner diameter (Thermo Scientific) with molecular nitrogen as carrier gas and 1 µl injection volume in splitless injection mode. The temperature profile setting was as follows: 40°C (3 min), 40–170°C (15°C min<sup>-1</sup>), 170–300 (100°C min<sup>-1</sup>). Products were quantified based on calibration curves from commercially available standards.

Concentrations of 6-hydroxyhexanoic acid were determined by HPLC using a Dionex Ultimate 3000 apparatus (Thermo Scientific) equipped with an Acclaim® OA column (Thermo Scientific). Samples were acidified with 1 M HCl to a pH of 3.0. Applied gradients were based on the solvents A, an aqueous 100 mM sodium sulfate solution (pH=3, adjusted with methanesulfonic acid), and B, acetonitrile. A sample volume of 10–20 µl was injected. Flow and the column temperature were kept constant at 0.4 ml min<sup>-1</sup> and 60 °C, respectively. The gradient profiles for analysis and equilibration were 5 % B for 2 min, 5– 30 % B in 6 min, 30–80 % B in 1 min, 80 % B for 1 min and 80-5 % B in 2 min, 5 % B for 5.5 min, respectively. Detection was accomplished via a UV spectrometer at 210 nm.

#### 4 Determination of Gibbs free energy, equilibrium constant, and equilibrium concentrations for CDH reaction

The Gibbs free energy was calculated according to the group contribution method<sup>[13]</sup>. The groups and compounds that have to be taken into account are highlighted in Fig. S1. Table S3 shows the groups and their contribution.

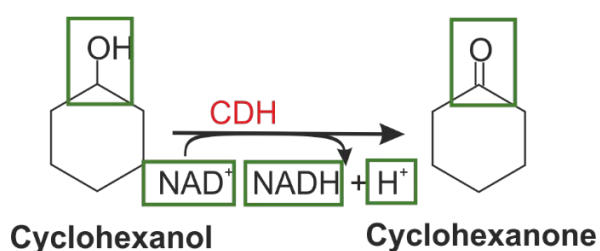


**Figure S1: Reaction scheme for CDH.** All relevant groups for the calculation of the Gibbs free energy according to the group contribution method are marked in green.

**Table S3: Group contributions for CDH reaction.**

Group	Occurrence <sup>1</sup>	Contribution [kcal mol <sup>-1</sup> ] <sup>2</sup>	Total contribution
H+	1	-9.5	-9.5
NADH - NAD <sup>+</sup>	1	4.74	4.74
-CO- (ring)	1	-30.1	-30.1
Alcohol	-1	-41.5	41.5
-CH< (ring)	-1	4.84	-4.84
<b>Total</b>			<b>1.8 kcal mol<sup>-1</sup></b>

<sup>1</sup>1 = 1 group is formed, -1 = one group is consumed

<sup>2</sup>according to<sup>[14]</sup> and<sup>[13]</sup>

Determination of equilibrium constant  $K'$ :

$$\Delta G^{0'} = -RT \ln K'$$

$$K' = 10^{\frac{-\Delta G^{0'}}{2.303 RT}}$$

$$R = 1.98 \times 10^{-3} \text{ kcal mol}^{-1} \text{K}^{-1} \quad T = 303 \text{ K (30}^\circ\text{C)}$$

$$K' = 10^{\frac{-\Delta G^{0'}}{1.3812}}$$

$$\text{with } \Delta G^{0'} = 1.8 \text{ kcal mol}^{-1} \quad K' = 0.0497$$

Determination of equilibrium concentration ratio:

$$K'_{pH=7} = \frac{[\text{Cyclohexanone}] \times [\text{NADH}]}{[\text{Cyclohexanol}] \times [\text{NAD}^+]}$$

$$\frac{[\text{Cyclohexanone}]}{[\text{Cyclohexanol}]} = K'_{pH=7} \times \frac{NAD^+}{NADH}$$

with  $\frac{[NAD^+]}{[NADH]} = 10.6$  [15]

$$\frac{[\text{Cyclohexanone}]}{[\text{Cyclohexanol}]} = 0.53 \quad \frac{[\text{Cyclohexanol}]}{[\text{Cyclohexanone}]} = 1.90$$

Figure S2 shows the time courses of experimentally determined cyclohexanol/cyclohexanone concentration ratios applying different initial concentrations of the two substrates. After 16 h, the reactions reached their equilibrium with concentration ratios in the same range independently of the type and concentration of substrate added. The averaged cyclohexanol/cyclohexanone concentration ratio after 16 h amounted to  $1.95 \pm 0.29$ , agreeing very well with the ratio of 1.90 calculated via the group contribution method assuming an intracellular  $NAD^+$  to  $NADH$  ratio of 10.6.

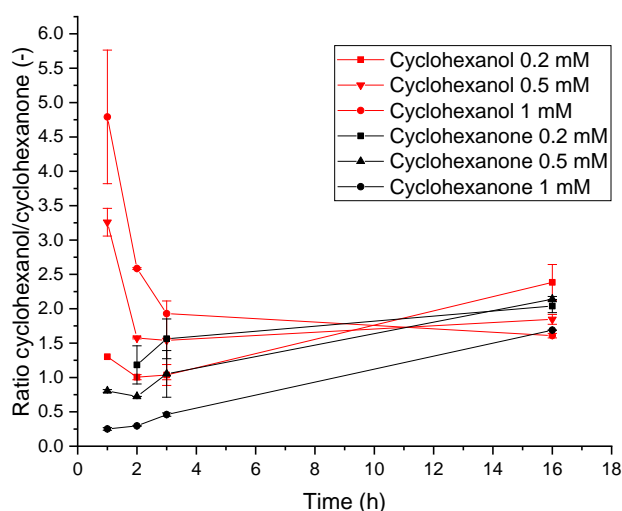


**Figure S2: Time courses of experimentally determined ratios of cyclohexanol and cyclohexanone concentrations with *P. taiwanensis* VLB120 pSEVA\_CDH as biocatalyst.** Three different concentrations of cyclohexanol and cyclohexanone were added to a  $0.25 \text{ g}_{\text{CDW}} \text{ L}^{-1}$  resting cell suspension in KPi-g buffer. Bioconversions were conducted in 2 mL reaction tubes with a liquid volume of 1 mL for 1, 2, 3, and 16 h in a thermoshaker (30 °C, 1,500 rpm). The bars represent average values and standard deviations of two independent biological replicates. The average experimental errors over all measurements for the ratio cyclohexanol/cyclohexanone is 8.9 %.

**5 Nucleotide sequence of lactonase gene from *Acidovorax* sp. CHX-100**

ATGGGCACCTCACCCCAATCCGATTTTCTGCGTGCGCTGTACCAGTCCTGGTCGGACCGCATGGCCGCCAAT  
CCCGCGCTGACCATCGCCGACCTGCGCAGCCTGTTCGACGAGTGGCATCAACCGACGCTCGAGCCCCAAGAC  
GTGACCTACAAGTCGGAAGTGCTCGCCGGTGTGGAAGCCATCTGGGCCCTGCCCCAAGGCGCTGACGCCAA  
GAAGGTCATCCTGTACACGCACGGCGGGCGGCTTTGCCGTGGGGTTCGGCCGCCAGCCATCGTAAGCTGGCCG  
GTCATCTGGCCAAGCACCTGGGCGTGACTGCGGTGGTGATCGACTACCGCCGGGCACCCGAGCATCCGTACC  
CGGCCAGATCGAGGATTCGACGGCTGTCTACAAAGAACTGCTGGCGCGTGGTTTCAAGGCGGCCGACATC  
GTCACCAGCGGGCGACTCGGCGGGCGGCAACCTGGCTATCTCCACCGTGCTGAAGCTGCGCCAGGACGGCGTG  
GCGCTGCCGGGCGCGGTCATCGCCTTTTCGCCCTGGCTCGACATGGAGCATGTTCGGCAAGACACTGCAGACC  
AACGCGGCCACGGACGCCCTGGTGAGCAAGGCCGTGCTGGAGGGCATGTTCGGGCATGTTCTGGGGGAGAA  
GGGCTCGCGCACCGACCCGCTGGCCAATCCGCTGAAGGCCGACTACACCGGCTTTCCGCGCCTGTACATCAA  
CGCCGGCAGTGCCGAAACCCTGCTAGACAACGCGCAGGATCTGGCGCGCATCGCCAAGGCTGCCGGCGTGA  
ACGTCACGCTGTGCGGTGGTTGACGGCATGCAGCACGTCTTCCCGTTCCTGGCGGGCCGAGCCCCCGAGGCCG  
ACGACGAGCTGCGGCGCATTGCCAGTGGTTCAAGCGCGCCTGA

## 6 Determination of growth rate and turnover number for Cyp

**Table S4:** Growth rate and whole-cell Cyp activity, concentration, and turnover number for *P. taiwanensis* VLB120 strains containing the different constructs used and developed in this study.

Plasmid	Growth rate [h <sup>-1</sup> ]	Specific Cyp activity <sup>a</sup> [U g <sub>CDW</sub> <sup>-1</sup> ]	Cyp concentration <sup>b</sup> [nmol g <sub>CDW</sub> <sup>-1</sup> ]	Turnover number [nmol min <sup>-1</sup> nmol <sup>-1</sup> ]
No plasmid	0.47 ± 0.01	-	-	-
pSEVA244_T	0.359 ± 0.004	-	-	-
pSEVA_Cyp	0.370 ± 0.002	55.6 ± 2.4	134.1 ± 3.2	414.6
pSEVA_Cyp_CDH	0.311 ± 0.003	44.8 ± 0.1	115.9 ± 5.0	386.5
pSEVA_CL_1	0.289 ± 0.002	47.8 ± 0.4	89.9 ± 6.7	533.5
pSEVA_CL_2	0.373 ± 0.004	43.4 ± 1.9	93.1 ± 9.5	466.2
pSEVA_6HA_1	0.312 ± 0.003	38.0 ± 0.6	98.7 ± 2.2	385.0
pSEVA_6HA_2	0.370 ± 0.008	44.8 ± 0.2	107.8 ± 13.0	415.6

<sup>a</sup> bioconversions with 0.5 g<sub>CDW</sub> L<sup>-1</sup> of cells in Erlenmeyer flasks, 10 min assay time, addition of 9.2 mM cyclohexane (180 μM in aqueous phase). Data for the plasmids pSEVA\_CL\_1, CL\_2, 6HA\_1, 6HA\_2 are derived from the experiments shown in Figs. 3BD, 4B, and S3B.

<sup>b</sup> determined via CO difference spectroscopy



## 7 Construction and characterization of *P. taiwanensis* VLB120 (pSEVA\_6HA\_1)

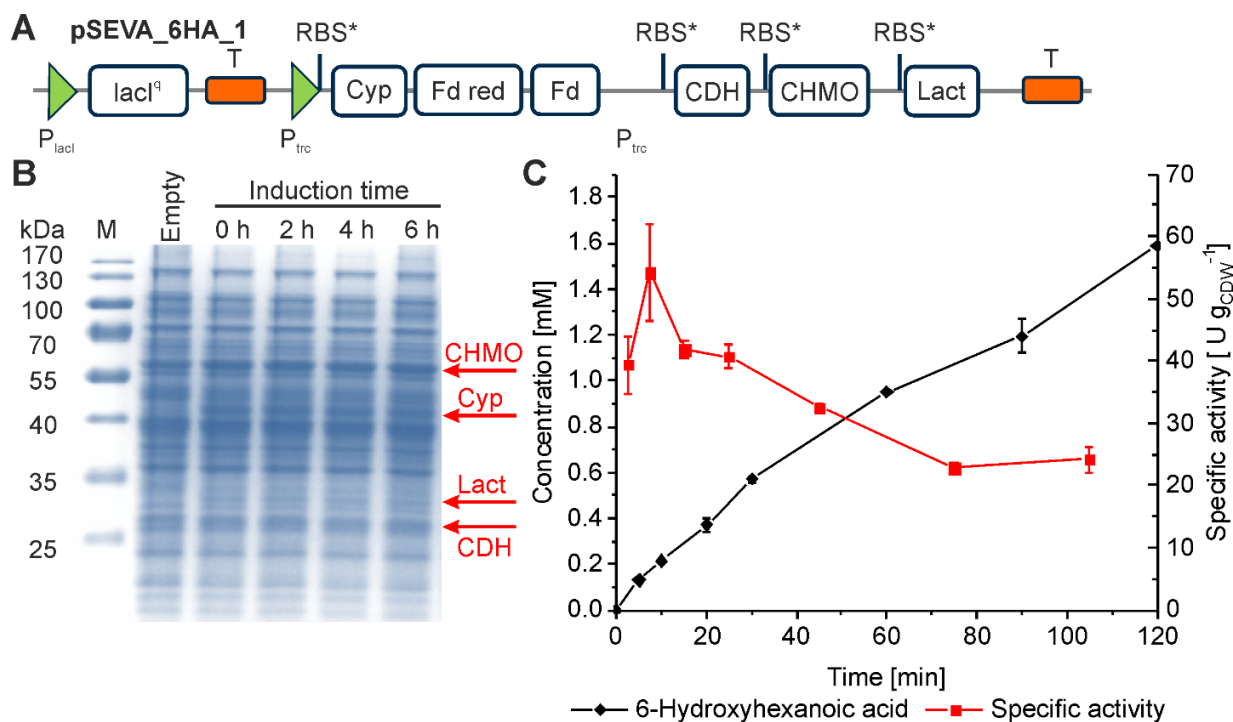


**Figure S3:** Construction and characterization of *P. taiwanensis* VLB120 (pSEVA\_6HA\_1). (A) Graphical representation of expression units in the plasmid pSEVA\_6HA\_1. (B) SDS-PAGE analysis showing bands for Cyp (47.4 kDa), CDH (26.5 kDa), CHMO (58.8 kDa), and Lact (32.2 kDa) after different times of induction and compared with cells containing an empty vector. (C) Time courses for the 6HA concentration and the whole-cell activity for 6HA formation in resting cell bioconversions as described in the legend of Fig. 3. Graph represents average values and standard deviations of two independent biological replicates. The average experimental errors over all measurements for 6HA concentrations, and whole-cell activities are 2.7 and 6.8 %, respectively.

## 8 References

- [1] K.-H. Choi, H. P. Schweizer. *Nat. Protoc.* **2006**, *1*, 153.
- [2] J. Sambrook, D. W. Russell, *Molecular cloning: a laboratory manual*, Cold Spring Harbor Laboratory, Cold Spring Harbor, NY 2001.
- [3] D. G. Gibson, L. Young, R.-Y. Chuang, J. C. Venter, C. A. Hutchison, H. O. Smith. *Nat. Methods* **2009**, *6*, 343.
- [4] D. Hanahan. *J. Mol. Biol.* **1983**, *166*, 557.
- [5] K. A. Köhler, C. Rückert, S. Schatschneider, F.-J. Vorhölter, R. Szczepanowski, L. M. Blank, K. Niehaus, A. Goesmann, A. Pühler, J. Kalinowski. *J. Biotechnol.* **2013**, *168*, 729.
- [6] R. Karande, D. Salamanca, A. Schmid, K. Buehler. *Biotechnol. Bioeng.* **2017**, *115*, 312.
- [7] L. Schäfer, R. Karande, B. Bühler. *Front. Bioeng. Biotechnol.* **2020**, *8*, 140.
- [8] S. Cornelissen, M. K. Julsing, A. Schmid, B. Bühler. *J. Ind. Microbiol. Biotechnol.* **2012**, *39*, 275.
- [9] S. Cornelissen, S. Liu, A. T. Deshmukh, A. Schmid, B. Bühler. *J. Ind. Microbiol. Biotechnol.* **2011**, *38*, 1359.
- [10] T. Omura, R. Sato. *J. Biol. Chem.* **1964**, *239*, 2370.
- [11] B. Halan, A. Schmid, K. Buehler. *Biotechnol. Bioeng.* **2010**, *106*, 516.
- [12] U. K. Laemmli. *Nature* **1970**, *227*, 680.
- [13] M. L. Mavrovouniotis. *Biotechnol. Bioeng.* **1990**, *36*, 1070.
- [14] M. D. Jankowski, C. S. Henry, L. J. Broadbelt, V. Hatzimanikatis. *Biophys. J.* **2008**, *95*, 1487.
- [15] M. R. Leonardo, Y. Dailly, D. P. Clark. *J. Bacteriol.* **1996**, *178*, 6013.

# 4 Front. Catal. (2021), 1, art. 683248, Supplementary Material

## Plasmid construction

*Acidovorax* sp. CHX100 was cultivated for 4 days in nutrient broth (NB) medium (Sambrook & Russell, 2001) for DNA isolation. The lactonase gene was amplified with the primers PLS017 and PLS018 (Table S2.4.1), Gibson Assembly of the resulting fragment and HindIII-digested pSEVA244\_T (Chapter 2.1) gave rise to pSEVA\_Lact.

**Table S2.4.1:** Primers used for cloning with indicated **fragment binding region**, **overlap to vector**, and **RBS**.

Primer#	Function	Sequence
PLS017	Lact fwd	TCTAGAGTCGACCTGCAGGCATGCA TAGTGGAGGT TACTAG ATGGGCACCTCACCCAATC
PLS018	Lact rev	TTTTCCCAGTCACGACGCGCCGCATCAGGCGCGCTTGAACCAC

## Semi-dry Western blot analysis

Cell disruption was performed by 3 passes through a French press (Thermo Electron Corporation, Waltham, MA/USA). The protein concentration was determined via Bradford assay (Bradford, 1976), and 20 µg total protein amount were loaded on a SDS-PAGE gel including a 3 µL Strep-Tag protein ladder (iba Lifesciences, Göttingen, Germany). One nitrocellulose membrane (NitroBind, 0.45 µm, 200x200 mm, GVS Filter Technology, Bologna, Italy), six Whatman papers, and the SDS-PAGE gel were pre-incubated in transfer buffer for 5 min at 4°C. The transfer sandwich was assembled as follows: 3 Whatman papers, membrane, SDS page, 3 Whatman papers. The transfer was performed for 30 min at 44 mA and 5 V. Afterward, the membrane was blocked with 20 mL 5% BSA in T-TBS buffer for 1 h at 4°C. Biotin blocking was performed by adding 20 µL biotin to the blocking solution and incubation for 10 min at 4 °C. One µl Strep-Tactin antibody solution (iba Lifesciences) was added followed by overnight incubation at 4°C. Five washing steps were performed with T-TBS for 5 min each. The membrane was imaged via the Fluor Chem FC3 imaging system (ProteinSimple, San Jose, CA/USA) after 5 min incubation in WesternBright ECL (Advansta, San Jose, CA/USA).

## Additional Supplementary Figures

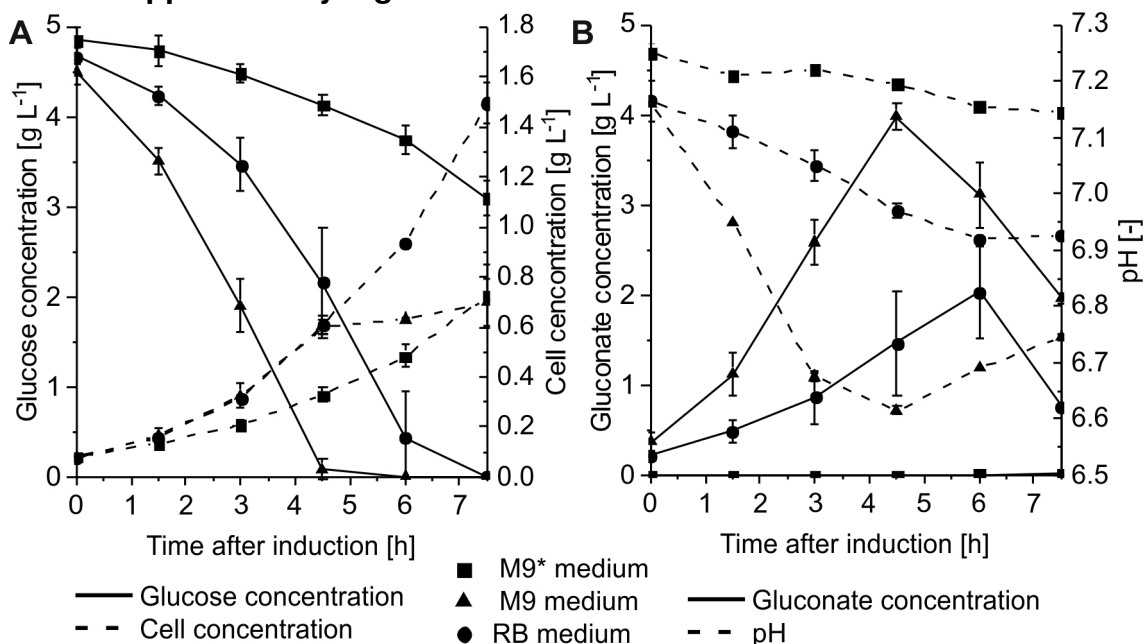


**Figure S2.4.1:** Physiological characterization of *P. taiwanensis\_6HA*. Cells were cultivated in M9\* (square), M9 (triangle), or RB medium (circle) containing 0.5 % (w/v) glucose and were induced by IPTG at  $OD_{450} = 0.5$ . **(A)** Time courses of glucose and cell concentration after induction. **(B)** Time courses of gluconate concentration and pH after induction.

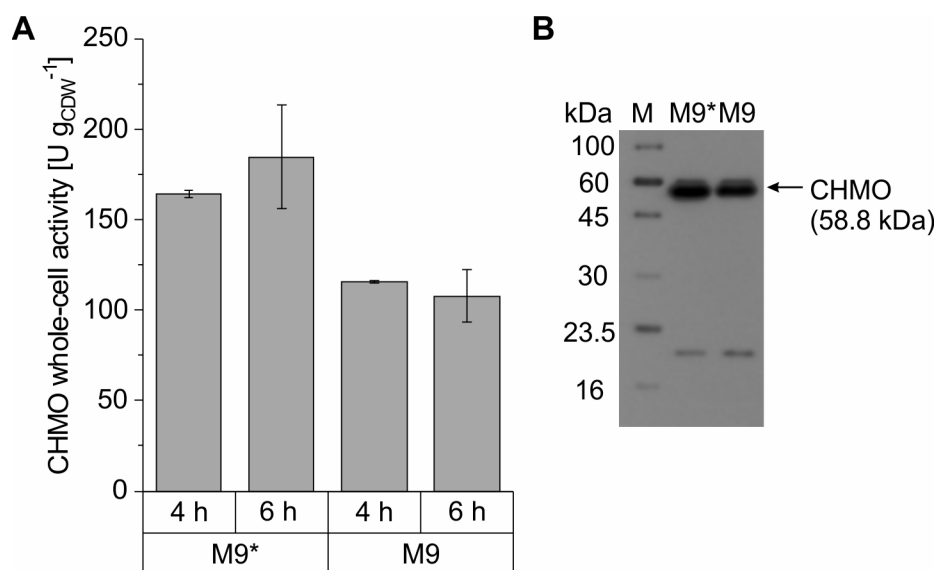


**Figure S2.4.2:** Comparison of CHMO activity **(A)** and protein amount **(B)** in M9- and M9\* grown *P. taiwanensis* VLB120 (pSEVA\_CHMO). **(A)** Cells were cultivated in M9\* or M9 medium containing 0.5 % (w/v) glucose and were harvested after 4 or 6 h of induction by IPTG. After resuspension in Kpi-buffer containing 1 % (w/v) glucose to a biomass concentration of  $0.25 \text{ g}_{\text{CDW}} \text{ L}^{-1}$ , 1 mL liquid volume was transferred to a Pyrex tube and equilibrated for 10 min at  $30^\circ\text{C}$ . Reactions were started by adding 12 mM cyclohexanone and stopped after 10 min. Graph represents average values and standard deviations of two independent biological replicates. The average experimental error over all activity measurements is 7.6 %. **(B)** Cell samples for Western blot analysis were taken after 6 h of induction and disrupted via French press.  $20 \mu\text{g}$  total protein were loaded. CHMO was detected via its C-terminal Strep-tag.

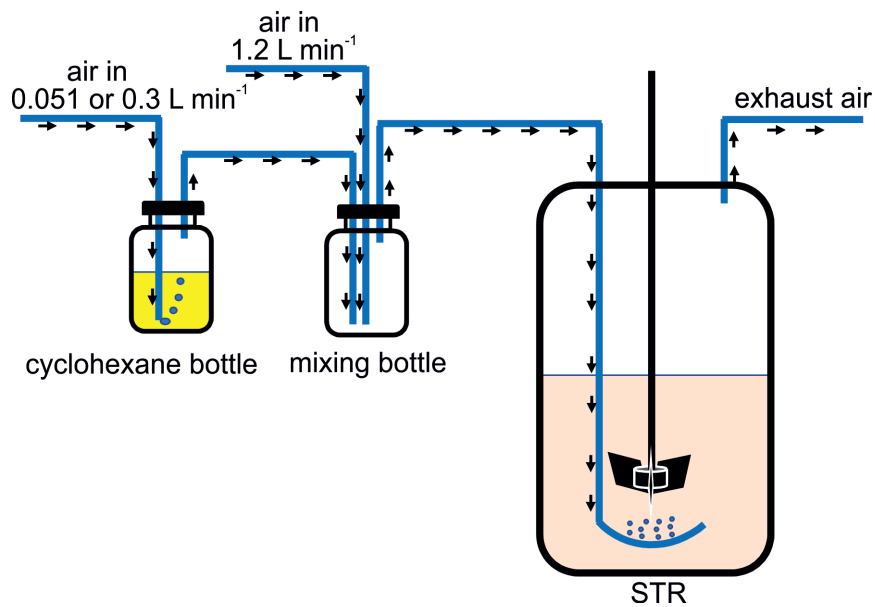


**Figure S2.4.3:** Stirred-tank bioreactor (STR) setup for continuous cyclohexane feed via the gas phase. Pressurized air with a defined flow rate (0.051 or 0.3 L min<sup>-1</sup>) is bubbled through a cyclohexane-filled bottle to obtain a cyclohexane-saturated air stream, which is subsequently mixed in the mixing bottle with the main air stream (1.2 L min<sup>-1</sup>). By varying the flow rate of the cyclohexane-saturated air stream, defined gas phase cyclohexane concentrations can be directed into the STR.

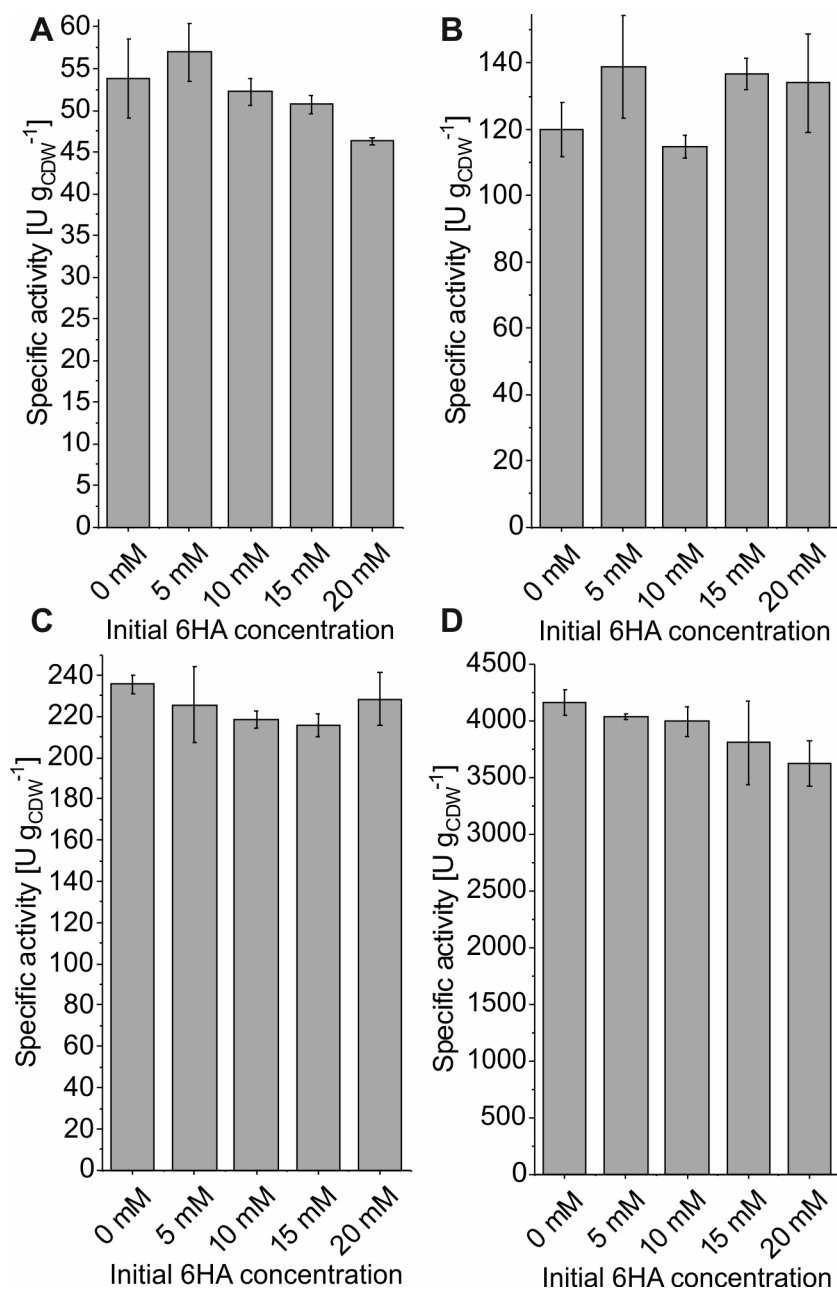


**Figure S2.4.4:** Effect of 6HA on specific Cytochrome P450 monooxygenase (**A**), cyclohexanol dehydrogenase (**B**), cyclohexanone monooxygenase (**C**), and lactonase (**D**) activity. Cells were cultivated in M9\* medium containing 0.5 % (w/v) glucose and harvested after 6 h of induction by IPTG. Cells were resuspended to a biomass concentration of  $0.25 \text{ g}_{\text{CDW}} \text{ L}^{-1}$  in Kpi-buffer containing 1 % (w/v) glucose and defined concentrations of 6HA, of which 10 mL were transferred into 100 mL screw-capped Erlenmeyer flasks (**A**, **D**) or 1 mL into 2 mL reaction tubes (**B**, **C**). After equilibration for 10 min at  $30^\circ\text{C}$ , reactions were started by adding pure cyclohexane to a concentration of 5 mM with respect to the aqueous phase volume (**A**), 5 mM cyclohexanol (**B**), 5 mM cyclohexanone (**C**), or 10 mM  $\epsilon$ -CL (**D**) and stopped after 10 min (**A**) or 5 min (**B**, **C**, **D**). Graphs represent average values and standard deviations of two independent biological replicates. The average experimental errors over all activity measurements is 4.9 %.

**5 Microb. Biotechnol. (2021), 14(3), p. 1011-1025, incl. Supplementary Material**

# One-pot synthesis of 6-aminohexanoic acid from cyclohexane using mixed-species cultures

Lisa Bretschneider,  Martin Wegner, Katja Bühler, Bruno Bühler and Rohan Karande

Department of Solar Materials, Helmholtz-Centre for Environmental Research –UFZ, Permoserstrasse 15, Leipzig, 04318, Germany.

## Summary

**6-Aminohexanoic acid (6AHA) is a vital polymer building block for Nylon 6 production and an FDA-approved orphan drug. However, its production from cyclohexane is associated with several challenges, including low conversion and yield, and severe environmental issues. We aimed at overcoming these challenges by developing a bioprocess for 6AHA synthesis. A mixed-species approach turned out to be most promising. Thereby, *Pseudomonas taiwanensis* VLB120 strains harbouring an upstream cascade converting cyclohexane to either  $\epsilon$ -caprolactone ( $\epsilon$ -CL) or 6-hydroxyhexanoic acid (6HA) were combined with *Escherichia coli* JM101 strains containing the corresponding downstream cascade for the further conversion to 6AHA.  $\epsilon$ -CL was found to be a better ‘shuttle molecule’ than 6HA enabling higher 6AHA formation rates and yields. Mixed-species reaction performance with 4 g l<sup>-1</sup> biomass, 10 mM cyclohexane, and an air-to-aqueous phase ratio of 23 combined with a repetitive oxygen feeding strategy led to complete substrate conversion with 86% 6AHA yield and an initial specific 6AHA formation rate of  $7.7 \pm 0.1$  U g<sub>CDW</sub><sup>-1</sup>. The same cascade enabled 49% 7-aminoheptanoic acid yield from cycloheptane. This combination of rationally engineered strains allowed direct 6AHA production from cyclohexane in one pot with high conversion and yield under environmentally benign conditions.**

## Introduction

Synthetic fibres, especially Nylon 6 and Nylon 66, account for 95% of the total polyamide production

(Bellussi and Perego, 2000), with applications in the automotive, textile, electronics and packaging industries (Moody and Needles, 2004; BASF, 2020). The industrial synthesis of Nylon 6 from cyclohexane, with a scale of 4.2 million tons year<sup>-1</sup>, involves multiple reaction steps and thus is highly resource-intensive (Ritz *et al.*, 1986). With an industrial history of 75 years, it suffers from a low cyclohexane per pass conversion of 10–15%, multiple unit operations at high temperature and pressure variations, huge efforts necessary for intermediate product isolation, extensive waste generation, and formation of explosive intermediates (Fischer *et al.*, 2010; Wittcoff *et al.*, 2012). Thus, there is a growing demand to develop sustainable synthetic routes that allow high substrate conversion and product yield, with reduced waste generation and energy consumption (Bellussi and Perego, 2000). In this context, the one-pot (bio)synthesis of 6-aminohexanoic acid (6AHA as precursor of Nylon 6) from cyclohexane would offer a greener and more sustainable process route.

Sattler and coworkers demonstrated an *in vitro* approach combining 6 isolated enzymes to synthesize 6AHA from cyclohexanol (Sattler *et al.*, 2014). Although balancing the enzyme ratio in the *in vitro* approach seems to be more straightforward than *in vivo*, finding the right enzymes with matching kinetics and catalytic efficiencies to synthesize 6AHA without accumulation of intermediate products turned out to be challenging (Sattler *et al.*, 2014). However, the tedious purification of all enzymes, the provision of necessary cofactors and their respective regeneration systems, and enzyme instability under process conditions favour the use of whole-cell biocatalysts (Duetz *et al.*, 2001; Walton and Stewart, 2004; Leak *et al.*, 2009; Schrewe *et al.*, 2013; Ladkau *et al.*, 2014).

In past decades, advances in the metabolic engineering toolbox enabled the rational design and expression of complex biosynthetic pathways in a single host for the production of high-value chemicals (Ladkau *et al.*, 2014). Although cascades involving more than 5 steps have been rationally engineered (Jeschek *et al.*, 2017), several challenges including redox imbalance, excess metabolic burden, poor expression levels, and toxicity issues often resulted in low product yields (Muschiol *et al.*, 2015; Rudroff, 2019). In this context, significant progress has been achieved by segregating complex pathways via the use of more than one engineered microbial strain and thus distributing the metabolic burden (Zhang and

Received 5 October, 2020; revised 14 December, 2020; accepted 14 December, 2020.

\*For correspondence. E-mail rohan.karande@ufz.de; Tel. +49 341 235 48 22 71; Fax. +49 341 235 45 1286.

*Microbial Biotechnology* (2021) 14(3), 1011–1025  
doi:10.1111/1751-7915.13744

© 2020 The Authors. *Microbial Biotechnology* published by Society for Applied Microbiology and John Wiley & Sons Ltd. This is an open access article under the terms of the Creative Commons Attribution-NonCommercial License, which permits use, distribution and reproduction in any medium, provided the original work is properly cited and is not used for commercial purposes.



Wang, 2016; Jones and Wang, 2018). For example, the coupling of limonene synthesis and oxyfunctionalization in one *Escherichia coli* strain resulted in low perillyl acetate yield, which could be improved by distributing this complex reaction cascade among two recombinant *E. coli* strains (Willrodt *et al.*, 2015). Recently, the Nylon 66 monomer adipic acid (AA) has been synthesized from cyclohexane employing a consortium of three *E. coli* strains achieving a conversion of 42% and > 99% AA yield (Wang *et al.*, 2020).

In this study, we aimed at 6AHA production from cyclohexane in a one-pot approach with high conversion and yield. For this purpose, previously established *Pseudomonas taiwanensis* VLB120 strains containing cascades for the conversion of cyclohexane to  $\epsilon$ -caprolactone ( $\epsilon$ -CL) and/or 6-hydroxyhexanoic acid (6HA) (Schäfer *et al.*, 2020) served as the basis. The respective biosynthetic pathways involve a cytochrome P450 monooxygenase (Cyp), a cyclohexanol dehydrogenase (CDH), a cyclohexanone monooxygenase (CHMO), and, facultatively, a lactonase (Lact). In this study, we set out to amend this cascade by the alcohol dehydrogenase AlkJ from *Pseudomonas putida* GPo1 (van Beilen *et al.*, 2001) and the  $\omega$ -transaminase CV2025 from *Chromobacterium violaceum* (Ladkau *et al.*, 2016) to finally synthesize 6AHA from cyclohexane (Fig. 1A). In order to enable modularity and a high overall pathway flux, we distributed the pathway genes among two vectors and also considered a mixed-species approach, which requires efficient shuttling of appropriate pathway intermediates among the strains (Jones and Wang, 2018). Finally, the operation of resulting systems was investigated by varying biomass amounts, gas–liquid phase ratios, and cyclohexane amounts in the aqueous phase to maximize substrate conversion and 6AHA yield.

## Results

In our previous study, *P. taiwanensis* VLB120 was established as a platform organism to produce the polycaprolactone monomers  $\epsilon$ -CL and 6HA from cyclohexane (Schäfer *et al.*, 2020). In the present work, we aimed to extend this biocatalytic reaction cascade for the production of 6AHA, the building block of Nylon 6 serving an even larger market (4.2 million tons per annum) than polycaprolactone (25,000 tons per annum) (Ritz *et al.*, 1986; Weissmehl and Arpe, 2008).

### *The alcohol dehydrogenase AlkJ and the transaminase CV2025 as suitable enzymes for the conversion of 6HA to 6AHA*

In a previous study, an *in vitro* cascade for 6AHA synthesis from cyclohexanol has been demonstrated (Sattler

*et al.*, 2014). However, all tested alcohol dehydrogenases were unable to catalyse 6HA oxidation to 6-oxohexanoic acid. Therefore, a complex strategy of esterase-catalysed capping of the acid group of 6HA with methanol, followed by oxidation of the alcohol group, transamination, and ester hydrolysis was pursued and allowed 6AHA production with a 24% yield. We set out to address 6HA oxidation directly and hypothesized that the membrane-associated alcohol dehydrogenase AlkJ from *P. putida* GPo1 (van Beilen *et al.*, 1994) bears high respective potential. AlkJ has been reported to convert aliphatic alcohols and  $\omega$ -hydroxyfatty acid methyl esters to corresponding aldehydes with high specific activity, for example 79 U g<sub>CDW</sub><sup>-1</sup> for 12-hydroxydodecanoic acid methyl ester oxidation in *E. coli* cells (Schrewe *et al.*, 2014). Beside its promising substrate spectrum, the irreversible nature of AlkJ-catalysed alcohol oxidation constitutes a crucial advantage. Ubiquinone serves as electron acceptor for AlkJ, which thereby feeds electrons into the respiratory electron transport chain (Kirmair and Skerra, 2014). It remained to be elucidated, if AlkJ also accepts 6HA as substrate. For the conversion of the resulting product 6-oxohexanoic acid to 6AHA, the transaminase CV2025 (TA) originating from *C. violaceum* was selected. This enzyme is known to be active on long-chain aldehydes and amines carrying carboxylic acid groups (Kaulmann *et al.*, 2007). It has successfully been applied together with AlkJ in a cascade hosted by *E. coli* JM101 to synthesize Nylon 12 monomers with fatty acid methyl esters as substrates (Ladkau *et al.*, 2016). Here, we first tested AlkJ and TA cascade in *E. coli* JM101 (*E. coli*\_6HA) for the conversion of 6HA to 6AHA.

Figure 2A demonstrates that the AlkJ-TA combination indeed catalyses the desired conversion of 6HA to 6AHA. A maximum specific whole-cell activity of  $14.7 \pm 1.2$  U g<sub>CDW</sub><sup>-1</sup> was achieved applying a 6HA concentration above 2.5 mM. Kinetic analyses involving the variation of the 6HA concentration revealed that as much as 1.5–2 mM 6HA was necessary to achieve half-maximal activity, an indication for a substrate uptake limitation (fitting with the Monod equation was not possible in this case). 6HA has a negative charge at the neutral pH applied, and its uptake may thus suffer from limited transfer over the cytoplasmic membrane. To investigate and circumvent such a 6HA uptake limitation, we constructed an *E. coli* strain (*E. coli*\_CL), which, in addition to AlkJ and TA, encodes the highly active lactonase (Lact) derived from *Acidovorax* sp. CHX100 and is thus prone to accept uncharged  $\epsilon$ -CL as a substrate.  $\epsilon$ -CL can be expected to readily diffuse through outer membrane pores as well as the inner membrane. Indeed, *E. coli*\_CL converted  $\epsilon$ -CL into 6AHA with a high maximal activity of  $39.4 \pm 3.2$  U g<sub>CDW</sub><sup>-1</sup> (measured applying

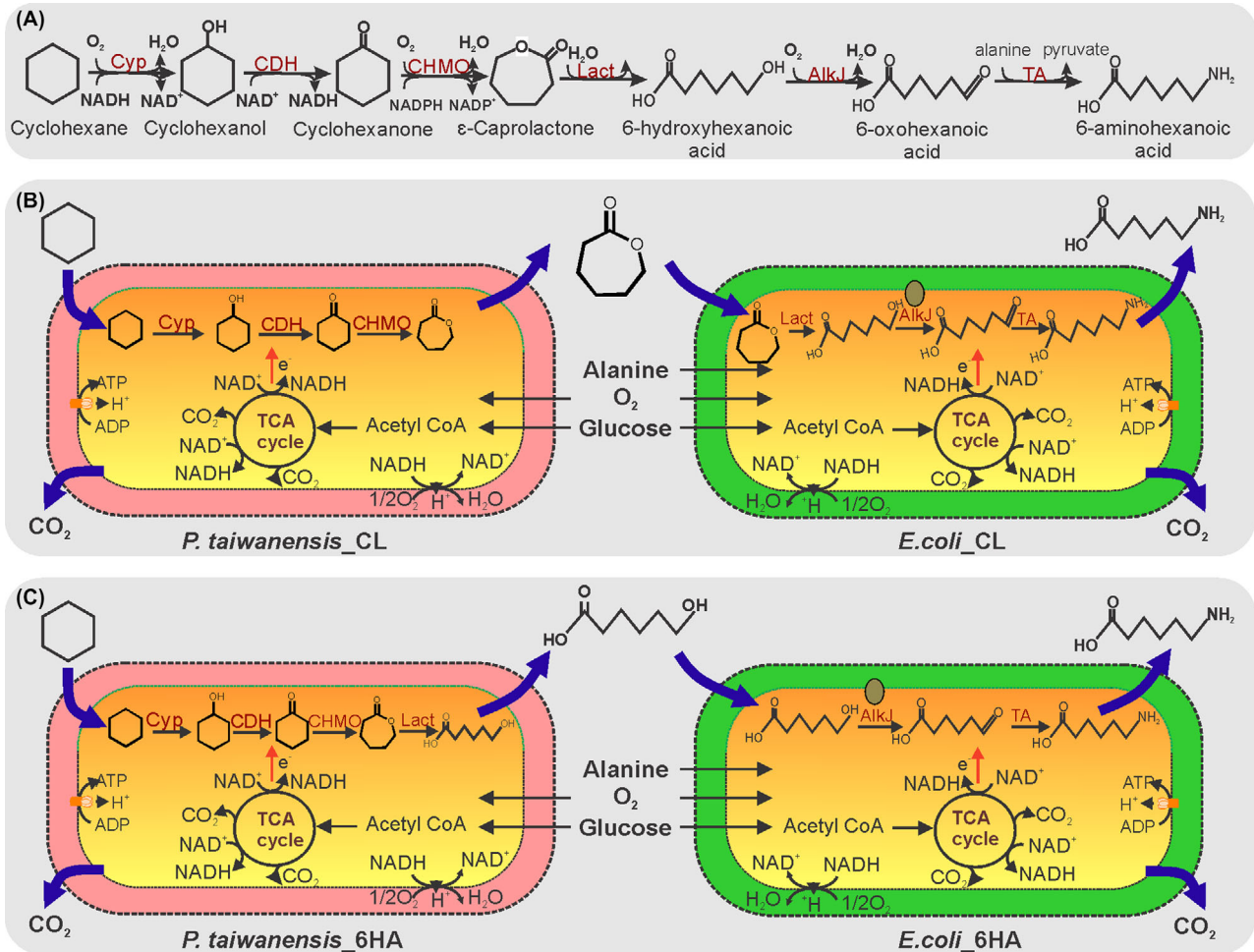


**Fig. 1.** Mixed-species strategies to produce 6-aminohexanoic acid (6AHA). A. Reaction scheme for the conversion of cyclohexane to 6AHA employing the enzymes Cytochrome P450 monooxygenase (Cyp), cyclohexanol dehydrogenase (CDH), cyclohexanone monooxygenase (CHMO), lactonase (Lact), alcohol dehydrogenase (AlkJ) and  $\omega$ -transaminase (TA), (B) combination of *P. taiwanensis* VLB120 (pSEVA\_CL\_2) (*P. taiwanensis*\_CL) and *E. coli* JM101 (pJ10Lact, pAlaDTA) (*E. coli*\_CL) with  $\epsilon$ -caprolactone ( $\epsilon$ -CL) as shuttling compound, and (C) combination of *P. taiwanensis* VLB120 (pSEVA\_6HA\_2) (*P. taiwanensis*\_6HA) and *E. coli* JM101 (pJ10, pAlaDTA) (*E. coli*\_6HA) with 6-hydroxyhexanoic acid (6HA) as shuttling compound.

2.5 and 5 mM  $\epsilon$ -CL) and featured an apparent  $\epsilon$ -CL-related substrate uptake constant ( $K_S$ ) of around 0.6 mM (fitted using the Monod equation) proving the substrate uptake limitation with 6HA as substrate (Fig. 2B). Next, the product formation pattern of *E. coli*\_CL was analysed to get insight into enzyme activities and the rate-limiting step (Fig. 2C). An immediate accumulation of 6HA with *E. coli*\_CL showed that the specific activity for the lactonase-catalysed first step ( $559 \pm 6 \text{ U g}_{\text{CDW}}^{-1}$ ) was 14-fold higher than that for the downstream steps catalysed by AlkJ and TA. This demonstrated that the AlkJ-catalysed alcohol oxidation was the rate-limiting step to produce 6HA from  $\epsilon$ -CL. After overnight incubation, most of the intermediate product 6HA was converted to the main product 6AHA and a minor amount of adipic acid (AA) as a by-product. Overall, 6 mM of  $\epsilon$ -CL were

transformed to 86% 6AHA, 9% intermediate product 6HA, and 5% overoxidation product AA.

#### *A mixed-species approach enables 6AHA production from cyclohexane*

As a next step, we aimed to design a complete enzyme cascade catalysing the conversion of cyclohexane to 6AHA in one strain. From our previous work, *P. taiwanensis* VLB120 (pSEVA\_CL\_2) (*P. taiwanensis*\_CL) and *P. taiwanensis* VLB120 (pSEVA\_6HA\_2) (*P. taiwanensis*\_6HA) strains were available catalysing the conversion of cyclohexane to  $\epsilon$ -CL and 6HA as main products with initial specific whole-cell activities of  $43.4 \pm 1.9$  and  $44.8 \pm 0.2 \text{ U g}_{\text{CDW}}^{-1}$  respectively (Schäfer *et al.*, 2020). These strains do not show any accumulation of pathway

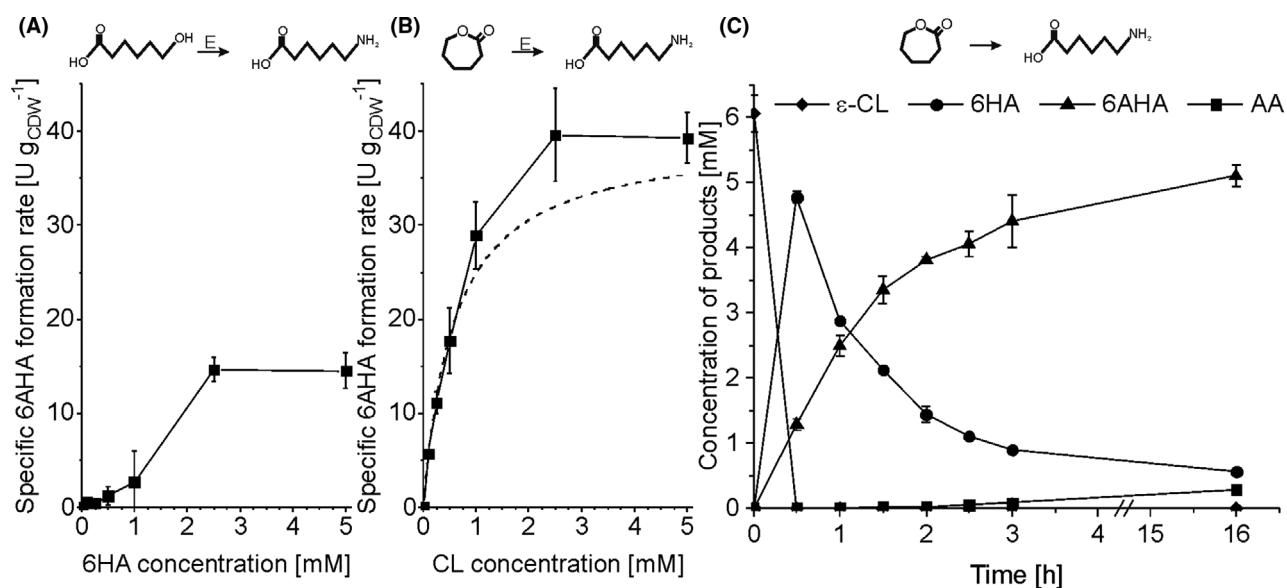


**Fig. 2.** Consecutive 6HA oxidation and transamination by recombinant *E. coli*. Panels A and B show specific 6AHA formation activities of *E. coli\_6HA* (A) and *E. coli\_CL* (B) at different initial substrate concentrations. Biotransformation assays were performed with a biomass concentration of  $0.5 \text{ g}_{\text{CDW}} \text{ l}^{-1}$  in 10 ml liquid volume in 100 ml screw-capped and closed flasks for 30 min. The assay was started by  $\epsilon$ -CL or 6HA addition. The dashed line in panel B depicts the curve according to Monod-type kinetics in order to determine the substrate concentration, at which the half-maximal rate is reached. C. Time-resolved product formation pattern for *E. coli\_CL*. Biotransformation assays were performed with a biomass concentration of  $1.5 \text{ g}_{\text{CDW}} \text{ l}^{-1}$  in 40 ml liquid volume in closed screw-capped 250 ml flasks and were started by adding 6 mM  $\epsilon$ -CL. Means and error bars refer to two independent experiments. The average experimental errors over all measurements for specific 6AHA formation rates,  $\epsilon$ -CL concentrations, 6HA concentrations, 6AHA concentrations and AA (adipic acid) concentrations are 32.7%, 4.6%, 2.0%, 5.3% and 3.9% respectively. E: *E. coli*-catalysed reactions.

intermediates at any time. However, the transfer of the *alkJ* containing *Pseudomonas*-compatible plasmids (Table S1, Entries 9, 11, 12) (Silva-Rocha *et al.*, 2013) into *P. taiwanensis* VLB120 did not yield any 6HA oxidation activity, which disqualified *P. taiwanensis* as host for the expression plasmids studied. Possible reasons for the missing activity include improper folding and membrane association of AlkJ. On the other side, the transformation of *E. coli* JM101 with the plasmids pSEVA\_CL\_2 or pSEVA\_6HA\_2 did not give any colonies, possibly due to a high metabolic burden on the cells. Thus, a single strain approach employing *E. coli* or *Pseudomonas* as host strains appeared not to be feasible with the expression plasmids tested.

To circumvent these complications, we evaluated a mixed-species approach with recombinant *Pseudomonas* and *E. coli* cells for the catalysis of an upper and a lower part of the cascade respectively. For this purpose, the complex biocatalytic cascade for the production of 6AHA from cyclohexane was rationally segregated into two parts, an upstream cascade encoded by *P. taiwanensis*\_CL or *P. taiwanensis*\_6HA for the conversion of cyclohexane to  $\epsilon$ -CL or 6HA and a downstream cascade catalysed by *E. coli*\_CL or *E. coli*\_6HA for the conversion of  $\epsilon$ -CL or 6HA to the target product 6AHA respectively (Fig. 1B and C). In the former case,  $\epsilon$ -CL served

as the shuttling compound (Fig. 1B, 3+3 approach), whereas this was the role of 6HA in the latter case (Fig. 1C, 4+2 approach). Both mixed-species approaches were investigated regarding cyclohexane conversion, specific rates, accumulation of intermediates, and 6AHA yield applying a strain ratio of 1:1, a total biomass concentration of  $3 \text{ g}_{\text{CDW}} \text{ l}^{-1}$ , and 5 mM cyclohexane (referred to the aqueous phase volume). In both combinations, cyclohexanol, cyclohexanone and  $\epsilon$ -CL concentrations remained below  $50 \mu\text{M}$ . The specific activities within the first 3 h of reaction for total product formation and referring to the total cell concentration (both strains) were  $8.1 \pm 1.2$  (Fig. 3A) and  $9.0 \pm 0.8 \text{ U g}_{\text{CDW}}^{-1}$  (Fig. 3B) for the 3 + 3 and 4 + 2 cascades respectively. Consequently, the *Pseudomonas*-catalysed upper cascade was functional, with approximately 40% of its maximal activity. The specific activity for 6AHA formation was constant over the first 3 h with  $4.3 \pm 0.7 \text{ U g}_{\text{CDW}}^{-1}$  for the 3 + 3 cascade, corresponding to 20% of its maximal activity (Fig. 2B), whereas, for the 4 + 2 cascade, it increased with time from below  $1 \text{ U g}_{\text{CDW}}^{-1}$  in the first hour to  $4.3 \pm 0.2 \text{ U g}_{\text{CDW}}^{-1}$  in the third hour. The latter cascade with a high apparent  $K_S$  of *E. coli*\_6HA for the shuttling compound 6HA (Fig. 2A) resulted in an overall slower 6AHA formation and 22% higher 6HA accumulation as

compared to the 3 + 3 cascade with  $\epsilon$ -CL as major shuttling compound (Fig. 3B). Thereby, the 3 + 3 cascade reached a yield of  $0.56 \text{ mol}_{6\text{AHA}} \text{ mol}_{\text{cyclohexane}}$ . These results favour the 3 + 3 cascade for 6AHA production from cyclohexane.

However, the accumulation of the intermediate product 6HA (27%), and the by-product AA (ca. 16%) due to inherent aldehyde dehydrogenase activities asked for further optimization to enhance the 6AHA yield. Aldehydes such as 6-oxohexanoic acid are generally very toxic to living cells (Feron *et al.*, 1991) so that 'generic' dehydrogenases immediately convert them to their less toxic alcohol or acid derivatives (Wierckx *et al.*, 2011). In this context, we aimed to enhance the rate for the downstream cascade by increasing the concentration of *E. coli* cells to  $4 \text{ g}_{\text{CDW}} \text{ l}^{-1}$  while keeping the *P. taiwanensis* cell concentration constant at  $1.5 \text{ g}_{\text{CDW}} \text{ l}^{-1}$ . This strategy, however, did not prevent 6HA and AA accumulation (Fig. S2). Whereas *P. taiwanensis*\_CL showed similar activity as in the experiment shown in Fig. 3, *E. coli*\_CL activity for 6AHA formation was low at only 10% of its maximal activity.

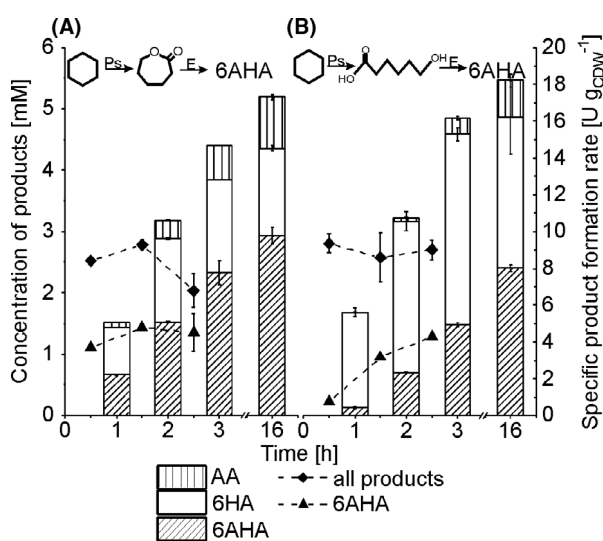


**Fig. 3.** Product formation from cyclohexane with the dual-species approach. The panels show the product concentrations accumulated after different reaction times (bars) and specific whole-cell activities over 3 h for 6AHA and overall product formation (curves). A 1:1 strain ratio was applied for the strain combinations *P. taiwanensis*\_CL/*E. coli*\_CL (A) and *P. taiwanensis*\_6HA/*E. coli*\_6HA (B). Bio-transformations were performed with a total biomass concentration of  $3.0 \text{ g}_{\text{CDW}} \text{ l}^{-1}$  in 10 ml liquid volume in closed screw-capped 100 ml flasks and were started by adding 5 mM cyclohexane (referred to the aqueous phase volume). Intermediate concentrations not depicted in the graphs remained below  $50 \mu\text{M}$ . Means and error bars refer to two independent experiments. The average experimental errors over all measurements for specific product formation rates, 6HA concentrations, 6AHA concentrations and AA concentrations are 7.5%, 5.4%, 4.0% and 12.0% respectively. E: *E. coli*-based catalyst; Ps: *P. taiwanensis*-based catalyst.

#### Impact of mixed-species biomass concentration on catalytic performance and product formation pattern

Further critical factors possibly affecting cyclohexane conversion and 6AHA yield include the high volatility (vapour pressure: 0.12 atm), low water solubility ( $43 \text{ mg l}^{-1}$  at  $25^\circ\text{C}$ ), and toxicity of cyclohexane (National Center for Biotechnology Information, 2020). When added to the liquid phase in a closed flask, cyclohexane quickly evaporates and saturates the headspace, thus making the gas-liquid mass transfer a parameter, possibly influencing reaction performance. Furthermore, cyclohexane significantly affected *P. taiwanensis* VLB120 growth, with its growth rate being reduced by half at 0.4–0.5 mM cyclohexane in the aqueous phase (data not shown). Besides cyclohexane, oxygen availability and mass transfer also may influence the catalytic performance. Cyp and CHMO require oxygen as their direct co-substrate whereas AlkJ uses it as the terminal electron acceptor via the respiratory electron transport chain. A general impact of substrate (cyclohexane and  $\text{O}_2$ ) availability was investigated by varying the biomass concentration utilizing a constant strain ratio of 1:1.

With  $1 \text{ g}_{\text{CDW}} \text{ l}^{-1}$  biomass, specific activities within the first 2 h of reaction amounted to  $18.9 \pm 1.7 \text{ U g}_{\text{CDW}}^{-1}$  for total product accumulation and  $9.8 \pm 1.6 \text{ U g}_{\text{CDW}}^{-1}$  for 6AHA formation (Fig. 4 AB), which was 2-fold higher than the activity achieved with  $3 \text{ g}_{\text{CDW}} \text{ l}^{-1}$  (Fig. 3A). Thereby, the upper cascade was operated at 87% of its maximal rate. After 2 h of reaction, these specific activities started to decrease significantly (Fig. 4A). Whereas the oxygen concentration still was around 15% (v/v) in the air phase and thus not limiting, the aqueous cyclohexane concentration stabilized and even slightly increased after 2 h of reaction (Fig. 4C). This cyclohexane level may have become rate-limiting or, more probably, inhibitory or toxic (over time – together with the products accumulated). After 16 h, a final cyclohexane conversion of 80% was achieved with a 6AHA yield of 47% (Fig. 4A and C). A volumetric rate of  $0.59 \text{ mM}_{6\text{AHA}} \text{ h}^{-1}$  was accomplished over the first 2 h.

With  $2 \text{ g}_{\text{CDW}} \text{ l}^{-1}$  biomass, cyclohexane was completely converted within the first 4 h of reaction. Within the first hour, specific rates amounted to  $15.8 \pm 1.3 \text{ U g}_{\text{CDW}}^{-1}$  for total product formation and  $7.4 \pm 1.2 \text{ U g}_{\text{CDW}}^{-1}$  for 6AHA formation and thus were similar to the initial rates achieved with  $1 \text{ g}_{\text{CDW}} \text{ l}^{-1}$ . However, the 2-fold higher cell concentration increased the volumetric rate to  $0.86 \pm 0.12 \text{ mM}_{6\text{AHA}} \text{ h}^{-1}$  within the first 2 h. Within 4 h, the total product formation activity decreased from  $16 \text{ U g}_{\text{CDW}}^{-1}$  to  $6 \text{ U g}_{\text{CDW}}^{-1}$ , which correlated with the drop in the aqueous cyclohexane concentration (virtually depleted after 4 h) and thus cyclohexane limitation (Fig. 4B and C). A further increase of the biomass

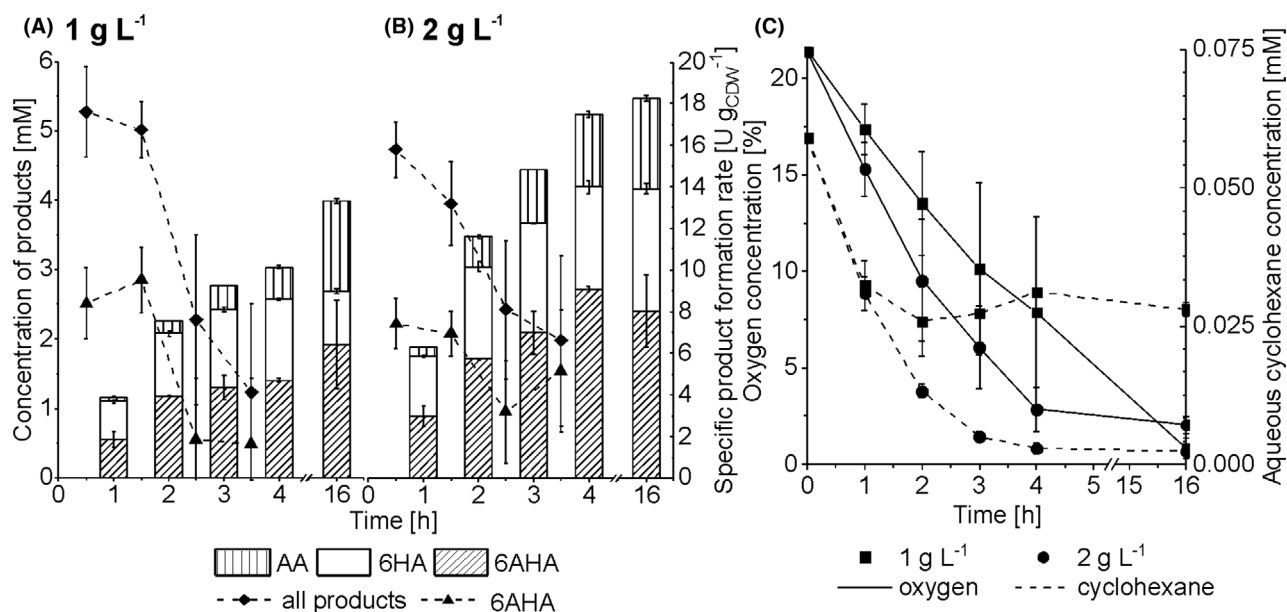


**Fig. 4.** Impact of mixed-species biomass concentration. Panels A and B show product concentrations accumulated after different reaction times (bars) and specific whole-cell activities over 4 h for 6AHA and overall product formation (curves). A 1:1 strain ratio was applied for the strain combination *P. taiwanensis*\_CL/*E. coli*\_CL with a total biomass concentration of 1.0 (panel A) or 2.0 g<sub>CDW</sub> l<sup>-1</sup> (panel B). Reactions were performed in 25 ml liquid volume in closed screw-capped 250 ml flasks and were started by adding 5 mM cyclohexane (referred to the aqueous phase volume). Intermediates not depicted in the graphs accumulated to less than 50  $\mu$ M. Panel C shows the courses of oxygen concentrations in the gas phase (solid lines) and of aqueous cyclohexane concentrations (dashed lines). Means and error bars refer to two independent experiments. The average experimental errors over all measurements for specific product formation rates, 6HA concentrations, 6AHA concentrations, AA concentrations, oxygen concentrations and cyclohexane concentrations are 53.7%, 3.6%, 12.5%, 3.4%, 21.1% and 14.4% respectively. The high error for specific product formation rates results from the low product concentration changes.

concentration, as applied in the experiment shown in Fig. 3A, was thus not considered beneficial under the conditions applied. The oxygen content in the air phase had dropped below 2% after 4 h, which may have limited the catalytic activity of the downstream cascade (i.e. the respiration-dependent AlkJ activity) and thus further conversion of the accumulated 6HA (Fig. 4B and C). This resulted in a final conversion of 99% and a 6AHA yield of 44%. Overall, reaction conditions that overcome substrate limitation, oxygen limitation, and toxification were considered to be necessary to maximize the 6AHA yield.

#### *Host-intrinsic dehydrogenase activity and oxygen availability severely influence the 6AHA yield*

The interplay between cyclohexane and oxygen availability and mass transfer on 6AHA yield was further investigated by changing the air-to-liquid phase ratio from 11 to 23 and 5 by using 12.5 and 50 ml of liquid volume, respectively, in the closed Erlenmeyer flasks (Fig. 5). A biomass concentration of 3 g<sub>CDW</sub> l<sup>-1</sup> was applied to avoid a potential toxification by a prolonged presence of a high cyclohexane concentration. The reaction was initiated by adding 5 mM of cyclohexane to the aqueous phase, which, in a gas-liquid equilibrium,

corresponded to aqueous phase concentrations of 28 and 128  $\mu$ M with 12.5 and 50 ml liquid volume respectively (Fig. 5). At these concentrations, the upstream cascade in *P. taiwanensis* VLB 120 was expected to run at maximum reaction velocity or zero-order kinetics for 128  $\mu$ M substrate and first-order kinetics for 28  $\mu$ M substrate. By such variation of the initial reaction rate, we aimed to investigate its impact on cyclohexane conversion and 6AHA formation.

For 12.5 ml reaction volume, initial specific activities of total product formation ( $6.3 \pm 1.0$  U g<sub>CDW</sub><sup>-1</sup>) and 6AHA formation ( $3.1 \pm 0.4$  U g<sub>CDW</sub><sup>-1</sup>) were stable over 2 h (Fig. 5A). Due to cyclohexane limitation, the initial specific activities of total product formation were 25% lower than that in the same experiment with an air-to-liquid phase ratio of 11 (Fig. 3A). Again, host-intrinsic dehydrogenases, possibly in combination with AlkJ, affected high-level AA formation (53%), with a minimal amount of 6HA (6%) remaining at the end of the experiment. For 50 ml reaction volume, a high initial total specific activity of  $19.0 \pm 0.1$  U g<sub>CDW</sub><sup>-1</sup> in the first hour rapidly dropped to  $1.2 \pm 0.2$  U g<sub>CDW</sub><sup>-1</sup> in the second hour (Fig. 5B) correlating with a decrease in the gas-phase O<sub>2</sub> concentration from 21% to 2% within the first hour (Fig. 5C). The activity decrease can thus be attributed to O<sub>2</sub> limitation

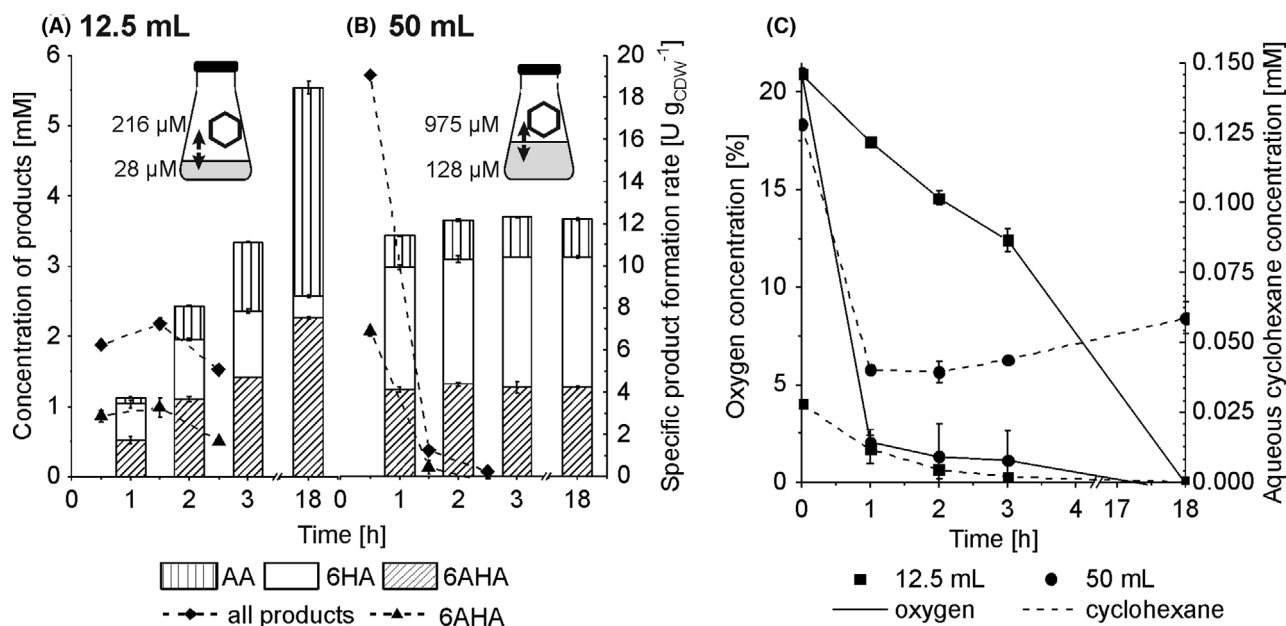


**Fig. 5.** Assessing the effect of O<sub>2</sub> and cyclohexane availability on by-product formation. Panels A and B show product concentrations accumulated after different reaction times (bars) and specific whole-cell activities over 3 h for 6AHA and overall product formation (curves). A 1:1 strain ratio was applied for the strain combination *P. taiwanensis*\_CL/*E. coli*\_CL with a total biomass concentration of 3.0 g l<sup>-1</sup> in 12.5 (A) or 50 ml (B) liquid volume in 250 ml screw-capped and closed flasks. The biotransformation was started by adding 5 mM cyclohexane (referred to the aqueous phase volume). Intermediates that are not depicted in the graphs accumulated to less than 50 μM. The schemes of the reaction flasks show the calculated initial cyclohexane concentrations (μM) in the aqueous and gas phases in equilibrium. Panel C shows the courses of oxygen concentrations in the gas phase (solid lines) and of aqueous cyclohexane concentrations (dashed lines). Means and error bars refer to two independent experiments. The average experimental errors over all measurements for specific product formation rates, 6HA concentrations, 6AHA concentrations, AA concentrations, oxygen concentrations and cyclohexane concentrations are 39.2%, 3.4%, 3.2%, 2.3%, 14.2% and 22.9% respectively.

resulting in a final conversion of 73% and a 6AHA yield of 35% (Fig. 5B). From these results, we conclude that O<sub>2</sub> limitation and host-intrinsic dehydrogenase activity can severely affect the 6AHA yield.

#### Overcoming oxygen limitation and tuning cyclohexane hydroxylation rate to maximize 6AHA yield

Based on the results obtained, we aimed to select one-pot reaction conditions that allow complete cyclohexane conversion and maximum 6AHA yield. For this purpose, oxygen limitation was overcome by using a low liquid reaction volume of 12.5 ml in a 250 ml flask, an intermediary total biomass concentration of 2 g<sub>CDW</sub> l<sup>-1</sup>, and the addition of pure oxygen into the flask whenever the head-space oxygen concentration dropped below 10% (Fig. 6A and C). Thereby, the low reaction volume with 5 mM cyclohexane (with respect to the liquid volume) also was chosen to establish low cyclohexane concentrations in the aqueous phase and thus minimize potential toxication effects. The results obtained so far indicated that high cyclohexane levels especially hampered lower cascade performance (Figs 3-5), which is well conceivable as it couples to the respiratory chain considered to be especially sensitive to solvent toxicity due to its location

in the cytoplasmic membrane (Buitelaar *et al.*, 1990; Uribe *et al.*, 1990; Vermuë *et al.*, 1993; Revilla *et al.*, 2007). At the chosen reaction conditions, cyclohexane was completely converted and, indeed, 6AHA was the main product with 82% yield (14% AA, 4% 6HA, Fig. 6A). The initial activity of 8.5 ± 0.5 U g<sub>CDW</sub><sup>-1</sup> for total product formation indicates that the upper cascade was substrate limited, whereas the lower cascade could sustain a similar activity of 7.7 ± 0.1 U g<sub>CDW</sub><sup>-1</sup>. These balanced rates of both cascade parts finally enabled the high 6AHA yield (Table 1). Additionally, we tested the conversion of 10 mM cyclohexane applying a total biomass concentration of 4 g<sub>CDW</sub> l<sup>-1</sup> in the same reaction set-up to evaluate the importance of synchronizing biomass and substrate concentration in the set-up chosen (Fig. S3). The initial specific activities for total product (9.7 ± 1.2 U g<sub>CDW</sub><sup>-1</sup>) and 6AHA (7.7 ± 0.1 U g<sub>CDW</sub><sup>-1</sup>) formation coincided with those obtained with 2 g<sub>CDW</sub> l<sup>-1</sup> and 5 mM cyclohexane (Table 1), resulting in 100% cyclohexane conversion and 86% 6AHA yield. Thereby, the higher substrate and biomass concentrations enabled a 2-fold increase in final 6AHA titre and volumetric productivity. Cyclohexane conversion and 6AHA yield obviously depend on substrate and biomass concentrations together with the avoidance of oxygen limitation.

## Evidence for an extended substrate scope

The potential of the constructed catalysts and the mixed-species set-up was further evaluated for cycloheptane as a biotransformation substrate. By applying similar reaction conditions as for cyclohexane, complete conversion of 5 mM cycloheptane was obtained (Fig. 6B, Table 1). The initial activity for total product formation amounted to  $8.5 \pm 0.1 \text{ U g}_{\text{CDW}}^{-1}$  and thus was comparable to the cyclohexane conversion activity obtained in the optimized set-up. After 18 h of biotransformation, 51% pimelic acid (PA), 48% 7-aminoheptanoic acid (7AHA) and 1% 7-hydroxyheptanoic acid (7HA) had accumulated (Fig. 6B). For the selected reaction conditions, the specific initial activity for 7AHA formation of  $3.5 \pm 0.1 \text{ U g}_{\text{CDW}}^{-1}$  was lower than that for 6AHA formation (Table 1). Further optimization of reaction conditions is necessary for maximizing the 7AHA yield. However, the productivity and final 7AHA titre could again be doubled by doubling cycloheptane and biocatalyst concentrations (Table 1, Fig. S3B and C). Overall, the results obtained with cycloheptane as substrate indicate the broad applicability of the constructed strains and mixed-species set-up.

## Discussion

In recent years, co-cultures have been applied to synthesize various compounds such as antibiotic building blocks (Zhang and Stephanopoulos, 2016), biofuels (Shin *et al.*, 2010), monoterpenoids (Willrodt *et al.*, 2015) or intermediates for polymer production (Zhang *et al.*, 2015; Wang *et al.*, 2020). In comparison with a single-species culture, the co-culture approaches are rationally designed to distribute the metabolic burden of long and complex biocatalytic pathways to different strains (Jones and Wang, 2018). However, the use of defined co-cultures requires the selection of compatible strains, easy access to shuttling compounds, and optimization of reaction conditions to achieve good biocatalytic performance.

## Selection of biocatalysts to establish a mixed-species approach

The ability of AlkJ to oxidize  $\omega$ -hydroxyacids and its tolerance towards the carboxylic acid moiety in 6HA were key findings in this work enabling the establishment of a more direct route for the transformation of cyclohexane to 6AHA compared previous studies (Sattler *et al.*,

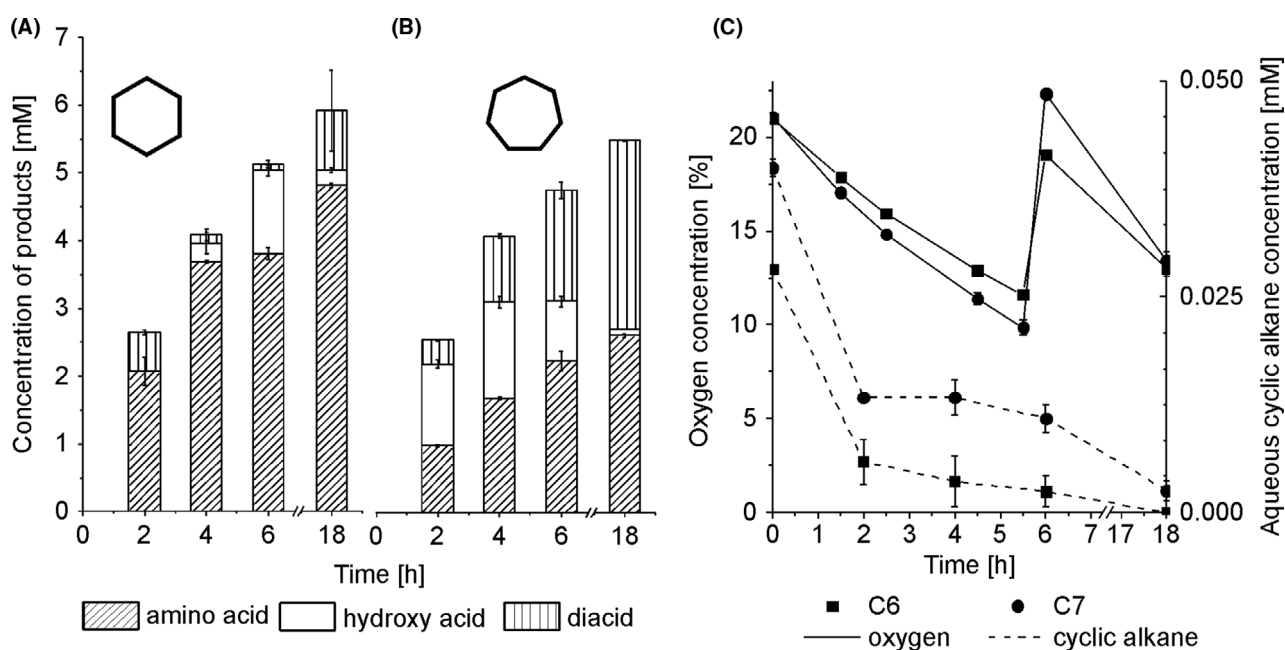


**Fig. 6.** Conversion of 5 mM cyclohexane (C6) or cycloheptane (C7) under optimized conditions. Panels A and B show product concentrations accumulated after different reaction times. A 1:1 strain ratio was applied for the strain combination *P. taiwanensis*\_CL/*E. coli*\_CL with a total biomass concentration of  $2.0 \text{ g l}^{-1}$  in 12.5 ml liquid volume in 250 ml screw-capped and closed flasks. Biotransformations were started by adding 5 mM of cyclohexane (A) or cycloheptane (B) (referred to the aqueous phase volume). Intermediates that are not depicted in the graphs accumulated to less than  $50 \mu\text{M}$ . Panel C shows the courses of oxygen concentrations in the gas phase (solid lines) and of aqueous cyclohexane concentrations (dashed lines). Means and error bars refer to two independent experiments. The average experimental errors over all measurements for 6HA concentrations, 6AHA concentrations, AA concentrations, 7-hydroxyheptanoic acid concentrations, 7-aminoheptanoic acid concentrations, pimelic acid concentrations, oxygen concentrations, cyclohexane concentrations and cycloheptane concentrations are 25.6%, 3.4%, 52.0%, 5.0%, 2.1%, 3.8%, 1.5%, 65.6% and 15.7% respectively.

**Table 1.** Selected reaction parameters for the conversion of cyclohexane and cycloheptane

Initial substrate concentration <sup>b</sup>	Cyclohexane <sup>a</sup>		Cycloheptane <sup>a</sup>	
	5 mM	10 mM	5 mM	10 mM
Final 6-AHA titre [g l <sup>-1</sup> ]	0.63 ± 0.01	1.25 ± 0.10	0.34 ± 0.01	0.61 ± 0.04
6AHA productivity [mM h <sup>-1</sup> ]	0.92 ± 0.01 (4 h)	1.85 ± 0.01 (4 h)	0.42 ± 0.01 (4 h)	0.66 ± 0.03 (4 h)
	0.27 ± 0.01 (18 h)	0.53 ± 0.04 (18 h)	0.15 ± 0.01 (18 h)	0.26 ± 0.02 (18 h)
Conversion [%]	100	100	100	100
Selectivity for 6AHA [%]	81.6 ± 7.7	85.8 ± 2.7	47.7 ± 0.1	49.2 ± 1.2
Total initial activity <sup>c</sup> [U g <sub>CDW</sub> <sup>-1</sup> ]	8.5 ± 0.5	9.7 ± 1.2	8.5 ± 0.1	7.0 ± 0.7
Initial 6AHA formation activity <sup>c</sup> [U g <sub>CDW</sub> <sup>-1</sup> ]	7.7 ± 0.1	7.7 ± 0.1	3.5 ± 0.1	2.7 ± 0.1

a. A strain ratio of 1:1 was applied for the strain combination *P. taiwanensis*\_CL/*E. coli*\_CL with a total biomass concentration of 2.0 g l<sup>-1</sup> (5 mM) or 4.0 g l<sup>-1</sup> (10 mM) in 12.5 ml liquid volume in 250 ml screw-capped and closed flasks. Biotransformations were started by adding 5 or 10 mM of cyclohexane or cycloheptane (referred to the aqueous phase volume). Means and errors refer to two independent experiments. The average experimental errors over all measurements for final 6AHA titres, 6AHA productivity, conversions, selectivities for 6AHA and initial activities are 4.1%, 2.8%, 0, 3.8% and 4.5% respectively.

b. Referred to in aqueous phase.

c. For 4 h.

2014). Although AlkJ originated from the *Pseudomonas* genus (van Beilen *et al.*, 2001) and can efficiently be synthesized in *E. coli* (Schrewe *et al.*, 2014; Ladkau *et al.*, 2016), recombinant expression of *alkJ* in *P. taiwanensis* VLB120 was not successful. On the other hand, employing *E. coli* for cyclohexane conversion was also not feasible, probably due to the high metabolic burden caused by the cytochrome P450 and Baeyer–Villiger monooxygenases. Even leaky expression of respective genes may have prevented successful transformation. For these enzymes, *E. coli* often does not constitute an optimal host organism (Biggs *et al.*, 2016; Jones and Wang, 2018). Reasons include cofactor demand (e.g. heme), uncoupling involving the formation of reactive oxygen species, and drainage of cellular resources (redox equivalents, building blocks). More fine-tuned gene expression appears to be required to solve issues hampering upper and lower pathway expression in *E. coli* and *P. taiwanensis*, respectively, and finally may enable the establishment of a single strain catalysing 6AHA production from cyclohexane. However, the approach to distribute this complex biocatalytic pathway among *P. taiwanensis* and *E. coli* proved to be suitable for efficient 6AHA synthesis from cyclohexane and allowed to overcome the issues encountered in the single-species approaches. A similar approach was successful for the production of oxygenated taxanes (Zhou *et al.*, 2015) and of ethanol from xylan (Shin *et al.*, 2010). Besides alleviation of metabolic burden, mixed-species/strain approaches can be employed to circumvent inhibitory effects of pathway intermediates (Martínez *et al.*, 2016), to meet cofactor and precursor requirements (Jones *et al.*, 2016), or simply to establish physical compartmentalization for the prevention of sideproduct formation (Chen *et al.*, 2017). Consequently, mixed-species cultures constitute a solid approach for the efficient

operation of otherwise inefficient complex pathways/cascades by exploiting the capacities of two or more strains.

#### Selection of appropriate shuttle compounds in a mixed-species approach

The export and subsequent import of a shuttle compound that connects the pathway between the different species is a prerequisite for the efficient operation of a mixed-species set-up. The transport of organic acids, alcohols, simple sugars, amino acids, certain flavonoids and alkaloids can be realized by the selection of appropriate microbes (Zhang and Wang, 2016). The inner and outer membranes of Gram-negative bacteria, such as *E. coli* and *P. taiwanensis*, represent barriers for the diffusion of hydrophilic and large hydrophobic compounds, respectively (Leive, 1974). In this study,  $\epsilon$ -CL and 6HA were investigated as possible shuttling compounds. Their small size (< 600 Da) allows them to pass the outer membrane by non-specific transmembrane pores (Denyer and Maillard, 2002; Nikaido, 2003). The inner membrane allows for passive diffusion of hydrophobic molecules but demands specific transport proteins for more hydrophilic compounds (Chen, 2007). 6HA is more polar than  $\epsilon$ -CL and charged at the applied pH, leading to hampered transport of 6HA, as only its protonated form diffuses at a reasonable rate through the cytoplasmic membrane. This slower diffusion as compared to the  $\epsilon$ -CL is reflected by the higher substrate concentration required for half-maximal activity (Fig. 2A and B). In certain cases, transporters such as AlkL, a hydrophobic outer membrane pore facilitating the passage of large hydrophobic molecules (Julsing *et al.*, 2012), ShiA as a transporter for 3-dehydroshikimic acid (Zhang *et al.*, 2015), or glycoside transporters (Shin *et al.*, 2010) are required to enhance the transfer over the cellular



membrane. The membrane transfer rate of pathway intermediates thus can constitute a major limitation for the performance of a mixed-species approach. A careful selection of the intermediate or strain can enhance conversion.

#### Optimization of reaction conditions to maximize product yield

Co-cultivation of different species in growth mode is challenging due to possibly fluctuating community structures caused by differing induction times and growth rates (Jones and Wang, 2018). Avoidance of growth by the omission of a growth substrate other than the energy source, for example the N-source, constitutes a more straightforward approach. The different species can be grown separately according to their specific requirements (e.g. induction time, temperature) and then combined in defined ratios in a resting cell format (Willrodt *et al.*, 2015; Martínez *et al.*, 2016). In this study, a closed reaction system was required to avoid the loss of the volatile substrate cyclohexane. Figure 7 gives a schematic overview on substrate mass transfer and reaction rates. Gas-liquid mass transfer rates for cyclohexane ( $m_1$ ) and  $O_2$  ( $m_2$ ) have a direct influence on  $r_1$ , the lumped rate of the three upper cascade reactions involving two oxygenases (Schäfer *et al.*, 2020), and  $r_3$ , the rate of AlkJ-catalysed 6HA oxidation, which is linked to the respiratory chain (Kirmair and Skerra, 2014). Furthermore, intrinsic dehydrogenases in both strains can convert 6-oxohexanoic acid into the by-product AA ( $r_5$ ,  $r_6$ ), thus minimizing 6AHA yield (Karande *et al.*, 2017; Schäfer *et al.*, 2020). Thereby,  $r_5$  in *P. taiwanensis* also involves dehydrogenase-catalysed 6HA oxidation. The challenge was to minimize 6HA accumulation and AA formation.

Optimization of reaction conditions led us to utilize a gas-liquid phase ratio of 23 with biomass and cyclohexane concentrations of  $2 \text{ g}_{\text{CDW}} \text{ l}^{-1}$  and 5 mM, respectively, as well as additional  $O_2$  supply to avoid limitations of  $r_1$  and  $r_3$  (Fig. 6A and C). Under these conditions,  $m_1$  governed overall cascade performance with the upstream cascade ( $r_1 = 1.02 \text{ mM h}^{-1}$  (all products considered, first 4 h of reaction)) operated under first-order kinetics (Table 1, Fig. 6A and C). The effect of  $m_2$  was minimized combining an appropriate biomass concentration with an  $O_2$  feed. Due to the very high activity of the lactonase, the 6HA formation rate always was equal to the rate of  $\epsilon$ -CL formation,  $r_1 = r_2$ . In set-ups only containing *E. coli*\_CL (Fig. 2C) or *P. taiwanensis*\_CL (Fig. S4), AA was formed at  $r_5 = 0.019$  or  $r_6 = 0.041 \text{ mM h}^{-1}$ , respectively (see Supporting Information, Section 3 for calculation details). However, within the first 4 h in the optimized mixed-species set-up (Fig. 6A), AA production rates ( $r_5 + r_6 = 0.03 \text{ mM h}^{-1}$ ) were well below the sum of

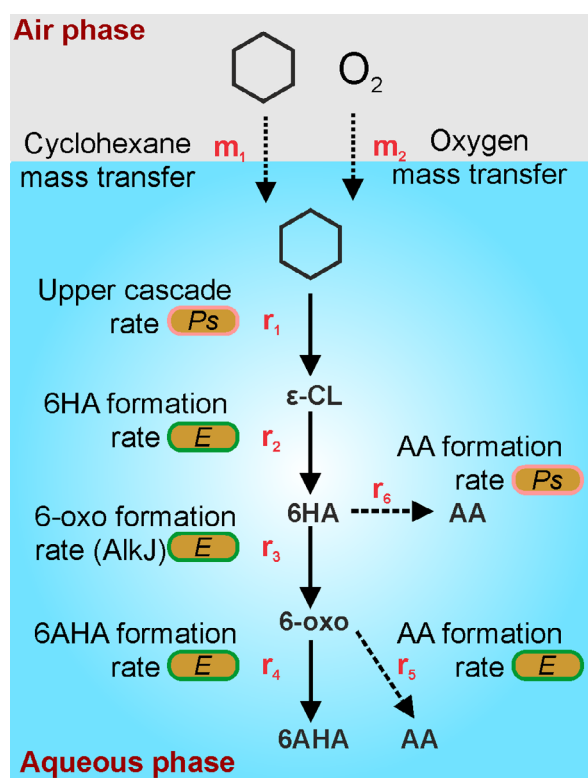


**Fig. 7.** Schematic representation of substrate mass transfer rates and cascade reaction rates in the mixed-species set-up designed in this study. The scheme refers to the consortium composed of *P. taiwanensis*\_CL (*Ps*) and *E. coli*\_CL (*E*).  $m_1$ , gas-liquid cyclohexane mass transfer;  $m_2$ , gas-liquid  $O_2$  mass transfer;  $r_1$ , upper cascade reaction rate lumping the three reactions catalysed by *P. taiwanensis*\_CL;  $r_2$ , rate of lactonase-catalysed  $\epsilon$ -CL hydrolysis;  $r_3$ , rate of AlkJ-catalysed 6HA oxidation;  $r_4$ , rate of transaminase-catalysed 6AHA formation;  $r_5$ , rate of dehydrogenase-catalysed AA formation in *E. coli*\_CL;  $r_6$ , rate of dehydrogenase-catalysed AA formation in *P. taiwanensis*\_CL. If  $m_1 < r_{1,\text{max}}$ , the cascade performance is governed by cyclohexane mass transfer (substrate limitation). If  $m_2 < 2r_{1,\text{max}} + r_{3,\text{max}}$ ,  $O_2$  mass transfer becomes limiting. The high lactonase activity available led to  $r_1 = r_2$ .  $r_2 > r_3$  leads to 6HA accumulation and possibly AA formation via  $r_6$ .  $r_3 > r_4$  can lead to AA formation via  $r_5$ .  $r_1 = r_2 = r_3 = r_4$  enables high 6AHA yield.

these rates. Thereby,  $r_6$  may have been limited by 6HA availability/uptake. The volumetric 6AHA formation rate  $r_4$  reached  $0.92 \text{ mM h}^{-1}$  (Table 1), which almost equalled  $r_3 = 0.92 - 0.95 \text{ mM h}^{-1}$ , and thus enabled 100% cyclohexane conversion and 82% selectivity for 6AHA formation within 18 h. The step-wise assessment of crucial reaction parameters and their optimization allowed full cyclohexane conversion, which was not achieved previously (Wang *et al.*, 2020). In comparison with the biological process, a one-step chemical process using Mn/AIVPO resulted in 9.8% of cyclohexane conversion and 72.9% of selectivity to  $\epsilon$ -caprolactam (You *et al.*, 2008).

Substrate limitation was selected in this study to minimize inhibition/toxication by cyclohexane and to avoid extensive 6HA accumulation. In the experiment shown in

Fig. 5A, the lower cascade did not reach its maximum rate and could not keep up with the upper cascade, although  $O_2$  was not limiting and the necessary cyclohexane limitation was in place (Fig. 5C). This may be due to the different cyclohexane : biomass ratio applied ( $1.67 \text{ mmol g}_{CDW}^{-1}$ ) compared to the experiments shown in Fig. 6 ( $2.5 \text{ mmol g}_{CDW}^{-1}$ , applied at two different concentration levels). This effect of the cyclohexane : biomass ratio and a possible interconnection with TA instability as indicated by AA accumulation (Fig. 5A) remain to be further investigated.

The low aqueous cyclohexane concentrations in the optimized set-up also can be considered beneficial regarding biocatalyst stability. With a logP of 3.44, cyclohexane is expected to cause membrane disintegration at a concentration above 0.6 mM (Sikkema *et al.*, 1994) and, already at lower concentrations, can have effects on membrane fluidity, electron transduction, and, consequently, reactions connected to metabolism (Sikkema *et al.*, 1994). Thus, cyclohexane can affect  $r_1$  (via redox metabolism),  $r_3$  (via electron transport chain),  $r_4$  (via alanine uptake and regeneration) and  $r_5/r_6$  (via redox metabolism). The establishment of an appropriate feeding regime will be crucial for future reaction engineering and scale up.

Further optimization may include strain ratio variation to equilibrate the rates of upstream and downstream cascades as demonstrated by Wang *et al.* (2020). The system presented here has been optimized regarding cyclohexane conversion and 6AHA yield and not specific activity. A higher *E. coli*\_CL share can be considered promising to limit 6HA accumulation but has been tested without success (Fig. S2). However,  $O_2$  depletion kinetics (Figs 4 and 5) indicate that cells were  $O_2$ -limited at the high cell concentration and low gas : liquid phase ratio applied in the respective experiment. Thus, strain ratio variation should be combined with a strategy to overcome  $O_2$  limitation. Further, suppression of AA formation can be targeted via the knockout of 6-oxohexanoic acid oxidation catalysing dehydrogenases in both strains.

7AHA could be synthesized from cycloheptane by the same enzymes and mixed-species set-up, although the titre achieved was 2-fold lower than that obtained for 6AHA, going along with stronger overoxidation to PA. It is known that AlkJ also converts longer-chain substrates such as 12-oxododecanoic acid methyl ester with high activity (Schrewe *et al.*, 2014). Thus, competition among TA and host dehydrogenases for 7-oxoheptanoic acid may be critical. In a previous study, it has been shown that the *C. violaceum* TA prefers small aliphatic and aromatic molecules (e.g. glyoxylate, butanal, benzaldehyde, phenylacetaldehyde) (Kaulmann *et al.*, 2007). Hence, TA affinity for 7-oxoheptanoic acid constitutes a promising

target to optimize the 7AHA yield, with enzyme engineering and screening of alternative TAs as possible approaches (Guo and Berglund, 2017).

## Conclusion and future perspectives

This is the first study that demonstrates a one-pot biocatalytic synthesis of 6AHA and 7AHA from cycloalkanes with 100% conversion and high selectivities (86% and 49% respectively), which outcompete the one-pot chemical process with yields below 10% (You *et al.*, 2008). Due to coexpression issues for the 8 genes required, the cascade was apportioned among *P. taiwanensis* and *E. coli*. As a shuttle compound,  $\epsilon$ -CL turned out feasible as it readily diffuses through cell membranes enabling high 6AHA production rates. In shake flasks, the interplay between the cyclohexane and  $O_2$  mass transfer and respective reaction rates was found to be critical for attaining a high 6AHA yield. Respective optimization of reaction conditions finally enabled the complete conversion of 10 mM cyclohexane with 86% 6AHA yield. For the technical scale, sophisticated feeding regimes and reaction engineering are prone to facilitate the balancing of oxygen and cyclohexane mass transfer and conversion rates. Suitable concepts include two-liquid phase systems (Kuhn *et al.*, 2012) or a feed of cyclohexane-saturated air. Furthermore, the mixed-species phototrophic biofilm concept enabling continuous photosynthetic  $O_2$  supply and operation at high cell densities (Hoschek *et al.*, 2019) may be adapted for 6AHA production from cyclohexane. Besides the *in situ* oxygen supply, the utilization of light as the energy source and water as the electron source enabling redox cofactor regeneration constitutes another possible advantage of this approach, when cascade parts are implemented in phototrophic microbes.

## Experimental procedures

### Chemicals and media

Adipic acid was purchased from AppliChem (Darmstadt, Germany), 7-aminoheptanoic acid from chemPUR (Karlsruhe, Germany). 6-hydroxyhexanoic acid, 7-hydroxyheptanoic acid and cycloheptane were acquired from abcr (Karlsruhe, Germany). All other chemicals used in this study were obtained from Carl Roth GmbH + Co KG (Karlsruhe, Germany), Merck KGaA (Darmstadt, Germany) and Sigma Aldrich (Steinheim, Germany) in the highest purity available. Cells were grown in lysogeny broth medium (Sambrook and Russell, 2001) or M9\* medium (Panke *et al.*, 1999) with a pH of 7.2 supplemented with 0.5% (w/v) glucose as sole carbon source. Thiamine ( $10 \text{ mg l}^{-1}$ ), kanamycin ( $50 \text{ } \mu\text{g ml}^{-1}$ ) and chloramphenicol ( $35 \text{ } \mu\text{g ml}^{-1}$ ) were added when appropriate.

### Strains, plasmids and molecular biology methods

The used strains and plasmids are listed in Table S1. *E. coli* JM101 and *P. taiwanensis* VLB120 were used for biotransformation studies and *E. coli* DH5 $\alpha$  for cloning purposes. The preparation of electrocompetent *Pseudomonas* and *E. coli* cells was performed as described earlier (Sambrook and Russell, 2001; Choi and Schweizer, 2006), and the vectors were introduced by electroporation (2500 V; Eppendorf Eporator<sup>®</sup>, Hamburg, Germany). DNA manipulation methods and agarose gel electrophoresis were performed as described by Sambrook and Russell (2001). Enzymes (Phusion High-Fidelity Polymerase, T5 exonuclease, Taq ligase, restriction enzymes, Fast Alkaline Phosphatase) and buffers were purchased from Thermo Scientific Molecular Biology (St. Leon-Rot, Germany) or New England Biolabs (Frankfurt/Main, Germany) and oligonucleotides from Eurofins Genomics (Ebersberg, Germany). Plasmids were isolated using the peqGOLD Plasmid Miniprep Kit I from peqLab (Erlangen, Germany) and purified via NucleoSpin Gel and PCR Clean-up from Macherey–Nagel (Düren, Germany) according to supplier protocols. The Gibson Master Mix was prepared according to (Gibson *et al.*, 2009). For detailed information, see Supporting Information (Section 1, Table S2).

### Growth of bacterial cultures

Cultivations were carried out at 30°C and 200 rpm in a Multitron shaker (Infors, Bottmingen, Switzerland). Microorganisms were cultivated in an LB pre-culture for ~ 20 h, from which an M9\* pre-culture (1% v/v) was inoculated and incubated for another 12–16 h. This pre-culture was used to inoculate an M9\* main culture at a starting OD of 0.2. Heterologous gene expression was induced with 1 mM isopropyl  $\beta$ -D-1-thiogalactopyranoside (IPTG) for *P. taiwanensis* strains or 1 mM IPTG and 0.025% (v/v) (0.22 mM) dicyclopropyl ketone (DCPK) for *E. coli* strains when the cultures reached an OD of ~ 0.5. Incubation was continued for another 5 h until cells were harvested for the biotransformation experiments.

### Biotransformation experiments

*E. coli* (pJ10, pAlaDTA) (*E. coli*\_CL), *E. coli* (pJ10Lact, pAlaDTA) (*E. coli*\_6HA), *P. taiwanensis* VLB120 (pSEVA\_CL\_2) (*P. taiwanensis*\_CL), and *P. taiwanensis* VLB120 (pSEVA\_6HA\_2) (*P. taiwanensis*\_6HA) were cultivated as described above. The cells were harvested by centrifugation (10 min, 3,214 g, room temperature) and resuspended in 100 mM potassium phosphate buffer (pH 7.4) supplemented with 1% (w/v) glucose and

50 mM L-alanine (reaction buffer) and thereby combined at different cell densities and strain ratios. The biotransformation assay was conducted in 100 or 250 ml screw-capped baffled Erlenmeyer flasks (total volumes of 123 ml and 300 ml respectively). The cell suspensions (volumes indicated in Table S3) were adapted for 10 min in a rotary incubator (30°C, 200 rpm). Biotransformation was initiated by adding pure substrate (cyclohexane, cycloheptane) to the concentration indicated in the text. The flask threads were wrapped with PTFE tape, and the lid contained a two-layered septum with Teflon facing the inner side of the flask and silicone facing outwards. A total of 1.5 ml samples were taken with a syringe at different time intervals. One ml sample was extracted with 0.5 ml ice-cold diethyl ether containing 0.2 mM n-decane as an internal standard. After 2 min extraction by vortexing and centrifugation, the organic phase was dried over water-free Na<sub>2</sub>SO<sub>4</sub> before it was transferred to a GC vial for analysis. The rest of the samples was centrifuged (4°C, 10 min, 17,000 g), and the supernatant was stored for HPLC analysis. Gas-phase samples (100  $\mu$ l) were taken from the flask using a gas-tight syringe (Hamilton, Reno, NV, USA). The activity is given in U g<sub>CDW</sub><sup>-1</sup> (units per gram cell dry weight), where 1 U corresponds to 1  $\mu$ mol product formed within 1 min reaction time. For specifications of biotransformation, set-ups refer to Table S3 in the Supporting Information. For analytical methods refer to Section 2 in the Supporting Information.

### Acknowledgements

We acknowledge the use of the facilities of the Centre for Biocatalysis (MiKat) at the Helmholtz Centre for Environmental Research, which is supported by European Regional Development Funds (EFRE, Europe funds Saxony) and the Helmholtz Association. LB and RK were funded by the ERA-IB-Project PolyBugs ID:16006 and the Sächsisches Ministerium für Wissenschaft und Kunst (SMWK) Project ID: 100318259. The authors would like to thank Prof. Dr. Andreas Schmid for helpful discussions and Dr. Monika Möder and Steffi Schrader from the Department of Analytical Chemistry, Helmholtz Centre for Environmental Research – UFZ, for the help with HPLC-MS/MS.

### Conflict of interest

None declared.

### Funding information

We acknowledge the use of the facilities of the Centre for Biocatalysis (MiKat) at the Helmholtz Centre for

Environmental Research, which is supported by European Regional Development Funds (EFRE, Europe funds Saxony) and the Helmholtz Association. LB and RK were funded by the ERA-IB-Project PolyBugs ID: 16006 and the Sächsisches Ministerium für Wissenschaft und Kunst (SMWK) Project ID: 100318259.

## References

- BASF. (2020). *products & markets* [WWW document]. [http://www2.BASF.us/businesses/plasticportal/products\\_and\\_markets.htm](http://www2.BASF.us/businesses/plasticportal/products_and_markets.htm).
- Bellussi, G., and Perego, C. (2000) Industrial catalytic aspects of the synthesis of monomers for nylon production. *Cattech* **4**: 4–16.
- Biggs, B.W., Lim, C.G., Sagliani, K., Shankar, S., Stephanopoulos, G., De Mey, M., and Ajikumar, P.K. (2016) Overcoming heterologous protein interdependency to optimize P450-mediated Taxol precursor synthesis in *Escherichia coli*. *PNAS* **113**: 3209–3214.
- Buitelaar, R., Vermue, M., Schlatmann, J., and Tramper, J. (1990) The influence of various organic solvents on the respiration of free and immobilized cells of *Tagetes minuta*. *Biotechnol Tech* **4**: 415–418.
- Chen, R.R. (2007) Permeability issues in whole-cell bioprocesses and cellular membrane engineering. *Appl Microbiol Biotechnol* **74**: 730–738.
- Chen, Z., Sun, X., Li, Y., Yan, Y., and Yuan, Q. (2017) Metabolic engineering of *Escherichia coli* for microbial synthesis of monolignols. *Metab Eng* **39**: 102–109.
- Choi, K.-H., and Schweizer, H.P. (2006) mini-Tn7 insertion in bacteria with single *attTn7* sites: example *Pseudomonas aeruginosa*. *Nat Protoc* **1**: 153–161.
- National Center for Biotechnology Information (2020). *Compound Summary: Cyclohexane* [WWW document]. URL <https://pubchem.ncbi.nlm.nih.gov/compound/Cyclohexane>.
- Denyer, S.P., and Maillard, J.Y. (2002) Cellular impermeability and uptake of biocides and antibiotics in Gram-negative bacteria. *J Appl Microbiol* **92**: 35S–45S.
- Duetz, W.A., Van Beilen, J.B., and Witholt, B. (2001) Using proteins in their natural environment: potential and limitations of microbial whole-cell hydroxylations in applied biocatalysis. *Curr Opin Biotechnol* **12**: 419–425.
- Feron, V., Til, H., De Vrijer, F., Woutersen, R., Cassee, F., and Van Bladeren, P. (1991) Aldehydes: occurrence, carcinogenic potential, mechanism of action and risk assessment. *Mutat Res Genet Toxicol* **259**: 363–385.
- Fischer, J., Lange, T., Boehling, R., Rehfinger, A., and Klemm, E. (2010) Uncatalyzed selective oxidation of liquid cyclohexane with air in a microcapillary reactor. *Chem Eng Sci* **65**: 4866–4872.
- Gibson, D.G., Young, L., Chuang, R.-Y., Venter, J.C., Hutchison, C.A., and Smith, H.O. (2009) Enzymatic assembly of DNA molecules up to several hundred kilobases. *Nat Methods* **6**: 343–345.
- Guo, F., and Berglund, P. (2017) Transaminase biocatalysis: optimization and application. *Green Chem* **19**: 333–360.
- Hoschek, A., Heuschkel, I., Schmid, A., Bühler, B., Karande, R., and Bühler, K. (2019) Mixed-species biofilms for high-cell-density application of *Synechocystis* sp. PCC 6803 in capillary reactors for continuous cyclohexane oxidation to cyclohexanol. *Bioresour Technol* **282**: 171–178.
- Jeschek, M., Gerngross, D., and Panke, S. (2017) Combinatorial pathway optimization for streamlined metabolic engineering. *Curr Opin Biotechnol* **47**: 142–151.
- Jones, J.A., Vernacchio, V.R., Sinkoe, A.L., Collins, S.M., Ibrahim, M.H.A., Lachance, D.M., *et al.* (2016) Experimental and computational optimization of an *Escherichia coli* co-culture for the efficient production of flavonoids. *Metab Eng* **35**: 55–63.
- Jones, J.A., and Wang, X. (2018) Use of bacterial co-cultures for the efficient production of chemicals. *Curr Opin Biotechnol* **53**: 33–38.
- Julsing, M.K., Schrewe, M., Cornelissen, S., Hermann, I., Schmid, A., and Bühler, B. (2012) Outer membrane protein AlkL boosts biocatalytic oxyfunctionalization of hydrophobic substrates in *Escherichia coli*. *Appl Environ Microbiol* **78**: 5724–5733.
- Karande, R., Salamanca, D., Schmid, A., and Buehler, K. (2017) Biocatalytic conversion of cycloalkanes to lactones using an in-vivo cascade in *Pseudomonas taiwanensis* VLB120. *Biotechnol Bioeng* **115**: 312–320.
- Kaulmann, U., Smithies, K., Smith, M.E., Hailes, H.C., and Ward, J.M. (2007) Substrate spectrum of  $\omega$ -transaminase from *Chromobacterium violaceum* DSM30191 and its potential for biocatalysis. *Enzyme Microb Technol* **41**: 628–637.
- Kirmair, L., and Skerra, A. (2014) Biochemical analysis of recombinant AlkJ from *Pseudomonas putida* reveals a membrane-associated, flavin adenine dinucleotide-dependent dehydrogenase suitable for the biosynthetic production of aliphatic aldehydes. *Appl Environ Microbiol* **80**: 2468–2477.
- Kuhn, D., Julsing, M.K., Heinzle, E., and Bühler, B. (2012) Systematic optimization of a biocatalytic two-liquid phase oxyfunctionalization process guided by ecological and economic assessment. *Green Chem* **14**: 645–653.
- Ladkau, N., Assmann, M., Schrewe, M., Julsing, M. K., Schmid, A., and Bühler, B. (2016) Efficient production of the Nylon 12 monomer  $\omega$ -aminododecanoic acid methyl ester from renewable dodecanoic acid methyl ester with engineered *Escherichia coli*. *Metab Eng* **36**: 1–9.
- Ladkau, N., Schmid, A., and Bühler, B. (2014) The microbial cell—functional unit for energy dependent multistep biocatalysis. *Curr Opin Biotechnol* **30**: 178–189.
- Leak, D.J., Sheldon, R.A., Woodley, J.M., and Adlercreutz, P. (2009) Biocatalysts for selective introduction of oxygen. *Biocatal Biotransformation* **27**: 1–26.
- Leive, L. (1974) The barrier function of the Gram-negative envelope. *Ann N Y Acad Sci* **235**: 109–129.
- Martínez, I., Mohamed, M.E.-S., Rozas, D., García, J.L., and Díaz, E. (2016) Engineering synthetic bacterial consortia for enhanced desulfurization and revalorization of oil sulfur compounds. *Metab Eng* **35**: 46–54.
- Moody, V., and Needles, H.L. (2004) 3 - Major fibers and their properties. In *Tufted Carpet: Textile Fibers, Dyes, Finishes, and Processes*. Moody, V., and Needles, H.L. (eds). Norwich: William Andrew Publishing, pp. 35–59.
- Muschiol, J., Peters, C., Oberleitner, N., Mihovilovic, M.D., Bornscheuer, U.T., and Rudroff, F. (2015) Cascade

- catalysis—strategies and challenges *en route* to preparative synthetic biology. *ChemComm* **51**: 5798–5811.
- Nikaido, H. (2003) Molecular basis of bacterial outer membrane permeability revisited. *Microbiol Mol Biol Rev* **67**: 593–656.
- Panke, S., Meyer, A., Huber, C.M., Witholt, B., and Wubolts, M.G. (1999) An alkane-responsive expression system for the production of fine chemicals. *Appl Environ Microbiol* **65**: 2324–2332.
- Revilla, A.S., Pestana, C.R., Pardo-Andreu, G.L., Santos, A.C., Uyemura, S.A., Gonzales, M.E., and Curti, C. (2007) Potential toxicity of toluene and xylene evoked by mitochondrial uncoupling. *Toxicol In Vitro* **21**: 782–788.
- Ritz, J., Fuchs, H., Kieczka, H., and Moran, W.C. (1986) Caprolactam. In *Ullmann's Encyclopedia of Industrial Chemistry*. Gerhartz, W. (ed). Weinheim: Wiley-VCH, pp. 31–50.
- Rudroff, F. (2019) Whole-cell based synthetic enzyme cascades—light and shadow of a promising technology. *Curr Opin Chem Biol* **49**: 84–90.
- Sambrook, J., and Russell, D. W. (2001) *Molecular Cloning: A Laboratory Manual*. Cold Spring Harbor, NY: Cold Spring Harbor Laboratory.
- Sattler, J.H., Fuchs, M., Mutti, F.G., Grischek, B., Engel, P., Pfeffer, J., *et al.* (2014) Introducing an in situ capping strategy in systems biocatalysis to access 6-aminohexanoic acid. *Angew Chem Int Ed* **53**: 14153–14157.
- Schäfer, L., Bühler, K., Karande, R., and Bühler, B. (2020) Rational engineering of a multi-step biocatalytic cascade for the conversion of cyclohexane to polycaprolactone monomers in *Pseudomonas taiwanensis*. *Biotechnol J* **15**: 2000091.
- Schrewe, M., Julsing, M.K., Bühler, B., and Schmid, A. (2013) Whole-cell biocatalysis for selective and productive C-O functional group introduction and modification. *Chem Soc Rev* **42**: 6346–6377.
- Schrewe, M., Julsing, M.K., Lange, K., Czarnotta, E., Schmid, A., and Bühler, B. (2014) Reaction and catalyst engineering to exploit kinetically controlled whole-cell multistep biocatalysis for terminal FAME oxyfunctionalization. *Biotechnol Bioeng* **111**: 1820–1830.
- Shin, H.-D., McClendon, S., Vo, T., and Chen, R.R. (2010) *Escherichia coli* binary culture engineered for direct fermentation of hemicellulose to a biofuel. *Appl Environ Microbiol* **76**: 8150–8159.
- Sikkema, J., de Bont, J.A., and Poolman, B. (1994) Interactions of cyclic hydrocarbons with biological membranes. *J Biol Chem* **269**: 8022–8028.
- Silva-Rocha, R., Martínez-García, E., Calles, B., Chavarría, M., Arce-Rodríguez, A., de las Heras, A., *et al.* (2013) The Standard European Vector Architecture (SEVA): a coherent platform for the analysis and deployment of complex prokaryotic phenotypes. *Nucleic Acids Res* **41**: D666–D675.
- Uribe, S., Rangel, P., Espínola, G., and Aguirre, G. (1990) Effects of cyclohexane, an industrial solvent, on the yeast *Saccharomyces cerevisiae* and on isolated yeast mitochondria. *Appl Environ Microbiol* **56**: 2114–2119.
- van Beilen, J.B., Kingma, J., and Witholt, B. (1994) Substrate specificity of the alkane hydroxylase system of *Pseudomonas oleovorans* GPo1. *Enzyme Microb Technol* **16**: 904–911.
- van Beilen, J.B., Panke, S., Lucchini, S., Franchini, A.G., Röthlisberger, M., and Witholt, B. (2001) Analysis of *Pseudomonas putida* alkane-degradation gene clusters and flanking insertion sequences: evolution and regulation of the *alk* genes. *Microbiology* **147**: 1621–1630.
- Vermuë, M., Sikkema, J., Verheul, A., Bakker, R., and Tramper, J. (1993) Toxicity of homologous series of organic solvents for the gram-positive bacteria *Arthrobacter* and *Nocardia* Sp. and the gram-negative bacteria *Acinetobacter* and *Pseudomonas* Sp. *Biotechnol Bioeng* **42**: 747–758.
- Walton, A.Z., and Stewart, J.D. (2004) Understanding and improving NADPH-dependent reactions by nongrowing *Escherichia coli* cells. *Biotechnol Prog* **20**: 403–411.
- Wang, F., Zhao, J., Li, Q., Yang, J., Li, R., Min, J., *et al.* (2020) One-pot biocatalytic route from cycloalkanes to  $\alpha$ ,  $\omega$ -dicarboxylic acids by designed *Escherichia coli* consortia. *Nat Commun* **11**: 1–10.
- Weisssermel, K., and Arpe, H.-J. (2008) *Industrial Organic Chemistry*. Hoboken, NJ: John Wiley & Sons, p. 511.
- Wierckx, N., Koopman, F., Ruijsenaars, H.J., and de Winde, J.H. (2011) Microbial degradation of furanic compounds: biochemistry, genetics, and impact. *Appl Microbiol Biotechnol* **92**: 1095–1105.
- Willrodt, C., Hoschek, A., Bühler, B., Schmid, A., and Julsing, M.K. (2015) Coupling limonene formation and oxyfunctionalization by mixed-culture resting cell fermentation. *Biotechnol Bioeng* **112**: 1738–1750.
- Wittcoff, H.A., Reuben, B.G., and Plotkin, J.S. (2012) *Industrial Organic Chemicals*. Hoboken, NJ: John Wiley & Sons.
- You, K., Mao, L., Chen, L., Yin, D., Liu, P., and Luo, H.A. (2008) One-step synthesis of  $\epsilon$ -caprolactam from cyclohexane and nitrosyl sulfuric acid catalyzed by VPO supported transition metal composites. *Catal Commun* **9**: 2136–2139.
- Zhang, H., Li, Z., Pereira, B., and Stephanopoulos, G. (2015) Engineering *E. coli*-*E. coli* cocultures for production of muconic acid from glycerol. *Microb Cell Fact* **14**: 134.
- Zhang, H., and Stephanopoulos, G. (2016) Co-culture engineering for microbial biosynthesis of 3-amino-benzoic acid in *Escherichia coli*. *Biotechnol J* **11**: 981–987.
- Zhang, H., and Wang, X. (2016) Modular co-culture engineering, a new approach for metabolic engineering. *Metab Eng* **37**: 114–121.
- Zhou, K., Qiao, K., Edgar, S., and Stephanopoulos, G. (2015) Distributing a metabolic pathway among a microbial consortium enhances production of natural products. *Nat Biotechnol* **33**: 377.

### Supporting information

Additional supporting information may be found online in the Supporting Information section at the end of the article.

**Fig. S1.** Oxygen measurement by GC. The panels show the GC chromatograms for a sample of 100% nitrogen (A) and air (B).

**Fig. S2.** Application of *P. taiwanensis* and *E. coli* strains at a lower strain ratio. The panels show the product concentrations accumulated after different reaction times (bars) and specific whole-cell activities over 3 h for 6AHA and overall product formation (curves). For the strain combinations *P. taiwanensis*\_CL/*E. coli*\_CL (A) and *P. taiwanensis*\_6HA/*E. coli*\_6HA (B), biotransformations were performed with biomass concentrations of 1.5 and 4 gCDW l<sup>-1</sup>. *P. taiwanensis* and *E. coli* strains, respectively, in 25 ml liquid volume in closed screw-capped 250 ml flasks and were started by adding 5 mM cyclohexane (referred to the aqueous phase volume). Intermediate concentrations not depicted in the graphs remained below 50 μM. Means and error bars refer to two independent experiments. The average experimental errors over all measurements for specific product formation rates, 6HA concentrations, 6AHA concentrations, and AA concentrations are 6.6%, 5.7%, 4.9%, and 20.0%, respectively.

**Fig. S3.** Conversion of 10 mM cyclohexane (A) or cycloheptane (B) under optimized conditions. Panels A and B show product concentrations accumulated after different reaction times. A 1:1 strain ratio was applied for the strain combination *P. taiwanensis*\_CL/*E. coli*\_CL with a total biomass concentration of 4.0 g l<sup>-1</sup> in 12.5 ml liquid volume in 250 ml screw-capped and closed flasks. Biotransformations were

started by adding 10 mM of cycloalkanes (referred to the aqueous phase volume). Intermediates that are not depicted in the graphs accumulated to less than 50 μM. Panel C shows the courses of oxygen concentrations in the gas phase (solid lines) and of aqueous cyclohexane (C6) and cycloheptane (C7) concentrations (dashed lines). Means and error bars refer to two independent experiments. The average experimental errors over all measurements for 6HA concentrations, 6AHA concentrations, AA concentrations, 7-hydroxyheptanoic acid concentrations, 7-aminoheptanoic acid concentrations, pimelic acid concentrations, oxygen concentrations, cyclohexane concentrations, and cycloheptane concentrations are 67.1, 6.2%, 3.8%, 26.9%, 9.9%, 17.6%, 3.3%, 26.2%, and 12.0%, respectively.

**Fig. S4.** Conversion of 6HA to AA by *P. taiwanensis* VLB120. Growing cells were inoculated in M9\* medium at an OD450 of 0.2. After 2 h of growth (OD450 ~ 0.4, time point 0 h), 1 mM (squares) or 5 mM (triangles) 6HA was added and growth (dashed lines) as well as AA formation (solid lines) were recorded. Means and error bars refer to two independent experiments. The average experimental errors over all measurements for the AA concentration and OD450 are 6.7% and 2.7%, respectively. over all measurements for the AA concentration and OD450 are 6.7% and 2.7%, respectively.

**Table S1.** Strains and plasmids used in this study.

**Table S2.** Primers used for cloning.

**Table S3.** Specifications for biotransformation experiments.

## Supporting Information

# One-pot synthesis of 6-aminohexanoic acid from cyclohexane using mixed-species cultures

### Table of Contents

1	Plasmid constructions .....	2
2	Analytical methods .....	3
3	Calculation of $r_5$ and $r_6$ in single species setups.....	5
4	Supplementary Tables.....	6
5	Supplementary Figures .....	9
6	References.....	13

## 1 Plasmid constructions

The strains and plasmids used in this study are listed in Table S1. The primers used for plasmid constructions are listed in Table S2.

### 1.1 Construction of pJ10Lact

The lactonase gene originates from *Acidovorax* sp. CHX100 and belongs to the same gene cluster as the cyclohexanol dehydrogenase and cyclohexanone monooxygenase genes. It consists of 903 bp. The gene sequence has been published before (Schäfer *et al.*, 2020).

*Acidovorax* sp. CHX100 was cultivated for 4 days in nutrient broth (NB) medium (Sambrook *et al.*, 2001) for DNA isolation performed with the peqLab GOLD kit for genomic DNA isolation. The lactonase gene was amplified with primers PLS019 and PLS020 and purified via agarose gel extraction (969 bp). pJ10 (Schrewe *et al.*, 2013) was digested with Sall and purified. The fragments were fused via Gibson Assembly (Gibson *et al.*, 2009) to yield pJ10Lact.

### 1.2 Construction of pSEVA244\_T\_AlkJ\_TA\_AlaD

The AlkJ gene was amplified from pJ10 (Schrewe *et al.*, 2014) with the primers PLS034 and PLS035 and fused to XmaJI-digested pSEVA244\_T (Schäfer *et al.*, 2020) via Gibson Assembly yielding pSEVA\_244\_T\_AlkJ. The TA gene was amplified from pAlaDTA (Ladkau *et al.*, 2016) with primers PLS039 and PLS040 and fused to BamHI-digested pSEVA\_244\_T\_AlkJ yielding pSEVA\_244\_T\_AlkJ\_TA. The AlaD gene was amplified from pAlaDTA (Ladkau *et al.*, 2016) with primers PLS041 and PLS042 and fused to HindIII-digested pSEVA\_244\_T\_AlkJ\_TA yielding pSEVA\_244\_T\_AlkJ\_TA\_AlaD.

### 1.3 Construction of pSEVA634\_T\_AlkJ\_TA and pSEVA634\_T\_AlkJ\_TA\_AlaD.

Gm<sup>R</sup> and pBBR1 origin of replication were amplified from pSEVA6311::DGC-244 using the primers PLS045A and PLS051. The *lac*-regulatory system (*lac*<sup>R</sup>-*P<sub>trc</sub>*) with AlkJ and TA or AlkJ, TA, and AlaD genes was amplified with primers PLS052 and PLS053 from pSEVA244\_T\_AlkJ\_TA or pSEVA244\_T\_AlkJ\_TA\_AlaD, respectively. Both fragments were assembled yielding pSEVA634\_T\_AlkJ\_TA or pSEVA634\_T\_AlkJ\_TA\_AlaD.



## 2 Analytical methods

Suspended biomass concentrations were determined by measuring the optical density at a wavelength of 450 nm using a Libra S11 spectrophotometer (Biochrom, Cambridge, UK). One OD<sub>450</sub> unit corresponds to 0.186 g<sub>CDW</sub> L<sup>-1</sup> for *P. taiwanensis* (Halan *et al.*, 2010) and 0.166 g<sub>CDW</sub> L<sup>-1</sup> for *E. coli* JM101 (Lindmeyer *et al.*, 2015).

Concentrations of cyclohexane, cycloheptane, cyclohexanol, cyclohexanone, and ε-CL were measured by GC (Trace 1310, Thermo Scientific, Waltham, MA) equipped with a flame ionization detector and a TR-5MS GC Column (dimensions: 15m length, 0.25 mm inner diameter (Thermo Scientific) with molecular nitrogen as carrier gas, 1 µl injection volume, and a split ratio of 7. The temperature profile applied was as follows: 40°C (1 min), 40–80°C (10°C min<sup>-1</sup>), 80–320°C (100°C min<sup>-1</sup>), 320°C (5.6 min). Products were quantified based on calibration curves established with commercially available standards.

Concentrations of 6-hydroxyhexanoic acid and adipic acid were quantified by HPLC as described before (Schäfer *et al.*). For the detection of 6-aminohexanoic acid by HPLC, a Dionex Ultimate 3000 system (Thermo Scientific) was equipped with a Primesep 100 column (5 µm particle size, dimensions: 4.6\* 250 mm) from SIELC Technologies (Wheeling, IL, USA). Mobile phases were composed of 0.4 % (v/v) trifluoroacetic acid in MilliQ water (A), 0.1 % (v/v) formic acid in MilliQ water (B), and acetonitrile (C). Ten µl of sample was injected. The flow and the column temperature were kept constant at 1.45 ml min<sup>-1</sup> and 32°C, respectively. The gradient profile was as follows: 70 % B, 30 % C for 2 min; 70-46.8 % B, 30 % C in 12 min; 46.8-25 % B, 30 % C in 1 min; 25-5 % B, 30-95 % C in 0.5 min; 5 % B, 95 % C for 2 min; 5-42.5 % B, 95-5 % C in 0.5 min; 42.5 % B, 5 % C for 2 min; 42.5-70 % B, 5-30 % C in 0.5 min; 70 % B, 30 % C for 1 min. Detection was accomplished via a charged aerosol detector (Corona™ Veo™ RS, Thermo Scientific).

The compounds were identified with HPLC-MS/MS using an Agilent 1290 Infinity series HPLC system (Agilent Technologies, Waldbronn, Germany) coupled to a QTrap® 6500+ mass

spectrometer (AB Sciex, Darmstadt, Germany) and controlled by Analyst® 1.7.0 software. Chromatographic separation was performed on a Poroshell 120 column (3 mm x 150mm x 2.0 µm, Agilent Technologies) at 40 °C. Phases A and B consisted of MilliQ® water and 0.1 % (v/v) formic acid in acetonitrile, respectively. Five µL of the sample were injected and the flow rate amounted to 0.4 mL min<sup>-1</sup>). The following gradient profile was applied: 95 % A for 2 min, 95-50 % A for 4 min, 50-10 % A for 3 min, 10-95 % A for 1 min, 95 % A for 2 min. Electrospray-ionization (ESI) was conducted in polarity switching mode with a source temperature of 500 °C and ion spray voltage of 5.5 kV (positive mode) or 4.5 kV (negative mode). For each compound, two mass transitions were detected in multiple reaction monitoring (sMRM) employing an entrance potential of 10 V.

O<sub>2</sub> was quantified using a Trace 1310 gas chromatograph (Thermo Fisher Scientific, Waltham, MA) equipped with a TG-BOND Msieve 5A capillary column (30 m, I.D.: 0.32 mm, film thickness: 30 µm, ThermoFisher Scientific) and a thermal conductivity detector operating at 100 °C with a filament temperature of 300 °C and a reference gas flow rate of 2 mL min<sup>-1</sup>. Argon gas was applied as carrier gas at a constant flow rate of 5 mL min<sup>-1</sup>. The injection temperature was set to 50 °C, and a split ratio of 2 was applied. The oven temperature was kept constant at 35 °C for 5 min. Nitrogen was used as the internal standard. Although the gas-tight syringe was used for headspace sampling, the presence of a small amount of air in the needle was inevitable. We quantified the amount of oxygen in the needle by sampling 100% nitrogen gas. A sample of 100% nitrogen contained 1.58 ± 0.22% oxygen (Figure S1). A respective correction was included for headspace samples with a measured oxygen concentration below 5%.

### 3 Calculation of $r_5$ and $r_6$ in single species setups

The capacities of *E. coli* and *P. taiwanensis* VLB120 to form AA from the AlkJ product 6-oxohexanoic acid ( $r_5$ ) and 6HA ( $r_6$ ), respectively, were estimated as follows:

$r_5$  was estimated from the conversion of  $\epsilon$ -CL by *E. coli*\_CL shown in Figure 2C, where AA accumulated as a by-product. Within 3 h of biotransformation,  $0.086 \pm 0.001$  mM AA accumulated in the medium (Figure 2C) translating into a specific activity of  $0.32 \pm 0.01$  U  $\text{g}_{\text{CDW}}^{-1}$  ( $1.5 \text{ g}_{\text{CDW}} \text{ L}^{-1}$  of biomass used). This translates into a volumetric rate of  $0.019 \text{ mM}_{\text{AA}} \text{ h}^{-1}$  for  $r_5$ .

$r_6$  was estimated from the conversion of 6HA in a shake flask culture of *P. taiwanensis* VLB120 (Figure S4). 6HA was added to concentrations of 1 and 5 mM, for which similar AA accumulation kinetics were observed. The average specific AA formation rate amounted to  $0.69 \pm 0.14$  U  $\text{g}_{\text{CDW}}^{-1}$  translating into a volumetric rate of  $0.041 \text{ mM}_{\text{AA}} \text{ h}^{-1}$  for  $r_6$ .

## 4 Supplementary Tables

**Supplementary Table S1:** Strains and plasmids used in this study

	Characteristics	Reference
<b>Strains</b>		
<i>E. coli</i>		
DH5α	<i>supE44ΔlacU169(Φ80lacZΔM15) hsdR17 recA1 endA1 gyrA96 thi-1 relA1</i>	(Hanahan, 1983)
JM101	<i>supE thi-1 Δ(lac-proAB) F'[traD36 proAB+lacIqlacZΔM15]</i>	(Messing, 1979)
<i>P. taiwanensis</i> VLB120	solvent tolerant, styrene degrading bacterium, isolated from forest soil	(Köhler <i>et al.</i> , 2013)
<b>Plasmids</b>		
pAlaDTA	p15A ori, carries <i>lacI</i> , <i>lacUV5</i> promoter, <i>alaD</i> , and <i>cv2025</i> , Cam <sup>R</sup>	(Ladkau <i>et al.</i> , 2016)
pJ10	broad-host-range vector pCom10 ( <i>alk</i> regulation system) carrying <i>alkJ</i> , Km <sup>R</sup>	(Schrewe <i>et al.</i> , 2014)
pJ10Lact	pJ10 derivative carrying lactonase gene after <i>alkJ</i> , Km <sup>R</sup>	This study
pSEVA_CL_2	ColE1/pRO1600 ori, carries <i>lacI</i> <sup>q</sup> , <i>P<sub>trc</sub></i> promoter, Cyp genes, <i>P<sub>trc</sub></i> , <i>cdh</i> , <i>chmo</i> , Km <sup>R</sup>	(Schäfer <i>et al.</i> , 2020)
pSEVA_6HA_2	ColE1/pRO1600 ori, carries <i>lacI</i> <sup>q</sup> , <i>P<sub>trc</sub></i> promoter, Cyp genes, <i>P<sub>trc</sub></i> , <i>cdh</i> , <i>chmo</i> , <i>lact</i> , Km <sup>R</sup>	(Schäfer <i>et al.</i> , 2020)
pSEVA244_T_AlkJ_TA_AlaD	ColE1/pRO1600 ori, carries <i>lacI</i> <sup>q</sup> , <i>P<sub>trc</sub></i> promoter, <i>alkJ</i> ( <i>P. putida</i> GPo1), <i>tA</i> ( <i>C. violaceum</i> ), <i>alaDH</i> ( <i>B. subtilis</i> ), Km <sup>R</sup>	This study
pSEVA6311::DGC-244	pBBR1 ori, Cyclohexanone regulatory system ( <i>ChnR</i> , <i>P<sub>chnB</sub></i> ), diguanylate cyclase from <i>Caulobacter crescentus</i> , Gm <sup>R</sup>	gift from Daniel Volke
pSEVA634_T_AlkJ_TA_AlaD	pBBR1 ori, carries <i>lacI</i> <sup>q</sup> , <i>P<sub>trc</sub></i> promoter, <i>alkJ</i> ( <i>P. putida</i> GPo1), <i>tA</i> ( <i>C. violaceum</i> ), <i>alaDH</i> ( <i>B. subtilis</i> ), Gm <sup>R</sup>	This study
pSEVA634_T_AlkJ_TA	pBBR1 ori, carries <i>lacI</i> <sup>q</sup> , <i>P<sub>trc</sub></i> promoter, <i>alkJ</i> ( <i>P. putida</i> GPo1), <i>tA</i> ( <i>C. violaceum</i> ), , Gm <sup>R</sup>	This study

**Supplementary Table S2:** Primers used for cloning.

Primer#	Function	Sequence
PLS019	Lact fwd	<u>CTACCATAGATTCCGGACGGTTTCAG</u> <b>TAGTGGAGGT</b> TACTAGATGGG <b>CACCTCACCCAATC</b>
PLS020	Lact rev	<u>GCCAAAACAGAAGCTTGGCTGCAGG</u> <b>TCAGGCGCGCTTGAACCAC</b>
PLS034	AlkJ fwd	<u>TGTGAGCGGATAACAATTTACACCTACTAGAG</u> <b>TAGTGGAGGT</b> TAC TAG <b>ATGTACGACTATATAATCGTTG</b>
PLS035	AlkJ rev	<u>GAGCTCGAATTCGCGCGGCCGCGGCTTACATGCAGACAGCTATC</u>
PLS039	TA fwd	<u>CGCGAATTCGAGCTCGGTACCCGGG</u> <b>TAGTGGAGGT</b> TACTAGATGC <b>AGAAACAGCGTACCACCTCTCAG</b>
PLS040	TA rev	<u>GCATGCCTGCAGGTCGACTCTAGAGCTA</u> <b>TTTTTCGAACTGCGGGTG</b> <b>GCTCCA</b> <u>AGCGCTGGCGAGGCCACGCGCTTTG</u>
PLS041	AlaD fwd	<u>TCTAGAGTCGACCTGCAGGCATGCA</u> <b>TAGTGGAGGT</b> TACTAGATGAT <b>CATAGGGGTTCTAAAGAG</b>
PLS042	AlaD rev	<u>TTTTCCAGTCACGACGCGGCCGCACTA</u> <b>TTTTTCGAACTGCGGGTG</b> <b>GCTCCA</b> <u>AGCGCTAGCACCCGCCACAGATG</u>
PLS045A	Gm <sup>R</sup> and pBBR1 ori fwd	<b>CTTGGACTCCTGTTGATAGATC</b>
PLS051	Gm <sup>R</sup> and pBBR1 ori rev	<b>CGCTCTCCTGAGTAGGAC</b>
PLS052	<i>lacI<sup>q</sup></i> _P <sub>trc</sub> with genes fwd	<u>CGGATTTGTCCTACTCAGGAGAGCGTTCACCGACAAACAACAGAT</u> <b>AAAAC</b>
PLS053	<i>lacI<sup>q</sup></i> _P <sub>trc</sub> with genes rev	<u>CTGGATCTATCAACAGGAGTCCAAGACTAGTCGCCAGGGTTTTTC</u>

The following labeling is used: **binding region**, overlap to vector, scar, **RBS**, **Stop codon**, **Strep-Tag**, **Spacer**

**Supplementary Table S3:** Specifications for biotransformation experiments.

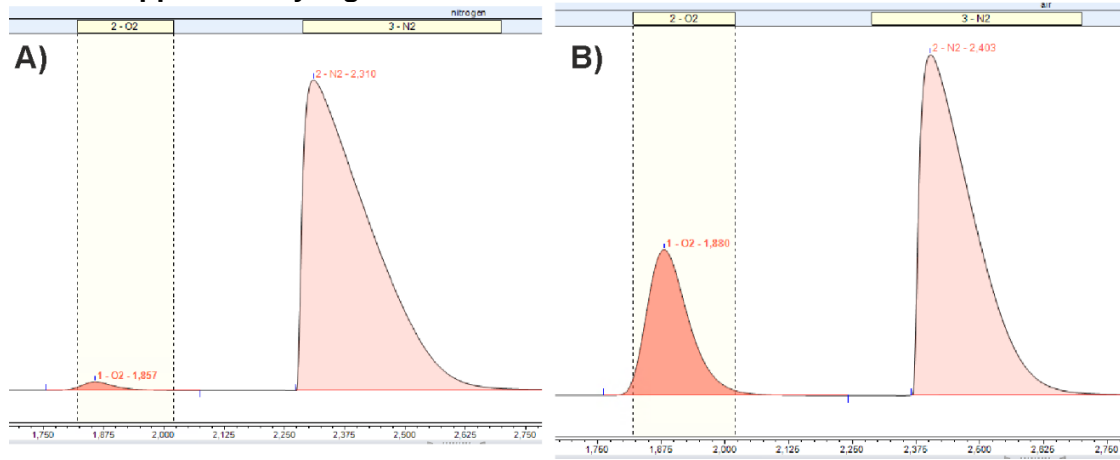
Experiment shown in	<i>E. coli</i> cell concentration [g <sub>CDW</sub> L <sup>-1</sup> ]	Ratio VLB120 / <i>E. coli</i>	Flask volume [mL]	Liquid volume [mL]	Initial substrate concentration [mM] <sup>b</sup>
Fig. 2A, B	0.5	n.a. <sup>a</sup>	100	10	5 (6OH or ε-CL)
Fig. 2C	1.5	n.a.	250	40	5 (ε-CL)
Fig. 3	1.5	1	100	10	5
Fig. 4	0.5, 1	1	250	25	5
Fig. 5	1.5	1	250	12.5, 50	5
Fig. 6, Table 1	1	1	250	12.5	5 <sup>c</sup>
Fig. S2	1.5	0.375	100	10	5
Fig. S3, Table 1	1.5	1	250	12.5	10 <sup>c</sup>

<sup>a</sup> n.a., not applicable

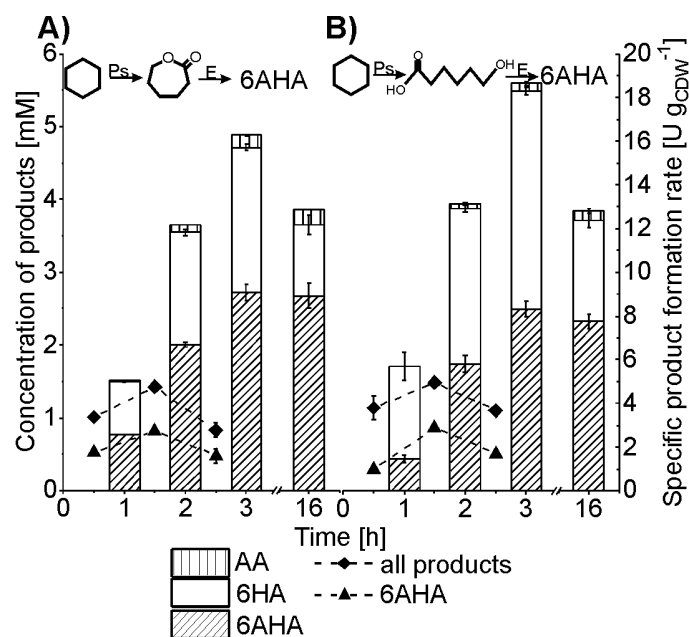
<sup>b</sup> refers to the concentration of cyclohexane if not stated otherwise

<sup>c</sup> also cycloheptane was applied in stated concentrations

## 5 Supplementary Figures



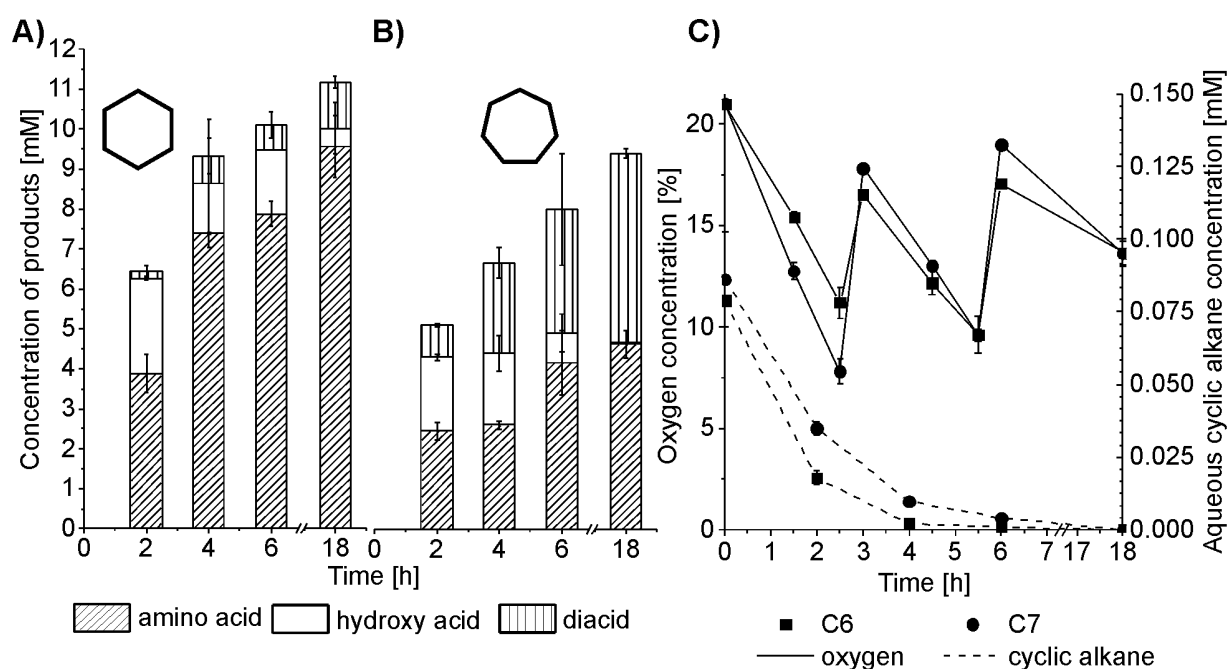
**Supplementary Figure S1: Oxygen measurement by GC.** The panels show the GC chromatograms for a sample of 100% nitrogen (A) and air (B).



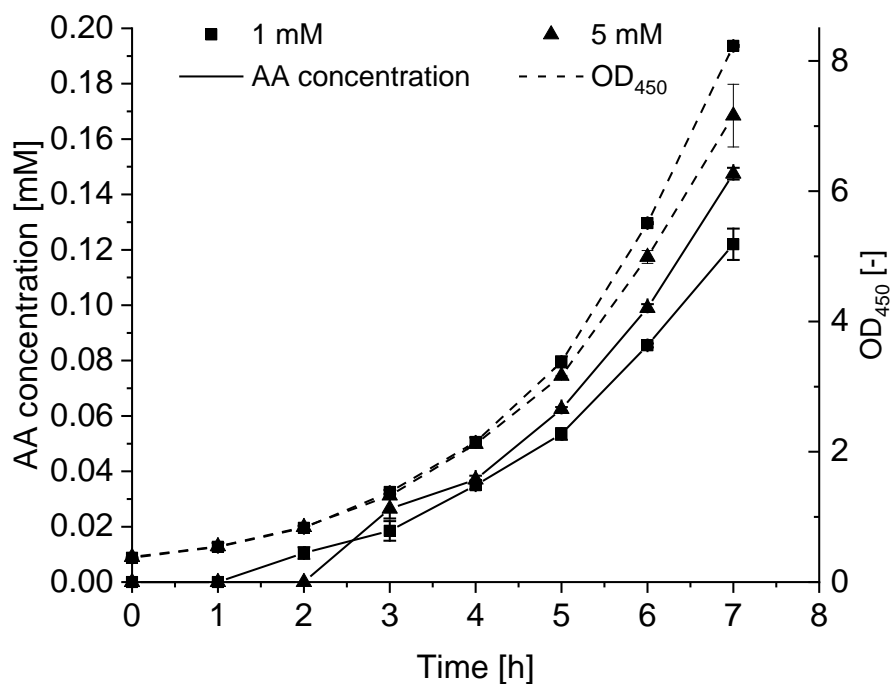
**Supplementary Figure S2: Application of *P. taiwanensis* and *E. coli* strains at a lower strain ratio.**

The panels show the product concentrations accumulated after different reaction times (bars) and specific whole-cell activities over 3 h for 6AHA and overall product formation (curves). For the strain combinations *P. taiwanensis*\_CL / *E. coli*\_CL (A) and *P. taiwanensis*\_6HA / *E. coli*\_6HA (B), biotransformations were performed with biomass concentrations of 1.5 and 4 g<sub>CDW</sub> L<sup>-1</sup> *P. taiwanensis* and *E. coli* strains, respectively, in 25 mL liquid volume in closed screw-capped 250 mL flasks and were started by adding 5 mM cyclohexane (referred to the aqueous phase volume). Intermediate concentrations not depicted in the graphs remained below 50 μM. Means and error bars refer to two independent experiments. The average experimental errors over all measurements for specific product formation rates, 6HA concentrations, 6AHA concentrations, and AA concentrations are 6.6, 5.7, 4.9, and 20.0 %, respectively.





**Supplementary Figure S3: Conversion of 10 mM cyclohexane (A) or cycloheptane (B) under optimized conditions.** Panels A and B show product concentrations accumulated after different reaction times. A 1:1 strain ratio was applied for the strain combination *P. taiwanensis*\_CL / *E. coli*\_CL with a total biomass concentration of  $4.0 \text{ g L}^{-1}$  in 12.5 mL liquid volume in 250 mL screw-capped and closed flasks. Biotransformations were started by adding 10 mM of cycloalkanes (referred to the aqueous phase volume). Intermediates that are not depicted in the graphs accumulated to less than  $50 \mu\text{M}$ . Panel C shows the courses of oxygen concentrations in the gas phase (solid lines) and of aqueous cyclohexane (C6) and cycloheptane (C7) concentrations (dashed lines). Means and error bars refer to two independent experiments. The average experimental errors over all measurements for 6HA concentrations, 6AHA concentrations, AA concentrations, 7-hydroxyheptanoic acid concentrations, 7-aminoheptanoic acid concentrations, pimelic acid concentrations, oxygen concentrations, cyclohexane concentrations, and cycloheptane concentrations are 67.1, 6.2, 3.8, 26.9, 9.9, 17.6, 3.3, 26.2, and 12.0 %, respectively.



**Supplementary Figure S4: Conversion of 6HA to AA by *P. taiwanensis* VLB120.** Growing cells were inoculated in M9\* medium at an OD<sub>450</sub> of 0.2. After 2 h of growth (OD<sub>450</sub>~0.4, time point 0 h), 1 mM (squares) or 5 mM (triangles) 6HA was added and growth (dashed lines) as well as AA formation (solid lines) were recorded. Means and error bars refer to two independent experiments. The average experimental errors over all measurements for the AA concentration and OD<sub>450</sub> are 6.7 and 2.7 %, respectively.

## 6 References

- Gibson, D.G., Young, L., Chuang, R.-Y., Venter, J.C., Hutchison, C.A., and Smith, H.O. (2009) Enzymatic assembly of DNA molecules up to several hundred kilobases, *Nat Methods* **6**: 343-345.
- Halan, B., Schmid, A., and Buehler, K. (2010) Maximizing the productivity of catalytic biofilms on solid supports in membrane aerated reactors, *Biotechnol Bioeng* **106**: 516-527.
- Hanahan, D. (1983) Studies on transformation of *Escherichia coli* with plasmids, *J Mol Biol* **166**: 557-580.
- Köhler, K.A., Rückert, C., Schatschneider, S., Vorhölter, F.-J., Szczepanowski, R., Blank, L.M., *et al.* (2013) Complete genome sequence of *Pseudomonas sp.* strain VLB120 a solvent tolerant, styrene degrading bacterium, isolated from forest soil, *J Biotechnol* **168**: 729-730.
- Ladkau, N., Assmann, M., Schrewe, M., Julsing, M.K., Schmid, A., and Bühler, B. (2016) Efficient production of the Nylon 12 monomer  $\omega$ -aminododecanoic acid methyl ester from renewable dodecanoic acid methyl ester with engineered *Escherichia coli*, *Metab Eng* **36**: 1-9.
- Lindmeyer, M., Meyer, D., Kuhn, D., Bühler, B., and Schmid, A. (2015) Making variability less variable: matching expression system and host for oxygenase-based biotransformations, *J Ind Microbiol Biotechnol* **42**: 851-866.
- Messing, J. (1979) A multipurpose cloning system based on the single-stranded DNA bacteriophage M13, *Recombinant DNA technical bulletin* **2**: 43-48.
- Sambrook, J., and Russell, D.W. (2001) *Molecular cloning: a laboratory manual*. Cold Spring Harbor, NY: Cold Spring Harbor Laboratory.
- Schäfer, L., Bühler, K., Karande, R., and Bühler, B. (2020) Rational Engineering of a Multi-Step Biocatalytic Cascade for the Conversion of Cyclohexane to Polycaprolactone Monomers in *Pseudomonas taiwanensis*, *Biotechnol J* **15**: 2000091.
- Schäfer, L., Karande, R., and Bühler, B. (2020) Maximizing biocatalytic cyclohexane hydroxylation by modulating cytochrome P450 monooxygenase expression in *P. taiwanensis* VLB120, *Front Bioeng Biotechnol* **8**: 140.

Schrewe, M., Julsing, M.K., Lange, K., Czarnotta, E., Schmid, A., and Bühler, B. (2014) Reaction and catalyst engineering to exploit kinetically controlled whole-cell multistep biocatalysis for terminal FAME oxyfunctionalization, *Biotechnol Bioeng* **111**: 1820-1830.

Schrewe, M., Ladkau, N., Bühler, B., and Schmid, A. (2013) Direct Terminal Alkylamino-Functionalization via Multistep Biocatalysis in One Recombinant Whole-Cell Catalyst, *Adv Synth Catal* **355**: 1693-1697.

## 6 Supplementary Material for Chapter 2.6

### Strain construction

All primers can be found in Table S2.6.1.

pSEVA244\_T\_ADH was constructed from pSEVA244\_T (Chapter 2). *Acidovorax* sp. CHX100 was cultivated for 4 days in NB medium for DNA isolation performed with the peqLab kit for genomic DNA isolation. The ADH gene (gene no. 1088) (Meyer *et al.*, 2003) was amplified with PLS026 and PLS027 and fused into XmaJI-digested pSEVA244\_T via Gibson assembly (Gibson *et al.*, 2009) to yield pSEVA244\_T\_ADH. The AldDH gene was also amplified from the *Acidovorax* sp. CHX100 genome (gene no. 1089) (Meyer *et al.*, 2003) using the primers PLS028 and PLS029 and ligated into KpnI-digested pSEVA244\_T to yield pSEVA244\_T\_AldDH. Amplification of the AldDH gene with the primers PLS037 and PLS038 and ligation into BamHI-digested pSEVA244\_T\_ADH yielded pSEVA244\_T\_ADH\_AldDH. Similarly, pSEVA244\_T\_alkJ was generated by amplifying alkJ from pJ10 (Schrewe *et al.*, 2013b) using the primers PLS034 and PLS035 and ligation into XmaJI-digested pSEVA244\_T. This vector also was subjected to AldDH gene insertion into its BamHI-site giving rise to pSEVA244\_T\_alkJ\_AldDH.

Gm<sup>R</sup> and pBBR1 origin of replication were amplified from pSEVA6311::DGC-244 using PLS045A and PLS051. The *lac*-regulatory system (*lacIq*-P<sub>trc</sub>) with the ADH and AldDH genes/ alkJ and AldDH genes were amplified from pSEVA244\_T\_ADH\_AldDH/ pSEVA244\_T\_alkJ\_AldDH with PLS052 and PLS053. Both fragments were assembled yielding pBL\_AA\_Ac/ pBL\_AA\_alkJ. The empty plasmid pSEVA634\_T was generated by fusing the Gm<sup>R</sup>-pBBR1 fragment with the *lac*-regulatory system, which was amplified with PLS052 and PLS053 from pSEVA244\_T.

Gm<sup>R</sup> and RK2 origin of replication were amplified from pSEVA628S using PLS045A and PLS051. The *lac*-regulatory system (*lacIq*-P<sub>trc</sub>) with the ADH and AldDH genes/ alkJ and AldDH genes were amplified from pSEVA244\_T\_ADH\_AldDH/ pSEVA244\_T\_alkJ\_AldDH with PLS052 and PLS053. Both fragments were assembled yielding pRKL\_AA\_Ac/ pRKL\_AA\_alkJ.

The empty plasmid pSEVA624\_T was generated by fusing the Gm<sup>R</sup>-RK2 fragment with the *lac*-regulatory system, which was amplified with PLS052 and PLS053 from pSEVA244\_T. ADH and AldDH genes were amplified from pSEVA244\_T\_ADH\_AldDH with PLS054 and PLS055 and fused with HindIII- and NdeI-digested pSEVA638::DGC-244 to yield pBX\_AA\_Ac.

Genome integration was performed according to Choi & Schweizer (2006). pUC18R6K-mini-Tn7T-Gm and pTNS2 were a gift from Herbert Schweizer (Addgene plasmid 65022 and 64968). The *lac*-regulatory system (*lacI<sup>q</sup>*-P<sub>trc</sub>) with the ADH and AldDH genes were amplified from pSEVA244\_T\_ADH\_AldDH with PLS049 and PLS050 and inserted in BamHI- and KpnI-digested pUC18R6K-mini-Tn7T-Gm to yield pUC18\_mini\_Tn7\_Gm\_LacIq-adh-aldDH. 50 ng of pUC18\_mini\_Tn7\_Gm\_LacIq-adh-aldDH and 50 ng of pTNS2 were transformed to 100  $\mu$ L competent *P. taiwanensis* VLB120\_Strep and incubated for 1.5 h at 37°C. Cells were plated on LB agar plated containing 30  $\mu$ g mL<sup>-1</sup> gentamycin and 100  $\mu$ g mL<sup>-1</sup> streptomycin.

**Table S2.6.1:** Primer used during the cloning. **binding region**, overlap to vector, scar, **RBS**, **Stop codon**, **Strep-Tag**, and **Spacer**.

Primer#	Function	Sequence
PLS026	ADH fwd	TGTGAGCGGATAACAATTTACACCTACTAGAG TAGTGGAGGT TACTAGATGCGCTGTTATTGCGTG
PLS027	ADH rev	GAGCTCGAATTCGCGCGGCCGCGGCCTA TTTTTCGAACT GCGGGTGGCTCCA AGCGCTTGGGATCAGTACGGCAC
PLS028	AldDH fwd single	GGCCGCGCGAATTCGAGCTCGGTAC TAGTGGAGGT TACTAGATGTATCCCCAACTCAGC
PLS029	AldDH rev single	TCGACTCTAGAGGATCCCCGGGTACCTA TTTTTCGAACT GCGGGTGGCTCCA AGCGCTATTAAGTTGCGAAATGAACTTG
PLS034	AlkJ fwd	TGTGAGCGGATAACAATTTACACCTACTAGAG TAGTG GAGGT TACTAGATGTACGACTATATAATCGTTG
PLS035	AlkJ rev	GAGCTCGAATTCGCGCGGCCGCGGC TTACATGCAGACAGCTATC
PLS037	AldDh fwd	CGCGAATTCGAGCTCGGTACCCGGG TAGTG GAGGT TACTAGATGTATCCCCAACTCAGC
PLS038	AldDH rev	GCATGCCTGCAGGTCGACTCTAGAGCTA TTTTTCGAACT GCGGGTGGCTCCA AGCGCTATTAAGTTGCGAAATGAACTTG
PLS049	LacI <sup>q</sup> _ADH_AldDH for integration fwd	TCGATCATGCATGAGCTCACTAGTG AATTAATTGACCCATCGAATGGTG
PLS050	LacI <sup>q</sup> _ADH_AldDH for integration rev	GGCCTGCAAGGCCTTCGCGAGGTAC ACTAGTCGCCAGGGTTTTTC
PLS045A	pSEVA resistance and ori fwd	CTTGGACTCCTGTTGATAGATC
PLS051	pSEVA resistance and ori rev	CGCTCTCCTGAGTAGGAC
PLS052	LacI <sup>q</sup> _ADH_AldDH for pSEVA fwd	CGGATTTGTCCTACTCAGGAGAGCG TTCACCGACAAACAACAGATAAAAC
PLS053	LacI <sup>q</sup> _ADH_AldDH for pSEVA rev	CTGGATCTATCAACAGGAGTCCAAG ACTAGTCGCCAGGGTTTTTC
PLS054	ADH_AldDH for pSEVA638 fwd	ATTCGAGCTCTTAGGAGGAAAAACA TAGTGGAGGTTACTAGATGCGCTG
PLS055	ADH_AldDH for pSEVA638 rev	TTTTCCAGTCACGACGCGGCCGCA TGCATGCCTGCAGGTCCG

### Gene sequence of alcohol dehydrogenase (ADH) gene from *Acidovorax* sp. CHX100 (no. 1088)

ATGCGCTGTTATTGCGTGATGCACCATTCAAAGCCGCTTGAAC TTGTCGAGCGGGAGACA  
CCGCAGCCCGTGGGAACCGAAGTGCTCGTGCGGGTGAAGGCTGCGGGCCTTTGCCACA  
CGGATCTGCACATCTGGGAAGGCTTTTACGACCTGGGCGGGCGGCAAGCGCATGAACCT  
GGCAGACCGTGGCATCAAGCCACCCATCATCCTCAGCCACGAAATCTGTGGCGAGGTG  
GTGGCGGCCGGGCCGGACGCAGGCGAAGTCCCCACGGCTCCCGCTTCGTGATCCACC

---

CCTGGATTGGCTGCGGTGAATGCCCCACCTGCCTGCGCGGCGATGAAAACCTGTGCCT  
GAAGGGCCGCGCCCTTGGCGTGGCACGCCCGGTGGCTTTGCCGATTACGTGATCGTT  
CCCCACCCGCGCTACCTGGTCAACATCGACGGTCTGGACGATGCCGAGGCGGCGCCTC  
TGGCCTGCGCGGGCGTAACAACCTACAGCGCCATCAAGAAGCTGGGCGACGGCATCCA  
CCACGAGCCCGTCGTCATCATCGGCGCCGGCGGGCCTGGGCCTGATGGCCATCGAGGTG  
CTCAAGGCCCTGGGCGGCAAAGGCGCCATCGTGGTGGACATCGACCCTGCCAAGCGCG  
AAGCCGCACTGGCCGAGGCGCTCTGGCGGTGATTGACGGCAAGGCTGCCGATGCGGC  
CGCCAGATCATCGCGGCGACCGAAGGCGGTGCCGGCCAGATTCTGGATCTGGTGGGC  
GCGTCCGCCACCGTATCGCTGGCCATGCAAAGCGCCCGGCGCGGCGGCCACATCGTCA  
TCTGCGGCCTGATGGGCGGCGACCTGACCATCTCGCTGGCCACCATCCCGCTGCGCCC  
GCTGTGCATCGAGGGCAGCTACGTTGGCACCCCTGTCCGAACTGCAAGAACTGGTGGAG  
CTGGTCAAGCGCACCGGCATGAAGTCTATTCCGGTGTGCGCGCCCGCCGATGTCCCAGG  
TGAACCAGGCCATCGACGACCTGCACCACGGCAAGGTGATCGGGCGTGCCGTACTGAT  
CCCATGA (1,053 bp)

**Gene sequence of aldehyde dehydrogenase (AldDH) gene from *Acidovorax* sp.  
CHX100 (no. 1089)**

ATGTATCCCCAACTCAGCCTCTACATCGACGGACAAATGCTGCGCGGCGAAGGCCGC  
CGCGAGCAGGATGTCTGAACCCCGCCAACAACCAGGTGATCGGCCAGCTGCCGCAT  
GCCACCCAGGCCGACCTAGACATGGCGCTGTCAGCGGCACAGCGCGCCTTCGCGTCCG  
TGGCGCACAGCTCGGCGATGCAGCGCGCGCAGGTGCTGAAAGCCGTCCGAGGATTG  
ATCCGCGAACGTGCGCCGCAAATTGGCCGCAACCTCACCTGGAGCAGGGCAAGCCCC  
TGGCCGAGGGCGTGGGCGAAGTGGCCATCTGCGCCGAGCACGCCGAGTGGCATGCCG  
AGGAATGCCGGCGCATCTACGGCCGCCTTATTCCGCCGCGCGATGCCAACGTGCAGC  
AGACCGTGCTGCGCGAACCCATCGGCGTGTGCGTGGCGTTCTCGCCCTGGA ACTTCC  
CGTTCAGCCAGGCCTTTCGCAAGGTGGTTCGCGGCCATTGGCGCCGGGTGCACGGTTAT  
CCTCAAGGGCTCCAGCGACACACCGGCCTCGGTGCAGGCGATCGCCGAGCTCTTTCATG  
ACGCCGGCTTGCCACCGGGCGTGTGTAACGTGGTGTCCGGCGATTCCGGGATGATCTC  
GGACTACCTGATCCGCTCGCCATCGTGCGAAGATTTCTTCACGGGCTCCACGCCC  
GTCGGGCAGCAGCTGGCTGCGCTGGCCGGTGCGAACATGAAGCGCAGCACCATGGAGC  
TTGGCGGCCACGCGCCCGTATCGTTTGTGACGATGCGGACATCGACCGGGCAGCAGA  
CGTGCTGTCTGGCTTCAAGTTCGCAACGCGGGACAGGTGTGCATTTCCCCACGCGCT  
TTTATGTGCAGGACGGTGTGTACGACCGTTTCGTGCAACGATTTCGCGCAGCGGGCGCAG  
GCCCTGGCGGTTCGGTACGGGCTGGTTGAAACCAACCGCATGGGGCCGCTGGCGCAAC  
CGCGCCGCGTTGCCGCCATGGAGGGCTTCGTGGAAGACGCCCGCCAGCGCGGGCGCCAA  
GATCGTGGCGGGCGGCCATCGGCTGCAAGGCGACGGCAACTTCTTCGCCCCACGGTG  
CTGGCTGACTTGCCGACGACTCGCGCTTCATGACCGAGGAGCCCTTCGGCCCGATGG  
CCGGCATGGTGCATTCAAGACGGTGGAGAAGTGCTCGCGCGCGCCAACAGCCTGCC  
CTTCGGCCTGGCGTCGTATGCCTTCACCACGTCACTGAATAACGCGCACCAGATCTCG  
CGCGGGCTTGAAGCGGGCATGGTGTCCATCAACCACATCGGGCTGGCGCTGGCCGAGA  
CACCGTTCGGTGGCATCAAGGAAAGTGGCTATGGCAGCGAGGGCGGCAGCGAAACCTT  
CGACGGCTACCTGACCACCAAGTTCATTTGCAACTTAATTGA (1,431 bp)

### Determination of co-factor specificity of ADH and AldDH

*P. taiwanensis* VLB120 (pSEVA244\_T\_ADH) and *P. taiwanensis* VLB120 (pSEVA244\_T\_AldDH) were cultivated followed by Strep-tag-mediated enzyme isolation as described before (Chapter 2.2) yielding  $0.06 \text{ mg mL}^{-1}$  ADH and  $0.01 \text{ mg mL}^{-1}$  AldDH. Activity assays were performed at  $30^\circ\text{C}$  in a total volume of 1 mL in 100 mM Kpi buffer (pH=7.4) with 20  $\mu\text{L}$  of the purified enzyme fraction(s), 0.2 mM cofactor(s) and 1 mM of 6HA. NAD(P)H formation was followed by monitoring the absorbance at 340 nm using a Cary Bio 300 UV-visible spectrophotometer (Varian, Palo Alto, USA, Figures S2.6.1 and S2.6.2).

### Additional Supplementary Figures and Tables

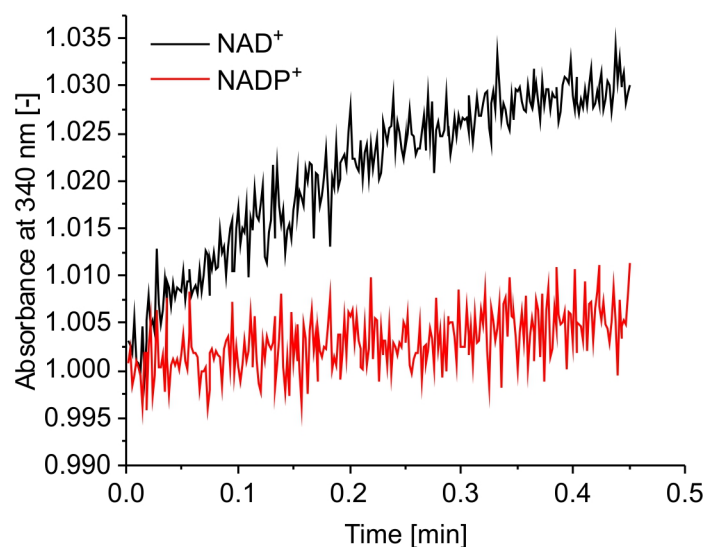


**Figure S2.6.1:** Cofactor preference of ADH. The graph shows the increase in absorbance at 340 nm after addition of NAD<sup>+</sup> (black) or NADP<sup>+</sup> (red) to a reaction mixture containing the substrate 6HA and ADH prepared as described in section 3.7.



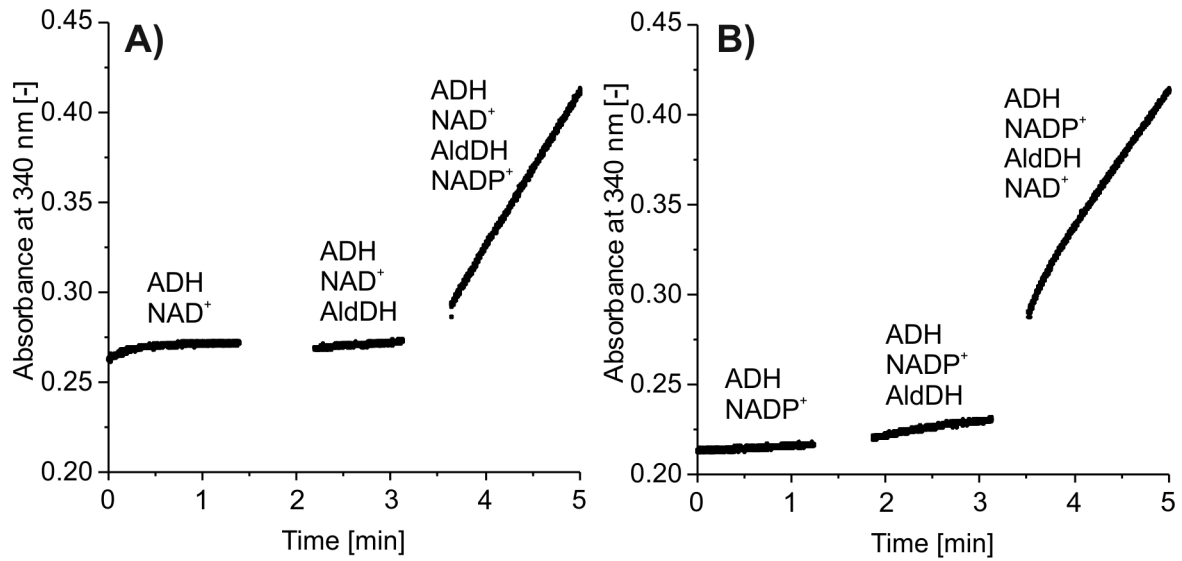


**Figure S2.6.2:** Cofactor preference of AldDH. Assays were conducted with 6HA as substrate following absorbance at 340 nm. **(A)** ADH and NAD<sup>+</sup> were incubated for 1 min. Then, AldDH was added to the reaction mixture, which did not lead to a significant absorption increase indicating that dehydrogenase-mediated conversion was neglectable. This changed upon NADP<sup>+</sup> addition after another 3 min. **(B)** ADH and NADP<sup>+</sup> were incubated for 1 min. Then, AldDH was added to the reaction mixture, which again did not lead to a significant change in the absorption slope. NAD<sup>+</sup> addition after another 3 min led to a strong absorption increase.



**Figure S2.6.3:** Genomic organization of cyclohexane degradation genes in *Acidovorax* sp. CHX100. The genes encoding a lactonase (Lact), a cyclohexanone monooxygenase (CHMO), a cyclohexanol dehydrogenase (CDH), a protein of unknown function (?), a putative alcohol dehydrogenase (ADH), and a putative aldehyde dehydrogenase (AldDH) form an operon presumably controlled via one promoter (P) upstream of the Lact gene and spanning a genomic region of 7 kb. Cyp genes are not part of this operon.

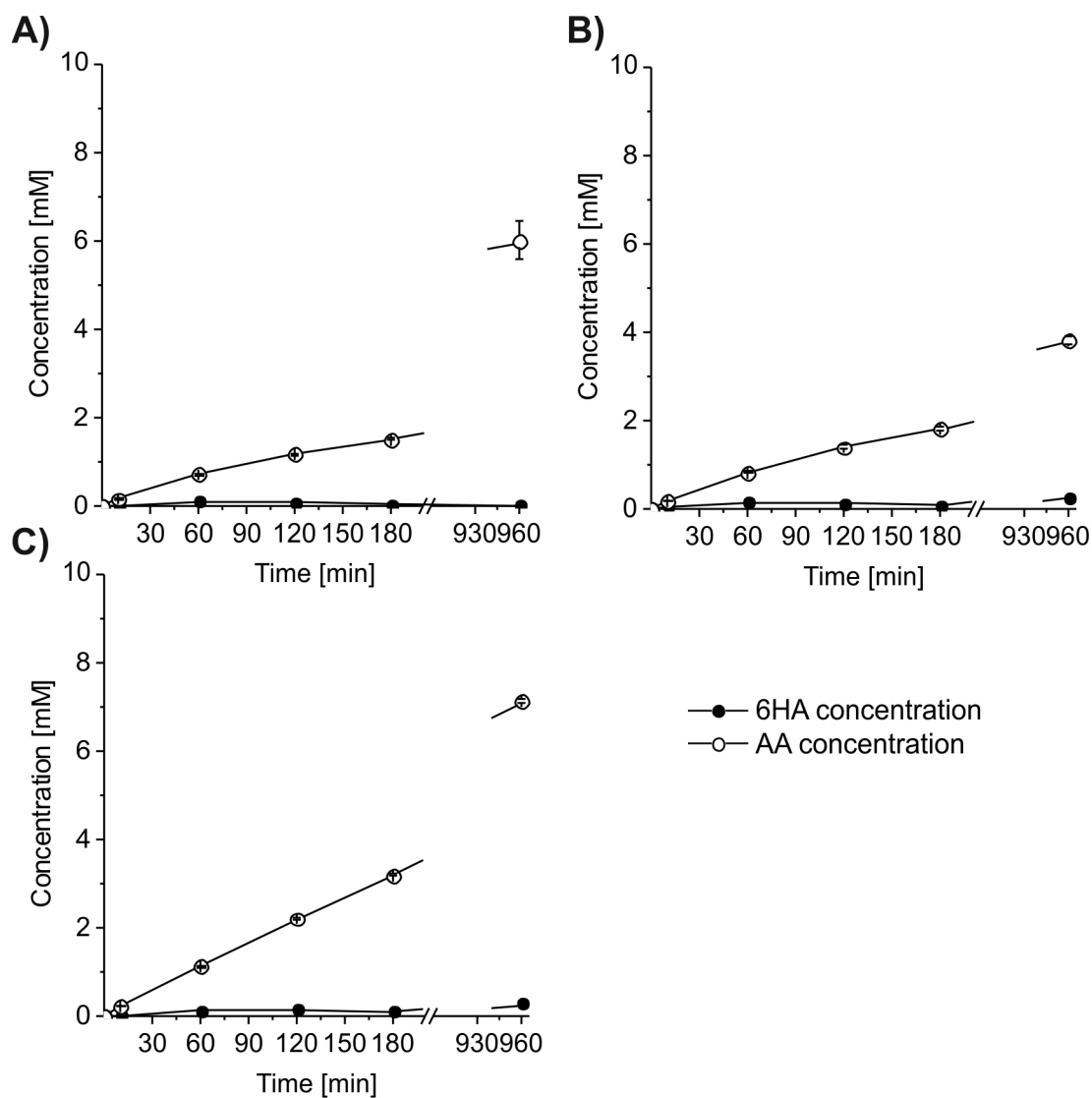


**Figure S2.6.4:** Resting cell assays employing *P. taiwanensis* VLB120 pSEVA\_6HA\_2 + pBL\_AA\_Ac (A), pRKL\_AA\_Ac (B), or pBX\_AA\_Ac (C). 6HA and AA concentrations are depicted for the experiment shown in 2.6.3C, D. Graphs represent average values and standard deviations of two independent biological replicates. The average experimental errors over all measurements for the 6HA and AA concentrations are 9.4 and 2.7 %, respectively.

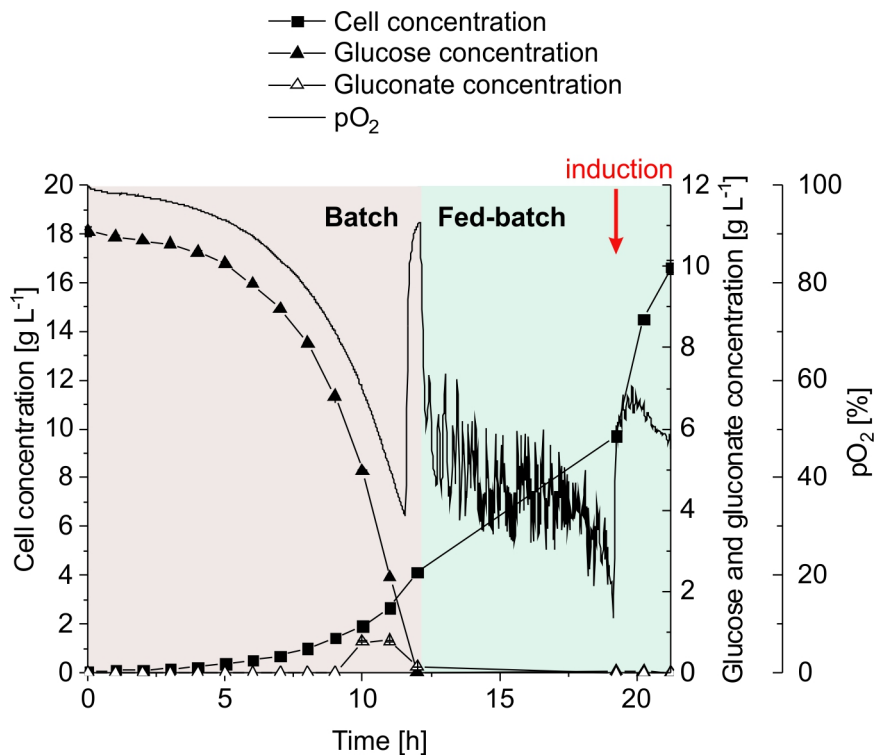


**Figure S2.6.5:** Batch and fed-batch phases of the cultivation of *P. taiwanensis* VLB120 (pSEVA\_6HA\_2, pBX\_AA\_Ac) in a stirred-tank bioreactor under glucose-limited conditions. Time courses of cell, glucose, gluconate, and dissolved oxygen ( $pO_2$ ) concentrations are shown during growth of cells used for the experiment presented in 2.6.5. The cells were induced for 2 h. Graphs represent average values and standard deviations of two technical replicates.

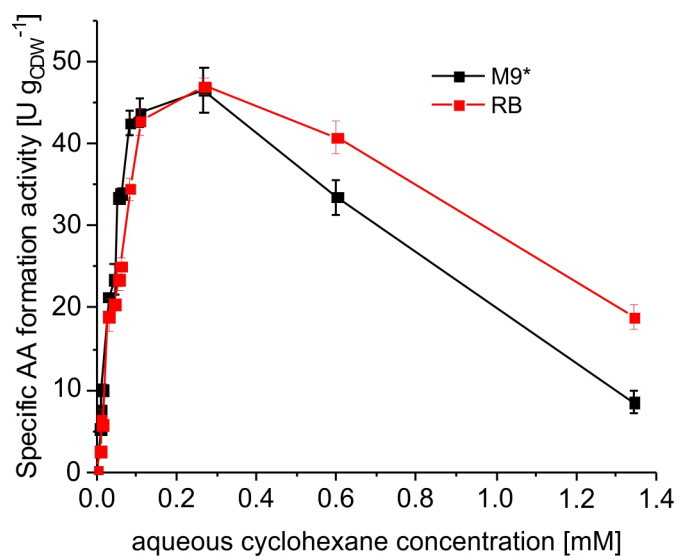


**Figure S2.6.6:** Specific AA formation activity as a function of the aqueous cyclohexane concentrations. *P. taiwanensis* VLB120 (pSEVA\_6HA\_2, pBX\_AA\_Ac) was cultivated in M9\* medium with 0.5% (w/v) glucose, induced by IPTG and 3MB, and harvested after 4 h. After resuspension in Kpi-buffer containing 1% glucose (w/v) to a biomass concentration of  $0.5 \text{ g}_{\text{CDW}} \text{ L}^{-1}$ , 10 mL liquid volume were transferred to 100 mL screw-capped Erlenmeyer flasks and equilibrated for 10 min at  $30^\circ\text{C}$ . Reactions were started by adding different volumes of pure cyclohexane and stopped after 10 min. Given aqueous cyclohexane concentrations represent measured values. Average values and standard deviations of two independent biological replicates are shown. The average experimental errors over all activity measurements is 6.0 %.

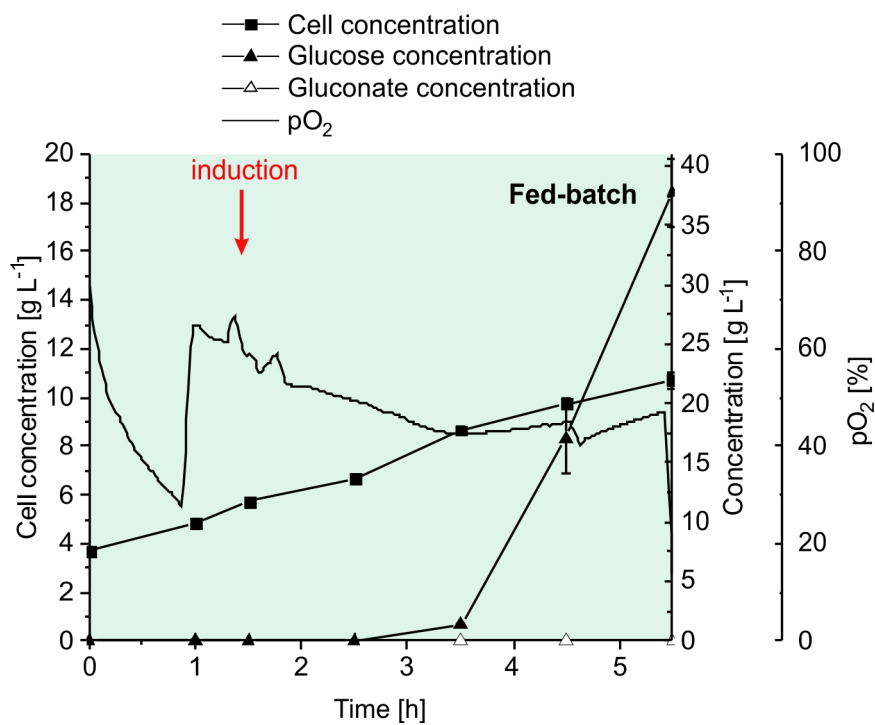


**Figure S2.6.7:** Fed-batch phase in a stirred-tank bioreactor with *P. taiwanensis* VLB120 (pSEVA\_6HA\_2, pBX\_AA\_Ac) growing under glucose-excess conditions. Time courses of cell, glucose, gluconate, and dissolved oxygen (pO<sub>2</sub>) concentrations are shown during growth of cells used for the experiment presented in 2.6.6. The stirrer speed was increased from 1,000 to 1,500 rpm 1 h after the start of exponential feeding for a  $\mu$  of 0.3 h<sup>-1</sup>. The cells were induced for 4 h. Graphs represent average values and standard deviations of two technical replicates.

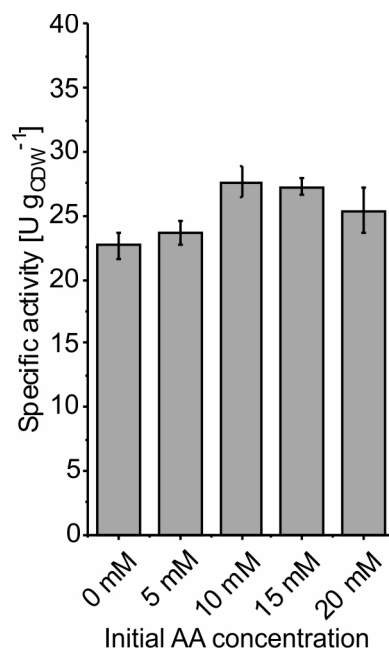


**Figure S2.6.8:** Impact of AA on the specific activity of *P. taiwanensis* VLB120 (pSEVA\_6HA\_2, pBX\_AA\_Ac). Cells were cultivated in M9<sup>+</sup>-containing shake flasks, induced for 4 h, harvested, and resuspended in Kpi-buffer (1 % (w/v) glucose, varying AA concentrations, pH 7.4) to a biomass concentration of 1.5 g<sub>CDW</sub> L<sup>-1</sup>. Biotransformations were conducted in 5 mL liquid volume within 100 mL screw-capped Erlenmeyer flasks, started by adding 5.5 µL pure cyclohexane (corresponding to 10 mM referring to aqueous phase volume) and terminated after 1 h. Graphs represent average values and standard deviations of two independent biological replicates. The average experimental errors over all measurements for the specific activities is 4.5 %.

# Curriculum Vitae

Name Lisa Bretschneider geb. Schäfer  
Born October 22, 1992 in Riesa  
Nationality German  
Academic Degree Master of Science (Molecular Bioengineering)

## Education

2017-2021 **PhD studies** at MLU Halle-Wittenberg & in the group Applied Biocatalysis in the Department of Soalr Materials, Helmholtz-Centre for Environmental Research - UFZ, leipzig, Germany

2015-2017 **Master studies** in Molecular Bioengineering, University of Technology Dresden, Master thesis: Immobilization of MatB for its use in micro(bio)reactors at Leibniz-Institut für Polymerforschung Dresden e.V.

2012-2015 **Bachelor studies** in Molecular Biotechnology, University of Technology Dresden, Bachelor thesis: The Role of Rab proteins in Hedgehog signaling at Max-Planck Institute of Molecular Cell Biology and Genetics

2004-2012 **Abitur** at Werner-Heisenberg-Gymnasium Riesa, Germany

## Publications

Schäfer, L.; Karande, R.; Bühler, B (2020): Maximizing biocatalytic cyclohexane hydroxylation by modulating cytochrome P450 monooxygenase expression in *P. taiwanensis*. *Frontiers in Bioengineering and Biotechnology*, 8, 140.

Schäfer, L.; Bühler, K.; Karande, R.; Bühler, B. (2020): Rational Engineering of a Multi-Step Biocatalytic Cascade for the Conversion of Cyclohexane to Polycaprolactone Monomers in *Pseudomonas taiwanensis*. *Biotechnology Journal*, 15(11), 2000091.

Bretschneider, L.; Wegner, M.; Bühler, K.; Bühler, B.; Karande, R. (2020): One-pot synthesis of 6-aminohexanoic acid from cyclohexane using mixed-species cultures. *Microbial Biotechnology*, 14(3), 1011-1025

Bretschneider, L.; Heuschkel, I.; Ahmed, A.; Bühler, K.; Karande, R.; Bühler, B. (2021): Characterization of different biocatalyst formats for BVMO-catalyzed cyclohexanone oxidation. *Biotechnology and Bioengineering*, 118(7), 2719-2733.

Bretschneider, L.; Heuschkel, I.; Wegner, M.; Lindmeyer, M.; Bühler, K.; Karande, R.; Bühler, B. (2021): Conversion of cyclohexane to 6-hydroxyhexanoic acid using recombinant *Pseudomonas*

---

*taiwanensis* in a stirred-tank bioreactor. *Frontiers in Catalysis*, 1, 683248.

Bretschneider, L.; Heuschkel, I.; Bühler, K.; Karande, R.; Bühler, B. (2021): Rational orthologous pathway and biochemical process engineering for adipic acid production using *Pseudomonas taiwanensis* VLB120. *Metabolic Engineering*, manuscript submitted.

## **Presentations**

Influence of different DNA elements on protein amount, active protein and activity for a cytochrome P450 monooxygenase, 1<sup>st</sup> *Pseudomonas* Grassroots Meeting, 8.-9.11.2018, Frankfurt/Main, Germany

Construction of *in vivo* cascades for the sustainable production of monomers. 6<sup>th</sup> Joint Conference of the DGHM VAAM, 8.-11.03.2020, Leipzig, Germany

Biocatalytic characterization of cyclohexanone monooxygenase (CHMO) derived from *Acidovorax* sp. CHX100 in an isolated enzyme, whole cell, and biofilm format, 2<sup>nd</sup> *Pseudomonas* Grassroots Meeting, 7.-8.11.2019, Leiden, The Netherlands

## **Poster**

Schäfer, L.; Karande, R.; Schmid, A.; Bühler, K.; Bühler, B.: Maximizing biocatalytic cyclohexane hydroxylation by modulating cytochrome P450 monooxygenase expression in *P. taiwanensis* VLB120, 14<sup>th</sup> International Symposium on Biocatalysis and Biotransformations (BioTrans), 7.-11.7.2019, Groningen, The Netherlands

## **Selbstständigkeitserklärung**

Hiermit erkläre ich, Lisa Bretschneider (geb. Schäfer), an Eides statt, dass ich die vorliegende Dissertation selbstständig und ohne fremde Hilfe verfasst habe, dass keine anderen als die von mir angegebenen Quellen und Hilfsmittel verwendet und die den verwendeten Werken wörtlich oder inhaltlich entnommenen Stellen als solche kenntlich gemacht worden sind.

Die Dissertation hat in der gegenwärtigen bzw. in einer anderen Fassung noch keiner Prüfungsbehörde vorgelegen.

---

Leipzig, 07.06.2021